Volume 51 Numbers 20–21 2004 ISSN 0967-0645

DEEP-SEA RESEARCH PART II

or:
nn D. Milliman

st Editors:
E. Morales
B. Lange

Oceanography in the eastern South Pacific: Part I

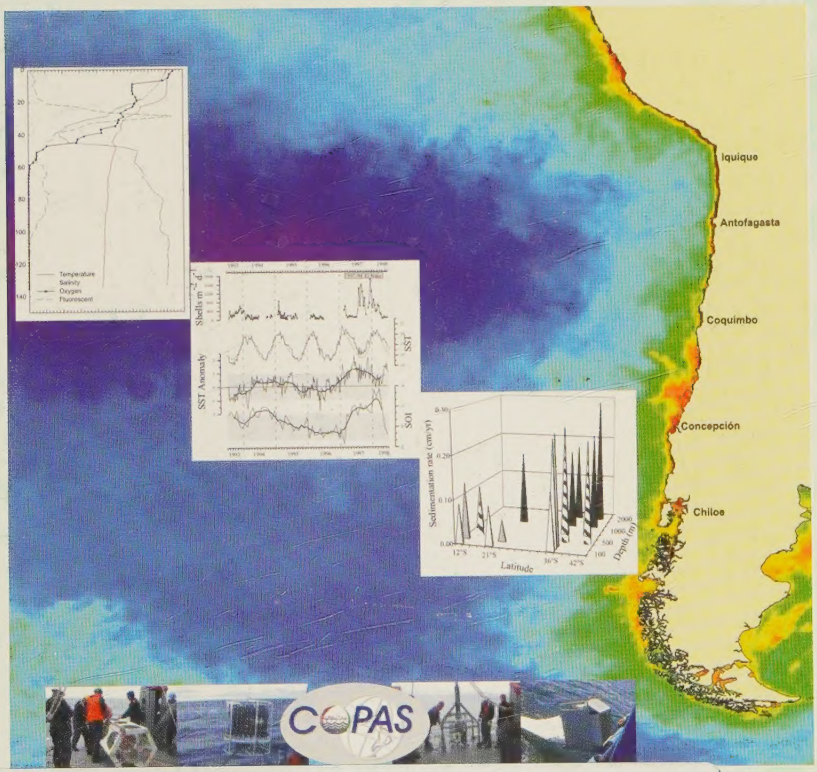

Library
Pacific Islands Fisheries Science Center
Nat'l Marine Fisheries Service

Received Feb 2005

www.elsevier.com/locate/dsr2

DEEP-SEA RESEARCH II

http://www.elsevier.com/locate/dsr2

Editor

PROFESSOR JOHN D. MILLIMAN: *Virginia Institute of Marine Science, School of Marine Science, The College of William and Mary, P.O. Box 1346, Gloucester Point, VA 23062–1346, USA*
E-mail: milliman@vims.edu

Associate Editors

J.W. MURRAY (*Chemistry*): *School of Oceanography, WB-10, University of Washington, Seattle, WA 98195, U.S.A. E-mail: jmurray@ocean.washington.edu*

FRIEDRICH A. SCHOTT: *Institut für Meereskunde an der Universität Kiel, Düsternbrooker Weg 20, D-24105 Kiel, Germany. E-mail: fschott@ifm.uni-kiel.de*

SHARON L. SMITH: *The Rosenstiel School, University of Miami, 4600 Rickenbacker Causeway, Miami, FL 33149, USA. E-mail: ssmith@rsmas.miami.edu*

Founder Editor: DR. MARY SEARS

Publishing Offices Elsevier Ltd, The Boulevard, Langford Lane, Kidlington, Oxford OX5 1GB, UK. Tel: + 44(0) 1865 843000; Fax: + 44(0) 1865 843010.

Advertising information. Advertising orders and enquiries can be sent to: ***USA, Canada and South America:*** Mr Tino DeCarlo, The Advertising Department, Elsevier Inc., 360 Park Avenue South, New York, NY 10010-1710, USA; phone: (+1) (212) 633 3815; fax: (+1) (212) 633 3820; e-mail: t.decarlo@elsevier.com. ***Europe and ROW:*** Katrina Barton, Advertising Department, Elsevier Ltd., 84 Theobald's Road, London WC1X 8RR, UK; phone (+44) 207 611 4117; fax: (+44) 207 611 4463; e-mail: k.barton@elsevier.com

USA mailing notice: *Deep-Sea Research II* (ISSN 0967-0645) is published annually in 26 issues by Elsevier Ltd. (P.O. Box 211, 1000 AE Amsterdam, The Netherlands). Annual subscription price in the USA US$ 3152 (valid in North, Central and South America), including air speed delivery.
USA POSTMASTER: Send address changes to *Deep-Sea Research II*, 655, Avenue of the Americas, New York, NY 10010.
AIRFREIGHT AND MAILING in the USA by Publications Expediting Inc., 200 Meacham Avenue, Elmont, NY 11003. Periodical postage rate paid at Jamaica, NY 11431.

Subscription Information

Published annually in 26 issues. Information on published and forthcoming issues can be found at the journal website.

Publication information: *Deep-Sea Research Part II* (ISSN 0967–0645). For 2004, volume 51 is scheduled for publication. Subscription prices are available upon request from the Publisher or from the Regional Sales Office nearest you or from this journal's website (http://www.elsevier.com./locate/dsr2). Further information is available on this journal and other Elsevier products through Elsevier's website: (http://www.elsevier.com). Subscriptions are accepted on a prepaid basis only and are entered on a calendar year basis. Issues are sent by standard mail (surface within Europe, air delivery outside Europe). Priority rates are available upon request. Claims for missing issues should be made within six months of the date of despatch.

Author enquiries. For enquiries relating to the submission of articles (including electronic submission), the preparation of electronic artwork, the status of accepted articles, author Frequently Asked Questions and any other enquiries relating to Elsevier, please consult http://authors.elsevier.com
Contact details for questions arising after acceptance of an article, especially those relating to proofs, are provided when an article is accepted for publication. Authors can also keep a track on the progress of their accepted article, and set up e-mail alerts informing them of changes to their manuscripts status, by using the "Track a paper" feature of Elsevier's Author Gateway (http: //authors.elsevier.com).

Orders, claims, and journal enquiries: please contact the Customer Service Department at the Regional Sales Office nearest you:
Orlando: Elsevier, Customer Service Department, 6277 Sea Harbor Drive, Orlando, FL 32887-4800, USA; phone: (+1) (877) 8397126 [toll free number for US customers], or (+1) (407) 3454020 [customers outside US]; fax: (+1) (407) 3631354; e-mail: usjcs@elsevier.com
Amsterdam: Elsevier, Customer Service Department, PO Box 211, 1000 AE Amsterdam, The Netherlands; phone: (+31) (20) 4853757; fax: (+31) (20) 4853432; e-mail: nlinfo-f@elsevier.com
Tokyo: Elsevier, Customer Service Department, 4F Higashi-Azabu, 1-Chome Bldg, 1-9-15 Higashi-Azabu, Minato-ku, Tokyo 106-0044, Japan; phone: (+81) (3) 5561 5037; fax: (+81) (3) 5561 5047; e-mail: jp.info@elsevier.com
Singapore: Elsevier, Customer Service Department, 3 Killiney Road, #08-01 Winsland House I, Singapore 239519; phone: (+65) 63490222; fax: (+65) 67331510; e-mail: asiainfo@elsevier.com

♾ The paper used in this publication meets the requirements of ANSI/NISO Z39. 48-1992 (Permanence of Paper).

© **2004 Elsevier Ltd. All rights reserved.**

Back Issues: Back issues of all previously published volumes are available direct from Elsevier Offices. Complete volumes and single issues can be purchased for 1999–2003. Earlier issues are available in high quality photo-duplicated copies as complete volumes only. Back volumes on microfilm are available from UMI, 300 North Zeeb Road, Ann Arbor, MI 48106-1346, USA.

Cover image: General overview of chlorophyll distribution in the Humboldt Current system off Chile and southern Peru from satellite color data (SeaWiFS) during spring 2003 (http://seawifs.gsfc.nasa.gov/SEAWIFS.html). Insets (from left to right): Vertical profile of oceanographic variables off Iquique (northern Chile) during April 2002 (COPAS data set). Foraminifer flux (warm water species) in relation to ENSO variability (Marchant et al., this issue). Sedimentation rates across and along the Chile-Peru continental margin (Muñoz et al., this issue). Bottom photographs, from COPAS picture gallery (from left to right): Preparing the new mooring with sediment traps for deployment off Concepción. Rosette water sampler system and CTD. Sediment collection with Multicorer. Zooplankton sampling with a multinet Hydrobios.

DEEP-SEA RESEARCH

PART II

Topical Studies in Oceanography

Oceanography in the eastern South Pacific: Part I

Guest Editors

Carmen E. Morales **Carina B. Lange**

Centro de Investigación Oceanográfica en el
Pacífico Sur-oriental (FONDAP-COPAS) and
Departamento de Oceanografía
Facultad de Ciencias Naturales y Oceanográficas
Universidad de Concepción
Casilla 160-C, Concepción, Chile

ELSEVIER

STATEMENT POLICY

Deep-Sea Research Part II: Topical Studies in Oceanography Publishes the topical issues arising from the many international and interdisciplinary projects which are undertaken.

Shorter research papers are welcomed for *Deep-Sea Research Part I: Oceanographic Research Papers*. Acceptable topics for papers include:

(1) the results of original scientific research
(2) theoretical work of evident oceanographic applicability
(3) the solution of some instrumental or laboratory problem with evidence of its successful use, and
(4) applications of oceanography.

Papers dealing with research on continental shelves (water depths shallower than 100–200 m) in most cases should be submitted to our sister journal *Continental Shelf Research*.

Progress reports and review articles may be invited by the Editor but these are generally more appropriate for *Progress in Oceanography*.

© 2004 Elsevier Ltd. All rights reserved.

This journal and the individual contributions contained in it are protected under copyright by Elsevier Ltd, and the following terms and conditions apply to their use:

Photocopying
Single photocopies of single articles may be made for personal use as allowed by national copyright laws. Permission of the publisher and payment of a fee is required for all other photocopying, including multiple or systematic copying, copying for advertising or promotional purposes, resale, and all forms of document delivery. Special rates are available for educational institutions that wish to make photocopies for non-profit educational classroom use.

Permissions may be sought directly from Elsevier Global Rights Department, P.O. Box 800, Oxford OX5 1DX, UK; phone: (+44) 1865 843830, fax: (+44) 1865 853333, e-mail: permissionselsevier.co.uk. You may also contact Global Rights directly through Elsevier's home page (http://www.elsevier.com), by selecting 'Obtaining Permissions'.

In the USA, users may clear permissions and make payments through the Copyright Clearance Center, Inc., 222 Rosewood Drive, Danvers, MA 01923, USA; phone: (+1) (978) 7508400, fax: (+1) (978) 7504744, and in the UK through the Copyright Licensing Agency Rapid Clearance Service (CLARCS), 90 Tottenham Court Road, London W1P 0LP, UK; phone: (+44) 20 7631 5555; fax: (+44) 20 7631 5500. Other countries may have a local reprographic rights agency for payments.

Derivative Works
Subscribers may reproduce tables of contents or prepare lists of articles including abstracts for internal circulation within their institutions. Permission of the publisher is required for resale or distribution outside the institution.

Permission of the publisher is required for all other derivative works, including compilations and translations.

Electronic Storage or Usage
Permission of the Publisher is required to store electronically any material contained in this journal, including any article or part of an article.

Except as outlined above, no part of this publication may be reproduced, stored in a retrieval system or transmitted in any form or by any means, electronic, mechanical, photocopying, recording or otherwise, without prior written permission of the publisher.

Address permissions requests to: Elsevier Global Rights Department, at the mail, fax and e-mail addresses noted above:

Notice
No responsibility is assumed by the Publisher for any injury and/or damage to persons or property as a matter of products liability, negligence or otherwise, or from any use or operation of any methods, products, instructions or ideas contained in the material herein. Because of rapid advances in the medical sciences, in particular, independent verification of diagnoses and drug dosages should be made.

Although all advertising material is expected to conform to ethical (medical) standards, inclusion in this publication does not constitute a guarantee or endorsement of the quality or value of such product or of the claims made of it by its manufacturer.

Oceanography in the eastern South Pacific: Part I

Volume 51 Nos. 20–21, 2004

CONTENTS

		Editorial
C.E. Morales and C.B. Lange	2345	Oceanographic studies in the Humboldt current system off Chile: an introduction
		Section I: Physical oceanogaphy
O. Leth, G. Shaffer and O. Ulloa	2349	Hydrography of the eastern South Pacific Ocean: results from the Sonne 102 cruise, May–June 1995
A. Valle-Levinson, W. Schneider, M. Sobarzo, M. Bello, L. Bravo, M. Castillo, L. Duarte, R. Fuenzalida, J.M. Gallegos, J. Garcés-Vargas, J. González, D. Gutiérrez, C. Molinet, M.S. Navarro, J. Pierini, E. Rodríguez-Rubio, A. Valdenegro, L. Vera and L. Zenteno	2371	Wind-induced exchange at the entrance to Concepción Bay, an equatorward facing embayment in central Chile
		Section II: Pelagic system and bentho-pelagic coupling
R. Escribano, G. Daneri, L. Farías, V.A. Gallardo, H.E. González, D. Gutiérrez, C.B. Lange, C.E. Morales, O. Pizarro, O. Ulloa and M. Braun	2389	Biological and chemical consequences of the 1997–1998 El Niño in the Chilean coastal upwelling system: a synthesis
V. Montecino, R. Astoreca, G. Alarcón, L. Retamal and G. Pizarro	2413	Bio-optical characteristics and primary productivity during upwelling and non-upwelling conditions in a highly productive coastal ecosystem off central Chile (~36°S)
L.A. Cuevas, G. Daneri, B. Jacob and P. Montero	2427	Microbial abundance and activity in the seasonal upwelling area off Concepción (~36°S), central Chile: a comparison of upwelling and non-upwelling conditions
M. Marchant, D. Hebbeln, S. Giglio, C. Coloma and H.E. González	2441	Seasonal and interannual variability in the flux of planktic foraminifera in the Humboldt Current System off central Chile (30°S)
H.E. González, D. Hebbeln, J.L. Iriarte and M. Marchant	2457	Downward fluxes of faecal material and microplankton at 2300 m depth in the oceanic area off Coquimbo (30°S), Chile, during 1993–1995

Section III: Benthic systems, sedimentation an elemental cycling in sediments

V.A. Gallardo, M. Palma, F.D. Carrasco, D. Gutiérrez, L.A. Levin and J.I. Cañete — 2475 — Macrobenthic zonation caused by the oxyge minimum zone on the shelf and slope o central Chile

L. Farías, M. Graco and O. Ulloa — 2491 — Temporal variability of nitrogen cycling i continental-shelf sediments of the upwellin ecosystem off central Chile

V. Molina, L. Farías, M. Graco, C. Rivera, L. Pinto and V.A. Gallardo — 2507 — Benthic nitrogen regeneration under oxyge and organic matter spatial variability o Concepción (~36°S), central Chile

P. Muñoz, C.B. Lange, D. Gutiérrez, D. Hebbeln, M.A. Salamanca, L. Dezileau, J.L. Reyss and L.K. Benninger — 2523 — Recent sedimentation and mass accumulatio rates based on ^{210}Pb along the Peru–Chil continental margin

CONTENTS direct

This journal is part of **ContentsDirect**, the ***free*** alerting service which sends tables o contents by e-mail for Elsevier books and journals. You can register for **ContentsDirec** online at: **www.elsevier.com/locate/contentsdirect**

ELSEVIER

Deep-Sea Research II 51 (2004) 2345–2348

DEEP-SEA RESEARCH
PART II

www.elsevier.com/locate/dsr2

Editorial

Oceanographic studies in the Humboldt current system off Chile: an introduction

The eastern South Pacific (ESP) Ocean is one of the least explored regions of the global ocean. This vast region holds one of the most productive marine systems in the world, the Humboldt current system (HCS), which includes the coastal upwelling ecosystems off Peru and Chile. Wind-driven upwelling of sub-surface, cold, nutrient-rich and CO_2-saturated waters triggers a significant exchange of heat and gases between the ocean and the atmosphere. In turn, the nutrient input into the euphotic zone enhances the biological production of autotrophs in the surface waters. This production is, to a great extent, transferred through the pelagic web into the large fisheries of the region and/or is exported to the benthic system and ultimately buried in the sediment where it accumulates as organic-rich mud.

Coastal upwelling areas of eastern boundary systems are characterized by strong short-term (days-weeks) and high mesoscale variability in the physical–chemical conditions (Hill et al., 1998). The ecosystems along the ESP also are known to be subject to strong seasonal to inter-annual variability (Barber and Chavez, 1986; Tarazona et al., 1988; Alheit and Bernal, 1993; Thomas, 1999; Hebbeln et al., 2000; Hidalgo and Escribano, 2001; Ulloa et al., 2001). In general, the intra-seasonal variability associated with coastal-trapped waves and the inter-annual variability associated with the El Niño southern oscillation (ENSO) cycle link the HCS with the equatorial Pacific (Enfield et al., 1987; Hormazabal et al., 2001).

The ESP is also characterized by holding one of the most extensive and intense oxygen minimum zones (OMZ) of the global ocean. Off Peru and Chile, these low-oxygen waters constitute the main source of coastal upwelling (Brandhorst, 1971; Blanco et al., 2001; Atkinson et al., 2002). Through the biologically mediated process of denitrification, the OMZ contributes to the global sink of nitrogen in the ocean and acts as a source of the greenhouse gas N_2O to the atmosphere (Codispoti and Christensen 1985; Codispoti et al., 1986). The vertical distribution of the OMZ, whose shallowness can at times impinge on the euphotic layer, is greatly modified by El Niño events, involving a higher oxygenation of the surface and subsurface layers and leading to potentially large changes in ecosystem structure, productivity, trophic transfers, and biogeochemical cycling (Morales et al., 1999; Ulloa et al., 2001). Immediately below the OMZ, lies the Antarctic intermediate water (AAIW), which is considered to be formed mainly at ~55°S (west of southern Chile), and from here to spread to the entire Southern Hemisphere and the tropics. This water mass carries the imprint of global warming and seems to be a sensitive indicator of anthropogenic perturbation, as proposed by climate models (Shaffer et al., 2000).

The responses of the HCS' coastal upwelling ecosystems and adjacent oceanic zones to the various sources of variability, both in space and time, have been poorly analyzed until most recently. Moreover, little else is known about the

0967-0645/$ - see front matter © 2004 Elsevier Ltd. All rights reserved.
doi:10.1016/j.dsr2.2004.08.008

communities inhabiting the OMZ and on the effects of this condition upon the cycling of carbon and nitrogen in the water column and in the sediments. Some of the most important limitations until now have been the lack of long-term time-series studies, comparison and integration of data gathered during different cruises and in different regions of the HCS, and, above all, a short-sight in the need for long-term support of multidisciplinary and multi-approach research in this region. Today, the newly born "Center for Oceanographic Research in the eastern South Pacific (COPAS)", funded by the Fund for Advanced Research in Priority Areas (FONDAP) of the National Commission for Scientific and Technological Research (Lange and Ulloa, 2003), represents a great opportunity and an exciting challenge to overcome all or most of those limitations. This special volume is one step towards achieving the COPAS goals.

This special volume on the physics, biology, biogeochemistry and sediments of the ESP is primarily focused on the HCS off Chile. In this region, at least two large coastal upwelling zones can be identified, based upon their hydrographic and ecosystem characteristics: the northern (18–30°S) and the central–south regions (30–40°S). Upwelling is rather continuous in the north (Shaffer et al., 1999; Blanco et al., 2001), generally displaying low chlorophyll-*a* levels except very close to the coast (Thomas, 1999; Morales et al., 2001), but strongly seasonal (austral spring-summer) in the central-south region (Shaffer et al., 1999; Thomas et al., 2001; Atkinson et al., 2002), with very high chlorophyll-*a* levels ($>10\,mg\,m^{-3}$) over the wider shelf and shelf break areas during the upwelling period (Ahumada et al., 1991; Thomas, 1999). In both cases, the winds from the south and south-west are favorable for upwelling (see review in Strub et al., 1998).

In this volume, a total of 11 original pieces of research on the HCS off Chile are presented, including the physical and chemical settings, the biological and ecological context in both pelagic and benthic communities, the biogeochemical cycling in the water column and the sediments, together with the recycling, export and sedimentation of organic/inorganic matter, as well as the characteristics of the seafloor environment. Within the physical context, a comprehensive database of all the available hydrographic data for the ESP region off Chile has been compiled by Leth et al. these authors analyzed three full-depth sections covering northern, central and southern Chile (along 28, 35, and 43°S, from the coast to 86–88°W), in terms of the general circulation in the region. These results sustain most of previous but sparse observations in the region (i.e. the poleward Peru–Chile undercurrent, with a descending core and peak velocities of $\sim10\,cm\,s^{-1}$) and also contribute with new insights such as mechanisms of property transport. The study by Valle-Levinson et al. though more local in nature, deals with one of the poorly known aspects along the Chilean coast, i.e. the wind induced circulation around bays. In this case, short-term hydrographic and velocity observations were analyzed during the upwelling season in terms of wind-induced exchange at the entrance to Concepción Bay (~36°S), in central-south Chile. The circulation pattern revealed a downwind flow in the upper layer being delimited by the pycnocline and upwind flow below, under weak internal friction.

A comprehensive synthesis on the structure and functioning of the HCS ecosystems in the coastal upwelling region off Chile is presented by Escribano et al.; it focuses on the biological and chemical consequences of the 1997–1998 El Niño. Overall, this synthesis proposes a refreshing view of the impacts of ENSO on the HCS ecosystems, neatly summarized in a diagram that contrasts normal to La Niña conditions with El Niño events. The ideas proposed in this study will guide much of our research in the coming years. The bio-optical characteristics and primary productivity during upwelling and non-upwelling conditions in the highly productive coastal ecosystem off Concepción are described in Montecino et al., representing one of the few studies in the region tackling the productivity subject in a functional manner. Cuevas et al. deal with the microbial communities in the same area, also comparing upwelling and non-upwelling conditions in terms of primary and bacterial production, and bacterial and flagellate

abundances; they discuss the relevance of the microbial food web in this upwelling system.

Studies on the vertical flux or export rates in the HCS are scarce but possible due to the existence of a long-term (10 + years) mooring system deployed in the oceanic area off Coquimbo (~30°S; 185 km from the coast; ~4500 m water depth), adjacent to an upwelling center. It includes a sediment trap positioned at ~2300 m water depth. Marchant et al. describe the seasonal and inter-annual variability in the vertical flux of planktic foraminifers in this area, covering the period 1993–1998, and including the 1997–1998 El Niño event, which had only a limited impact on this flux. González et al. summarize the amount and variability in the downward carbon and carbonate fluxes, and identify their main sources (i.e., faecal material and microplankton), during the 1993–1995 period.

Most of our knowledge on the benthic systems and elemental cycling in the sediments in the HCS off Chile derive from studies carried out in the area off Concepción. Gallardo et al. illustrate the effects of the OMZ on the macrobenthic zonation in the shelf and slope, and show that the global hypothesis on diversity and density being lower within the core of an OMZ rather than beneath it in deeper, more oxygenated waters (Rosenberg et al., 1983; Mullins et al., 1985; Wishner et al., 1995) is not valid in this area, but only for diversity. Farías et al. analyze the temporal variability of nitrogen recycling in continental-shelf sediments of the upwelling ecosystem off Concepción. Their results show that the sediments act as a large sink for nitrate here, though the intense denitrification is coupled with nitrification. Complementing this study, Molina et al. describe the benthic nitrogen regeneration processes under the influence of spatial variability in oxygen and organic matter in the sediments off Concepción. As a reflection of the processes occurring in the water column and in the sediments of the HCS region, Muñoz et al. present data on recent sedimentation and mass accumulation rates based on ^{210}Pb along the Peru–Chile continental margin. This study supports the distinction of two main areas within the HCS now based on sedimentation controls, central Peru to northern Chile and central to southern Chile.

Overall, the studies included in this special volume provide an integrated view of the oceanography of the HCS off Chile and adjacent areas and reflect the substantial progress made during recent years in discovering or re-discovering the essentials of this system. No doubt this first volume will serve as a reference for the many scientific problems in the region, old and new, that need to be tackled. Investigations in the HCS should be focused on those essentials that distinguish it from other eastern boundary systems, using new available technologies and multidisciplinary approaches.

Acknowledgements

We are thankful to many colleague scientists who encouraged us to compile this volume as part of an integrated activity of our FONDAP-COPAS Center. We thank the authors of the papers in this issue and the many reviewers who contributed their time and efforts to provide thoughtful reviews of the manuscripts. Most of the work reported in this volume was supported by the Chilean National Commission for Scientific and Technological Research (CONICYT) and the University of Concepción. We are indebted to Mrs. Danielle Barriga for invaluable technical assistance, and a large quota of patience, as our Editorial Assistant. The editorial support of DSR II Editor, Dr. John D. Milliman, is also acknowledged. The Hanse Institute for Advanced Studies in Delmenhorst, Germany, provided support to CBL for part of the editorial work. Facilities and funding for the editorial expenses were made available by the FONDAP-COPAS Center at the University of Concepción, Chile.

References

Ahumada, R., Matrai, P., Silva, N., 1991. Phytoplankton biomass distribution and relationship to nutrient enrichment during an upwelling event off Concepción Bay (Chile). Boletín de la Sociedad de Biología, Concepción (Chile) 62, 7–19.

Alheit, J., Bernal, P., 1993. Effects of physical and biological changes on the biomass yield of the Humboldt Current

Ecosystem. In: Sherman, K., Alexander, L.M., Gold, B.D. (Eds.), Large Marine Ecosystems. American Association for the Advancement of Science Press, Washington, DC, pp. 53–58.

Atkinson, L.P., Valle-Levinson, A., Figueroa, D., De Pol-Holz, R., Gallardo, V.A., Schneider, W., Blanco, J.L., Schmidt, M., 2002. Oceanographic observations in Chilean coastal waters between Valdivia and Concepción. Journal of Geophysical Research 107 (C7) 10.1029/2001JC000991.

Barber, R.T., Chavez, F.P., 1986. Ocean variability in relation to living resources during the 1982–83 El Niño. Nature 319, 279–285.

Blanco, J.L., Thomas, A.C., Carr, M.E., Strub, P.T., 2001. Seasonal climatology of hydrographic conditions in the upwelling region off northern Chile. Journal of Geophysical Research 106, 11451–11467.

Brandhorst, W., 1971. Condiciones oceanográficas estivales frente a la costa de Chile. Revista de Biología Marina, Valparaíso (Chile) 4, 34–84.

Codispoti, L.A., Christensen, J.P., 1985. Nitrification, denitrification and nitrous oxide cycling in the eastern tropical South Pacific Ocean. Marine Chemistry 16, 277–300.

Codispoti, L.A., Friederich, G.E., Packard, T.T., Glover, H.E., Kelly, P.J., Spinrad, R.W., Barber, R.T., Elkins, J.W., Ward, B.B., Lipschultz, F., Lostaunau, N., 1986. High nitrite levels off northern Peru: a signal of instability in the marine denitrification rate. Science 233, 1200–1202.

Enfield, D.B., Cornejo-Rodríguez, M.P., Smith, R.L., Newberger, P.A., 1987. The equatorial source of propagating variability along the Peru coast during the 1982–1983 El Niño. Journal of Geophysical Research 92 (C13), 14335–14346.

Hebbeln, D., Marchant, M., Wefer, G., 2000. Seasonal variations of the particle flux in the Peru–Chile Current under "normal" and under El Niño conditions. Deep-Sea Research II 47, 2101–2128.

Hidalgo, P., Escribano, R., 2001. Succession of pelagic-copepod species during the period 1996/1998 in northern Chile: the influence of the 1997–98 El Niño. Hydrobiologia 453, 153–160.

Hill, A.E., Hickey, B., Shillington, F.A., Strub, P.T., Brink, K.H., Barton, E.D., Thomas, A.C., 1998. Eastern ocean boundaries coastal segment. In: Robinson, A.R., Brink, K.H. (Eds.), The Sea. The Global Coastal Ocean. Regional Studies and Synthesis, vol. 11. Wiley, New York, pp. 29–67.

Hormazabal, S., Shaffer, G., Letelier, J., Ulloa, O., 2001. Local and remote forcing of sea surface temperature in the coastal upwelling system off Chile. Journal of Geophysical Research 106 (C8), 16657–16671.

Lange, C.B., Ulloa, O., 2003. Center for Oceanographic Research opens in Chile. EOS Transactions American Geophysical Union 84 (7), 61.

Morales, C.E., Hormazabal, S.E., Blanco, J.L., 1999. Interannual variability in the mesoscale distribution of the depth of the upper boundary of the oxygen minimum layer off northern Chile (18–24S): implications for the pelagic system and biogeochemical cycling. Journal of Marine Research 57, 909–932.

Morales, C.E., Blanco, J.L., Braun, M., Silva, N., 2001. Chlorophyll-*a* distribution and mesoscale processes in upwelling and adjacent oceanic zones off northern Chile (summer–autumn 1994). Journal of the Marine Biological Association, UK 81, 193–206.

Mullins, H.T., Thompson, J.B., McDougall, K., Vercoutere, T.L., 1985. Oxygen minimum zone edges effects: evidence from the central California coastal upwelling system. Geology 13, 491–494.

Rosenberg, R., Arntz, W.E., Chumán de Flores, E., Flores, L.A., Carbajal, G., Finger, I., Tarazona, J., 1983. Benthos biomass and oxygen deficiency in the upwelling system off Peru. Journal of Marine Research 41, 263–279.

Shaffer, G., Hormazabal, S., Pizarro, O., Salinas, S., 1999. Seasonal and interannual variability of currents and temperature off central Chile. Journal of Geophysical Research 104 (C12), 29951–29961.

Shaffer, G., Leth, O., Ulloa, O., Bendtsen, J., Daneri, G., Dellarossa, V., Hormazabal, S., Sehlstedt, P.I., 2000. Warming and circulation changes in the eastern South Pacific Ocean. Geophysical Research Letters 27, 1247–1250.

Strub, P., Mesias, J., Montecino, V., Ruttlant, J., 1998. Coastal ocean circulation off western South America. In: Robinson, A., Brink, K. (Eds.), The Sea, The Global Coastal Ocean, vol. 11. Wiley, New York, pp. 272–313.

Tarazona, J., Salzwedel, H., Arntz, W.E., 1988. Oscillations of macrobenthos in shallow water off the Peruvian central coast induced by El Niño 1982–83. Journal of Marine Research 46, 593–611.

Thomas, A.C., 1999. Seasonal distributions of satellite-measured phytoplankton pigment concentration along the Chilean coast. Journal of Geophysical Research 104, 25877–25890.

Thomas, A.C., Carr, M.E., Strub, P.T., 2001. Chlorophyll variability in eastern boundary currents. Geophysical Research Letters 18, 3421–3424.

Ulloa, O., Escribano, R., Hormazabal, S., Quiñones, R.A., Ramos, M., González, R.R., 2001. Evolution and biological effects of the 1997–98 El Niño in northern Chile. Geophysical Research Letters 28 (8), 1591–1594.

Wishner, K.L., Ashijan, C.J., Gelfman, C., Gowing, M.M., Kann, L., Levin, L.A., Mullineaux, L.S., Saltzman, J., 1995. Pelagic and benthic ecology of the lower interface of the Eastern Tropical Pacific oxygen-minimum zone. Deep Sea Research 42, 93–115.

Carmen E. Morales, Carina B. Lange
Centro de Investigación Oceanográfica en el Pacífico Sur-Oriental (FONDAP-COPAS) and Departamento de Oceanografía, Universidad de Concepción, Casilla 160-C, Concepción, Chile
E-mail address: camorale@udec.cl
URL: http://www.copas.cl

ELSEVIER

Deep-Sea Research II 51 (2004) 2349–2369

DEEP-SEA RESEARCH
PART II

www.elsevier.com/locate/dsr2

Hydrography of the eastern South Pacific Ocean: results from the Sonne 102 cruise, May–June 1995

Ole Leth[a,b,*], Gary Shaffer[a,c], Osvaldo Ulloa[a,b,d]

[a]*Programa Regional de Oceanografía Física y Clima (PROFC), Universidad de Concepción, Casilla 160-C, Concepción, Chile*
[b]*Centro de Investigación Oceanográfica en el Pacífico Sur-Oriental (FONDAP-COPAS), Universidad de Concepción, Casilla 160-C, Concepción, Chile*
[c]*Department of Geophysics, Danish Center for Earth System Science, University of Copenhagen, Juliane Maries Vej 30, 2100 Copenhagen Ø, Denmark*
[d]*Departamento de Oceanografía, Universidad de Concepción, Casilla 160-C, Concepción, Chile*

Accepted 26 July 2004

Abstract

Full-depth conductivity temperature–depth/hydrographic measurements were taken in May June 1995 along 28 15′, 35°15′, and 43°15′S from the Chilean coast to 86–88°W from the R.V. *Sonne*. Sections of potential temperature, salinity, neutral density, and oxygen are presented to illustrate the water-column structure in this sparsely sampled region. A more comprehensive database on all available hydrographic data from the region was compiled. These data and available meteorological data are used to help in the interpretation of the Sonne results. A number of important features found in the sections are discussed, including a shallow salinity minimum (apparently ventilated from south of ~37°S), salt fingering as a possible mechanism to transport high-salinity subtropical water into the shallow salinity minimum, Equatorial Subsurface Water, Subantarctic Mode Water, and Antarctic Intermediate Water. Geostrophic calculations of alongshore flow show the poleward Peru–Chile Undercurrent at each of the three sections with a poleward descending core and peak velocities of ~10 cm s^{-1}. As in earlier works, a deep Pacific outflow is found near the Chilean coast, part of a clockwise deep circulation in the Chile Basin.
© 2004 Elsevier Ltd. All rights reserved.

1. Introduction

The eastern South Pacific is one of the least-explored and least-sampled regions of the global ocean. Only a few transects with high-quality hydrographic measurements have crossed the area and few of these have been repeated. An expedition was carried out in 1995 on board the R.V.

*Corresponding author. Programa Regional de Oceanografía Física y Clima (PROFC), Universidad de Concepción, Casilla 160-C, Concepción, Chile. Fax: +56 41 23 9900.
E-mail address: okl@profc.udec.cl (O. Leth).

0967-0645/$ - see front matter © 2004 Elsevier Ltd. All rights reserved.
doi:10.1016/j.dsr2.2004.08.009

Sonne (cruise 102) as a joint geological and oceanographical effort to study paleoproductivity, ocean circulation, and carbon cycling in the Peru–Chile Current system. The hydrographic data were collected by the Ocean and Climate group at the University of Copenhagen in co-operation with several Chilean colleagues. Here, some of these data are presented and findings based upon the data are discussed.

The zonal sections of the Sonne cruise constitute a partial repetition in the eastern South Pacific Ocean of the transpacific sections from the 1967 SCORPIO expedition (Eltanin cruises 28 and 29) (Stommel et al., 1973). A detailed comparison of the two hydrographic data sets was conducted by Shaffer et al. (2000). The results indicate warming at intermediate depths in the eastern South Pacific Ocean and apparent changes in the deep ocean circulation off Chile between the two occupations 28 years apart. This study complements well similar studies of decadal changes in the intermediate and deep-ocean water masses from the western part of the South Pacific (Bindoff and Church, 1992; Bindoff and McDougall, 1994; Johnson and Orsi, 1997). The sparse number of repeated hydrographic transects in the South Pacific contrasts with much more extensive observations in the North Atlantic, where there is strong evidence of large-scale changes in the ocean climate (e.g., Parrilla et al., 1994; Bryden et al., 1996; Joyce et al., 1999).

This paper deals with the basic hydrographic properties of the eastern South Pacific Ocean based on the Sonne sections and its relation to the general circulation in the region. In addition, a more comprehensive data set is compiled for the eastern South Pacific Ocean based on all of the available hydrographic data sampled since 1965. This data set is used to put the observed properties of the Sonne sections into a more general context and to elaborate some of the hydrographic differences observed between the SCORPIO stations and the reoccupied Sonne stations, as discussed by Shaffer et al. (2000).

2. Methods

Three hydrographic sections were occupied from May to June 1995 on board the R.V. *Sonne* along 28°15′, 35°15′, and 43°15′S from the Chilean coast to 88, 88, and 86°W, respectively (Fig. 1). In the following, these sections will be referred to by their nominal latitudes. The sections transversed the gap between the coast and the meridional World Ocean Circulation Experiment (WOCE) section P19 along 88°W, occupied in March 1993. A total of 42 full-depth conductivity–temperature–depth (CTD) and hydrographic stations were taken with a spacing of 0.25° longitude over the continental shelf, shelf break, and slope, gradually increasing to 2° longitude to the west. On the cruise, a Neil Brown Instrument Systems Mark IIIC/WOCE CTD was used and placed in a rosette with Niskin bottles. The CTD was lowered to within 20 m of the bottom. Samples drawn from the Niskin bottles were analyzed for concentrations of dissolved oxygen, silica, phosphate, nitrate, nitrite, helium, tritium, and to calibrate the CTD conductivity sensor. Here, we will only be concerned with the temperature, salinity, and dissolved oxygen data. Since the rosette only

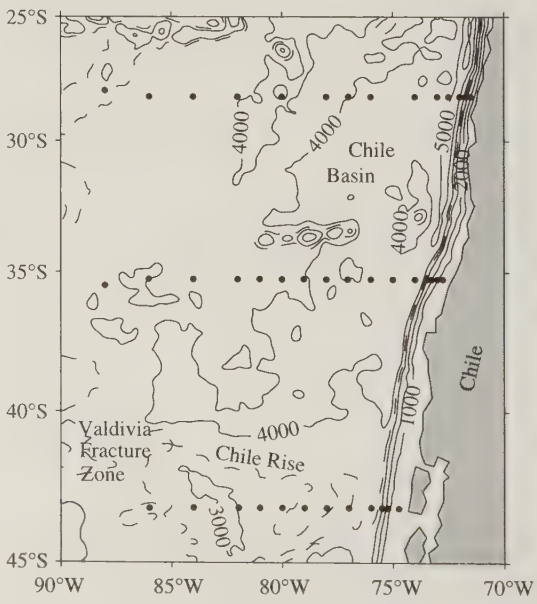

Fig. 1. Positions of full-depth CTD/hydrographic stations (filled circles) occupied during the Sonne 102 cruise, May–June 1995. Isobaths are shown for each 1000 m with solid contours. Additionally, the isobath for 3500 m is shown (dashed line).

carried 24 Niskin bottles, an additional shallow cast was usually taken at each full-depth station to increase the resolution of the upper 500 m. Together with recent WOCE sections occupied in the eastern South Pacific, the Sonne data form a considerable increment in the number of full-depth hydrographic observations from this region.

Water sample salinities on the R.V. *Sonne* were measured on a Guildline Model 8410 Portasal laboratory salinometer, standardized using International Association for the Physical Sciences of the Oceans Standard Seawater (SSW) batch P126. Standardization was done after about 12 samples. Pre- and post-cruise calibrations of the CTD by the manufacturer revealed a drift of $0.0008\,^{\circ}\mathrm{C\,month^{-1}}$ in temperature and an insignificant drift in pressure. After calibration and bin averaging, the final CTD data were reported every 2 dbar. Due to standardization problems of the salinometer, data from the station at 88°W and 28°S are not included here. The final CTD temperature and salinity appear to be accurate within 0.003 °C and 0.005, respectively; pressure measurements are believed to have better than 0.1% accuracy (Leth, 1997).

Initially, an examination was performed between the SCORPIO and Sonne data in the Pacific deep and basin water on isotherms of potential temperature (θ). SCORPIO data were interpolated onto Sonne locations along isotherms using semi-Hermite splines (Akima, 1970), and great care was taken not to interpolate the data through bathymetric features in the deep ocean. The horizontal interpolation was done for $\theta<1.57\,^{\circ}\mathrm{C}$ (pressure >2961 dbar) at 43°S, for $\theta<1.39\,^{\circ}\mathrm{C}$ (pressure >3680 dbar) at 35°S, and for $\theta<1.62\,^{\circ}\mathrm{C}$ (pressure >2672 dbar) at 28°S. In all three sections, there was a systematic offset in salinity of about 0.006, with Sonne data being fresher over the pressure range. The procedure was later repeated with linear interpolation and also by interpolating the (higher resolution) Sonne data onto SCORPIO positions. This, however, did not change the results. The pressure range covers the deeper part of the Circumpolar Deep Water, which fills the Chile Basin from above the Chile Rise and from the Southeast Pacific Basin through gaps and fracture zones in the Chile Rise.

Throughout the Sonne cruise, the salinometer worked satisfactorily. After the cruise, when we became aware of the offset mentioned above, the salinometer was tested for linearity (linear drift). The linearity of the instrument was examined by standardizing it with SSW batch P126 (salinity of 34.995) and checking the difference between the instrument reading and reference SSW batches 30L6 (salinity of 30.072) and 38H3 (salinity of 38.003). The salinity offset was found to be less than 0.001, much less than the observed difference between Sonne and SCORPIO data. This difference can be explained by the different sampling procedures for Sonne and SCORPIO (plastic Niskin bottles versus epoxy lined brass Nansen bottles) and differences between labeled and actual salinity of the applied SSW batches (P126 on Sonne and P46 on SCORPIO) (Mantyla, 1987).

Comparisons also were made between the WOCE section P19 and the SCORPIO sections where they intersect at 28 and 43°S. At 43°S, WOCE salinities were found to be 0.004 lower for $\theta<1.38\,^{\circ}\mathrm{C}$ (pressure >3351 dbar). At 28°S, however, WOCE salinities were found to be 0.002 higher than SCORPIO salinities for $\theta<1.65\,^{\circ}\mathrm{C}$ (pressure >2585 dbar). A comparison between Sonne and WOCE salinities at the 35°S crossing gave an agreement within 0.001. Accurate oxygen data are only available from the Sonne section at 28°S. The accuracy of the oxygen measurements from the Sonne bottle casts is believed to be $\pm 0.6\,\mu\mathrm{mol\,kg^{-1}}$.

3. Results and discussion

Figs. 2–5 show objectively interpolated (Roemmich, 1983) and contoured potential temperature, salinity, and neutral density (γ_n) (Jackett and McDougall, 1997) for the sections at 28, 35, and 43°S, and oxygen for the section at 28°S. Prior to the objective interpolation, the CTD data were smoothed with a 6 dbar half-width Hanning filter. The smoothed data were then objectively interpolated to every 0.1° in longitude and every 20 m in the vertical. Each interpolated grid point was estimated from the 36 nearest data points. A

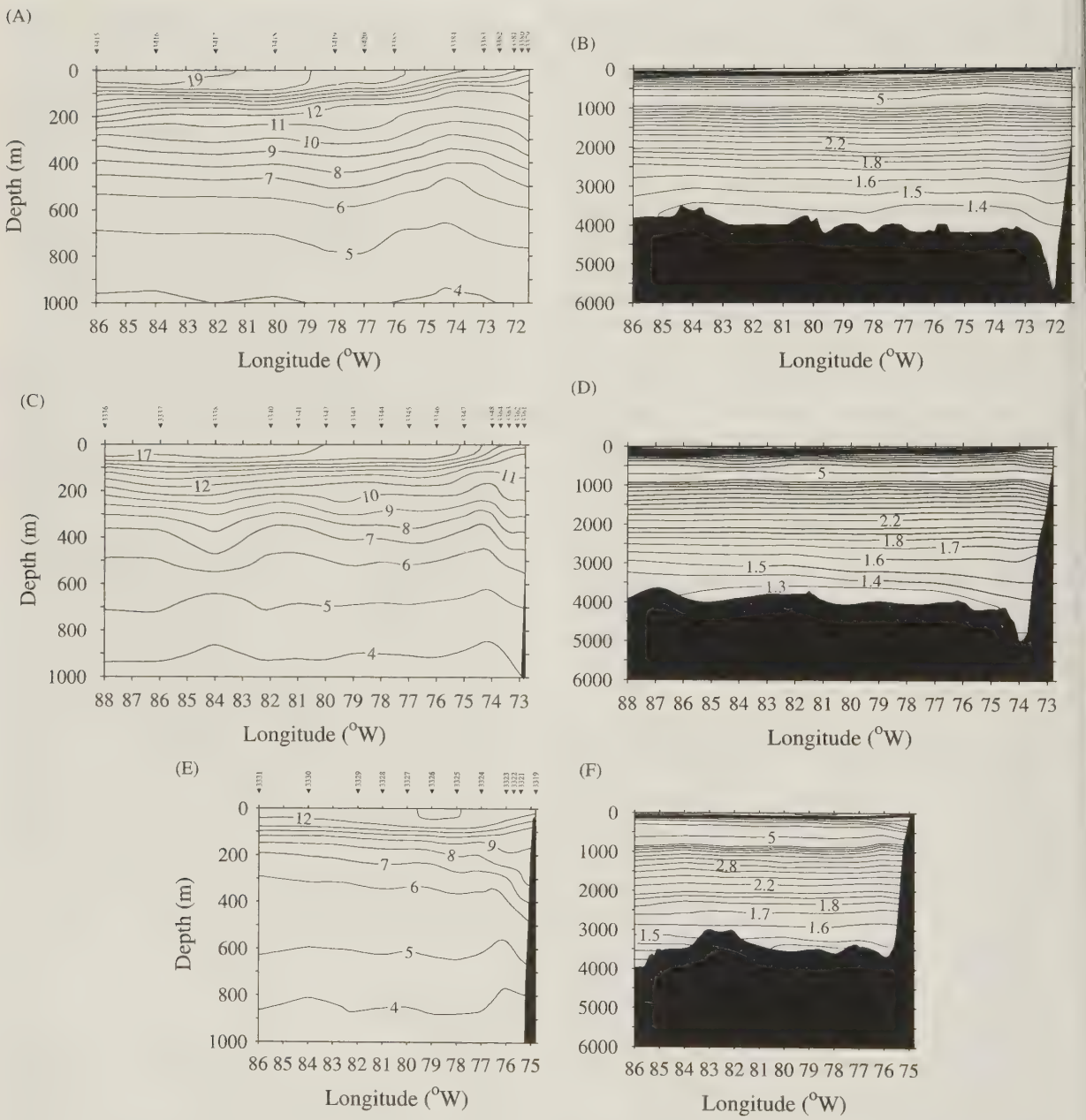

Fig. 2. Potential temperature (°C), based on CTD data from the Sonne 102 cruise along 28°S (A, B), 35°S (C, D), and 43°S (E, F). These sections are shown in Fig. 1. (Left panels) Potential temperature of the upper 1000 m with a contour interval of 1 °C. Numbers on upper *X*-axis refer to Sonne oceanographic stations. (Right panels) Potential temperature down to the bottom with contour intervals of 0.1 C for potential temperatures less than 2 C, 0.2 C for potential temperatures between 2 and 4 C, and 1 C for potential temperatures greater than 4 °C.

Gaussian-shaped covariance function was used in the interpolation with a horizontal correlation scale of two times the station spacing and a linearly increasing vertical correlation scale from 10 m at the surface to 100 m at 1000 m depth. Below 1000 m, the correlation scale was a constant

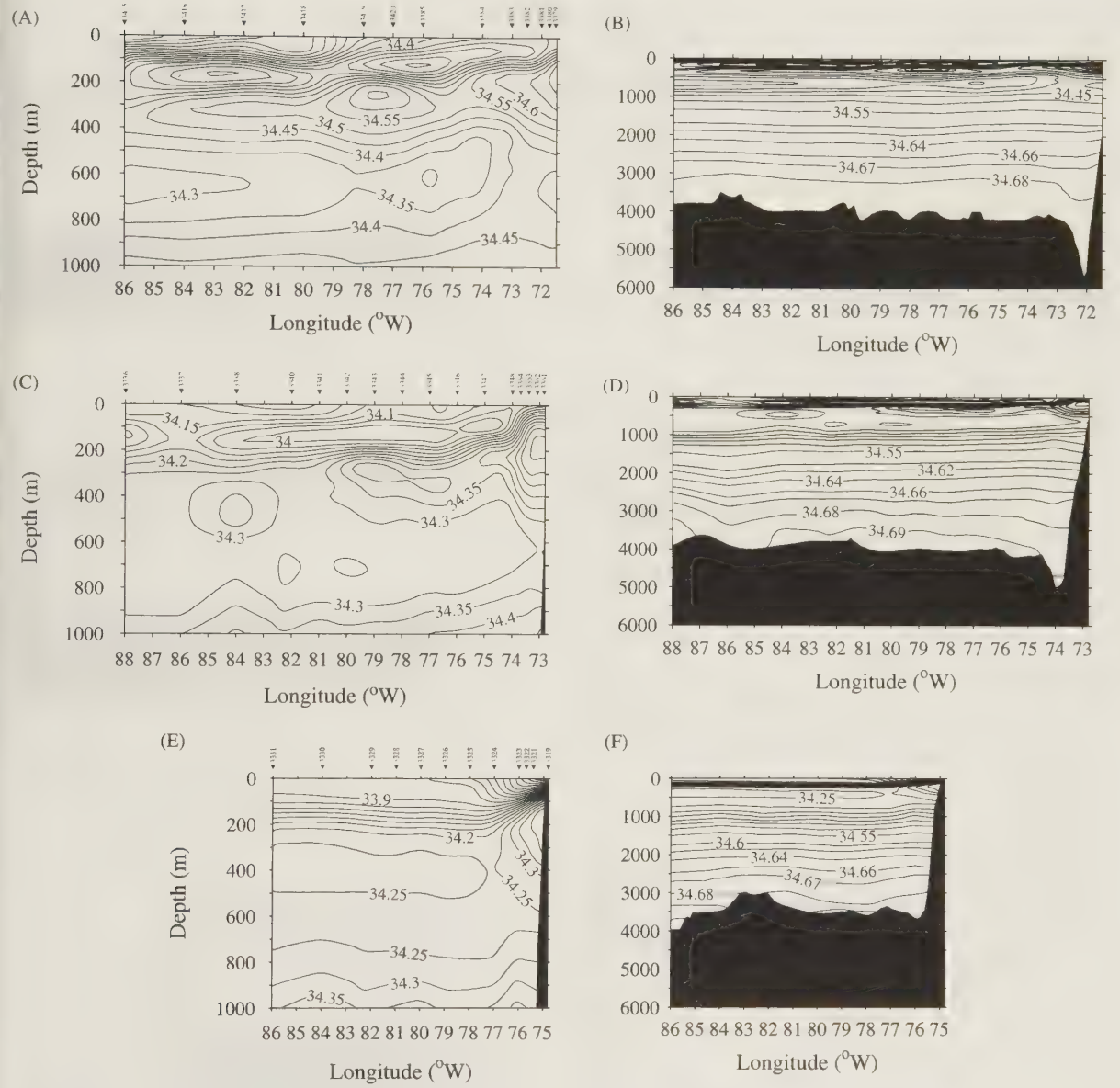

Fig. 3. Salinity, based on CTD data from the Sonne 102 cruise along 28°S (A, B), 35°S (C, D), and 43°S (E, F). These sections are shown in Fig. 1. (Left panels) Salinity of the upper 1000 m with a contour interval of 0.05. Numbers on upper X-axis as in Fig. 2. (Right panels) Salinity down to the bottom with contour intervals of 0.05 for salinities less than 34.6, 0.02 for salinities between 34.6 and 34.66, and 0.01 for salinities greater than 34.66.

100 m. For the oxygen data, variable correlation scales were used both horizontally and vertically to accommodate an increase in spacing of the bottle data with increasing depth.

In order to facilitate the interpretation of the Sonne data, horizontal maps of meteorological data, selected hydrographic properties, and derived geostrophic velocities also were prepared for

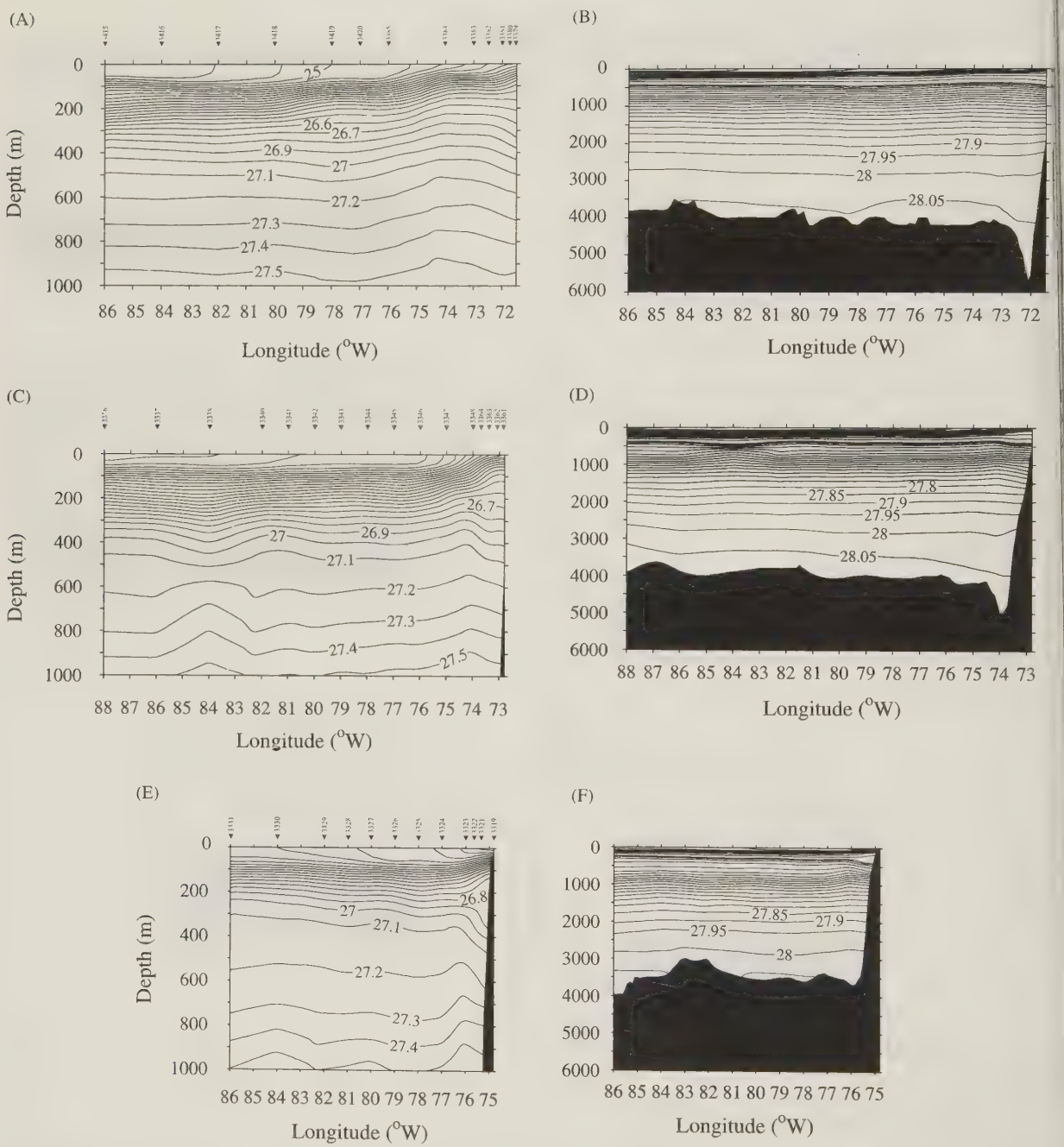

Fig. 4. Neutral density ($kg\,m^{-3}$), based on CTD data from the Sonne 102 cruise along 28°S (A, B), 35°S (C, D), and 43°S (E, F). These sections are shown in Fig. 1. (Left panels) Neutral density of the upper 1000 m with a contour interval of $0.1\,kg\,m^{-3}$. Numbers on upper X-axis as in Fig. 2. (Right panels) Neutral density down to the bottom with contour intervals of $0.2\,kg\,m^{-3}$ for neutral densities less than 27 and $0.05\,kg\,m^{-3}$ for neutral densities greater than $27\,kg\,m^{-3}$.

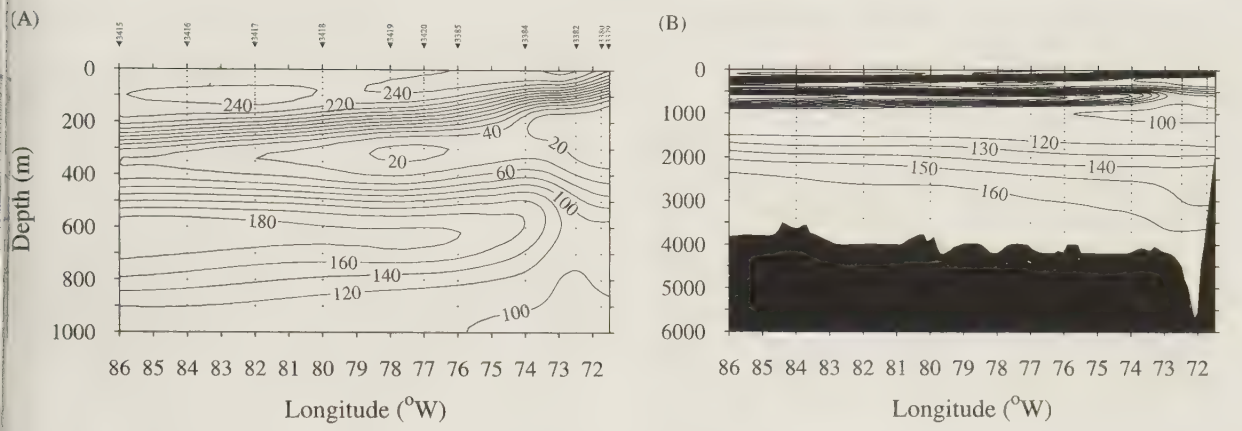

Fig. 5. Oxygen (μmol kg $^{-1}$) based on the bottle data from the Sonne 102 cruise along 28 S. This section is shown in Fig. 1. (Left panel) Oxygen of the upper 1000 m with a contour interval of 20 μmol kg^{-1}. Numbers on upper X-axis as in Fig. 2. (Right panel) Oxygen down to the bottom with a contour interval of 20 μmol kg^{-1} for oxygen less than 120 and 10 μmol kg^{-1} for oxygen greater than 120 μmol kg^{-1}.

the eastern South Pacific Ocean, east of 110°W and between 10 and 50°S.

3.1. Upper waters

The two northernmost sections of the Sonne cruise (28 and 35°S) were taken at the eastern edge of the South Pacific Subtropical Gyre such that temperature and salinity generally increase westward above the main thermocline (Figs. 2A, C, 3A, and C). Near the coast, the thermocline outcrops and an alongshore front is present. A similar feature also is seen in the density and oxygen sections and is associated with prevailing equatorward winds and coastal upwelling, bringing relatively cold and oxygen-poor water to the surface. Between about 15 and 33°S of the WOCE section P19, a shallow thermostad with a temperature of ~17 °C was reported by Tsuchiya and Talley (1998), sandwiched between the seasonal and the main thermocline. This section was taken during the summer, and the thermostad was explained as a relic of the previous winter convection. On our section along 28°S, taken at the onset of winter, no such strong thermostad was present but a well-defined thermocline was seen below ~50 m in the west and at shallower depths toward the coast (Fig. 2A). A characteristic band of low salinity was observed near the base of the thermocline, between 100 and 300 m, in the western portion of the 28°S section (Fig. 3A) and at somewhat shallower depths in the 35°S section (Fig. 3C), where it sloped upward toward the coast. In the Sonne sections, the salinity minimum was centered on $\gamma_n = 25.7\,\mathrm{kg\,m^{-3}}$ and corresponded to an approximate temperature range of 11–15 °C. A similar shallow salinity minimum also was seen in the zonal WOCE section P6 along 32°S (Wijffels et al., 2001) and in the SCORPIO section at 28°S, encompassing the area between the coast to about 86°W. This salinity minimum was present, but appeared very diffuse, in the zonal WOCE section P21 along 17°S (Tsimplis et al., 1998), and was absent as far south as 43°S.

The sign and magnitude of the vertical salinity gradient above the shallow salinity minimum and the sign and magnitude of the vertical temperature gradient suggest that double-diffusive convection, such as salt fingering, can take place. This property already has been demonstrated to the west of our sections (Tsuchiya and Talley, 1998; Wong and Johnson, 2003). Here, we extend these calculations toward the Chilean coast.

A uniquely defined and suitable measure for classifying the double-diffusive regimes of a stratified water column is given by the Turner

angle (Tu) (e.g., Ruddick, 1983), defined as

$$Tu = \tan^{-1}\left(\alpha\frac{\partial\theta}{\partial z} - \beta\frac{\partial S}{\partial z}, \alpha\frac{\partial\theta}{\partial z} + \beta\frac{\partial S}{\partial z}\right),$$

where α is the thermal expansion coefficient, β is the haline contraction coefficient, S is the salinity, and z is oriented positive upward. Double diffusion may occur as salt fingering in the $45° < Tu < 90°$ interval and as layering in the $-90° < Tu < -45°$ interval. In the $-45° < Tu < 45°$ interval, the water column is stably stratified with respect to both temperature and salinity, whereas a Turner angle in the second or third quadrant corresponds to a gravitationally unstable water column.

To evaluate the Turner angle, the vertical gradients of potential temperature and salinity were calculated as least-squares fit over 10 dbar from the 2-dbar bin-averaged CTD data, and α and β were calculated according to McDougall (1987). The Turner angle is shown in Fig. 6 for selected density surfaces along 28 and 35°S. The selected density surfaces are located immediately above and within the core ($\gamma_n = 25.7\,\mathrm{kg\,m^{-3}}$) of the shallow salinity minimum.

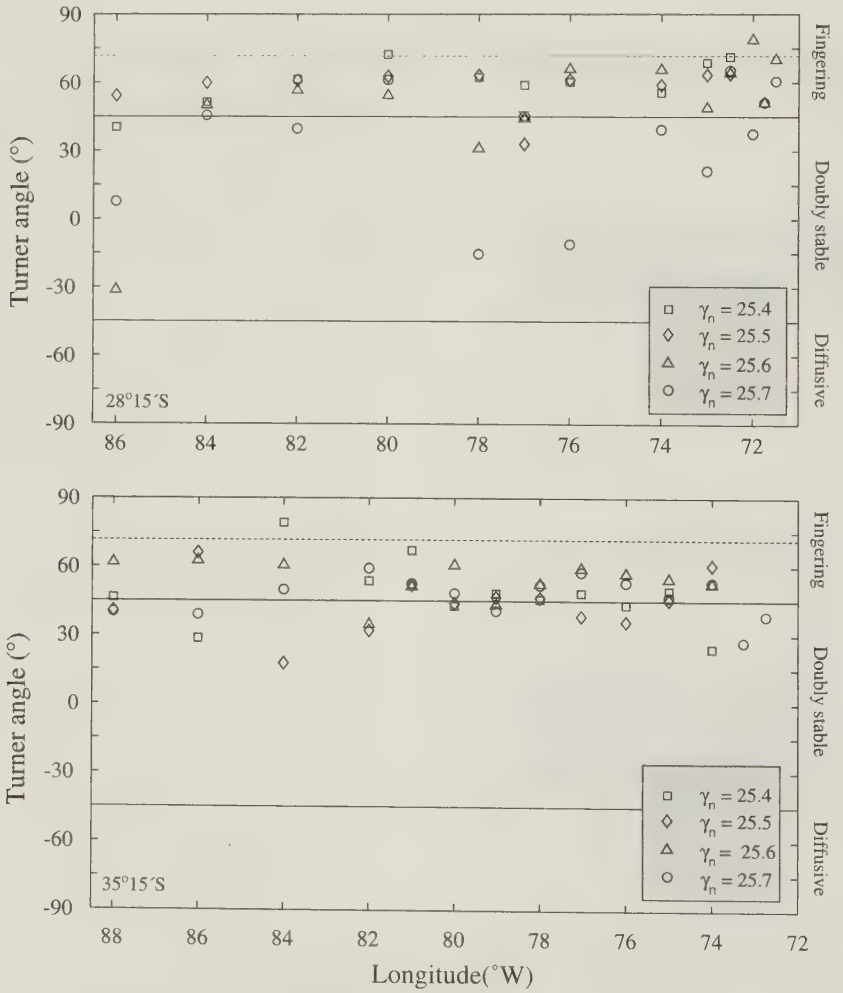

Fig. 6. Turner angle at $\gamma_n = 25.4$, 25.5, 25.6, and $25.7\,\mathrm{kg\,m^{-3}}$ calculated from the CTD data of the Sonne 102 cruise along 28 S (upper panel) and 35 S (lower panel). Turner angles between 45 and 90 suggest that double diffusion through salt fingering is possible. Strong salt fingering may occur for Turner angles larger than 71.6°, indicated by the dashed line (Ruddick, 1983).

West of 77°W, the 25.4 kg m^{-3} isopycnal is located deeper than 100 m at 28°S, whereas at 35°S, the 25.4 kg m^{-3} isopycnal is deeper than 80 m and the 25.7 kg m^{-3} isopycnal is deeper than 100 m. At these depths, below the mixed layer, wind induced mixing can be considered small. Double diffusion is possible via salt fingering within a thick band of 40–60 m immediately above the shallow salinity minimum (Fig. 6). Strong salt fingering seems to be favored in only a few cases (above dashed line in Fig. 6). It should be noted that the vertical salinity gradient changes sign around $\gamma_n = 25.7$ kg m^{-3}, and this explains why most of the stations at this density surface appear to be stably stratified with respect to double diffusion. A vertical staircase structure in salinity may be identified at some of the stations within the band west of 77°W, which indicates that salt fingering is present (not shown here). However, the structures are weak, thus indicating that salt fingering is not very active. At these relatively shallow depths, a relatively large vertical velocity shear may exist that will have a tendency to smooth property gradients, inhibiting double diffusion. The double diffusion will act to erode the shallow salinity minimum from above as it is advected northward in the South Pacific Subtropical Gyre.

The density surface of the core of the shallow salinity minimum outcrops south of about 41°S and near the coast (Fig. 7), and it slopes downward toward the west in a bowl-shaped manner, as expected from the anticyclonic circulation of the South Pacific Subtropical Gyre, exceeding depths of 250 m near 110°W and 20°S. The data used to construct the horizontal maps are of mixed quality and of different vertical resolutions, including both high-resolution CTD casts and bottle casts with variable vertical resolutions. Most of the historical data (i.e., prior to the WOCE and Sonne sections) are from bottle casts and the vertical resolution of standard bottle depths between 150 and 300 m is 50 m, which is inadequate to resolve features with a typical vertical scale of about 100 m. The resolution is higher at shallower depths. Thus, the salinity minimum is probably badly resolved in the northwest corner of Fig. 7, but may be resolved sufficiently well elsewhere.

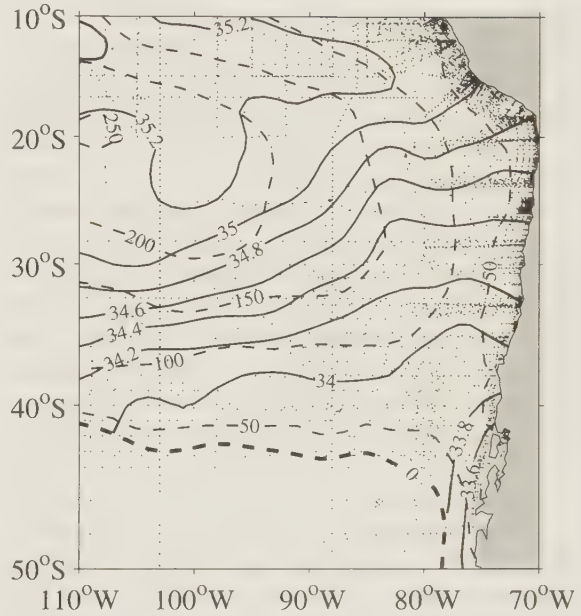

Fig. 7. Salinity and pressure (dbar) on $\gamma_n = 25.7$ kg m^{-3}. Salinity is shown with solid contours and a contour interval of 0.2. Pressure is shown with dashed contours and a contour interval of 50 dbar. The plot is based on all available hydrographic data from the eastern South Pacific Ocean between January 1965 and December 2001.

The shallow salinity minimum seems to be a common feature of the eastern boundary current systems of the Pacific and Atlantic Oceans (Reid, 1973). In the eastern South Pacific Ocean, the shallow salinity minimum spreads equatorward along the continent and extends westward to about 160°W between ~8 and 16°S, but does not cross the equator (Reid, 1973). Wyrtki (1967) explained the shallow salinity minimum in the eastern South Pacific Ocean as the result of Subantarctic Surface Water sinking as it moves equatorward within the Peru–Chile Current, and pointed out that the sinking and formation of the shallow salinity minimum takes place around 35°S. West of 90°W, it seems to coincide with the Subtropical Front, a narrow zone that marks the transition between warm subtropical waters to the north and colder Subantarctic waters to the south (Stramma et al., 1995).

With the geostrophic and hydrostatic layered model of Luyten et al. (1983), the shallow salinity

minimum of the eastern North Pacific Ocean was explained by Talley (1985) as a result of wind-driven ventilation of the thermocline along the eastern rim of the North Pacific Subtropical Gyre. The properties of the salinity minimum are set by the conditions in the mixed layer into which isopycnals outcrop, and the rate at which water moves into the thermocline along isopycnals is set by the Ekman pumping via the wind stress curl. As water is subducted below the lighter water above and is no longer in contact with the mixed layer, its potential vorticity is conserved in the model. The winter mixed-layer salinity of the outcropping zone and wind patterns determine the deepest density layer in which the minimum occurs. This is because the deepest mixed layer is usually found in winter when the vertical stability is weakest and the water column is most susceptible to possible Ekman pumping.

Essentially, the same model was applied by De Szoeke (1987) for the South Pacific Ocean and, to a high degree, the results resembled those of the North Pacific, with a ventilated region along the southern and eastern rim of the Subtropical Gyre. Huang and Qui (1998) analyzed observational data and estimated the annual mean subduction rate into the South Pacific Subtropical Gyre, but their analysis was not targeted to specific water masses. The preferred ventilation of the South Pacific thermocline from the southeast between ~30 and 40°S also may be inferred from a series of salinity and temperature plots on neutral density surfaces presented and discussed by You et al. (1995). The salinity in the mixed layer decreases poleward along the Chilean coast, so water that is pumped into the thermocline from the mixed layer and moves equatorward will have lower salinity than the water above. Below, the water is bounded by the salinity maximum of Equatorial Subsurface Water (ESSW), centered at ~180 m (Figs. 3A and C). Hence, the necessary conditions for a shallow salinity minimum are present. ESSW also is known as Subtropical Underwater and has recently been studied by O'Connor et al. (2002).

To diagnose the annual rate at which water enters the thermocline in the eastern South Pacific, or is sucked into the mixed layer from the thermocline there, we calculated the annual mean subduction rate, $\bar{S}$ (Marshall et al., 1993). $\bar{S}$ is defined as

$$\bar{S} = -\bar{w}_{-h} - \bar{\mathbf{u}}_{-h} \cdot \nabla_{\mathrm{H}} h, \tag{1}$$

where h is the depth of the winter mixed-layer base when it is deepest, $\bar{w}_{-h}$ and $\bar{\mathbf{u}}_{-h} = (\bar{u}, \bar{v})_{-h}$ are the annual mean vertical and horizontal velocity components at the mixed-layer base, and $\nabla_{\mathrm{H}} = (\partial/\partial x,\ \partial/\partial y)$, where x and u are positive toward the east, y and v are positive toward the north, and w is positive upward. The overbars denote annual averages. The vertical velocity, $\bar{w}_{-h}$, in Eq. (1) is calculated from the Ekman pumping and a term due to the divergence of the meridional flow within the mixed layer

$$\bar{w}_{-h} = \frac{1}{\rho} \nabla_{\mathrm{H}} \times \frac{\bar{\tau}}{f} - \frac{\beta}{f} \int_{-h}^{0} \bar{v}\, \mathrm{d}z,$$

where $\rho = 1025\,\mathrm{kg\,m^{-3}}$ is a constant reference density, $\bar{\tau} = (\bar{\tau}_x, \bar{\tau}_y)$ is the annual mean wind stress vector, f is the Coriolis parameter, and β is its meridional derivative. The lateral injection term, $\bar{\mathbf{u}}_{-h} \cdot \nabla_{\mathrm{H}} h$, in Eq. (1) gives the transfer of horizontal flow in the mixed layer into the thermocline through the sloping mixed-layer base.

The annual mean Ekman pumping was calculated from the European Remote Sensing Satellite scatterometer winds, ERS-1 and ERS-2 (Bentamy et al., 1998) between August 1991 and August 2000. Eight gaps of up to three weeks during 1992 were filled by linear interpolation. The depth of the deepest winter mixed layer, defined as the depth where γ_{n} is $0.125\,\mathrm{kg\,m^{-3}}$ greater than at the surface, was calculated by combining all available bottle and CTD salinity observations (in all 5403 stations) and late winter (August and September) bottle, CTD, and Expendable Bathythermograph (XBT) temperature observations (in all 1067 bottle and CTD stations, and 3121 XBT stations) from the National Oceanographic Data Archive between January 1965 and December 2001, including our Sonne sections. We also included the recent WOCE sections P6, P18, P19, and P21 for the region. The data were interpolated (Akima, 1970) onto standard depths and objectively mapped with a constant horizontal correlation scale of 5° longitude and 5° latitude and γ_{n} calculated. We use annual rather than late winter salinities due to

sparse data coverage, especially in the southern half of the region. Seasonal salinity changes are generally small at the depths considered, except near the coast of southern Chile where large fresh water runoff is present during autumn and summer (Davila et al., 2002). Annual mean geostrophic velocity at the base of the winter mixed layer was calculated from all available temperature and salinity data, assuming a level of no motion at $\gamma_n = 28.054\,kg\,m^{-3}$. This density level corresponds to a mean depth of ~3700 m and is equivalent to the depth of $\sigma_4 = 45.83\,kg\,m^{-3}$ chosen in Shaffer et al. (2004) for the region.

The late winter mixed-layer depth (Fig. 8A) is less than 50 m near the South American coast and deepens toward the west and southwest. The geostrophic velocity at the mixed-layer base (Fig. 8B) reflects the anticyclonic Subtropical Gyre north of ~45°S and the cyclonic circulation south of ~45°S, due to eastward flow of the Antarctic Circumpolar Current and poleward flow of the Cape Horn Current along the coast of southern Chile. Because of substantial equatorward flow in the Subtropical Gyre, the vertical velocity at the base of the mixed layer (Fig. 8D) is reduced by up to 40% of the surface Ekman pumping (Fig. 8C), whereas the transfer of water from the thermocline into the mixed layer is enhanced near the coast. Lateral injection through the spatially varying base of the mixed layer (Fig. 8E) shows an irregular pattern with regions of alternating signs but of similar magnitude. These regions appear because of the strong zonal velocity components along ~15 and ~40°S and shallow ridges and troughs in the gridded mixed layer, perhaps an artifact of the sparse data coverage. The resulting estimate of the net subduction rate (Fig. 8F) shows a field quite different from that of the Ekman pumping alone. Subduction, still positive across most of the region, is now also prominent near the coast. Apparently, the low-salinity water of the shallow salinity minimum in the eastern South Pacific Ocean can be subducted directly into the thermocline near 37°S and then carried eastward and equatorward by the Peru–Chile Current. A similar mechanism seems to apply to the formation of the shallow salinity minimum in the North Pacific (Yuan and Talley, 1992). Integration of the local subduction rate over the ventilation region for the shallow salinity minimum, here defined between $\gamma_n = 25.4$ and $26.2\,kg\,m^{-3}$ and east of 110°W, gives an estimated transport of low-salinity water into the thermocline of 2.8 Sv ($1\,Sv = 10^6\,m^3\,s^{-1}$), with equal contributions from the vertical and lateral components.

The shallow salinity minimum shows a high oxygen concentration, and its base is marked by a very strong oxygen concentration gradient (Fig. 5A). This strong gradient presumably marks the boundary between recently ventilated waters from the south and poorly ventilated waters of equatorial origin below (e.g., Reid, 1973; Blanco et al., 2001).

In the three Sonne sections, a core of high-salinity water is observed near the coast (Figs. 3A, C, and E), centered at a depth of about 180 m and clearly bounded above by the shallow salinity minimum and below by a weaker salinity minimum at about 650 m. Along 28°S, the core of high-salinity water is seen to coincide with low oxygen concentrations (Fig. 5A). The salinity maximum and oxygen minimum are associated with the poleward transport of ESSW within the Peru–Chile Undercurrent (PCU) (Silva and Neshyba, 1979). As ESSW is advected poleward along the coast of Chile, it is markedly diluted between 35 and 43°S due to mixing with ambient water. The salinity maximum decreases by ~0.1 between 28 and 35°S, but by >0.2 between 35 and 43°S. There are probably several explanations for this. For instance, the coastline is more irregular between 35 and 43°S than farther to the north, leading to higher dissipation and mixing. The wind also is more variable in strength and direction south of 35°S, which may reduce or change the sign of the local wind stress curl and thereby affect the local alongshore pressure gradient. The alongshore pressure gradient is believed to be important for driving the undercurrent and advecting ESSW poleward along the Chilean coast (see McCreary and Chao, 1985). The salinity maximum extends westward as a more or less continuous band at 28 and 35°S, with a thickness of 200–300 m centered approximately on the $26.6\,kg\,m^{-3}$ isopycnal. Within this band, a second core of increased salinity and low oxygen is visible near 78°W at 28°S and

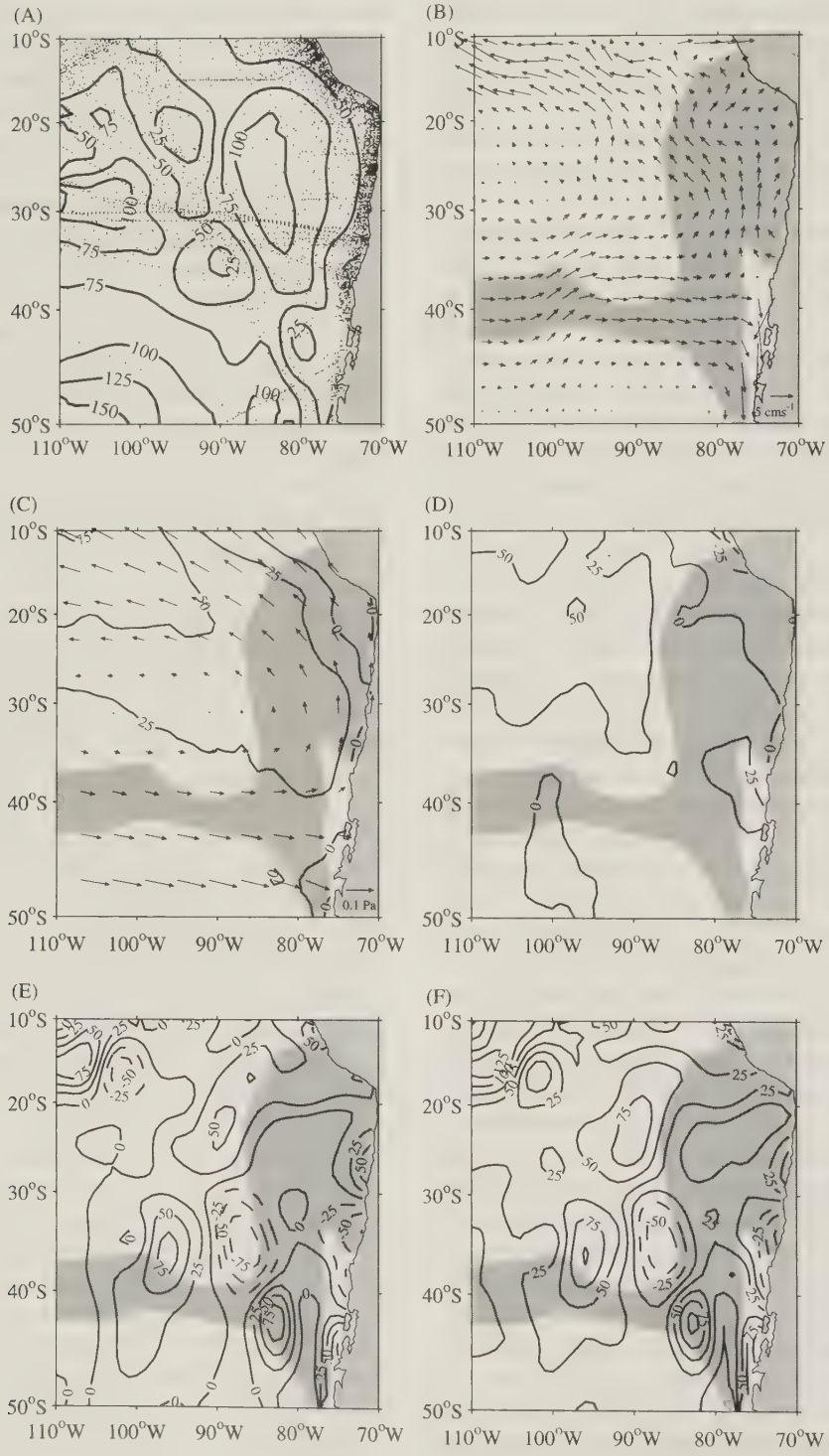
(A)
(B)
(C)
(D)
(E)
(F)
10°S
20°S
30°S
40°S
50°S
110°W
100°W
90°W
80°W
70°W
5 cms⁻¹
0.1 Pa

near 79°W at 35°S. A similar offshore salinity maximum and oxygen minimum is seen in the SCORPIO section at 28°S and in the WOCE section P6 (32°S), but is absent in the SCORPIO and Sonne sections at 43°S. The rather constant offshore position of this second core may indicate another poleward current of equatorial origin, separated from the PCU within our latitude band, maybe a subsurface signature of the Peru–Chile Counter Current. However, the position is ~200 km farther offshore than predicted by Strub et al. (1995). Also, the two salinity maxima and oxygen minima are separated by only a few degrees longitude and are neither well resolved nor traceable in the horizontal salinity and oxygen maps based on the available data. The offshore salinity maximum cannot be identified in the WOCE section P21 (17°S), where salinity at all longitudes seems to decrease monotonically with depth within the main thermocline (Tsimplis et al., 1998). However, there is a very weak local salinity maximum over the shelf off Peru at 150 m, which marks the PCU.

We calculated the geostrophic velocity based on our CTD data with the $\gamma_n = 28.054\,\mathrm{kg\,m^{-3}}$ level of no motion (Fig. 9). The geostrophic velocity field shows a rich structure in the upper ~1000 m on scales of 100–300 km, much of which is probably related to mesoscale eddies in the Peru–Chile Current system. The geostrophic calculations reveal a maximum poleward velocity within the PCU of $7.6\,\mathrm{cm\,s^{-1}}$ centered at 163 m (28°S), $11.8\,\mathrm{cm\,s^{-1}}$ at 190 m (35°S), and $9.5\,\mathrm{cm\,s^{-1}}$ at 253 m (43°S). Evidence of a poleward descending core in the PCU also may be found in Silva and Neshyba (1979) and in other eastern boundary current systems as well. Mittelstaedt (1976) and Barton (1989) found that the core of the undercurrent near the northwestern coast of Africa goes deeper as it extends poleward. McCreary and Chao (1985) and Clarke (1989) explained the poleward descending core within the framework of linear, stratified, and wind-driven theory, a poleward decrease in the vertical stratification, and a widening of the shelf. Theory also predicts a poleward decrease in the velocity previously documented for the PCU (Silva and Neshyba, 1979); however, this is not evident in the Sonne data.

The transport of the PCU also was estimated from the derived velocities in the three sections. The undercurrent may be defined by salinities greater than 34.6, 34.45, and 34.3 at 28, 35, and 43°S, respectively. With this definition, the area-averaged poleward transport was found to be 1.3, 1.3, and 1.1 Sv at the respective latitudes, consistent with estimates based on long current meter observations at 30°S (Shaffer et al., 1999).

3.2. Mode and intermediate waters

The Subantarctic Mode Water (SAMW) is distinguishable from Antarctic Intermediate Water (AAIW) in the western part of the South Pacific Ocean by its thermostad, pycnostad, and lower density (Piola and Georgi, 1982). Farther to the east, the two water masses tend toward equal hydrographic properties; off southern Chile, where the densest SAMW is found, the AAIW salinity minimum is found immediately below the SAMW thermostad. In WOCE section P19 along 88°W, the thermostad can be traced from at least 50°S and northward to 37°S; however, the pycnostad can be traced all the way to 28°S (Tsuchiya and Talley, 1998). In our 43°S section, east of WOCE section P19, the thermostad is clearly visible from

Fig. 8. (A) Depth (in m) of the late winter mixed layer defined as the depth where γ_n is $0.125\,\mathrm{kg\,m^{-3}}$ greater than at the surface. The contour interval is 25 m. (B) Annual mean geostrophic velocity at the mixed-layer base relative to a level of no motion at $\gamma_n = 28.054\,\mathrm{kg\,m^{-3}}$ (corresponding to a mean depth of ~3700 m). Velocity vectors are shown at every second grid point and a reference vector is supplied in the lower right corner. (C) Annual mean Ekman pumping velocity (in $\mathrm{m\,yr^{-1}}$) and wind stress vectors. Wind stress vectors are shown at every fourth grid point and a reference vector is supplied in the lower right corner. (D) Annual mean vertical pumping velocity at the mixed-layer base ($-\bar{w}_{-h}$, in $\mathrm{m\,yr^{-1}}$). (E) Annual mean lateral subduction rate through the mixed-layer base ($-\bar{\mathbf{u}}_{-h} \cdot \nabla_H h$, in $\mathrm{m\,yr^{-1}}$). (F) Net subduction rate through the mixed-layer base ($\bar{S}$, in $\mathrm{m\,yr^{-1}}$). The contour intervals in C–F are $25\,\mathrm{m\,yr^{-1}}$. Notice that, per definition, positive values in C–F denote transports into the thermocline. The shaded region in B–F shows the ventilation region of the shallow salinity minimum between $\gamma_n = 25.4$ and $26.2\,\mathrm{kg\,m^{-3}}$, and east of 110°W.

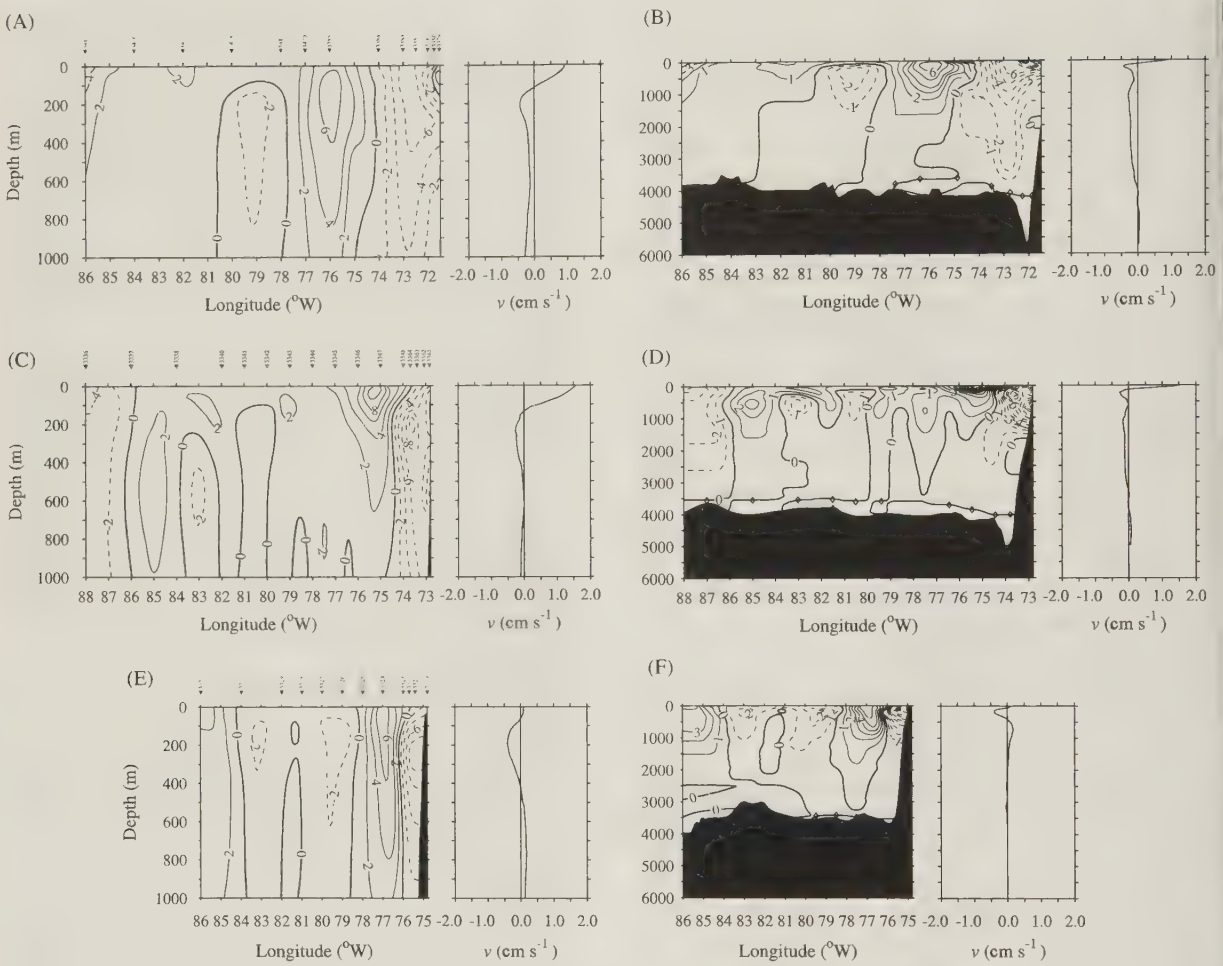

Fig. 9. Geostrophic velocity and sectional-averaged geostrophic velocity ($cm\,s^{-1}$) calculated with levels of no motion at $\gamma_n = 28.054\,kg\,m^{-3}$ based on CTD data from the Sonne cruise along 28°S (A, B), 35°S (C, D), and 43°S (E, F). These sections are shown in Fig. 1. (Left panels) Geostrophic velocity of the upper 1000 m with a contour interval of $2\,cm\,s^{-1}$. Numbers on upper X-axis as in Fig. 2. (Right panels) Geostrophic velocity down to the bottom with contour intervals of $1\,cm\,s^{-1}$. Positive values (solid contours) indicate flow to the north. The levels of no motion are indicated with diamonds.

~200 km off the coast and confined between ~5 and 6 °C (Fig. 2E). The pycnostad is confined between about $\gamma_n = 27.1$ and $27.26\,kg\,m^{-3}$, corresponding to a depth interval from ~300 to 600 m (Fig. 4E).

SAMW at 43°S contains a weak salinity maximum in excess of 34.26 at $\gamma_n = 27.16\,kg\,m^{-3}$ (Fig. 3E). The weak salinity maximum may originate from the relatively high-salinity water found on the same density surface over the continental slope as a diluted form of ESSW. A similar weak salinity maximum is not seen in the SCORPIO data at the same latitude. Farther north (at 35°S), the thermostad is substantially weakened (Fig. 2C), but the pycnostad is still present between $\gamma_n = 27.1$ and $27.26\,kg\,m^{-3}$ (Fig. 4C), about 150 m deeper than at 43°S (Fig. 4E). The thermostad cannot be identified at 28°S and the pycnostad can only be weakly identified (Figs. 2A and 4A). SAMW is believed to be formed in the eastern South Pacific Ocean about 5–10° latitude south of our study region (McCartney, 1977).

McCartney (1977) suggests a mechanism whereby late winter heat loss to the atmosphere results in deep convection and the formation of a relatively homogeneous water mass, which then spreads equatorward from the formation area via the South Pacific Subtropical Gyre.

In their comparison of the Sonne and SCORPIO sections at 43°S, Shaffer et al. (2000) found evidence for warming of up to 0.08 °C on neutral density levels and of up to 0.2 °C on pressure levels in the SAMW depth range and in the upper AAIW parts. At 28°S, no significant warming was observed in the depth range of SAMW, but such warming was observed below ~650 m. One explanation for why no warming was observed in SAMW at 28°S may be that the temperature signal is not carried that far north, where only the pycnostad of SAMW can be (weakly) identified.

The vertical gradient in salinity is generally low as far south as 43°S, and AAIW is defined by a weak salinity minimum of ~34.24 on the 27.26 kg m^{-3} isopycnal. This density level corresponds to a depth of ~650 m (Fig. 4E). Farther north, as the influence of more saline, equatorial water masses increases above the salinity minimum, the vertical contrast is sharpened. At 35°S, the core of AAIW is located about 50 m deeper than at 43 and 28°S. This is consistent with a participation of AAIW in the anticyclonic circulation of the Subtropical Gyre below the main thermocline (Johnson, 1972; Reid, 1986). Pressure on the density surface of AAIW attains a meridional maximum along an axis crossing the Pacific at 35°S and a zonal maximum at 160°W, which, for example, can be inferred from the maps of Johnson (1972). The core of AAIW is characterized by patches of salinity slightly less than 34.25 at 35°S, which ascend by about 50 m along isopycnals going eastward from 88°W to about 150 km from the coast. From there, the isopycnals slope steeply downward toward the continental slope. At 28°S, AAIW is centered at ~650 m with a core salinity slightly in excess of 34.28 and maximum oxygen values slightly above 190 μmol kg^{-1}. The increases in salinity (from 34.24 to 34.28) and (density preserving) temperature (from 4.8 to 5.1 °C) equatorward along the AAIW core between 43 and 28°S suggest isopycnal mixing with water from lower latitudes and probably also diapycnal mixing.

Upward sloping isopycnals eastward from ~77°W to ~100–250 km from the coast and downward sloping isopycnals from there to the continental slope are evident in the three sections, suggesting an equatorward flow east of 77°W and a poleward flow closer to the coast. The dynamic calculation relative to $\gamma_n = 28.054$ kg m^{-3} (Fig. 9) shows poleward flow near the coast reaching as deep as 1700 m in all three sections. Between most station pairs, however, poleward flow is present all the way down to the reference levels of zero velocity. Below 1000 m, the velocities are <5 cm s^{-1} and decrease uniformly with depth. The deep poleward flow over the continental slope within our latitudinal band also is evident in the circulation patterns derived by Reid (1986) for the South Pacific Ocean, and in recent geostrophic calculations based on WOCE section P6 along 32°S (Wijffels et al., 2001; Shaffer et al., 2004). In

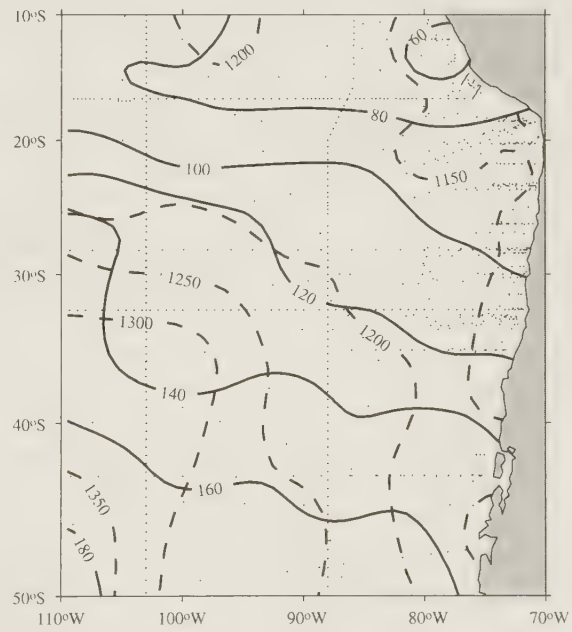

Fig. 10. Oxygen (μmol kg^{-1}) and pressure (dbar) at $\gamma_n = 27.64$ kg m^{-3}. Oxygen is shown with solid contours and a contour interval of 20 μmol kg^{-1}. Pressure is shown with dashed contours and a contour interval of 50 dbar. The plot is based on all available hydrographic data from the eastern South Pacific Ocean between January 1965 and December 2001.

Reid's analysis, the poleward flow extends west to about 100°W. Wijffels et al. (2001) applied inverse calculation methods constrained with specified mass and silicate transports and velocity observations from floats and current meter moorings. Their preferred solution showed poleward flow within ~1000 km from the Chilean coast and below ~600 m of ~15 Sv, with a core of strong southward flow at a depth of ~3000 m on the Chilean slope. Shaffer et al. (2004) used the heat balance of the deep Chile and Peru basins and direct current observations to determine the level of no motion in the eastern boundary current there to be at $\sigma_4 = 45.83\,\mathrm{kg\,m^{-3}}$. They found weak equatorward flow above the main thermocline and poleward flow within ~1600 km from the Chilean coast and below ~1000 m of ~10 Sv. Of this, 4.4 Sv was confined within 425 km off the coast (the nearshore boxes east of 76°W in their Fig. 6). Table 1 shows the geostrophic transports between the coast and 86°W for our three Sonne sections calculated using the same levels of no motion and layer boundaries as in Shaffer et al.

Table 1
Layer boundaries, mean depths, and transport estimates between the Chilean coast and 86 °W at 28, 32, 35, and 43 °S

Layer number	Layer boundary	Z_m (m)	Transport (Sv)			
			28°S	32°S[a]	35°S	43°S
	Surface	0				
1			1.3	2.8	3.0	0.1
		121				
	26.04 kg m^{-3}					
2			−2.1	1.5	−0.8	−1.6
		374				
	27.01 kg m^{-3}					
3			−2.9	1.7	−0.4	0.2
		1064				
	27.56 kg m^{-3}					
4			−2.6	−2.4	−2.2	0.1
		2197				
	27.93 kg m^{-3}					
5			−3.1	−4.7	−3.0	−0.3
		3680				
	28.054 kg m^{-3}					
6			0.0	0.4	0.3	0.0
	Sea floor					

[a]Transport estimates at 32°S are derived from the work of Shaffer et al. (2004).

(2004). For completeness, we have included comparable transport estimates at 32°S derived from the work of Shaffer et al. (2004).

3.3. Deep and basin waters

Below AAIW and above the crests of the basins, Pacific Deep Water appears as very homogeneous water. Most properties change slowly and monotonically with depth in most places, making the depth interval rather featureless. For example, salinity increases uniformly with depth while potential temperature decreases with depth in the three Sonne sections. However, other tracers, such as dissolved oxygen and silica, may be useful to identify the influence of water from remote sources in the North Atlantic and around Antarctica. Oxygen profiles at 28°S show a wide minimum between ~800 and 1500 m with concentrations $< 120\,\mu\mathrm{mol\,kg^{-1}}$. Closer to the coast, at 71°45.0′W (station 3380), the concentration is as low as $93.3\,\mu\mathrm{mol\,kg^{-1}}$ at 900 m depth (Fig. 5B). The deep oxygen minimum can barely be separated from the shallower minimum associated with ESSW near the continental slope, but farther offshore it is clearly separated by the intermediate oxygen maximum of recently ventilated AAIW in the depth interval of ~500–800 m. In the transpacific SCORPIO sections (Warren, 1973) and WOCE section P6, the oxygen minimum appears all the way across the Pacific, although not as strong west of 110°W. The low oxygen concentrations between 800 and 1500 m appear to originate from immediately south of the equator (Tsuchiya and Talley, 1998). At least in part, the outflow from the Pacific Ocean in this depth interval can be seen as a compensation of the deep inflow from the Southern Ocean, which upwells at northern latitudes, as suggested by Wunsch et al. (1983). From there, the water returns south, crossing the equator in the east between ~100 and 120°W and flowing along the Chilean slope, where the lowest-oxygen concentrations also are observed (Reid, 1986).

The meridional extent of the deep oxygen minimum in the eastern South Pacific is most clearly seen in WOCE section P19 (Tsuchiya and Talley, 1998). The low-oxygen core over the

Chilean slope descends poleward from ~1000 m ($\gamma_n = 27.55\,kg\,m^{-3}$) at 28°S to ~1500 m ($\gamma_n = 27.8\,kg\,m^{-3}$) at 43°S and shows a slight poleward increase in concentration (Warren, 1973). This suggests that some vertical exchange is taking place, mainly by mixing water in from below the oxygen minimum. Fig. 10 shows the oxygen concentration and pressure of the deep oxygen minimum on the $27.64\,kg\,m^{-3}$ isopycnal based on historical data. The southward flow near the coast discussed above is consistent with this distribution, exhibiting the lowest oxygen concentrations near the coast. The geostrophic velocity, relative to $\gamma_n = 28.054\,kg\,m^{-3}$, of the low-oxygen core in the Sonne section east of 86°W is indeed poleward with a mean value of $-1.0\,cm\,s^{-1}$.

Shaffer et al. (2000) observed warming and a decrease in oxygen concentrations between 1967 and 1995 on neutral density surfaces at depths between 650 and 1200 m at 28°S. For example, temperature was found to have increased by 0.03 °C on $\gamma_n = 27.64\,kg\,m^{-3}$ and oxygen seems to have decreased by $3.5\,\mu mol\,kg^{-1}$ between 1967 and 1995. These results suggest a change in circulation at mid-depths during recent decades, whereby subtropical water masses have moved farther south along the Chilean coast. To quantify this change, meridional and zonal temperature and oxygen gradients are calculated on the $27.64\,kg\,m^{-3}$ isopycnal at 28°S. Meridional temperature and oxygen gradients are calculated as least-squares fit to the available hydrographic data between 20 and 35°S and east of 90°W, neglecting stations within 150 km of the coast, and the zonal gradients are calculated from the Sonne and SCORPIO data only. The meridional temperature and oxygen gradients are found to be $3.4 \pm 0.4 \times 10^{-7}\,°C\,m^{-1}$, and $-3.0 \pm 0.5 \times 10^{-5}\,\mu mol\,kg^{-1}\,m^{-1}$, respectively, and the zonal temperature and oxygen gradients are found to be $0.5 \pm 0.2 \times 10^{-7}\,°C\,m^{-1}$ and $-0.9 \pm 0.2 \times 10^{-5}\,\mu mol\,kg^{-1}\,m^{-1}$, respectively. The gradients given are positive toward the north and east, and the confidence limits are calculated to the 90% level, assuming a Student's t-distribution of the data. However, the Student's t-test assumes statistical independence of the data, which may not hold for closely spaced stations in time and space. From the above analysis, the observed hydrographic changes at mid-depths at 28°S seem to be best explained by a seaward/poleward excursion of the water masses by ~100–400 km and may indicate enhancement in the deep poleward flow along Chile.

The Chile Basin is filled from the south through gaps and fracture zones in the Chile Rise (Lonsdale, 1976). The Chile Rise crosses the eastern South Pacific in a northwestward direction from the continental slope near 45°S and intersects our southernmost (zonal) section at 82°W (Fig. 1). To display some of the hydrographic properties near the bottom more clearly than section wide maps allow, the westernmost station and a station in the eastern part of the Chile Basin, near the continental slope, are shown for each section in Fig. 11.

All of the stations were taken within the Chile Basin except the station at 86°W and 43°S (station 3331), which was taken in the Southeast Pacific Basin near the sill of the Valdivia fracture zone (Fig. 1). The salinity maximum of Lower Circumpolar Deep Water (modified North Atlantic Deep Water) defined by salinities >34.70 can be identified in the deepest bottle at station 3331. This water mass is apparently restricted from moving farther north by the Chile Rise. At depths over 3400 m, the temperature is significantly higher in the Chile Basin than it is to the south of the Chile Rise at corresponding depths. As noted by Tsuchiya and Talley (1998), the temperature in the western portion of the basin corresponds much better to the temperature at the crest of the Chile Rise (compare station 3336 with station 3331 in Fig. 11), suggesting that at least part of the water in the western part of the Chile Basin is renewed over the Chile Rise rather than through the gaps and fracture zones. The highest temperatures and lowest salinities, thus the lightest water, are found on the eastern side of the basin. This suggests a southward geostrophic flow relative to the bottom. The Sonne data and the part of the WOCE section P19 that crosses the western part of the Chile Basin both show lighter water in the northern part, suggesting an eastward geostrophic flow relative to the bottom (Tsuchiya and Talley, 1998). Thus, a cyclonic circulation pattern would be expected in

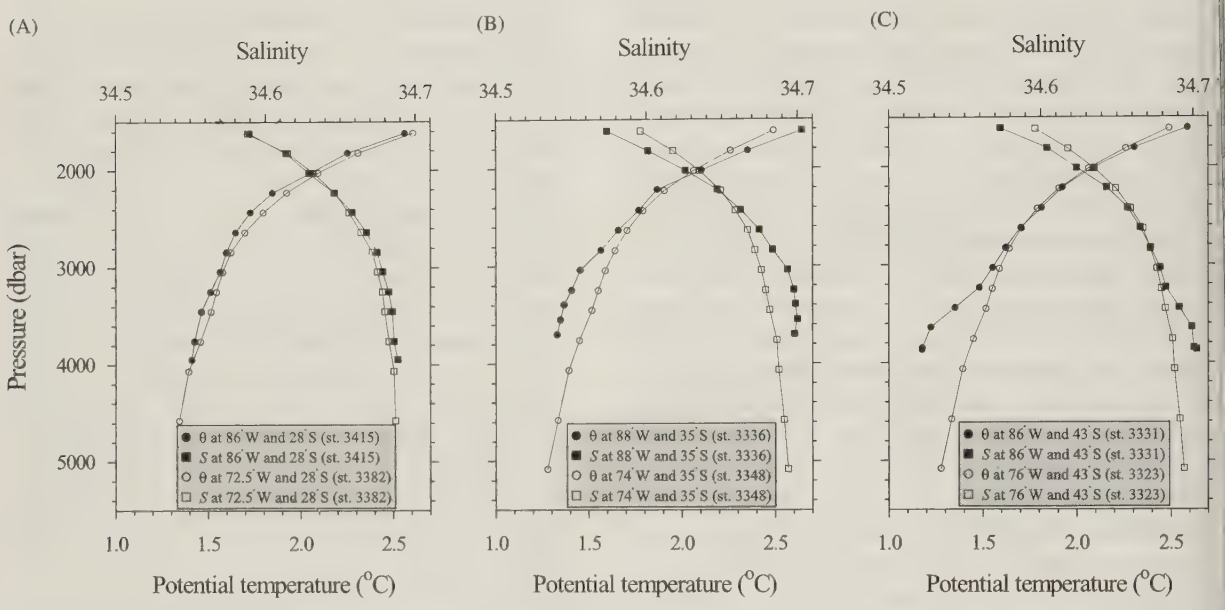

Fig. 11. Potential temperature (°C) and salinity at bottle depths below 1600 m for selected stations from the Sonne cruise along (A) 28°S, (B) 35°S, and (C) 43°S.

the basin. A similar circulation pattern was derived by Reid (1986) at 3500 m.

4. Summary

Three full-depth hydrographic sections along nominal latitudes of 28, 35, and 43°S from the coast of Chile to 86–88°W were occupied during the Sonne cruise 102 in 1995. To help in the interpretation of these data, a more comprehensive database was prepared, based on all available hydrographic data from the region since 1965. Above the main thermocline, the temperature at the two northernmost sections was rather similar at corresponding depths, whereas the southern section was significantly colder. This may indicate that winter cooling has set in at higher latitudes. The main thermocline slopes weakly upward to ~100 km from the coast. From there to the coast, isotherms incline strongly upward. The weak upward slope of the thermocline is associated with the anticyclonic circulation of the South Pacific Subtropical Gyre. The strongly inclined isotherms are associated with the wind-driven coastal upwelling circulation. This interpretation is consistent with the thermocline at 43°S, appearing rather flat.

A layer of relatively low salinity was observed at 28 and 35°S near the base of the thermocline and centered on $\gamma_n = 25.7\,\mathrm{kg\,m^{-3}}$, but was absent at 43°S. Immediately above this shallow salinity minimum, the water column was found to be favorable for double diffusion via salt fingering (at a few stations the conditions were favorable for strong salt fingering). However, the process did not appear to be very active. The occurrence of the shallow salinity minimum seems to be best explained by subduction of Subantarctic Surface Water that enters the region from the southwest near 37°S. There, the density surface outcrops in the base of the mixed layer and conditions are favorable for subduction. It was found that ~2.8 Sv enters the thermocline in the density range of the shallow salinity minimum and east of 110°W. After the water is subducted, it is advected equatorward at the rim of the Subtropical Gyre underneath the subtropical water.

The characteristic band of high-salinity and low-oxygen water between $\sim\gamma_n = 26.2$ and $26.9\,\mathrm{kg\,m^{-3}}$ (corresponding approximately to the

100–350 m depth interval near the coast) marks the poleward advection of ESSW. As the coast is approached, the isopycnals tilt downward and define the PCU. Dynamic calculations relative to $\gamma_n = 28.054\,kg\,m^{-3}$ revealed maximum poleward velocities between 7.6 and $11.8\,cm\,s^{-1}$ within the PCU and a poleward descending core. There is some evidence in the literature of a poleward descending core in the PCU (Silva and Neshyba, 1979). Whether a poleward descending core is an intrinsic feature of all major eastern boundary current systems still remains unclear. Another salinity maximum and oxygen minimum was observed ~600 km offshore of the PCU. Whether or not it was associated with the Peru–Chile Counter Current could not be determined.

Off Chile, SAMW is found immediately above AAIW and can be traced by a thermostad of 5–6 °C and a pycnostad of $\gamma_n = 27.1$–$27.26\,kg\,m^{-3}$. At 43°S, the thermostad and pycnostad were clearly visible in the 300–600 m depth interval. This depth interval also contained a weak salinity maximum. The pycnostad could further be identified northward at 35°S and weakly at 28°S, whereas the thermostad could only be weakly identified at 35°S.

AAIW was seen in all three sections, although it was weakly defined at 43°S because of the much lower vertical property contrast there. Farther to the north, the core of AAIW could clearly be identified by its relatively lower salinity and higher oxygen concentration. A deep poleward flow within ~150–200 km of the coast and in the depth range of AAIW and below was inferred from dynamic calculations. This deep poleward flow near the coast of Chile also has been suggested by other investigators (e.g., Warren, 1973; Wunsch et al., 1983; Wijffels et al., 2001; Shaffer et al., 2004).

Below AAIW, the most characteristic feature in the Sonne data presented here was a minimum in oxygen concentrations in the 800–1500 m depth interval, with the lowest concentrations being observed over the continental slope. From geostrophic calculations, the flow in this depth interval and below appears to be southward along the eastern boundary of the South Pacific Ocean. It has been suggested that this southward flow may have increased over the last decades (Shaffer et al., 2000).

The Chile Basin appears to be ventilated mainly from levels above the Chile Rise by the upper portion of Circumpolar Deep Water. The lower portion of Circumpolar Deep Water, characterized by relatively high salinities of North Atlantic origin, was clearly restricted from progressing north from the Southeast Pacific Basin by the Chile Rise. Within the Chile Basin, the lightest water was found toward the east and north, which suggests a southward and eastward flow relative to the bottom.

Acknowledgements

We thank the captain, crew, and organizers of the R.V. *Sonne* cruise 102 for their help. Comments and suggestions from three reviewers helped improve this manuscript. This work was supported by the Danish Natural Science Research Council, the Carlsberg Foundation, the Danish National Research Foundation, and the Chilean National Research Council. O.L. acknowledges the FONDECYT grant No. 3000025.

References

Akima, H., 1970. A new method of interpolation and smooth curve fitting based on local procedures. Journal of the Association for Computing Machinery 17, 589–602.

Barton, E.D., 1989. The poleward undercurrent on the eastern boundary of the subtropical North Atlantic. Coastal Estuarine Studies 34, 82–95.

Bentamy, A., Grima, N., Quilfen, Y., 1998. Validation of the gridded weekly and monthly wind fields calculated from ERS-1 scatterometer wind observations. Global Atmospheric Ocean Systems 6, 373–396.

Bindoff, N.L., Church, J.A., 1992. Warming of the water column in the southwest Pacific Ocean. Nature 357, 59–62.

Bindoff, N.L., McDougall, T.J., 1994. Diagnosing climate changes and ocean ventilation using hydrographic data. Journal of Physical Oceanography 24, 1137–1152.

Blanco, J.L., Thomas, A.C., Carr, M.E., Strub, P.T., 2001. Seasonal climatology of hydrographic conditions in the upwelling region off northern Chile. Journal of Geophysical Research 106, 11451–11467.

Bryden, H.L., Griffiths, M.J., Lavín, A.M., Millard, R.C., Smethie, W.M., 1996. Decadal changes in water mass

characteristics at 24°N in the subtropical North Atlantic Ocean. Journal of Climate 9, 3162–3186.

Clarke, A.J., 1989. Theoretical understanding of eastern ocean boundary poleward undercurrents. In: Neshyba, S.J., Mooers, C.N.K., Smith, R.L., Barber, R.T. (Eds.), Poleward Flows Along Eastern Ocean Boundaries. Springer, New York, pp. 26–39.

Davila, P.M., Figueroa, D., Muller, E., 2002. Freshwater input into the coastal ocean and its relation with the salinity distribution off austral Chile (35–55°S). Continental Shelf Research 22, 521–534.

De Szoeke, R.A., 1987. On the wind-driven circulation of the South Pacific Ocean. Journal of Physical Oceanography 17, 613–630.

Huang, R., Qui, B., 1998. The structure of the wind-driven circulation in the subtropical South-Pacific Ocean. Journal of Physical Oceanography 28, 1173–1186.

Jackett, D.R., McDougall, T.J., 1997. A neutral density variable for the world's oceans. Journal of Physical Oceanography 27, 237–263.

Johnson, G.C., Orsi, A.H., 1997. Southwest Pacific Ocean water-mass changes between 1968/69 and 1990/91. Journal of Climate 19, 306–316.

Johnson, R.E., 1972. Antarctic Intermediate Water in the South Pacific Ocean. In: Fraser, R. (Ed.), Oceanography of the South Pacific Ocean. National Commission for UNESCO, Wellington, New Zealand, pp. 55–69.

Joyce, T.M., Pickart, R.S., Millard, R.C., 1999. Long-term hydrographic changes at 52 and 66°W in the North Atlantic Subtropical Gyre & Caribbean. Deep-Sea Research II 46, 245–278.

Leth, O.K., 1997. Calibration report of the Sonne cruise 102 CTD data. Technical Report, University of Copenhagen, Denmark (14pp).

Lonsdale, P., 1976. Abyssal circulation of the Southeastern Pacific and some geological implications. Journal of Geophysical Research 81, 1163–1176.

Luyten, J.R., Pedlosky, J., Stommel, H., 1983. The ventilated thermocline. Journal of Physical Oceanography 13, 292–354.

Mantyla, A.W., 1987. Standard seawater comparison updated. Journal of Physical Oceanography 17, 543–548.

Marshall, J.C., Nurser, A.J.G., Williams, R.G., 1993. Inferring the subduction rate and period over the North Atlantic. Journal of Physical Oceanography 23, 1315–1329.

McCartney, M.S., 1977. Subantarctic Mode Water. In: Angel, M. (Ed.), A Voyage of Discovery. George Deacon 70th Anniversary Volume. Deep-Sea Research 24(Suppl.), 103–119.

McCreary, J.P., Chao, S.Y., 1985. Three-dimensional shelf circulation along an eastern ocean boundary. Journal of Marine Research 43, 13–36.

McDougall, T.J., 1987. Neutral surfaces. Journal of Physical Oceanography 17, 1950–1964.

Mittelstaedt, E., 1976. On the currents along the Northwest African coast south of 22° North. Deutsche Hydrographische Zeitschrift 29, 97–117.

O'Connor, B.M., Fine, R.A., Maillet, K.A., Olson, D.B., 2002. Formation rates of subtropical underwater in the Pacific Ocean. Deep-Sea Research I 49, 1572–1590.

Parrilla, G., Lavín, A., Bryden, H., Garcia, M., Millard, R., 1994. Rising temperatures in the subtropical North Atlantic Ocean over the past 35 years. Nature 369, 48–51.

Piola, A.R., Georgi, D.T., 1982. Circumpolar properties of Antarctic Intermediate Water and Subantarctic Mode Water. Deep-Sea Research 29, 687–711.

Reid, J.L., 1973. The shallow salinity minimum of the Pacific Ocean. Deep-Sea Research 20, 51–58.

Reid, J.L., 1986. On the total geostrophic transport of the Pacific Ocean: flow patterns, tracers and transports. Progress in Oceanography 16, 1–61.

Roemmich, D., 1983. Optimal estimation of hydrographic station data and derived fields. Journal of Physical Oceanography 13, 1544–1549.

Ruddick, B., 1983. A practical indicator of the stability of the water column to double-diffusive activity. Deep-Sea Research 30, 1105–1107.

Shaffer, G., Hormazabal, S., Pizzaro, O., Salinas, S., 1999. Seasonal and interannual variability of currents and temperature over the slope of central Chile. Journal of Geophysical Research 104, 29951–29961.

Shaffer, G., Leth, O., Ulloa, O., Bendtsen, J., Daneri, G., Dellarossa, V., Hormazabal, S., Sehlstedt, P.I., 2000. Warming and circulation changes in the eastern South Pacific Ocean. Geophysical Research Letter 27, 1247–1250.

Shaffer, G., Hormazabal, S., Pizarro, O., Ramos, M., 2004. Circulation and variability in the Chile Basin. Deep-Sea Research I 51, 1367–1386.

Silva, N., Neshyba, S., 1979. On the southernmost extension of the Peru–Chile Undercurrent. Deep-Sea Research 26, 1387–1393.

Stommel, H., Stroup, E.D., Reid, J.L., Warren, B.A., 1973. Transpacific hydrographic sections at lats. 43°S and 28°S: the SCORPIO expedition-I. Preface. Deep-Sea Research 20, 1–7.

Stramma, L., Peterson, R.G., Tomczak, M., 1995. The South Pacific Current. Journal of Physical Oceanography 25, 77–91.

Strub, P.T., Mesías, J.M., James, C., 1995. Altimeter observations of the Peru–Chile countercurrent. Geophysical Research Letter 22, 211–214.

Talley, L.D., 1985. Ventilation of the Subtropical North Pacific: the shallow salinity minimum. Journal of Physical Oceanography 15, 633–649.

Tsimplis, M.N., Bacon, S., Bryden, H.L., 1998. The circulation of the subtropical South Pacific derived from hydrographic data. Journal of Geophysical Research 103, 21443–21468.

Tsuchiya, M., Talley, L.D., 1998. A Pacific hydrographic section at 88°W: water-property distribution. Journal of Geophysical Research 103, 12899 12918.

Warren, B.A., 1973. Transpacific hydrographic sections at lats. 43°S and 28°S: the SCORPIO expeditions-II. Deep water. Deep-Sea Research 20, 9–38.

Wijffels, S.E., Toole, J.M., Davis, R., 2001. Revisiting the South Pacific subtropical circulation: a synthesis of World Ocean Circulation Experiment observations along 32°S. Journal of Geophysical Research 106, 19481–19513.

Wong, A.P.S., Johnson, G.C., 2003. South Pacific Eastern Subtropical Mode Water. Journal of Physical Oceanography 33, 1493–1509.

Wunsch, C., Hu, D., Grant, B., 1983. Mass, heat, salt and nutrient fluxes in the South Pacific Ocean. Journal of Geophysical Research 13, 725–753.

Wyrtki, K., 1967. Circulation and water masses in the eastern Equatorial Pacific Ocean. International Journal of Oceanology and Limnology 1, 117–147.

You, Y., McDougall, T.J., Schmitt, R.W., 1995. Dianeutral motion, water mass conversion, and nonlinear effects on the density ration in the Pacific thermocline. Journal of Physical Oceanography 25, 1891–1904.

Yuan, X., Talley, L.D., 1992. Shallow salinity minima in the North Pacific. Journal of Physical Oceanography 22, 1302–1316.

ELSEVIER

Deep-Sea Research II 51 (2004) 2371–2388

DEEP-SEA RESEARCH
PART II

www.elsevier.com/locate/dsr2

Wind-induced exchange at the entrance to Concepción Bay, an equatorward facing embayment in central Chile

A. Valle–Levinson[a,*], W. Schneider[b,i], M. Sobarzo[b], M. Bello[c], L. Bravo[b], M. Castillo[c], L. Duarte[b], R. Fuenzalida[b,j], J.M. Gallegos[d], J. Garcés–Vargas[b], J. González[d], D. Gutiérrez[e], C. Molinet[f], M.S. Navarro[d], J. Pierini[g], E. Rodríguez–Rubio[b], A. Valdenegro[d], L. Vera[h], L. Zenteno[f]

[a]*Center for Coastal Physical Oceanography, Department of Ocean, Earth and Atmospheric Sciences, Old Dominion University, Crittenton Hall, 768 West 52nd Street, Norfolk, Virginia 23529, USA*
[b]*Departamento de Oceanografía, Universidad de Concepción, Casilla 160–C, Concepción, Chile*
[c]*Servicio Hidrográfico y Oceanográfico de la Armada, Errázuriz 232, Valparaíso, Chile*
[d]*Universidad Católica de Valparaíso, Casilla 4059, Valparaíso, Chile*
[e]*Instituto del Mar, Esquina Gamarra con General Valle s/n, Chucuito, Callao, Peru*
[f]*Centro Universitario de la Trapananda, Universidad Austral de Chile, Portales 73, Coyhaique, Chile*
[g]*Instituto Argentino de Oceanografía, Universidad Nacional del Sur, C.C. 804, 8000–Bahia Blanca, Argentina*
[h]*Instituto Oceanografico de la Armada, Base Naval Sur, Casilla 5940, Guayaquil, Ecuador*
[i]*Centro de Investigación Oceanográfica en el Pacífico Sur–Oriental (FONDAP–COPAS), Universidad de Concepción, Casilla 160–C, Concepción, Chile*
[j]*Universidad Arturo Prat, Avenida Arturo Prat 2120, Iquique, Chile*

Accepted 20 July 2004

Abstract

Hydrographic and underway water velocity profiles were measured at the entrance to Concepción Bay, an equatorward facing embayment in central Chile, in order to illustrate the wind-induced exchange flow. Observations took place over a 25-h period (5–6 January 2002) during the austral summer, which is characterized by upwelling winds in the region. One portion of the observational transect was directly influenced by the wind and the other was protected from such influence by an island. The portion of the transect influenced by wind showed a surface layer, delimited by a pycnocline, moving downwind owing to the direct action of wind stress. This surface transport should have caused an onshore decrease of surface elevation that would drive upwind flow below the surface layer. The portion of the transect protected by the island was influenced by its wake and perhaps forced by a semidiurnal tide. This study is one of the few observational examples of wind-induced flow that documents the wind-induced exchange pattern under weak internal friction (low Ekman number). This pattern consists of downwind flow in an upper layer delimited by the pycnocline and upwind flow below.
© 2004 Elsevier Ltd. All rights reserved.

*Corresponding author. Tel.: +1 757 683 5578; fax: +1 757 683 5550.
E-mail address: arnoldo@ccpo.odu.edu (A. Valle–Levinson).

0967-0645/$ - see front matter © 2004 Elsevier Ltd. All rights reserved.
doi:10.1016/j.dsr2.2004.08.010

1. Introduction

Studies on wind-induced circulation in shallow (<100 m) coastal embayments with bathymetry consisting of a channel flanked by shoals have been carried out for nearly three decades. Early research illustrated a pattern of downwind flow over shoals and upwind flow in channels. This wind-driven pattern was shown theoretically (Csanady, 1973), in laboratory experiments (Fischer, 1976), in field observations (Hearn et al., 1987), and in numerical results (Signell et al., 1990). The topic of wind-induced flow in coastal embayments has gained increased interest in recent years because of the nature of its spatial structure (e.g., Wong, 1994; Glorioso and Davies, 1995; Friedrichs and Hamrick, 1996; Mathieu et al., 2002; Winant, 2004). Because of the difficulty in obtaining water velocity measurements along a transect during periods of considerable wind forcing, the great majority of these efforts have been theoretical, using analytical and numerical approaches. Recent observations by Valle–Levinson et al. (2001a, b, 2002) have illustrated some aspects of the vertical and lateral structures of wind-induced exchange under moderately to strongly frictional conditions, which arise from tidal forcing in relatively shallow systems. The purpose of this investigation was to document, on the basis of observations, the transverse structure of wind-induced exchange at a semi-enclosed embayment characterized by weak internal friction and simple morphology. The transverse structure under weak internal friction distinguishes this study from previous work, which dealt mostly with strong internal friction. The present study documents the transverse structure of the wind-induced exchange in Concepción Bay, an equatorward facing embayment in central Chile. Weak internal friction is related to feeble tidal currents in this relatively deep bay (~50 m uniformly across the entrance), allowing the development of a well-defined pycnocline.

Equatorward facing embayments usually present upwelling and productivity attributed to changes in coastline morphology and bathymetry (e.g., Figueroa and Moffat, 2000). These embayments are oriented so that upwelling winds blow offshore along the bay's axis, providing ideal natural laboratories for studying wind-induced effects in semi-enclosed systems. In addition, because these embayments are perpendicular to the direction of internal Kelvin wave propagation, they may act as regions of energy dampening (Valle–Levinson et al., 2003a). Such wave dampening may allow periodic pulses of nutrient injections into the photic zone that would help explain, in conjunction with local upwelling dynamics, the high productivity of these systems. Other examples of equatorward facing embayments are the Gulf of Arauco in central Chile; Monterey Bay and Morro Bay in central California, USA; San Quintín Bay in México; and Walvis Bay in namibia.

The wind-induced exchange illustrated in this study was observed with shipborne measurements, collected during a diurnal cycle, of underway current velocity profiles at the bay's entrance. These velocity observations, together with salinity and temperature profiles, also allow the characterization of the transverse structure of tidal properties and hydrography at the entrance to the bay. This work presents a depiction of the study area, followed by the data collection and analysis scheme. The description of salient hydrographic features sets the stage for the presentation of subtidal flows and the diurnal and semidiurnal variability associated with flow distributions across the bay entrance.

2. Study area

Concepción Bay, located along Chile's central coast (36.6°S), is an embayment with an approximate rectangular 'U' shape that opens equatorward and is characterized by a marked change in the general coastline orientation from N–S to E–W (Fig. 1). The bay extends almost 16 km from head to mouth (N–S) and ~9 km from the Tumbes Peninsula on the west to Tomé Point on the east. Its surface area is ~144 km^2. The bay's bathymetry is relatively smooth, with isobaths roughly following the coastline. On the northwestern end of the bay, the general isobath curvature is interrupted by Quiriquina Island, which separates the commu-

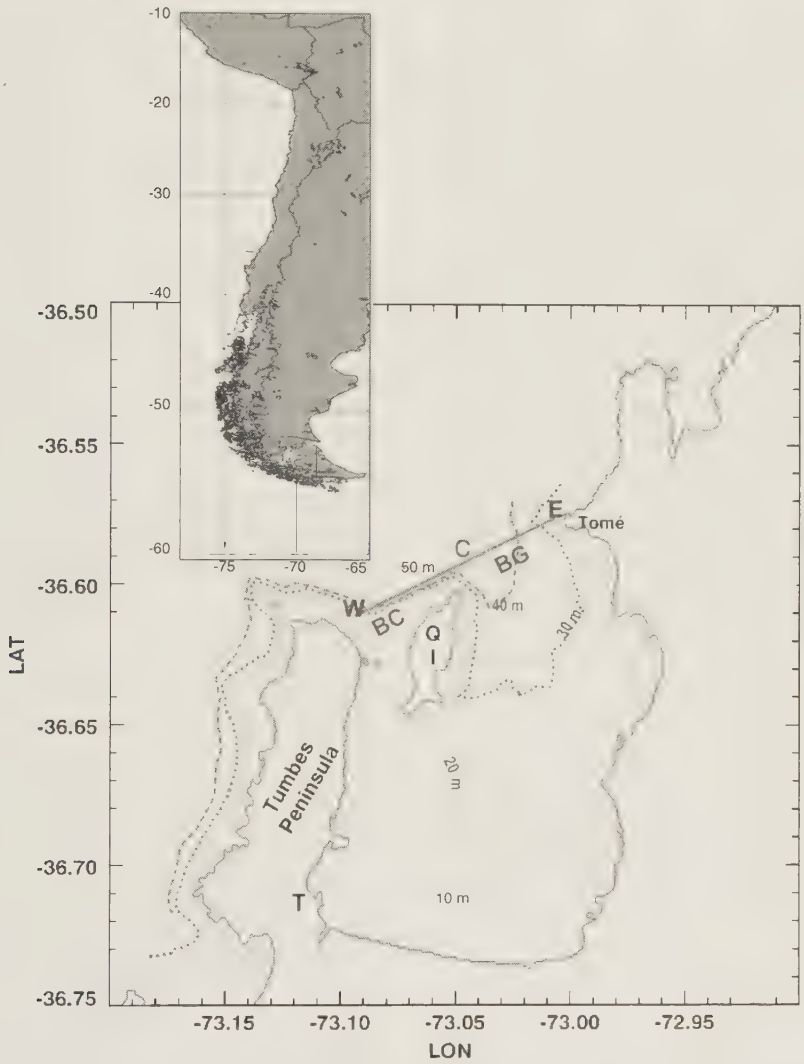

Fig. 1. Map of study area in central Chile showing ADCP sampling transect and CTD stations W, C, and E, with approximate bathymetry. Quiriquina Island (QI) separates Boca Grande (BG) from Boca Chica (BC). Talcahuano is shown at T and Concepción's Airport is located beyond the abscissa, at the '-73.05' label.

nication between the bay and the adjacent ocean into two openings: Boca Grande (~5 km wide and typically 45 m deep) and Boca Chica (~2 km wide and typically 10 m deep). As documented in this study, most water enters/leaves Concepción Bay through Boca Grande.

Wind forcing in the bay area presents a well-defined semi-annual signal. The southwesterly and upwelling favorable winds observed during most of the austral spring and summer (September–March) shift to predominantly northerly and northwesterly winds in late autumn and winter (May–July); transitional periods of variable winds occur in April and August (Saavedra, 1980; Sobarzo et al., 1997; Parada et al., 2001). Winds are the main driving agent of the bay's non-tidal circulation (Sobarzo et al., 1997). Autumn–winter winds are associated with synoptic-scale winds that affect the Chilean coast. Spring–summer winds feature a sea-breeze regime with an onshore

component (eastward) peaking at ~3–5 m s^{-1} in the afternoon (between 15 and 20 h) and reversing to a weakly offshore component at night. The summer regime develops because the large air temperature gradients between the land and ocean are boosted by the coastal ocean's relatively cold waters (typically 11–15 °C) and the relatively large heat fluxes from the atmosphere.

The bay receives buoyancy forcing from local (atmospheric) and advective (upwelling) heat fluxes. Freshwater inputs to the bay are negligible in the summer but may be important during the rainy winter season. During the summer, atmospheric heat fluxes exhibit appreciable diurnal variations related to extended periods of solar radiation during the day.

Tides in Concepción Bay are mixed with semidiurnal dominance. Typical neap to spring tidal ranges at the bay's head, in Talcahuano, oscillate between 0.7 m and 1.2 m. Although this increased tidal forcing could cause fortnightly variations in the bay's sub-tidal flows, no such variations were registered during 17 days of observations by Sobarzo et al. (1997), as wind effects masked any sub-inertial tidal modulation. Since the present study was carried out during neap tides, the influence of tidal forcing on the patterns observed was weak.

3. Data collection and analysis

The 25-h-long observation carried out during the austral summer at the mouth of Concepción Bay, central Chile (Fig. 1), was designed to document the transverse structure of the wind-induced exchange flow, the tidal flows, and the hydrography of this equatorward facing embayment. Even though this study represents a snapshot of different possible scenarios of wind-induced water exchange, the observed conditions are expected to be typical of summer, on the basis of previous time series measurements by Sobarzo et al. (1997). Underway measurements of velocity profiles and surface temperatures were obtained on board the RV Kay Kay of the Universidad de Concepción, during 5–6 January 2002. The underway measurements were combined with conductivity–temperature–oxygen–fluorescence–depth profiles (CTD) obtained at three stations (Fig. 1) along a transect across the bay's mouth. The transect was repeated 16 times during the 25 h of observations and the 3 CTD stations were occupied at least eight times in that period. For convenience, and owing to the marked differences in hydrographic and flow distributions, the transect was divided into two portions. The portion related to Boca Chica goes from Tumbes Peninsula to ~4 km from shore (Fig. 1), and that associated with Boca Grande is the region >4 km from shore.

The CTD stations were located at each end of the transect (stations W and E) and over its deepest part (station C) (Fig. 1). Station C (Central) was only occupied in eastward traverses, for a total of eight casts. Eight casts also were made at station W (West), but 10 were obtained at station E (East), where sampling began and ended. A SeaBird SBE 25 with dissolved oxygen and fluorescence sensors recorded the hydrographic data. Processing for sensor alignment, loop editing, and 1-m bin averaging was effected with the manufacturer's software. Processed data were used to produce average profiles and time series evolution at each of the three stations, reflecting the stratification conditions under which the wind-induced flow developed.

Underway water velocity profiles were measured with an RD Instruments 307.2 kHz acoustic Doppler current profiler (ADCP), which was mounted on a catamaran, pointing downward, and towed from the starboard side of the ship at typical speeds of 2.5 m s^{-1}. The ADCP transducers were located at 0.5 m from the surface and recorded 2-m bins. The first usable bin was centered at a depth of ~3.1 m. Each velocity profile consisted of 30 bins recorded from 15 pings averaged over 1 min. Navigation data were obtained with a Trimble 2000 Global Positioning System and used to calibrate the ADCP compass following Joyce (1989). The ADCP data also were trimmed with the criteria outlined in Valle-Levinson and Atkinson (1999). Furthermore, these data were rotated to the axis of maximum variance (principal axis), which aligned with the bathymetry (35° counterclockwise from east). The trimmed

and rotated ADCP data constituted the "corrected data" used for analyses.

The corrected ADCP data closest to the surface were used in conjunction with water temperature (recorded by the same instrument at the transducer's head) to construct a map in the distance-time domain of the intratidal variability of near-surface temperatures and currents at the sampling transect. The map was generated by interpolation to a uniform grid of 100 m in the horizontal and 0.5 h in time using Delaunay triangulations (Fang and Piegl, 1992, 1993), allowing the description of the transverse structure of near-surface wind-induced flow and its modifications by tidal forcing during the study period.

Corrected ADCP profiles were interpolated onto a uniform grid of 200 m in the horizontal and 2 m in the vertical, also using Delaunay triangulations. Subtidal flows were determined at each grid point from a least-squares fit of semidiurnal and diurnal harmonics plus a subtidal contribution (V_0) to the observations (V), i.e., through minimization of the difference between both sides of the following relationship:

$$V = V_0 + V_2 \sin(\omega_2 t + \varphi_2) + V_1 \sin(\omega_1 t + \varphi_1), \quad (1)$$

where V is the vector of observations with cross-bay and principal-axis components (u, v), $V_{2,1}$ are the amplitudes of the semidiurnal and diurnal tidal currents, $\omega_{2,1}$ are the semidiurnal ($2\pi/12$ h) and diurnal ($2\pi/24$ h) frequencies, and $\varphi_{1,2}$ are the phases of both constituents relative to midnight (UT), 5 January. Special attention here is placed on the description of the subtidal contribution, V_0, although tidal properties also are described.

Two criteria are used to examine the validity of Eq. (1) in representing the actual variability of the flow at each grid point of the observational transect: goodness of fit (γ) and root mean squared errors (rmse) between observations and fit. The goodness of fit yields the fraction of variability in the observed flows explained by (1), e.g., for the u component of the flow:

$$\gamma = \frac{\sum_{i=1}^{N} (\bar{u}_i - u'_i)^2}{\sum_{i=1}^{N} (\bar{u}_i - u_i)^2} \times 100, \quad (2)$$

where the subscript i indicates each of the observations ($N = 16$ repeated transects) made at each grid point. The overbar denotes the average of the N observations and the prime indicates the flow predicted by (1). A perfect fit would represent $u' = u$ or $\gamma = 100$.

The distribution of γ throughout the sampling transect shows reasonable values for both flow components over the northeastern end of the transect in regions >4 km (Fig. 2), i.e., in Boca Grande. The greatest values of γ are found near the surface, which is the area that behaves most similarly to Eq. (1). The relatively low values of γ ($<80\%$) shown in most of the distribution suggest that the greatest portion of the section is likely influenced by forcing other than semidiurnal and diurnal tidal forcing, which are the forcings given by (1). Complementary to γ is the rmse distribution that shows rather small values over Boca Grande and the greatest values, i.e., the poorest performance of (1), in Boca Chica (Fig. 3). Removal of the diurnal constituent to the fit in Eq. (1) increases the rmse and reduces γ substantially (not shown). The effect of removing the semidiurnal constituent from the fit is less dramatic. This represents a diagnostic of the importance of diurnal forcing on the observations. Diurnal forcing is not necessarily tidal, as the tide was semidiurnal (Fig. 4A), but is most likely related to wind forcing as presented next.

4. Results and discussion

Tides and wind were the forcing agents that influenced Concepción Bay during the observation period. The study took place during neap tides, which were mostly semidiurnal with a range of ~0.8 m (Fig. 4A). Wind measured at the head of the bay (at Concepción's airport) exhibited well-defined diurnal variability, reflecting a sea-breeze regime (Fig. 4C). Typical wind speeds were ~7 m s^{-1} that translated into wind stresses of 0.07 Pa, calculated as in Large and Pond (1981). Tides were weak and winds were moderate during the experiment, so that flow and hydrographic variability were expected to be mostly influenced by wind forcing.

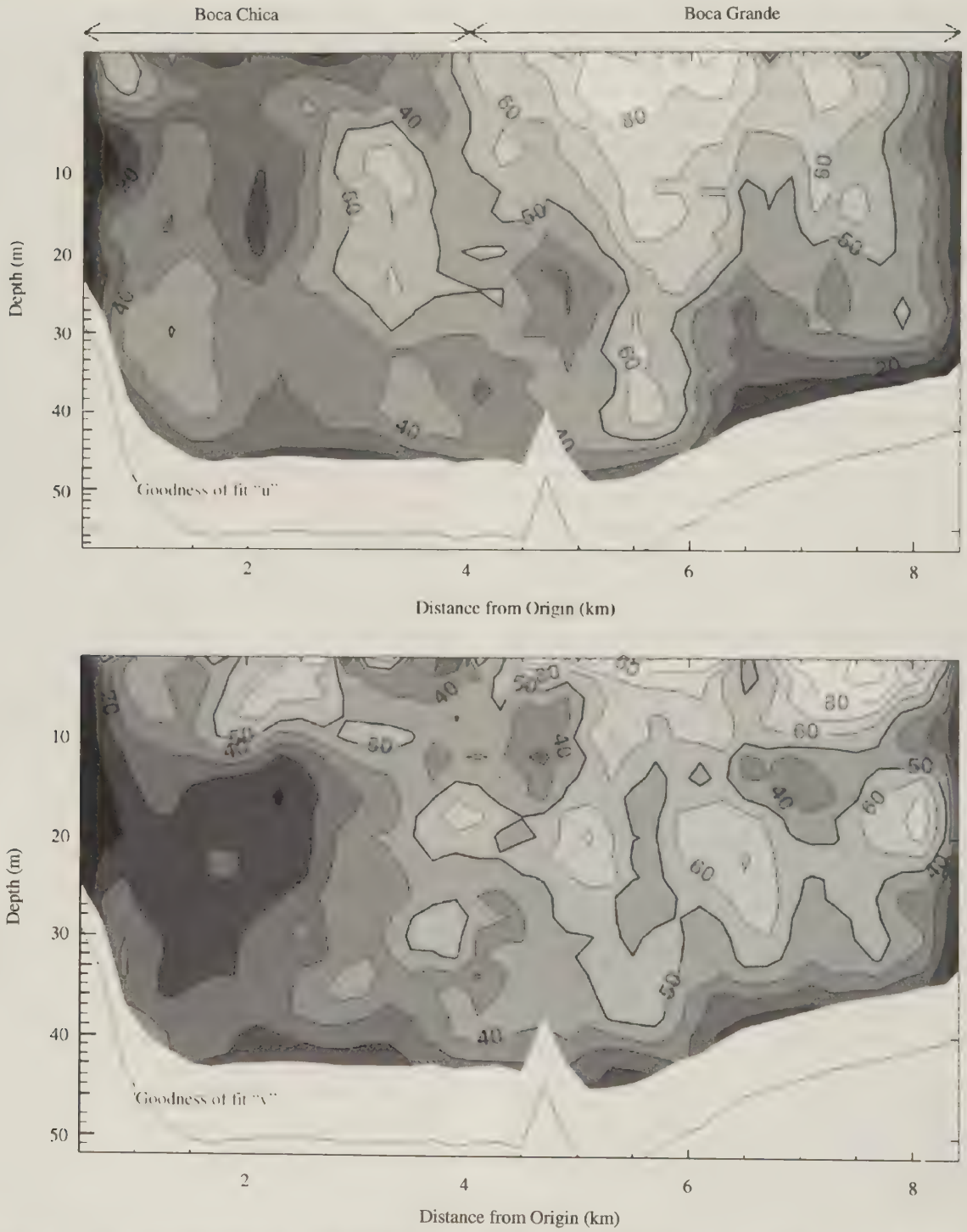

Fig. 2. Distribution (looking seaward) of the goodness of fit related to the representation of the observations by Eq. (1) $I = V_0 + V_2\sin(\omega_2 t + \varphi_2) + V_1\sin(\omega_1 t + \varphi_1)$. Contour interval is 10% and the 50% contour appears as a thick line. Origin is at Pt. Tumbes.

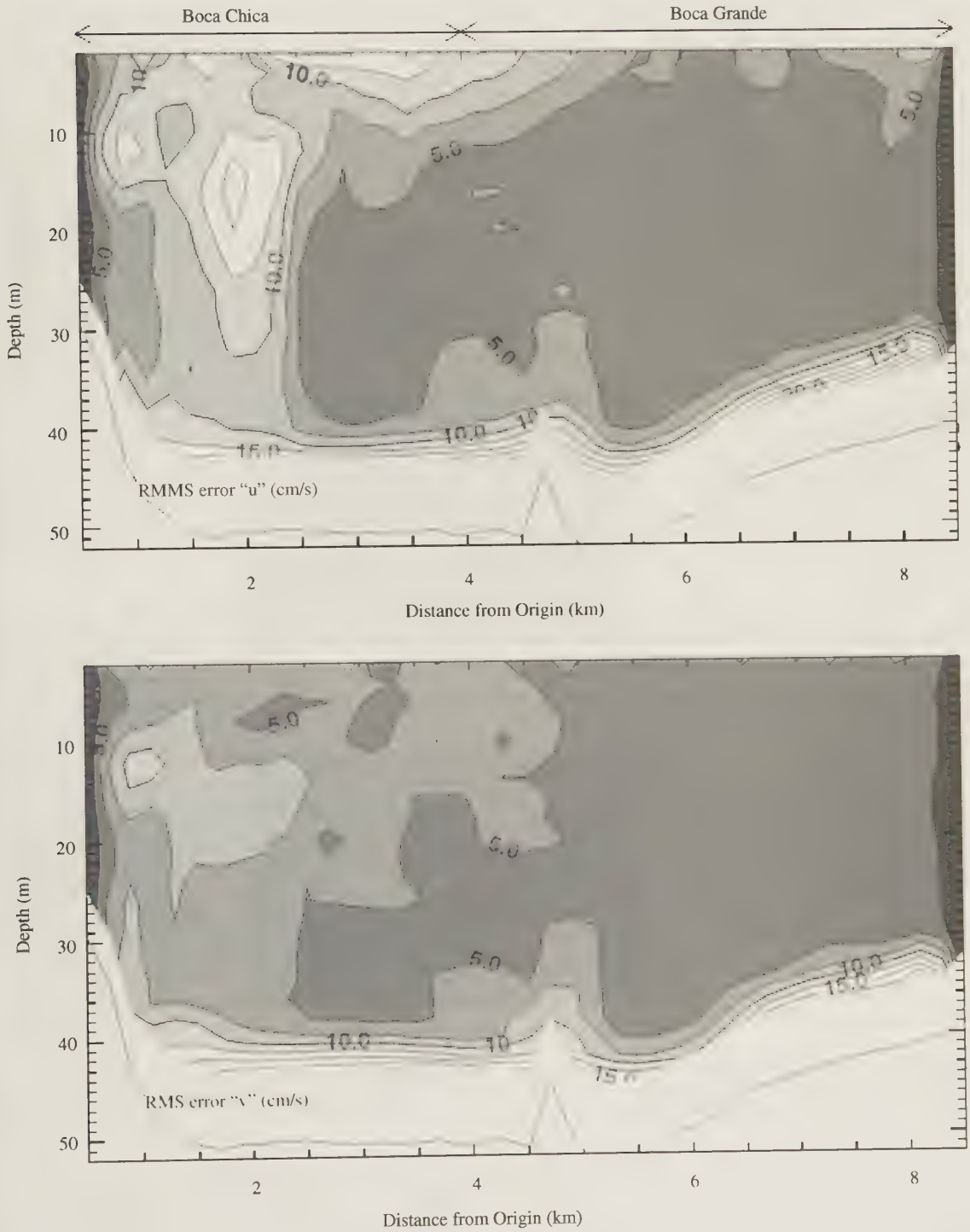

Fig. 3. Distribution (looking seaward) of the root mean square error (in $\mathrm{cm\,s^{-1}}$) between observed values and those predicted by Eq. (1): $V = V_0 + V_2\sin(\omega_2 t + \varphi_2) + V_1\sin(\omega_1 t + \varphi_1)$. Contour interval is $2.5\,\mathrm{cm\,s^{-1}}$. Origin is at Pt. Tumbes.

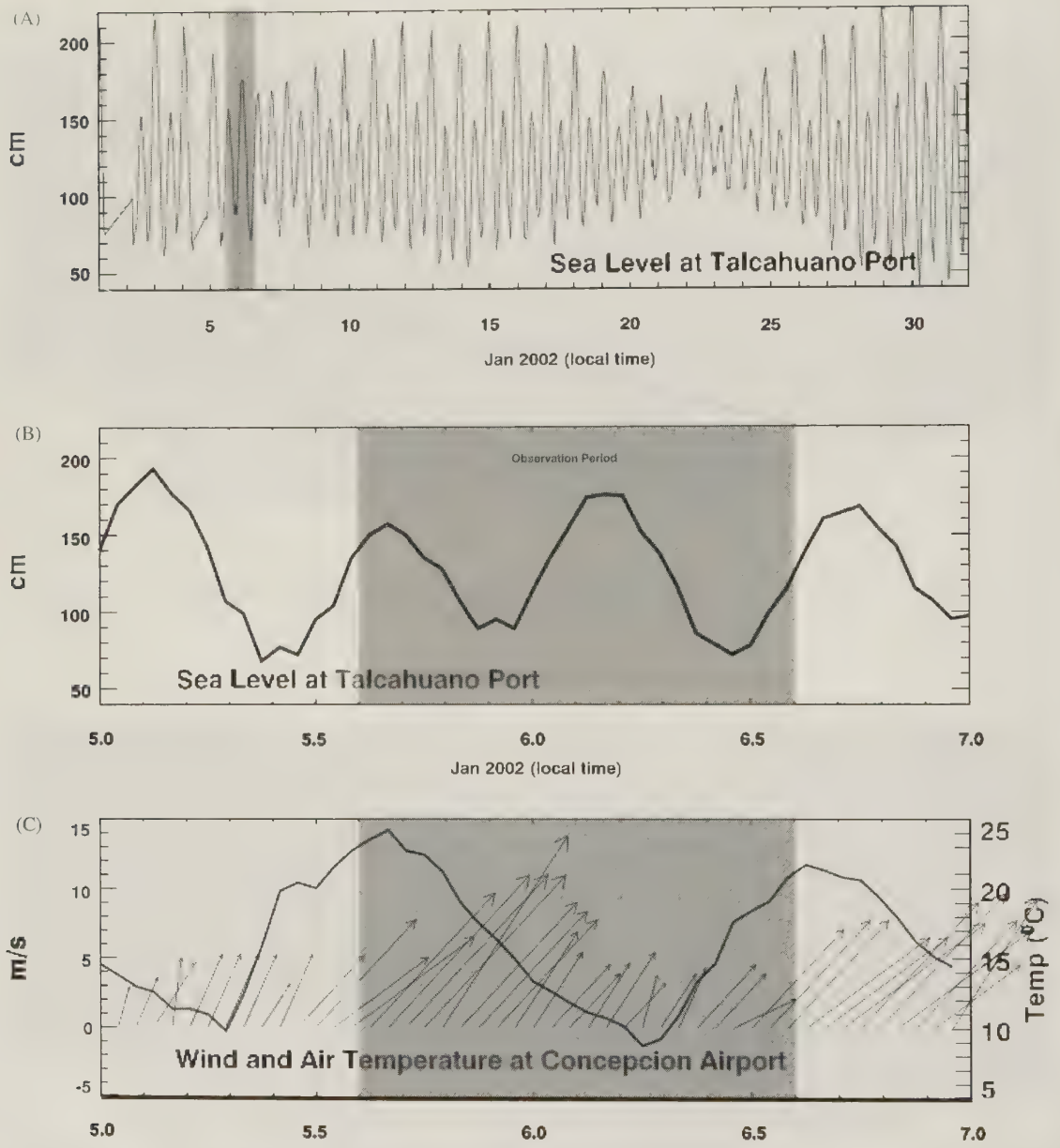

Fig. 4. Tidal and wind forcing during the measurement period. Tides (in meters) as measured in Talcahuano, in the southwestern corner of Concepción Bay (A, B). Wind velocity and air temperature at Concepción's airport, ~5 km south of the bay (C). Vectors point in the direction toward which the wind blows.

4.1. Hydrographic variables

The mean profiles of the basic hydrographic variables (temperature, salinity, and density) at the sampling locations (W, E, and C) showed three relatively well-defined regions in the water column (Fig. 5): (A) a 3–4 m deep near-surface mixed layer, (B) a pycnocline between 4 and 10 m depth, where mean density changed by $\sim 1\,kg\,m^{-3}$, and (A) a nearly homogenous bottom layer. The

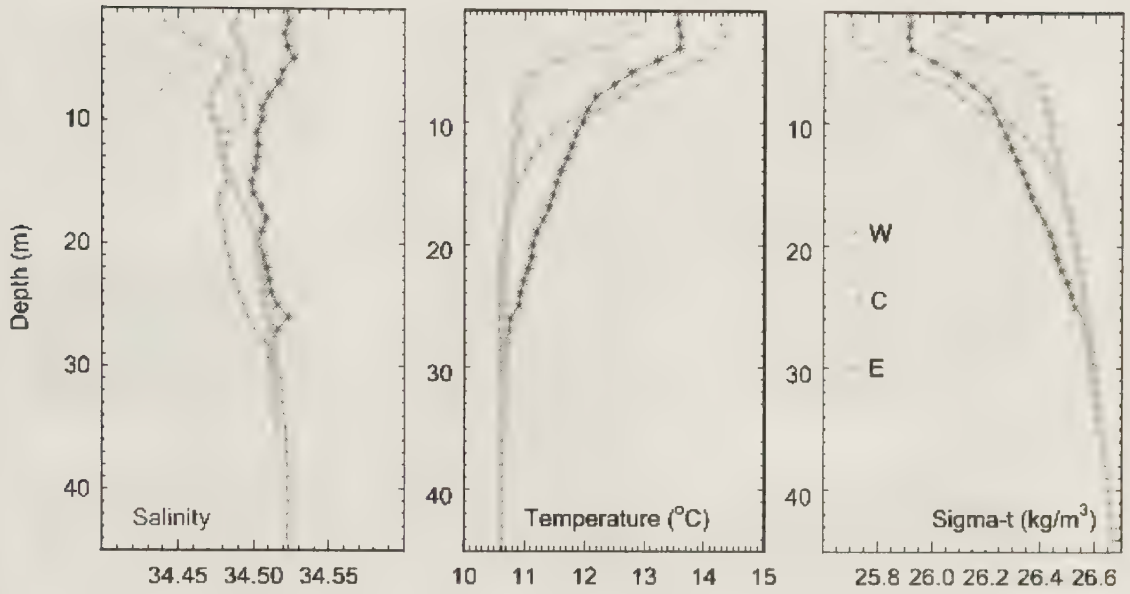

Fig. 5. Average salinity, temperature, and density anomaly profiles throughout the sampling period at the three CTD stations.

surface mixed layer was best defined in the middle of the transect (station C) (Fig. 5), as there were other mixing/stratifying influences at the shallower ends. Nonetheless, the presence of a pycnocline that decoupled bottom waters from direct surface forcing was indeed clear. The pycnocline was caused mainly by thermal gradients that reflected a mean decrease of more than 2 °C. The salinity field had a negligible influence on the density field as it showed very weak spatial (<0.1 from end to end of the transect) and temporal variations (Fig. 6).

At each of the three CTD cast sites, all hydrographic variables, except salinity, exhibited predominantly diurnal fluctuations that were most evident in the upper 30 m of the water column (Fig. 6). Station C, in the middle of the transect, also showed semidiurnal fluctuations coherent with the tide in the form of upward excursions during ebbing. All three stations had a marked pycnocline (0.1 kg m^{-3} per m depth) that appeared to tilt upward from west to east at any given time, consistent with Earth's rotation effects. This tilt was inferred from the pycnocline depth at stations W and E. Temperature and dissolved oxygen changed together with density anomaly and delineated two distinct layers: a stratified surface layer that extended to 7–15 m depth, separated by a relatively strong pycnocline (or thermocline or oxycline) from a bottom mixed layer of cold, suboxic/anoxic upwelling-related waters (Ahumada et al., 1983; Arcos and Wilson, 1984). The layer of maximum fluorescence appeared to follow the pycnocline's oscillations, suggesting that the relatively strong pycnocline acted as a barrier for fluorescent particles, perhaps phytoplankton, as found by Sharples et al. (2001). The insulating effects of the pycnocline were also evident in the non-tidal, diurnal, and semidiurnal flow distributions.

4.2. Subtidal flow

The subtidal flow, represented by the first term on the right-hand side of Eq. (1), showed upper-layer outflow and lower-layer inflow (Fig. 7A and C). The surface outflow was not perfectly aligned with the wind at Concepcion's airport because of the likely spatial gradients induced by the coastal topography. The observed net exchange pattern essentially coincided with the straight average of the 16 transect repetitions and is, therefore,

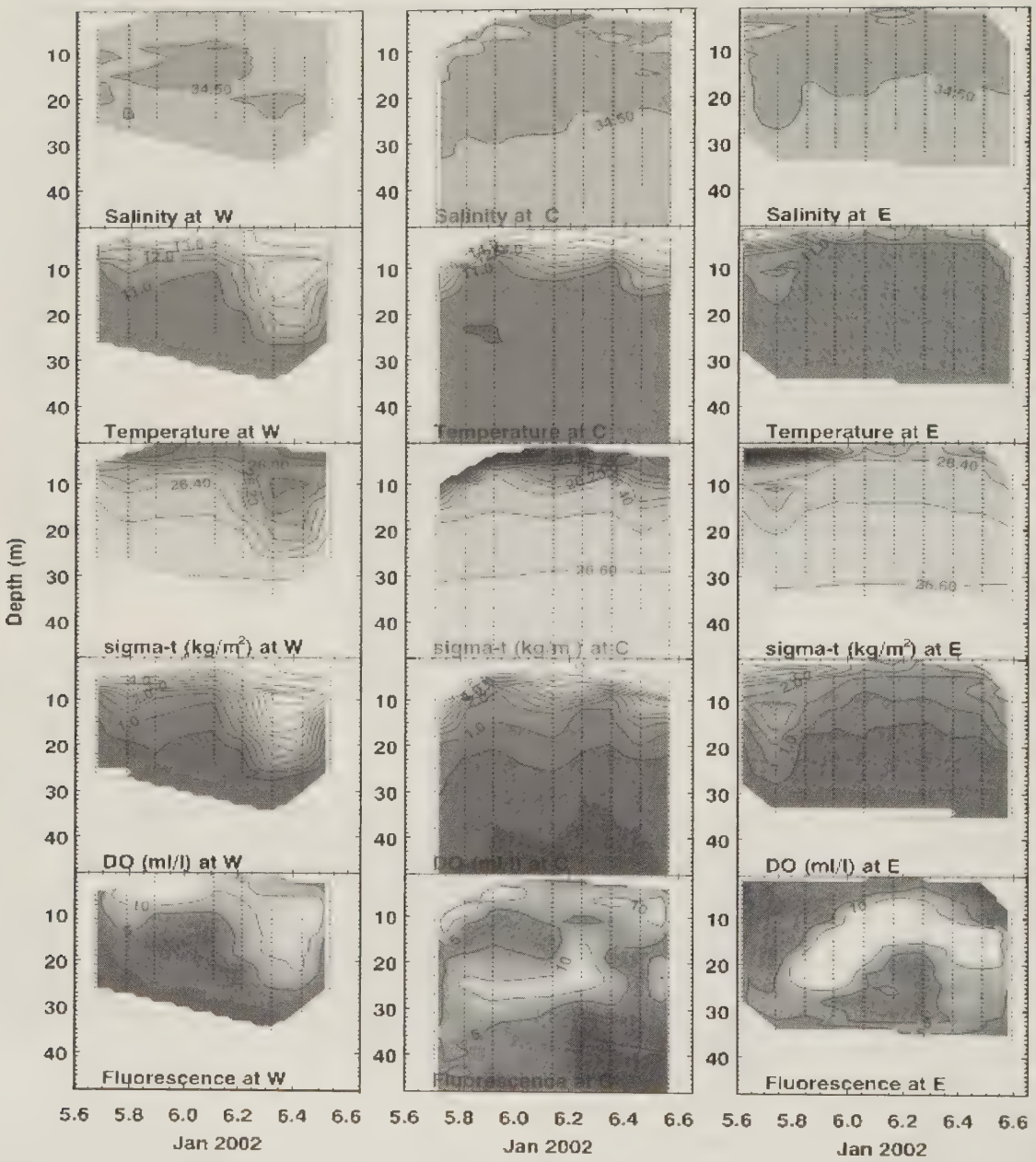

Fig. 6. Time series (25 h) in local time of hydrographic variables at each of the 3 CTD stations. Contour intervals for salinity, temperature, density, dissolved oxygen, and fluorescence are 0.05, 0.5 °C, 0.1 kg m^{-3}, 0.5 ml L^{-1}, and 5, respectively. The units of fluorescence are approximate units of chlorophyll–*a* (mg m^{-3}), although these were not verified in the field.

independent of the quality of the fit represented by (1).

The exchange flows could be the result of the combination of three main different forcing agents: wind stress, baroclinic (density) gradients, and/or tidal rectification through non-linear interactions of tidal flow with bathymetry. A southerly wind, as observed, should produce northward

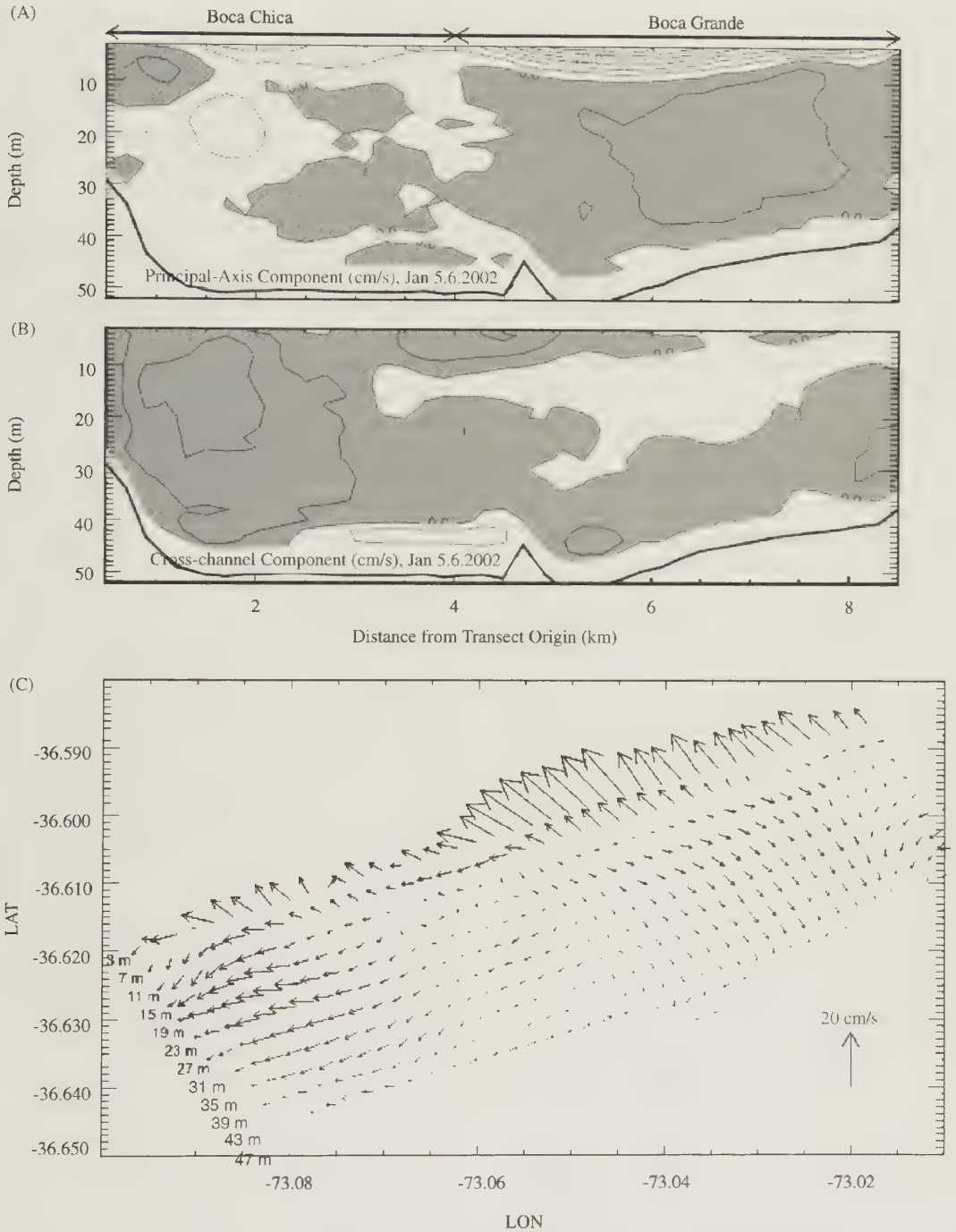

Fig. 7. Subtidal flow V_0 at the entrance to Concepción Bay (looking seaward inside from the bay). (A) Principal-axis component contoured at 2.5 cm s^{-1} intervals. Shaded areas denote inflows. (B) Component of the flow perpendicular to the principal-axis component contoured at 2.5 cm s^{-1} intervals. Shaded areas denote flow toward Tumbes Peninsula (to the left). (C) Vector representation at different depths. Each depth has been displaced in latitude and longitude for better visualization. The uppermost bin (3 m) is drawn at the actual coordinates.

(downwind) surface flow and upwind near-bottom flow as in Figs. 7A and C. Also, buoyant water inside the bay, a consequence of increased warming in the shallow bay relative to the adjacent ocean, would produce a net exchange pattern as in Fig. 7. Furthermore, a rectified tidal flow would produce net exchange flows opposite to those observed (e.g., Ianniello, 1979). From a typical momentum balance, the wind-stress (τ) contribution may be characterized as $\tau/(\rho H_0)$, where ρ and H_0 are typical water density and depth of frictional influences, respectively. Taking τ as 0.07 Pa, ρ of $1026\,\mathrm{kg\,m^{-3}}$, and H_0 of 10 m, the wind-stress contribution to the observed flows was $6.8\times10^{-6}\,\mathrm{m\,s^{-2}}$. The baroclinic pressure gradient may be characterized as $gH/\rho\ (\Delta\rho/\Delta x)$, where g is the acceleration owing to gravity ($9.8\,\mathrm{m\,s^{-2}}$), H is the water depth (45 m), and $\Delta\rho/\Delta x$ is a typical along bay density gradient, taken as $10^{-6}\,\mathrm{kg\,m^{-4}}$ (or $0.01\,\mathrm{kg\,m^{-3}}$ in 10 km), on the basis of our near-bottom cross-bay observations (Fig. 5). The estimate of the along-bay density gradient is likely overvalued because cross-bay gradients are expected to be larger than the along-bay gradients, as suggested by the bay's bathymetry. Even though the baroclinic contribution to the net exchange flow was likely overestimated at $4.3\times10^{-7}\,\mathrm{m\,s^{-2}}$, it was at the very least 10 times lower than the wind-stress contribution. This is equivalent to a Wedderburn number of 5–10 (e.g., Monismith, 1986; Geyer, 1997), which indicates a dominance of wind over baroclinicity in driving the flows. The tidally rectified flow will be proportional to the bottom stress, or C_dU^2/H. Taking the non-dimensional drag coefficient (C_d) as 0.0025 and U as $0.05\,\mathrm{m\,s^{-1}}$, the contribution to the observed flow from tidal rectification was $1.6\times10^{-7}\,\mathrm{m\,s^{-2}}$. It is likely, then, that the observed subtidal flows were produced mostly by wind stress.

There are three interrelated aspects of the distribution of net exchange flows throughout the transect that are worth mentioning. First, the thickness of the outflow/inflow layers corresponds to the layers circumscribed by the pycnocline. Second, the wind-induced exchange is typical of a weak internal friction response. And third, the flow patterns may reflect the effects of the earth's rotation. The interrelation among these three aspects is explained next.

The wind stress drives downwind flow at the surface and its influence is felt throughout a layer of frictional influence where the vertical eddy viscosity, A_z, remains non-zero, i.e., allowing a vertical exchange of momentum. At the pycnocline, the vertical exchange of momentum is suppressed because $A_z\sim0$ and, thus, limits the wind influence in the water column. The downwind transport sets up a barotropic pressure gradient in the form of a sea level slope because of the presence of a coast that hinders the horizontal resupply of mass. This sea level slope, whose surface tilts up in the wind direction, in turn drives upwind flow below the pycnocline.

The wind-induced exchange pattern portrayed in Fig. 7 is rarely observed in shallow estuaries or embayments because frictional effects would tend to produce downwind flow over the shallow flanks and upwind flow in a deep channel (Csanady, 1973; Hunter and Hearn, 1987; Wong, 1994; Friedrichs and Hamrick, 1996). The dynamic shallowness of the embayment is ultimately dictated by the ratio of Ekman layer to total depth (Winant, 2004) or analogously by the Ekman number (Kasai et al., 2000; Valle–Levinson et al., 2003b), i.e., by the ratio of friction to Earth's rotation influences (A_z/fH^2). In the case of our observations, the Ekman number was ~0.004, taking a conservatively high value of A_z ($7\times10^{-4}\,\mathrm{m^2\,s^{-1}}$), an f of $8.5\times10^{-5}\,\mathrm{s^{-1}}$, and an H of 45 m at the mouth of Concepción Bay. The value of the eddy viscosity was derived from the ratio between wind stress (0.07 Pa) and the vertical shear above the pycnocline ($0.1\,\mathrm{m\,s^{-1}}$ change in 10 m). Under such a low Ekman number, the exchange flow is theoretically expected to be as observed (Kasai et al., 2000). Furthermore, the low Ekman number should indicate effects of Earth's rotation on the exchange flows.

The earth's rotation effects are manifested by lateral asymmetries in inflows/outflows (Valle–Levinson et al., 2003b; Winant, 2004) as observed in the principal-axis component (Fig. 7A) that shows the strongest ouflows over the left portion of Boca Grande (region >4 km) and strongest inflows over the right portion. The asymmetries were restricted

o Boca Grande because the region < 4 km was in he lee of Quiriquina Island. Additional Earth's otation effects would be manifested by a trans-verse flow directed to the left at the surface and to he right at depth. This pattern was not very obust in the observations, but was identifiable in portions of Boca Grande. A structure similar to he subtidal flow was observed in the structure of diurnal variability in flow.

4.3. Diurnal and semidiurnal flow variability

The temporal variations of surface temperature and flow throughout the transect (Fig. 8) featured a clear diurnal signal in temperature, but a less clear one in flow. Diurnal variability in surface temperature was expected from the diurnal heating/cooling cycle (Valle–Levinson et al., 2003a) and the weak tidal forcing during the observation period. It is noteworthy that the coolest water was found off Tomé Point between 7 and 8 AM (local time or between 6.4 and 6.45 on Fig. 8), which was the time of strongest surface outflow and weakening of the upwelling wind (Fig. 4C). It is likely that this coolest water upwelled as a result of wind-driven flow influenced by rotation that would cause near-surface divergence at Tomé Point. The dominant periods of variability in flow were masked by the interaction of semidiurnal and diurnal forcing from tides and wind. Surface flows remained practically unidirectional throughout the transect and observation period, most markedly in Boca Grande. Over this section of the bay entrance, surface outflow weakened but did not reverse direction, which translated into net surface outflow. Only within Boca Chica (~2–3.5 km) (Fig. 8) were there direction reversals with an apparent semidiurnal periodicity. The vertical structure of the diurnal and semidiurnal flow variations is explored next.

The vertical structure of diurnal variations in flow are depicted in terms of the amplitude and phase of the diurnal harmonic obtained with the fit given in Eq. (1). The distributions of amplitude and phase reflected the combined influences of a diurnal sea breeze and diurnal tidal forcing, as it is impossible to separate their effects in this time series or in any customary time series. The amplitude of the diurnal variability (Fig. 9A) exhibited the greatest values in the upper layer circumscribed by the pycnocline. Maxima appeared shifted to the left region of Boca Grande (looking seaward), which is the part of the mouth cross-section unprotected from southerly winds. Below this layer of greatest amplitudes, the diurnal variability was nearly uniform. The phase of such diurnal variations nicely illustrated the two layers in Boca Grande (Fig. 9B), where a phase difference of ~12 h was appreciable between the upper and lower layers. A phase lag of 12 h in a 24 h signal indicates oppositely moving flows. Such is the response expected from a sea breeze acting on an embayment like Concepción Bay; downwind flow at the surface and upwind at depth, driven by the onshore set-down established by the wind. Given the spatial structure of the distributions of amplitude and phase, and given that tidal forcing was rather weak, it is highly likely that the spatial structure of the diurnal response in Concepción Bay was produced by a sea breeze. The sea breeze response, in turn, must have influenced the subtidal flow by shaping the net outflow/inflow patterns observed in the transect.

The vertical structure of semidiurnal amplitude confirmed weak semidiurnal tidal forcing in Boca Grande, but showed comparable amplitude to diurnal forcing in Boca Chica (Fig. 10A). The phase of the semidiurnal tidal flow was relatively small in the vertical and exhibited a weak structure in the transverse direction (Fig. 10B). In contrast to the large phase changes observed in the diurnal variations, the phase structure of the semidiurnal variations suggested a barotropic or unidirectional response to tidal forcing. The better-defined semidiurnal signal in Boca Chica than in Boca Grande was attributed to the sheltering effects of Quiriquina Island from southerly wind forcing. However, the Boca Chica portion of the transect exhibited poor fits as shown in Figs. 2 and 3, and the semidiurnal variability in that region should be taken cautiously. Overall, the distribution of semidiurnal and diurnal parameters at the entrance to Concepción Bay suggested predominance of wind forcing in Boca Grande and tidal forcing and/or island wake effects in Boca Chica as the main

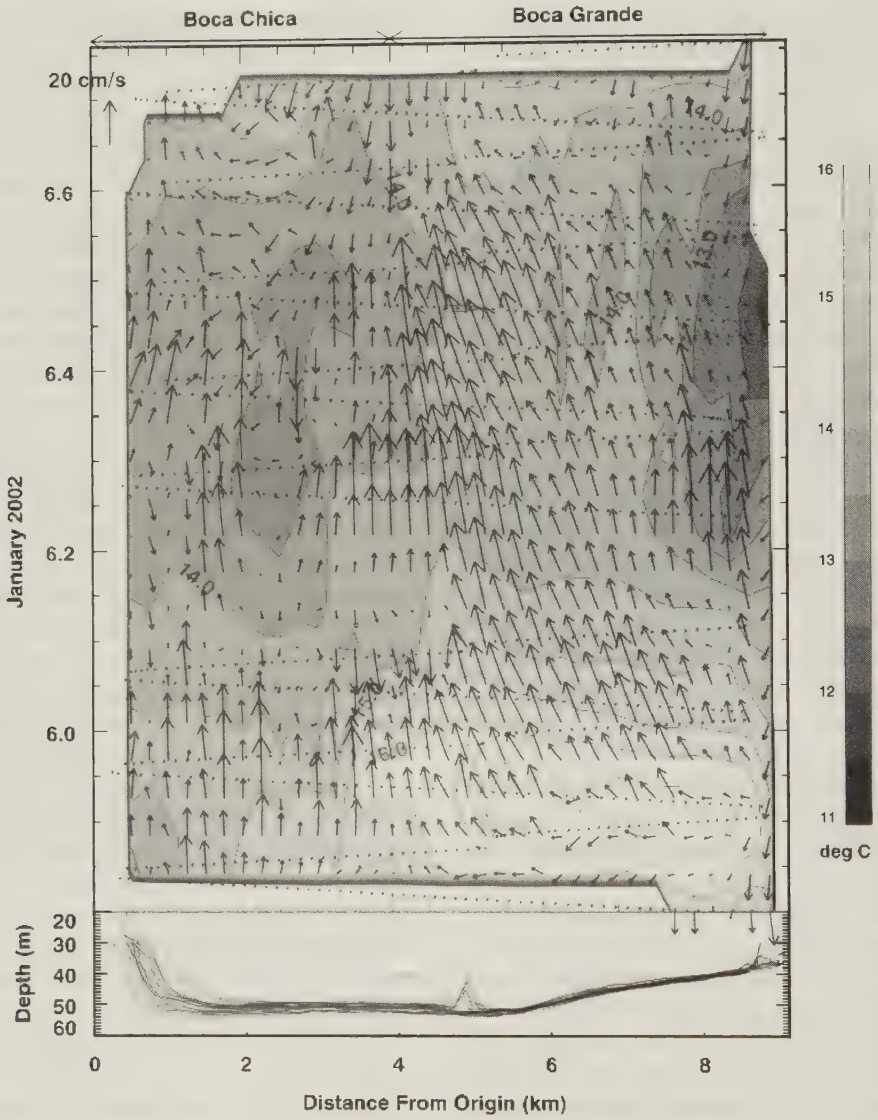

Fig. 8. Upper panel: Near-surface temperature (contours) and total flow V (vectors) presented in the distance (from Pt. Tumbes) versus time (UT) domain. Temperature contour interval is 0.5 °C. Dots represent observation locations and times. The lower panel shows the bathymetry measured at each of the 16 transect repetitions.

agents causing variability in diurnal or smaller periods. Inertial influences, which are expected to be relevant in the area, could not be elucidated with our sampling period. In order to distinguish between diurnal (24 h) and inertial (~20 h) influences, the sampling period should be at least 5 days (Rayleigh criterion).

5. Summary

This study presents one of the few observational examples available to date of the transverse structure of wind-induced exchange in an embayment under weak internal friction. This pattern consists of downwind flow at the surface and

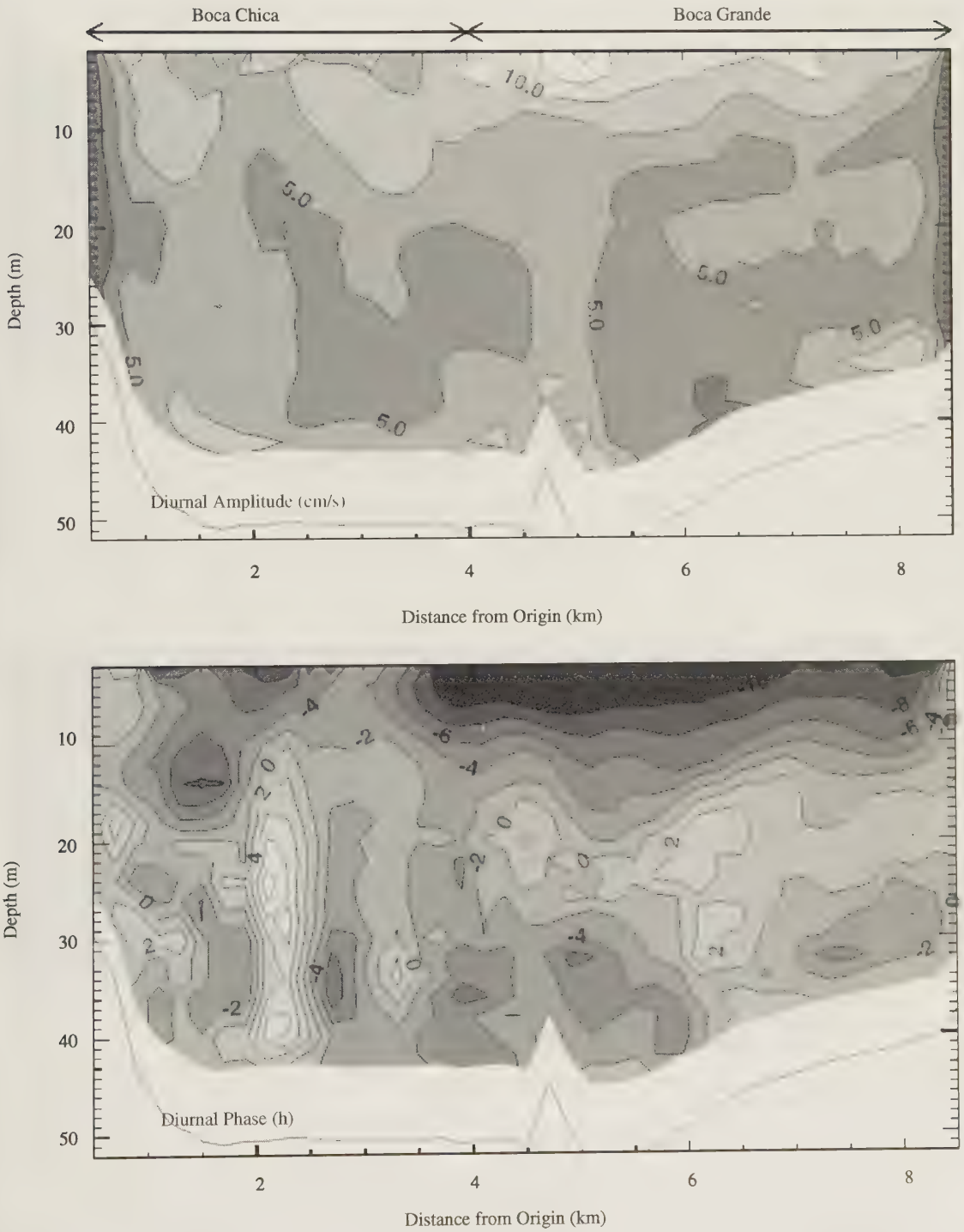

Fig. 9. Amplitude (upper panel) and phase (lower panel) of diurnal variations in observed flow. Amplitude contour interval is 2.5 cm s^{-1} and phase contour interval is 2 h.

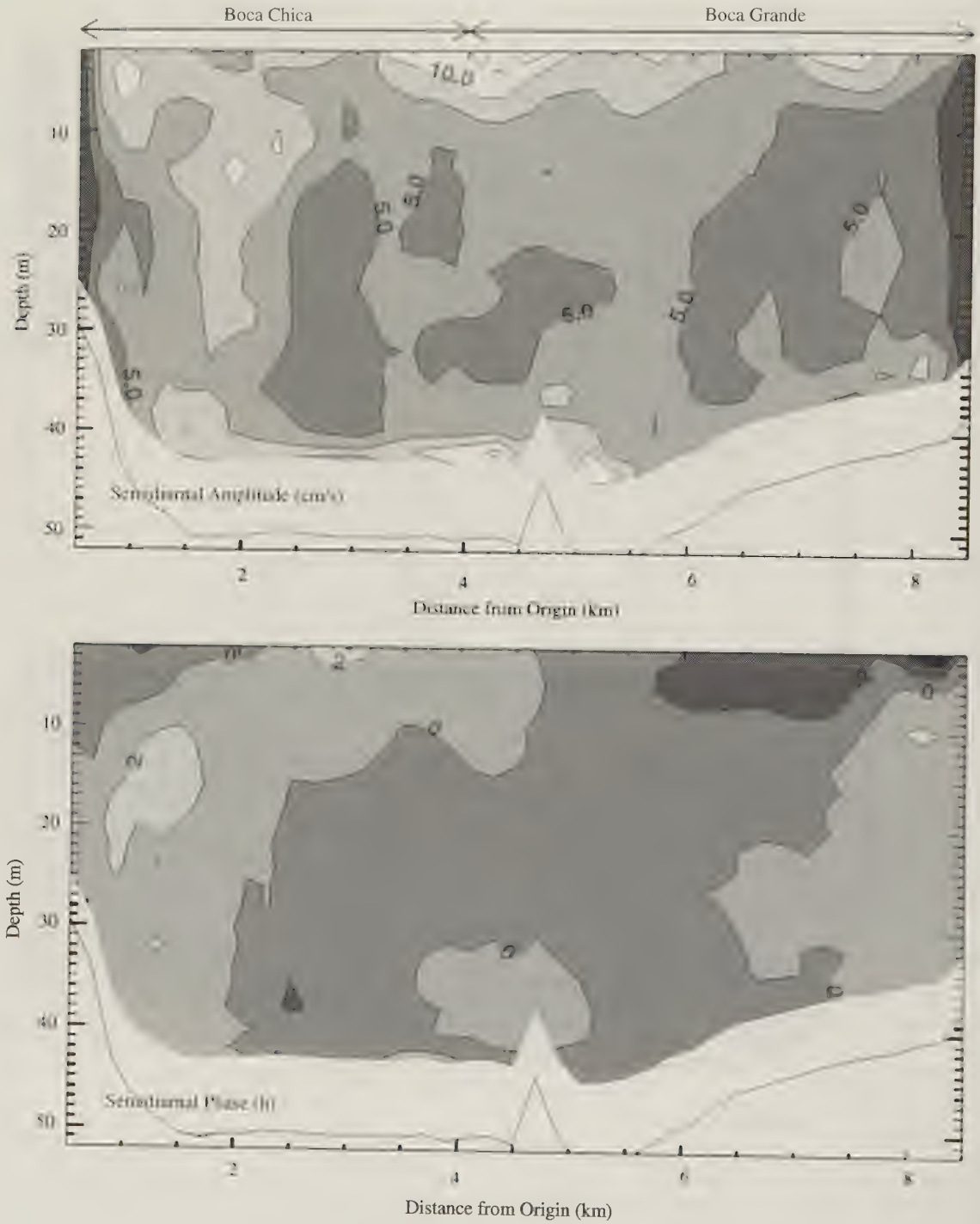

Fig. 10. Amplitude (upper panel) and phase (lower panel) of semidiurnal variations in observed flow. Amplitude contour interval is 2.5 cm s^{-1} and phase contour interval is 2 h.

pwind flow at depth, and contrasts with the heoretical frictional pattern in a shallow channel/ hoal bathymetry of downwind flow over shoals nd upwind flow in channels. The latter pattern is nore likely to be observed in instances when riction overwhelms Coriolis accelerations (i.e., arge Ekman number). The pattern observed in Concepción Bay is expected when Coriolis accel- rations are important (small Ekman number). Coriolis effects on wind-induced exchange, then, vill be appreciable in systems where the local vater depth is a few times greater than the Ekman ayer depth (Winant, 2004). In Concepción Bay, luring our study period, the ratio of local water lepth (~50 m) to Ekman depth (5–10 m) was 5:10. The effects of Coriolis accelerations were identified n Boca Grande, which was the portion of the ransect directly affected by southerly winds. This ype of wind (upwelling-favorable) blows along the nain axis of equatorward facing embayments and hould produce local responses consisting of sea evel slopes and two-layered flows. A similar wind- nduced response was observed in the Gulf of Arauco, another equatorward facing embayment ust south of Concepción Bay (Valle–Levinson et al., 2003a). Both of these examples illustrate wind-driven flow under stratified conditions in which a pycnocline limits the vertical transfer of horizontal momentum in the water column. Whether the two-layer response persists under weakly stratified conditions, typical of winter, remains to be elucidated. On the basis of theoretical considerations from semi-analytical (Winant, 2004) and numerical results (Sanay, 2003), an inflow/outflow pattern similar to that observed in the summer should be expected in winter for the particular case of Concepción Bay. This is because the depth of the system is a few times greater than the depth of frictional influence (Ekman depth), which would grow only slightly in the well-mixed conditions during the winter relative to that under stratified conditions.

Another noteworthy aspect of this investigation, although particular to the study area, was that the wind-induced response was restricted to the portion of the cross section directly affected by the wind, i.e., Boca Grande. The presence of an island, Quiriquina, near the bay mouth, protected a portion of the bay entrance (Boca Chica) from southerly wind influences and could have generated island wake effects (e.g., Wolanski et al., 1984). The Boca Chica portion of the bay mouth's transect may have been influenced by weak tidal forcing. This type of forcing was overwhelmed by wind forcing in Boca Grande. It would be worthwhile to repeat the experiment with northerly wind conditions in order to avoid the island wake effects and under weakly stratified conditions to compare expected theoretical responses to observed patterns.

Acknowledgments

Data were collected during a course of the Second Austral Summer Institute (2002, Procesamiento de datos obtenidos con un ADCP remolcado), financed by an agreement between the Universidad de Concepción (Chile), Woods Hole Oceanographic Institution (USA), and the Fundación Andes (Chile). This manuscript was completed while A.V.L. was on research leave at the Centro de Investigación Científica y Educación Superior de Ensenada, Estación La Paz, Baja California Sur. A.V.L. received funding from the US National Science Foundation (NSF), Projects No. 9812206 and No. 9983685. The Captain and crew of the R/V Kay Kay of the Universidad de Concepción are acknowledged for their dedication and help during the experiment. This is a contribution of the FONDAP–COPAS Center (Project No. 150100007).

References

Ahumada, R., Rudolph, A., Martínez, V., 1983. Circulation and fertility of waters in Concepcion Bay. Estuarine Coastal and Shelf Science 16, 95–105.

Arcos, D., Wilson, R.E., 1984. Upwelling and the distribution of chlorophyll a within the bay of Concepcion, Chile. Estuarine Coastal and Shelf Science 18, 25–35.

Csanady, G.T., 1973. Wind-induced barotropic motion in long lakes. Journal of Physical Oceanography 3, 429–438.

Fang, T., Piegl, L., 1992. Algorithm for Delaunay triangulation and convex hull computation using a sparse matrix. Computer Aided Design 24, 425–436.

Fang, T., Piegl, L., 1993. Delaunay triangulation using a uniform grid. IEEE Computer Graphics and Applications, 36–47.

Figueroa, D., Moffat, C., 2000. On the influence of topography in the induction of coastal upwelling along the Chilean coast. Geophysical Research Letters 27 (23), 3905–3908.

Fischer, H.B., 1976. Mixing and dispersion in estuaries. Annual Review of Fluid Mechanics 8, 107–133.

Friedrichs, C.T., Hamrick, J.M., 1996. Effects of channel geometry on cross sectional variations in along channel velocity in partially stratified estuaries. In: Aubrey, D.G., Friedrichs, C.T. (Eds.), Buoyancy Effects on Coastal and Estuarine Dynamics. Coastal and Estuarine Studies, vol. 53, American Geophysical Union, pp. 283–300.

Geyer, W.R., 1997. Influence of wind on dynamics and flushing of shallow estuaries. Estuarine Coastal and Shelf Science 44, 713–722.

Glorioso, P.D., Davies, A.M., 1995. The influence of eddy viscosity formulation, bottom topography, and wind wave effects upon the circulation of a shallow bay. Journal of Physical Oceanography 25, 1243–1264.

Hearn, C.J., Hunter, J.R., Heron, M.L., 1987. The effects of a deep channel on the wind-induced flushing of a shallow bay or harbor. Journal of Geophysical Research 92, 3913–3924.

Hunter, J.R., Hearn, C.J., 1987. Lateral and vertical variations in the wind-driven circulation in long, shallow lakes. Journal of Geophysical Research 92, 13106–13114.

Ianniello, J.P., 1979. Tidally induced residual currents in estuaries of constant breadth and depth. Journal of Marine Research 35, 755–785.

Joyce, T.M., 1989. On in situ "calibration" of shipboard ADCPs. Journal of Atmospheric and Oceanic Technology 6, 169–172.

Kasai, A., Hill, A.E., Fujiwara, T., Simpson, J.H., 2000. Effect of the Earth's rotation on the circulation in regions of freshwater influence. Journal of Geophysical Research 105 (C7), 16961–16969.

Large, W.G., Pond, S., 1981. Open ocean momentum flux measurements in moderate to strong winds. Journal of Physical Oceanography 11, 324–336.

Mathieu, P.P., Deleersnijder, E., Cushman-Roisin, B., Beckers, J.M., Bolding, K., 2002. The role of topography in small well-mixed bays, with application to the lagoon of Mururoa. Continental Shelf Research 22, 1379–1395.

Monismith, S., 1986. An experimental study of the upwelling response of stratified reservoirs to surface shear stress. Journal of Fluid Mechanics 171, 407–439.

Parada, C.E., Sobarzo, M.A., Figueroa, D., Castro, L., 2001. Circulation of the Arauco Gulf in a seasonal transitional period: a new approach. Investigaciones Marinas 29 (1) 11–23 (In Spanish).

Saavedra, N., 1980. La presión y la dirección del viento e Concepción. Tralka (Chile) 1, 153–162.

Sanay, R., 2003. Wind-induced exchange in semi-enclose basins. Ph.D. Dissertation, Old Dominion University Norfolk, VA, 150pp.

Sharples, J., Moore, C.M., Rippeth, T.P., Holligan, P.M. Hydes, D.J., Fisher, N.R., Simpson, J.H., 2001. Phyto plankton distribution and survival in the thermocline. Limnology & Oceanography 46 (3), 486–496.

Signell, R.P., Beardsley, R.C., Grabor, H.C., Capotondi, A. 1990. Effect of wave–current interaction on wind-driven circulation in narrow, shallow embayments. Journal o Geophysical Research 95, 9671–9678.

Sobarzo, M., Figueroa, D., Arcos, D., 1997. The influence o winds and tides in the formation of circulation layers in a bay, a case study: Concepción Bay, Chile. Estuarine Coasta and Shelf Science 45, 729–736.

Valle-Levinson, A., Atkinson, L., 1999. Spatial gradients in the flow over an estuarine channel. Estuaries 22 (2A), 179–193.

Valle-Levinson, A., Wong, K., Bosley, K., 2001a. Observations of the wind-induced exchange at the entrance to Chesapeake Bay. Journal of Marine Research 59 (3), 391–416.

Valle-Levinson, A., Delgado, J.A., Atkinson, L.P., 2001b. Reversing water exchange patterns at the entrance to a semiarid coastal lagoon. Estuarine Coastal and Shelf Science 53, 825–838.

Valle-Levinson, A., Wong, K.C., Bosley, K.T., 2002. Effects of Hurricane Floyd on the exchange at the Chesapeake Bay Entrance. Continental Shelf Research 22, 1715–1730.

Valle-Levinson, A., Atkinson, L.P., Figueroa, D., Castro, L., 2003a. Flow induced by upwelling winds in an equatorward facing bay: Gulf of Arauco, Chile. Journal of Geophysical Research 108 (C2), 3054.

Valle-Levinson, A., Reyes, C., Sanay, R., 2003b. Effects of bathymetry and Earth's rotation on estuary/ocean exchange. Journal of Physical Oceanography 33 (11), 2375–2393.

Winant, C.D., 2004. Three dimensional wind-driven flow in an elongated, rotating basin. Journal of Physical Oceanography 34 (2), 462–476.

Wolanski, E., Imberger, J., Heron, M.L., 1984. Island wakes in shallow coastal waters. Journal of Geophysical Research 89, 10533–10569.

Wong, K.-C., 1994. On the nature of transverse variability in a coastal plain estuary. Journal of Geophysical Research 99, 14209–14222.

ELSEVIER

Deep-Sea Research II 51 (2004) 2389–2411

DEEP-SEA RESEARCH
PART II

www.elsevier.com/locate/dsr2

Biological and chemical consequences of the 1997–1998 El Niño in the Chilean coastal upwelling system: a synthesis

Rubén Escribano[a,b,*], Giovani Daneri[a,c], Laura Farías[a,d,e], Víctor A. Gallardo[a,c], Humberto E. González[a,f], Dimitri Gutiérrez[g], Carina B. Lange[a,c], Carmen E. Morales[a,b], Oscar Pizarro[a,e,h], Osvaldo Ulloa[a,c,e], Mauricio Braun[i]

[a]*Centro de Investigación Oceanográfica en el Pacífico Sur-Oriental (FONDAP-COPAS), Universidad de Concepción, Casilla 160-C, Concepción, Chile*

[b]*Departmento de Oceanografía, Estación de Biología Marina, Universidad de Concepción, Casilla 42, Dichato, Concepción, Chile*

[c]*Centro de Ciencias y Ecología Aplicada (CEA), Universidad del Mar, Campus Valparaíso, Carmen 446, Placeres, Valparaíso, Chile*

[d]*Departamento de Oceanografía, Universidad de Concepción, Casilla 160-C, Concepción, Chile*

[e]*Programa Regional de Oceanografía Física y Clima (PROFC), Casilla 160-C, Concepción, Chile*

[f]*Instituto de Biología Marina, Universidad Austral de Chile, Casilla 567, Valdivia, Chile*

[g]*Instituto del Mar del Peru (IMARPE), Apartado 22, Callao, Lima, Peru*

[h]*Departamento de Física de la Atmósfera y del Océano, Universidad de Concepción, Casilla 160-C, Concepción, Chile*

[i]*Instituto de Fomento Pesquero (IFOP), Casilla 8-V, Valparaíso, Chile*

Accepted 27 July 2004

Abstract

The coastal upwelling ecosystem of the Humboldt Current System off Peru and Chile exhibits strong interannual variability due to changes in the oceanographic conditions related to the El Niño (EN) Southern Oscillation. It is generally believed that major changes occur in the community structure and biological production of this system as a consequence of El Niño-La Niña periods. This paper presents a summary of the information available on the physical, chemical, and biological responses of the Chilean upwelling zone resulting from the strong 1997–1998 EN event. Oceanographic changes for the whole region included the intrusion of oceanic, low-nutrient, warmer, and more oxygenated waters into the coastal areas, with positive sea-surface temperature anomalies lasting until the winter of 1998. Off northern Chile, small-sized phytoplankton prevailed and chlorophyll-*a* fluctuated widely during most of the EN event, although inshore levels were consistently high. Zooplankton assemblages shifted to smaller species during the warm phase; the total biomass, however, did not change. Primary production rates and the vertical flux of carbon were

*Corresponding author. Departmento de Oceanografía, Center for Oceanographic Research in the eastern South Pacific (FONDAP-COPAS), PO Box 42, Dichato, Concepcion, Chile. Tel.: +56 451 683247; fax: +56 41 683902.

E-mail address: rescribano@udec.cl (R. Escribano).

0967-0645/$ - see front matter © 2004 Published by Elsevier Ltd.
doi:10.1016/j.dsr2.2004.08.011

not greatly affected. The total anchovy catch for 1997 held stable, reaching up to 1 million tons. In 1998, the catch decreased to 400,000 tons before recovering to 1.2 million tons in 1999 and 2000. Off central/southern Chile, the 'normal' seasonal regime (spring/summer benthic hypoxia) was replaced by oxygenation near the bottom and lower carbon input as a result of the EN event. Macrofaunal biomass increased significantly in the inshore sediments during the warm phase, then diminished in the following spring/summer period. The decreased macrofaunal biomass was associated with the disappearance of filamentous bacterial mats and increased benthic bioturbation. The overall productive capacity of the Chilean upwelling systems seems to have recovered rapidly after the EN decline, suggesting weaker ecological impacts than those observed in the seasons after the 1972–1973 and 1982–1983 events.
© 2004 Published by Elsevier Ltd.

1. Introduction

The coastal upwelling zone of the Humboldt Current System (HCS) in the eastern South Pacific (ESP) is well known for its rich biological productivity, as reflected in the large anchovy, sardine (Ryther, 1969; Cushing, 1990), and jack mackerel (Alheit and Bernal, 1993) fisheries in the area. This high production is mostly sustained by the fertilizing effect of wind-driven coastal upwelling, which pumps nutrients into the euphotic zone over the continental shelf (Barber and Smith, 1981). The HCS is, however, subject to strong interannual variability due to the El Niño Southern Oscillation (ENSO). Perhaps because of the catastrophic collapses of the Peruvian fishery after the 1972–1973 El Niño (EN) event, much of the knowledge regarding EN effects in the region comes from the Peruvian ecosystem. Several studies have dealt with the physical variability (Enfield and Allen, 1980; Smith, 1983; Huyer et al., 1987; Enfield, 1989; Fahrbach et al., 1991) and the biological consequences of EN events on the pelagic system (Barber and Chavez, 1983, 1986; Thomas et al., 2001), benthic communities (Arntz et al., 1987; Tarazona et al., 1988; Arntz and Tarazona, 1990), and fisheries (Alamo and Bouchon, 1987; Arntz and Tarazona, 1990). In general terms, this research suggests that upwelling is greatly reduced during warm ENSO phases, causing, in turn, a significant reduction in primary production and a dramatic impoverishment of the entire marine ecosystem (see Artnz and Farhbach, 1996 for a review).

In terms of ENSO effects, the upwelling systems off the Chilean coast remain the least-studied parts of the HCS. Studies of the upwelling system off northern Chile (18–30°S) show interannual fluctuations in anchovy catches (Blanco et al., 2001) and changes in surface chlorophyll-*a* (Chl-*a*) levels associated with the 1996–1998 transition from La Niña to EN conditions (Thomas et al., 2001; Blanco et al., 2002; Carr et al., 2002). Data from regular monitoring of the biological and chemical conditions off Chile's coast is limited, as is the background information necessary to assess the ecosystem's response to ENs. Little attention has been paid to ENSO-related biogeochemical changes in the HCS (Guillen, 1987; Wilkerson et al., 1987). Nevertheless, carbon (C) and nitrogen (N) fluxes play a key role in the regulation of oceanic production (Walsh, 1991), as greenhouse gases are actively exchanged with the atmosphere (CO_2, N_2O) during upwelling and a shallow, intense oxygen minimum zone (OMZ) is found in the water column (Codispoti et al., 1986; Morales et al., 1999) and over the continental shelf (Gallardo et al., 1995). The concurrence of the recent 1997–1998 EN with a number of multidisciplinary studies in different regions along the Chilean coast provided important information on the physical, chemical, and biological responses of the HCS to the EN. This paper consolidates the information available on the main biological and chemical consequences of the 1997–1998 EN in the coastal upwelling systems off Chile.

1.1. Environmental setting and study areas

The two main upwelling regions of the Chilean HCS are identified by previous and current research, large-scale fishery zones, and oceanographic and biogeochemical conditions (Fig. 1). The northern region (18–30°S) experiences year-round coastal

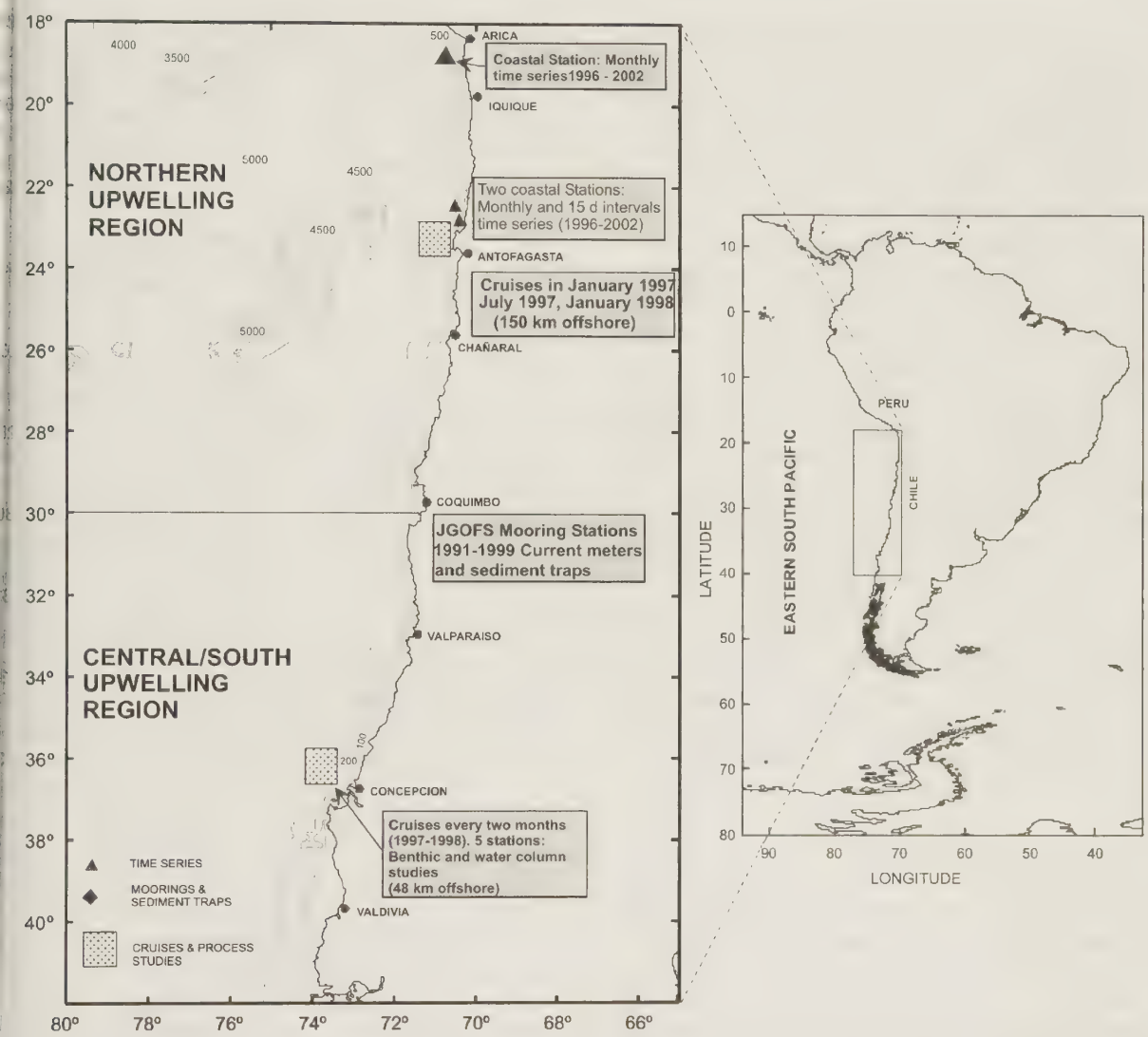

Fig. 1. The study area in the HCS off Chile, including the two major coastal upwelling regions, northern and central/southern Chile, limited by the subtropical convergence (30°S) in the eastern South Pacific. The sources of data used in this synthesis, location of the sampling stations, and type of observations along the Chilean coast are also illustrated.

upwelling and moderate winds (5–10 m s^{-1}), with maximum winds coming from the S-SW during spring–summer (Pizarro et al., 1994). Water mass distribution (Robles et al., 1976; Silva and Sievers, 1981) and large-scale circulation patterns have been reviewed by Strub et al. (1998), whereas the seasonal climatology of the oceanographic conditions has been reported by Blanco et al. (2001). Wind-driven coastal upwelling usually promotes the ascent of equatorial subsurface waters so that a persistent OMZ (< 0.5 mL O_2 L^{-1}) penetrates the euphotic layer (<50 m depth) close to the coast (Morales et al., 1999). The continental shelf is very narrow or almost non-existent (<20 km wide) and high levels of biomass/productivity are mostly restricted to a very narrow coastal band (Morales et al., 1996a; Daneri et al., 2000). The northern upwelling system sustains a strong pelagic fishery, at times attaining

5–6 million tons per year and accounting for ~40% of total annual Chilean fish landings.

The central/southern upwelling region (30–40°S) is highly seasonal, with intense events during the spring and summer (Cáceres and Arcos, 1991; Strub et al., 1998; Figueroa and Moffat, 2000). The continental shelf (20–60 km), some 30 km wider than in the north, is interrupted by submarine canyons (Fig. 1). Rainfall and river runoff are important in this area and low salinity waters (<33.8) may extend far offshore (>30 km) during winter and early spring (Strub et al., 1998; Faúndez et al., 2001). The central/southern OMZ, deeper (>50 m) and less intense (>0.5 mL O_2 L^{-1}) than the northern one, has produced some of the highest primary production rates (10 g C m^{-2} d^{-1}) ever recorded (Fossing et al., 1995; Daneri et al., 2000). This high primary production is thought to sustain the region's large fisheries, including jack mackerel landings of 3 million tons between 1990 and 1996 (Arcos et al., 2001). In the shelf sediments, extended periods of suboxia affect the benthic environment, favoring high biomass development in the form of giant bacterium *Thioploca* mats (Gallardo, 1977; Gallardo et al., 1995).

2. Observations and measurements

This synthesis uses data collected in various locations, manners, and times; Fig. 1 presents a summary of the sampling sites and observations. Time-series data are from serial observations maintained by the Chilean Institute for Fishery Research (IFOP) during the last 5 years at four coastal stations off northern Chile (unpublished data); the information used here comes from two such stations: Arica (~18°S) and Antofagasta (~23°S). Monthly observations began in May 1997, and comprise discrete water samples for temperature, salinity, and Chl-*a* (Table 1) down to 50 m water depth. Temperature was measured with reversed-calibrated thermometers, salinity with an Autolab salinometer, and Chl-*a* by filtration onto GF/F filters and by fluorometric determination (Parsons et al., 1984). No information on the depth of the photic layer is available to estimate the depth-integrated values, so Chl-*a* maximum

Table 1
Summary of time-series measurements at coastal stations off Chile during 1996–2000

Station locations	Frequency	Period	Measurements
Arica (18°S) one fixed coastal station	Monthly	1996–2002	Discrete depths: temperature, salinity, Chl-*a*
Antofagasta (23°S) [1] one fixed coastal station	Monthly	1996–2002	Discrete depths: temperature, salinity, Chl-*a*
Antofagasta (23°S) [2] one fixed coastal station	Every 15 days	Jun. 1996 –Jan. 1998	CTDO, fluorescence, zooplankton
Concepcion (36°S) 5 stations in a transect	Every 2 months	Mar. 1997 –Dec. 1998	CTDO, Chl-*a*, benthic fauna, C and N in sediments

The stations off Arica and Antofagasta [1] are routinely sampled by the IFOP. The Antofagasta [2] station was part of a local study (Ulloa et al., 2001) and the Concepción sampling consisted of an inshore–offshore transect, also as part of a local study by the University of Concepción (Gutiérrez et al., 2000; Sellanes, 2002; Farías et al., 2004).

values from each profile were used to estimate monthly anomalies by subtracting the 4-year monthly means. This information was used to analyze the temporal variation of the phytoplankton biomass. In addition, a coastal station near Antofagasta was sampled every 15 days, from July 1996 to January 1998, to obtain CTDO data, fluorescence profiles, and zooplankton samples (details in Escribano and McLaren, 1999) (Table 1).

Routine measurements of sea-surface temperature (SST) and sea level were taken from the database of the Hydrographic Service of the Chilean Navy (SHOA), which is made up of data collected over the last 10–20 years from tide gauges in several ports along the Chilean coast. SST is routinely measured with nearshore temperature sensors and loggers (~1 m depth) at each port. SST anomalies were calculated by subtracting the mean annual signal from the time series; the mean annual signal was estimated at each site by adjusting four harmonics with periods of 1, $\frac{1}{2}$, $\frac{1}{3}$, and $\frac{1}{4}$ year to a monthly SST time-series stretching from January 1980 to December 2000. Wind-stress anomalies were calculated from satellite data using the same methodology, although, in the case of wind stress, the basal period for estimating the annual signal was January 1992 to December 2002.

Information on currents was taken from a mooring station on the continental slope (water depth, 875 m) off Coquimbo (30°19′S–71°47′W). This is a long-term deployment initiated as part of the Chilean JGOFS program (Shaffer et al., 1999; Hormazabal et al., 2002). The present analysis uses data collected by a current meter at 220 m depth between October 1997 and October 1999. Several CTD (calibrated SeaBird-25 and EG&G Mark-III) casts were made near this mooring station (30°21′S–71°55′W) in November 1997 (EN condition) and July 1998 (non-EN condition). A second mooring station in the oceanic area off Coquimbo (~30°S–73°W; water depth of ~4300 m), provided the time series of the vertical flux of fecal C and its relative contribution to total particulate carbon. The data were obtained from a sediment trap located at ~2300 m depth between 1993 and 1998 (see details in González et al., 2004).

Additional information on the water column was taken from two process-oriented cruises conducted off Antofagasta during July 1997 and January 1998 (González et al., 1998, 2000; Daneri et al., 2000; Iriarte et al., 2000). These data include CTDO profiles, primary production rates, zooplankton and phytoplankton biomass and composition, and vertical fluxes of organic carbon (methods described in González et al., 1998). The data for the area off Concepcion (~36°S) come mainly from benthic studies and bimonthly cruises (1997–1998) carried out along a cross-shelf transect (five stations) from the middle of Concepción Bay to the outer shelf (~50 km offshore). These cruises included CTDO (Sea Bird-25) and nutrient profiles, nutrient concentrations, benthic fauna abundance, and the vertical flux of organic matter to the sediments. Methodological details are provided in Gutiérrez et al. (2000) and Farías et al. (2002).

3. Results

3.1. SST evolution during the 1997–1998 EN in the HCS

The 1997–1998 EN event began developing late in 1996 in the western equatorial region in response to the weakening and reversal of the trade winds (Chavez et al., 2002). NOAA satellite data for the ESP (Fig. 2) showed a positive SST anomaly, or pre-EN conditions, during January 1997. Although the region had almost returned to normal in March 1997, the first Kelvin wave was observed off the Chilean coast in April–May 1997 (Ulloa et al., 2001). After May 1997, warm conditions prevailed and positive SST anomalies (1–3 °C) lasted for up to 14 months, reaching maximum intensity in late 1997 and early 1998. The subtropical area of the ESP had started to cool by March 1998, although positive SST anomalies were observed until the end of 1998.

Positive SST anomalies were observed along the Chilean coast during 1997–1998 (Fig. 3). Five-day average anomalies, taken from the daily SST data collected at different ports (Arica, Antofagasta, Coquimbo, Valparaíso, and Talcahuano),

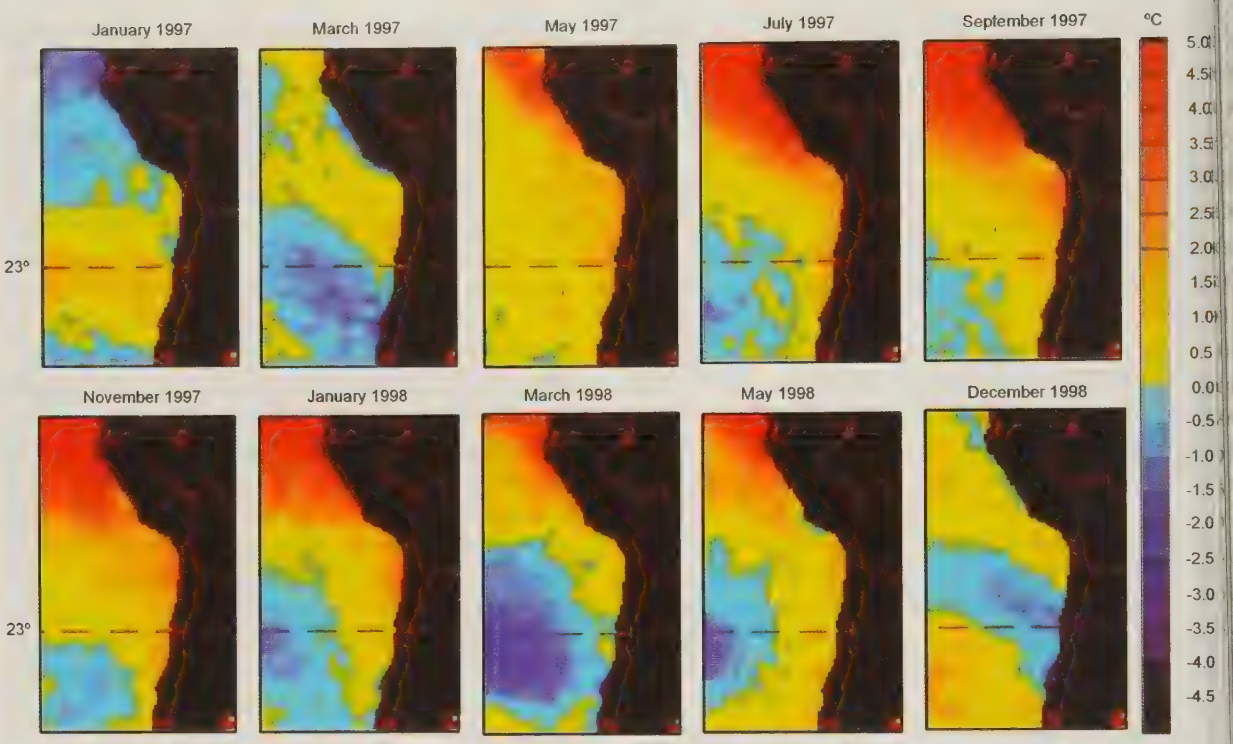

Fig. 2. Monthly means of SST anomalies from satellite information (NOAA satellite data) for the eastern South Pacific region during 1997 and 1998.

exhibited fairly synchronous warm and cold periods, revealing the effects of remotely forced ENSO variability acting on local conditions. Off northern Chile (Arica to Coquimbo), there were two positive peaks in SST anomalies (Fig. 3) associated with the passage of two Kelvin waves of equatorial origin (Ulloa et al., 2001). Further south (Valparaiso to Talcahuano), the two-peak pattern of the north was less clear. An abrupt cooling of the nearshore waters occurred all along the coast off Chile between August and September 1998.

Upwelling driven by local wind forcing also could cause the fluctuations in the SST measured at each of these ports. Ekman transport data estimated for the region from the ERS 1 and ERS 2 satellites (Fig. 4) show strong seasonal variation between 5° and 40°S, moderate intra-seasonal variability south of 25°S, and latitudinal variability from the coast off northern Peru to central/southern Chile. Negative Ekman transport values indicate favorable conditions for offshore advection and coastal upwelling. When superimposed over the seasonal variation, the offshore Ekman transport appears to be greater during 1997. This increase, however, actually took place off Peru. In the Chilean upwelling area (18–40°S), the seasonal pattern remained similar to that of both previous and subsequent years. Upwelling favorable winds, therefore, were present even during the EN conditions of the spring and summer season. These observations are consistent with the negative Ekman transport anomalies measured off Peru and Chile (less pronounced) in austral winter 1997. Seasonal and intra-seasonal scale anomalies in the wind field may have resulted from the influence of ENSO-related atmospheric disturbances of equatorial origin (e.g., Hormazabal et al., 2002). In any case, such variation seems to interact strongly with equatorial Kelvin waves, thus greatly moderating the EN's expression in the ESP, causing variability in upwelling frequency and intensity, in both time and space.

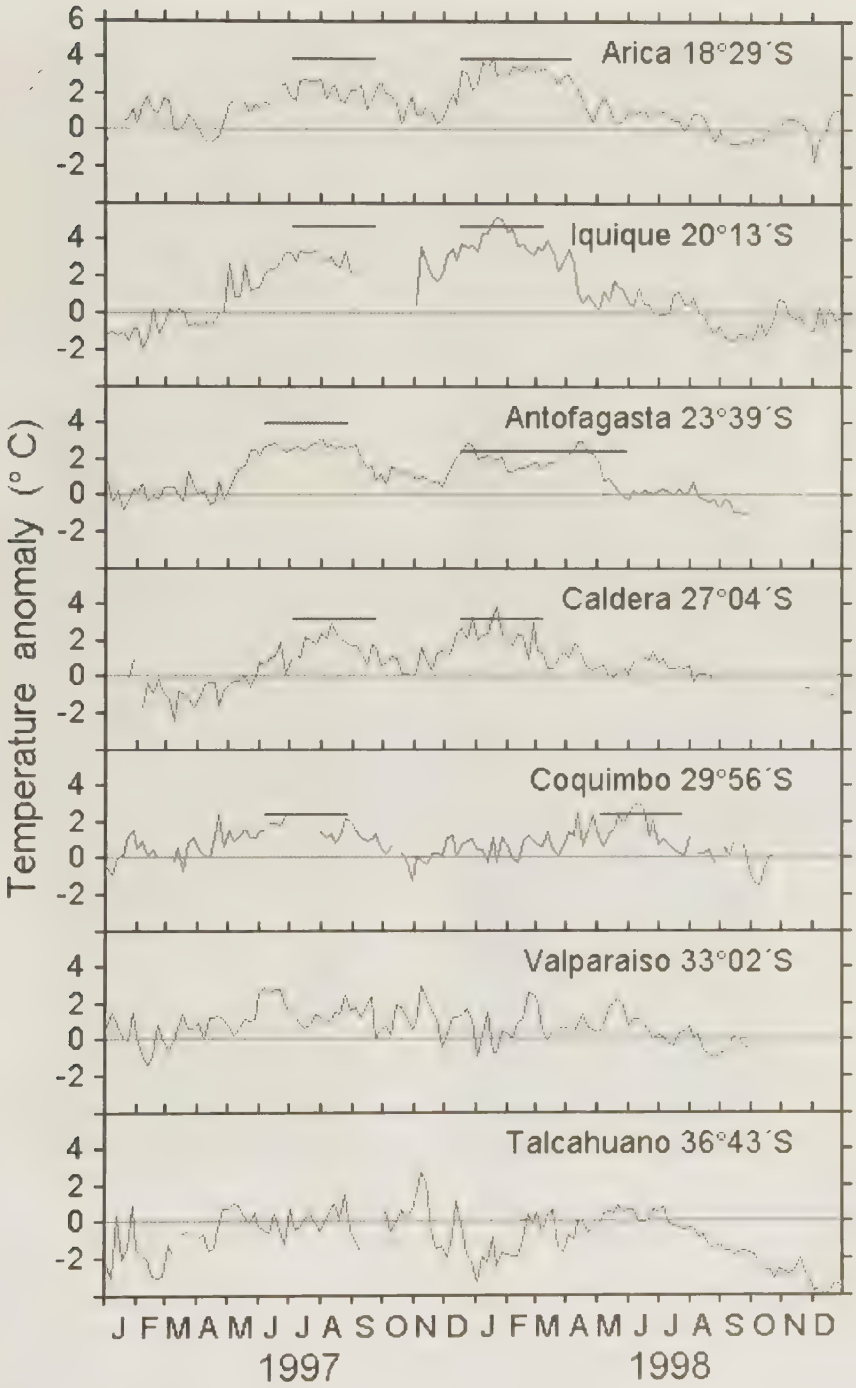

Fig. 3. SST anomalies along the Chilean coast from January 1997 to December 1998. Values are 5 day averages estimated from daily observations provided by the Hydrographic and Oceanographic Service of the Chilean Navy (SHOA). The thicker horizontal lines illustrate the two positive peaks observed off northern Chile.

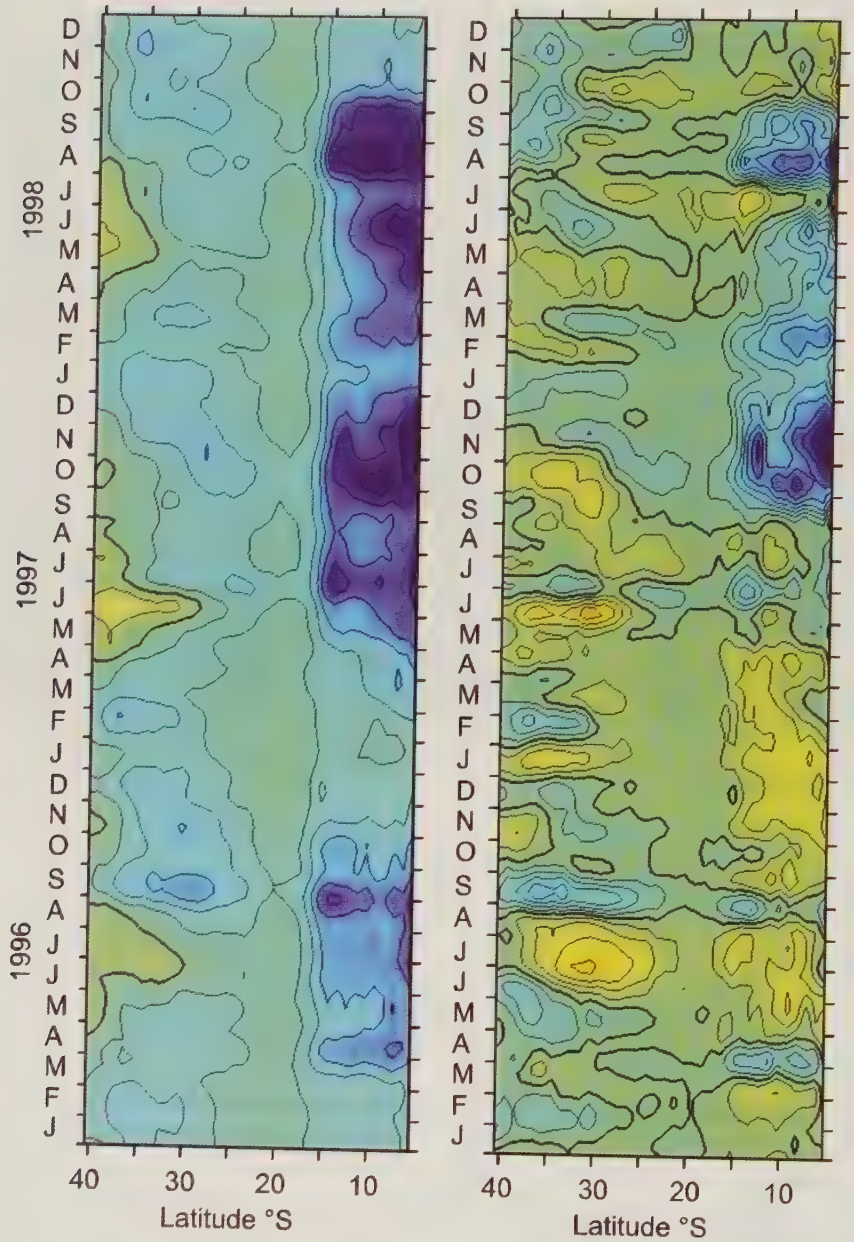

Fig. 4. Offshore Ekman transport (left) and its anomaly (right) along the western coast of South America between 5.5° and 41.5°S, during 1996–1998. Negative (offshore) values are in blue, contours are every $0.5\,m^2\,s^{-1}$ in the left panel and $0.2\,m^2\,s^{-1}$ in the right one; the thick line shows the zero contour. Ekman transport was estimated using weekly wind-stress data derived from ERS 1 and 2 satellite observations. Weekly data were low-passed using a five-point triangular filter.

3.2. Physical–chemical consequences

The onset of the 1997–1998 EN event was marked by a significant deepening of the thermocline at the coastal stations off Arica and Antofagasta (Fig. 5). The 15 °C isotherm descended to below 50 m and two Kelvin waves were observed (May and December 1997). These

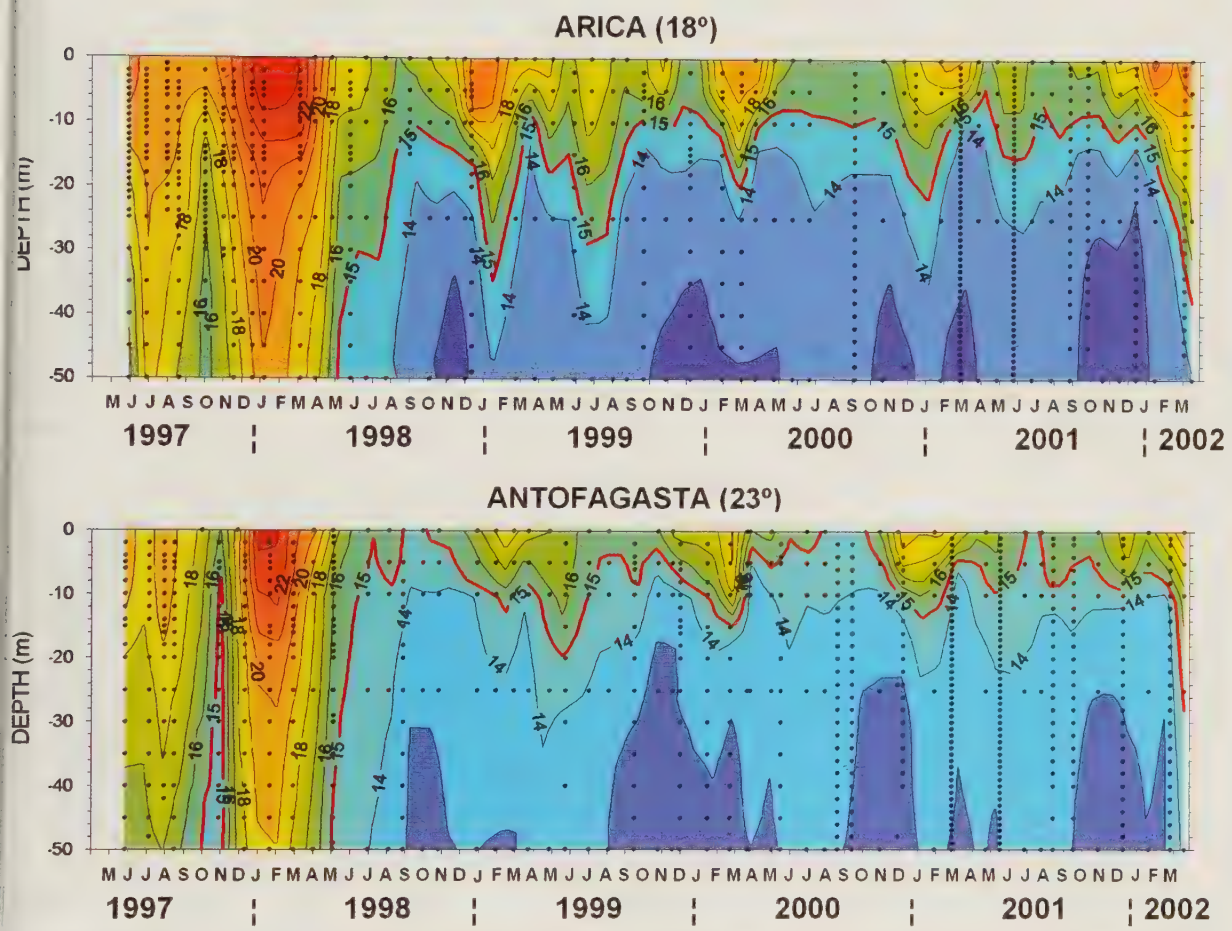
ARICA (18°)
DEPTH (m)
0
-10
-20
-30
-40
-50
M J J A S O N D J F M A M J J A S O N D J F M A M J J A S O N D J F M A M J J A S O N D J F M A M J J A S O N D J F M
1997
1998
1999
2000
2001
2002
ANTOFAGASTA (23°)
DEPTH (m)
0
-10
-20
-30
-40
-50
M J J A S O N D J F M A M J J A S O N D J F M A M J J A S O N D J F M A M J J A S O N D J F M A M J J A S O N D J F M
1997
1998
1999
2000
2001
2002

Fig. 5. Time series of temperature (°C) at two coastal stations off northern Chile from May 1997 to March 2002, illustrating the warming of the entire water column upon the arrival of two Kelvin waves by May and December 1997.

alterations in the vertical thermal structure were the same as those reported in the time series off Antofagasta (Ulloa et al., 2001). A sharp increase in salinity in the upper 50 m was also associated with the Kelvin waves; values which are usually <34.8 in this layer passed 35.0 during this period (Fig. 6).

CTD profiles from November 1997 (EN) and October 1998, taken off Coquimbo, indicate that the whole water column (down to 600 m) became warmer (Fig. 7a) and more saline (Fig. 7b) during the EN event. The structure of the water mass changed and the shallow salinity minimum disappeared during the warm period (Fig. 7c). Although seasonal variations in this coastal mooring's alongshore component of currents at 220 m depth (Fig. 8) are large, alterations in the Peru–Chile Undercurrent flow are not evident. Two maxima in the southward flow do coincide with the May and December 1997 Kelvin waves; however, poleward flow also occurs during these months in other years. The normally shallow nearshore OMZ ($<1\,mL\,O_2\,L^{-1}$) deepened with the arrival of the Kelvin waves.

The oxygenation of the water column increased at the two coastal stations off northern Chile (Arica and Antofagasta) during the EN event. The O_2 concentrations of $>4\,mL\,L^{-1}$ in the upper 40 m are noteworthy, as under normal conditions, the OMZ is a prominent feature of the 0–50 m layer

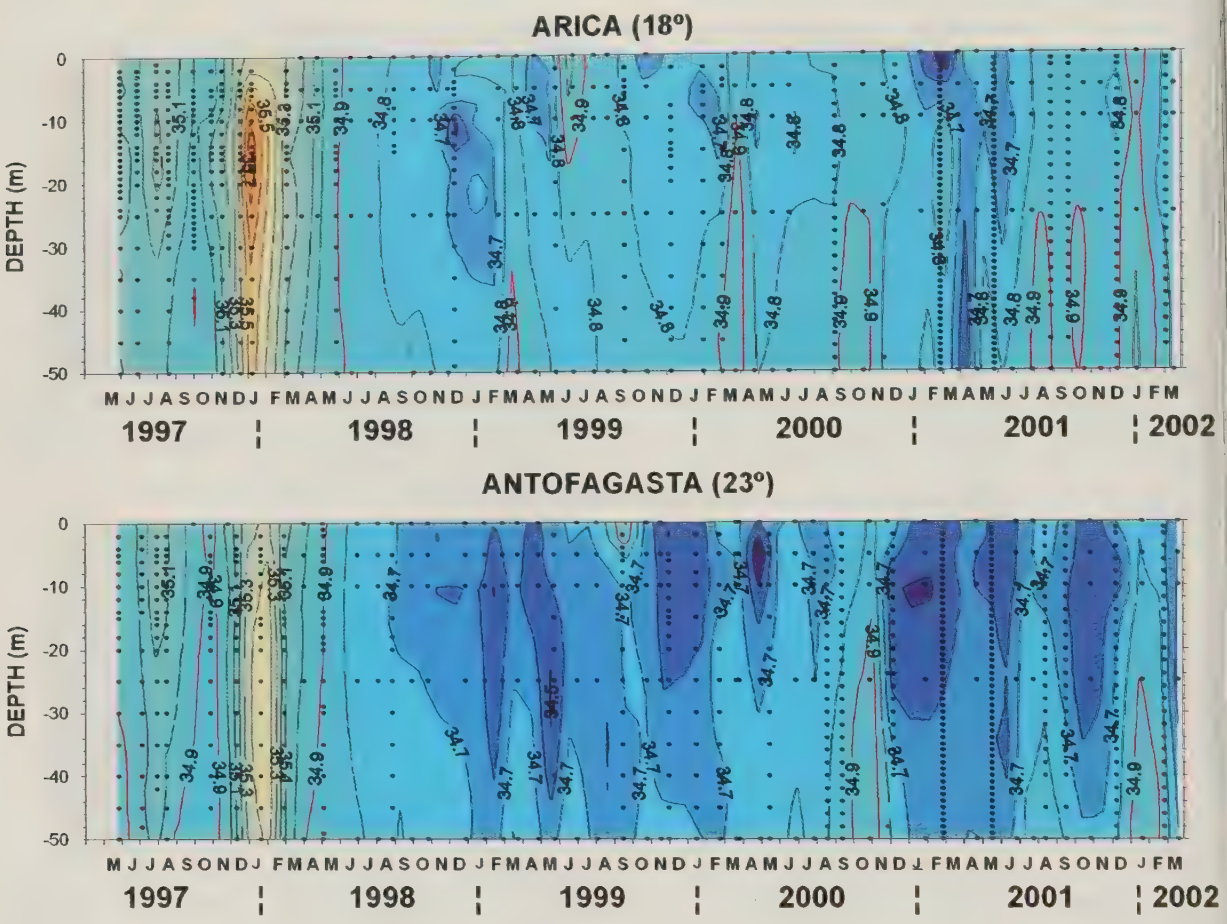
ARICA (18°)
DEPTH (m)
0
-10
-20
-30
-40
-50
M J J A S O N D J F M A M J J A S O N D J F M A M J J A S O N D J F M A M J J A S O N D J F M
1997
1998
1999
2000
2001
2002
ANTOFAGASTA (23°)
DEPTH (m)
0
-10
-20
-30
-40
-50
M J J A S O N D J F M A M J J A S O N D J F M A M J J A S O N D J F M A M J J A S O N D J F M
1997
1998
1999
2000
2001
2002

Fig. 6. Time series of salinity at two coastal stations off northern Chile from May 1997 to March 2002, illustrating the increase in salinity in the water column upon the arrival of two Kelvin waves by May and December 1997.

(Fig. 9). In the central/southern region (Concepción), the OMZ is usually shallow in coastal waters (50–100 m depth) during normal upwelling conditions. The OMZ deepened during the EN event (May, August, and November 1997) and returned to typical conditions in March and November 1998, with low oxygen ($<2\,mL\,L^{-1}$) at depths as shallow as 30 m (Fig. 10). The deepening of the OMZ in May 1998 apparently resulted from suppressed upwelling under non-EN conditions.

Nutrient information from the 1997–1998 EN is scarce. Nitrate concentrations were measured at three coastal stations off Antofagasta in January 1998. In the nearshore zone (~2 km from the coast), nitrate levels were variable but still $>5\,\mu M$ in the upper 50 m layer. However, at the coastal front (~18 km from the coast) and the offshore (~36 km from the coast) stations, there was very little nitrate in the same layer (Fig. 11). Changes in the nitrate concentrations of the same top layer in the central/southern region (off Concepción) were not obvious in the May 1997 and 1998 data, although the maximum levels at depths below 50 m decreased during the latter period (Fig. 12).

The vertical flux of organic C was investigated off Antofagasta, Coquimbo, and Concepción. The vertical flux of particulate organic carbon (POC) off Antofagasta, based on short-term deployments, was lower in July 1997 (EN condition) than in January 1997 (pre-EN condition)

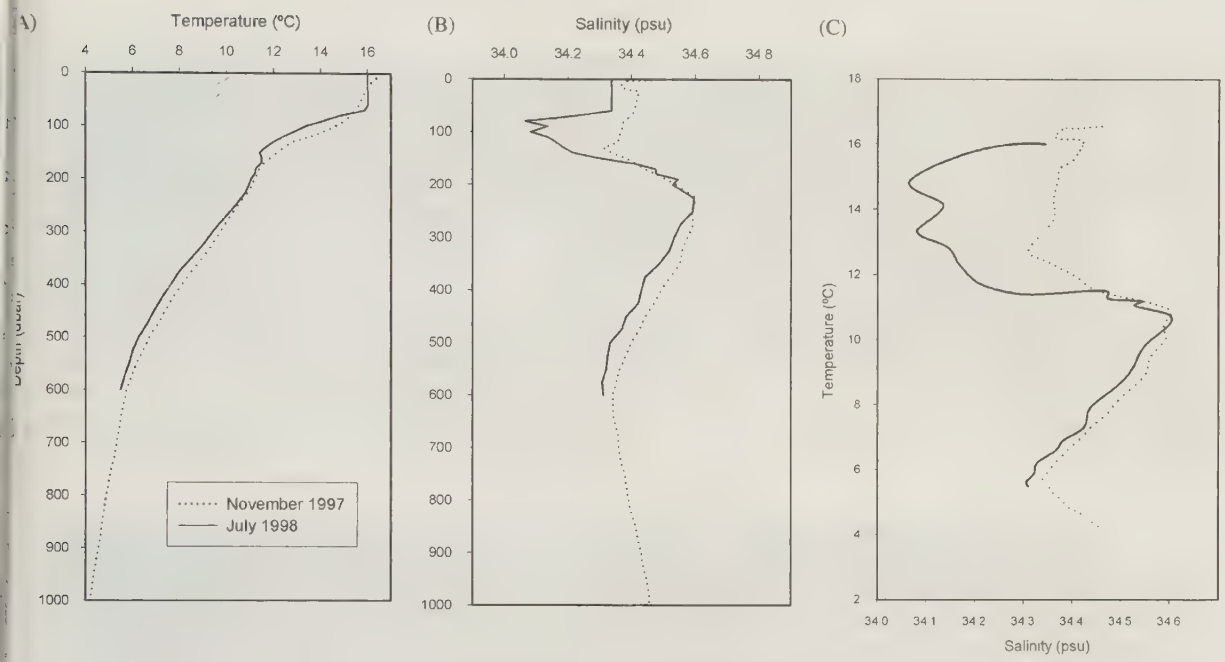

Fig. 7. Vertical profiles of temperature (A) and salinity (B) and the corresponding T-S diagram (C) from CTD data obtained off Coquimbo, near the mooring station (30°21.3′S–71°55′W), during November 1997 (EN condition; fine line) and July 1998 (thick line). Plots are mean data from seven CTD casts for November 1997 and three casts for July 1998.

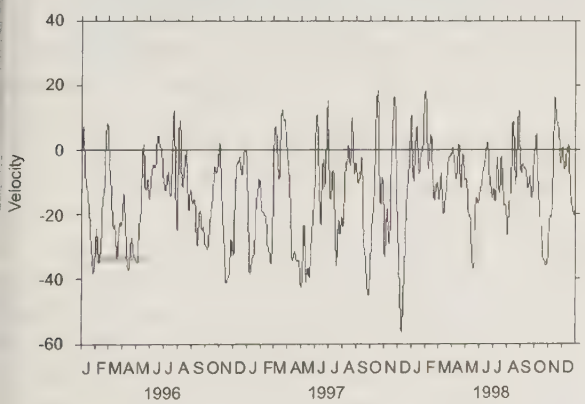

Fig. 8. Alongshore velocity ($cm\,s^{-1}$) at 220 m depth over the slope, at about 15 km from the coast off Coquimbo (30°S). Positive values are approximately equatorward. Daily means were estimated from hourly data and then low-passed using a seven-point triangular filter. The long-term mean of the alongshore velocity at this location is about $-13\,cm\,s^{-1}$.

(Table 2), although the possibility that this may have been an expression of the different seasonal conditions of summer (January) and winter (July) cannot be discarded. The time series for the flux of fecal C and its contribution to total particulate carbon from the long-standing sediment trap off Coquimbo (~2300 m depth) did not show a notable difference between 1997 and previous years (Fig. 13). Fecal C contributed ~30% on average to total C sedimentation, and the seasonal pattern of variability observed during 1993–1996 seemed not to be remarkably different from that of 1997–1998, suggesting that vertical fluxes of organic matter, in terms of fecal C, did not alter during the EN event. However, in the same area, the annual flux of siliceous plankton was markedly lower during EN (1997–1998) compared to non-EN (1993–1994) years (Romero et al., 2001). Meantime, in the coastal zone off Concepción, the vertical fluxes of C and N were found to be significantly reduced in the summer 1998 (EN condition) in comparison with the summer 1999 and 2000, as estimated from the amount of Chl-*a* and total C and N in the sediments over the continental shelf (Farías et al., 2004).

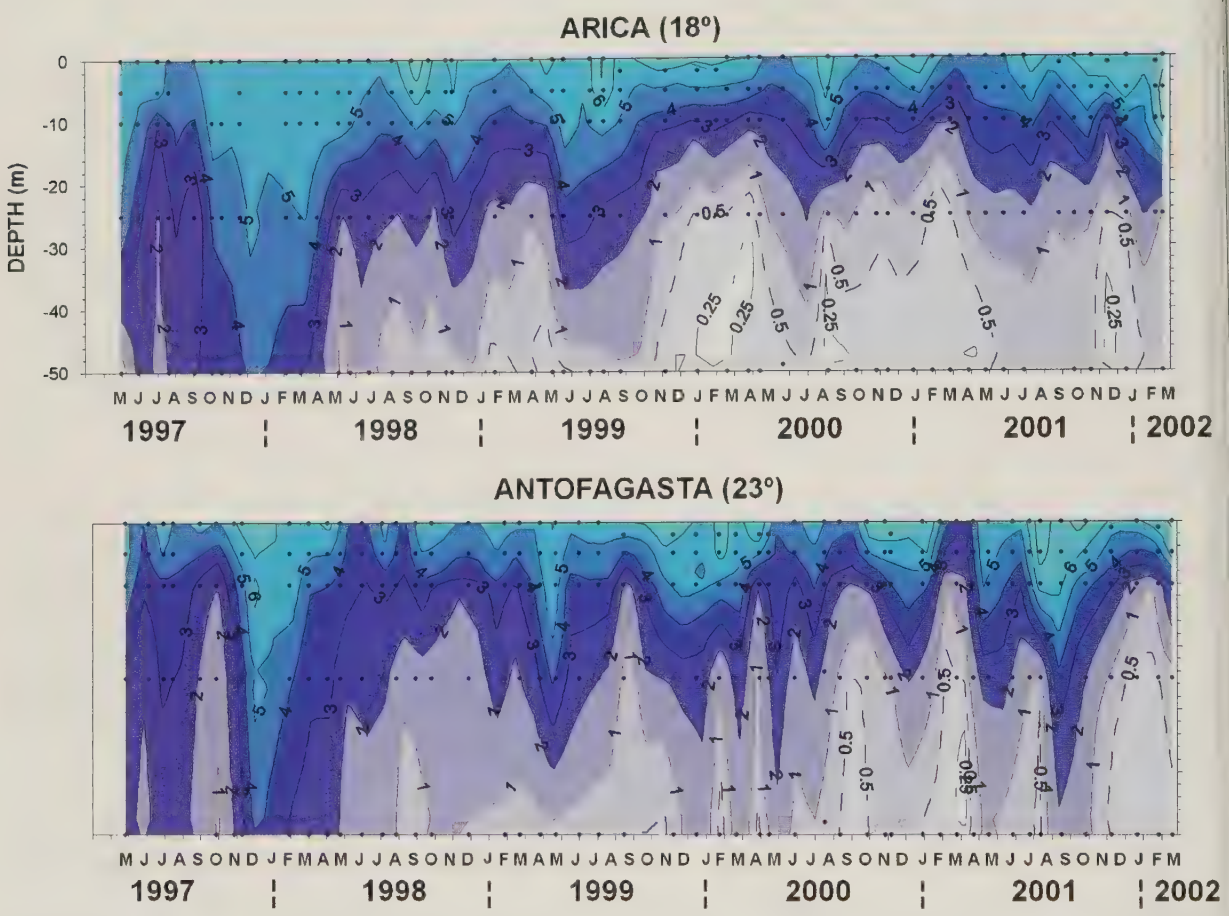
ARICA (18°)
DEPTH (m)
0
-10
-20
-30
-40
-50
M J J A S O N D J F M A M J J A S O N D J F M A M J J A S O N D J F M A M J J A S O N D J F M A M J J A S O N D J F M
1997
1998
1999
2000
2001
2002
ANTOFAGASTA (23°)
M J J A S O N D J F M A M J J A S O N D J F M A M J J A S O N D J F M A M J J A S O N D J F M A M J J A S O N D J F M
1997
1998
1999
2000
2001
2002

Fig. 9. Time series of dissolved oxygen (mL L^{-1}) at the coastal stations off Arica and Antofagasta (northern Chile) from May 1997 to March 2002, illustrating the abrupt deepening of the oxycline and retrieval of the OMZ from nearshore waters upon the arrival of two Kelvin waves in May and in December 1997.

3.3. Biological consequences

Information on primary production rates is still too limited (Daneri et al., 2000) to allow a precise comparison of EN and non-EN levels in the coastal upwelling regions off Chile (Table 3). The estimates of pre-EN (January 1997) and EN (July 1997) primary production made off Antofagasta do not differ, either for coastal or offshore waters, from estimates made during subsequent years in coastal and oceanic areas off northern and central/southern Chile (González et al., 1998; Daneri et al., 2000, unpublished data). More information is available on changes in phytoplankton biomass, measured as Chl-*a* concentration, derived from the time-series studies at the nearshore stations off Arica and Antofagasta during the 1997–2000 period (Fig. 14). Chl-*a* levels appeared to be reduced in the upper 50 m during 1997 compared to subsequent years. Even though monthly anomalies of Chl-*a* maximum in the water column remained negative during 1997, variation both in time and between stations was very high. In fact, Ulloa et al. (2001) found no significant differences in Chl-*a* concentrations between EN and non-EN months in the time series off Antofagasta between June 1996 and January 1998.

The analysis of planktonic communities off Antofagasta during cruises undertaken in January and July 1997 revealed that small-sized species,

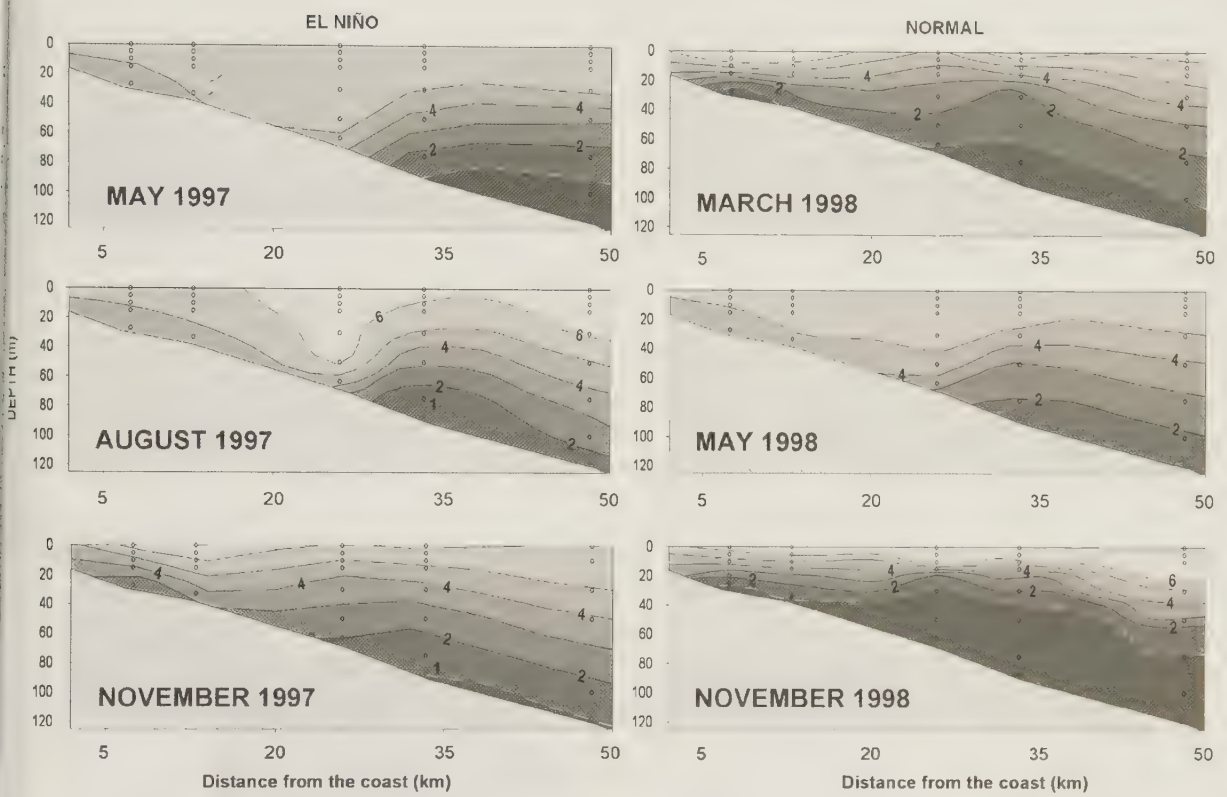

Fig. 10. Dissolved oxygen (mL L $^{-1}$) distribution in the water column off central/southern Chile, near Concepción (36°S), during 1997 and 1998. Contours are from CTDO profiles at five stations over a cross-shelf transect. The broken line shows the 1 mL L $^{-1}$ oxyline, representing the behavior of the OMZ (data from Sellanes, 2002).

including small diatoms and autotrophic flagellates, dominated the phytoplankton during EN conditions, whereas large diatoms prevailed under normal upwelling conditions (Iriarte et al., 2000). Zooplankton time-series data off Antofagasta also displayed a shift towards small-sized species during EN, although total biomass in the nearshore did not suffer abrupt collapses when compared with the previous year (Ulloa et al., 2001). During normal upwelling, the coastal zooplankton community was commonly dominated by large copepods, such as *Eucalanus* spp., and euphausiids, mainly the endemic HCS species, *Euphausia mucronata* (Hidalgo and Escribano, 2001; Fernández et al., 2002). During the warm event, the abundance of small-sized copepods, such as *Oithona* spp. and *Paracalanus parvus*, increased and the occurrence of euphausiids and the large *Eucalanus* spp. decreased (González et al., 2002). Larval stages of euphausiids, however, seemed to increase in abundance during EN months (Fernández et al., 2002). The abundant, medium-sized copepod *Calanus chilensis* also increased in number in the nearshore during EN conditions, although the female adults were reduced in body size in the warmer waters (Ulloa et al., 2001).

Information on the responses of the benthic community to the 1997–1998 EN was obtained from the shelf off Concepción and is described in detail in Gutiérrez et al. (2000). An important consequence of the deepening of the OMZ during EN events is the contact of oxygenated waters with the normally suboxic or anoxic sediments on the shelf, causing changes in bottom communities. Under normal upwelling conditions (and cold La

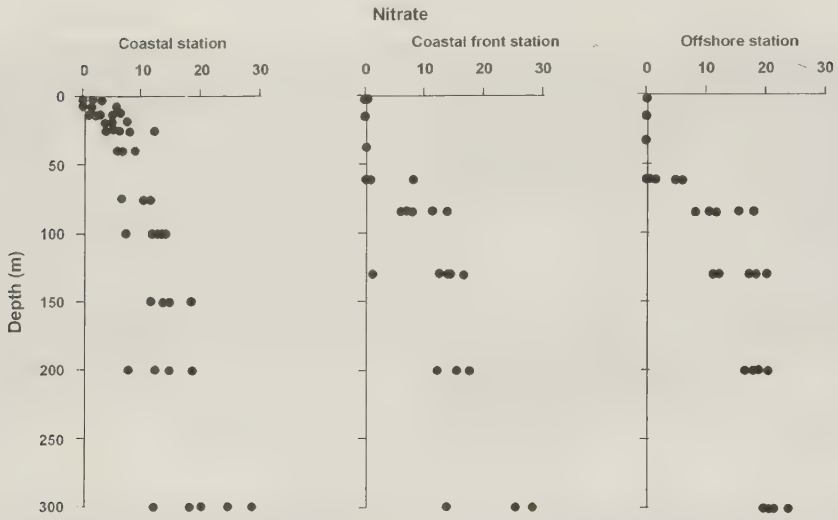

Fig. 11. Vertical profiles of nitrate concentration (μM) obtained in the coastal zone off northern Chile, near Mejillones (23°S), during January 1998 at three stations located in the nearshore, the coastal front, and offshore (~36 km from the coast).

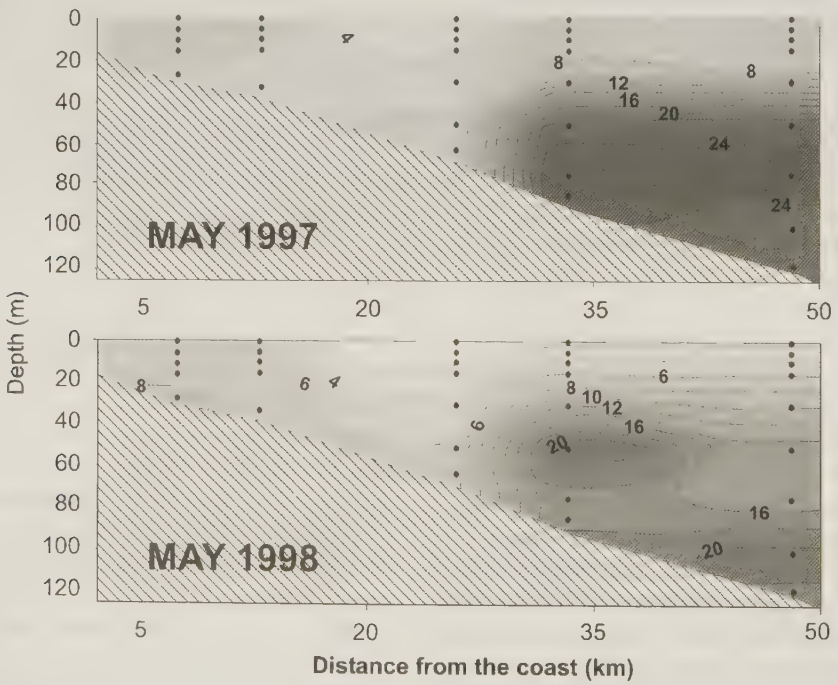

Fig. 12. Nitrate concentration (μM) in the water column off central/southern Chile, near Concepción (36°S), in May 1997 and May 1998 (data from Sellanes, 2002).

Niña phases), a reduced environment dominates the shelf bottom, promoting the growth of large mats of the giant filamentous bacteria *Thioploca*. During the EN months, the greater oxygenation of the bottom sediments was associated with a sharp decrease in *Thioploca* biomass. The response of the

macro-benthic assemblages varied according to distance from the shore. Macrofaunal biomass increased in mid-bay sediments and decreased in shelf sediments during EN. The bioturbation of sediments, however, intensified at all sampling sites during EN, possibly as a consequence of changes in community structure as the relative contribution of different functional groups was altered. Also, the organic matter deposited on the shelf became oxidized and was released from the sediments during the warm event.

Table 2
Ranges of vertical flux of POC as estimated from floating sediment traps off Antofagasta (23°S) under pre-El Niño conditions (January 1997) and during El Niño (July 1997)

Depth (m)	Location	POC (mg C m^{-2} d^{-1})	
		January 1997	July 1997
65	Coastal	166.8–176.4	71.4–164.3
	Offshore	125.1–141.6	32.3–103.6
100	Coastal	117.9–119.0	35.0–40.9
	Offshore	19.8–No data	18.3–47.3

Data from González et al. (1998).

4. Discussion

A conceptual model of the response of the HCS ecosystem off Chile to the 1997–1998 EN was designed in an attempt to integrate the above information. This particular event was considered to be one of the most intense recorded (McPhaden,

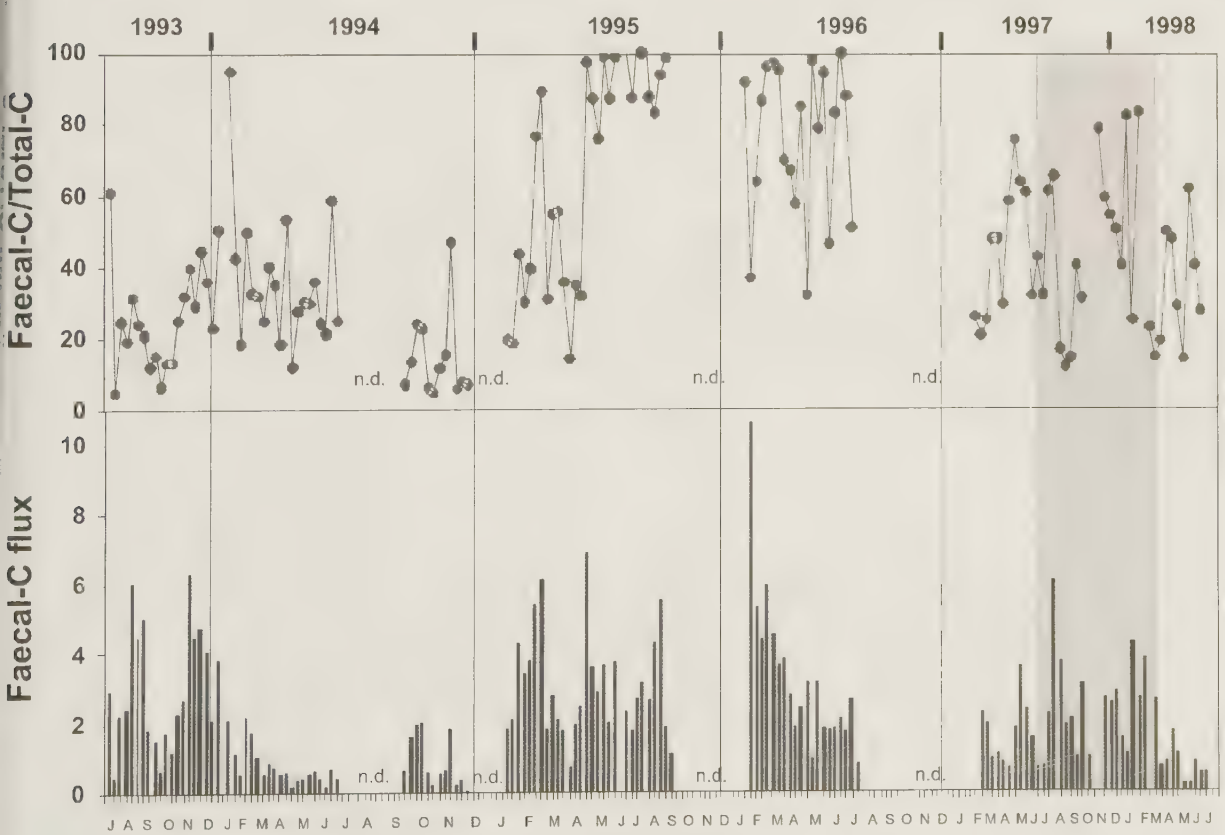
1993
1994
1995
1996
1997
1998
Faecal-C/Total-C
Faecal-C flux
n.d.
J A S O N D J F M A M J J A S O N D J F M A M J J A S O N D J F M A M J J A S O N D J F M A M J J A S O N D J F M A M J J

Fig. 13. Time series of the vertical flux of fecal carbon (mg C m^{-2} d^{-1}) and the proportion of fecal carbon over total organic carbon (%), estimated from sediment traps located at 2300 m at the deep-mooring station off Coquimbo (30 S), from 1993 to 1998. The shaded area denotes the 1997–1998 EN event.

Table 3
Water-column integrated estimates (mean ± SD) of primary production rates in the Chilean coastal upwelling system during 1997–2000

Period	Location	Primary production ($g C m^{-2} d^{-1}$)		Source
		Coastal	Offshore	
January 1997 pre-El Niño cruise	Antofagasta (23°S)	3.17 ± 1.81	0.82 ± 0.29	González et al. (1998)
July 1997 El Niño cruise	Antofagasta (23°S)	2.03 ± 1.40	1.56 ± 1.18	González et al. (1998)
October 1998 spring cruise	Concepción (36°S)	4.13 ± 2.56	0.32	Daneri et al. (2000)
2000 summer cruise	Iquique (20°S)	3.3	0.3	Single estimate (Unpublished data)

Values were all obtained by in situ incubations and integrated over the photic layer (1% of light level). A single measurement was available for Iquique.

1999). The model summarizes the main alterations in the physical and chemical environment and the biological consequences for the pelagic and benthic systems by comparing a cold phase (normal upwelling) with a warm ENSO phase (Fig. 15). The model is largely based on the northern upwelling region. Since satellite data showed positive SST and sea-level anomalies during the 1997–1998 EN event to be greatest between 5° and 15°S but extending beyond 40°S (Carr et al., 2002), similar, less intense changes are expected for the central/southern region.

During a "normal" cold condition (Fig. 15, upper panel), the SSTs in the coastal upwelling area vary between 15 and 18 °C, coastal fronts are well developed (Sobarzo and Figueroa, 2001; Marín et al., 2001), and the cold (~12 °C), nutrient-rich, equatorial subsurface waters ascend in the nearshore, shoaling the OMZ and creating a low-oxygen environment near the surface waters (Blanco et al., 2001, 2002). These conditions favor higher NO_3 inputs into the photic zone. Primary production is expected to be higher and mostly sustained by NO_3 (new production). The resulting high biomass values that are associated with reducing conditions in subsurface waters will, in turn, favor higher sedimentation and accumulation rates of organic matter on the shelf (Carr, 2003). Phytoplankton is distributed mainly in the upper 50-m layer, within a shallow photic zone (~60 m) (González et al., 1998) and restricted to the nearshore band (Escribano, 1998; Escribano and Hidalgo, 2000; Morales et al., 2001). Similar observations have been made for the zooplankton and small pelagic fish, whose vertical distributions and diel migrations seem restricted by a shallow OMZ (Judkins, 1980; Jarre et al., 1991; Morales et al., 1996b; Escribano and Hidalgo, 2000; Escribano et al., 2000; Rojas et al., 2002). The structure of this highly concentrated pelagic ecosystem is dominated by large species of diatoms, euphausiids, and large-sized copepods (Iriarte et al., 2000; Hidalgo and Escribano, 2001; Ulloa et al., 2001).

During the warm ENSO phase (Fig. 15, lower panel), surface waters become warmer (>20 °C), coastal fronts weaken or disappear (Blanco et al., 2002), and the photic layer deepens to below 100 m (González et al., 1998). In conjunction with changes in the coastal zone's water mass composition, the thermocline, oxycline, and OMZ deepen, oxygenating the subsurface waters overlying the shelf and shelf break (Blanco et al., 2002). Upwelling may continue during this phase (Carr et al., 2002), but a deeper nutricline limits the input of new nutrients into the photic zone, favoring regenerated production (Carr, 2003). The limited data available on nutrients off Chile suggest that NO_3 is reduced except close inshore. The deepening of the thermocline may occur under conditions of sustained upwelling and may even be increased by Ekman pumping (Halpern, 2002). This deepening may allow a vertical expansion of the photic-oxygenated layer and, along with the disappearance of coastal fronts, would result in a higher dispersion—both vertical and horizontal—of plankton and fish (clupeids) (Escribano, 1998; Escribano et al., 2000; Ulloa et al., 2001). The

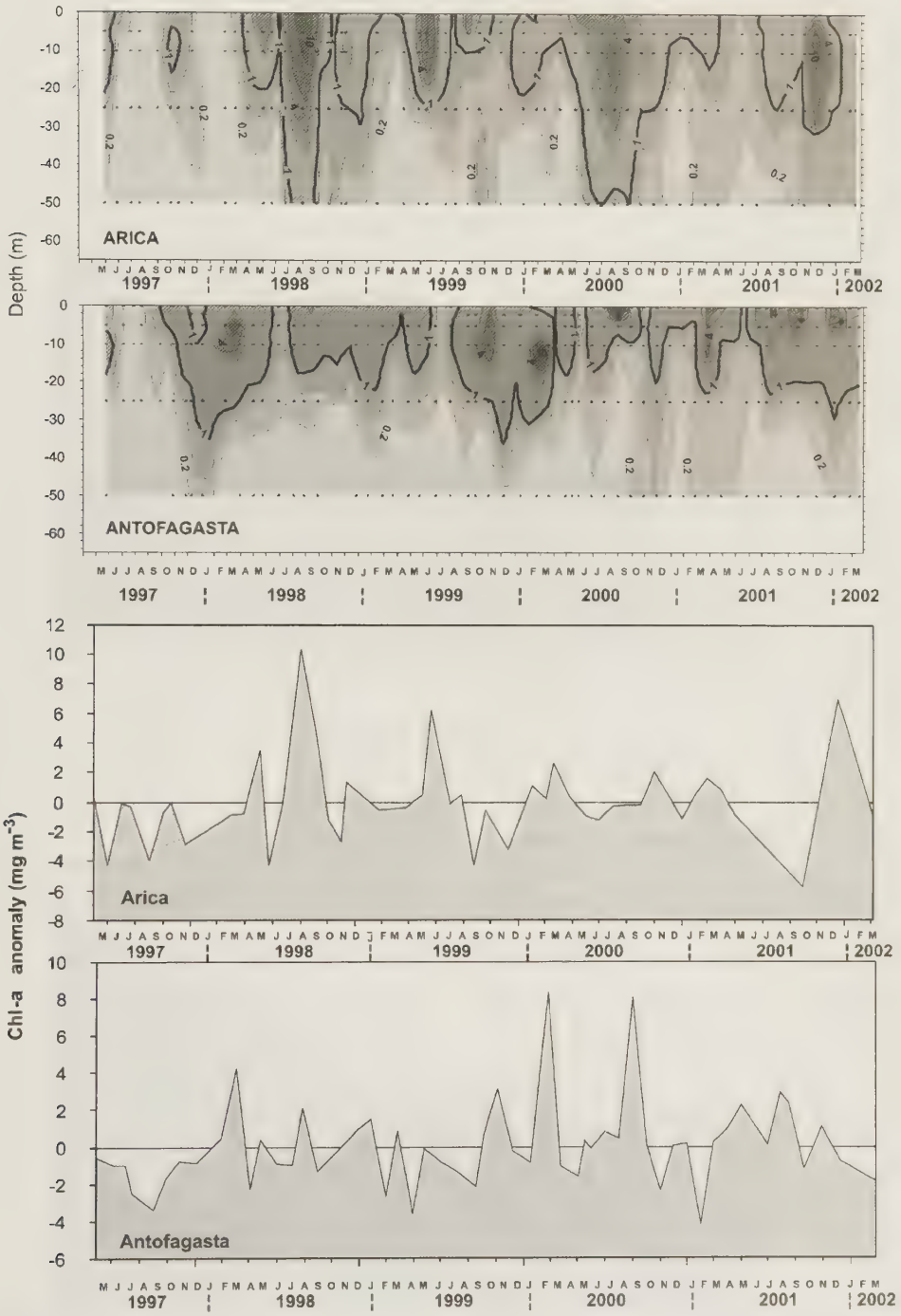

Fig. 14. Time series of Chl-*a* concentration (upper panels) and corresponding anomalies (lower panels) in Arica and Antofagasta (northern Chile) from May 1997 to March 2002. Units are in mg Chl-*a* m^{-3}. Between May 1997 and February 1998, a decrease in Chl-*a* occurred at both stations, being less pronounced off Antofagasta. Negative monthly anomalies in maximum values of Chl-*a* prevailed during 1997 at both stations.

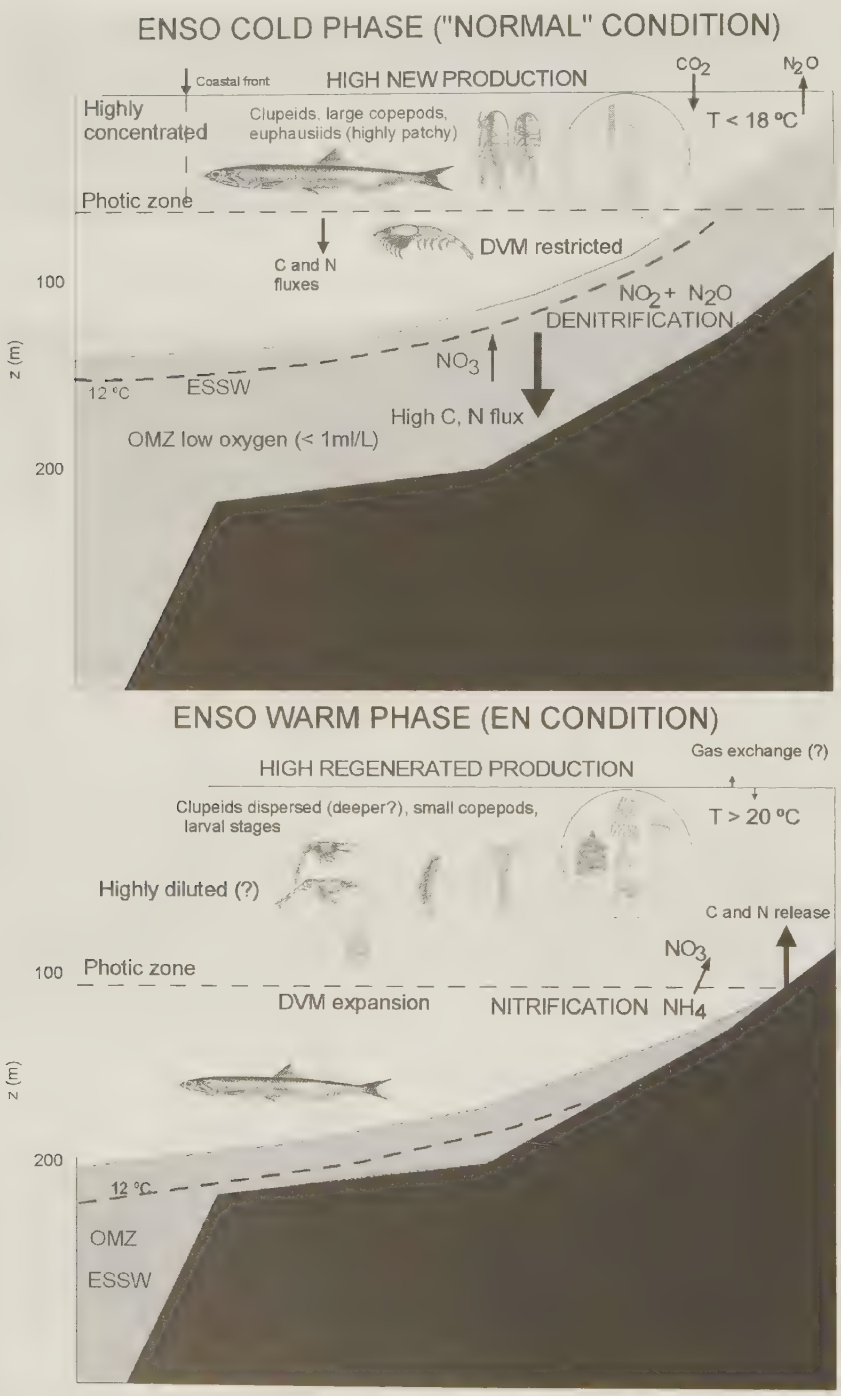

Fig. 15. Conceptual model summarizing the main oceanographic changes and their chemical and biological consequences during the two phases of the ENSO in the Chilean coastal upwelling ecosystem: "normal" upwelling condition (upper panel) and the EN condition (lower panel). The model is mostly based on information derived from the northern region (18–30°S), but similar—though less intense—responses are expected for the central/south (30–40°S) upwelling region. The 12 °C isotherm represents the average temperature of the ESSW (Equatorial subsurface water) within 100–200 m and thus illustrates the retrieval of the OMZ from the coastal zone under EN conditions.

elagic ecosystem appears to be dominated by ower trophic levels, including flagellates, small iatoms and copepods, larval stages of euphau- ids, and gelatinous species (Fernández et al., 002; González et al., 2002).

During normal or cold events, the denitrification ates within the OMZ and the accumulation of N_2O close to the surface waters are expected to ntensify (Codispoti et al., 1986; Morales et al., 999). During active upwelling, a strong initial utgassing of CO_2 and N_2O, both greenhouse ases, is expected in the areas of an intense and hallow OMZ, probably with a net outsourcing rom the ocean albeit the potential increase in new roduction by the phytoplankton community. During EN, the oxygenation of the water column would result in lower denitrification rates (Morales t al., 1999) and in a reduced supply of organic natter to deeper waters, and also in the release of rganic matter from the shelf sediments (Gutiérrez t al., 2000). EN events may favor higher itrification, potentially contributing NO_3 to the hotic layer. The expansion of the habitable olume for planktonic communities may allow an increase in the total community aerobic espiration by small organisms (microplankton), thus affecting the production/respiration ratio (Eissler and Quiñones, 1999). The sea to atmosphere exchange of CO_2 is likely to be reduced unless upwelling favorable winds remain during the EN event, as was the case off Coquimbo in July 1997 (Torres et al., 2003). Altogether, these changes alter the region's biogeochemical cycling and the gas exchange between the sea and the atmosphere, a key issue considering the potential loss of biologically available N from the ocean. The nature and magnitude of the alterations however, remain, to be assessed.

The oceanographic alterations during the 1997–1998 EN caused a reduction in surface Chl-*a* in the ESP region, especially off northern Chile, according to satellite data (Thomas et al., 2001; Blanco et al., 2002; Carr et al., 2002). However, the Chl-*a* levels, which appear relatively high in the coastal waters, seem reduced offshore (Carr et al., 2002), suggesting that the satellite data resolution (9 km) used in these studies does not provide accurate information for the nearshore band. Also, surface Chl-*a* does not adequately reflect the phytoplankton biomass vertically integrated over the euphotic zone, which deepens during EN. The in situ data from the two coastal stations off northern Chile showed lower Chl-*a* during 1997, although negative maximum Chl-*a* anomalies also occurred through 2002. Although the maximum Chl-*a* in the water column was very low ($0.1–0.2\,\mu g\,L^{-1}$) at both stations in August 1997, the highest values ($2.4\,\mu g\,L^{-1}$) did not coincide in time: Arica peaked in May 1997 and Antofagasta in October 1997. Thus, in addition to cross-shelf variation, timing and latitudinal variability also need to be considered when evaluating EN effects on phytoplankton biomass. Moreover, if the integrated phytoplankton biomass remains unchanged in the water column upon an increase in the depth of the euphotic zone, for example, due to nutrient limitation, lower biomass per unit volume will be found; this could explain the lower surface Chl-*a* values described by Thomas et al. (2001) during the warm 1997–1998 event. Changes in Chl-*a* also may be related to the shift to small-sized species in the phytoplankton community structure during EN (Iriarte et al., 2000), a relationship that warrants further study.

The observed changes in the species composition of planktonic assemblages during EN may have important consequences for the trophic structure and biogenic fluxes in the coastal waters of the HCS. The shift towards small-sized classes during EN would favor regenerated production and the microbial food web as the dominant pathways of C and N, sustaining the productivity of the coastal areas (Carr, 2003). When small copepods dominate the zooplankton, a smaller contribution to the vertical flux of POC and fecal pellets is expected (González et al., 2000). Abundant small-sized species, like cyclopoid copepods, may substantially reduce the vertical flux of particulates by feeding on phytodetritus and fecal pellets. In contrast, when large copepods and euphausiids are abundant, an intense vertical flux of their fecal material is expected, allowing greater amounts of organic matter to sink faster. Such changes in phytoplankton and zooplankton community structures also can affect the food spectrum available for higher trophic levels.

The full impact of the 1997–1998 EN on HCS fishery resources is far from clear. The strong fishery of small pelagic anchovy and sardines in northern Chile was not noticeably affected in 1997, as was the Peruvian anchovy industry as a result of the 1982–1983 EN (see Arntz and Fahrbach, 1996 for a review). Our data indicate that food levels, at least in nearshore waters where anchovy normally spawn (Castro et al., 2000), might have been sufficient for larval survival. In fact, winter spawning took place as usual during the 1997–1998 EN and high concentrations of anchovy eggs were collected in the annual IFOP survey (Oliva et al., 1998). This year's class, however, produced lower landings in 1998 (Oliva et al., 2000). Abnormally high surface temperatures and changes in the larval food spectrum (shift to smaller size classes) probably caused greater egg and larvae mortalities, but insufficient knowledge of the food requirements for clupeid larvae off northern Chile hinders any assessment of the food effect. Acoustic anchovy surveys during EN and normal conditions indicated that the adult population deepened and even tended to remain near the bottom, at depths around 60 m, in coastal waters during the warm event (IFOP, unpublished information). This particular change in behavior during EN also was observed in Peruvian waters (Gutiérrez, 2001). Arcos et al. (2001) analyzed the effects of the 1997–1998 EN on the jack mackerel fishery off central/southern Chile. The oceanographic conditions altered by EN triggered changes in migratory routes and nursery distributions of this species, in turn reducing availability of the resource for the local fishery industry. Anchovy and the common sardine, *Strangomera bentincki*, are also important resources in this region, and, as suggested for the northern area, a reduction in recruitment was reported for both species, affecting the stock during subsequent years (1998–1999) (Cubillos and Arcos, 2002).

In the conceptual scheme presented here (Fig. 15), the strong alterations in the physical–chemical environment and the biological responses during the 1997–1998 EN have been emphasized. However, the apparent weak level of ecological impact, compared to previous events, seems to be an important feature of this EN in the HCS off Chile. Despite the strong variability of the in situ Chl-*a* presented here, it is likely that primary production in the nearshore was sustained at similar levels during this warm event supporting the production of zooplankton since the total biomass did not suffer major changes (Ulloa et al., 2001). In the California Current System, ecological impacts of this event also were considered to be less extensive. Chavez et al. (2002) suggested that the onset of the event occurred at the time when the Pacific decadal oscillation was shifting from a warm to a cold phase, resulting in weaker ecological effects as compared to the 1982–1983 and 1991–1992 events that took place during a warm phase and produced drastic ecological impacts. It is likely that long-term climate regimes of the Pacific Ocean play an important role in regulating the ecosystem responses to alternating EN–La Niña events.

Acknowledgments

We are grateful to Drs. A. Thomas, S. Hormazabal, and J.T. Pennington for valuable comments that improved the manuscript. We thank SHOA (Hydrographic Service of the Chilean Navy) for providing SST and sea-level data. Information from coastal time series in Arica and Antofagasta were obtained through the project "Bio-oceanographic Monitoring of Regions I and II (MOBIO)", funded by the Fishery Research Fund of Chile (FIP), and carried out by the Instituto de Fomento Pesquero (IFOP). This work is a contribution from the Center for Oceanographic Research in the eastern South Pacific (COPAS) funded by Chile's CONICYT-FONDAP Program (Project No. 150100007).

References

Alamo, A., Bouchon, M., 1987. Changes in the food and feeding of the sardine (*Sardinops sagax*) during the years 1980–1984 off the Peruvian coast. Journal of Geophysical Research 92, 411–415.

Alheit, J., Bernal, P., 1993. Effects of physical and biological changes on the biomass yield of the Humboldt Current Ecosystem. In: Sherman, K., Alexander, L.M., Gold, B.D. (Eds.), Large Marine ecosystems. American Association

for the Advancement of Science Press, Washington, DC, pp. 53–58.

Arcos, D.F., Cubillos, L.A., Nuñez, S.P., 2001. The jack mackerel fishery and El Niño 1997–98 effects of Chile. Progress in Oceanography 49, 597–617.

Arntz, W.E., Fahrbach, E., 1996. El Niño Experimento Climático de la Naturaleza. Fondo de Cultura Económica, Mexico, DF, 312pp.

Arntz, W.E., Tarazona, J., 1990. Effects of the El Niño on benthos, fish and fisheries off the South American Pacific coast. In: Glynn, P.W. (Ed.), Global Ecological Consequences of the 1982–83 El Niño—Southern Oscillation. Elsevier Oceanography Series, Amsterdam, pp. 323–360.

Arntz, W.E., Brey, T., Tarazona, J., Roble, A., 1987. Changes in the structure of a shallow sandy-beach community in Peru during an El Niño event. In: Payne, A.I.L., Gulland, J.A., Brink, K.H. (Eds.), The Benguela and Comparable Ecosystems. South African Journal of Marine Sciences 5, 645–658.

Barber, R.T., Chavez, F.P., 1983. Biological consequences of El Niño. Science 22, 1203–1210.

Barber, R.T., Chavez, F.P., 1986. Ocean variability in relation to living resources during the 1982–83 El Niño. Nature 319, 279–285.

Barber, R.T., Smith, R.L., 1981. Coastal upwelling ecosystems. In: Analysis of Marine Ecosystems. Academic Press, New York, pp. 31–68.

Blanco, J.L., Thomas, A.C., Carr, M.E., Strub, P.T., 2001. Seasonal climatology of hydrographic conditions in the upwelling region off northern Chile. Journal of Geophysical Research 106, 11451–11467.

Blanco, J.L., Carr, M.-E., Thomas, A.C., Strub, P.T., 2002. Hydrographic conditions off northern Chile during the 1996–1998 La Niña and El Niño. Journal of Geophysical Research 107 (C3).

Cáceres, M., Arcos, D.F., 1991. Varibilidad en la estructura espacio-temporal de un area de surgencia frente a la costa de Concepción, Chile. Investigación Pesquera (Chile) 36, 27–38.

Carr, M.-E., 2003. Simulation of carbon pathways in the planktonic ecosystem off Peru during the 1997–1998 El Niño and La Niña. Journal of Geophysical Research 108 (C12), 3380.

Carr, M.-E., Strub, P.T., Thomas, A.C., Blanco, J.L., 2002. Evolution of 1996–1999 La Niña and El Niño conditions off the western coast of South America: a remote sensing perspective. Journal of Geophysical Research 107 (C12), 3236.

Castro, L.R., Salinas, G.R., Hernandez, E.H., 2000. Environmental influences on winter spawning of the anchoveta *Engraulis ringens* off Central Chile. Marine Ecology Progress Series 197, 247–258.

Chavez, F.P., Pennington, J.T., Castro, C.G., Ryan, J.P., Michisaki, R.P., Schlining, B., Walz, P., Buck, K.R., McFadyen, A., Collins, C.A., 2002. Biological and chemical consequences of the 1997–1998 El Niño in central California waters. Progress in Oceanography 54, 205–232.

Codispoti, L.A., Friederich, G.E., Packard, T.T., Glover, H.E., Kelly, P.J., Spinrad, R.W., Barber, R.T., Elkins, J.W., Ward, B.B., Lipschultz, F., Lostaunau, N., 1986. High nitrate levels off northern Peru: a signal of instability in the marine denitrification rate. Science 233, 1200–1202.

Cubillos, L.A., Arcos, D.F., 2002. Recruitment of common sardine (*Strangomera bentincki*) and anchovy (*Engraulis ringens*) off central-south Chile in the 1990s and the impact of the 1997–1998 El Niño. Aquatic Living Resources 15, 87–94.

Cushing, D.H., 1990. Plankton production and year class strength in fish populations: an update of the match/mismatch hypothesis. Advances in Marine Biology 26, 250–294.

Daneri, G., Dellarossa, V., Quiñones, R., Jacob, B., Montero, P., Ulloa, O., 2000. Primary production and community respiration in the Humboldt Current System off Chile and associated oceanic areas. Marine Ecology Progress Series 197, 41–49.

Eissler, Y., Quiñones, R.A., 1999. Microplanktonic respiration off northern Chile during El Niño 1997 -1998. Journal of Plankton Research 21, 2263–2283.

Enfield, D.B., 1989. El Niño, past and present. Review Geophysical 27, 159–187.

Enfield, D.B., Allen, J.S., 1980. On the structure and dynamics of monthly mean sea level anomalies along the Pacific coast of North and South America. Journal of Physical Oceanography 10, 557–578.

Escribano, R., 1998. Population dynamics of *Calanus chilensis* in the Chilean Eastern Boundary Humboldt Current. Fisheries Oceanography 7, 245–251.

Escribano, R., Hidalgo, P., 2000. Spatial distribution of copepods in the north of the Humboldt Current region off Chile during coastal upwelling. Journal of the Marine Biological Association, UK 80, 283–290.

Escribano, R., McLaren, I.A., 1999. Production of *Calanus chilensis* in the upwelling area of Antofagasta, northern Chile. Marine Ecology Progress Series 177, 147–156.

Escribano, R., Marín, V., Irribarren, C., 2000. Distribution of *Euphausia mucronata* at the upwelling area of Peninsula Mejillones: the influence of the oxygen minimum layer. Scientia Marina 64, 69–77.

Fahrbach, E., Trillmich, F., Arntz, W.E., 1991. The time sequence and magnitude of physical effects of the El Niño in the eastern Pacific. In: Trillmich F., Ono, K.A. (Ed.), Pinnipeds and El Niño Responses to Environmental Stress. Springer, Berlin, pp. 8–21.

Farías, L., Graco, M., Molina, V., Gutierrez, D., Gallardo, V.A., Ulloa, O., 2002. Nitrogen cycling in sediments from central Chile (36°S): seasonal and interannual variability. Investigaciones Marinas, Valparaíso, Chile (Extended Abstract) 30, 167–168.

Farías, L., Graco, M., Ulloa, O., 2004. Temporal variability of nitrogen cycling in continental-shelf sediments of the upwelling ecosystem off central Chile. Deep-Sea Research II, this issue [doi:10.1016/j.dsr2.2004.07.029].

Faúndez, P.B., Morales, C.E., Arcos, D., 2001. Variabilidad espacial y temporal en la hidrografía invernal del sistema de

bahías frente a la VIII región (Chile centro-sur). Revista Chilena de Historia Natural 74, 817–831.

Fernández, D., Escribano, R., Hidalgo, P., 2002. Distribución de eufáusidos en el sistema de surgencia de la Península de Mejillones (23°S) asociada a condiciones previas y durante El Niño 1997/98. Investigaciones Marinas Valparaíso, Chile 31, 56–72.

Figueroa, A.D., Moffat, C., 2000. On the influence of topography in the induction of coastal upwelling along the Chilean coast. Geophysical Research Letters 27, 3905–3908.

Fossing, H., Gallardo, V.A., Jorgensen, B.B., Huttel, M., Nielsen, L.P., Schultz, H., Canfield, D., Forster, S., Glud, R.R., Gundersen, J.K., Ramsing, N.B., Teske, A., Thamdup, B., Ulloa, O., 1995. Concentration and transport of nitrate by the mat-forming sulphur bacterium *Thioploca*. Nature 374, 713–715.

Gallardo, V.A., 1977. Large benthic microbial communities in sulfide biota under Peru–Chile subsurface countercurrent. Nature 268, 331–332.

Gallardo, V.A., Carrasco, F.D., Roa, R., Cañete, J.I., 1995. Ecological patterns in the benthic macrobiota across the continental shelf off central Chile. Ophelia 40, 167–188.

González, H.E., Daneri, G., Figueroa, D., Iriarte, J.L., Lefèvre, N., Pizarro, G., Quiñones, R., Sobarzo, M., Troncoso, A., 1998. Producción primaria y su destino en la trama trófica pelágica y océano profundo e intercambio océano-atmósfera de CO_2 en la zona norte de la Corriente de Humboldt (23°S): Posibles efectos del evento El Niño, 1997–98 en Chile. Revista Chilena de Historia Natural 71, 429–458.

González, H.E., Ortiz, V.C., Sobarzo, M., 2000. The role of faecal material in the particulate organic carbon flux in the northern Humboldt Current, Chile (23°S), before and during the 1997–1998 El Niño. Journal of Plankton Research 22, 499–529.

González, H.E., Pagés, F., Sobarzo, M., Escribano, R., 2002. Effects of the 1997/98 El Niño on the oceanographic conditions and zooplankton community structure in the coastal upwelling system off northern Chile. Investigaciones Marinas Valparaíso, Chile (extended abstract) 30, 112–114.

González, H.E., Hebbeln, D., Iriarte, J.L., Marchant, M., 2004. Downward fluxes of faecal material and microplankton at 2,300 m depth in the oceanic area off Coquimbo (30°S), Chile, during 1993–1995. Deep-Sea Research II, this issue [doi:10.1016/j.dsr2.2004.07.027].

Guillen, O., 1987. Relación NO_3/SiO_3 durant El Niño 1982–83. Boletín ERFEN 21, 3–9.

Gutiérrez, M., 2001. Efectos del evento El Niño 1997–98 sobre la distribución y abundancia de anchoveta (*Engraulis ringens*). In: Tarazona, J., Arntz, W., Castillo de Maruenda, E. (Eds.), El Niño en America Latina: Impactos biológicos y sociales. Consejo Nacional de Ciencia y Tecnología, Lima Perú. Editorial Omega, SA, pp. 55–72.

Gutiérrez, D., Gallardo, V.A., Mayor, S., Neira, C., Vasquez, C., Sellanes, J., Rivas, M., Soto, A., Carrasco, F., Baltazar, M., 2000. Effects of dissolved oxygen and fresh organic carbon on the bioturbation potential of macrofauna in sublittoral bottoms off central Chile, during the 1997–98 El Niño. Marine Ecology Progress Series 202, 81–99.

Halpern, D., 2002. Offshore Ekman transport and Ekman pumping off Peru during the 1997–1998 El Niño. Geophysical Research Letter 29(5), 10.1029/2001GLO14097, 2002.

Hidalgo, P., Escribano, R., 2001. Succession of pelagic–copepod species during the period 1996/1998 in northern Chile: the influence of the 1997–98 El Niño. Hydrobiologia 453, 153–160.

Hormazabal, S., Shaffer, G., Pizarro, O., 2002. Tropical Pacific control of intraseasonal oscillations off Chile by way of oceanic and atmospheric pathways. Geophysical Research Letters 29(6), 10.1029/2001GLO13481. 5-4.

Huyer, A., Smith, R.L., Paluszkiewicz, T., 1987. Coastal upwelling off Peru during normal and El Niño times, 1981–1984. Journal of Geophysical Research 92, 297–308.

Iriarte, J.L., Pizarro, G., Troncoso, V.A., Sobarzo, M., 2000. Primary production and biomass size-fractioned phytoplankton off Antofagasta, Chile (23–24°S) during pre-El Niño and El Niño 1997. Journal of Marine Systems 26, 37–51.

Jarre, A., Munck, P., Pauly, D., 1991. Two approaches for modeling fish stock interactions in the Peruvian upwelling ecosystem. ICES Marine Symposium 193, 171–184.

Judkins, D.C., 1980. Vertical distribution of zooplankton in relation to the oxygen minimum off Peru. Deep-Sea Research 27A, 475–487.

Marín, V.H., Escribano, R., Delgado, L.E., Olivares, G., Hidalgo, P., 2001. Nearshore circulation in a coastal upwelling site off the northern Humboldt Current System. Continental Shelf Research 21, 1317–1329.

McPhaden, M.J., 1999. Genesis and evolution of the 1997–98 El Niño. Science 283, 950–954.

Morales, C.E., Blanco, J.S., Braun, M., Reyes, H., Silva, N., 1996a. Chlorophyll-*a* distribution and associated oceanographic conditions in the upwelling region off northern Chile during the winter and spring 1993. Deep-Sea Research I 43, 267–289.

Morales, C.E., Braun, M., Reyes, H., Blanco, J.L., Davies, A., 1996b. Anchovy larval distribution in the coastal zone off northern Chile: the effect of low dissolved oxygen concentration and of a cold-warm sequence 1990–95. Investigaciones Marina Valparaíso, Chile 24, 77–96.

Morales, C.E., Hormazabal, S.E., Blanco, J.L., 1999. Interannual variability in the mesoscale distribution of the depth of the upper boundary of the oxygen minimum layer off northern Chile (18–24°S): implications for the pelagic system and biogeochemical cycling. Journal of Marine Research 57, 909–932.

Morales, C.E., Blanco, J.L., Braun, M., Silva, N., 2001. Chlorophyll-*a* distribution and mesoscale processes in upwelling and adjacent oceanic zones off northern Chile (summer–autumn 1994). Journal of the Marine Biological Association, UK 81, 193–206.

Oliva, J., Braun, M., Castillo, J., Blanco, J., Rojas, O., 1998. Evaluación del stock desovante de la anchoveta en la I y II

Regiones (1997). Instituto de Fomento Pesquero. Informe Final Proyecto FIP (Chile) 97-01, 133pp.

Oliva, J., Barría, P., Braun, M., Catasti, V., Claramunt, G., Díaz, E., Escribaño, R., Herrera, G., Montenegro, C., Oliva, M., Pizarro, J., Pizarro, P., Serra, R., Rojas, O., Reyes, H., 2000. Evaluación del stock desovante de anchoveta en la I y II Regiones. Informe Final FIP (Chile) 2000-06, 114pp.

Parsons, T.R., Maita, Y., Lalli, C.M., 1984. A Manual of Chemical and Biological Methods for Seawater Analysis. Pergamon Press, Oxford, 173pp.

Pizarro, O., Hormazabal, S., González, A., Yañez, E., 1994. Variabilidad del viento, nivel del mar y temperatura en la costa norte de Chile. Investigaciones Marina, Valparaíso, Chile 22, 85–101.

Robles, F., Alarcón, E., Ulloa, A., 1976. Las masas de agua en la región norte de Chile y sus variaciones estacionales en un período frío (1967) y en períodos cálidos (1969, 1971–1973). Reunión de Trabajo sobre el fenómeno conocido como "El Niño". Guayaquil, Ecuador, 4–12 de Diciembre de 1974, No. 185, pp. 94–196.

Rojas, P., Escribano, R., Marín, V., 2002. The influence of coastal upwelling on fish larvae distribution off Mejillones Peninsula, northern Chile. Fisheries Oceanography 11, 233–244.

Romero, O.E., Hebbeln, D., Wefer, G., 2001. Temporal and spatial variability in export production in the SE Pacific Ocean: evidence from siliceous plankton fluxes and surface sediment assemblages. Deep-Sea Research I 48, 2673–2697.

Ryther, J.H., 1969. Photosynthesis and fish production in the sea. Science 166, 72–76.

Sellanes, J., 2002. Efectos de El Niño 1997–98 sobre los indicadores bioquímicos de la calidad de la materia orgánica sedimentaria y la meiofauna en un área de surgencia costera de Chile central. Ph.D. Thesis Dissertation, Department of Oceanography, Universidad de Concepción, Chile, 189pp.

Shaffer, G., Hormazabal, S., Pizarro, O., Salinas, S., 1999. Seasonal and interannual variability of currents and temperature off central Chile. Journal of Geophysical Research 104 (C12), 29951–29961.

Silva, S.N., Sievers, H.A., 1981. Masas de agua y circulación en la región de la rama costera de la Corriente de Humboldt: latitudes 18°S–33°S (Operación Oceanográfica MARCH-ILE X-ERFEN I). Ciencia y Tecnología del Mar CONA 5, 5–50.

Smith, R.L., 1983. Peru coastal current during El Niño: 1976 and 1982. Science 221, 1397–1399.

Sobarzo, M., Figueroa, D., 2001. The physical structure of a cold filament in a Chilean upwelling zone Peninsula Mejillones, Chile, 23°S. Deep-Sea Research I 48, 2699–2726.

Strub, P., Mesias, J., Montecino, V., Rutllant, J., 1998. Coastal ocean circulation off western South America. In: Robinson, A., Brink, K. (Eds.), The Sea, vol. 11. The Global coastal ocean. First Workshop on Coastal Ocean Advanced Science and Technology Studies (COASTS) IOC, Liege. Wiley, New York.

Tarazona, J., Salzwedel, H., Arntz, W.E., 1988. Oscillations of macrobenthos in shallow water off the Peruvian central coast induced by El Niño 1982–83. Journal of Marine Research 46, 593–611.

Thomas, A.C., Blanco, J.L., Carr, M.E., Strub, P.T., Osses, J., 2001. Satellite-measured chlorophyll and temperature variability off northern Chile during the 1996–1998 La Niña and El Niño. Journal of Geophysical Research 106 (C1), 899–915.

Torres, R., Turner, D.R., Ruttlant, J., Lefevre, N., 2003. Continued CO_2 outgassing in an upwelling area off northern Chile during the development phase of El Niño 1997–1998 (July 1997). Journal of Geophysical Research 108 (C10), 3336.

Ulloa, O., Escribano, R., Hormazabal, S., Quiñones, R.A., Ramos, M., González, R.R., 2001. Evolution and biological effects of the 1997 98 El Niño in northern Chile. Geophysical Research Letters 28 (8), 1591–1594.

Walsh, J.J., 1991. Importance of continental margins in the marine biogeochemical cycling of carbon and nitrogen. Nature 350, 53–55.

Wilkerson, F.P., Dugdale, R.C., Barber, R.T., 1987. Effects of El Niño on new, regenerated, and total production in eastern boundary upwelling systems. Journal of Geophysical Research 92, 347 353.

ELSEVIER

Deep-Sea Research II 51 (2004) 2413–2426

DEEP-SEA RESEARCH
PART II

www.elsevier.com/locate/dsr2

Bio-optical characteristics and primary productivity during upwelling and non-upwelling conditions in a highly productive coastal ecosystem off central Chile (~36°S)

Vivian Montecino[a,*], Rosa Astoreca[a,b], Gadiel Alarcón[c], Leira Retamal[a,d], Gemita Pizarro[e]

[a]*Departamento de Ciencias Ecológicas, Facultad de Ciencias, Universidad de Chile, Casilla, 653 Santiago, Chile*
[b]*Ecologie des Systèmes Aquatiques-ESA, Université Libre de Bruxelles, Campus Plaine-CP 221, Boulevard du Triomphe, B-1050 Bruxelles, Belgium*
[c]*Centro de Investigación Oceanográfica en el Pacífico Sur-Oriental (FONDAP-COPAS), Departamento de Oceanografía, y Programa Regional de Oceanografía Física y Clima (PROFC), Universidad de Concepción, Casilla 160-C, Concepción, Chile*
[d]*Département de Biologie, Université Laval, Québec, Canada, G1K 7P4*
[e]*Instituto de Fomento Pesquero, E. Abello 0552, Punta Arenas, Chile*

Accepted 24 July 2004

Abstract

Variability of several bio-optical and photosynthetic properties of phytoplankton in the highly productive coast off Concepción, central Chile (~36°S) was quantified during contrasting seasons at offshore, shelf, and nearshore sites. During October 1998 (upwelling) and July 1999 (non-upwelling), 21 stations were sampled for chlorophyll-*a*, pigment spectral light absorption, primary production, and attenuation coefficients ($k\lambda$) of downwelling irradiance ($E_d(\lambda)$); $k\lambda$ was used to estimate the depth of the euphotic zone (Z_{eu}). Primary production was measured through ^{14}C-fixation experiments using simulated in situ and in situ incubations with water from six depths within the Z_{eu}. The photosynthetic parameters (α^B, P^B_{max}) were obtained through photosynthesis-irradiance experiments with samples from two Z_{eu} depths. Bio-optical properties showed large spatial variability during both seasons, including spectral in vivo phytoplankton absorption ($a_{ph}(\lambda)$), pigment specific phytoplankton absorption ($a^*(\lambda)$) within the upper 25 m, and water-column transmittance ($T(\lambda)$), calculated for the upper 10 m using $E_d(\lambda)$ at four wavelengths. Under non-upwelling conditions, $a^*(\lambda)$, $T(\lambda)$, and α^B presented higher values whereas $a_{ph}(\lambda)$ values decreased accordingly. Under upwelling conditions, primary productivity ranged from 0.7 to 7.5 g C m^{-2} d^{-1} at the coastal stations and was <0.6 g C m^{-2} d^{-1} at the oceanic stations; in the non-upwelling season, values over the entire area ranged from 0.2 to 1.9 g C m^{-2} d^{-1}. The significant correlations found among bio-optical properties and physiological parameters highlight both the short- and long-term changes in the area's environmental conditions. The combination of three independent biological parameters—α^B, P^B_{max}, and $a_{ph}(442)$—accounted for most of the horizontal and vertical variability among and within

*Corresponding author. Tel.: +56 2 678 7405 or 271 2977; fax: +56 2 272 7363.
E-mail address: clorofil@uchile.cl (V. Montecino).

0967-0645/$ - see front matter © 2004 Elsevier Ltd. All rights reserved.
doi:10.1016/j.dsr2.2004.08.012

stations for each cruise. These results support a distinction of different functional zones for the two contrasting upwelling conditions.
© 2004 Elsevier Ltd. All rights reserved.

1. Introduction

Physiological and bio-optical parameters are basic tools in the study of phytoplankton primary production (PP). The absorption and scattering coefficients are the inherent optical properties (IOPs) that control the underwater light environment. Therefore, IOPs are used to describe the behavior of living particles, such as phytoplankton cells, associated non-algal particles (biogenic detritus and heterotrophic organisms), and other absorbing components such as colored dissolved organic matter (CDOM) (Bricaud et al., 1998). The water column, which operates as a bio-optical system, is composed of and modulated by the radiation flux and its absorption by particulate and dissolved matter (i.e. phytoplankton and CDOM, respectively). From an ecosystem point of view, trophic regimes based on photosynthetic carbon fixation (ranging from oligotrophic to eutrophic) can be analyzed in terms of the relationship between light availability and phytoplankton light absorption in the PAR range (400–700 nm) and changes therein in both space and time. On a regional scale, the optical properties in the water column (i.e. the chlorophyll specific absorption coefficient of phytoplankton $a^*(\lambda)$) also allow the identification of spatial differences related to photosynthetic performance. The optical properties in different areas will depend on local factors with both light and phytoplankton composition being directly or indirectly modulated by nutrients, mixing, or turbulence (Kiørboe, 1993).

The quantification of regional variability is essential in understanding phytoplankton dynamics across regions. Moreover, global PP estimates, using satellite-derived data, can be made by incorporating the regional variability into larger scales. The starting point for understanding the trophic status of large oceanic areas (Platt et al., 1995) is to estimate the relationship between PP and IOP data at the smallest scale, since the physiological parameters of phytoplankton are known to vary largely in space and time (Kyewalyanga et al., 1998; Sathyendranath et al., 1999). In the case of coastal waters, productive upwelling areas are characterized by a distribution of phytoplankton biomass with sharp surface boundaries and typical shapes. Moreover, in the Humboldt Current System (HCS), the usually high phytoplankton biomass values (>1 mg chlorophyll-$a\,m^{-3}$) off Perú and Chile (Walsh, 1981; Thomas et al., 2001; Nixon and Thomas, 2001) are associated with the upwelling processes that, in turn, are affected by local topography, the continental shelf width, and short-term variations in wind strength, as well as seasonal, intraseasonal, and interannual variability (Montecino et al., 1998; Rutllant and Montecino, 2002). In this physically heterogeneous system, large spatial bio-optical variability can be expected considering that integrated light availability is driven by physical processes (Siegel et al., 1995) and by changes in the phytoplankton assemblage composition, which involve differences in efficiency levels for light or nutrient utilization (Cullen and MacIntyre, 1998). Along the Chilean coast, however, this variability has been poorly studied.

Upwelling off central Chile is seasonal. During about half of the year (October–March), wind-driven coastal upwelling fertilizes the surface waters promoting high primary production off Concepción (Daneri et al., 2000). During the rest of the year, winds are not favorable for upwelling and phytoplankton biomass and PP diminish considerably (Cuevas et al., 2004; Farías et al., 2004). Stuart et al. (2004) recently showed significant spatial variability in the bio-optical characteristics during the upwelling season off Concepción, but no results were reported on the non-upwelling season and no PP measurements were included.

The present study was undertaken to quantify the variability of bio-optical properties and related

physiological parameters (i.e. light transmittance, phytoplankton light absorption, photosynthetic parameters), describing the interactions between spectral light availability and the changes in the efficiency of phytoplankton light utilization. It is hypothesized that wide differences could be found between oceanic and coastal water columns in the very productive area off Concepción. Consequently, we propose that different geographical sites could be aggregated through the combination of their biological and optical properties, thus defining particular functional zones.

2. Methods

This study was conducted during two 15-day cruises in austral spring (October 1998, upwelling) and winter (July 1999, non-upwelling), onboard the R/V Abate Molina, between Punta Nugurne (35°58′42″S 72°47′18″W) and Punta Lavapié (37°08′54″S 73°35′00″W). Sampling was carried out at a total of 21 oceanographic stations, distributed over and adjacent to the 40–80 km broad continental shelf, a ~360-km transect off Concepción and the southern upwelling area of Punta Lavapié (Fig. 1). Stations were classified and enumerated according to bottom depth as being either oceanic, coastal, or shelf stations (Table 1). SeaWiFS images were processed with SeaDAS 4.2, applying standard NASA methodology and the daily EPTOMS & NCEP meteorology. Satellite chlorophyll-*a* (C_{sat}) was obtained using the OC-4 algorithm (O'Reilly et al., 1998). During both cruises, surface radiation measurements and vertical profiles were made with a multispectral (7-channel) radiometer (Satlantic) composed of the SeaWiFS Profiling Multichannel Radiometer (SPMR) for downwelling irradiance ($E_d(\lambda)$) and the Multichannel Visible Detector System (MVDS). $E_d(\lambda)$ raw data were converted to binary data and binned in 1-m increments using the Prosoft 6d software. The depth of the euphotic zone (Z_{eu}) was estimated with the attenuation coefficient of the most penetrating downwelling irradiance ($k_d(\lambda)$) in the PAR range, either at 555 or 489 nm bands. Irradiance transmittance ($T(\lambda)$) was calculated in the upper 10 m using the median $E_d(\lambda)$ values as follows:

$$(E_d(\lambda, 0-10\,\mathrm{m})/E_d(\lambda, 0^-)) * 100$$

(Barnard et al., 1999).

The transmittance spectra from all stations were grouped according to the shape of each single slope between 489 and 555 nm in order to characterize different water types; the median spectrum was then calculated for each group. To find a representative spectrum for each water type, these shapes were tested to be significantly different at $p<0.05$ using the Kruskal–Wallis test.

At all stations, water samples from six depths (0–100 m) were filtered onto glass-fiber filters (0.7 μm nominal size) for fluorometric analysis of chlorophyll-*a* (Chl-*a*) and phaeopigments (Phaeo) (Jeffrey et al., 1997). For the in vivo phytoplankton light absorption, water samples were collected from selected stations and depths and filtered (500 ml in coastal and 1000 ml in oceanic stations) using GF/F filters (Whatmann). The filtration was done under dim light, and all filters were kept frozen in liquid nitrogen. Replicates of filtered samples from the spring cruise were analyzed in Canada according to Stuart et al. (1998, 2004). The in vivo light absorption spectra of particles, $a_p(\lambda)$, were measured using the filter technique of Mitchell et al. (2000), at 1 nm resolution in a Shimadzu UV-1203 spectrophotometer. To determine the absorption by detrital material, pigments were extracted using hot methanol. Detritus absorption ($a_d(\lambda)$) was corrected using exponential curve adjustments for each sample: $a_d(\lambda) = a_d(\lambda_0) \exp[-S(\lambda-\lambda_0)]$; this allowed the calculation of the coefficient describing the exponential slope of the absorption curve (S) (Roesler et al., 1989; Hoepffner and Sathyendranath, 1993). To obtain the phytoplankton light absorption spectra ($a_{ph}(\lambda)$), the values of $a_d(\lambda)$ were subtracted from $a_p(\lambda)$. The specific absorption coefficients of phytoplankton ($a^*(\lambda)$) were calculated by dividing the $a_{ph}(\lambda)$ estimates at 442 and 676 nm, by the sum of Chl-*a* plus Phaeo concentration (Sathyendranath et al., 1999). The path-length amplification factor was corrected using the algorithm of Cleveland and Weidemann (1993). The scattering was corrected

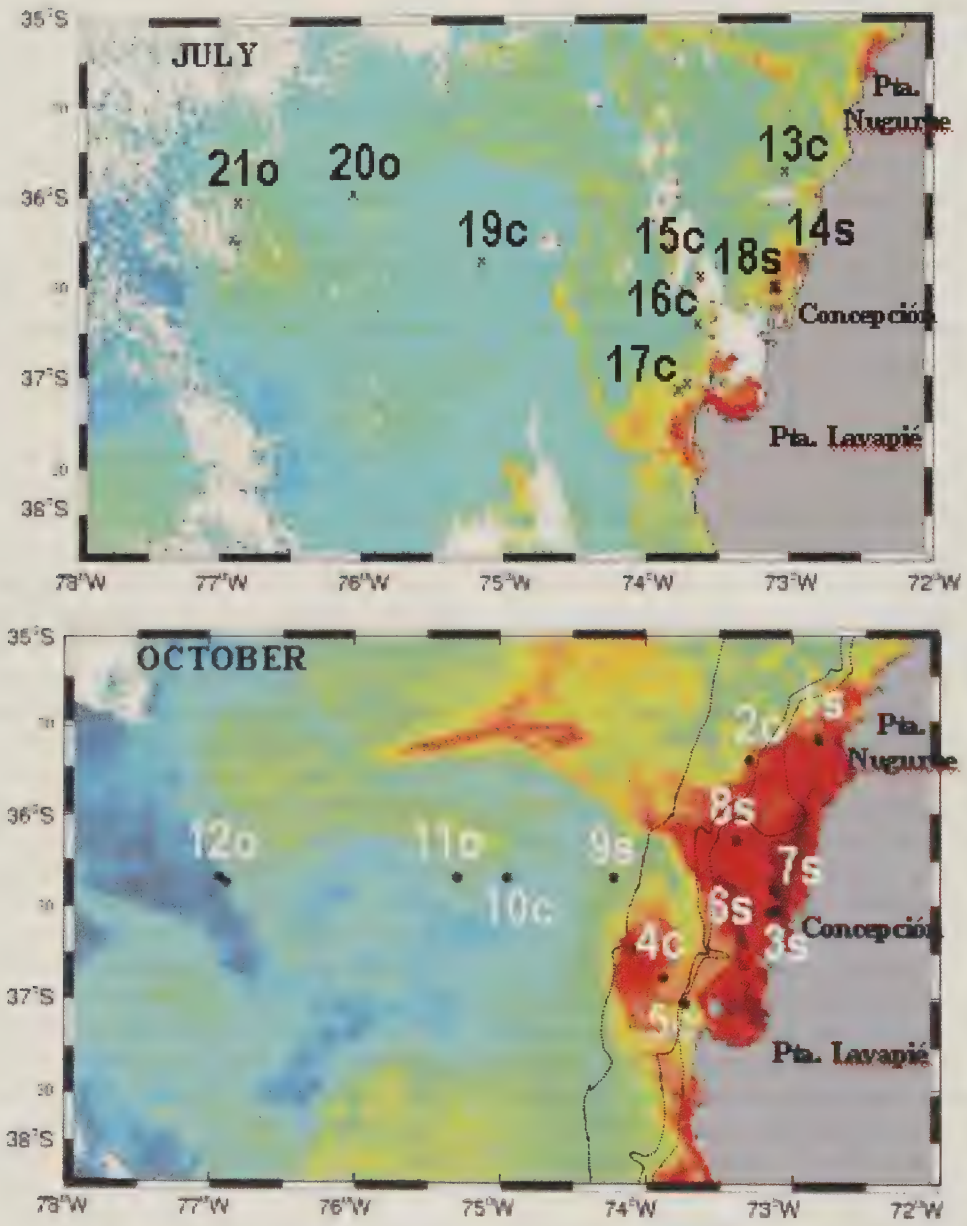

Fig. 1. The location of the study area off Concepción, Chile (arrow), off the Pacific coast of South America (left panel). SeaWiFs Chl-*a* (C_{sat}) color images (right panel) for austral spring, 23 October 1998 (upper right), and austral winter, 15 July 1999 (bottom right) showing C_{sat} distribution during upwelling and non-upwelling conditions. The color bar indicates the Chl-*a* concentrations (mg m^{-3}). Depth contours for 200, 600 and 3000 m are also given in the October image. The sampling station numbers are followed by letters corresponding to their location (s = shelf, c = coastal, o = oceanic), and the largest numbers for each cruise correspond to the offshore stations.

subtracting the absorption between 700 and 750 nm from each spectrum as suggested by Mitchell et al. (2000).

On deck incubations for simulated in situ PP measurements were conducted almost daily with samples from six depths in the Z_{eu}. After sampling

Table 1
Dates, location, and station numbers during spring (October 1998, Oct) and winter (July 1999, Jul) cruises. Depth (m) and fluorometer Chl-*a* (mg m^3) of samples used in the photosynthesis versus irradiance experiments. Photosynthetic parameters α^B [mg C (mg Chl-*a*)$^{-1}$ h^{-1} (μmol quanta m^{-2} s^{-1})$^{-1}$] and P^B_{max} [mg C (mg Chl-*a*)$^{-1}$ h^{-1}]. Z_{eu} is the euphotic depth (m) used for the calculations of daily integrated primary production (PP) that are given separately for the simulated in situ (SIS) or in situ (IS) incubation procedures in mg C m^{-2} d^{-1}

Dates[a]	Location[b]	Station[c]	Depth	Chl-*a*	α^B	P^B_{max}	Z_{eu}	Daily PP	
								SIS	IS
5-Oct	Shelf	1s	3	26.16	0.033	3.52			
	Shelf	1s	10	26.13	0.022	3.12			
	Coastal	2c	0	6.96	xx	3.12	26.2	7.48	
	Coastal	2c	19	7.07	0.023	3.82			
7-Oct	Shelf	3s	5	3.58	0.025	2.43			
	Coastal	4c	10	0.24	0.016	1.52			
8-Oct	Coastal	5c1					38.0		0.68
	Coastal	5c2					x	1.14	
9-Oct	Coastal	5c3					32.2	1.95	
	Coastal	5c4	10	6.05	0.021	1.71			
	Coastal	5c4	17	4.43	0.019	1.74			
0-Oct	Shelf	6s					16.4	1.08	
1-Oct	Shelf	7s1					18.2	3.18	
2-Oct	Shelf	7s2	5	14.52	0.023	3.63	18.9		
	Shelf	7s2	10	14.39	0.02	3.04			
3-Oct	Shelf	8s1					11.7	4.06	
	Shelf	8s2	10	20.81	0.018	3.3			
4-Oct	Shelf	9s	10	16.14	0.019	2.84	19.0		
	Coastal	10c	3	3.79	0.03	1.38			
	Coastal	10c	10	3.78	0.021	1.18			
25-Oct	Oceanic	11o					78.0	0.49	
26-Oct	Oceanic	12o1					104.0	0.2	
26-Oct	Oceanic	12o2	10	0.44	0.011	1.21			
27-Oct	Oceanic	12o3					130.0		0.3
	Oceanic	12o4					x	0.59	
16-Jul	Coastal	13c1	17	1.06	0.043	3.97			
16-Jul	Coastal	13c1	25	0.98	0.019	2.7			
16-Jul	Coastal	13c2					58.8		0.63
15-Jul	Shelf	14s	5	1.89	0.026	4.82	56.9		
15-Jul	Shelf	14s	17	1.12	0.023	2.12			
15-Jul	Coastal	15c						0.5	
14-Jul	Coastal	16c						0.81	
13-Jul	Coastal	17c3	0	1.00	0.046	7.02			
13-Jul	Coastal	17c3	10	1.01	0.032	4.88			
13-Jul	Coastal	17c2					54.0		0.17
12-Jul	Coastal	17c1					59.3	0.66	
11-Jul	Shelf	18s2					52.5		0.32
10-Jul	Shelf	18s1					66.1	1.93	
9-Jul	Coastal	19c					76.2	1.15	
8-Jul	Oceanic	20o					72.6	0.35	
7-Jul	Oceanic	21o3							0.19
6-Jul	Oceanic	21o2					102.0		0.15
5-Jul	Oceanic	21o1	0	0.23	0.066	2.76			
5-Jul	Oceanic	21o1	25	0.25	0.029	3.99			

[a]Dates are in reverse chronological order in July, so that the largest numbers in each cruise correspond to the offshore stations.
[b]Location according to bottom depth: shelf < 200 m, coastal > 500 m, oceanic > 3000 m.
[c]Letters after Station number refer to s = shelf, c = coastal, o = oceanic, and number after letter represent different casts. x = same as previous cast, xx = outlier.

(around noon), 20 μCi Na $H^{14}CO_3$ were added to three transparent and two opaque 100 ml bottles for each depth. These bottles were immediately placed in six cylinders at sea-surface temperature and exposed to surface irradiance (Io) (from 90% to 0.2%) over a period of 5–7 h (Montecino and Quiroz, 2000). Whenever possible, in situ PP incubations from early morning to dawn also were done at the six original depths, following the same protocol. For daily PP calculations, the integration of Baines et al. (1994) was used. The photosynthesis-irradiance experiments (*P–E* curves) were performed with two depth samples: one from the near surface (3–10 m) and one from the Chl-*a* maximum within the mixed layer (< 25 m depth). Both samples were inoculated separately with 1 μCi Na $H^{14}CO_3$ per ml, filling immediately after 18 vials per depth that were placed in a thermoregulated miniaturized incubator; the two sets of vials were incubated for 1 h, as described in Montecino et al. (1996). The photosynthetic parameters P^B_{max}, maximum photosynthetic rate normalized by Chl-*a* and α^B, the Chl-*a* specific initial slope of the *P–E* curve, were obtained from a non-linear fit of the P^B versus *E* data to the hyperbolic tangent model of Jassby and Platt (1976). No offset was established for these *P–E* curves (Markager et al., 1999).

Definition of trophic regimes, from oligotrophic to hypertrophic, was done according to the simple classification proposed by Nixon (1995). These values, based on yearly carbon fixation rates, were expressed as daily rates so as to make them comparable with the results of this study. Values are as follows (in $g C m^{-2} d^{-1}$): <0.27 for oligotrophic, 0.27–0.82 for mesotrophic, 0.82–1.37 for eutrophic, and >1.37 for hypertrophic waters.

Discriminate analysis was used to distinguish the station or sample groups with similar parameter combinations. Four parameters (α^B, P^B_{max}, $a_{ph}(442)$, and the $a^*(442)/a^*(676)$ ratio), previously identified by cluster analysis, were used to characterize the different groups. Parameter values were log-transformed to overcome differences in their magnitudes. One of the selected variables—the $a^*(442)/a^*(676)$ ratio—was disregarded by the software because of its high correlation with $a_{ph}(442)$.

3. Results

Off Concepción, the distribution of satellite Chl-*a* (C_{sat}) is shown through the SeaWiFs images from 23 October 1998 and 15 July 1999 for the upwelling (austral spring) and non-upwelling season (winter), respectively (Fig. 1). In the October image, the offshore gradients are noticeable, and three large regions can be identified: the shelf and coastal regions (highest C_{sat} values), the open-ocean region (lowest values), and an intermediate zone (upwelling plume). In the July image, C_{sat} differences between the coastal and the intermediate zone are subtler. This pattern is also observed in the in situ abundance of phytoplankton biomass; surface Chl-*a* values ranged from 0.35 to ~25 $mg m^{-3}$ in the upwelling season and were restricted to ⩽1.5 $mg m^{-3}$ in the non-upwelling season. In October, shelf stations differed from the rest in showing a stratified distribution and the highest surface values; in July, the coastal stations attained the largest Chl-*a* values (Fig. 2). The depth of the euphotic zone (Z_{eu}) increased from the coast toward the open ocean and had different ranges on each cruise (Table 1): >100 m in October and <50 m in July.

Fig. 3 shows the large variability in $a^*(\lambda)$ estimates between cruises. In the different zones, the $a^*(\lambda)$ spectra in October are flattened (Fig. 3A) with respect to those in July, where the two maximum absorption peaks in the blue (~442 nm) and red (~676 nm) regions are well-defined (Fig. 3B). In both seasons, the oceanic spectra were characterized by a slight shift of the blue peak to longer wavelengths. At 442 nm, the spectra from the upwelling region at Punta Lavapié (Station 5) showed the lowest values in October and intermediate values in July. The maximum $a^*(442)$ values were 0.024 m^2 (mg Chl-*a* + Phaeo)$^{-1}$ in October and 0.047 m^2 (mg Chl-*a* + Phaeo)$^{-1}$ in July.

Spectral transmittance ($T(\lambda)$) in surface waters from the upper 10 m samples showed a distinct pattern between the upwelling and non-upwelling seasons and also in space. The transmittance data from the October cruise (Fig. 4A) allowed the separation of three water types: high, intermediate, and low $T(\lambda)$ values over the 400–555 nm range. In

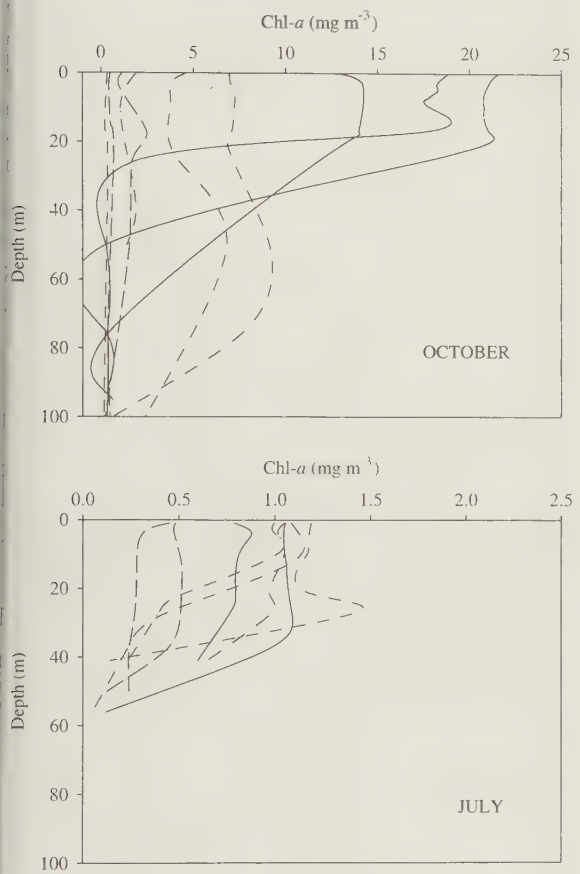

Fig. 2. Vertical Chl-*a* profiles during the upwelling (October 1998) and non-upwelling (July 1999) seasons, distinguishing between shelf (continuous line), coastal (dash–dot–dot line), and oceanic (long dash line) stations. Notice the 10 fold decrease of the Chl-*a* axis for the July cruise.

the upwelling season, $T(442)$ values over the whole area ranged from 6% to 88%. The $T(\lambda)$-intermediate water types were those of the upwelling plume (Punta Lavapié), which can be identified by their similar transmittance values (50–55% at $T(489)$ and $T(555)$), producing a flat spectral shape. The intermediate pattern differs significantly from the spectral shape of oceanic waters, in which an increasing slope was obtained between $T(555)$ and $T(489)$, and are also different from the shelf waters, in which the slope decreased between $T(555)$ and $T(489)$. In the non-upwelling season, the $T(442)$ values over the entire area varied less, ranging from 42% to 78%. Therefore, only two water types were identified: oceanic and intermediate (Fig. 4B). Mean Chl-*a* values from the upper 10 m are also clearly different between water columns: <10, 10–40, and $>100\,\mathrm{mg\,m^2}$ for high, intermediate, and low transmittance water types, respectively (Fig. 4C).

Phytoplankton light absorption $a_{ph}(442)$ and $T(442)$ displayed a logarithmic relationship (Fig. 5), with similar slopes ($p<0.01$) in the data from the two cruises, including the smaller range of $a_{ph}(\lambda)$ values during the July cruise and those with a larger range from the same October 1998 cruise measured separately by Stuart et al. (2004). Combining the data of both cruises, daily PP—from simulated in situ measurements—was significantly correlated with Z_{eu}-integrated Chl-*a* ($R^2=0.96$, $n=15$, $p<0.0001$), though there was a greater variability at concentrations $<60\,\mathrm{mg\ Chl\text{-}a\,m^{-2}}$ ($R^2=0.45$, $n=9$, $p<0.15$; Fig. 6). In October, PP ranged between 0.68 and $7.48\,\mathrm{g\,C\,m^{-2}\,d^{-1}}$ at coastal and shelf stations, including simulated in situ and in situ incubations, and was $<0.59\,\mathrm{g\,C\,m^{-2}\,d^{-1}}$ at oceanic stations (Table 1); in July, the values ranged between 0.15 and $1.93\,\mathrm{g\,C\,m^{-2}\,d^{-1}}$ in the whole area. Nevertheless, the frequency distribution of daily PP ($n=22$) indicated that the two dominant frequencies for both cruises corresponded to mesotrophic (0.27–$0.82\,\mathrm{g\,C\,m^{-2}\,d^{-1}}$) and eutrophic ($0.82$–$1.37\,\mathrm{g\,C\,m^{-2}\,d^{-1}}$) waters. The PP difference found between cruises ($\chi^2=6.32$, $p<0.05$) is given by the significant difference ($t_s=1.74$, $p<0.05$) in the hypertrophic water range ($>1.37\,\mathrm{g\,C\,m^{-2}\,d^{-1}}$), since the analysis indicated that the oligotrophic water range ($<0.27\,\mathrm{g\,C\,m^{-2}\,d^{-1}}$) was similar for both periods.

When considering all available data on the photosynthetic parameters, α^B and P^B_{max}, both were significantly higher in July than in October (Table 2). Moreover, using a smaller data set, based on the coincident α^B and $a^*(442)$ measurements, the relationship between α^B and $a^*(442)$ clearly shifted between cruises (Fig. 7). In July, the non-upwelling season, a larger variability especially in the α^B axis was obtained.

To assess the degree of similar characteristics between stations or depths in each cruise, discriminant functions (DFs) were analyzed by

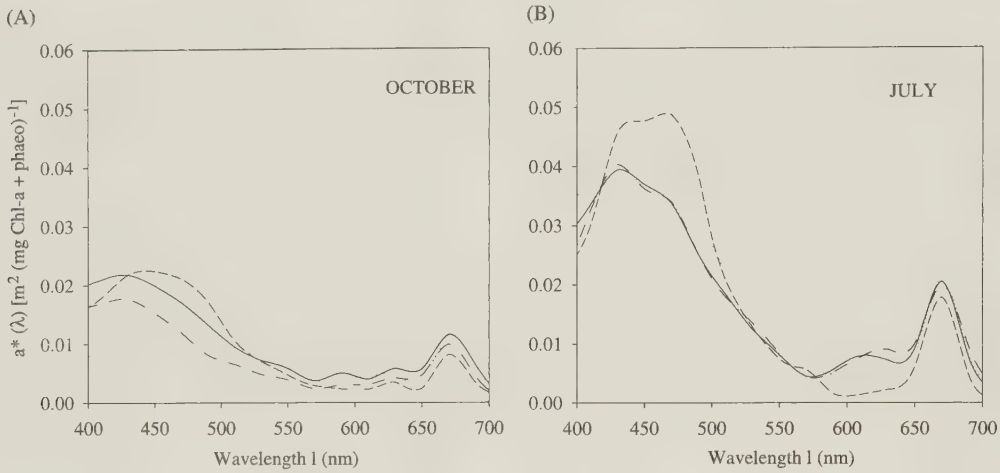

Fig. 3. In vivo specific (fluorometric Chl-a + Phaeo) absorption [$a^*(\lambda)$] during (A) October 1998 and (B) July 1999 cruises. The $a^*(\lambda)$ spectra between 400 and 700 nm correspond to 10 m depth samples from representative coastal, shelf, upwelling center (Punta Lavapié, south of 37°S), and oceanic sites (200 nautical miles). Same notation as in Fig. 2 plus dotted line for upwelling center samples.

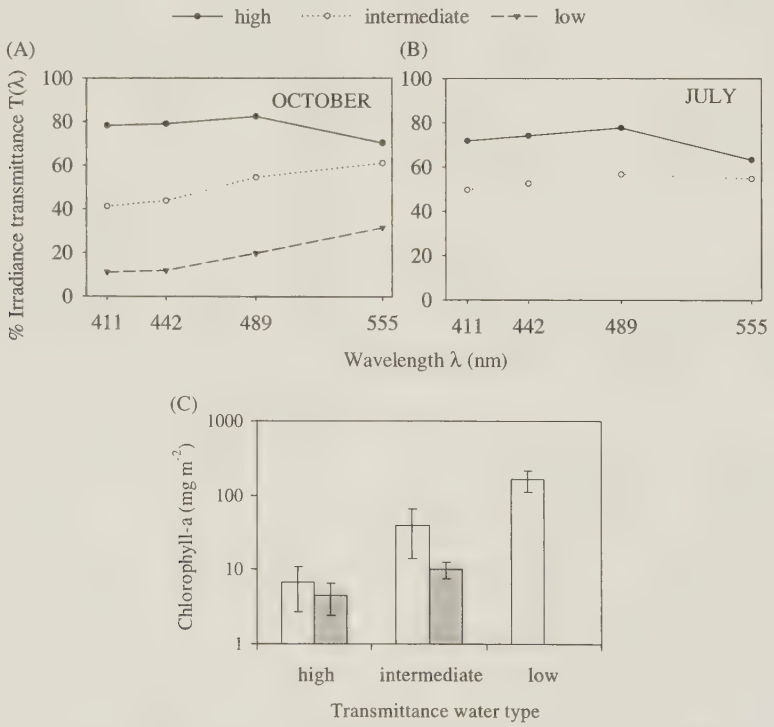

Fig. 4. Mean spectral surface transmittance $T(\lambda)$ between 411 and 555 nm during October 1998 and July 1999 cruises. October 1998 (A): oceanic, upwelling center (Punta Lavapié) and coastal or shelf stations characterizing high, intermediate, and low transmittance waters, respectively ($n = 13$). July 1999 (B) only high (oceanic stations) and intermediate (all other sites) transmittance water types were found ($n = 11$). Water type transmittance with respect to integrated (0–10 m) values of Chl-a during October 1998 (clear bar) and July 1999 (gray bar) cruises (C), distinguishing between high ($<6.8\,mg\,m^2$), intermediate (10.1 39.5 mg m^2), and low (163.6 mg m^2) T water types.

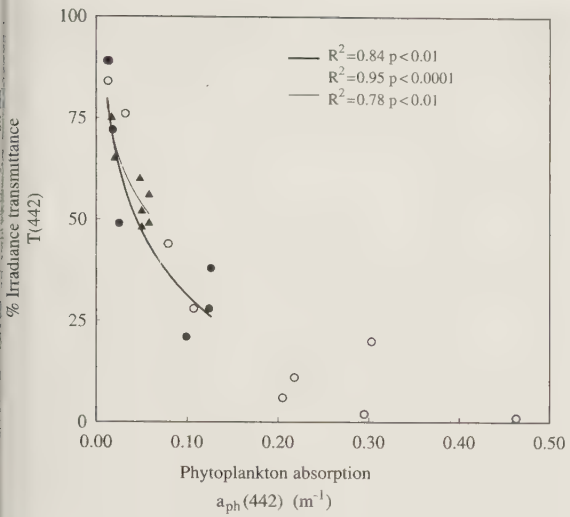

Fig. 5. Relationship between phytoplankton absorption ($a_{ph}(442)$) from surface waters with transmittance ($T(442)$): October 1998 cruise (solid circles) and July 1999 cruise (solid triangles) data represent mean values for the upper 10 m layer; open circles represent data for the same October 1998 cruise, as measured separately by Stuart et al. (2004). The value of R_2 and ANOVA probability for each relationship is given.

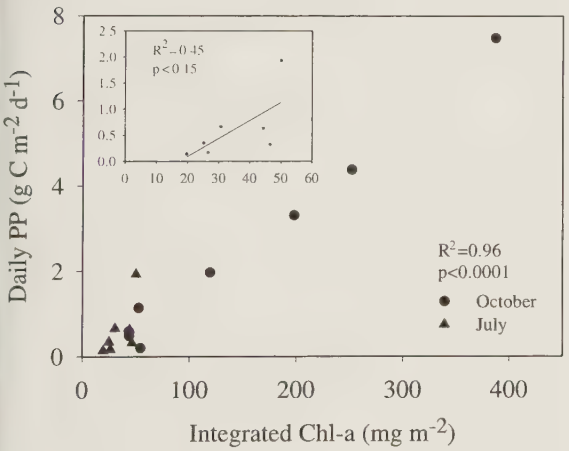

Fig. 6. Relationship between Z_{eu} integrated Chl-a and daily PP, combining data from both the October 1998 and July 1999 cruises. The insert shows an enlargement of the results < 60 mg Chl-a m^{-2}.

combining three parameters: α^B, P^B_{max}, and $a_{ph}(442)$. Three significant DFs were found for October ($p<0.001$) and two for July ($p<0.05$). In October 70.7% and 28.4% of the total variance

Table 2
Non parametric Mann–Whitney test comparing the photosynthetic parameters of the P–E curve: α^B [mg C mg Chl-a^{-1} h^{-1} (μmol quanta m^{-2} s^{-1})$^{-1}$] and P^B_{max} [mg C (mg Chl-a)$^{-1}$ h^{-1}] between cruises (n = number of cases, U = test statistics)

Variable	Median	n	U	P
α^B				
Spring (October)	0.021	15	27	0.033*
Winter (July)	0.031	8		
P^B_{max}				
Spring (October)	2.84	15	25	0.024*
Winter (July)	3.98	8		

*$p<0.05$.

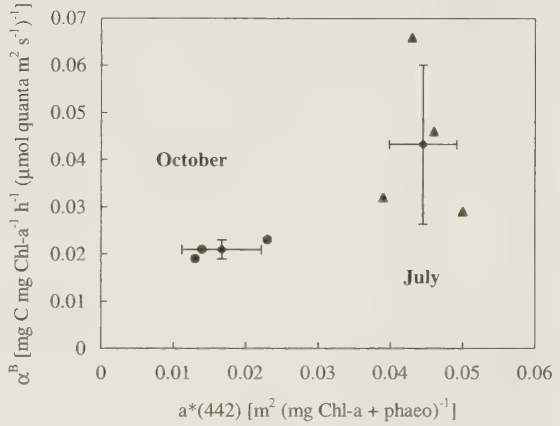

Fig. 7. Distribution of the values on Chl-a + Phaeo specific absorption coefficient at 442 nm [a*(442)] Versus the initial slope (α^B) of the P–E curves at different stations but from coincident sample depths (0–25 m) during the October 1998 (dots) and July 1999 (triangles) cruises. The mean value and standard error is also shown for each cruise.

was explained by DF-I and DF-II with 0.959 and 0.905 canonical correlation values, respectively. The stations were better separated by DF-I than by DF-II (Fig. 8A). The first DF was highly associated with $a_{ph}(442)$ and P^B_{max} and the second with α^B. One of the resulting groups was formed with stations from the shelf, except for one coastal station (2c, 19 m). This group presented higher $a_{ph}(442)$ and P^B_{max} values than the other group. The two DFs found in July explained 95.7% and 4.3% of total variance with 0.977 and 0.700 canonical correlation values, respectively. The highest variability between groups was found for

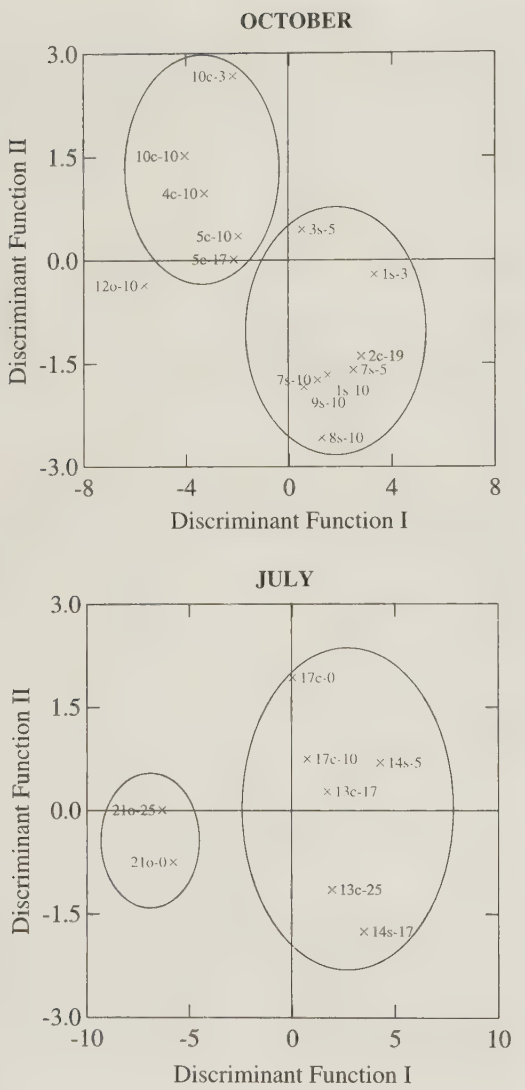

Fig. 8. Distribution of the stations for the two first DFs as the result of combining three parameters [α^B, P^B_{max}, and $a_{ph}(440)$] obtained during the upwelling (October 1998) and non-upwelling (July 1999) cruises. The sample depth of each station is given next to the station name.

DF-I (Fig. 8B). DF-I was highly associated with $a_{ph}(442)$, whereas DF-II was associated with P^B_{max}. Two groups are separated according to DF-I, one with high and the other one with low $a_{ph}(442)$ values. In the first group, a separation exists between samples from shallow depths (<17 m), showing higher P^B_{max} values, and those from deeper depths, showing lower P^B_{max} values. These results indicate that the horizontal variability of the system could be higher during the upwelling season.

4. Discussion

The spatial and temporal distribution of bio-optical properties and the variability of phytoplankton photosynthesis are key variables in the definition of carbon export ratios. In this context the bio-optical parameters measured in the highly productive coastal upwelling zone off Concepción (~36°S), along with biomass abundance and physiological characteristics of phytoplankton, revealed large seasonal variability under upwelling (October) and non-upwelling (July) conditions.

The bio-optical parameters and the carbon fixation rates were significantly variable among geographically similar sites. The largest differences were observed from the shelf to the oceanic direction, especially during October. These differences have been used elsewhere to define the limits and the size of productive habitats in terms of concentration of surface Chl-*a* equal to 1 mg m^{-3} (Nixon and Thomas, 2001). Off Concepción, where the 200 m isobath approaches the coast only at the Bio-Bio submarine canyon, the large area of high Chl-*a* concentrations found in October and the persistence of high PP values can be attributed to wind driven coastal upwelling and increased residence time of upwelled waters over the 60-km-wide shelf (Peterson et al., 1988). C_{sat} and in situ surface Chl-*a* values were below 1 mg m^{-3} at only a few sites, including the two oceanic stations (Figs. 1 and 2). Therefore, in the present study, Chl-*a* was the main state variable controlling the bio-optical properties on the regional scale.

The seasonality of the bio-optical properties is described by a 2-fold increase in the values of $a^*(\lambda)$ and higher $T(\lambda)$ percentages in July 1999, whereas $a_{ph}(\lambda)$ values decreased (Figs. 3–5). The same difference occurs spatially when the oceanic sites are compared with the nearshore ones for all of these parameters. Phytoplankton absorption variability off Concepción (0.010–0.460 m^{-1}) is comparable to the $a_{ph}(440)$ range for Canadian

estuarine waters (from 0.020 to 0.300 m^{-1}), as reported by Babin et al. (1993). The specific phytoplankton absorption, ranging from 0.012 to 0.047 m^2 (mg Chl-*a*+*Phaeo*)$^{-1}$ for $a^*(442)$, agrees well with the range of 0.030–0.060 m^2 (mg Chl-*a*+Phaeo)$^{-1}$ reported for coastal water off Perú (Bricaud and Stramski, 1990) but are lower than the 0.100 m^2 (mg Chl-*a*+Phaeo)$^{-1}$ value reported for the southern California Current (Sosik and Mitchell, 1995). These light absorption results indicate that phytoplankton assemblages in these nearshore and offshore waters have special bio-optical characteristics, particularly during non-upwelling conditions; this reasoning is based on $a^*(440)$ results that never exceeded values of 0.100 m^2 (mg Chl-*a*+Phaeo)$^{-1}$ as reported for oligotrophic sites (Bricaud et al., 1995; Babin et al., 1996).

Related to the photosynthetic parameters, and from the analysis of the entire data set, the slightly higher α^B values obtained in the non-upwelling season (Table 2) could be explained by the significant increase in $a^*(\lambda)$. This is shown in the $a^*(442)$ versus α^B relationship (Fig. 7), with both parameters drawn from coincident samples. It is this increase in $a^*(442)$ that allows an enhancement of the phytoplankton light-limited efficiency—α^B—in the *P* versus *E* relationship. P^B_{max} experienced a 30% increase from the upwelling to the non-upwelling season (2.84 in October 1998 to 3.98 mg C mg Chl-a^{-1} h^{-1} in July 1999) (Table 2), though both mean values were below the annual mean of 5.20 mg C mg Chl-a^{-1} h^{-1} reported previously for this area (Montecino et al., 1998). Moreover, unweighted quantum yield estimations showed that seasonal variability was small (V. Montecino, unpublished data). During the upwelling season, the maximum values of $a^*(442)$, α^B and P^B_{max} were close to the minimum values during the non-upwelling one. Most probably, these changes are related to changes in species composition, including size composition, and, therefore, changes in optical cross-section in the non-upwelling season. Some of these results are also comparable to the seasonal patterns of photosynthetic parameters in a lower latitude upwelling area (off Coquimbo, 30°S), where α^B was higher in winter than in spring (Montecino et al., 1996), explained by changes in $a^*(\lambda)$ and species composition. At this northern site, the decrease in Chl-*a* specific primary production (P^B) during spring–summer was explained by an increase in phytoplankton cell size (Montecino and Quiroz, 2000). Therefore, and according to allometric considerations, the decrease in cell size should occur preferentially under light limitation, notwithstanding interspecific variability and photo-acclimatization.

Cell size is known to affect photosynthetic parameters and light absorption. By specifying the cell size of the dominant organisms, more than 80% of the variability in the spectral shape of the phytoplankton absorption coefficient was recently explained by Ciotti et al. (2002). Off Concepción, fractionated PP throughout the October cruise (V. Montecino, unpublished data) indicated that the highest carbon-fixation rates (> 10.0 mg C m^{-3} d^{-1}) at specific depths had a negligible contribution (< 10%) from the smaller size fraction (< 8 μm). Moreover, HPLC analysis of pigment composition revealed high fucoxanthin/Chl-*a* ratios at the nearshore stations, indicative of phytoplankton being dominated by diatoms (Stuart et al., 2004). This is opposite to results found in high-nutrient upwelling areas off northern Chile (Antofagasta and Coquimbo), where upwelling interacts with a narrower continental shelf (Montecino et al., 1998; Montecino and Quiroz, 2000). Furthermore, the inverse relationship of PP with the photosynthetic parameter α^B has been related to the predominance of small-sized phytoplankton off Antofagasta (23°S) and off Coquimbo (30°S) (Iriarte et al., 2000; Montecino and Quiroz, 2000).

Photosynthetic parameters and other relevant biological and environmental factors should not be considered separately when explaining temporal similarities or differences in PP and biomass (Sathyendranath et al., 1999). Results from this study help in understanding the large PP variability known for this area, with monthly averages between 0.30 and 5.90 g C m^2 d^{-1} (Daneri et al., 2000). They also explain the maxima of 9.60 g C m^2 d^{-1} and of 19.90 g C m^2 d^{-1} reported by Fossing et al. (1995) and Daneri et al. (2000), respectively. Measurements during 1998 and 1999

showed that only three stations out of 11 had values falling in the oligotrophic range. The frequency of PP values falling in the eutrophic–hypertrophic ranges represented 50% of the different locations during the October cruise and 18% of the results obtained in the July cruise. This corroborates that the HCS system off Concepción is one of the most productive areas in the world, even during non-upwelling conditions. The present empirical evidence about the adjustments of phytoplankton assemblages to light availability further supports the interseasonal maintenance of production levels in this highly productive nearshore region. The differences in phytoplankton performance can be attributed to biological and physical factors; however, nutrient concentrations ($\sim$1 μM $P\text{-}PO_4$) and temperature conditions ($\sim$12.0 °C) were very similar between the two cruises. This temperature similarity is due to the presence of Equatorial subsurface waters that replace the Subantarctic waters found nearshore during winter. The composition of phytoplankton assemblages between cruises changed from *Chaetoceros–Thalassiosira* and dinoflagellates to pennate diatom populations, whereas the abundance decreased from 10^9 to 10^7 cells ml^{-1} (H. González, pers. comm.). Probably by being exposed to a more turbulent mixed layer, specific populations were prevented from remaining under the appropriate light conditions (>50 m euphotic water column). Therefore, the highest $a^*(\lambda)$ range in winter (Fig. 3) is likely to be related to differences in the assemblage's cell size structure, pigment packaging, and pigment composition, already discussed in relation to photosynthetic parameters variability.

As described for the California Current (Abbott and Letelier, 1998; Hayward and Venrick, 1998), differences between offshore and inshore regimes found over a smaller spatial scale in the present study also can be attributed to population differences in cell size or growth strategies. The variability shown by the majority of the continental shelf samples in light absorption and in photosynthetic parameters (Fig. 8) can be attributed either to the local effect of upwelled waters or to the runoff influence of the Bio-Bio and Itata rivers. The analysis of these phytoplankton parameters identified two spatial patterns: one wit more horizontal variability than the other. Th three groups formed in spring revealed th horizontal heterogeneity of the system wher the particle load, including Chl-*a*, was highes over the shelf contributing to low-transmittanc waters. This was probably a result of the upwelle waters segregating the nearshore stations into tw groups. The evidence that those stations closer t the upwelling plume differ from the other tw groups (Fig. 4), indicative of the tight physical– biological coupling, allows the identification o different water types expanding on the oceanic anc coastal waters types of Jerlov, and the classifica tion in clear and green waters of Barnard et al (1999). The second pattern, obtained in the non upwelling season, indicates that the largest varia bility occurred mostly on the vertical scale. One of the groups included the surface samples and the other the deeper samples, revealing a more horizontal homogeneity of the system.

Related to the known environmental effects on phytoplankton photosynthesis (Platt and Jassby, 1976; Bouman et al., 2003), the seasonal differences in the phytoplankton size structure, biomass, absorption properties, and light-limited efficiency found in the inshore–offshore sites off Concepción occurred over relatively small spatial scales. Since several studies have examined the variability of model parameters (Babin et al., 1993; Bricaud et al., 1995; Sosik, 1996), estimates of annual primary production and remote sensing applications on a regional scale require consideration, not only of the alongshore variability, but also of the vertical variability in this surface waters (Fig. 8). This small scale variability leads to a final consideration related to the association of high production with high phytoplankton biomass, which, facing a sustained increase in the organic matter supply rate (Baines et al., 1994; Nixon, 1995), could ultimately cause eutrophication in these continental shelf or nearshore ecosystems. The combination of daily PP with bio-optical parameters (such as the decrease in transmittance) obtained in different cruises and sites clearly identified the sites that are most susceptible to eutrophication. These areas are those adjacent to the Concepción Bay and the most productive coastal and shelf

ctor north of 36°30′S (Rio Itata–Punta Nugurne) Table 1).

To summarize, based on the bio-optical patterns ound in nature that result from the interactions etween spectral light availability and the changes the efficiency of phytoplankton light utilization, e have shown differences in coastal water ructure and small-scale environmental condi- ons in time for the area off Concepción. Through hysical or biological separation/aggregation of eographical zones, we have also demonstrated hat the water column operates as a compound io-optical system. In addition to the paired elationships between parameters, such as $a_{ph}(\lambda)$ ith $T(\lambda)$, biomass with PP, and $a^*(\lambda)$ with α^B, the ombination of three biological parameters ac- ount for the differences among and within tations for upwelling and non-upwelling condi- ions, allowing a more detailed understanding of ow this system shifts seasonally.

Acknowledgements

This research was supported by grants from CONICYT (FONDAP-Humboldt and FONDECYT No. 1960875), the Universidad de Chile (V. Montecino), NASA (A. Thomas), and GLOBEC (T. Strub). The invaluable help of S. Pegau during V.M.'s visit to Oregon State University (USA) and of G. Yuras in providing images and a bathymetric chart for Fig. 1 are acknowledged. We thank V. Lutz, V. Stuart, and O. Ulloa for helpful comments during earlier versions of this manuscript and three anonymous reviewers for their important suggestions.

References

Abbott, M., Letelier, R., 1998. Decorrelation scales of chlorophyll as observed from bio-optical drifters in the California Current. Deep-Sea Research II 45, 1639–1667.

Babin, M., Therriault, J.C., Legendre, L., Condal, A., 1993. Variations in the specific absorption coefficient for natural phytoplankton assemblages: impact on estimates of primary production. Limnology and Oceanography 38, 154–177.

Babin, M., Morel, A., Claustre, H., Bricaud, A., Kolber, Z., Falkowski, P., 1996. Nitrogen- and irradiance-dependent variations of the maximum quantum yield of carbon fixation in eutrophic, mesotrophic and oligotrophic marine systems. Deep-Sea Research I 43, 1241–1272.

Baines, S., Pace, M., Karl, D., 1994. Why does the relationship between sinking flux and planktonic primary production differ between lakes and oceans? Limnology and Oceanography 39, 213–226.

Barnard, A., Zaneveld, J., Pegau, W., Mueller, J., Maske, H., Lara, R., Alvarez, S., Cervantes, R., Valdez, E., 1999. Determinación de niveles de PAR a partir de perfiles del coeficiente de absorción a 490 nm. Ciencias Marinas 25, 487–507.

Bouman, H., Platt, T., Sathyendranath, S., Li, W., Stuart, V., Fuentes, C., Maass, H., Horne, E., Ulloa, O., Lutz, V., Kyewalyanga, M., 2003. Temperature as indicator of optical properties and community structure of marine phytoplankton: implications for remote sensing. Marine Ecology Progress Series 258, 19–30.

Bricaud, A., Stramski, D., 1990. Spectral absorption coefficients of living phytoplankton and nonalgal biogenous matter: a comparison between the Peru upwelling area and the Sargasso Sea. Limnology and Oceanography 35, 562–582.

Bricaud, A., Babin, M., Morel, A., Claustre, H., 1995. Variability in the chlorophyll-specific absorption coefficients of natural phytoplankton: analysis and parameterization. Journal of Geophysical Research 100, 13321–13332.

Bricaud, A., Morel, A., Babin, M., Allali, K., Claustre, H., 1998. Variations of light absorption by suspended particles with chlorophyll a concentration in oceanic (case I) waters: analysis and implications for bio-optical models. Journal of Geophysical Research 103, 31033–31044.

Ciotti, A.M., Lewis, M.R., Cullen, J.J., 2002. Assessment of the relationships between dominant cell size in natural phytoplankton communities and the spectral shape of the absorption coefficient. Limnology and Oceanography 47, 404–417.

Cleveland, J., Weidemann, A., 1993. Quantifying absorption by aquatic particles: a multiple scattering correction for glass-fiber filters. Limnology and Oceanography 38, 1321–1327.

Cuevas, L.A., Daneri, G., Jacob, B., Montero, P., 2004. Microbial abundance and activity in the seasonal upwelling area off Concepción (~36°S), central Chile: a comparison of upwelling and non-upwelling conditions. Deep-Sea Research II, this issue [doi:10.1016/j.dsr2.2004.07.026].

Cullen, J., MacIntyre, J., 1998. Behavior, physiology and the niche of depth-regulating phytoplankton. In: Anderson, D.M., Cembella, A.D., Hallegraeff, G.M. (Eds.), NATO ASI Series. Berlin, Heidelberg, vol. G 41, pp. 559–579.

Daneri, G., Dellarossa, V., Quiñones, R., Jacob, B., Montero, P., Ulloa, O., 2000. Primary production and community respiration in the Humboldt current system off Chile and associated oceanic areas. Marine Ecology Progress Series 197, 41–49.

Farías, L., Graco, M., Ulloa, O., 2004. Temporal variability of nitrogen cycling in continental-shelf sediments of the upwelling ecosystem off central Chile. Deep-Sea Research II, this issue [doi:10.1016/j.dsr2.2004.07.029].

Fossing, H., Gallardo, V.A., Joergensen, B.B., Huttel, M., Nielsen, L.P., Schulz, H., Canfield, D.E., Foster, S., Glud, R.N., Gundersen, J.K., Kuver, J., Ramsing, N.B., Teske, A., Thamdrup, B., Ulloa, O., 1995. Concentration and transport of nitrate by the mat-forming sulphur bacterium *Thioploca*. Nature 374, 713–715.

Hayward, T.L., Venrick, E.L., 1998. Nearsurface pattern in the California Current: coupling between physical and biological structure. Deep-Sea Research II 45, 1617–1638.

Hoepffner, N., Sathyendranath, S., 1993. Determination of the major groups of phytoplankton pigments from the absorption spectra of total particulate matter. Journal of Geophysical Research 98, 22789–22803.

Iriarte, J.L., Pizarro, G., Troncoso, V.A., Sobarzo, M., 2000. Primary production and biomass of size-fractionated phytoplankton off Antofagasta, Chile (23–24 S) during pre-El Niño and El Niño 1997. Journal of Marine Systems 26, 37–51.

Jassby, A.D., Platt, T., 1976. Mathematical formulation of the relationship between photosynthesis and light for phytoplankton. Limnology and Oceanography 21, 540–547.

Jeffrey, S.W., Mantoura, R.F., Wright, S.W., 1997. Phytoplankton Pigments in Oceanography. UNESCO Publishing, Paris, pp. 1–661.

Kiørboe, T., 1993. Turbulence, phytoplankton cell size, and the structure of pelagic food webs. Advances in Marine Biology 29, 1–72.

Kyewalyanga, M., Platt, T., Sathyendranath, S., Lutz, V., Stuart, V., 1998. Seasonal variations in physiological parameters of phytoplankton across the North Atlantic. Journal of Plankton Research 20, 17–42.

Markager, S., Vincent, W.F., Tang, E.P., 1999. Carbon fixation by phytoplankton in high Arctic lakes: implications of low temperature for photosynthesis. Limnology and Oceanography 44, 597–607.

Mitchell, G., Bricaud, A., Carder, K., Cleveland, J., Ferrari, G., Gould, R., Kahru, M., Kishino, M., Maske, H., Moisan, T., Moore, L., Nelson, N., Phinney, D., Reynolds, R., Sosik, H., Stramski, D., Tassan, S., Trees, C., Weidemann, A., Wieland, J., Vodacek, A., 2000. Determination of spectral absorption coefficients of particles, dissolved material and phytoplankton for discrete water samples. In: Fargion, G.S., Mueller, J.L. (Eds.), Ocean Optics Protocols for satellite Ocean Color Sensor Validation, Revision 2. NASA, Greenbelt, Maryland, pp. 125–153.

Montecino, V., Quiroz, D., 2000. Specific primary production and phytoplankton cell size structure in an upwelling area off the coast of Chile (30°S). Aquatic Science 62, 364–380.

Montecino, V., Pizarro, G., Quiroz, D., 1996. Dinámica fitoplanctónica en el sistema de surgencia frente a Coquimbo (30°S) a través de la relación funcional entre fotosíntesis e irradianza (P-I). Gayana Oceanología 4, 139–151.

Montecino, V., Pizarro, G., Quiroz, D., 1998. Primary production off the Chilean coast. Proceedings Aha Huliko'a Hawaiian Winter Workshop: Biotic impact of extratropical climate variability in the Pacific. University of Hawaii at Manoa, pp. 69–76.

Nixon, S., 1995. Coastal marine eutrophication: a definitio social causes, and future concerns. Ophelia 4 199–219.

Nixon, S., Thomas, A., 2001. On the size of the Perú upwellir ecosystem. Deep-Sea Research I 48, 2521–2528.

O'Reilly, J.E., Maritorena, S., Mitchell, B.G., Siegel, D.A Carder, K.L., Garver, S.A., Kahru, M., McClain, C., 199 Ocean color chlorophyll algorithms for Sea WiFS. Journa Geophysical Research 103, 24937–24953.

Peterson, W.T., Arcos, D.F., McManus, G.B., Dam, H Bellantoni, D., Johnson, T., Tiselius, P., 1988. Th nearshore zone during coastal upwelling: daily variabilit and coupling between primary and secondary productio off Central Chile. Progress in Oceanography 20, 1–40.

Platt, T., Jassby, A., 1976. The relationship between photo synthesis and light for natural assemblages of coasta marine phytoplankton. Journal of Phycology 12, 421–430.

Platt, T., Sathyendranath, S., Longhurst, A., 1995. Remot sensing of primary production in the ocean: promise and fulfillment. Philosophical Transactions of the Royal Society of London B 348, 191–202.

Roesler, C., Perry, M.J., Carder, K.L., 1989. Modeling in situ phytoplankton absorption from total absorption spectra in productive inland marine waters. Limnology and Oceanography 34, 1510–1523.

Rutllant, J., Montecino, V., 2002. Multiscale upwelling forcing cycles and biological response off north-central Chile. Revista Chilena de Historia Natural 75, 217–231.

Sathyendranath, S., Stuart, V., Irwin, B., Maass, H., Savidge G., Gilpin, L., Platt, T., 1999. Seasonal variations in bio-optical properties of phytoplankton in the Arabian Sea. Deep-Sea Research II 46, 633–653.

Siegel, D., Michaels, A., Sorensen, J., O'Brien, M., Hammer, M., 1995. Seasonal variability of light availability and utilization in the Sargasso Sea. Journal of Geophysical Research 100, 8695–8713.

Sosik, H., 1996. Bio-optical modeling of primary production: consequences of variability in quantum yield and specific absorption. Marine Ecology Progress Series 143, 225–238.

Sosik, H., Mitchell, G., 1995. Light absorption by phytoplankton, photosynthetic pigments and detritus in the California current system. Deep-Sea Research I 42, 1717–1748.

Stuart, V., Sathyendranath, S., Platt, T., Maass, H., Irwin, B.D., 1998. Pigments and species composition of natural phytoplankton populations: effect on the absorption spectra. Journal of Plankton Research 20, 187–217.

Stuart, V., Ulloa, O., Alarcón, G., Sathyendranath, S., Major, H., Head, E., Platt, T., 2004. Bio-optical characteristics of phytoplankton populations in the upwelling system off the coast of Chile. Revista Chilena de Historia Natural 77, 87–105.

Thomas, A.C., Blanco, J.L., Carr, M.E., Strub, P.T., Osses, J., 2001. Satellite-measured chlorophyll and temperature variability off northern Chile during the 1996–1998 La Niña and El Niño. Journal of Geophysical Research 106, 899–915.

Walsh, J.J., 1981. A carbon budget for overfishing off Perú. Nature 290, 300–304.

ELSEVIER

Deep-Sea Research II 51 (2004) 2427–2440

DEEP-SEA RESEARCH
PART II

www.elsevier.com/locate/dsr2

Microbial abundance and activity in the seasonal upwelling area off Concepción (~36°S), central Chile: a comparison of upwelling and non-upwelling conditions

L. Antonio Cuevas[a,b,*], Giovanni Daneri[b,c], Bárbara Jacob[b,c], Paulina Montero[b,c]

[a] *Programa de Postgrado en Oceanografía, Departamento de Oceanografía, Universidad de Concepción, Casilla 160-c, Concepción, Chile*
[b] *Centro de Investigación Oceanográfica en el Pacífico Sur-Oriental (FONDAP-COPAS), Universidad de Concepción, Casilla 160-C, Concepción, Chile*
[c] *Centro de Ciencias y Ecología Aplicada (CEA), Universidad del Mar, Carmen 446, Valparaíso, Chile*

Accepted 25 July 2004

Abstract

The contribution of bacteria and nanoflagellates to marine carbon flux was studied in the upwelling area off Concepción, central Chile (~36°S), at coastal shelf and oceanic stations, during October 1998 (austral spring, upwelling season) and July 1999 (austral winter, non-upwelling season). During the spring cruise, euphotic-zone integrated primary production ranged from 1200 to 8740 and from 320 to 540 mg C $m^{-2} d^{-1}$ and bacterial production from 238 to 760 and from 91 to 102 mg C $m^{-2} d^{-1}$ at coastal shelf and adjacent oceanic stations, respectively. Bacterial growth in coastal shelf waters was higher (0.4–1.3 d^{-1}) than at the oceanic stations (0.2 d^{-1}). In the same station order, the abundance ranges for heterotrophic nanoflagellates were 0.7–33.9 $\times 10^5$ and 0.2–56.9 $\times 10^5$ cells L^{-1} and, for autotrophic nanoflagellates, 3.8–32.1 $\times 10^5$ and 0–30.4 $\times 10^5$ cells L^{-1}, respectively. During the non-upwelling conditions, primary production was lower at the coastal shelf stations (481–1710 mg C $m^{-2} d^{-1}$) and slightly higher (415–865 mg C $m^{-2} d^{-1}$) at the oceanic stations. Bacterial production (< 100 mg C $m^{-2} d^{-1}$) and bacterial growth rates (< 0.2 d^{-1}) were also lower. Heterotrophic nanoflagellates (0.6–39.6 $\times 10^5$ and 1.9–59.9 $\times 10^5$ cells L^{-1}) and autotrophic nanoflagellates (0.4–22.6 $\times 10^5$ and 0–12.5 $\times 10^5$ cells L^{-1}) had similar abundances than those at coastal shelf and oceanic stations during the spring. Under upwelling conditions, bacterial production represented 4.3–22.4% (coastal) and 18.9–28.6% (oceanic) of the primary production, whereas wintertime production was lower at the coastal stations (4.7–13.5%) but remained similar at the oceanic stations (11.9–26.8%). Significant correlations were found between primary and bacterial production for the spring cruise, and between bacterial abundance and (a) chlorophyll-*a*, (b) dissolved organic carbon (DOC), and (c) heterotrophic nanoflagellates (all data). This suggests that a significant

*Corresponding author. Tel./fax: +56 41 68 3033.
E-mail address: lcuevas@udec.cl (L.A. Cuevas).

0967-0645/$ - see front matter © 2004 Elsevier Ltd. All rights reserved.
doi:10.1016/j.dsr2.2004.07.026

fraction of the primary production is channeled through bacteria and, subsequently, through heterotrophic nanoflagellates reflecting the importance of microbial food webs in carbon cycling in the upwelling system off central Chile.
© 2004 Elsevier Ltd. All rights reserved.

1. Introduction

The Humboldt Current System (HCS) and associated oceanic areas are of great importance to global carbon cycling due to the large standing stock of particulate organic carbon (POC) and high rates of primary production (PP) (Daneri et al., 2000). The HCS is an Eastern Boundary Current System typified by the occurrence of coastal upwelling. The presence of a shallow, nutrient-rich, oxygen-depleted, subsurface water mass, as well as interannual variations associated with El Niño events are typical of this system (Strub et al., 1998). The high productivity is driven mainly by coastal upwelling processes that fertilize the photic zone with inorganic nutrients. The area off Concepción (~36°S) is probably the most productive upwelling ecosystem along the Chilean coast (Daneri et al., 2000). Important commercial pelagic and demersal fisheries take place in the area, accounting for a significant proportion (> 40%) of Chilean fish landings. Concepción's continental margin is the widest shelf area along the HCS (up to 90 km from the coast) and is confined by the outlets and submarine canyons associated with the Itata and Bio-Bio rivers. The oceanography of the area is physically complex because of the widely variable climatic, topographic, and meteorological conditions, which are mainly determined by the position of the Pacific anticyclonic system that influences the annual pattern of wind direction and strength (Strub et al., 1998). Mesoscale structures (i.e. upwelling plumes, shelf-break fronts, filaments, eddies shedding from the coast) are common features in the coastal transition zone off Concepción (Fig. 1 in Montecino et al., 2004).

Highly productive upwelling systems commonly have been characterized as having a short food chain composed of large-sized phytoplankton, zooplankton, and pelagic fish. However, a large proportion of the total flux of organic matter is, most likely, being channeled through bacteria and associated food webs. Heterotrophic bacteria are important agents of carbon cycling in oceanic ecosystems; bacteria, together with some flagellate communities, may be responsible for the major consumption of biogenic carbon (Sherr, 1988; Sherr and Sherr, 1988; Fuhrman, 1999). Bacterial production (BP) is the key process by which dissolved organic matter (DOM) is channeled through the microbial loop, and estimates of BP and bacterivory can be combined to establish the importance of the microbial loop and microbial food webs in marine ecosystems. Bacterial abundance (BA) in marine environments, which rarely exceeds 10^{10} cells L^{-1}, is mostly controlled by predation or substrate availability (Azam et al., 1983; Billen et al., 1990), although more recently partial control of bacteria by viruses also has been reported (Proctor and Fuhrman, 1990; Fuhrman and Noble, 1995; Fuhrman, 1999).

Bacterial predation by protists (most commonly heterotrophic flagellates and small ciliates) has been shown to be important in controlling bacterioplankton abundance through a range of different ecosystems (review in Sanders et al., 1992). Heterotrophic nanoflagellate abundance has been found to be highly correlated with abundance of their prey (bacteria and picoplanktonic algae). Sometimes, however, weak correlations have been found between these flagellates and bacteria. This suggests that flagellate biomass cannot always be supported by the available bacteria and, thus, must be supported by other food sources such as autotrophic picoplankton (Sherr and Sherr, 1992), viruses (González and Suttle, 1993), or directly by dissolved organic carbon (DOC) (Sherr, 1988; Tranvik et al., 1993). Nanoflagellates include both heterotrophic and phototrophic forms, since some chlorophyll-containing nanoflagellates have been shown to ingest bacterioplankton (Caron et al., 1990) and, in other cases, autotrophic nanoflagellates can potentially

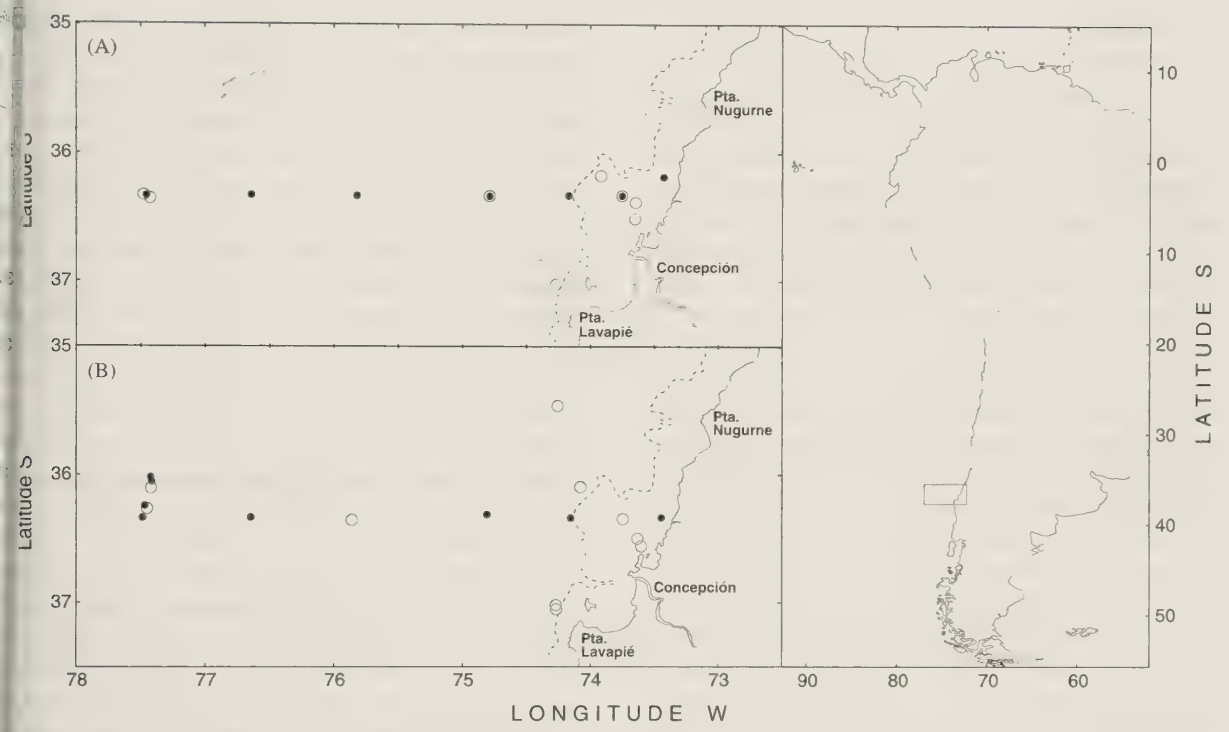

Fig. 1. Sampling area for the two MIRC cruises off Concepción. (A) spring (October 1998, upwelling) and (B) winter (July 1999, non-upwelling). Black dots: onshore–offshore transects; white circles: 48 h stations.

contribute to primary productivity and nutrient regeneration.

There are few studies on bacterial dynamics and carbon flow through bacterioplankton and associated food web organisms in upwelling areas. Typical upwelling values for the flow of organic matter through bacteria are between 3% and 55% of the total autotrophic productivity (McManus and Peterson, 1988; Ducklow, 1993; Painting et al., 1993; Wiebinga et al., 1997; Ducklow, 2000). Although it is generally recognized that the coupling between primary and bacterial production becomes tighter in oligotrophic systems, bacteria also have been shown to rapidly respond to the pulsed production cycles typical of upwelling areas (McManus and Peterson, 1988). Bacteria are an important component of the upwelling ecosystems off Chile. Troncoso et al. (2003) demonstrated that, depending on environmental conditions, bacteria are capable of processing a significant proportion of the organic matter produced by phytoplankton in three upwelling ecosystems along Chilean coast. These authors interpreted the significant correlation between BP and PP, coupled with a lack of correlation between temperature and BP, as an indication that substrate availability is more important than temperature in limiting bacterial activity and abundance in the HCS off Chile. The potential role of nanoflagellates in controlling BA in the upwelling system of the HCS off Chile, however, has received little attention. The present study uses new data to examine the spatial variability and association between BA, production, turnover time, and nanoflagellate abundance with the sources of organic matter (PP and DOC) on the coastal shelf region and in the adjacent oceanic region in the Concepción upwelling ecosystem. The aim of our study is to provide a more complete assessment of the importance of microbial-mediated carbon fluxes together with the factors that control BA in this highly productive upwelling area.

2. Methods

2.1. Field sampling

Sampling took place in the Concepción upwelling ecosystem and adjacent oceanic areas aboard the R.V. *Abate Molina* during two Multidisciplinary Intensive Research Cruises (MIRC I and II), as part of the FONDAP-Humboldt Research Program. The MIRC I cruise took place in October (austral spring) 1998 and the MIRC II cruise in July (austral winter) 1999. A coast to offshore transect, starting at 5 nautical miles from the coast and ending 200 n mile offshore, plus four 48-h process stations (YY1 to YY4) were sampled (11 stations each cruise; Fig. 1). During both cruises, distinct coast to offshore, cold, high pigment filaments extending up to 100 n mile from the coast were present (Fig. 1 in Montecino et al., 2004). In this study, the "coastal shelf stations" refer to stations sampled within the continental shelf and 100 n mile offshore, whereas the "oceanic stations" refer to stations offshore of this (>100 n mile).

2.2. Sample collection and hydrographic measurements

Water samples for BA, heterotrophic and autotrophic nanoplankton abundance (HNF and ANF), chlorophyll-*a* (Chl-*a*), and DOC were taken from within the top 350 m of the water column (9–12 samples per profile). BP and PP were measured within the euphotic zone. The water column structure data were obtained from a continuous CTD register using a Neil Brown (MK III) equipped with oxygen sensors, in vivo fluorescence Sea-Tech (FL 3000), and a scalar PAR sensor (Biospherical Instrument, Mod. QSP-200L). The General Oceanic rosette was equipped with 12 Niskin bottles (5 L).

2.3. Bacterial abundance

Discrete 50-mL seawater samples were collected directly from Niskin bottles into sterile tubes and preserved in the dark with glutaraldehyde (2% final concentration) at 4°C. Bacterial counting was done using epifluorescence microscopy following the methodology of Porter and Feig (1980). Two to five mL of seawater containing bacteria were stained with DAPI (4′ 6-diamidino 2-phenylindole) to a final concentration of 72 μM and collected onto black, 25 mm, polycarbonate filters (0.2 μm pore size). Ten to twenty random fields (minimum 400 cells) were counted with a Zeiss Axioskop epifluorescence microscope (1000×) equipped with quartz optics with UV excitation.

2.4. Bacterial biomass and biovolume

Bacterial organic carbon (BOC, or bacterial cellular carbon) was estimated using the equation:

$$\mathrm{BOC\ (fg)} = 90.06 \times \mathrm{BVOL\ (\mu m^3)}^{0.59},$$

where BVOL = bacterial volume (Simon and Azam, 1989). Two epifluorescence microscopy pictures were taken for each sample. The cell volume was determined by measuring the longest cell axis on enlarged microphotography (12,500×). Between 100 and 200 cells were measured; care was taken to measure the size of the bacterial cell wall and not the fluorescent halo around the bacteria. The bacterial volume was calculated using the equation

$$\mathrm{BVOL\ (\mu m)^3} = (d^2 \times \pi/4) \times (l - d) + (\pi \times d^3/6),$$

where d = diameter and l = length (Watson et al., 1977). BOC was determined in a complete profile at only one station (coastal) during spring and at two stations (coastal and oceanic) during the winter cruise.

2.5. Bacterial production

BP was measured through the incorporation of [methyl-^{3}H]-thymidine into the DNA (Fuhrman and Azam, 1982; modified by Wicks and Robarts, 1987). The collection of discrete seawater samples from the process stations at six light intensities (from 100% to 1%) and PP measurements were done simultaneously. At the sampling stations, the euphotic zone range from 17 to 58 m (spring) and from 41 to 63 m (winter) and was shallower towards the coast. Ten mL of seawater from each

epth were transferred to sterile tubes (three replicates and one blank). The blank was poisoned with 0.2-μm filtered formaldehyde. The samples were incubated with [methyl-^{3}H]-thymidine (50.1 Ci × mmol^{-1} specific activity) to a final concentration of 10 nM (saturation concentration) and maintained in the dark in a water bath provided with running surface seawater. The incubation was stopped after 1 h with the addition of cold analytical trichloroacetic acid 50% w/v. After 10 min of extraction, the tube contents were filtered (0.45 μm pore size). In accordance with Wicks and Robarts (1987), the sample was treated with 5 mL of phenol–chloroform solution (50% w/v) after filtering. After applying a vacuum, 5 mL of cold analytical ethanol (80% v/v) were added to each sample. The DNA was extracted and the dried filters were transferred to plastic liquid scintillation vials, where they were kept cool until radioisotopic analysis. In the laboratory, the vials were treated with analytical ethyl acetate and 10 mL of liquid scintillate Ecolite (+) (ICN). The incorporation of [methyl-^{3}H]-thymidine was measured in dpm using the ^{3}H technique in a Packard (Mod. 1600 TR) liquid scintillation counter. The counting efficiency was calculated from the non-quenched standard of ^{3}H-toulene. The thymidine uptake was transformed into cell production by using a constant of 2×10^{18} cells per mole of thymidine incorporated (Fuhrman and Azam, 1982). At the same time, the experiments of BP samples from the same Niskin bottles were collected for BA and biomass. Bacterial growth (μ) was calculated as a ratio of BP over biomass. This calculation allowed an estimation of the daily BP and biomass.

2.6. Heterotrophic and autotrophic nanoflagellate abundance, volume, and production

Ten mL of seawater were collected onto black, 25-mm × polycarbonate filters (0.8 μm pore size; Nuclepore), stained in vivo with Proflavine (3-6-diamine-acridine hemi-sulfate) to a final concentration of 0.033% w/v, according to Haas (1982), and fixed with 6% glutaraldehyde (final concentration). The microscopy preparations were stored at −20°C in the dark. Forty random fields were counted with a Zeiss-Axioskop epifluorescence microscope equipped with quartz optics with blue excitation and a 1000 × magnification.

ANF and HNF were counted separately. The red autofluorescence of cells containing chlorophyll was used to identify ANF. All non-pigmented organisms below 10 μm in size were classified as HNF. In the same filter, 30 cells were measured and the flagellate volume was calculated using the Chrzanowski and Simek (1990) equation

$$\mathrm{HNFVOL}\ (\mu\mathrm{m})^3 = [(\pi/6) \times l] \times w^2,$$

where HNFVOL = heterotrophic nanoflagellate volume, w = width, and l = length.

A growth efficiency of 33% was used to calculate the production of flagellates (HNF and ANF) (Hansen et al., 1997).

2.7. Bacterial grazing rates

HNF grazing rates on bacteria were calculated using the Peters (1994) model. This model includes data from lentic, lotic, and marine systems ($R^2 = 75$, $n = 329$, $p < 0.001$) and estimates potential specific grazing rate (GR, bacteria HNF^{-1} h^{-1}). This model was chosen because it considers a greater number of variables, including temperature (T), prey abundance (BA), prey volume (BVOL), predator abundance (HNFA), and predator volume (HNFVOL):

$$\log GR = -2.701 - 0.344[\log BVOL] + 0.477[\log HNFVOL] + 0.489[\log AB] - 0.270[\log HNFA] + 0.033\,T.$$

The volume of HNF was determined from the same samples from which bacterial volume were obtained. The specific grazing rate was estimated for each cruise independently and was used to estimate the overall carbon flux from bacteria to its predators (i.e. GR multiplied by HNF abundance).

2.8. Primary production (PP) and chlorophyll-a

Water-column integrated PP was estimated from changes in the dissolved oxygen concentrations of light and dark bottle incubations. Water

samples were collected from light depths corresponding to 100%, 80%, 53%, 32%, 8%, and 1% of the surface incident PAR radiation. Samples from each depth were dispensed in glass bottles (125 mL nominal volume) and incubated in situ from dawn to dusk in a drifting array. This procedure is fully described in Daneri et al. (2000). Chl-*a* data from the same cruises were provided by H. González (unpublished data).

2.9. Dissolved organic carbon

Ten mL aliquots were drawn directly into clean, pre-combusted glass ampoules from the Niskin bottles. The samples were flame sealed and stored at −20 °C until analysis in the laboratory. Only the shallower samples from within the euphotic zone (i.e. 58 and 63 m during the spring and winter cruises, respectively) were filtered through pre-combusted (450 °C) glass-fiber filters (Whatman GF/F). Deeper-water samples were not filtered, as POC becomes a minor fraction of the total organic carbon at depth. In the laboratory, the DOC samples were analyzed using a TOC 5000 SHIMADZU DOC analyzer. Water samples were acidified with 10 µl of concentrated phosphoric acid (final pH of 2) and decarbonated by purging with CO_2-free gas (high purity air) for 10 min. The carrier gas utilized was a high purity air (<1 ppm of CO_2 and CO). At least four injections were made per sample, and the results were accepted when the coefficient of variation of the samples was within 2%. Prior to analysis, the furnace was given a series of injections of freshly prepared Milli-Q water. The signal of Milli-Q high purity water was used as an instrument blank. In order to minimize sample carryover, deep-water samples were run first. Calibration standards were prepared with potassium hydrogen phthalate.

2.10. Statistical analyses

Kruskal–Wallis non-parametric test and Mann–Whitney mean differences analyses were used to examine and compare the association between seasonal and between coastal shelf and oceanic stations of the following variables: BP, PP, Chl-*a*, DOC, BA, and HNF.

3. Results

3.1. Chlorophyll-a and primary production

The highest euphotic-zone integrated Chl-*a* values (53.3–248.5 mg m^{-2}) were observed in the coastal shelf stations during the spring cruise (MIRC I, October 1998, upwelling). In the oceanic area, these values were 16 fold lower (6.6–12.1 mg m^{-2}). During the winter cruise (MIRC II, July 1999, non-upwelling), the integrated Chl-*a* values in the coastal shelf zone fluctuated between 25.2 and 49.2 mg m^{-2}, and between 13.3 and 26.5 mg m^{-2} at the oceanic stations. During both cruises, significant differences were found between coastal shelf and oceanic stations ($n = 85$, $U = 229$, $p < 0.01$ during spring and $n = 115$, $U = 886$, $p < 0.01$ during the winter).

The PP values in the euphotic zone (Table 1) in both coastal shelf stations and oceanic stations showed a trend similar to the integrated Chl-*a* values. During the upwelling cruise, the average euphotic-zone integrated PP ranged from 1200 to 8740 mg C m^{-2} d^{-1} in the coastal shelf zone; in the oceanic area, they were an order of magnitude lower (320–540 mg C m^{-2} d^{-1}). During the non-upwelling cruise, coastal PP values varied between 500 and 1710 mg C m^{-2} d^{-1} and oceanic PP between 415 and 865 mg C m^{-2} d^{-1}. Significant differences were found between the coastal and the oceanic stations during the spring ($n = 39$, $U = 18$, $p < 0.01$) and the winter ($n = 49$, $U = 171$, $p < 0.05$).

3.2. DOC, bacterial biomass, growth, and production

During the upwelling cruise, surface DOC values were close to 100 µM along the whole transect (coast to 200 n mile offshore) (Fig. 2A). Values <100 µM were observed between 100 and 250 m depth, but increased below 300 m at 200 n mile offshore. This subsurface peak coincided with low dissolved oxygen concentration (<2 mL O_2 L^{-1}), associated with the Equatorial subsurface water (data not shown). However, near the coast, a similar increase in DOC at depth was not

Table 1
Primary production (PP) and bacterial production (BP) during spring and winter cruises. Stations are presented from nearshore to offshore

Season	Station	Distance offshore (nm)	Lat. S	Long. W	PP ($mg C m^{-2} d^{-1}$)	BP ($mg C m^{-2} d^{-1}$)	BGR d^{-1}	BP/PP (%)
Spring	YY-3a	11.0	36° 30.74′	73° 09.18′	5500	238.6	0.60	4.3
(upwelling,	YY-4a	13.2	36° 23.00′	73° 08.80′	4460	310.3	0.89	6.9
October)	YY-2a	28.7	36° 10.67′	73° 25.47′	4300	292.7	0.67	6.8
	YY-1a	29.0	37° 01.20′	73° 46.57′	3040	517.9	1.03	17.0
	M4	35.4	35° 42.01′	73° 19.62′	8740	561.2	0.35	6.4
	YY-1b	36.0	36° 52.60′	73° 53.70′	1200	268.3	0.59	22.4
	YY-5a	199.8	36° 19.80′	76° 58.63′	320	91.3	0.17	28.5
	YY-5b	196.5	36° 21.51′	76° 55.81′	540	102.3	0.17	18.9
Winter (non-	YY-2b	5.3	36° 33.59′	73° 06.05′	481	64.7	0.04	13.5
upwelling,	YY-2a	10.2	36° 30.11′	73° 07.86′	1100	66.4	0.06	6.0
July)	T2	20.0	36° 19.98	73° 15.16	1710	79.8	0.05	4.7
	YY-3a	28.6	37° 01.30′	73° 46.12′	885	80.3	0.08	9.1
	YY-3b	28.9	37° 03.22′	73° 45.95′	500	63.2	0.05	12.6
	YY-4	36.7	36° 05.83′	73° 34.64′	569	64.1	0.06	11.3
	T5	120.0	36° 20.00	75° 19.31	865	103.3	0.10	11.9
	YY-1a	199.7	36° 16.09′	76° 57.10′	440	75.0	0.13	17.0
	YY-1b	198.8	36° 06.37′	76° 55.23′	415	111.3	0.18	26.8

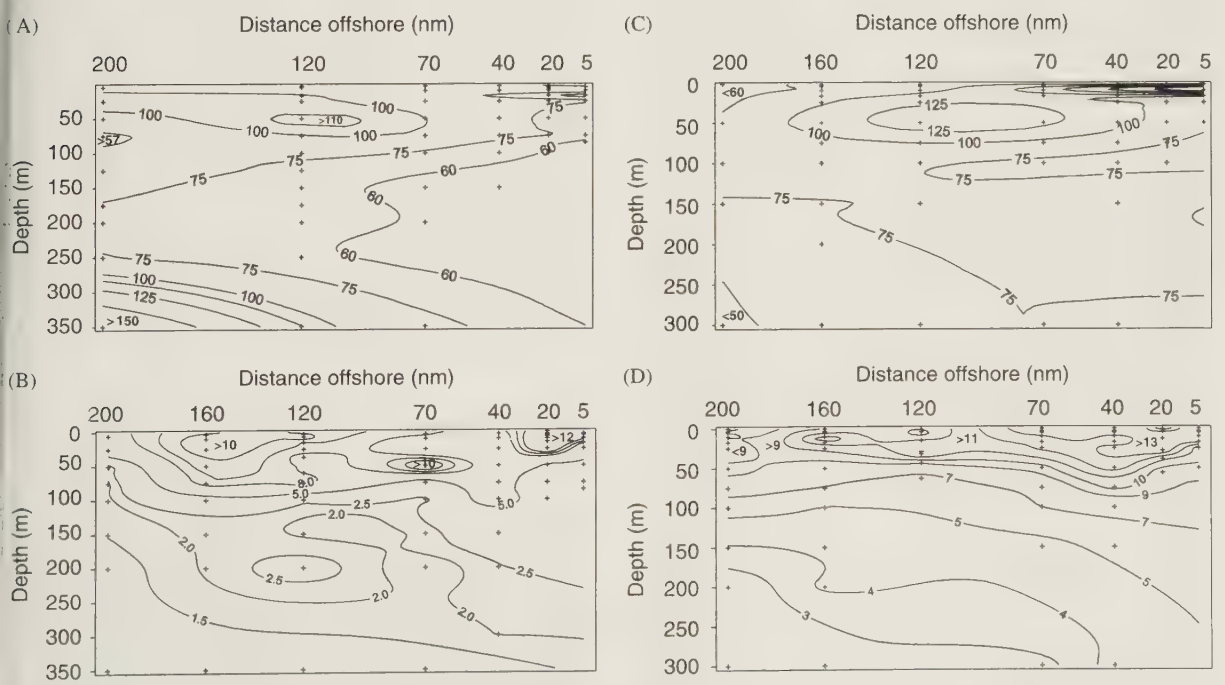

Fig. 2. Distribution of the dissolved organic carbon (DOC; A, C) and bacterial abundance (B, D) during the spring (A, C) and winter (B, D), along the 200 n mile transect. DOC units: μM; bacterial abundance units: 10^6 cells L^{-1}.

observed in oxygen-depleted waters. No significant differences were found between coastal shelf and oceanic stations ($n = 39$, $U = 92$, $p > 0.05$). Bacterial abundance was 10^9 cells L^{-1} in shallow water (<100 m), with maximum values at 20 n mile, 120–160 n mile, and a subsurface maximum (75 m) at 70 n mile from the coast (Fig. 2B). Based on a single station, bacterial cell volume was estimated to be $0.14 \pm 0.07\ \mu m^3$, whereas bacterial cell carbon was 27 fg C. Integrated bacterial biomass ranged from 348 to 1611 mg C m^{-2} (coastal shelf stations) and from 527 to 618 mg C m^{-2} (oceanic stations). The coastal shelf range, however, was biased by the high value measured at station M4 (1611 mg C m^{-2}); the exclusion of this value brought the range down to 348–596 mg C m^{-2}, implying higher bacterial biomass towards the oceanic stations. The integrated bacterial biomass difference between coastal shelf and oceanic stations was significant ($n = 101$, $U = 822$, $p < 0.01$).

During the winter non-upwelling cruise, DOC surface concentrations >100 μM were found between 70 and 160 n mile offshore, whereas DOC concentrations <100 μM were mostly found below 100 m depth (Fig. 2C). No statistically significant differences were found between coastal shelf and oceanic stations ($n = 46$, $U = 191$, $p > 0.05$). Bacterial abundance was $>10^9$ cells L^{-1} in the upper 75 m (Fig. 2D) and bacterial cell volume was $0.10 \pm 0.06\ \mu m^3$ (coastal shelf stations) and $0.06 \pm 0.04\ \mu m^3$ (oceanic stations). The average bacterial cell carbon was 22 fg C (coastal shelf stations) and 16 fg C (oceanic stations) (Mann–Whitney $U = 2$; $p < 0.01$). The integrated bacterial biomass was higher than the bacterial biomass in spring, varying between 1067 and 1579 mg C m^{-2} (coastal shelf stations) and between 589 and 1002 mg C m^{-2} (oceanic stations). The mean difference between coastal shelf and oceanic stations was significant ($n = 108$, $U = 223$, $p < 0.01$).

BP during spring upwelling was close to 500 mg C m^{-2} d^{-1} at the coastal shelf stations compared to 100 mg C m^{-2} d^{-1} at the oceanic stations (Table 1), with a significant difference between them ($n = 60$, $U = 50$, $p < 0.01$). Bacterial growth rates at the coastal shelf stations were higher (0.10–1.03 d^{-1}) than at the oceanic stations (0.17 d^{-1}). The 0.10 d^{-1} value was related to one station close to 100 n mile offshore; the exclusion of this station brought the range up to 0.35–1.03 d^{-1} (Table 1).

During winter, BP was similar at all the stations ($n = 60$, $U = 318$, $p > 0.05$), ranging from 63 to 111 mg C m^{-2} d^{-1}; in general, the higher values were found at the oceanic stations. The winter BP values showed a 6-fold drop in relation to the spring values (Table 1). The bacterial growth rate during the winter cruise was <0.18 d^{-1} (with lowest values at the coastal shelf stations: 0.04–0.08 d^{-1}; Table 1).

On an average, a higher proportion of photosynthetic carbon production was channeled through bacteria in the spring (10.7% for coastal shelf and 23.7% for oceanic stations); in the winter, the percentage of the PP contributing to BP fell to 9.5% and 18.6%, respectively. In both cases, the bacterial carbon flux (as a % of PP) was higher under oligotrophic conditions (>100 n mile offshore) (Table 1). The correlation between DOC and BA was not significantly different between the spring and winter cruises. Pooling the data together from both cruises gave a weak but significant correlation ($r = 0.41$; $n = 83$; $p < 0.01$) between DOC and BA (Fig. 3A). The correlation between Chl-*a* and BA was also significant in both spring ($r = 0.66$; $n = 76$; $p < 0.01$) and winter cruises ($r = 0.37$; $n = 218$; $p < 0.01$) (Fig. 3B). The correlation between PP and BP (Fig. 3C) was significant in spring ($r = 0.42$; $n = 44$; $p < 0.01$) but not in winter ($r = 0.17$; $n = 54$; $p > 0.1$). No significant correlation was found between temperature and BP during spring ($n = 49$, $U = 235$, $p > 0.05$) and winter ($n = 41$, $U = 136$, $p > 0.05$).

3.3. Nanoflagellates and grazing rates on bacteria

Heterotrophic and autotrophic nanoflagellate abundances were similar in terms of magnitude. HNF and ANF were more abundant ($>10 \times 10^5$ cells L^{-1}) in the upper 100 m of the water column, with no ANF below this depth (Fig. 4). In spring, the maximum HNF values ($>40 \times 10^5$ cells L^{-1}) were obtained at 200 n mile offshore (Fig. 4A) and the highest ANF values ($>30 \times 10^5$ cells L^{-1}) were found at the surface at

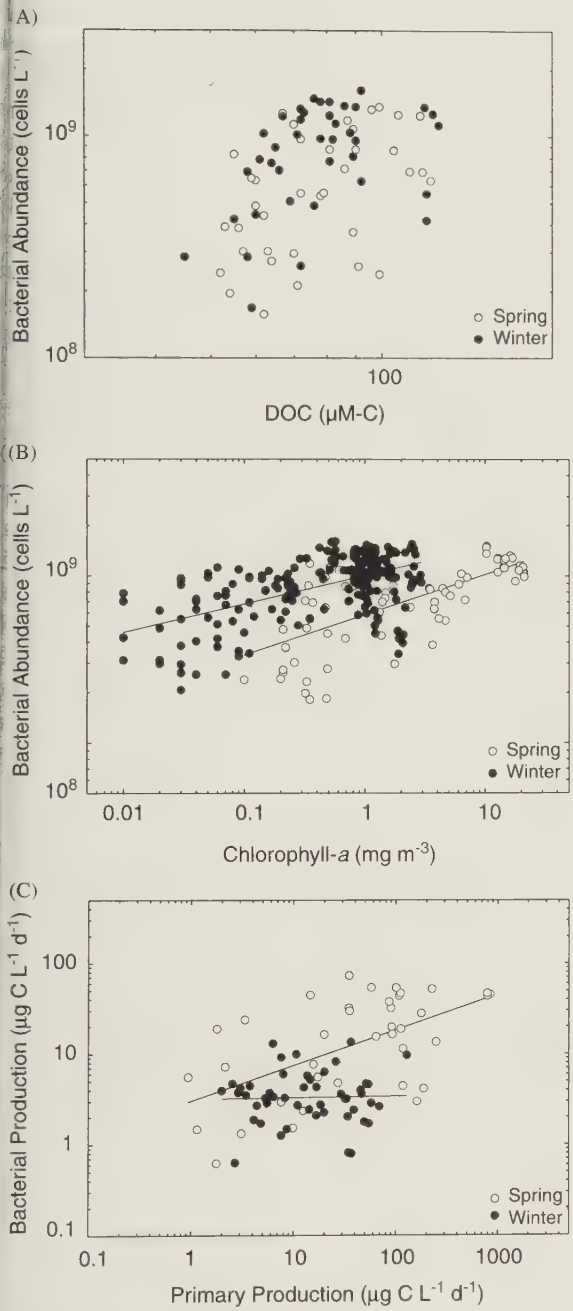

Fig. 3. Relationship between (A) dissolved organic carbon (DOC) and bacterial abundance, (B) chlorophyll-*a* and bacterial abundance, and (C) primary productivity and bacterial production during the spring-upwelling and winter non-upwelling cruises (log–log scale). Black lines represent the slopes for each season, dotted lines represent 95% confident intervals.

120 n mile, at 75 m depth, and at 40 and 160 n mile offshore (Fig. 4B). No significant differences were found between coastal shelf and oceanic stations ($n = 91$, $U = 585$, $p > 0.05$ for HNF and $n = 100$, $U = 863$, $p > 0.05$ for ANF, respectively). In winter, HNF abundance values were $< 15 \times 10^5$ cells L^{-1} close to the coast and more than 20×10^5 cells L^{-1} at > 120 n mile offshore (Fig. 4C), with significant differences between coastal shelf and oceanic stations ($n = 79$, $U = 341$, $p < 0.01$), and a peak ($> 30 \times 10^5$ cells L^{-1}) at 160 n mile offshore. This peak coincided with a Chl-*a* maximum (> 2 mg m^{-3}) (H. González, unpublished data). A maximum in ANF abundance (20×10^5 cells L^{-1}) was found within the top 25 m depth at a coastal shelf station (20 n mile); higher values ($> 10 \times 10^5$ cells L^{-1}) also were found at oceanic stations (120 and 200 n mile offshore; Fig. 4D). No significant differences between coastal shelf and oceanic stations were found ($n = 72$, $U = 596$, $p > 0.05$). BA was strongly correlated with both spring ($r = 0.67$; $n = 112$; $p < 0.01$) and winter HNF abundance ($r = 0.58$; $n = 117$; $p < 0.01$) (Fig. 5), as expected when HNF are important bacterial consumers. Nanoflagellate cell volumes were similar during spring and winter cruises, but very different between coastal shelf (322.5 μm^3) and oceanic (47.3 μm^3) stations.

The Peters (1994) model for estimating bacterivory by HNF resulted in average specific grazing rates of 13.8 ± 4.9 bacteria HNF^{-1} h^{-1} during the spring cruise and of 10.0 ± 3.2 bacteria HNF^{-1} h^{-1} during the winter cruise. In spring the average total grazing was 1.25×10^6 bacteria L^{-1} d^{-1}, and in winter it was 3.58×10^6 bacteria L^{-1} d^{-1}. The amount of BP channeled through HNF grazing in spring represented 4.3% and, in winter, over 100% of the BP that would have been necessary to sustain the grazing pressure exerted by the HNF assemblages.

4. Discussion

The data obtained during this study show important differences between seasons and among coastal shelf and oceanic regions in terms of the

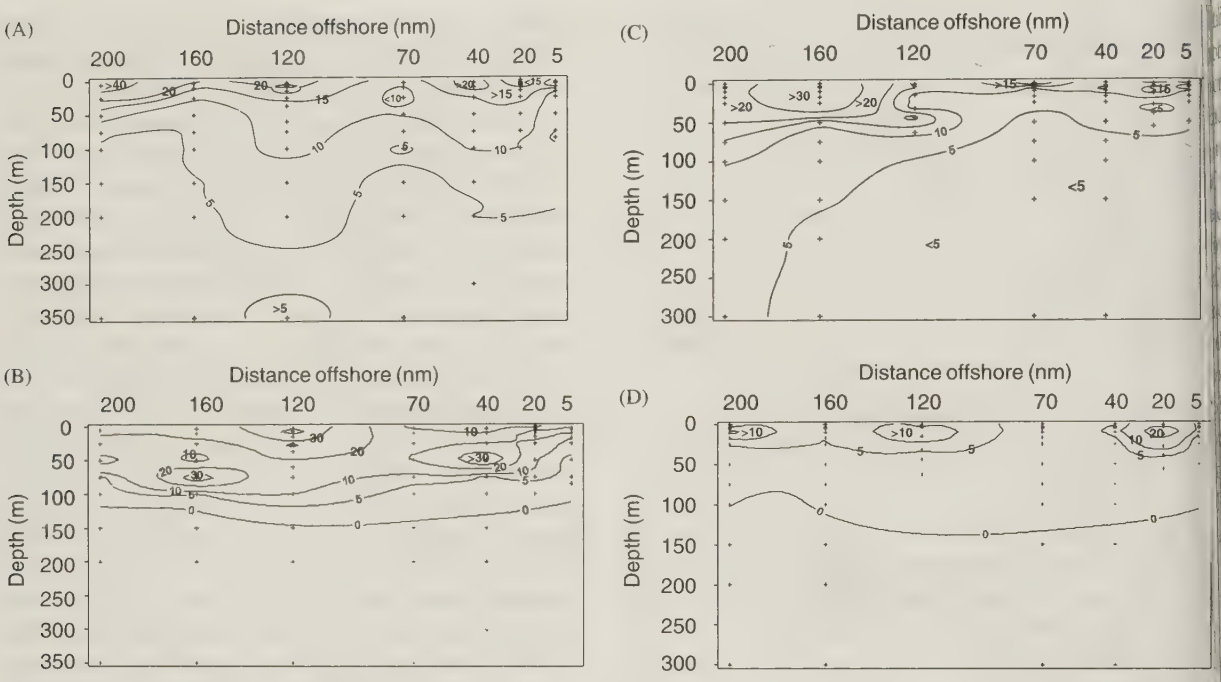

Fig. 4. Distribution of heterotrophic nanoflagellates (A, C) and autotrophic nanoflagellates (B, D) during the spring (A, B) and winter (C, D) cruises, along the 200 n mile transect. Abundance units: 10^5 cells L^{-1}.

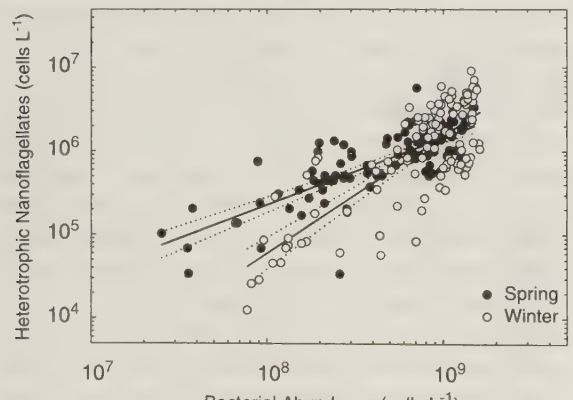

Fig. 5. Relationship between the abundances of heterotrophic nanoflagellates and bacteria during the spring, upwelling and winter, non-upwelling, conditions (log–log scale). Black lines represent the slopes for each season; dotted lines represent 95% confident intervals.

amount of PP and its subsequent utilization by microorganisms in the Concepción upwelling system. Wind-driven upwelling events in the HCS off Chile are more prominent in spring than in winter, when the weakening of the South Pacific anticyclone produces a wind pattern less favorable to upwelling. This phenomenon, coupled with a reduced light field, decreases the system's productivity in winter; this seasonality is particularly strong in the upwelling ecosystem off Concepción. During this study, the highest PP and Chl-*a* values were obtained during the spring (October 1998) upwelling cruise, whereas in the winter (July 1999) non-upwelling cruise, substantial drops in PP (~ 5-fold) and Chl-*a* (4-fold) were observed. The overall seasonal drop in the productivity of the Concepción upwelling system was also reflected in the BP values, which showed a 6-fold decrease from spring (upwelling) to winter (non-upwelling). Lower bacterial growth rates were also observed during the non-upwelling ($<0.2\,d^{-1}$) as compared to upwelling ($\sim 1.0\,d^{-1}$) conditions. The simultaneous drop in PP and BP that is reflected in the positive correlations between PP and BP and between bacterial abundance and Chl-*a* and DOC is, in all probability, indicative of a strong coupling between organic matter synthesis and

ilization by bacteria. This, coupled with a lack of rrelation between temperature and BP, seems to nfirm substrate availability as one of the key ctors influencing bacterial activity in the upwel- g system off Concepción, as reported by roncoso et al. (2003). Caution, however, is eded with this interpretation as the influence of her organic sources in the upwelling system off oncepción, such as river input, cannot be mpletely ruled out. Although substrate avail- ility (a bottom-up type of control) may be the edominant factor controlling bacterial activity in e HCS off Chile, the influence of top-down-type ocesses may also play an important role in the ansfer of organic carbon to higher trophic levels. NF are the principal consumers of heterotrophic cteria, exerting a grazing pressure capable of nstraining bacterial numbers (Sanders et al., 92). In this study, similar numbers of flagellates ere observed during both the spring and winter uises and, in general, flagellate and bacterial undances are comparable with data reported for her upwelling areas (Table 2). The maximum NF abundance in this study was found at -100 n mile from the coast, in the open ocean, where micro-heterotrophic pathways are usually dominant.

The results of this study's grazing model predict that, in spring, the HNF incorporate only a small fraction (<5%) of the BP (Fig. 6), lending further support, at least during situations of high productivity, to a bottom-up type of the control of BP in the Concepción upwelling system. Similar conclusions were drawn by Strom (2000), who reported that the influence of particle-feeding heterotrophs, such as protozoa, in more productive systems is somewhat diminished. The situation during the winter, however, was different. The grazing model predicted that HNF would be able to process over 100% of the BP (Fig. 6) and, therefore, we expected this grazing pressure to have a large impact on the bacterial abundance (BA). However, similar BA values were found in either spring or winter.

One possibility for sustaining HNF biomass, given the differences in trophic conditions during both upwelling and non-upwelling periods (i.e. low substrate availability; e.g. low PP and low BP), is the functioning of a highly coupled system in which the flagellate activity (grazing) stimulates

able 2
bundance and composition of microbial organisms in upwelling areas

acteria (10^9 cells L^{-1})	Flagellates (10^6 cells L^{-1})	Ciliates (10^5 cells L^{-1})	Comments	Reference
1–0.5	0.02–0.3	0.2–1.0	Over slope, Peru	Sorokin and Kogelschatz, 1978
1–0.5	0.01–0.9	0.1–0.3	Intensive coastal upwelling, Peru	
5–2.1	0.01–0.2	0.1–6.0	Phytoplankton bloom, Peru	
0–4.0	0.2–1.5		Active upwelling, Concepción	McManus and Peterson, 1988
.8–3.7	0.2–3.9		Relaxation, Concepción	
.8–3.3			Concepción Bay	Pantoja et al., 1989
.2–8.8			Upwelling center, Southern Benguela (summer)	Painting et al., 1993
.0–2.1			Upwelling SW Monsoon, Gulf of Aden	Wiebinga et al., 1997
.1–2.5			Oligotrophic SW Monsoon, Somali Basin	
.0–2.1			Upwelling NE Monsoon, Gulf of Aden	
.1–2.5			Oligotrophic NE Monsoon, Somali Basin	
.3–1.2	1.2–2.5		Langrangian study, Concepción Bay	Pacheco and Troncoso, 1998
.2–1.1	0.8–1.3		Pre-El Niño conditions, Antofagasta	Iriarte et al., 2000
.08–0.5			El Niño conditions, Antofagasta	
.2–0.7	1.5–3.0		Photic zone, depleted oxygen water column, Antofagasta	Pantoja, unpublished data
.3–1.4	0.07–3.4		Coastal upwelling, Concepción	This study
.2–0.6	0.2–5.7		Oceanic upwelling, Concepción	
.9–1.8	0.06–3.9		Coastal non-upwelling, Concepción	
.5–1.2	0.2–5.9		Oceanic non-upwelling, Concepción	

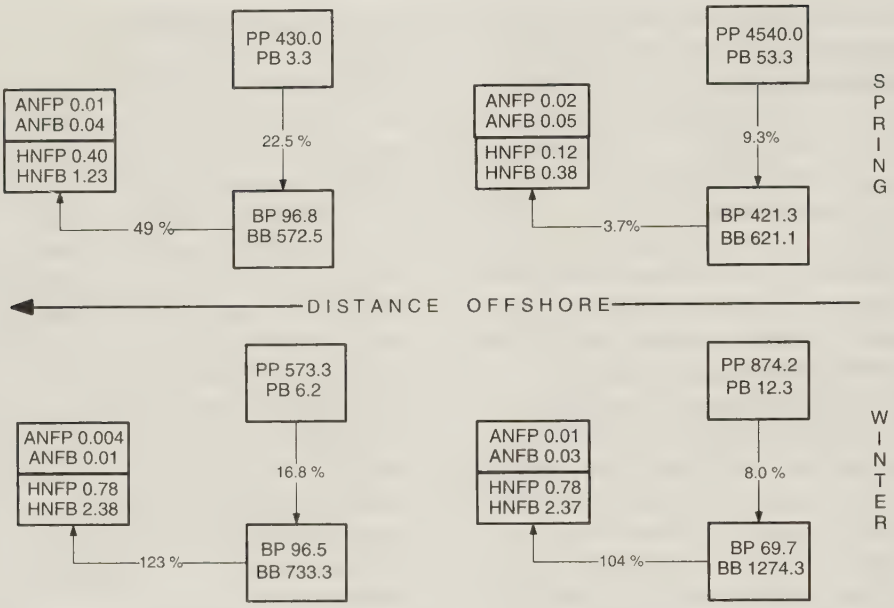

Fig. 6. Flux of microbial carbon during spring and winter seasons, and for coastal and oceanic areas. PP: Primary productivity, PB: Phytoplankton biomass, BP: Bacterial productivity, BB: Bacterial biomass, ANFP: Autotrophic nanoflagellates productivity, ANFB: Autotrophic nanoflagellates biomass, HNFP: Heterotrophic nanoflagellates productivity and HNFB: Heterotrophic nanoflagellates biomass. Productivities are in mg $C\,m^{-2}\,d^{-1}$ and biomasses in mg $C\,m^{-2}$.

BP by originating discrete sources of DOM or by producing regenerated inorganic nutrients (Bloem et al., 1988). However, this latter explanation seems somewhat unlikely as bacterioplankton cannot be supported exclusively by DOM regenerated from grazing. If the relatively high HNF biomass observed during the winter non-upwelling cruise were not being maintained by such a flagellate grazing-BP coupled system, it is possible that the flagellates were grazing on food sources other than bacteria. Sherr and Sherr (1988) pointed out that many flagellates do prey on phytoplankton as well as on bacteria. The idea that flagellates can feed on small phytoplankton is supported by our study, as the observed winter HNF peak coincided with peaks of Chl-*a* ($>2\,mg\,m^{-3}$), POC ($>0.2\,mg\,L^{-1}$), and PON ($>0.028\,mg\ L^{-1}$) measured 160 n mile offshore (H. González, unpublished data).

A drop in the specific activity (i.e. BP/BB) by bacteria ($0.57\pm0.57\,d^{-1}$ in spring and $0.07\pm0.05\,d^{-1}$ in winter) could be indicative that the winter bacteria were less active. The more dormant condition of the winter bacteria also is supported by changes in bacterial growth efficiency (BGE), which is an indicator of how active bacteria are in the water column and how efficiently they can incorporate organic substrates. Estimates of the daily BGE over incorporation rates of DOC within the photic layer can be obtained from

$$\mathrm{BGE} = \left[\frac{\mathrm{BP}}{\mathrm{BP}+\mathrm{BR}}\right] \times 100,$$

where BP = bacterial production, and BR = bacterial respiration, which can be estimated using the del Giorgio et al. (1997) equation

$$\mathrm{BR} = -3.67 + 0.75\ \log\ \mathrm{BA} + 0.059 \times T,$$

where BA = bacterial abundance (cells mL^{-1}) and T = in situ temperature (°C).

In coastal and open ocean environments, BGE ranges from 1% to 69%, (review in del Giorgio and Cole, 2000). In our study, estimated daily BGE values ranged from 34.9% in the spring to 8.2% in the winter, indicating a higher proportion of inactive or slow-growing bacteria in the winter. The inactive or slow-growing bacteria theory also

supported by the observed drop in bacterial llular carbon content, from the spring (27 fg cell^{-1}) to the winter (22 fg C cell^{-1} at coastal and fg C cell^{-1} at oceanic stations), since other udies have shown that larger cell volumes tend to associated with active bacteria (González et al., 990, 1993).

This study demonstrates that bacterioplankton nd organisms associated with microbial food ebs are important agents of carbon cycling in the oncepción upwelling system. A significant correlation between autotrophic organic matter and BP as observed during this study. This, coupled with lack of correlation between temperature and BP nd a lack of evidence that HNF can effectively ontrol bacterial biomass, points to the dominance f a bottom-up type of control of bacterial ctivity. The data also lend further support to a rong coupling between bacterial activity and pwelling driven productivity pulses in this important upwelling ecosystem.

cknowledgements

We thank the crew of the R.V. *Abate Molina*. .A.C. also thanks the microbiological laboratory f the EULA Center (Chile), especially M. Abarzúa, for the use of epifluorescent equipment. he comments and suggestions of three anonmous reviewers are greatly acknowledged. The hlorophyll-*a* data used in this study were kindly upplied by Dr. H. González. This work was unded by the FONDAP-Humboldt Program and he FONDAP-COPAS Center (Project No. 50100007). The editorial comments to the first ersion of the manuscript are also acknowledged.

References

Azam, F., Fenchel, T., Field, J.G., Gray, J.S., Meyer-Reil, L.A., Thingstad, F., 1983. The ecological role of water-column microbes in the sea. Marine Ecology Progress Series 10, 257–263.

Billen, G., Servais, P., Becquevort, S., 1990. Dynamics of bacterioplankton in oligotrophic and eutrophic aquatic environments: bottom-up or top-down control? Hydrobiology 207, 37–42.

Bloem, J., Starink, M., Bär-Gilissen, M.-J., Cappenberg, T., 1988. Protozoa grazing, bacterial activity and mineralization in two-stage continuous cultures. Applied Environmental Microbiology 54, 3113–3121.

Caron, D.A., Porter, K.G., Sanders, R.W., 1990. Carbon, nitrogen, and phosphorous budgets for the mixotrophic phytoflagellate *Poterioochromonas malhamensis* (Chrysophyceae) during bacterial ingestion. Limnology and Oceanography 35, 433–443.

Chrzanowski, T.H., Simek, K., 1990. Prey-size selection by freshwater flagellated protozoa. Limnology and Oceanography 35, 1429–1436.

Daneri, G., Dellarossa, V., Quiñones, R., Jacob, B., Montero, P., Ulloa, O., 2000. Primary production and community respiration in the Humboldt Current System off Chile and associated oceanic areas. Marine Ecology Progress Series 197, 41–49.

Ducklow, H.W., 1993. Bacterioplankton distributions and production in the northwestern Indian Ocean and Gulf of Oman, September 1986. Deep-Sea Research 40, 753–771.

Ducklow, H.W., 2000. Bacterial production and biomass in the oceans. In: Kirchman, D. (Ed.), Microbial Ecology of the Oceans. Wiley-Liss, New York, pp. 85–120.

Fuhrman, J.A., 1999. Marine viruses and their biogeochemical and ecological effects. Nature 399, 541–548.

Fuhrman, J.A., Azam, F., 1982. Thymidine incorporation as a measure of heterotrophic bacterioplankton production in marine surface waters: evaluation and field results. Marine Biology 66, 109–120.

Fuhrman, J.A., Noble, R.T., 1995. Viruses and protists cause similar bacterial mortality in coastal waters. Limnology and Oceanography 40, 1236–1242.

del Giorgio, P.A., Cole, J.J., 2000. Bacterial energetics and growth efficiency. In: Kirchman, D. (Ed.), Microbial Ecology of the Oceans. Wiley-Liss, New York, pp. 289–325.

del Giorgio, P.A., Cole, J.J., Cimbleris, A., 1997. Respiration rates in bacteria exceed phytoplankton production in unproductive aquatic systems. Nature 385, 148–151.

González, J.M., Suttle, C.A., 1993. Grazing by marine nanoflagellates on viruses and virus-sized particles: ingestion and digestion. Marine Ecology Progress Series 94, 1–10.

González, J.M., Sherr, E.B., Sherr, E.F., 1990. Size-selective grazing on bacteria by natural assemblages of estuarine flagellates and ciliates. Applied Environmental Microbiology 56, 583–589.

González, J.M., Sherr, E.B., Sherr, E.F., 1993. Differential feeding by marine flagellates on growing vs. starving, and on motile vs. non-motile, bacterial prey. Marine Ecology Progress Series 102, 257–267.

Haas, L.W., 1982. Improved epifluorescense microscopy for observing planktonic microorganisms. Annales de L'Institut Océanographique 58, 261–266.

Hansen, P.J., Bjørnsen, P.K., Hansen, B.W., 1997. Zopoplancton grazing and growth: scaling with the 2–2000 μm body size range. Limnology and Oceanography 42, 687–704.

Iriarte, J.L., Pizarro, G., Troncoso, V.A., Sobarzo, M., 2000. Primary production and biomass of size-fractionated

phytoplankton off Antofagasta, Chile (23–24°S) during pre-El Niño and El Niño 1997. Journal of Marine Systems 26, 37–51.

McManus, G.B., Peterson, W.T., 1988. Bacterioplankton production in the nearshore zone during upwelling off central Chile. Marine Ecology Progress Series 43, 11–17.

Montecino, V., Astoreca, R., Alarcón, G., Retamal, L., Pizarro, G., 2004. Bio-optical characteristics and primary productivity during upwelling and non-upwelling conditions in a highly productive coastal ecosystem off central Chile (~36°S). Deep-Sea Research II, this issue [doi:10.1016/j.dsr2.2004.08.012].

Pacheco, A., Troncoso, V.A., 1998. Tamaño celular, abundancia y productividad del bacterioplancton en la Bahía de Concepción, Chile: Un enfoque langrangiano. Gayana Oceanología 6, 35–48.

Painting, S.J., Lucas, M.I., Peterson, W.T., Brown, P.C., Hutchings, L., Mitchell-Innes, B.A., 1993. Dynamics of bacterioplankton communities during the development of an upwelling plume in the southern Benguela. Marine Ecology Progress Series 35, 35–53.

Pantoja, S., González, H., Bernal, P., 1989. Bacterial biomass and production in a shallow bay. Journal of Plankton Research 11, 599 604.

Peters, F., 1994. Prediction of planktonic protistan grazing rates. Limnology and Oceanography 39, 195–206.

Porter, K.G., Feig, Y.S., 1980. The use of DAPI for identifying and counting aquatic microflora. Limnology and Oceanography 25, 943–948.

Proctor, L.M., Fuhrman, J., 1990. Viral mortality of marine bacteria and cyanobacteria. Nature 343, 60–62.

Sanders, R.W., Caron, D.A., Berninger, U.G., 1992. Relationship between bacteria and heterotrophic nanoplankton in marine and fresh waters: an inter-ecosystem comparison. Marine Ecology Progress Series 86, 1–14.

Sherr, E., 1988. Direct use of high molecular weight polysaccharide by heterotrophic flagellates. Nature 335, 348–351.

Sherr, E.B., Sherr, B.F., 1988. Role of microbes in pelagic food webs: a revised concept. Limnology and Oceanography 33, 1225–1227.

Sherr, E.B., Sherr, B.F., 1992. Trophic roles of pelagic protists: phagotrophic flagellates as herbivores. Archive für Hydrobiologie 37, 165–172.

Simon, M., Azam, F., 1989. Protein content and protein synthesis of planktonic marine bacteria. Marine Ecology Progress Series 51, 201–213.

Sorokin, Y., Kogelschatz, J., 1978. Analysis of heterotrophic microplankton in an upwelling area. Hydrobiology 60, 195–208.

Strom, S.L., 2000. Bacteriovory: interaction between bacteria and their grazers. In: Kirchman, D. (Ed.), Microbial Ecology of the Oceans. Wiley-Liss, New York, pp. 351–386.

Strub, T., Mesias, J., Montecino, V., Rutllant, J., Salinas, S., 1998. Coastal ocean circulation off Western South America. In: Brink, K.H., Robinson, A. (Eds.), The Sea. Wiley, New York, pp. 273–313.

Tranvik, L.J., Sherr, E.B., Sherr, B.F., 1993. Uptake and utilization of 'colloidal DOM' by heterotrophic flagellates in seawater. Marine Ecology Progress Series 92, 301–309.

Troncoso, V.A., Daneri, G., Cuevas, L.A., Jacob, B., Montero, P., 2003. Bacterial carbon flow in the Humboldt Current System off Chile. Marine Ecology Progress Series 250, 1–12.

Watson, S.W., Novitsky, T.J., Quinby, H.L., Valois, F.W., 1977. Determination of bacterial number and biomass in the marine environment. Applied Environmental Microbiology 33, 940–946.

Wicks, R.J., Robarts, R.D., 1987. The extraction and purification of DNA labelled with [methyl-^{3}H] thymidine in aquatic bacterial production studies. Journal Plankton Research 9 (6), 1159–1166.

Wiebinga, C.J., Veldhuis, M.J.W., Baar, H.J.W., 1997. Abundance and productivity of bacterioplankton in relation to seasonal upwelling in the northwest Indian Ocean. Deep-Sea Research 44, 451–476.

ELSEVIER

Deep-Sea Research II 51 (2004) 2441–2455

DEEP-SEA RESEARCH
PART II

www.elsevier.com/locate/dsr2

Seasonal and interannual variability in the flux of planktic foraminifera in the Humboldt Current System off central Chile (30°S)

Margarita Marchant[a,*], Dierk Hebbeln[b], Susana Giglio[c,d,1], Cecilia Coloma[a,e], Humberto E. González[f]

[a]*Departamento de Zoología, Fac. Ciencias Naturales y Oceanográficas, Universidad de Concepción, Casilla 160-C, Código Postal 4080831, Concepción, Chile*

[b]*Geowissenschaften, Research Center Ocean Margins (RCOM), Universität Bremen, Postfach 330440, D-28334 Bremen, Germany*

[c]*Escuela de Ciencias del Mar, Facultad de Recursos Naturales, Universidad Católica de Valparaíso, Casilla 1020, Valparaíso, Chile*

[d]*Servicio Hidrográfico de la Armada, Av. Errázuriz 232, Playa Ancha, Valparaíso, Chile*

[e]*Programa de Magíster mención Zoología, Escuela de Graduados, Universidad de Concepción, Concepción, Chile*

[f]*Instituto de Biología Marina, Facultad de Ciencias, Universidad Austral de Chile, Campus Isla Teja, Casilla 567, Valdivia, and Centro de Investigación Oceanográfica en el Pacífico Sur-Oriental (FONDAP-COPAS), Chile*

Accepted 24 July 2004

Abstract

Seasonal and interannual changes in the flux of planktic foraminifers were studied in the Humboldt Current System off Coquimbo, Chile (30°S; 73°15′W), using material collected by time series sediment traps located at 2300 m water depth and 100 nautical miles from the coast. The almost continuous record spans 6 years (1993–1998) with a temporal resolution of 6–13 days. The seasonal flux pattern of planktic foraminifers was marked by high fluxes during austral late winter–early summer (August–January) and low fluxes during the fall–early winter period (March–July). Five species contributed ~90% of the total flux of planktic foraminifers: *Globigerina bulloides*, *Neogloboquadrina incompta*, *N. pachyderma*, *N. dutertrei*, and *Globigerinella calida*. Stable oxygen isotope variability in foraminifer shells appears to be driven by seasonal changes in surface seawater temperature; isotope data of *G. bulloides* and *N. incompta* (>212 and 150–212 μm size classes) suggest that water-column stratification dominates during the low-flux period and mixing during the high-flux period. The strong 1997–1998 El Niño event had only a limited impact on the planktic foraminifer flux. The most significant El Niño-related signal was a remarkable increase in the flux and abundance of species that, under normal conditions, only accounted for <10% of the total planktic foraminiferal assemblage.
© 2004 Elsevier Ltd. All rights reserved.

*Corresponding author. Tel.: +56 41 20 4228; fax: +56 41 23 8982.
E-mail address: mmarchan@udec.cl (M. Marchant).
[1]Now at: Programa de Doctorado en Oceanografía, Departamento Oceanografía, Universidad de Concepción, Chile.

0967-0645/$ - see front matter © 2004 Elsevier Ltd. All rights reserved.
doi:10.1016/j.dsr2.2004.08.013

1. Introduction

Eastern boundary current (EBC) systems are driven by coastal upwelling and belong to the most productive regions in the world's oceans (Berger et al., 1989). One such current system is the extensive (~30° latitude) and highly productive (>200 g $C\,m^{-2}\,year^{-1}$) Peru–Chile Current (PCC) or Humboldt Current System (Berger et al., 1987). The PCC, particularly off Chile, remains one of the least studied EBCs, and available information on particle fluxes is rather limited (Marchant et al., 1998; Hebbeln et al., 2000; Romero et al., 2001; González et al., 2004).

To increase the understanding of the dynamics of such upwelling and high-productivity systems, investigations of upwelling and productivity proxies are of special importance. The usefulness of planktic foraminifer tests in such studies has often been demonstrated. Information can be extracted from their flux (or concentration) and their faunal composition (Kroon and Ganssen, 1989; Sautter and Thunell, 1989; Ortiz and Mix, 1992) as well as from the stable isotope composition of their carbonate tests (Kroon and Ganssen, 1989; Sautter and Thunell, 1991; Donner and Wefer, 1994).

Information on the seasonal flux pattern of planktic foraminifers and their stable isotope composition in the PCC has been assessed previously (Marchant et al., 1998) through time-series sediment traps (1991–1994) located at 30°S and 73°15′W, ~100 nautical miles (nm) off Coquimbo, central Chile. Coastal upwelling and its associated filaments in this area result, even at the trap site, in relatively cold sea surface temperatures (SSTs; e.g., 14 °C in winter and 19 °C in summer (http://ingrid.ldgo.columbia.edu/SOURCES/.IGOSS/.nmc/.weekly/.sst/)). Although the prevailing winds are favorable to upwelling throughout the year (Strub et al., 1998), Coastal Zone Color Scanner (CZCS) data show enriched pigment concentrations only from July to October (e.g. Thomas, 1999; Thomas et al., 1994) or for the summer (SeaWiFS) (Thomas et al., 2001).

Marchant et al. (1998) found a distinct seasonal cycle in the flux of planktic foraminifers, with high fluxes between August and January and low fluxes during the rest of the year. The higher fluxes coincided with increased coastal upwelling, as indicated by stable oxygen isotope data. During the weak 1991–1992 El Niño (EN) event, fluxes were only slightly lower and the faunal composition reflected the warmer SSTs. However, there were only small differences between the average fluxes of the 1991–1992 EN and the following normal period (1993–1994), with 3000 and 4000 shells $m^{-2}\,day^{-1}$ in the >150 μm fraction, respectively.

This study extends the earlier planktic foraminifer flux record, analyzing a full 5-year record (22 July 1993–30 June 1998) of measurements from the oceanic station off Coquimbo in order to: (1) determine the daily average fluxes of individual planktic foraminifer species, (2) assess the seasonal and interannual variability of these fluxes, and (3) estimate the impact of the strong 1997–1998 EN event on the assemblage compositions and fluxes.

2. Material and methods

In addition to published foraminiferal flux and oxygen isotope data from the study site off Coquimbo (November 1991–April 1992, July 1993–July 1994) (Marchant et al., 1998; Hebbeln et al., 2000), new data collected between September 1994 and July 1998 are included here. During this period, time-series sediment traps (Kiel-SMT 230, cone-shaped, 0.5-m^2 collection area, 20 sample cups) were deployed at ~100 nm off Coquimbo, Chile (OCEMOS station) (Fig. 1) at 2300 m depth and approximately 2000 m above the seafloor. The traps were deployed and recovered six times (CH5–2, CH6–2, CH7–2, CH8–2, CH10–2, and CH11–1) (see Table 1 for details), thus providing a rather high temporal resolution of 6–13 days per sample. A current meter was located 20 m below each trap during the deployment period. Current velocities were normally well below 10 cm s^{-1} (S. Salinas, pers. comm.); thus trapping efficiency (Baker et al., 1988) was probably not significantly affected by the currents around the traps. The mid-dates of the sampling periods were used to graph the flux data.

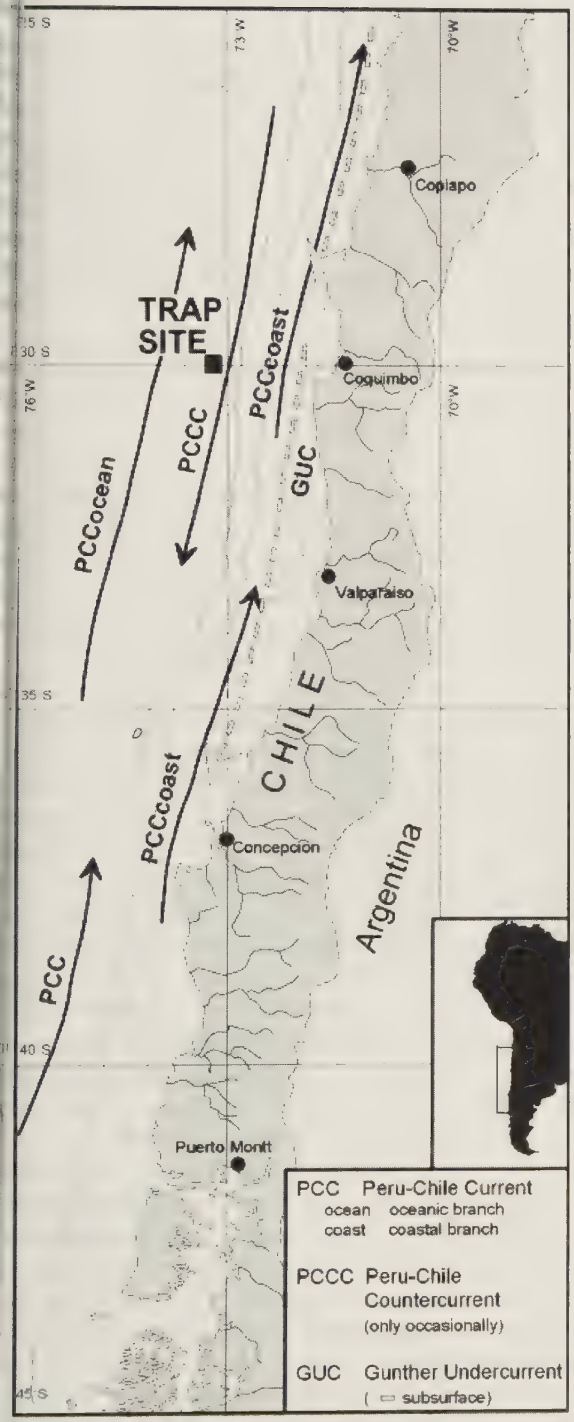

Fig. 1. Location of the mooring site (black square) at 30°S and 73°15′W in relation to ocean surface and subsurface currents in the SE Pacific off Chile (after Shaffer et al., 1995; Strub et al., 1998).

Before deployment, 1 ml of saturated $HgCl_2$ solution was added per 100 ml of sample solution (seawater from 2000 m water depth) to retard microbial degradation of the collected material (Lee et al., 1992). NaCl was added to the sampling cups to reach a final salinity of 38–40. After recovery, the samples were poisoned again with $HgCl_2$ (0.5 ml in 100 ml of seawater) and stored at 4 °C. In the laboratory, the samples were carefully wet-sieved through a 1-mm screen and split into aliquots by a rotary liquid splitter. The splitting procedure, sample preparation, and analysis are the same as those described in Fischer and Wefer (1991).

Carbonate contents of the collected material were determined with an elementary analyzer (Hereaus CHN-O-Rapid) on freeze-dried and homogenized material of a $\frac{1}{5}$ split. Total carbon (TC) contents were measured on untreated samples, and organic carbon (TOC) contents on HCl-treated samples. Carbonate contents were calculated according to the formula: $CaCO_3 = [(TC - TOC) \times 8.333]$ and refer to the <1 mm fraction; the >1 mm fraction was negligible in amount and dominated by undamaged zooplankton organisms, which are assumed to reflect "swimmers" that are not part of the passive particle flux.

The foraminiferal shells were individually picked from wet-sample splits ($\frac{1}{25}$) by pipette. After washing the tests and drying them at 50 °C, the foraminifers were divided into three size fractions: 63–150, 150–212, and >212 μm. All foraminifers were weighed to determine the foraminiferal carbonate flux. Data concerning the number of foraminifer shells and the species composition of the foraminiferal fauna were only obtained for the >150 μm fraction. The <150 μm fraction was not investigated in more detail due to taxonomic difficulties in identifying small juvenile forms. Investigated planktic foraminifer species were identified after Kennett and Srinivasan (1983), Hemleben et al. (1989), and Kemle-von Mücke and Hemleben (1999).

Two species of planktic foraminifera, *Neogloboquadrina incompta* [formerly referred to as *Neogloboquadrina pachyderma* (dex.), (Kemle-von Mücke and Hemleben, 1999)] and *Globigerina*

Table 1
Logistics of the sediment traps deployed in the study area off Coquimbo, Chile, between July 1993 and June 1998

Sediment trap	Sampling interval (d)	Latitude (°S)	Longitude (°W)	Water depth (m)	Trap depth (m)	Sampling period
CH 3-1	9	30°01.05′	73°11.00′	4360	2333	22 Jul. 1993–18 Jan. 1994
CH 4-1	8	30°00.30′	73°10.27′	4330	2303	25 Jan. 1994–04 Jul. 1994
CH 5-2	6	29°59.61′	73°13.23′	4410	2407	25 Sep. 1994–23 Jan. 1995
CH 6-2	6	29°57.30′	73°17.21′	4420	2393	28 Jan. 1995–28 May 1995
CH 7-2	11	29°57.40′	73°17.30′	4420	2498	07 Jun. 1995–13 Jan. 1996
CH 8-2	8	29°54.80′	73°17.97′	4430	2508	28 Jan. 1996–07 Jul. 1996
CH 9-2	No data available due to malfunctioning of the sediment trap					
CH 10-2	13	29°59.90′	73°16.75′	4500	2578	14 Feb. 1997–31 Oct. 1997
CH 11-1	12	29°58.80′	73°18.10′	4440	2526	03 Nov. 1997–30 Jun. 1998

bulloides, were analyzed for the stable oxygen isotope composition ($\delta^{18}O$) of their carbonate shells. Each measurement was performed on 15–30 individual shells of each species for the 150–212 μm and >212 μm size fractions. Stable isotope measurements were performed on a Finnigan MAT 251 mass spectrometer with an automated carbonate preparation device. The isotopic composition of the carbonate sample was measured on the CO_2 gas evolved by treatment with phosphoric acid at a constant temperature of 75 °C. The ratio of $^{18}O/^{16}O$ is given in ‰ relative to the PDB standard. A working standard (Burgbrohl CO_2 gas) was used for the measurement of the isotopic ratios of the samples. This standard gas was calibrated against the PDB standard using standards NBS 18, 19, and 20 of the National Bureau of Standards. Analytical standard deviation is about ±0.07‰ PDB (Isotope Laboratory, Bremen University).

3. Results

Of the 160 samples available, 133 were analyzed for planktic foraminifer species. The remaining samples were from so-called stagnation periods, when mass fluxes of unknown origin clogged the traps and no material was collected. In addition, no planktic foraminifers were found in five samples collected in October 1995, although these samples had a relatively high carbonate content, and, most likely, were affected by a preservation problem. The new data were integrated to previously published data collected in 1993–1994 (Marchant et al., 1998) in order to discuss the longest possible time series.

3.1. Carbonate flux and foraminiferal fluxes

The total carbonate flux (Fig. 2, upper panel) varied between almost 0 and ~180 mg m^{-2} day^{-1}, showing a weak seasonal pattern of higher fluxes in austral late winter–early summer (August–January) as compared to the fall–early winter period (March–July). The foraminiferal carbonate flux (>63 μm) reached maximum values of ~110 mg m^{-2} day^{-1} in early 1996 and, in general, followed the pattern of the total carbonate flux. The foraminiferal carbonate flux contributed, on average, ~40% to the total carbonate flux, but was significantly lower (<25%) during the second half of 1993, when the total carbonate flux had maximum values, and at the end of 1994.

The flux of foraminifer shells in the >150 μm fraction closely followed the foraminiferal carbonate flux (Fig. 2, lower panel); small foraminifers (<150 μm) only contributed about one-third of the foraminiferal carbonate flux. The highest foraminifer fluxes were observed during the early summer months, with peak values of 17,500 shells m^{-2} day^{-1} in 1994; 9300 shells m^{-2} day^{-1} in 1995; 13,400 shells m^{-2} day^{-1} in 1996; and 15,300 shells m^{-2} day^{-1} in 1997 (Fig. 2, lower panel).

A total of 27 species of planktic foraminifers (>150 μm) collected in the sediment trap between

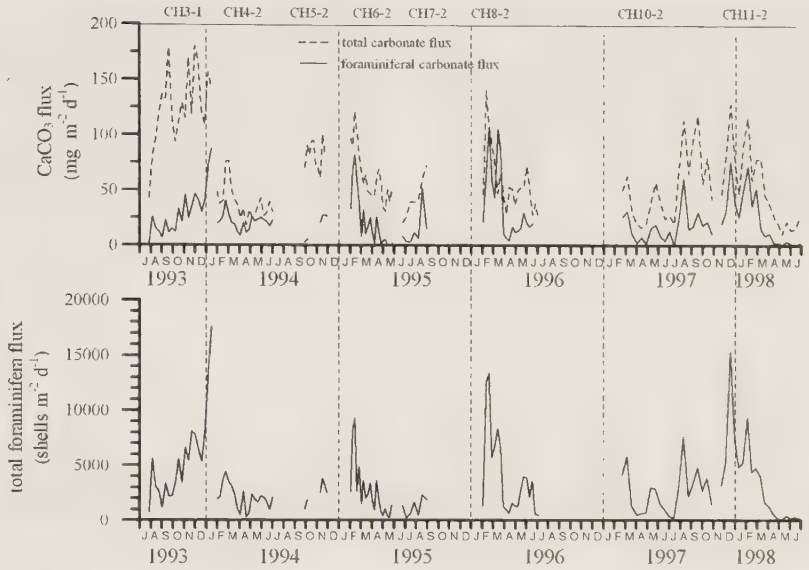
CH3-1
CH4-2
CH5-2
CH6-2
CH7-2
CH8-2
CH10-2
CH11-2
total carbonate flux
foraminiferal carbonate flux
CaCO3 flux (mg m-2 d-1)
total foraminifera flux (shells m-2 d-1)
J A S O N D J F M A M J J A S O N D J F M A M J J A S O N D J F M A M J J A S O N D J F M A M J J A S O N D J F M A M J
1993
1994
1995
1996
1997
1998

Fig. 2. Total carbonate and foraminiferal (>63 μm) carbonate fluxes (upper panel), and total flux of foraminifer shells (>150 μm) (lower panel) at trap site (30°S and 73°15′W) between July 1993 and June 1998.

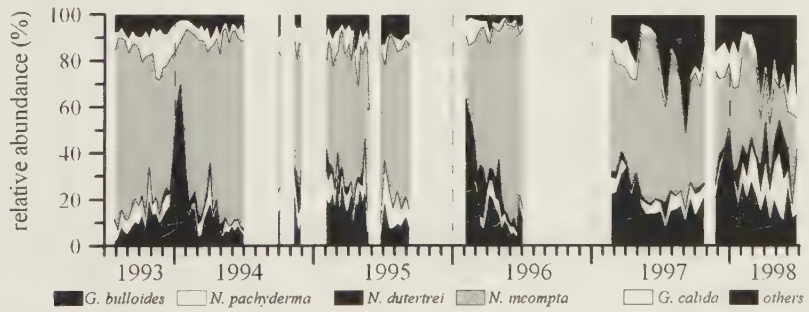

Fig. 3. Faunal composition (relative contribution) of the planktic foraminiferal flux (>150 μm) at the trap site (30°S and 73°15′W) between July 1993 and June 1998.

1993 and 1998 were identified. Five species accounted for approximately 90% of the total foraminiferal flux (Fig. 3): *G. bulloides*, *Globigerinella calida*, *Neogloboquadrina dutertrei*, *N. pachyderma*, and *N. incompta*. In 1997 and 1998, when the proportions of these five species decreased to <70% of the total assemblage, *Globorotalia crassaformis*, *Globigerinella siphonifera*, *Globigerinoides sacculifer*, *Globoquadrina conglomerata*, *Hastigerina digitata*, and *Pulleniatina obliquiloculata* together made up >20% of this total, though these species were rare before 1997. In addition, *Globigerinella digitata* and *Globorotalia tumida* were only found in the 1997–1998 samples.

Numerically, *N. incompta* was the dominant species, accounting for an average of 60% across most of the record; this percentage was higher in 1993–1994 and lower in 1998 (Fig. 3). The average *G. bulloides* contribution throughout the sampling period was 5–20%, with some individual summer peaks (60–70% in 1993–1994, 45–55% in 1996, and 40% in 1997–1998). Other contributions were smaller (<10%) but also

variable. *N. pachyderma* contributed 3–5% on average and showed relative maxima (up to 10%) during late winter–early summer periods. The average contribution of *G. calida* varied between 4% (1996) and 9% (1998), whereas *N. dutertrei* accounted for values from >8% (1996 and 1998) to <2% during the rest of record.

Among the five dominant species, the flux of *G. bulloides* shells was marked by extreme summer peaks in 1993–1994 (~12,000 shells m^{-2} day^{-1}), 1996 (~7000 shells m^{-2} day^{-1}), and 1997 (~6000 shells m^{-2} day^{-1}), whereas in the remaining period, the flux did not exceed 2000 shells m^{-2} day^{-1} (Fig. 4). *G. calida* showed extreme summer peaks in 1995 (~1200 shells m^{-2} day^{-1}) and 1998 (~800

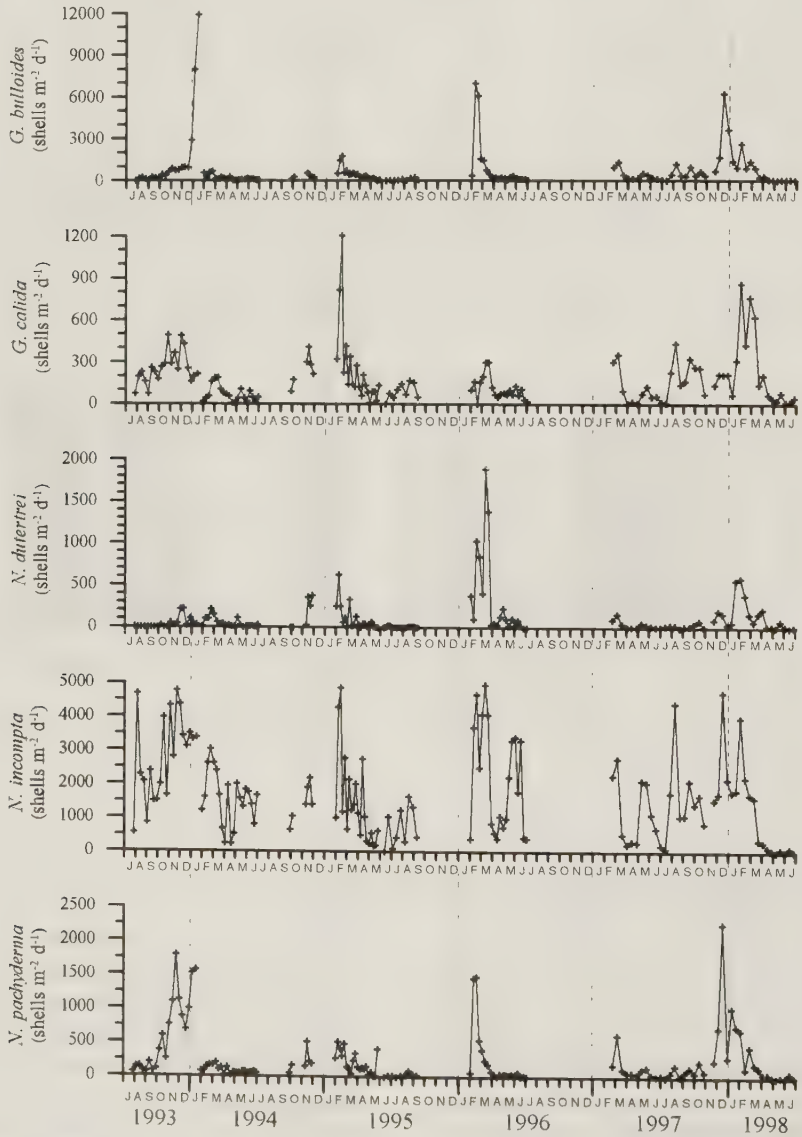

Fig. 4. Fluxes of the five most important planktic foraminifera species (>150 μm) at the trap site (30°S and 73°15′W) between July 1993 and June 1998.

ells m^{-2} day^{-1}); during all other periods it gistered less than ~500 shells m^{-2} day^{-1}, with wer fluxes in fall and winter. *N. dutertrei* resented very low fluxes (<200 shells m^{-2} day^{-1}), ith maxima in the summers of 1995 and 1998 ~600 shells m^{-2} day^{-1}) and the summer of 1996 ~1800 shells m^{-2} day^{-1}). The flux of *N. incompta* ached up to 5000 shells m^{-2} day^{-1}, with higher alues mainly occurring in late winter–early summer and lower values in fall–early winter. *N. pachyderma* fluxes peaked in spring–summer 1993 (~1800 shells m^{-2} day^{-1}), 1996 (~1500 shells m^{-2} day^{-1}), and at the end of 1997 (~2300 shells m^{-2} day^{-1}), with less-pronounced maxima in the summers of 1994–1995 and at the beginning of 1997 (~500 shells m^{-2} day^{-1}); the rest of the time, the fluxes were rather low (<200 shells m^{-2} day^{-1}) (Fig. 4).

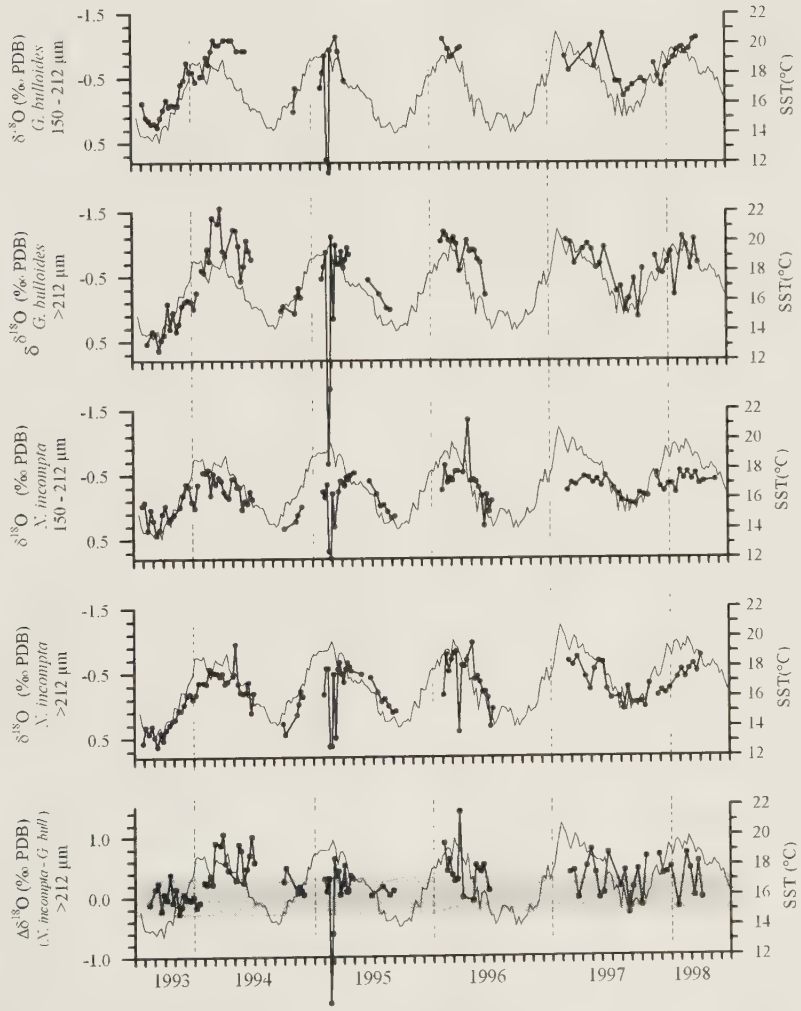

Fig. 5. Stable oxygen isotope data ($\delta^{18}O$) of *G. bulloides* and *N. incompta* for the two size classes (150–212 and >212 µm) collected at the trap site (30°S and 73°15′W) between July 1993 and June 1998 (bold lines with symbols). The $\Delta\delta^{18}O$ (*N. incompta G. bulloides*; >212 µm) is interpreted as a measure of the degree of mixing of the water column (see text); the gray shaded field indicates a well-mixed water column (see text). Sea-surface temperature (SST) data for the mooring site (thin lines) were obtained from http://ingrid.ldgo.columbia.edu/SOURCES/.IGOSS/.nmc/.weekly/.sst/.

3.2. Stable oxygen isotopes in G. bulloides and N. incompta

The $\delta^{18}O$ data for *G. bulloides* and *N. incompta* (150–212 μm and >212 μm) showed a continuous change from high winter (mainly August–September) values (~0.8–0‰ PDB) to low summer (mainly February–April) values (<−1‰ PDB for *G. bulloides* and <−0.5‰ PDB for *N. incompta*), reflecting the yearly summer sea-surface warming (Fig. 5). The most prominent deviations from the annual SST cycle occurred (a) in the first part of 1994, when the *G. bulloides* data were rather light, especially for the >212 μm fraction; (b) in spring–summer 1994–1995, when the *N. incompta* data for both fractions were relatively heavy; and (c) in 1997–1998, when the seasonal cycle was significantly smoothed in *N. incompta*, especially in the smaller fraction (Fig. 5). Extremely high $\delta^{18}O$ data in all four data sets appeared during the summer period (February–March) of 1995, which were enriched by 1–3‰.

Overall, the $\delta^{18}O$ values for *N. incompta* were heavier (i.e. colder) than those of *G. bulloides*, with maximum amplitudes of 1.5 and 2‰, respectively (Fig. 5). During the late winter–early summer period, $\delta^{18}O$ values of both species were similar, while during fall–early winter, in all records, the values of *G. bulloides* were considerably lighter than those of *N. incompta*.

4. Discussion

4.1. Variations in water column properties as deduced from stable oxygen isotopes

The occurrence of *G. bulloides* from subpolar to tropical regions suggests that the distribution and abundance of this species may be controlled primarily by food availability, rather than by a specific temperature range (Deuser et al., 1981; Thunell and Reynolds, 1984). This species is often mentioned as a typical indicator of upwelling conditions (Thiede, 1975; Reynolds and Thunell, 1985). *G. bulloides* lives in the surface mixed layer (Steens et al., 1992) and is most abundant above the thermocline (Fairbanks et al., 1982). In contrast, *N. incompta*, mainly confined to th subpolar zone (Bradshaw, 1959), is a deep-dwel ing species mostly living below the thermoclin (Fairbanks et al., 1982).

Between 1993 and 1998, the $\delta^{18}O$ values of th two size classes of *G. bulloides* and *N. incompt* showed a very similar pattern compared to th SST data (Fig. 5). This similarity became ever more obvious when comparing the winter season of the cold year (1993) and the warm year (1997) The difference in SST (~1.5 °C) corresponded to a comparable offset in the $\delta^{18}O$ data (~0.5‰).

In order to compare the stable oxygen isotope data of *G. bulloides* and *N. incompta* in terms o water column structure, any vital effects that may affect their isotope data have to be ruled out. For both species, vital effects have been described for oxygen isotope fractionation; however, for *G. bulloides* (Spero and Lea, 1996) and encrusted *N. incompta* (only encrusted shells were used in this study) (Kohfeld et al., 1996), this vital effect is of the order of −0.8‰ and therefore negligible when calculating the $\Delta\delta^{18}O$ for these species. For the calculation of the $\Delta\delta^{18}O$, we focused on the >212 μm fraction, as Spero and Lea (1996) recommended the use of bigger shells for paleoceanographic applications.

As mentioned earlier (Marchant et al., 1998), the larger amplitude in $\delta^{18}O$ of *G. bulloides* (2‰) in comparison with *N. incompta* (1.5‰) suggests a generally shallower, and thus more variable, habitat above the thermocline for *G. bulloides* and a deeper, relatively more stable, (sub) thermocline habitat for *N. incompta*. These interpretations are in accordance with temperature measurements at the mooring site, indicating a seasonal temperature range of ⩾8 °C for the 0–50 m layer and ⩾4 °C for the 50–100 m layer (Salinas et al., unpublished data) (Fig. 6A).

Based on their different depth habitats in a stratified water column, the oxygen isotope data of *G. bulloides* and *N. incompta* are expected to record a distinct temperature difference. In contrast, when strong upwelling deepens the surface mixed layer, the two species build their shells in a much less stratified water mass and the $\Delta\delta^{18}O$ ideally approaches 0. Under non-upwelling conditions, the species live at different depths within a

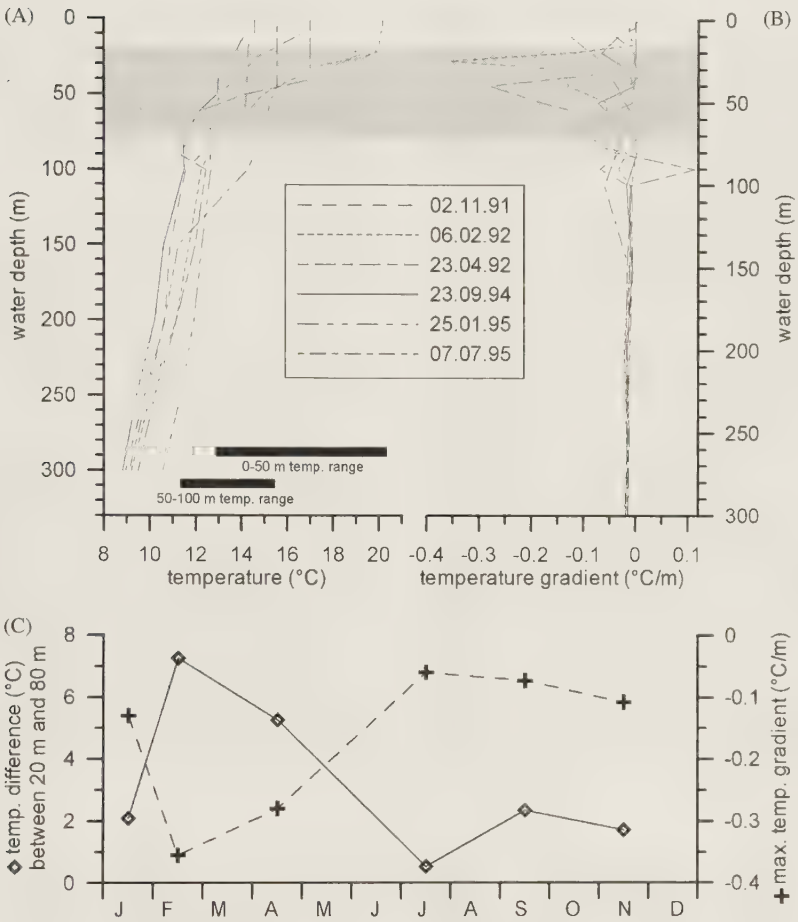

Fig. 6. (A) Temperature distribution in the upper water column at the sediment trap site during various sampling dates. Black bars indicate the temperature ranges in the 0–50 and 50–100 m intervals, respectively. (B) Temperature gradients from data in (A), expressed as the average temperature change per m unit. Gray shading in (A) and (B) marks the 20–80 m depth interval. (C) Stratification state in the upper water column indicated by the temperature difference between 20 and 80 m water depth (diamonds) and by the maximum temperature gradient (crosses) taken from (B). Plots are based on unpublished data from JGOFS-CHILE cruises (courtesy of L. Salinas, Pontificia Universidad Católica de Valparaíso, Chile).

stratified water column, resulting in a considerable $\Delta\delta^{18}O$ (we use $\pm 0.3‰$ as an empirically derived range indicating upwelling conditions; Marchant et al., 1998) (see Fig. 5).

Thus, late winter–early summer $\Delta\delta^{18}O$ values close to 0 point to homogenous conditions in both habitats, mainly in terms of temperature (i.e. a mixed water column, most likely related to upwelling; also high pigment concentrations in surface waters during summer) (Thomas et al., 2001). In contrast, diverging values during the late summer–early winter period reflect different conditions, which are probably induced by stratification of the water column under non-upwelling conditions. Such a pattern is also reflected in the temperature measurements at the mooring site (Salinas et al., unpublished data), which show maximum temperature gradients and higher temperature differences in the 20–80 m layer during February and April (Fig. 6B, C). At other sampling times (January, July, September, and November), considerably lower temperature

differences and gradients point to a much better mixed water column, as also reflected in the $\Delta\delta^{18}O$ data (Fig. 5). Continuing with the approach developed by Steens et al. (1992) and applied to the PCC by Marchant et al. (1998) and Hebbeln et al. (2000), we used the $\Delta\delta^{18}O$ of both species (*N. incompta* and *G. bulloides*; >212 μm fraction) as an indicator of upwelling intensity (Fig. 5). Over the entire study period, the $\Delta\delta^{18}O$ data varied between −0.3 and 1.5‰ (Fig. 5), except for the event in early 1995.

Focusing on a seasonality analysis, and in spite of the scatter in the data, there is an obvious difference between fall–early winter and late winter–early summer data (Fig. 7). Whereas during fall–early winter, many $\Delta\delta^{18}O$ data were >0.3‰, most of them were <0.3‰ for the late winter–early summer period. The scatter in the data indicate that the conditions were quite variable, with the fall–early winter season (March–June) characterized by a continuous change between upwelling events and periods of stratification, and the late winter–early summer (August–January) dominated by upwelling. Based on these data, we can differentiate between a upwelling-dominated period in late winter–ear summer and a stratification-affected period i fall–early winter, which is a rather consisten signal over the entire time series record (Fig. 7).

In February–March 1995, the $\delta^{18}O$ data showe an unusual pattern, with values enriched by 1–3‰ compared to the rest of the record (Fig. 5). As thes "outliers" were observed in both size classes of th two species, they most likely reflect a real oceanc graphic phenomenon. If these data were to reflec an extreme upwelling event, the SST should hav dropped by >10 °C. If they were to reflect a chang in salinity, the psu should have increased by ~1(However, neither explanation appears likely. Dur ing this event, there was neither a significant chang in the species assemblage of planktic foraminifera nor a change in their fluxes. Furthermore, the fluxe of the main flux constituents (lithogenic matter carbonate, biogenic opal, and organic matter) show no indication of an unusual advective even (Hebbeln, unpublished data) that could have resulted from the reworking of glacial (i.e. iso topically heavy) shelf or slope sediments.

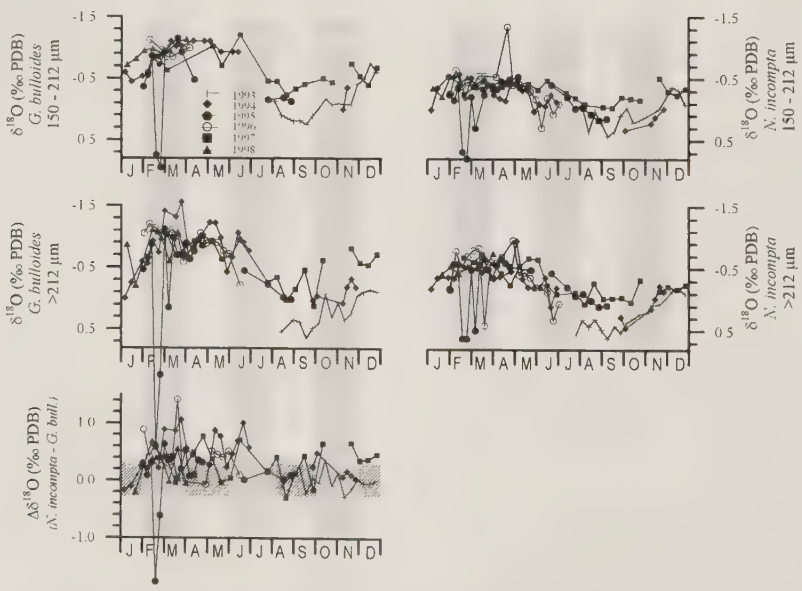

Fig. 7. Seasonal variability of stable oxygen isotope data ($\delta^{18}O$) of *G. bulloides* and *N. incompta* for the two size classes (150–212 and >212 μm) and for the $\Delta\delta^{18}O$ data (see text) collected at the trap site (30° S and 73° 15′W) between July 1993 and June 1998. The hatched field in the $\Delta\delta^{18}O$ graph is indicative of a well-mixed water column (see text). The vertical gray shadings indicate two month periods to facilitate data comparison.

Seasonal patterns in the fluxes of planktic foraminifers and other organisms

Highest total carbonate ($\sim$100 mg m^{-2} day^{-1}) and foraminiferal carbonate fluxes ($\sim$70 mg m^{-2} day^{-1}) occurred during the late winter–summer period (Fig. 8A, B), extending beyond the return of the isotope data to a more stratified setting. This pattern also was reflected in the total foraminiferal flux (Fig. 8D), which reached peak values of >10,000 shells m^{-2} day^{-1} in early summer. Thus, in contrast to diatoms (exemplified by the biogenic opal flux in Fig. 8F), which were characterized by a distinct high-flux event from August to October (the beginning of the upwelling period at this site) (Romero et al., 2001), the foraminifers were not closely related to the onset of upwelling conditions. Rather, they displayed a typical secondary producer pattern by following the primary producers (i.e. diatoms) slightly later.

Whereas the foraminiferal carbonate flux (>63 μm) only accounted, on average, for ~40% of the total carbonate flux (Fig. 2, 8E), the remaining fraction consisted largely of coccoliths (Marchant et al., 1998; González et al., 2004). Such coccoliths, assumed here to be the most important contributors to the non-foraminiferal $CaCO_3$ flux, had their highest fluxes between August and December (Fig. 8C). The flux of planktic foraminifers also started to increase in August and peaked between November and March. Thus, there seems to be a distinct sequence in the fluxes of organisms in response to the onset of upwelling conditions, characterized by a bloom of diatoms, accompanied and followed by a less pronounced but longer lasting bloom of coccolithophores, and finally, maximum fluxes of planktic foraminifers (Fig. 8). This pattern also was reflected in the varying contributions of carbonaceous organisms to the total $CaCO_3$ flux (Fig. 8E). While the planktic foraminifers contributed <35% between September and November, they accounted for >45% in January–February.

Annual planktic foraminiferal flux data can only be compiled for 1993–1994 (4000 shells m^{-2} day^{-1}) and 1997–1998 (3400 shells m^{-2} day^{-1}). These

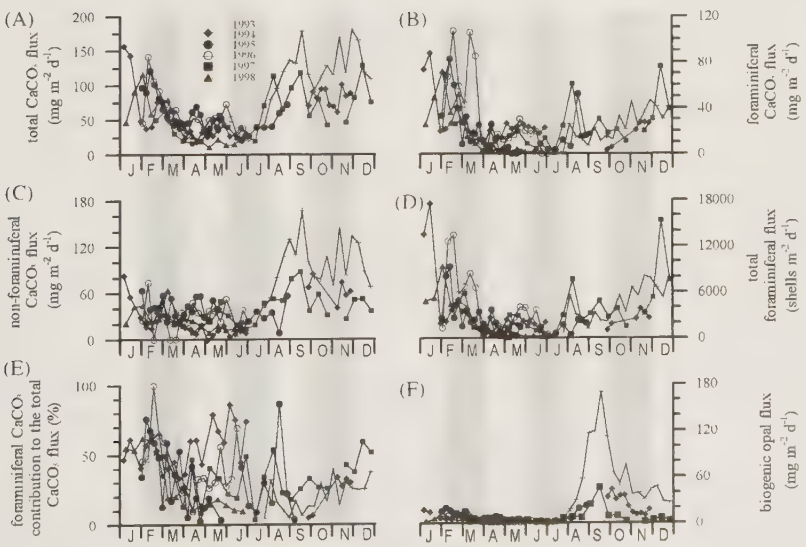

Fig. 8. Seasonal variability of (A) the total carbonate flux, (B) the foraminiferal and (C) the non-foraminiferal carbonate flux, (D) the total flux of foraminiferal shells (>150 μm), (E) the foraminiferal carbonate contribution to the total carbonate flux, and (F) the biogenic opal flux (D.H., unpublished data) at the trap site (30 S and 73 15′W) between July 1993 and June 1998. Vertical gray shadings as in Fig. 7.

numbers characterize the PCC area as a very productive region with respect to planktic foraminifers; in fact, in a Pacific-wide comparison (see Marchant et al., 1998), the PCC is only rivaled by Station Papa in the NE Pacific, where annual fluxes reach 3200 shells $m^{-2} day^{-1}$ (Reynolds and Thunell, 1989).

4.3. *The impact of El Niño on planktic foraminifera in the waters off Chile*

The Southern Oscillation Index (SOI) indicated two EN southern oscillation (ENSO) events during the study period (1993–1998): the long 1991–1995 period, which was marked by some punctuated events of prevailing EN conditions, and the strong 1997–1998 event (Fig. 9). The mooring site off central Chile is close to the southern limit of the detectable EN signal in the water column, as indicated by the weak SST anomalies of $<2°C$ associated with the stro 1997–1998 EN event (Fig. 9). However, t analysis of SSTs obtained in weekly intervals the mooring site showed a distinct EN-relate signal during the 1997–1998 EN event, whe SSTs increased by $>1°C$ compared to a 18-year weekly average (Fig. 9). In contras during 1994, when the SOI pointed to ENS conditions in the central Pacific, SSTs off Chi were within a 1 °C range from the average, which assumed to reflect normal conditions. Thus, f the period considered here, only the 1997–199 event resulted in EN conditions at the samplin site.

The most remarkable observations that can b attributed to this warm event were the significantl enhanced fluxes and relative abundances of th foraminifers combined as "other species", which under normal conditions, were far less importan (on average, $<10\%$ of the total foraminifera

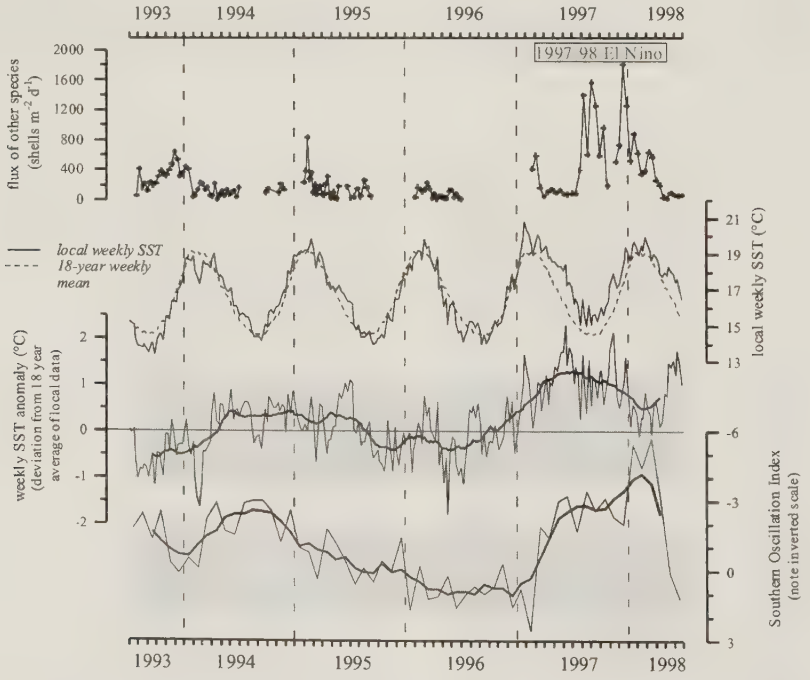

Fig. 9. The combined flux of less important planktic foraminiferer species ("other species") at the trap site (30°S and 73°15′W) between July 1993 and June 1998, in relation to the weekly local SST record. The difference between the SST record and its 18-year weekly mean is shown as the weekly SST anomaly (gray shading marks −1 to +1 C range), showing the strongest deviations from the mean during the 1997–1998 EN event, which is also indicated in the lowest numbers of the SOI (note inverted scale). SST data were obtained as in Fig. 5 and SOI data from http://ingrid.ldgo.columbia.edu/SOURCES/.Indices/.soi.

una) than the dominant species discussed above. nong these other species were mostly warm-ter species, such as *G. crassaformis*, *G. siphonia*, *G. sacculifer*, *G. conglomerata*, *H. digitata*, d *P. obliquiloculata* (Kemle-von Mücke and mleben, 1999). Some species (*G. digitata*, *G. lobus*, and *G. tumida*) occurred exclusively ring this EN event and were absent in the naining part of the time-series record. The antitatively most important "other species" ring this period were *H. digitata*, *Turborotalita inqueloba*, and *Globigerinita glutinata*. During e 1997–1998 El Niño event, the average con-bution of these "other species" increased to 20% (Fig. 3), and their combined fluxes reached lues of >1000 shells m^{-2} day^{-1} (Fig. 9). In ntrast, the dominant species showed no clear N-related signal.

The stable oxygen isotope data of the (sub) ermocline species, *N. incompta*, showed a ry smooth seasonal cycle during this EN event ig. 5), with normal winter data but very old" summer data. These "cold" summer data ere even "colder" than in the previous years, though the SST was slightly warmer in 997–1998. These "cold" summer data might oint to an even deeper habitat of *N. incompta* uring the EN event compared to the ormal years. This habitat shift was probably duced by a deepening of the thermocline the course of the EN event, a typical feature f an EN event along the South American est coast (Arntz and Fahrbach, 1996; Escribano t al., 2004).

In an earlier study of planktic foraminiferal uxes from this same site, Marchant et al. (1998) ompared a short record from the 1991–1992 EN, hen SST anomalies reached values $>1\,^{\circ}C$ in a w short pulses, to the normal record from 993–1994. Their results indicated that the 991–1992 EN, which was a significantly weaker vent off Chile than the 1997–1998 EN, was haracterized (1) by enhanced *N. dutertrei* and educed *N. pachyderma* fluxes and (2) by lower otal foraminiferal fluxes. The much longer ecord analyzed here indicates that these obser-ations cannot be clearly related to EN onditions.

Acknowledgments

We are grateful to M. Segl and B. Meyer-Schack, who performed the stable isotope measurements at the Isotope Laboratory, Bremen University. We acknowledge the officers and crews of the R/V Vidal Gormaz and R/V Abate Molina for their excellent seamanship, often under the most difficult conditions. Special thanks are due to S. Salinas for providing unpublished CTD-data from the sediment trap site. The comments and suggestions of three anonymous reviewers are appreciated. This work was supported by the German Bundesministerium für Bildung und Forschung through funding of the project "JGOFS-Chile". M.M. acknowledges financial support by the Deutscher Akademischer Austauschdienst (DAAD) and the Chilean National Commission for Science and Technology, through FONDECYT 2001, Project No. 1010912 and FONDAP-COPAS Project No. 150100007. Technical support from the Research Center Ocean Margins (Bremen University) and the Dirección de Investigación and Departamento de Zoología (Universidad de Concepción) is also acknowledged.

References

Arntz, W.E., Fahrbach, E., 1996. El Nino—Experimento climatico de la naturaleza: Causas fisicas y efectos biologicos. Fondo de Cultura Economica, Mexico 312pp.

Baker, E.T., Milburn, H.B., Tennant, D.A., 1988. Field assessment of sediment-trap efficiency under varying flow conditions. Journal of Marine Research 46, 573–592.

Berger, W.H., Fischer, K., Lai, C., Wu, G., 1987. Ocean productivity and organic carbon flux Part I Overview and maps of primary production and export productivity. University of California, San Diego SIO Reference, pp. 87–30.

Berger, W.H., Smetacek, V.S., Wefer, G., 1989. Ocean productivity and paleoproductivity—an overview. In: Berger, W.H., Smetacek, V.S., Wefer, G. (Eds.), Productivity of the Ocean: Present and Past. Dahlem Workshop Report. Wiley, New York, pp. 1–34.

Bradshaw, J.S., 1959. Ecology of living planktonic foraminifera in the north and equatorial Pacific Ocean. Contributions of the Cushman Foundation for Foraminiferal Research 10, Part 2, pp. 25–64.

Deuser, W.G., Ross, E.H., Hemleben, Ch., Spindler, M., 1981. Seasonal changes in species composition, numbers, mass, size, and isotopic composition, of planktonic foraminifera settling into the deep Sargasso Sea. Palaeogeography, Palaeoclimatology, Palaeoecology 33, 103–127.

Donner, B., Wefer, G., 1994. Flux and stable isotope composition of *Neogloboquadrina pachyderma* and other planktonic foraminifers in the Southern Ocean (Atlantic sector). Deep-Sea Research I 41, 1733–1743.

Escribano, R., Daneri, G., Farías, L., Gallardo, V.A., González, H.E., Gutiérrez, D., Lange, C.B., Morales, C.E., Pizarro, O., Ulloa, O., Braun, M., 2004. Biological and chemical consequences of the 1997–1998 El Niño in the Chilean coastal upwelling system: a synthesis. Deep-Sea Research II, this issue [doi:10.1016/j.dsr2.2004.08.011].

Fairbanks, R.G., Sverdlove, M., Free, R., Wiebe, P.H., Bé, A.W.H., 1982. Vertical distribution and isotopic fractionation of living planktonic foraminifera from the Panama Basin. Nature 298, 841–844.

Fischer, G., Wefer, G., 1991. Sampling, preparation and analysis of marine particulate matter. In: Hurd, D.C., Spencer, D.W. (Eds.), The Analysis and Characterization of Marine Particles, Geophysical Monograph 63, 391–397.

González, H.E., Hebbeln, D., Iriate, J.L., Marchant, M., 2004. Downward fluxes of faecal material and microplankton at 2300 m depth in the oceanic area off Coquimbo (30°S), Chile, during 1993–1995. Deep-Sea Research II, this issue [doi:10.1016/j.dsr2.2004.07.027].

Hebbeln, D., Marchant, M., Wefer, G., 2000. Seasonal variations of the particle flux in the Peru–Chile Current under "normal" and under El Niño conditions. Deep-Sea Research II 47, 2101–2128.

Hemleben, C., Spindler, M., Anderson, O.R., 1989. Modern Planktonic Foraminifera. Springer, New York, 335pp.

Kemle von-Mücke, S., Hemleben, C., 1999. Foraminifera. In: Boltovskoy, D. (Ed.), South Atlantic Zooplankton. Backhuys Publishers, Leiden, The Netherlands, pp. 43–73.

Kennett, J., Srinivasan, M., 1983. Neogene planktonic foraminifera – a phylogenetic atlas. Hutchinson Ross Publishing Company, Stroudsburg, 265pp.

Kohfeld, K.E., Fairbanks, R.G., Smith, S.L., Walsh, I.D., 1996. *Neogloboquadrina pachyderma* (sinistral coiling) as paleoceanographic tracers in polar ocean: evidence from Northeast Water Polynya plankton tows, sediment traps, and surface sediments. Paleoceanography 11, 679–699.

Kroon, D., Ganssen, G., 1989. Northern Indian Ocean upwelling cells and the stable isotope composition of living planktonic foraminifers. Deep-Sea Research 36, 1219–1236.

Lee, C., Hedges, J.I., Wakeham, S.G., Zhu, N., 1992. Effectiveness of various treatments in retarding microbial activity in sediment trap material and their effects on the collection of swimmers. Limnology and Oceanography 37, 117–130.

Marchant, M., Hebbeln, D., Wefer, G., 1998. Seasonal fl patterns of planktic foraminifera in the Peru–Chile Curre Deep-Sea Research I 45, 1161–1185.

Ortiz, J.D., Mix, A.C., 1992. The spatial distribution an seasonal succession of planktonic foraminifera in t California Current off Oregon, September 1987 – Septemb 1988. In: Summerhayes. C.P., Prell, W.L., Emeis, K.C (Eds.), Upwelling Systems: Evolution Since t Early Miocene, Geological Society Special Publication 6 pp. 197–213.

Reynolds, S.L., Thunell, R., 1985. Seasonal succession planktonic foraminifera in the subpolar North Pacifi Journal of Foraminiferal Research 15, 282–301.

Reynolds, S.L., Thunell, R., 1989. Seasonal succession planktonic foraminifera: results from a four-yea time-series sediment trap experiment in the Northea Pacific. Journal of Foraminiferal Research 19 (4 253–267.

Romero, O.E., Hebbeln, D., Wefer, G., 2001. Variability i export production in the SE Pacific Ocean during El Niñ and non-El Niño conditions: evidence from diatom fluxe and surface sediment assemblages. Deep-Sea Research 48 2673–2697.

Sautter, L.R., Thunell, R., 1989. Seasonal succession o planktic foraminifera: results from a four-year time-serie sediment trap experiment in the Northeast Pacific. Journa of Foraminiferal Research 19 (4), 253–267.

Sautter, L.R., Thunell, R., 1991. Seasonal variability in the $\delta^{18}O$ and $\delta^{18}C$ of planktonic foraminifera from an upwelling environment: sediment trap results from the San Pedro Basin, Southern California Bight. Paleoceanography 6 307–334.

Shaffer, G., Salinas, S., Pizarro, O., Vega, A., Hormazabal, S. 1995. Currents in the deep ocean off Chile (30°S). Deep-Sea Research I 42, 425–436.

Spero, H.J., Lea, D.W., 1996. Experimental determination of stable isotope variability in *Globigerina bulloides*: implications for paleoceanographic reconstructions. Marine Micropaleontology 28, 231–246.

Steens, T.N.F., Ganssen, G., Kroon, D., 1992. Oxygen and carbon isotopes in planktonic foraminifera as indicators of upwelling and upwelling-induced high productivity in sediments from the northwestern Arabian Sea. In: Summerhayes, C.P., Prell, W.L., Emeis, K.C. (Eds.), Upwelling Systems: Evolution since the Early Miocene, Geological Society Special Publication 64, pp. 107–119.

Strub, P.T., Mesias, J.M., Montecino, V., Rutllant, J., Salinas, S., 1998. Coastal ocean circulation off Western South America, coastal segment. In: Robinson, A.R., Brink, K.H. (Eds.), The Sea, The Global Coastal Ocean, Regional Studies and Synthesis, vol. 11. Wiley, New York, pp. 273–313.

Thiede, J., 1975. Distribution of foraminifera in surface waters of a coastal upwelling area. Nature 253, 712–714.

Thomas, A.C., 1999. Seasonal distributions of satellite-measured phytoplankton pigment concentration along the

Chilean coast. Journal of Geophysical Research 104, 25877 25890.

Thomas, A.C., Huang, F., Strub, P.T., James, C., 1994. Comparison of the seasonal and interannual variability of phytoplankton pigment concentrations in the Peru and California Current system. Journal of Geophysical Research 99 (C4), 7355–7370.

Thomas, A.C., Carr, M.-E., Strub, P.T., 2001. Chlorophyll variability in eastern boundary currents. Geophysical Research Letters 28, 3421–3424.

Thunell, R.C., Reynolds, L.A., 1984. Sedimentation of planktonic foraminifera: seasonal changes in species flux in the Panama Basin. Micropaleontology 30, 243–262.

ELSEVIER

Deep-Sea Research II 51 (2004) 2457–2474

DEEP-SEA RESEARCH
PART II

www.elsevier.com/locate/dsr2

Downward fluxes of faecal material and microplankton at 2300 m depth in the oceanic area off Coquimbo (30°S), Chile, during 1993–1995

Humberto E. González[a,b,*], Dierk Hebbeln[c], José L. Iriarte[d], Margarita Marchant[e]

[a]*Instituto de Biología Marina, Universidad Austral de Chile, Casilla 567, Valdivia, Chile*
[b]*Centro de Investigación Oceanográfica en el Pacifico Sur-Oriental (FONDAP-COPAS), Universidad de Concepción, Casilla 160-C, Concepción, Chile*
[c]*Geowissenschaften, Research Center Ocean Margins (RCOM), Universität Bremen, Postfach 330440, D-28334 Bremen, Germany*
[d]*Instituto de Acuicultura, Universidad Austral de Chile, Casilla 1327, Puerto Montt, Chile*
[e]*Departamento de Zoología, Universidad de Concepción, Casilla 160-C, CP 4080831 Concepción, Chile*

Accepted 27 July 2004

Abstract

Vertical fluxes of biogenic elements (carbon, carbonate) and their main sources (faecal material, foraminifers, and coccolithophorids) were studied during 1993–1995 with a sediment trap deployed at a depth of 2300 m in the oceanic area off the coastal upwelling system off Coquimbo, Chile (30°S). The average flux of particulate organic carbon (POC) was 6.8 mg $m^{-2} d^{-1}$. Faecal material made the main contribution to the total POC flux, averaging 2.1 mg C $m^{-2} d^{-1}$ (35%), followed by carbon-based tintinnids, with an average flux of 0.7 mg C $m^{-2} d^{-1}$ (9.3%). Zooplankton faecal material made up 17% of the vertical POC flux in spring and 44% in the other seasons. Faeces from euphausiids and appendicularians contributed the most to total faecal carbon flux (65%), whereas the faeces of copepods and protists were relatively minor (10%). The vertical flux of microzooplankton was dominated by tintinnids, foraminifers, and coccolithophorids, which, respectively, averaged 61×10^3, 68×10^3, and 26×10^3 individuals $m^{-2} d^{-1}$. Intra-annual variability in carbon flux seems to result mostly from seasonal changes in oceanographic conditions, such as Ekman transport offshore, which was highly correlated with the POC flux ($r^2 = 0.59$). Inter-annual variability, on the other hand, might result partly from remote forcing. Other factors, such as surface pigment distribution and the composition and abundance of both zooplankton and phytoplankton in the study area, also are discussed.

Average carbonate fluxes of foraminifers and coccosphere + coccolith were 56 and 7 mg $m^{-2} d^{-1}$, respectively, or 73% and 11% of the total carbonate flux. The sinking flux of $CaCO_3$ was significantly higher than that of POC throughout

*Corresponding author. Instituto de Biología Marina, Universidad Austral de Chile, Casilla 567, Valdivia, Chile. Tel.: +56 63 22 1559; fax: +56 53 22 1455.
E-mail address: hgonzale@uach.cl (H.E. González).

0967-0645/$ - see front matter © 2004 Elsevier Ltd. All rights reserved.
doi:10.1016/j.dsr2.2004.07.027

the year, averaging 90% of the total carbon and suggesting deep-water delivery of biogenic $CaCO_3$ to be the ma pathway for removing carbon from the upper-ocean biosphere in the study area.
© 2004 Elsevier Ltd. All rights reserved.

1. Introduction

The Humboldt Current System (HCS), stretching all along the west coast of South America, is one of the world's most productive coastal upwelling systems (Daneri et al., 2000) and might play an important role in modulating the nature and effects of global change in the region (Shaffer, 1993). Off Chile, the HCS can be subdivided into a northern (18–23°S) and a southern coastal sector (36–39°S), affected by year-round and seasonal upwelling events, respectively. Both sectors are main spawning and feeding areas for clupeiform fishes (Alheit and Bernal, 1993). Equatorward of 30°S, wind-driven coastal upwelling becomes an increasingly steady, year-round phenomenon associated with the relatively stable eastern rim of the SE Pacific subtropical anticyclone, characterized by modest seasonal changes in position and intensity (reviewed by Rutllant et al., 2004). Between 27 and 36°S, the synoptic-scale wind regime progressively modulates the southerlies (controlled by the subtropical anticyclone), producing 3–7-day cycles of enhancement relaxation of the prevailing equatorward winds (Garreaud et al., 2002).

Despite being an upwelling centre, no pelagic fish spawning has been reported in the area off Coquimbo, around 30°S (L. Castro, pers. comm.). Its absence could be a result of (1) the NW wind-vector anomalies at San Felix Island (weaker trades at 900 km offshore), implying a weak subtropical anticyclone and hence weaker upwelling-favourable winds at the coast off 30°S (Rutllant et al., 2004) or (2) the intense offshore Ekman transport and the narrow continental shelf, resulting in cold coastal temperature anomalies that extend hundreds of kilometres offshore (Parrish et al., 1984). Offshore transport of coastal-generated organic particles (i.e., plankton, detritus) has been reported in mesoscale physical features such as upwelling plumes and eddies along northern and central Chile (Thoma et al., 1994; Thomas, 1999). The fate of thi particulate organic matter (POM) off th study area is highly variable, part of it bein exported to and sequestered in deeper layers of th ocean.

Over geological to centennial time scales geochemical imbalances and global climate at th Earth's surface are closely tied to carbon seques tration by marine organisms (Ducklow et al. 2001). For example, the sinking of planktoni biota and their egestion products (i.e., faeca pellets produced by zooplankton) export carbo and other elements from the productive layer into deep waters. The quantity and composition o sinking matter, as measured with sediment traps are functions of variable components within the overlying pelagic system (Peinert et al., 1989 Legendre and Rassoulzadegan, 1996). Faeca production and the formation of phytoplankton aggregates are the main processes generating large particles with a settling rate high enough to escape the photic zone before being utilized by microbes and metazoans (e.g., Alldredge and Silver, 1988). A significant effort has been devoted to the study and quantification of "bulk" estimates of the vertical flux of particulates (e.g., Berger et al., 1989; Ittekkot et al., 1996; Neuer et al., 2002). However, only a few of these studies have included detailed microscopic analyses to assess the role of specific taxa (key species or functional groups) or faecal material in contributing to geochemical fluxes (Pilskaln and Honjo, 1987; Bathmann et al., 1990; Wassmann et al., 2000; Turner, 2002). A better understanding of the ecology and life cycles of such key species will provide new biological proxies to interpret the sedimentary record (Smetacek, 2003). Thus, the analysis of different types of sedimented faecal material will allow us to identify the main zooplanktonic groups contributing to the export of particulate organic carbon (POC).

Very little information is available on deep fluxes of carbon and other elements in the HCS. Annual patterns in the sedimentation of particles (Hebbeln et al., 2000a) and planktic foraminifers (Marchant et al., 1998) have been described, and the sedimentation of organic matter at 2300 m depth has been shown to be about 5.6 g dry weight $m^{-2} yr^{-1}$.

Here we present an analysis of downward fluxes of biogenic elements in association with their main constituents. The hypothesis that faecal material and foraminifers are the main contributors to the total flux of POC and carbonate, respectively, in bathypelagic waters of the HCS, was tested.

Materials and methods

An automated, cone-shaped sediment trap (SMT 230, Salzgitter Electronic, Kiel) was deployed at 2300 m in a 4700 m water column depth at a time series station located ~185 km off Coquimbo, Chile (30°S; 73°11′W) between July 1993 and May 1995 (Fig. 1). The trap had 20 cups (250 ml each) and a baffled catchment area of 0.5 m^2. The individual sample collection period varied between 6 and 9 days; time intervals with no data (Figs. 2–5) resulted from a trap failure. Before deployment, each collector cup was filled with a hypersaline NaCl–seawater solution, made from water collected at 2000 m, with 1% (v/v) saturated $HgCl_2$ added to retard bacterial activity in the trap (Lee et al., 1992). NaCl was added to the sampling cups to give a final salinity of 38–40. After recovery, the samples were poisoned again with $HgCl_2$ (0.5 ml/100 ml of sample solution) and stored at 4 °C. During 1997, surface-tethered, cylindrical sediment traps (122 cm^2 area and 8.3 aspect ratio) were deployed at 65, 100, 200, and 300 m water depth off Antofagasta (23°S) (Fig. 1), for periods of 1–3 days as follows: (1) January 1997: 16–18 (23°20′S; 71°52′W), 18–20 (23°40′S; 70°42′W), 26–27 (23°20′S; 71°52′W), and 28–31 (23°20′S; 70°42′W); (2) July 1997: 05–06 (23°20′S; 71°52′W), 08–11 (23°20′S; 70°42′W), 11–13 (23°00′S; 70°37′W), and 16–17 (23°20′S; 74°14′W); and (3) January 1998: 26–28 (22°47′S; 70°32′W). Part of this information (total POC fluxes) was published in González et al. (1998), and it is used here to illustrate the correlation between carbon faecal material flux and total carbon flux in sediment traps deployed in deep and surface layers of the HCS.

Organic carbon content was measured on decalcified samples (with 6 N HCl) using an elementary analyser (Heraeus, CHN-O-Rapid). Carbonate contents were calculated as $(C_{total}-C_{org}) \times 8.33$ (Hebbeln et al., 2000a). No measurements of pH or dissolved organic matter concentration were completed on the trap samples' supernatant. Therefore, the extent of carbonate dissolution or organic matter degradation occurring in the sample cups could not be estimated (Noji et al., 1999). Aliquots (250 ml; 1/16–1/25 of the total sample) of the collected material were used for microzooplankton (tintinnids, foraminifers, and coccolithophorids) and faecal material counting and sizing were done using standard microscopy methods (Utermöhl, 1958) and scanning electron microscopy. Samples were counted ~3–6 months after collection. Faeces collected were identified based on published descriptions (e.g., González, 1992a, b) and classified as copepod, euphausiid, appendicularian, protistan, or undetermined. Cylindrical faeces were assumed to be from copepods and euphausiids, and ellipsoid pellets to be from appendicularians. Ostracods may also produce ellipsoid or spherical faecal material (M. Angel, pers. comm.); however, the low numbers of ostracods usually collected in zooplankton catches in the study area (H. González, unpublished data collected during 2002 and 2003) suggest that the main contributors of ellipsoid pellets are indeed appendicularians. The total volume of faecal pellets collected was calculated after counting (50–300 pellets per cup sample) and sizing (length and width) all intact and broken faecal pellets. Faecal pellet carbon from sediment-trap samples was estimated after calculating the total volume and using an average volume-to-carbon ratio of 0.048 mg C mm^{-3} (González and Smetacek, 1994). Tintinnid carbon content was estimated, after measuring the lorica volume of the identified taxa, using a factor 0.08 pg C μm^3 (Garrison and Buck, 1989). Coccolith carbonate content was estimated as 114.7 pg

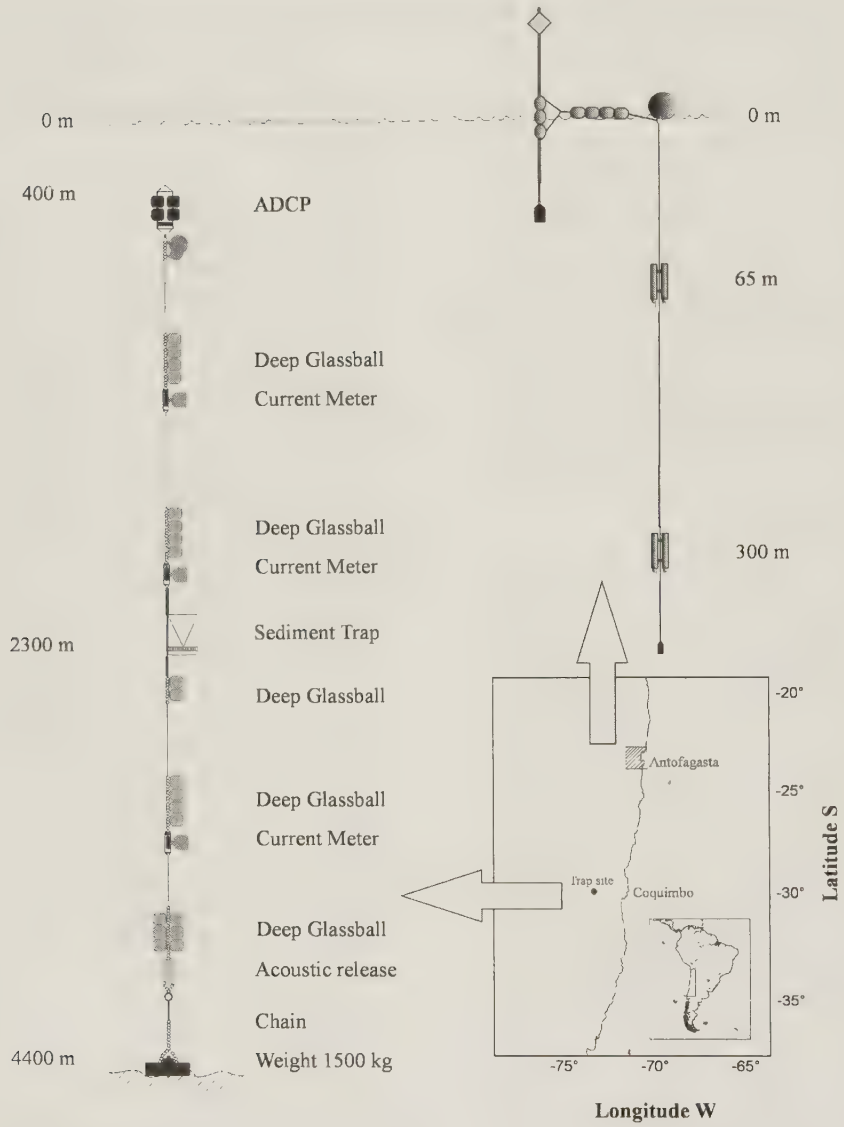

Fig. 1. Schematic drawing of the moored sediment trap deployed at 2300 m water depth off Coquimbo (30°S, left side) and the free-floating cylindrical sediment traps located between 65 and 300 m depth off Antofagasta (23°S, right side). The inset shows the sampling site locations in the general context of the Chilean coast.

$CaCO_3$, based on the average content of the dominant species (*Emiliania huxleyi* and *Coccolithus pelagicus*) (Young and Ziveri, 2000), and the coccosphere carbonate content was estimated as 2294.4 pg $CaCO_3$, assuming 20 coccoliths per coccosphere. Foraminifer-carbonate content was estimated after rinsing, drying, and weighing 50–100 individuals (ind) from each sample. For abundance estimates, >200 ind were counted from each sample; small juveniles were classified as foraminifers. Species data for foraminifers >150 μm in size are described by Marchant et al. (this volume). Selected samples—abundant in protists and minipellets of protistan origin—were treated with DAPI to better observe the presence or absence of protoplasm inside the mineral skeletons.

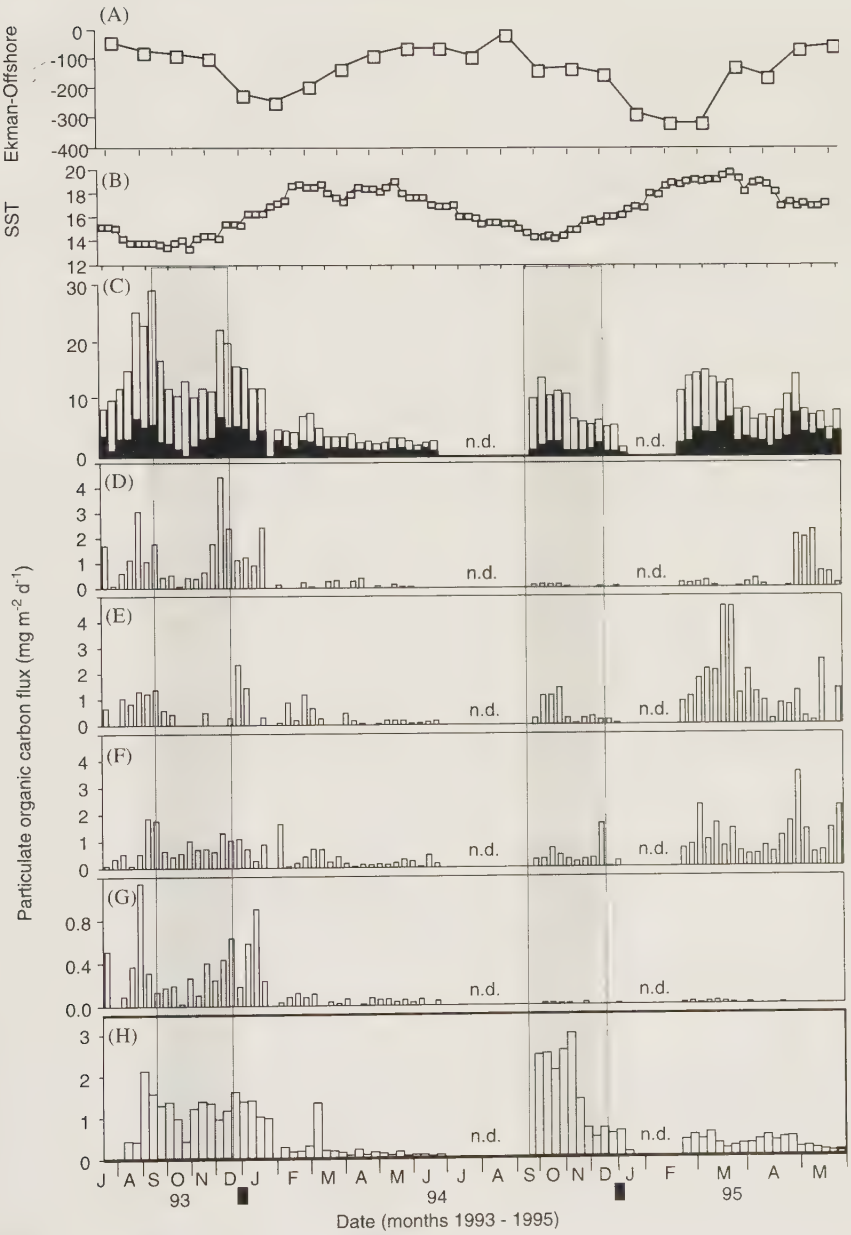

Fig. 2. (A) Weekly Ekman transport ($m^3 s^{-1}$) estimates off Coquimbo (calculations based on wind data from Punta Lengua de Vaca); (B) SST in °C; (C) total POC (white bars) and faecal material organic carbon (black bars) fluxes. POC fluxes of (D) undetermined, (E) euphausiid, (F) appendicularian, and (G) copepod faecal material, and (H) tintinnid-based organic carbon flux, at the sediment-trap site off Coquimbo from July 1993 to May 1995. n.d. = no data due to trap malfunction. Date-scale spacing is not constant because sample collection period varied between 6 and 9 days. Shaded areas enclose spring periods.

Statistical analysis of the data was carried out using the non-parametric Spearman rank correlation (Zar, 1984). Using wind data obtained from the Coquimbo meteorological station, the mean seasonal Ekman offshore transport (Bakun upwelling index) was calculated for the 100-m coastal

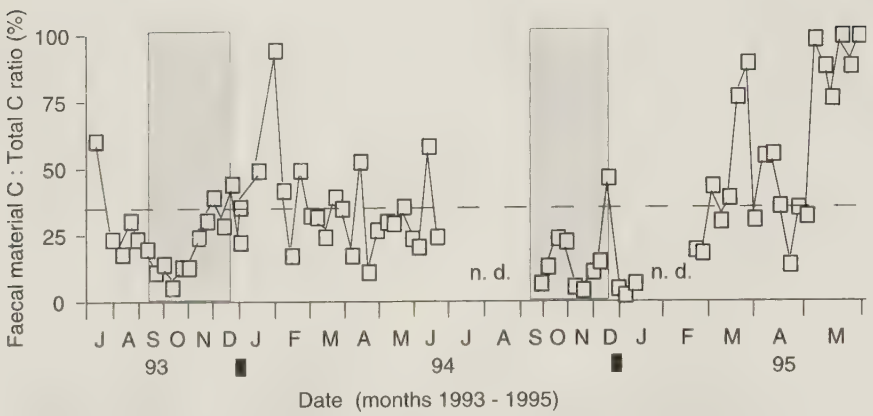

Fig. 3. Percentage of faecal pellet organic carbon from total organic carbon ($C_{\text{faecal material}}$:$C_{\text{total}}$) from July 1993 to May 1995 at the sediment-trap site off Coquimbo. Enclosed areas show spring periods when the ratios were lowest, and the horizontal dashed line indicates the total mean value of the ratio (35.4%).

line as $Mx = (\tau^y/\rho f) \times 100$, where τ^y is the wind stress, ρ the water density, and f the Coriolis parameter. Sea-surface temperatures (SST) were obtained from the NASA Physical Oceanography Distributed Active Archive Center at the Jet Propulsion Laboratory, California Institute of Technology, and wind speeds were obtained from a Campbell automatic meteorological station located at 30.25°S, near Punta Lengua de Vaca.

3. Results

3.1. Oceanographic conditions

Previous studies of the physical flow field at ~2 km depth in the trap deployment region (Shaffer et al., 1995, 1999, in press) have shown current velocities in the 2300–3400 m depth layer to average 0.3–0.6 cm s^{-1}. In other words, current speeds are slow enough to be confident that the particle catch efficiency by the trap was not significantly biased. In addition, the eddy kinetic energy at 3400 m depth (1.0 $cm^2 s^{-2}$) is among the lowest observed in the ocean (Shaffer et al., 1995).

The upwelling index showed that offshore transport confined to the Ekman layer (upper 50 m water column) increased during austral spring and summer (Fig. 2A), determined by the increment in the S, SW wind stress. SST displayed a marked seasonal variability, with minimum values in late winter/early spring (~14 °C) and maximum values in late spring and summer (~19 °C) (Fig. 2B).

3.2. Fluxes of particulate organic carbon, faecal matter, and tintinnids

The average total POC flux for the 1993–1995 period (Fig. 2C) amounted to 6.8 mg C $m^{-2} d^{-1}$; maximum values were observed during spring 1993 (September–December; average of 13.3 mg C $m^{-2} d^{-1}$), and minimum values during fall–winter 1994 (March–August; average of 1.9 mg C $m^{-2} d^{-1}$). Almost all POC maxima (values > 10 mg $m^{-2} d^{-1}$) coincided with maxima in faecal material fluxes (Fig. 2C). The average faecal pellet carbon flux was 2.1 mg C $m^{-2} d^{-1}$ for the 1993–1995 period. During the 1993 sampling period, the vertical flux of faecal material consisted mainly of degraded, undetermined faeces; appendicularian faeces dominated during September–November 1994 (Fig. 2F) and euphausiid faecal strings dominated during January–March 1995 (Fig. 2E). The overall contribution of faecal pellet carbon to the total POC flux was 35.4%, with average minimum values of 17% centred around spring (September–December) (Fig. 3). Average sizes (length and width, respectively) of the different faecal pellets were: 129 μm (range

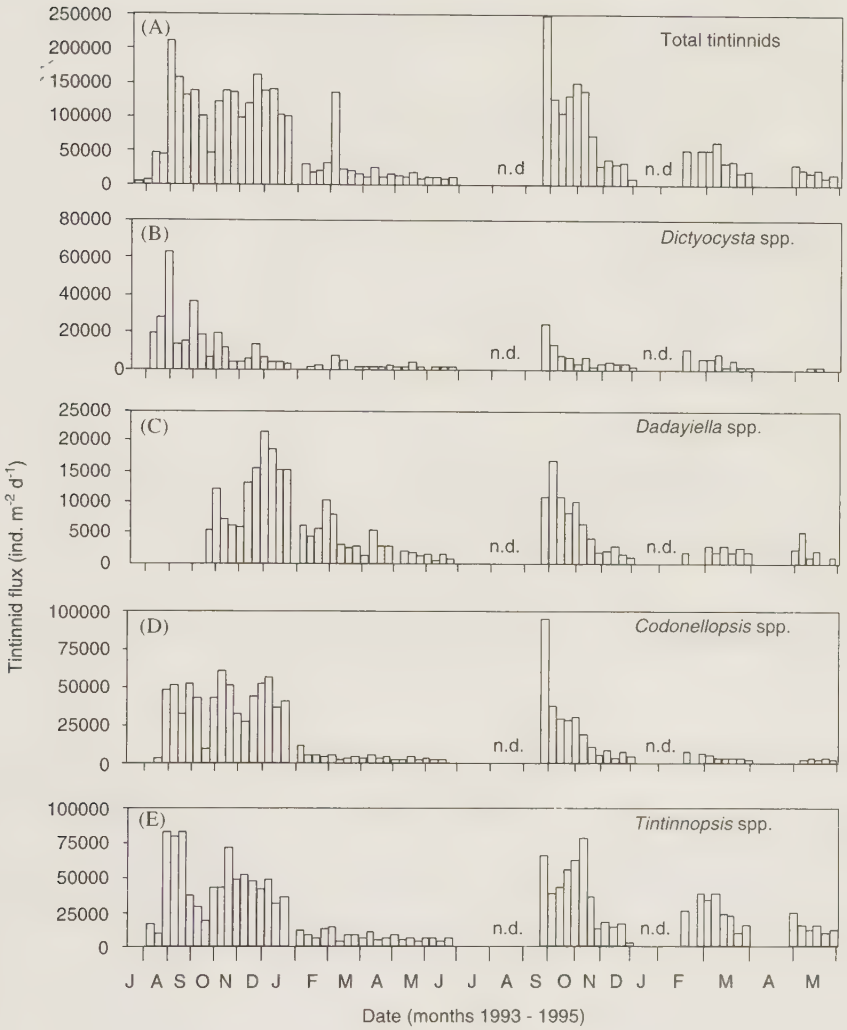

g. 4. Fluxes (ind $m^{-2} d^{-1}$) of total tintinnids (A) and individuals of the genera *Dictyocysta* (B), *Dadayiella* (C), *Codonellopsis* (D), nd *Tintinnopsis* (E) from July 1993 to May 1995 at the sediment-trap site off Coquimbo. n.d. = no data.

0–410 μm) and 46 μm (range 20–100 μm) or appendicularian pellets; 329 μm (range 00–850 μm) and 89 μm (range 35–320 μm) for uphausiid strings; and 83 μm (range 35–195 μm) nd 24 μm (range 15–70 μm) for copepod ellets.

The average carbon flux, attributed to tintinids, amounted to 0.7 mg $m^{-2} d^{-1}$, or 9.3% of the otal POC flux, and was highly variable; the ighest value (~3 mg $m^{-2} d^{-1}$) was observed in eptember–November 1994 (Fig. 2H). Throughut the study period, the average flux of tintinnids amounted to 61,000 ind $m^{-2} d^{-1}$ (Fig. 4A). Average fluxes (ind) of some of the dominant genera were 5700 (*Dictyocysta*, Fig. 4B), 4400 (*Dadayiella*; Fig. 4C), 14,900 (*Codonellopsis*, Fig. 4D) and 30,900 $m^{-2} d^{-1}$ (*Tintinnopsis*, Fig. 4E). The distribution of abundances among genera showed that the most abundant genera (*Tintinnopsis* and *Codonellopsis*) showed conspicuous maxima during spring and early summer, whereas the less abundant genera showed brief maxima either at the beginning (*Dictyocysta*) or at the end (*Dadayiella*) of spring (Fig. 4).

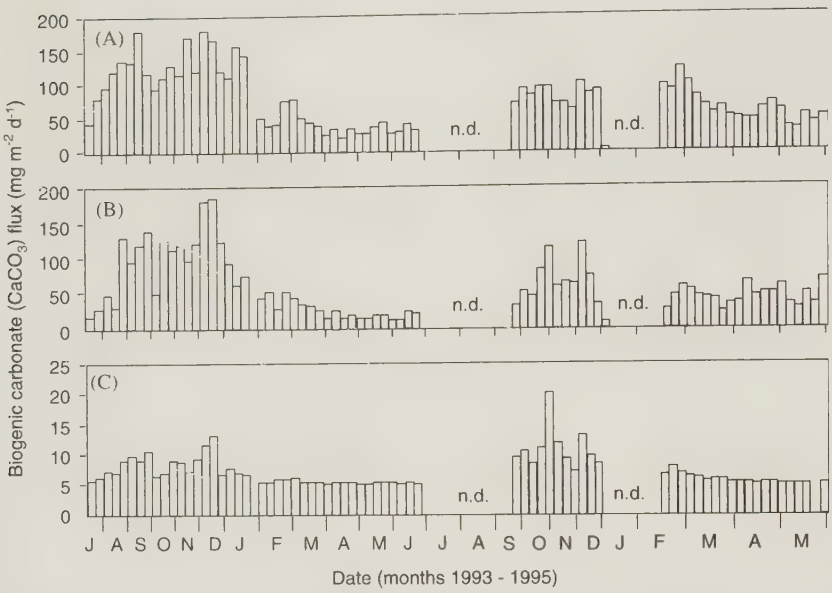

Fig. 5. Vertical fluxes of total biogenic carbonate (A) and its components: foraminifera carbonate (B) and coccolithophorids + coccoliths carbonate (C) (mg m $^{-2}$ d^{-1}) between July 1993 and May 1995 at the sediment-trap site off Coquimbo. n.d. = no data.

3.3. Carbonate and foraminifer/coccolithophore fluxes

The vertical fluxes of carbonate and POC at 30°S in the HCS off Chile are compared with other coastal and oceanic regions in Table 1. The contribution of the carbonate flux to the total carbon flux (POC + carbonate) was 90%, which is close to the contribution estimated from several other deep sediment traps (average 83%) deployed in different areas of the world oceans (Table 1).

Foraminifers contributed the most to the carbonate flux (Fig. 5A), averaging 55.7 mg m^{-2} d^{-1} (Fig. 5B) equivalent to and $\sim 68 \times 10^3$ ind m^{-2} d^{-1}. The dominant foraminifer species were *Globigerina bulloides*, *Globigerinella calida*, *Neogloboquadrina pachyderma* (sin.), *N. incompta* (dex.) and *N. dutertrei*, which together contributed ~85% of the large individuals (>150 μm) present in the samples (see Marchant et al., this volume). Adults and juvenile of the two dominant species, *N. incompta/pachyderma* and *G. bulloides*, of >212, 212–150, and 150–63 μm in diameter have an average carbonate content of 0.816, 0.030, and 0.0027 μg ind^{-1}, respectively.

Coccospheres + coccoliths made the second largest contribution to the carbonate flux, averaging 7 mg m^{-2} d^{-1} (Fig. 5C) and representing a flux of $\sim 26 \times 10^3$ coccospheres m^{-2} d^{-1}. In addition to the undamaged coccospheres, numerous detached coccoliths were always found covering the settling chamber bottoms. The majority of coccoliths retained in the trap were from *E. huxleyi* and *C. pelagicus*, with a minor contribution of others species such as *Gephyrocapsa oceanica*, *Pontosphaera syracusana*, and *Calcidiocus leptoporus*. The free coccoliths in the trap samples could have come from appendicularian faecal material, which was found to be full of coccoliths (Figs. 6A, C, and D) or from tintinnids, which agglutinate coccoliths in their lorica (Fig. 6E).

4. Discussion

4.1. Biological characteristics of the study area and their influence in timing deposition

High fluxes of total organic and inorganic carbon as well as particle constituents (faecal

Table 1
POC and $CaCO_3$ fluxes (mg $C\,m^{-2}\,d^{-1}$) estimated from deep sediment traps (range 500–3943 m depth) deployed in different areas of the world oceans

Study area	Depth (m)	POC flux (mg $C\,m^{-2}\,d^{-1}$)	$CaCO_3$ flux (mg $C\,m^{-2}\,d^{-1}$)	% $CaCO_3$ from $CaCO_3$ + POC	Reference
Panamá Bight	3560	12	122	91	Honjo (1982)
Station P (50°N; 145°W)	3800	3	60	95	Honjo (1984)
Equatorial pacific (12°S; 135°W)	3600	0.7	16	96	Honjo et al. (1995)
Arabian sea (14.5°N; 65°W)	2800	1.5	18	92	Nair et al. (1989)
Bay of Bengal (13°N; 84°E)	2300	2.6	17	87	Ittekkot et al. (1991)
Upwelling Guinea Basin (1°N; 11°W)	3943	5.5	54	91	Fischer and Wefer (1996)
East China Sea slope (25°11′N; 122°58′E)	1588	53	160	75	Hung et al. (2003)
Western Pacific (4°07′N; 136°17′E)	1769	6[a]	49	89	Kawahata et al. (2000)
Western Pacific (0°00′N; 175°19′E)	1357	2[a]	30	94	Kawahata et al. (2000)
Western Pacific (7°56′N; 175°00′E)	1637	1[a]	8	89	Kawahata et al. (2000)
W Pacific weak upwelling (0°N; 175°E)	1040	3[a]	39	93	Kawahata and Gupta (2003)
W Caroline Basin (2°59′N; 135°01′E)	1592	9[a]	78	90	Kawata et al. (1998)
W Caroline Basin (2°59′N; 135°01′E)	3902	8[a]	71	90	Kawata et al. (1998)
NW Africa (21.2°N; 20.7°W)	2195–3568	5.4	66	92	Fischer et al. (2004)
W Equatorial Atlantic (8°S; 28°W)	671–5031	1.4	15.4	92	Fischer et al. (2004)
SW Africa (20.1°S; 9.2°W)	1640–1717	10.5	58.6	85	Fischer et al. (2004)
Bransfield Strait (62°26′S; 57°31′W)	1588	12	14	54	Wefer et al. (1988)
Off Central California	1700	15[a]	29	66	Martin and Knauer (1983)
Off Central California	2000	15[a]	18	55	Martin and Knauer (1983)
S California Bight (33°33′N; 118°30′W)	879	35	53	60	Crisp et al. (1979)
S California Bight	824	22	120	85	Nelson et al. (1987)
S California Bight	500	32	99	76	Thunell et al. (1994)
S California Bight (34°14′N; 102°02′W)	540	87	152	64	Thunell (1998)
NW Gulf of Mexico (26°57′N; 94°46′W)	1404	12	115	90	Walsh and Gardner (1992)
East Hawaii (15°21′N; 151°28′W)	2778	1	12	92	Pilskaln and Honjo (1987)
Tropical Atlantic (13°30′N; 54°00′W)	3755	2	26	93	Pilskaln and Honjo (1987)
Panama Basin (5°21′N; 81°53′W)	2869	11	51	82	Pilskaln and Honjo (1987)
Humboldt Current System (30°S)	2300	7	61	90	Present study

[a]Assuming that half of the organic matter is POC.

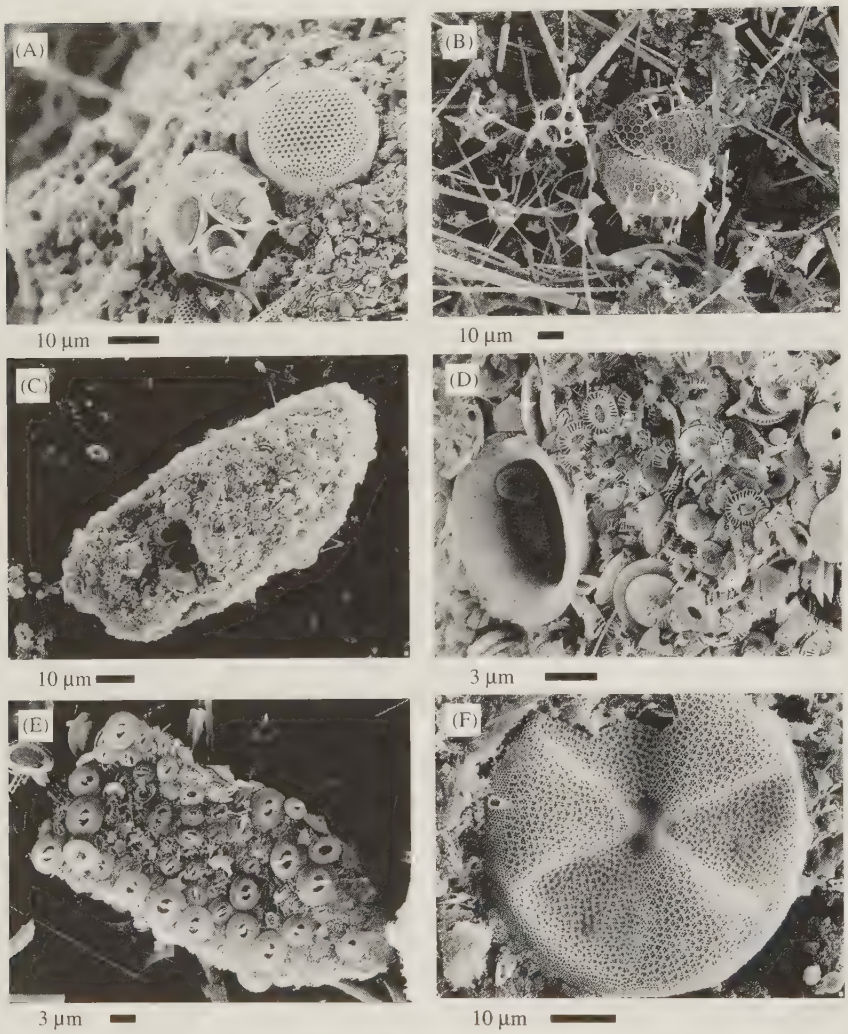

Fig. 6. SEM photographs of (A) the surface of a faecal pellet devoid of a peritrophic membrane showing the presence of abundant coccoliths, an undamaged coccosphere (*P. syracusana*), and a centric diatom (genus *Thalassiosira*); (B) general view of sedimented matter showing the presence of centric diatoms (genera *Chaetoceros*, *Thalassiosira*, and *Stephanopyxis*), radiolarians, and dinoflagellates (skeleton of *Actiniscus pentasterias*); (C) appendicularian faecal pellet loaded with different types of coccoliths; (D) a close view of an appendicularian faecal pellet showing a variety of coccoliths such as those of the taxa *E. huxleyi*, *C. pelagicus* and *P. syracusana*; (E) tintinnid (genus *Tintinnopsis*) lorica covered with agglutinated coccoliths. (F) Centric diatom (species *Actinoptychus senarius*) partially embedded in an aggregate. (A–C, F) Scale bar = 10 μm; (D, E) scale bar = 3 μm.

material and protist skeletons) were observed in spring and summer (Figs. 2 and 5), which partially coincide with maximum values in pigment concentrations reported for the study area. The pigment concentration off central Chile (30°S) ranged between 0.1 and 1.2 mg m^{-3} (Thomas, 1999), with maximum values occurring at different seasons of the year, depending on the satellite used to process the information: winter–spring (CZCS) or summer (SeaWiFS), the seasons of maximum and minimum upwelling-favourable winds, respectively (Thomas et al., 2001). The possible discrepancy between high organic and inorganic carbon flux estimates and low surface pigment

concentration estimates by satellite imagery, both taken in spring, may result from the development of a subsurface chlorophyll-*a* (Chl-*a*) maximum (not registered by satellite) and high integrated Chl-*a* concentrations in this season (Morales et al., 1996; González et al., 2000a). This study does not assess whether a subsurface Chl-*a* maximum layer might result in increased vertical fluxes of faecal pellets due to enhanced zooplankton grazing rates at this layer. However, in a coastal embayment of central Chile, copepod aggregation and maximum feeding activity indeed occurred at the depth of maximum Chl-*a* (Castro et al., 1991). Additionally, pico- and nano-phytoplankton were the main contributors to total Chl-*a* during winter, both in the northern HCS (Iriarte et al., 2000) and around our trap site (Hebbeln et al., 2000a), possibly reducing the wintertime vertical flux of particles. During the other seasons, large net-phytoplankton (>20 μm) predominate and are expected to have higher sinking rates due to larger cell sizes and a greater tendency to flocculate than smaller cells (Kiørboe, 1993).

From a temporal perspective, there is ~1 month time difference between the winter period of high pigment concentration in the surface water column and the early spring maximum fluxes of the particle constituents. If we assume that the faecal material was originally produced in the photic zone, then the time difference denotes a lag between production and sinking to 2300 m. If we assume an average settling velocity of $90\,m\,d^{-1}$ (Baldwin et al., 1998; Deuser et al., 1990), it would take the faecal material approximately a month to sink to 2300 m. Baldwin et al. (1998) reported ~50 days lag time between the Bakun upwelling index and the arrival of particulate matter to a sediment trap deployed at 3500 m depth in the NE Pacific. These authors estimated a sinking rate of $\sim 100\,m\,d^{-1}$, allowing for time between the upwelling of nutrients and the flux of material from the photic zone. Alldredge et al. (1987) indicated that the sinking rate of macrocrustacean (probably euphausiid) pellets ranged from 18 to $170\,m\,d^{-1}$. We did not consider the settling rates of aggregates of phytodetrital material because of their high variability; some studies have reported sustained residence of 5–16 days in surface waters (Riebesell, 1992), and others the dramatic and sudden arrival of phytodetritus material on the deep-sea floor (Lampitt, 1985; Rice et al., 1994).

The timing of organic matter delivery to the trap off Coquimbo seems to be dependent on the offshore transport of coastal POM in the upper water column (presumably via offshore-trending upwelling filaments) during intense spring upwelling activity when new production (Eppley and Peterson, 1979), and its subsequent export to the deep sea, is expected to be maximized. Supporting evidence for the offshore transport of particulates to the trap site in the spring and summer is the documentation of phytoplankton in offshore-trending upwelling filaments in the region, as well as the presence of abundant neritic diatoms in sediment-trap samples and bottom sediments (Strub et al., 1998; Thomas, 1999; Romero et al., 2001). The Ekman transport showed a relatively high correlation ($r^2 = 0.59$) with POC flux when subjected to a time lag of 1 month with respect to wind stress (estimated time for POC generated within the photic zone to reach the sediment trap at 2300 m depth) (Fig. 7, upper panel inset). Later in the year, other pulses of organic matter collected at 2300 m depth might be associated with "repackaging" of particles in faecal pellets (McCave, 1984; Lampitt, 1985) produced by large-size zooplankton such as euphausiids (see below).

Iriarte and González (2004) reported an average primary production (PP) rate of 2376 mg $C\,m^{-2}\,d^{-1}$ between January and July 1997 for the Antofagasta area (25°S). Simultaneously, an average vertical carbon flux of 83.7 mg $C\,m^{-2}\,d^{-1}$ was measured (González et al., 1998) using surface-tethered sediment traps deployed between 65 and 300 m depth (Fig. 7, bottom). The carbon flux at 300 m depth was only 3.5% of the photosynthetically produced carbon in the photic zone. Assuming carbon fluxes at 2300 m depth off Antofagasta are similar to those at the Coquimbo trap site, an average of 6.8 mg $C\,m^{-2}\,d^{-1}$ (8%) escaped degradation through the 300–2300 m water column before being exported to 2300 m depth. The average depth of the water column at 185 km off Antofagasta is ~4000 m, so, if similar degradation rates occur at bathy- and meso-pelagic layers, then

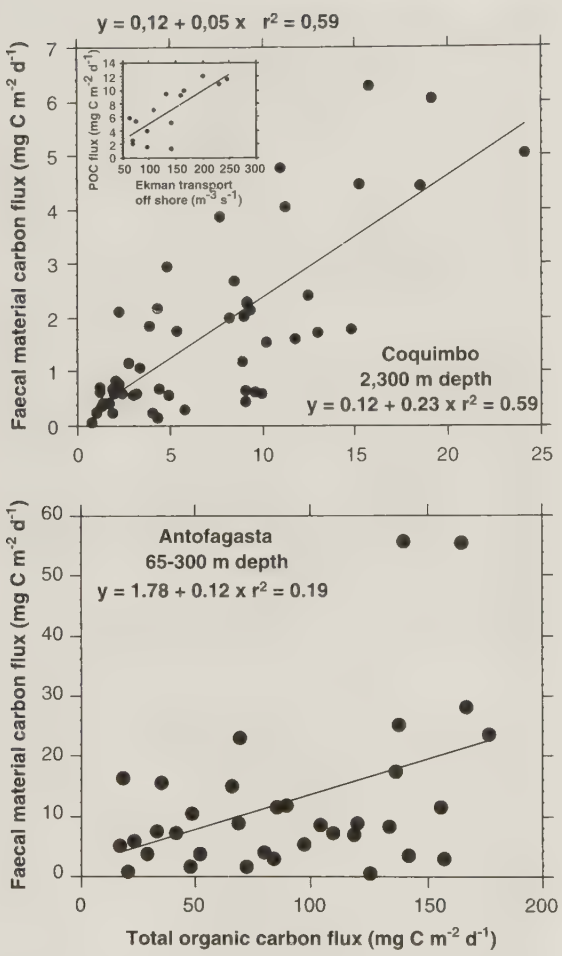
y = 0,12 + 0,05 x r² = 0,59
Faecal material carbon flux (mg C m⁻² d⁻¹)
POC flux (mg C m⁻² d⁻¹)
Ekman transport off shore (m⁻³ s⁻¹)
Coquimbo
2,300 m depth
y = 0.12 + 0.23 x r² = 0.59
Antofagasta
65-300 m depth
y = 1.78 + 0.12 x r² = 0.19
Total organic carbon flux (mg C m⁻² d⁻¹)

Fig. 7. Linear correlation between total organic carbon flux and faecal material-carbon flux from samples collected by using a moored sediment trap deployed at 2300 m water depth off Coquimbo (30°S) (upper panel), and from samples collected by using drifting sediment traps deployed at depths between 65 and 300 m off Antofagasta (23°S). The inset of the upper panel shows the linear correlation between POC flux and the Ekman transport offshore ($r^2 = 0.59$). The POC flux was shifted 1 month forward (estimated time for POC generated within the photic zone to reach the sediment trap at 2300 m depth) with respect to wind stress.

only 0.5 mg C m^{-2} d^{-1} (~0.02% of the PP) would potentially arrive to the seafloor sediments. Pantoja et al. (2004), estimated that about 0.04% of the particulate protein (THAA-C) generated during PP in the photic zone arrived to the sediments at 1200 m depth in the Iquique coastal upwelling system (20°24′S; 70°40′W).

4.2. Seasonal pattern of particulate organic carbon, faecal matter carbon, and tintinnid fluxes

Temporal variability of particulate carbon flux toward the deep sea seems to result from either annual, seasonal, episodic events, or a combination of all of these (Deuser, 1996). Off Coquimbo, faecal material was indeed mainly driven by seasonal variability, but other types of particles like marine snow (beyond the scope of this paper) might be influenced by episodic events such as the transit of coastal trapped waves (Djurfeldt, 1994) or inter-annual variability, illustrated by the high fluxes of *Chaetoceros* spp. observed during late winter–early spring 1993 (Romero et al., 2001), but not during late winter–early spring 1994 (H. González, unpublished information).

As was shown for the HCS off 23°S (González et al., 2000a), grazing off Coquimbo (30°S), as evidenced by faecal pellet fluxes, is probably an important process contributing particles to the vertical flux. Recognizable faecal material contributed a significant proportion of the total carbon collected in our sediment trap, averaging 35% (range 3–99%) for the whole study period (Fig. 3).

Sediment traps deployed in upper and deeper layers of the ocean are influenced by different processes (biological, physical, and chemical) that enhance or reduce the flux of particles, impeding flux comparisons between such traps. However, the relative contribution of certain types of particles (i.e., faecal pellets from appendicularians, foraminiferal tests, etc.) to total carbon flux can be compared between upper-ocean and deep-moored traps to provide a qualitative assessment of how carbon delivery mechanisms (i.e., particle type) change with depth. This, in turn, is a complicated function of mid-water advection, remineralization rates, and biological feeding interactions. Analysis of cylindrical sediment-trap samples deployed for short periods (~2 days) at 65–300 m water depths off Antofagasta showed no correlation between total POC sedimentation and faecal pellet carbon sedimentation ($r^2 = 0.19$) (Fig. 7, lower panel). At 2300 m depth, a positive correlation emerged ($r^2 = 0.59$) because the total flux of POC became enriched in faecal matter (Fig. 7, upper panel).

Possible explanations are (1) increased trap efficiency to collect faecal material in a deeper, quiescent environment; (2) higher settling rates for compact and large faecal pellets (i.e., as produced by appendicularians and euphausiids), allowing them to exit the upper zone of the ocean quickly (compared to marine snow and other types of particles) before being utilized; and (3) shallow-water grazing and mid-water defecation by vertically migrating animals (Zhang and Dam, 1998).

The faecal matter contribution to total POC flux probably underestimated the true importance of faecal material because a large and unknown quantity of degraded faecal material, which precluded quantification, was collected in the trap cups. We suggest that most of this material originated from euphausiid faecal strings, based on the reported abundance of such faecal matter in other areas of the HCS off northern Chile (González et al., 2000b). Correlations between the total POC flux and the fluxes of faecal material were only significant ($p<0.0001$) for appendicularian and undetermined faecal material. In addition, total faecal carbon fluxes were significantly correlated with fluxes of appendicularians, euphausiid, and undetermined faecal material fluxes, suggesting a prominent role of appendicularians and euphausiids in faecal pellet flux, and a minor role of copepod faecal pellet flux (Table 2).

The high correlation ($p<0.0001$) between total POC flux and opal flux is most probably the result of high density, and hence rapid sinking speeds, of aggregates (marine snow) loaded with abundant empty diatom frustules. The relatively high correlation between different groups of protists (e.g., foraminifers, coccolithophorids, radiolarians, and tintinnids) may indicate mass sedimentation of protist mineral skeletons within large particles (e.g., large faecal pellets or aggregates). Tintinnids, because of the composition of their loricae, are likely to be the only group that made a significant contribution to POC flux.

Most of the tintinnid loricae were empty, probably because the protoplasm attaches itself to the shell by a fragile strand that breaks apart easily as a result of mechanical or chemical disturbance (Boltovskoy et al., 1993). We do not know the ratio of empty to full loricae, so we have

Table 2
Spearman rank correlation, among microplankton, detritus, and different chemical components of the material sedimented at 2300 m depth in waters off Coquimbo during 1993–1995

	(1)	(2)	(3)	(4)	(5)	(6)	(7)	(8)	(9)	(10)	(11)	(12)	(13)	(14)
Total mass flux (1)	1													
Total organic carbon (2)	**0.942*****	1												
Opal (3)	**0.972*****	**0.923*****	1											
Total $CaCO_3$ (4)	**0.961*****	**0.897*****	**0.912*****	1										
Faecal material organic carbon (5)	**0.476*****	**0.581*****	0.399**	**0.525*****	1									
Tintinnid carbon (6)	**0.808*****	**0.778*****	**0.846*****	**0.798*****	0.310*	1								
Undetermined faeces carbon (7)	**0.481*****	**0.475*****	**0.419****	**0.470*****	**0.603*****	0.306*	1							
Krill strings carbon (8)	0.129 ns	0.294*	0.074 ns	0.150 ns	**0.638*****	0.051 ns	0.138 ns	1						
Appendicularian pellets carbon (9)	0.405**	**0.493*****	0.354*	**0.487*****	**0.745*****	0.342*	0.329*	0.404**	1					
Copepod pellet carbon (10)	0.445**	0.378*	0.391*	0.441**	0.218 ns	0.298 ns	0.373*	0.048 ns	−0.069 ns	1				
$CaCO_3$ from foraminifers (111)	0.235 ns	0.201 ns	0.143 ns	0.369*	0.115 ns	0.117 ns	0.081 ns	0.036 ns	0.158 ns	0.400**	1			
No. of foraminifers (12)	**0.772*****	**0.712*****	**0.755*****	**0.806*****	**0.502*****	**0.767*****	0.369*	0.100 ns	**0.545*****	0.264 ns	0.188 ns	1		
No. coccolithophorids (13)	**0.818*****	**0.714*****	**0.852*****	**0.796*****	0.148 ns	**0.820*****	0.195 ns	−0.129 ns	0.125 ns	0.381*	0.230 ns	**0.652*****	1	
No. of radiolarians (14)	**0.681*****	**0.581*****	**0.697*****	**0.654*****	0.128 ns	**0.603*****	0.441**	−0.160 ns	0.036 ns	**0.663*****	0.266 ns	0.556***	**0.686*****	1

$^{*}0.0011<p<0.01$; $^{**}0.00011<p<0.001$; $^{***}p<0.0001$; ns = not significant, $p>0.01$. $n=72$.

probably overestimated the carbon-based tintinnid flux. However, Gilron and Lynn (1989) reported that tintinnid lorical carbon accounts for 50–79% of the overall biomass of the ciliate, so if all the tintinnids were empty, the flux will be overestimated by 21–50%. The flux of tintinnids showed a coarse seasonal pattern; the high spring concentrations (which, in 1993, also included a part of late winter and early summer) decreased through summer to reach very low values during winter (Fig. 2H).

4.3. Carbonate flux

The ratio between coccolithophorid-carbonate flux and foraminifer-carbonate flux was 0.13 (SD = 0.06, $n = 72$), which is very low in comparison to the ratios of 4–6 reported for open-ocean, oligotrophic areas (Honjo, 1977; Deuser and Ross, 1989) and this is indicative of the importance of foraminifers in this coastal upwelling region. Foraminifers and coccoliths + coccospheres contributed 73% (SD = 28%, $n = 72$) and 11% (SD = 10%, $n = 72$) to the average carbonate flux, respectively. The present study includes foraminifers $<65\,\mu m$ in diameter, which are a large fraction (~45%) of the total abundance, significantly increasing the contribution foraminifers make to the total carbonate flux as compared with estimates that only consider ind $>65\,\mu m$ in diameter (~40%) (Marchant et al., this volume). The carbonate input of different groups of organisms to the sediments of the South Atlantic was dominated by coccolithophorids (oligotrophic areas) and foraminifers (more fertile, mesotrophic areas) (Baumann et al., 2004).

Faecal material from euphausiid and appendicularian origins usually contained both coccospheres and free coccoliths (Fig. 6A, C and D), suggesting that faecal material is an important vehicle for the export of these particles to the deep sea (Honjo, 1976; Pilskaln and Honjo, 1987; Gorsky et al., 1999). Fluxes of free coccoliths in our sediment-trap samples ranged from 3.5×10^5 to $1.2 \times 10^8\,m^{-2}\,d^{-1}$, that is, 2–5 orders of magnitude higher than the coccosphere flux. However, the free coccoliths were probably released from semi-degraded faecal material during the splitting procedure and sample manipulation. Macroaggregates and tintinnid loricae might also be vehicles for coccolith transport (Fig. 6E). The coccolith assemblages in the trap were dominated by *E. huxleyi* and *C. pelagicus*, the cosmopolitan species that tend to dominate the cold waters of some oceans (i.e., Milliman, 1980, for the Scottish Sea; Samtleben and Bickert, 1990, for the Norwegian Sea).

4.4. Carbon versus carbonate fluxes and biogeochemical significance

The contribution of the carbonate flux to the total carbon flux (POC + carbonate) was 90% at 30°S in the HCS off Chile, which is close to the contribution estimated from several other deep sediment traps (average $84 \pm 13\%$; $n = 27$) deployed in different areas of the world oceans (Table 1). An analysis of the most important flux components (carbonate, biogenic opal, and lithogenic) to annual organic carbon fluxes from the global ocean demonstrated that carbonate strongly determines organic carbon fluxes, suggesting a ballast effect of carbonate on the 'transfer efficiency' of organic carbon to the deep sea (Fischer et al., 2004).

The mean $C_{organic}$:$C_{carbonate}$ ratio for the whole period was 0.09 (SD = 0.03, $n = 72$). This ratio indicates a potential net export of carbonate to the deep sea, which is important in regulating marine carbon cycling and the ocean–atmosphere CO_2 exchange. The average $C_{organic}$:$C_{carbonate}$ ratio in the world ocean is reported to fluctuate between ~4 and <1 from the upper 500 m to the deep sea (>4000 m depth) (Broecker and Peng, 1982; Tsunogai and Noriki, 1991; Anderson and Sarmiento, 1994). According to Archer's (1991) model of $\%CaCO_3$ accumulation at the saturation horizon as a function of the $C_{organic}$:$C_{carbonate}$ ratio, our trap site would indicate that ~10% of the $CaCO_3$ dissolves at or above the saturation horizon: ~2000 m depth for aragonite and ~3500 m depth for calcite in the South Pacific (reviewed by Jansen, 2001). Above the saturation horizon, the water column is supersaturated with respect to calcite and the mechanisms underlying possible losses of $CaCO_3$ are not yet well

understood. However, dissolution in zooplankton guts (Jansen, 2001) and the existence of microzones where decomposition of organic matter lowers the pH sufficiently to dissolve calcite (Balch and Kilpatrick, 1996) have been mentioned as important mechanisms.

The carbonate flux in our samples was dominated by foraminifer tests. Foraminifer tests of the species *Globigerinoides sacculifer* from 100 to 900 μm in diameter presented sinking rates between 115 and 1500 m d^{-1}, necessitating from 22 to 1.6 days, respectively, to reach a 2500 m depth sediment trap (Bijma et al., 1994; Takahashi and Bé, 1984). Thus, the foraminifer-$CaCO_3$ flux at the trap site seemed to be affected by a combination of autocthonous, in situ exported (large sized) and alloctonous, laterally advected (small-sized) foraminifers. The POC flux, mainly composed by phytoplankton or low-density detritus, seems to be more affected by intra-annual variability related to upwelling strength, coastal PP, and offshore advection in particle-loaded filaments.

The fact that $CaCO_3$, rather than POC, was the main contributor to the particulate carbon flux (Table 1) is supported by studies of offshore marine sediments in central Chile that showed that the carbonate content in the sediments (~10%) is significatively higher than the organic carbon content (~0.8%) (Hebbeln et al., 2000b). Thus, the high fluxes of $CaCO_3$ represent a potential sediment reservoir as they do, in fact, result in significant accumulation in the underlying deep sediments, suggesting that the deep-water delivery of biogenic $CaCO_3$ is the main pathway by which carbon is removed from the upper-ocean biosphere in the study area.

Acknowledgements

We thank the captain and crew of the R.V. *Abate Molina* for support in the field work. We are very grateful to Drs. D. Karl, M. Angel, and C. Pilskaln for comments and suggestions which improved an earlier version of this manuscript. R. Silva (Electron Microscopy Section, Universidad Austral de Chile) collaborated in obtaining the photographs shown in Fig. 6. Special thanks go to E. Menschel for collaboration in sample analysis in the laboratory and to J. Rutllant for providing wind data from Coquimbo, which allowed the calculation of Ekman offshore transport. This study was funded by the German Bundesministerium through the JGOFS-Chile project; the Universidad Austral de Chile (Project No. DID S-199909); the FONDAP-COPAS Center (Fondap Project No. 150100007), and FONDECYT Project No. 1010912. Technical support from the Research Center Ocean Margins (Bremen University) and the Dirección de Investigación (Universidad de Concepción) is also acknowledged.

References

Alheit, J., Bernal, P., 1993. Effects of physical and biological changes on the biomass yield of the Humboldt Current System. In: Sherman, K., Alexander, L.M., Gold, B.D. (Eds.), Large Marine Ecosystems: Stress, Mitigation, and Sustainability. American Association for the Advance of the Science Press, Washington, DC, pp. 53–68.

Alldredge, A.L., Silver, A.W., 1988. Characteristics, dynamics and significance of marine snow. Progress in Oceanography 20, 41–82.

Alldredge, A.L., Gotschalk, C.C., MacIntyre, S., 1987. Evidence for sustained residence of macrocrustacean fecal pellets in surface waters off Southern California. Deep-Sea Research 34, 1641–1652.

Anderson, L.A., Sarmiento, J.L., 1994. Redfield ratios of remineralization determined by nutrient data analysis. Global Biogeochemical Cycles 8, 65–80.

Archer, D., 1991. Modeling the calcite lysocline. Journal of Geophysical Research 96, 17037–17050.

Balch, W.M., Kilpatrick, K., 1996. Calcification rates in the equatorial Pacific along 140°W. Deep-Sea Research II 43, 971–993.

Baldwin, R.J., Glatts, R.C., Smith Jr., K.L., 1998. Particulate matter fluxes into the benthic boundary layer at a long time-series station in the abyssal NE Pacific: composition and fluxes. Deep-Sea Research II 45, 643–665.

Bathmann, U., Peinert, R., Noji, T.T., Bodungen, B.v., 1990. Pelagic origin and fate of sedimenting particles in the Norwegian Sea. Progress in Oceanography 24, 117–125.

Baumann, K.-H., Böckel, B., Donner, B., Gerhardt, S., Henrich, R., Vink, A., Volbers, A., Willems, H., Zonneveld, K.A.F., 2004. Contribution of calcareous plankton groups to the carbonate budget of South Atlantic surface sediments. In: Wefer, G., Mulitza, S., Ratmeyer, V. (Eds.), The South Atlantic in the Late Quaternary: Reconstructions of Material Budgets and Current Systems. Springer, Berlin, pp. 81–99.

Berger, W.H., Smetacek, V.S., Wefer, G., 1989. Productivity of the Ocean: Present and Past. Wiley, Chichester, UK, pp. 1–34.

Bijma, J., Hemleben, C., Wellnitz, K., 1994. Lunar-influenced carbonate flux of the planktic foraminifer *Globigerinoides sacculifer* (Brady) from the central Red Sea. Deep-Sea Research I 41, 511–530.

Boltovskoy, D., Alder, V., Abelmann, A., 1993. Annual flux of Radiolaria and other shelled plankters in the eastern equatorial Atlantic at 853 m: seasonal variations and polycystine species-specific responses. Deep-Sea Research I 40, 1863–1895.

Broecker, W.S., Peng, T.-H., 1982. Tracers in the Sea. Lamont-Doherty Geological Observatory, Columbia University ELDEGEO Press, Columbia.

Castro, L.R., Bernal, P.A., González, H.E., 1991. Vertical distribution of copepods and the utilization of the chlorophyll *a*-rich layer within Concepción Bay, Chile. Estuarine, Coastal and Shelf Science 32, 243–256.

Crisp, P.T., Brenner, S., Kaplan, L.T., 1979. Organic chemical characterization of sediment trap particulates from San Nicolas, Santa Barbara, Santa Monica and San Pedro Basins, California. Geochimica et Cosmochimica Acta 43, 1791–1801.

Daneri, G., Dellarossa, V., Quiñones, R., Jacob, B., Montero, P., Ulloa, O., 2000. Primary production and community respiration in the Humboldt Current System off Chile and associated oceanic areas. Marine Ecology Progress Series 197, 41 49.

Deuser, W.G., 1996. Temporal variability of particle flux in the deep Sargasso Sea. In: Ittekkot, V., Schäfer, P., Honjo, S., Depetris, P.J. (Eds.), Particle Flux in the Ocean. SCOPE 57. Wiley, Chichester, UK, pp. 185–198.

Deuser, W.G., Ross, E.H., 1989. Seasonally abundant planktonic foraminifera of the Sargasso Sea: succession, deep-water fluxes, isotopic composition, and paleoceanographic implications. Journal of Foraminiferal Research 19, 268–293.

Deuser, W.G., Müller-Karger, F.E., Evans, R.H., Brown, O.B., Esaias, W.E., Feldman, G.C., 1990. Surface-ocean color and deep-ocean carbon flux: how close a connection? Deep-Sea Research 37, 1331–1344.

Djurfeldt, L., 1994. The influence of physical factors on a subsurface chlorophyll maximum in an upwelling area. Estuarine, Coastal and Shelf Science 39, 389–400.

Ducklow, H.W., Steinberg, D.K., Buesseler, K.O., 2001. Upper ocean carbon export and the biological pump. Oceanography 14, 50–58.

Eppley, R.W., Peterson, B.J., 1979. Particulate organic matter flux and planktonic new production in the deep ocean. Nature 282, 677–680.

Fischer, G., Wefer, G., 1996. Seasonal and interannual particle fluxes in the eastern equatorial Atlantic from 1989 to 1991: ITCZ migrations and upwelling. In: Ittekkot, V., Schafer, P., Honjo, S., Depetris, P.J. (Eds.), Particle Flux in the Ocean. Wiley, Chichester, UK, pp. 199–214.

Fischer, G., Wefer, G., Romero, O., Dittert, N., Ratmeyer, V., Donner, B., 2004. Transfer of particles into the deep Atlantic and the global ocean: control of nutrient supply and ballast production. In: Wefer, G., Mulitza, S., Ratmeyer, V. (Eds.), The South Atlantic in the Late Quaternary: Reconstructions of Material Budgets and Current Systems. Springer, Berlin, pp. 21–47.

Garreaud, R.D., Rutllant, J.A., Fuenzalida, H., 2002. Coastal lows along the subtropical West Coast of South America: mean structure and evolution. Monthly Weather Review 130, 75–88.

Garrison, D.L., Buck, K.R., 1989. Protozooplankton in the Weddell Sea, Antarctica: abundance and distribution in the ice-edge zone. Polar Biology 9, 341–351.

Gilron, G.L., Lynn, D.H., 1989. Estimates of in situ population growth rates of four tintinnine ciliate species near Kingston Harbour, Jamaica. Estuarine, Coastal and Shelf Science 29, 1–10.

González, H.E., 1992a. The distribution and abundance of krill faecal material and oval pellets in the Scotia and Weddell Seas (Antarctica) and their role in particle flux. Polar Biology 12, 81–91.

González, H.E., 1992b. Distribution and abundance of mini-pellets around the Antarctic Peninsula. Implications for protistan feeding behaviour. Marine Ecology Progress Series 90, 223–236.

González, H.E., Smetacek, V., 1994. The possible role of the cyclopoid copepod *Oithona* in retarding vertical flux of zooplankton faecal material. Marine Ecology Progress Series 113, 233–246.

González, H.E., Daneri, G., Figueroa, D., Iriarte, J., Lefevre, N., Pizarro, G., Quiñones, R., Sobrazo, M., Troncoso, A., 1998. Producción primaria y su destino en la trama trófica pelágica y océano profundo e intercambio océano-atmósfera de CO_2 en la zona norte de la Corriente de Humboldt (23°S): posibles efectos del evento El Niño, 1997–98 en Chile. Revista Chilena de Historia Natural 71, 429–458.

González, H.E., Sobarzo, M., Figueroa, D., Nöthig, E.-M., 2000a. Composition, biomass and potential grazing impact of the crustacean and pelagic tunicates in the northern Humboldt Current area off Chile: differences between El Niño and non-El Niño years. Marine Ecology Progress Series 195, 201–220.

González, H.E., Ortiz, V., Sobarzo, M., 2000b. The role of faecal material in the particulate organic carbon flux in the northern Humboldt Current, Chile (23°S), before and during the 1997–98 El Niño. Journal of Plankton Research 22, 499–529.

Gorsky, G., Chrétiennot-Dinet, M.J., Balnchot, J., Palazzoli, I., 1999. Picoplankton and nanoplankton aggregation by appendicularians: fecal pellet contents of *Megalocercus huxleyi* in the equatorial Pacific. Journal of Geophysical Research 104, 3381–3390.

Hebbeln, D., Marchant, M., Wefer, G., 2000a. Seasonal variations of the particle flux in the Peru–Chile current at 30°S under "normal" and under El Niño conditions. Deep-Sea Research II 47, 2101–2128.

Hebbeln, D., Lamy, F., Marchant, M., Klump, J., Wefer, G., 2000b. Present and past sedimentation along the Chilean continental slope. Zeitschrift für Angewandte Geologie 1, 125–132.

Honjo, S., 1976. Coccoliths: production, transportation and sedimentation. Marine Micropaleontology 1, 65–79.

Honjo, S., 1977. Biogenic carbonate particles in the ocean; do they dissolve in the water column. In: Andersen, N.R., Malahoff, A. (Eds.), The Fate of Fossil Fuel CO_2. Plenum Press, New York, pp. 269–294.

Honjo, S., 1982. Seasonality and interaction of biogenic and lithogenic particulate flux at the Panama Basin. Science 218, 883–884.

Honjo, S., 1984. Study of ocean fluxes in time and space by bottom-tethered sediment trap arrays: a recommendation. In: Global Ocean Flux Study. Proceeding of a Workshop. Natural Academic Press, Washington, DC, pp. 305–324.

Honjo, S., Dymond, J., Collier, R., Manganini, S.J., 1995. Export production of particles to the interior of Equatorial Pacific Ocean during 1992 EqPac Experiment. Deep-Sea Research II 42, 831–870.

Hung, J.-J., Lin, C.-S., Chung, Y.-C., Hung, G.-W., Liu, W.-S., 2003. Lateral fluxes of biogenic particles through the Mien-Hua canyon in the southern East China Sea slope. Continental Shelf Research 23, 935–955.

Iriarte, J.L., González, H.E., 2004. Phytoplankton size structure during and after the 1997/98 El Niño in a coastal upwelling area of the northern Humboldt Current System. Marine Ecology Progress Series 269, 83–90.

Iriarte, J.L., Pizarro, G., Troncoso, V., Sobarzo, M., 2000. Primary production and biomass of size-fractioned phytoplankton off Antofagasta, Chile (23–24°S) during pre-El Niño and El Niño 1997. Journal of Marine Systems 26, 37–51.

Ittekkot, V., Nair, R.R., Honjo, S., Ramaswami, V., Bartsch, M., Manganini, S.J., Desai, B.N., 1991. Enhanced particle fluxes in Bay of Bangal induced by injection of water. Nature 351, 385–387.

Ittekkot, V., Schäfer, P., Honjo, S., Depetris, P., 1996. Particle Flux in the Ocean. Wiley, Chichester, UK.

Jansen, H., 2001. Modelling the marine carbonate pump and its implications on the atmospheric CO_2 concentration. Dr. rer. nat. Thesis, Faculty of Physics, University of Bremen, pp. 1–128.

Kawahata, H., Gupta, L.P., 2003. El Niño/Southern Oscillation (ENSO) related variations in particulate export fluxes in the western and central Equatorial Pacific. Journal of Physical Oceanography 59, 663–670.

Kawahata, H., Suzuki, A., Ohta, H., 2000. Export fluxes in the Western Pacific Warm Pool. Deep-Sea Research I 47, 2061–2091.

Kawata, H., Yamamuro, M., Ohta, H., 1998. Seasonal and vertical variations of sinking particle fluxes in the West Caroline Basin. Oceanologica Acta 21, 521–532.

Kiørboe, T., 1993. Turbulence, phytoplankton cell size, and the structure of pelagic food webs. Advances in Marine Biology 29, 1–72.

Lampitt, R.S., 1985. Evidence for the seasonal deposition of detritus to the deep-sea floor and its subsequent resuspension. Deep-Sea Research 32, 885–898.

Lee, C., Hedges, J., Wakeham, S., Zhu, N., 1992. Effectiveness of various treatments in retarding microbial activity in sediment trap material and their effects on the collection of swimmers. Limnology and Oceanography 37, 117–130.

Legendre, L., Rassoulzadegan, F., 1996. Food-web mediated export of biogenic carbon in oceans: hydrodynamic control. Marine Ecology Progress Series 145, 179–193.

Marchant, M., Hebbeln, D., Wefer, G., 1998. Seasonal flux pattern of planktic foraminifera in the Peru–Chile current. Deep-Sea Research I 45, 1161–1185.

Marchant, M., Hebbeln, D., Giglio, S., Coloma, C., González, H.E., 2004. Seasonal and interannual variability in the flux of planktic foraminifera in the Humboldt Current System off central Chile (30°S). Deep-Sea Research II, this issue [doi:10.1016/j.dsr2.2004.08.013].

Martin, J.H., Knauer, G.A., 1983. VERTEX: manganese transport with $CaCO_3$. Deep-Sea Research 30, 411–425.

McCave, I.N., 1984. Size spectra and aggregation of suspended particles in the deep ocean. Deep-Sea Research 31, 329–352.

Milliman, J.D., 1980. Coccolithophorid production and sedimentation, Rockall Bank. Deep-Sea Research 27a, 959–963.

Morales, C., Blanco, J., Braun, M., Reyes, H., Silva, N., 1996. Chlorophyll-*a* distribution and associated oceanographic conditions in the upwelling region off northern Chile during the winter and spring 1993. Deep-Sea Research I 43, 267–289.

Nair, R.R., Ittekkot, V., Manganini, S.J., Ramaswamy, V., Haake, B., Degens, E.T., Desai, B.N., Honjo, S., 1989. Increased particle flux to the deep ocean related to monsoons. Nature 338, 749–751.

Nelson, J.R., Beers, J.R., Eppley, R.W., Jackson, J.A., McCarthy, J.J., Soutar, A., 1987. A particle flux study in the Santa Monica–San Pedro Basin off Los Angeles: particle flux, primary production, and transmissometer survey. Continental Shelf Research 7, 307–328.

Neuer, S., Davenport, R., Freudenthal, T., Wefer, G., Llinás, O., Rueda, M.-J., Steinberg, D.K., Karl, D.M., 2002. Differences in the biological pump at three subtropical ocean sites. Geophysical Research Letters 29, 1885–1888.

Noji, T.T., Børsheim, K.Y., Rey, F., Nortvedt, F.R., 1999. Dissolved organic carbon associated with sinking particles can be crucial for estimates of vertical carbon flux. Sarsia 84, 129–135.

Pantoja, S., Sepúlveda, J., González, H.E., 2004. Decomposition of sinking proteinaceous material during fall in the oxygen minimum zone off northern Chile. Deep-Sea Research I 51, 55–70.

Parrish, R.H., Bakun, A., Husby, D.M., Nelson, C.S., 1984. Comparative climatology of selected environmental processes in relation to eastern boundary current pelagic fish reproduction. In: Sharp, G.D., Csirke, J. (Eds.), Proceedings of the Expert Consultations to Examine Changes in Abundance and Species of Neritic Fish Resources, San José,

Costa Rica, 18–29 April 1983, vol. 3. FAO Fisheries Report, 291, pp. 731–777.

Peinert, R., Bodungen, B.v., Smetacek, V., 1989. Food web structure and loss rate. In: Berger, W.H., Smetacek, V., Wefer, G. (Eds.), Productivity of the Ocean: Present and Past. Wiley, New York, pp. 35–48.

Pilskaln, C.H., Honjo, S., 1987. The fecal pellet fraction of biogeochemical particle fluxes to the deep sea. Global Biogeochemical Cycles 1, 31–48.

Rice, A.L., Thurston, M.H., Bett, B.J., 1994. The IOSDL DEEPSEAS programme: introduction and photographic evidence for the presence and absence of a seasonal input of phytodetritus at contrasting abyssal sites in the northeastern Atlantic. Deep-Sea Research I 41, 1305–1320.

Riebesell, U., 1992. The formation of large marine snow and its sustained residence in surface waters. Limnology and Oceanography 37, 63–76.

Romero, O., Hebbeln, D., Wefer, G., 2001. Temporal and spatial variability in export production in the SE Pacific Ocean: evidence from siliceous plankton fluxes and surface sediment assemblages. Deep-Sea Research I 48, 2673–2697.

Rutllant, J.A., Rosenbluth, B., Hormazabal, S., 2004. Intraseasonal variability of wind-forced coastal upwelling off central Chile (30°S). Continental Shelf Research 24, 789 804.

Samtleben, C., Bickert, T., 1990. Coccoliths in sediment traps from the Norwegian Sea. Marine Micropaleontology 16, 39–64.

Shaffer, G., 1993. Effects of the marine biota on global carbon cycling. In: Heimann, M. (Ed.), The Global Carbon Cycle. Springer, Berlin, pp. 431–455.

Shaffer, G., Salinas, S., Pizarro, O., Vega, A., Hormazabal, S., 1995. Currents in the deep ocean off Chile (30°S). Deep-Sea Research I 42, 425–436.

Shaffer, G., Hormazabal, S., Pizarro, O., Salinas, S., 1999. Seasonal and interannual variability of currents and temperature off central Chile. Journal of Geophysical Research 104, 29951–29961.

Shaffer, G., Hormazabal, S., Pizarro, O., Ramos, M. Circulation and variability in the subtropical eastern South Pacific Ocean. Journal of Geophysical Research (in press).

Smetacek, V., 2003. Linking the biology of key species with ocean biogeochemistry. Ocean Biogeochemistry & Ecosystems Analysis. International Open Science Conference, 7–10 January 2003, Paris, France, Abstracts, p. 21.

Strub, P.T., Mesias, J., Montecino, V., Rutllant, J., Salinas, S., 1998. Coastal ocean circulation off western South America. In: Robinson, A.R., Brink, K.H. (Eds.), The Global Coastal Ocean. Regional Studies and Syntheses. Wiley, New York, pp. 273–314.

Takahashi, K., Bé, W.H., 1984. Planktonic foraminifera: factors controlling sinking speeds. Deep-Sea Research 31, 1477–1500.

Thomas, A.C., 1999. Seasonal distributions of satellite-measured phytoplankton pigment concentration along the Chilean coast. Journal of Geophysical Research 104, 25877–25890.

Thomas, A.C., Huang, F., Strub, P.T., James, C., 1994. Comparison of the seasonal and interannual variability of phytoplankton pigment concentrations in the Peru and California Current systems. Journal of Geophysical Research 99, 7355–7370.

Thomas, A.C., Carr, M.-E., Strub, P.T., 2001. Chlorophyll variability in eastern boundary currents. Geophysical Research Letters 28, 3421–3424.

Thunell, R.C., 1998. Particle fluxes in a coastal upwelling zone: sediment trap results from Santa Barbara Basin, California. Deep-Sea Research II 45, 1863–1884.

Thunell, R.C., Pilskaln, C.H., Tappa, E., Sautter, L.R., 1994. Temporal variability in sediment fluxes in the San Pedro Basin, Southern California Bight. Continental Shelf Research 14, 333–352.

Tsunogai, S., Noriki, S., 1991. Particulate fluxes of carbonate and organic carbon in the ocean. Is the marine biological activity working as a sink of the atmospheric carbon? Tellus 43, 256–266.

Turner, J.T., 2002. Zooplankton fecal pellets, marine snow and sinking phytoplankton blooms. Aquatic Microbial Ecology 27, 57–102.

Utermöhl, H., 1958. Zur Vervollkommnung der quantitativen Phytoplankton-Methodik. Internationale Vereinigung für Theoretische und Angewandte Limnologie 9, 1–39.

Walsh, I.D., Gardner, W.D., 1992. A comparison of aggregate profiles with sediment trap fluxes. Deep-Sea Research 39, 1817–1834.

Wassmann, P., Ypma, J.E., Tselepides, T., 2000. Vertical flux of faecal pellets and microplankton on the shelf of the oligotrophic Cretan Sea (NE-Mediterranean Sea). Progress in Oceanography 46, 241–258.

Wefer, G., Fischer, G., Fütterer, D., Gersonde, G., 1988. Seasonal particle flux in the Bransfield Strait (Antarctica). Deep-Sea Research 35, 891–898.

Young, J.R., Ziveri, P., 2000. Calculation of coccolith volume and its use in calibration of carbonate flux estimates. Deep-Sea Research II 47, 1679–1700.

Zar, J.H., 1984. Biostatistical Analysis. Prentice-Hall, Englewood Cliffs, NJ.

Zhang, X., Dam, H.G., 1998. Downward export of carbon by diel migrant mesozooplankton in the central equatorial Pacific. Deep-Sea Research II 44, 2191–2202.

ELSEVIER

Deep-Sea Research II 51 (2004) 2475–2490

DEEP-SEA RESEARCH
PART II

www.elsevier.com/locate/dsr2

Macrobenthic zonation caused by the oxygen minimum zone on the shelf and slope off central Chile

V.A. Gallardo[a,b,*], M. Palma[a,c], F.D. Carrasco[b], D. Gutiérrez[d], L.A. Levin[e], J.I. Cañete[f]

[a]*Centro de Investigación Oceanográfica en el Pacífico Sur-Oriental (FONDAP-COPAS), Universidad de Concepción, Casilla 160-C, Concepción, Chile*

[b]*Departamento de Oceanografía, Universidad de Concepción, Casilla 160-C, Concepción, Chile*

[c]*Programa de Doctorado en Ciencias Biológicas, Departamento de Zoología, Universidad de Concepción, Casilla 160-C, Concepción, Chile*

[d]*Dirección de Investigación Oceanográfica, Instituto del Mar del Perú (IMARPE), Casilla 22, Callao, Lima, Perú*

[e]*Integrative Oceanography Division, Scripps Institution of Oceanography, La Jolla, CA 92093-0218, USA*

[f]*Departamento de Ciencias Naturales, Facultad de Ciencias, Universidad de Magallanes, Casilla 113-D, Punta Arenas, Chile*

Accepted 20 July 2004

Abstract

The relationship between macrobenthic ($\geqslant 300\,\mu m$) zonation and the oxygen minimum zone (OMZ: $O_2 < 0.5\,ml\,L^{-1}$) was studied in shelf and slope sediments (122–840 m depth) off Concepción Bay, central Chile. Four study sites were sampled during March–April 1999 for abiotic factors, macrofaunal density, biomass, mean individual size, and diversity. Within the OMZ (122–206 m), the macrofaunal density was high (16,478–21,381 individuals m^{-2}) and 69–89% of the organisms were soft-bodied. Density was highest (21,381 individuals m^{-2}), biomass lowest (16.95 g wet weight m^{-2}), and individual size smallest (0.07 mg C individuals $^{-1}$) at the shelf break site (206 m). Polychaete worms made up 71% of the total abundance, crustaceans 16%, and mollusks only 2%. Total abundance beneath the OMZ (mid-slope site, ~840 m) was 49% crustaceans and 43% polychaetes. Although existing literature originally led to the hypothesis that both diversity and biomass within the OMZ would be lower than beneath the OMZ, in the present study this was only true for diversity. Biomass distribution, on the other hand, was concave along the depth gradient; the highest values were near the upper edge of (122 m) and beneath (840 m) the OMZ. Indices of the macrofaunal community structure varied in relation to bottom-water oxygen concentration, chlorophyll-*a*, phaeopigments, and sulfide concentration, but not in relation to grain size, C, N, mud, porosity, redox potential, a bottom-water temperature.

© 2004 Published by Elsevier Ltd.

*Corresponding author. Departamento de Oceanografía, Universidad de Concepción, Casilla 160-C, Concepción, Chile. Tel./fax: +56 41 20 4520.

E-mail address: vagallar@udec.cl (V.A. Gallardo).

0967-0645/$ - see front matter © 2004 Published by Elsevier Ltd.
doi:10.1016/j.dsr2.2004.07.028

1. Introduction

Since the time of the "Challenger" Expedition, scientists have noted nearly imperceptible changes in populations and communities across the wide horizontal areas of the ocean basins, but rapid changes with depth down the continental margins. The underlying causes of such vertical zonation remain one of deep-sea ecology's most difficult and elusive problems to date (Gage and Tyler, 1991). Early studies related the continental margin's major physiographical and hydrographical features to faunal boundaries and depth zonation. The shelf break, for example, is one of the most distinct physiographical features of the Earth's surface and marks the boundary between shallow shelf and deep-sea faunas. However, where oxygen-poor water masses overlie more oxygenated waters, as in the eastern South Pacific, depth zonation may be more tied to oxygen gradients (Gallardo, 1963; Mullins et al., 1985; Wishner et al., 1990; Arntz et al., 1991; Díaz and Rosenberg, 1995).

The Humboldt Current System (HCS) is characterized by an oxygen minimum zone (OMZ: $<0.5\,ml\ O_2\,L^{-1}$, 100–300 m depth), which is associated with the Poleward Undercurrent (PCU) and the Equatorial Subsurface Waters (ESSW) (Pizarro et al., 2002). The chemical conditions of central Chile's OMZ are dysoxic ($<1\,ml\,L^{-1}$), yielding a hypoxic physiological regime and specific biofacies; together these factors shape faunal zonation patterns (Tyson and Pearson, 1991; Rullkötter, 2000).

One of Chile's most productive marine zones is off the central coast. Coastal winds, shelf width, and diverse topographic features (embayments, capes, and submarine canyons) generate several upwelling centers and coastal eddies and contribute to high marine productivity (Cáceres and Arcos, 1991; Cáceres, 1992). During cold phases of the El Niño Southern Oscillation (ENSO), spring and summer upwelling events are more intense and more frequent (Strub et al., 1998; Figueroa and Moffat, 2000). These events transport nutrient-rich waters from the shallow ESSW mass to the photic zone (Hormazábal et al., 2001). Primary production rates typically vary from 0.5 to 5 g $C\,m^{-2}\,d^{-1}$ (Daneri et al., 2000), but can reach up to $9.9\,g\,C\,m^{-2}\,d^{-1}$ (Fossing et al., 1995). High primary production is accompanied by high carbon input to the sediments (Ahumada et al., 1989; Fossing et al., 1995; Gutiérrez et al., 2000; Farias et al., 2002). Total organic carbon (TOC) content ranges from 3% to 6% in the shelf surface sediments, where organic matter is largely composed of fresh, labile, particulate material of phytoplanktonic origin (Thamdrup and Canfield, 1996; Gutiérrez et al., 2000; Graco et al., 2001; Neira et al., 2001). Surface sediments, therefore, are highly reactive, with sulfate reduction rates as high as those in mudflat sediments (Ferdelman et al., 1997).

Environmental conditions influence benthic communities in other organically enriched, oxygen-deficient areas (Pearson and Rosenberg, 1978; Díaz and Rosenberg, 1995; Levin, 2003). Macrofaunal diversity and dominance are low and the numerical abundance of a few species is high within the OMZs of the Arabian Sea (Levin et al., 2000), west Africa (Sanders, 1969), the eastern tropical Pacific (Levin et al., 1991, 1994), and the Peru margin (Levin et al., 2002). Previous studies also have found high densities and low species richness for the benthic communities of central Chile's continental shelf (Gallardo, 1985; Carrasco and Gallardo, 1994), but little information is available about the slope communities. The macrofaunal benthic communities off Mejillones Peninsula in northern Chile (1061 and 1350 m depth), where upwelling is significant (Cañete et al., 1999), consist of small animals, low species richness, and low standing stock.

This study aims to (i) describe the macrobenthic community's composition, density, biomass, and diversity across central Chile's OMZ, (ii) identify the influence of oxygen deficiency and other abiotic factors on both the macrofaunal shelf and slope community structures, (iii) evaluate evidence for cross-margin biological zonation and identify possible causative factors, and (iv) compare the macrofaunal assemblages on the central Chile margin with those of other OMZs. Existing literature led us to hypothesize that the OMZ's macrofaunal biomass and diversity would be greatly reduced and its composition signifi-

cantly altered when compared to deeper, more oxygenated conditions.

This is the first known investigation of OMZ-induced zonation on the shelf and upper slope in the eastern South Pacific, following the work of Sanders (1969) at similar depths off Walvis Bay, West Africa, Nichols and Rowe (1977) off northwest Africa, Gallardo (1963) off Chile, and Frankenberg and Menzies (1968) and Rowe (1971a, b) off Peru; studies of deeper (mid-lower slope) depths were reviewed by Levin (2003).

2. Methods

2.1. Field work

Sediment and benthic samples were collected from four stations. The two stations within the OMZ were on the outer shelf (122–123 m) and the shelf break (203–209 m); the remaining two stations were at the lower OMZ edge (upper slope; 362–364 m) and beneath the OMZ (mid-slope; 806–903 m) (Fig. 1; Table 1). Henceforth, these sites will be referred to as OS-122, SB-206, US-364, and MS-840. Samples were collected on board the Chilean Navy's R/V *Vidal Gormaz*, from 29 March to 5 April 1999. A mini-multicorer with six tubes, 9.6 cm inner diameter (i.d.), was cast three to four times at each station for sediment collections and two to three tubes from each cast were used for sampling macrofauna. The sediment (2–20 cm) was sieved on board through a 300-μm mesh with filtered seawater (the first 2 cm of sediment unsieved) and then preserved in a buffered 10% seawater solution of formaldehyde. Sediment grain analyses were performed on wet multicorer samples (0–1 cm), using an ELZONE282 PC laser particle size analyzer. Parallel CTD and rosette casts were made for salinity, temperature, and dissolved oxygen (DO). DO was determined by the Winkler microtitration method (Knap et al., 1993), using from three to six replicates. Redox profiles were measured in 74-mm (i.d.) sediment sub-cores, using a platinum standard combination electrode with a calomel internal reference. Sub-samples for dissolved sulfide, TOC, total nitrogen (TN), and pigments (chlorophyll-*a* and phaeopigments) were

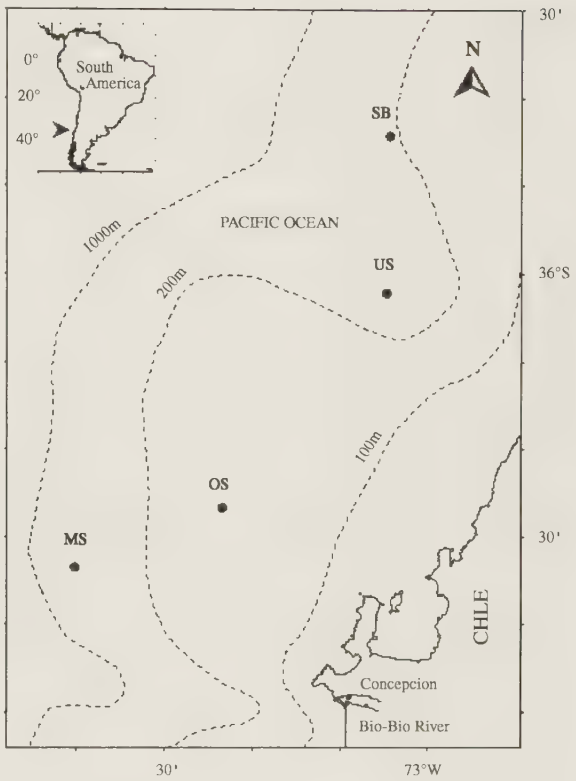

Fig. 1. Study sites on the continental margin off Concepción Bay, central Chile: OS = outer shelf site (122 m depth); SB = shelf break site (206 m); US = upper slope site (364 m); and MS = mid-slope site (840 m). The stations are not in a regular transect because of the difficulty in finding soft bottoms along a single straight transect across the continental margin.

taken with 36-mm (i.d.) tubes. Sulfides and pigments were sampled in two independent replicates (casts) from each station. Each sulfide sample was fixed with 2% zinc acetate until analysis. The pore water was extracted under a N_2 atmosphere with a squeezer, at 1 and 2 cm vertical intervals, in the first 15 cm of sediment.

2.2. Laboratory analyses

In the laboratory, the macrofauna was sorted, transferred to a 70% ethanol solution, identified to the lowest possible taxonomic level, counted, and weighed (alcohol wet weight). Taxa usually considered to be meiofauna (nematodes, copepods, and foraminifers) were neither counted nor used in

Table 1
Data collected from sampling sites on the margin off central Chile (29 March–5 April 1999)

Station	Depth (m)	No. of cores	Cast	Lat. (°S)	Long. (°W)
SB	209	3	MC-11	35°44.08	73°04.57
SB	203	2	MC-16	35°44.60	73°04.41
SB	207	3	MC-24	35°44.60	73°04.57
US	364	2	MC-1	36°02.40	73°05.10
US	362	3	MC-7	36°02.47	73°04.22
US	364	3	MC-10	36°02.31	73°05.17
US	364	3	MC-12	36°02.65	73°05.70
OS	122	3	MC-2	36°25.55	73°23.28
OS	122	3	MC-7	36°26.06	73°23.24
OS	123	3	MC-9	36°26.21	73°23.92
OS	122	3	MC-17	36°26.65	73°24.08
MS	806	2	MC-4	36°33.49	73°39.87
MS	810	3	MC-6	36°32.70	73°04.90
MS	903	3	MC-9	36°31.52	73°39.37

Sampling sites are: OS = outer shelf site; SB = shelf break site; US = upper slope site; and MS = mid-slope site. (MC = multicorer).

biomass determinations. Sulfides were determined colorimetrically following Cline (1969). Sulfide inventories were calculated by correcting for porosity (Berner, 1971), integrating the first 15 cm of sediment. A CHN elemental analyzer (Carlo Erba, model NA-1500) was used to determine TOC and TN from freeze-dried sediment samples at the Max Planck Institute for Marine Microbiology and Biogeochemistry (Bremen). Chlorophyll-*a* (chl-*a*) and phaeopigments (Phaeo) were analyzed fluorometrically in a sediment section of 0 to 1 cm. Samples were kept frozen at −80 °C and thawed before extraction. Thawed fractions of 0.2–0.3 g were mixed with 5 ml of 90% acetone in a vortex stirrer, sonicated for 10 min, and then centrifuged at 1500 rpm for 5 min. This extraction was done twice. Before reading fluorescence, and to obviate any potential interference arising from phaeo and carotenoids, a 0.5 ml aliquot of the pooled extract was diluted 20 times, both before and after acidification, with two drops of 10% HCl (Gutiérrez et al., 2000).

2.3. Data processing and statistical analyses

Prior to calculating density and biomass means and standard deviations, data from each multicore were pooled within a station and normalized per m^2. Body sizes were determined by converting the wet weight value to organic carbon (Brey et al., 1988). Species diversity was estimated using the Shannon H' ($\log_2$) index (Pielou, 1966), the J' index of equitability or evenness (Pielou, 1966), and the Simpson dominance D (Legendre and Legendre, 1979). A jackknife technique also was applied to calculate the Shannon H' and obtain parametric estimators of mean and variance (Sokal and Rohlf, 1981). Sanders–Hurlbert rarefaction curves were plotted to assess species richness corrected for sample size (Sanders et al., 1965; Hurlbert, 1971). Diversity analyses were performed with Biodiversity Pro ecological software (McAleece et al., 1997).

For multidimensional analyses, the species abundance data matrix was transformed according to $Y = \sqrt{\sqrt{x}}$. The similarity matrix was obtained with the Bray–Curtis index. Numerical classification was done with SIGTREE software (Nemec and Brinkhurst, 1998), using the UPGMA linkage method (Sneath and Sokal, 1973). Non-metric multidimensional scaling (NMDS) analysis was used for ordination (Gauch, 1982; Field et al., 1982; Gray et al., 1988), and the significance of differences between sites was examined by the ANOSIM randomization test (Clarke and Ainsworth, 1993). NMDS and multivariate analyses of relative dispersion were carried out on macrofaunal data. The relative index of multivariate

dispersion examines rank dissimilarity among replicate casts (i.e. heterogeneity within a station), where a value of 1 is the average dispersion among stations.

The correlations between environmental factors (depth, bottom-water oxygen, TOC, TN, C:N ratio, chl-*a*, redox potential, bottom water temperature, sediment sulfide concentration, grain size, and sorting coefficients) and community parameters (density, biomass, body size, and diversity parameters) were calculated with Pearson's '*r*' coefficient. The relationships between the environmental factors and the community ordination patterns were explored by the Bio-Env procedure (Clarke and Ainsworth, 1993).

3. Results

3.1. Physical setting

The lowest bottom-water oxygen levels (0.10 and 0.13 ml L^{-1}) were recorded at OS-122 and SB-206, well within the ESSW. Oxygen levels in the OMZ increased with depth, reaching 0.52 ml L^{-1} at US-364, which may be influenced by the upper boundary of the Antarctic Intermediate Waters (AAIW). The highest DO value (2.89 ml L^{-1}) was obtained at MS-840, clearly under the influence of the AAIW (Table 2). The sediments were mainly silt and clay (97.90–99.90% mud) and were poorly sorted at all sites (Table 2). At OS-122, the sediment was a soupy brown, somewhat oxidized mud at the surface, and occasional long *Thioploca* filaments were found down to 11 cm depth in the sediment. A compact layer of homogeneous gray clay went from 20 cm deep to the core bottoms (~40 cm). At SB-206, the sediment was heavily compacted but moderately burrowed. Oxidized sediments and patches of deep-dwelling fauna (maldanid polychaetes) were found down to 20 cm deep at US-364; empty chaetopterid polychaete tubes were observed protruding from core samples. Sediments from the deepest site appeared highly oxidized to the eye and were sticky to the touch. A few agglutinated branched foraminifers were visible at the sediment surface, empty maldanid polychaete tubes were found in the top 15 cm, and small (1–3 cm) reduced black patches were present deep within the sediment column.

OS-122 had the highest TOC (4.3%), TN (0.6%), chl-*a* (35.7 μg g^{-1}), and phaeo (277.7 μg g^{-1}) contents of the sampled stations, whereas SB-206 had the lowest values of these variables. The redox potential (Eh) was lower at OS-122 and SB-206 than at US-364 and MS-840 (Table 2). DO ($r = 0.980$; $p < 0.05$) and

Table 2
Summary of abiotic data at the study sites

Stations	OS	SB	US	MS
Average water depth (m)	122	206	364	840
Bottom water temperature (°C)	10.8	10.4	8.9	3.7
Bottom water oxygen (ml L^{-1})	0.10	0.13	0.52	2.89
Chlorophyll-*a* 0–1 cm (μg g^{-1})	35.7	12.9	13.3	13.4
Phaeopigments 0–1 cm (μg g^{-1})	277.7	126.6	131.3	150.9
Sulfide pool (μmol cm^{-2})	4.9	4.3	2.7	3.6
% TOC (0–1 cm)	4.3	1.1	3.1	2.1
% TN (0–1 cm)	0.6	0.2	0.4	0.3
C:N (molar) (0–1 cm)	8.5	7.6	8.7	8.4
Porosity (v/v) (0–1 cm)	0.9	0.7	0.8	0.9
Eh (mV) (0–1 cm)	135	121	198	257
% mud	99.5	97.9	99.6	98.9
Mean grain size (μm)	12.58	8.54	12.57	8.79
Sorting (ϕ)	6.31	6.87	6.31	6.83

Sampling sites are: OS = outer shelf site; SB = shelf break site; US = upper slope site; and MS = mid-slope site.

temperature ($r = 1.00$; $p < 0.05$) correlated positively with bottom-water depth. Chl-*a*, Phaeo, sulfide, and TOC, TN, porosity, redox potential, and the C:N ratio showed almost no correlation with bottom-water depth ($p > 0.05$).

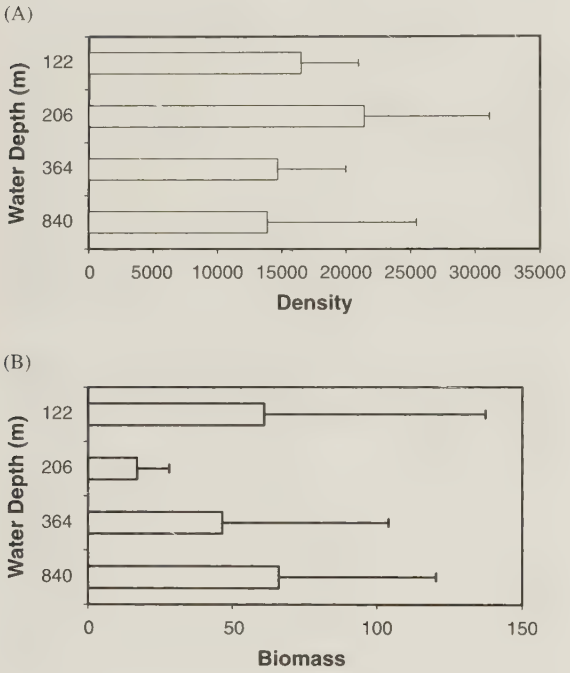

Fig. 2. (A) Mean density (ind m^{-2}) and (B) mean biomass (g wet wt m^{-2}) of macrofauna at each sampling depth (error bars indicate + one standard deviation).

3.2. Macrofaunal density, biomass, and body size

Mean densities ranged from ~16,480 ind m^{-2} at OS-122 to 21,380 individuals (ind) m^{-2} at SB-206, then diminished to 14,664 ind m^{-2} at US-364 and to 13,860 ind m^{-2} at MS-840; these differences were not statistically significant ($p > 0.05$) (Fig. 2A, Table 3a). The biomass distribution was concave along the depth gradient, with the lowest value at SB-206 (16,954 ± 12,805 g m^{-2}). The higher biomass found at the upper edge of the OMZ was similar to values beneath the OMZ (Fig. 2B). Macrofaunal individuals were small at all sites; polychaetes were the dominant group (Table 3; Fig. 3). The mean size of individual macrofauna in the study was 0.27 mg C ind^{-1}. The lowest body size was recorded at SB-206 (0.07 mg C ind^{-1}) and the highest at MS-840 (0.45 mg C ind^{-1}) (Table 4), although individual body size did not differ significantly among the stations ($p > 0.05$).

3.3. Species composition

A total of 71 species and morpho-species were identified from the four stations (Table 5). Polychaetes were dominant and characteristic of the ESSW-influenced OMZ and the OMZ edge sites (97% at OS-122, 70% at SB-206, and 74% at US-364) (Fig. 3). At MS-806, however, under the AAIW, polychaete abundance (43%) yielded to Crustacea (49%) and mollusks gained importance

Table 3
Mean density (ind m^{-2}, upper panel) and biomass (g wet wt m^{-2}, lower panel) and their standard deviation for the major groups and the total macrofauna on the continental margin off central Chile

Taxa	OS (Mean ± SD)	SB (Mean ± SD)	US (Mean ± SD)	MS (Mean ± SD)
Polychaeta	16,056 ± 4213	14,836 ± 7182	10,799 ± 4008	5915 ± 1618
Crustacea	130 ± 127	247 ± 327	2003 ± 1446	6762 ± 10,396
Mollusca	259 ± 438	18 ± 50	154 ± 117	900 ± 627
Other	35 ± 64	6179 ± 4258	1708 ± 3077	283 ± 320
Total	16,478 ± 4842	21,280 ± 11,817	14,664 ± 8648	13,860 ± 12,961
Polychaeta	53.6 ± 77.9	15.6 ± 10.5	35.8 ± 55.7	39.8 ± 22.9
Crustacea	6.6 ± 7.8	0.6 ± 1.5	4.9 ± 11.1	1 ± 1.5
Mollusca	0.1 ± 0.2	0.02 ± 0.1	1.4 ± 3.1	25.1 ± 34.9
Other	0.7 ± 1.6	0.8 ± 0.9	4.4 ± 13	0.3 ± 0.3
Total	60.9 ± 87.4	17 ± 12.9	46.5 ± 82.8	66.1 ± 59.6

Sampling sites are: OS = outer shelf site; SB = shelf break site; US = upper slope site; and MS = mid-slope site.

6.5%). The polychaete assemblage's composition varied considerably (Fig. 4); Cossuridae (*Cossura chilensis*), Spionidae (*Paraprionospio pinnata*), Cirratulidae (*Cirratulus cirratus*), Paraonidae (*Aricidea pigmentata*), and Nephtyidae (*Nephtys ferruginea*) were found at all sites, but only made up the greatest fraction of the total numbers at OS-122 and SB-206 (Table 5). At OS-122, *Mediomastus branchiferus* (11%) and *Paraprionospio pinnata* (10%) were also common. At SB-206, several species (e.g. *Cossura chilensis*, *Aricidea pigmentata*, and *Paraprionospio pinnata*) were found to have highly developed branchial structures (Fig. 5), a feature also noted by Lamont and Gage (2000). At US-364, the amphinomid *Paramphinome australis* comprised 42% of all polychaetes (4507 ± 1844 ind m^{-2}) and the archiannelid *Nerilidium* (unique to this station) 9%. At MS-840, polychaetes were less abundant and consisted mainly of *Aricidea pigmentata* (31%), *Euclymene* sp. (15%), and *Paramphinome australis* (14%). The relative crustacean abundance increased with increasing depth and DO (Fig. 3). Amphipods were collected at all sites, but never comprised more than 5% of the total abundance; they were most dense at MS-840 (371 ± 452 ind m^{-2}). Mysidacea also showed maximum values at MS-840 ($3990 \pm 10{,}227$ ind m^{-2}). At US-364, cumaceans were abundant (1528 ± 1536 ind m^{-2}). Mollusks, represented by the small bivalves of the genera *Thyasira* and *Nucula*, were present at OS-122. Although bivalves were absent at SB-206, they reappeared at US-364 (*Gari solida*, *Eunucula* sp., and one unidentified form) and were most dense at MS-840, where *Thyasira* sp., *Eunucula* sp., and other small, unidentified bivalves were found. Oligochaetes and nemerteans were most dense at OS-122 (4873 ± 3622 ind m^{-2}) and SB-206 (1201 ± 3396 ind m^{-2}).

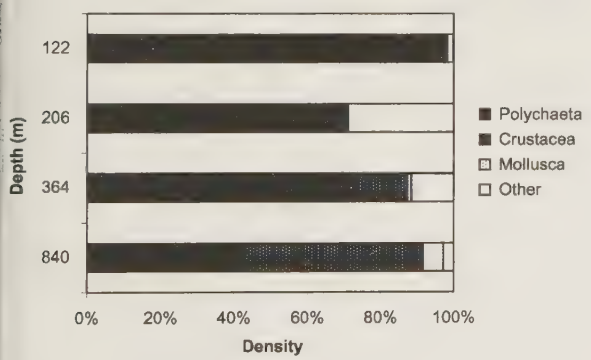

Fig. 3. Percent density of major macrofaunal taxa in the study area.

The dominant annelid species—in terms of biomass—was not the most abundant annelid species. Rather the annelid biomass was dominated by *Pectinaria* sp. (35%) and *Magelona phyllisae* (24%) at OS-122, by *Terebellides* sp. (28%), *Cirratulus cirratus* (18%), and *Cossura chilensis* (8%) at SB-206, by *Euclymene* sp. (43%) and *Terebellides* sp. (16%) at US-364, and by *Euclymene* sp. (90%) at MS-840.

3.4. Macrofaunal diversity

Macrofaunal species richness, estimated by rarefaction, was lowest within the OMZ ($E[S_{100}] = 11.8$–12.4) and highest beneath the OMZ ($E[S_{100}] = 21.1$) (Table 4 and Fig. 6), with relatively high values

Table 4
Diversity measures for the macrofauna (≥300 μm) on the continental margin off central Chile

Site	Depth	$r(n)$	S	BS	$H'(\log^2)$	$E(S_{100})$	H'_{jk}	SD	SE	H'_{max}	D	J'
OS	122	12 (4)	26	0.32	2.07	12.44	2.76	0.51	0.04	4.70	0.27	0.58
SB	206	8 (3)	31	0.07	2.89	11.82	3.05	0.69	0.09	4.95	0.18	0.58
US	364	11 (4)	38	0.22	3.54	18.49	3.65	0.43	0.04	5.25	0.14	0.68
MS	840	8 (3)	39	0.45	3.67	21.06	3.86	1.06	0.14	5.29	0.14	0.70

Code as follows: r = number of cores of 0.0071 m^{-2} each; (n) = number of the multicorer casts; S = total number of species per station; BS = mean individual body size (mg C ind^{-1}) (tested for significance); H' = Shannon diversity index; $E(S_{100})$ = rarefaction richness; H'_{jk} = Jackknifed Shannon diversity; SD = standard deviation; SE = standard error of the jackknifed Shannon index; H'_{max} = maximum theoretical diversity; D = Simpson Dominance; and J' = Equitability of Pielou. Sampling sites are: OS = outer shelf site; SB = shelf break site; US = upper slope site; and MS = mid-slope site.

Table 5
Species composition, density, and biomass expressed per m^2 at each depth on the continental margin off central Chile

	122 m				206 m				364 m				840 m			
	Density mean (SD) ($n=12$)		Biomass		Density mean (SD) ($n=8$)		Biomass		Density mean (SD) ($n=11$)		Biomass		Density mean (SD) ($n=8$)		Biomass	
Paraprionospio pinnata	1648	(539)	3.136	(1.929)	353	(213)	1.121	(1.115)								
Sphiophanes bombyx					18	(49)	0.002	(0.005)					18	(49)	0.321	(0.090)
Scolelepis sp.					35	(65)	0.012	(0.023)								
Nephtys ferruginea	1177	(939)	5.492	(5.317)	71	(75)	1.296	(2.721)	193	(221)	0.743	(1.124)	18	(49)	0.011	(0.030)
Aricidea pigmentata	1012	(899)	0.406	(0.414)	3760	(2324)	1.100	(0.848)	1733	(1691)	0.327	(0.408)	1853	(557)	0.371	(0.111)
Cirrophorus sp.													494	(727)	0.072	(0.111)
Cirratulus cirratus	1071	(644)	0.253	(0.153)	4713	(3565)	2.853	(2.507)	758	(510)	0.276	(0.291)	141	(151)	0.095	(0.186)
Tharyx sp.	94	(193)	0.042	(0.079)												
Mediomastus branchiferus	1789	(1385)	0.264	(0.256)	18	(49)	0.078	(0.220)					318	(308)	1.467	(1.602)
Capitella sp.	294	(733)	0.088	(0.136)									141	(272)	0.583	(1.099)
Cossura chilensis	7874	(3331)	6.159	(2.470)	4237	(1994)	1.275	(0.856)	231	(230)	0.014	(0.011)	424	(292)	0.115	(0.124)
Lumbrineris tetraura					18	(49)	1.347	(3.810)	257	(327)	2.39	(2.134)				
Lumbrineris chilensis					18	(49)	0.002	(0.005)								
Euclymene sp.	35	(122)	0.016	(0.057)	758	(1139)	1.022	(1.517)	77	(131)	15.831	(45.516)	900	(384)	35.748	(22.062)
Johnstonia sp.					18	(49)	0.886	(2.507)								
Terebellides sp.	212	(733)	1.138	(3.943)	18	(49)	4.371	(12.364)	116	(164)	5954	(11.124)	18	(49)	0.041	(0.115)
Syllidae sp.	12	(40)	0.022	(0.077)					347	(470)	0.019	(0.020)	106	(196)	0.011	(0.020)
Typosyllis sp.	24	(81)	0.055	(0.192)					13	(42)	0.001	(0.004)				
Exogone sp.									629	(822)	0.068	(0.096)	106	(146)	0.016	(0.002)
Haploscoloplos kerguelensis					18	(49)	0.147	(0.419)	334	(425)	1. 461	(2.064)				
Berkeleya sp.																
Nereis dorsolobata													18	(49)	0.005	(0.015)
Chaetopteridae sp. A	12	(40)	1.077	(3.731)									71	(106)	0.35	(0.835)
Magelona phyllisae	565	(430)	12.744	(41.386)									53	(405)	0.06	(0.120)
Pherusa sp.	24	(54)	0.73	(1.707)	18	(49)	0.002	(0.005)	13	(42)	0.001	(0.004)				
Polynoe sp.	35	(87)	0.75	(2.571)	317	(438)	0.013	(0.023)					52	(149)	0.277	(0.784)
Sabellidae sp. A	24	(54)	0.077	(0.199)	18	(49)	0.002	(0.005)	13	(42)	0.005	(0.017)				
Pectinaria sp.	12	(40)	18.792	(65.099)												
Sigambra bassi	141	(208)	2.314	(3.004)	18	(49)	0.002	(0.005)								
Paramphinome australis					317	(164)	0.051	(0.047)	4506	(1844)	0.386	(0.399)	847	(758)	0.071	(0.078)
Nerillidium sp.									963	(1348)	0.021	(0.027)				
Ophelina sp.					71	(199)	0.014	(0.040)	154	(147)	4.904	(6.438)	177	(146)	0.058	(0.050)
Protodorvillea sp.					71	(130)	0.004	(0.010)	308	(492)	0.022	(0.038)	53	(73)	0.046	(0.064)

Ampharetidae sp. A									13	(42)	0.881	(2.921)	71	(151)	0.023	(0.050)
Phyllodocidae sp. A					53	(149)	0.002	(0.005)								
Glycera sp.									13	(42)	0.135	(0.447)				
Goniada unicinigera													35	(65)	0.009	(0.017)
Aphroditidae sp.A									13	(42)	0.001	(0.004)				
Eunicidae sp. A									13	(42)	0.001	(0.004)				
Onuphis sp.									13	(42)	3.139	(10.412)				
Hesionidae sp. A									13	(42)	0.001	(0.010)				
Podarke sp.									64	(97)	0.004	(0.007)				
Tomopteridae sp. A									13	(42)	0.039	(0.128)				
Pontodoridae sp A.									13	(42)	0.969	(3.215)				
Cumacea sp. A									1527	(1536)	0.249	(0.369)	52	(73)	0.012	(0.018)
Ostracoda sp. A													159	(296)	0.026	(0.049)
Amphipoda sp. A	24	(54)	0.005	(0.011)	212	(345)	0.032	(0.042)	243	(290)	0.032	(0.037)				
Ampeliscidae sp. A													371	(452)	0.076	(0.092)
Phoxocephalidae sp. A													53	(49)	0.016	(0.045)
Isopoda sp. A													35	(99)	0.005	(0.015)
Tanaidacea sp. A					18	(49)	0.004	(0.010)	141	(218)	0.004	(0.066)	2101	(1126)	0.272	(0.154)
Mysidacea sp. A									64	(146)	0.298	(0.988)	3990	(10226)	0.574	(1.410)
Cancer sp.	12	(40)	0.393	(1.362)												
Eurypodius sp.									13	(42)	0.013	(0.043)				
Pleuroncodes monodon	94	(109)	6.151	(6.851)					13	(42)	3318	(11.004)				
Calianassa sp.					18	(49)	0.528	(1.493)								
Solenogaster					18	(49)	0.018	(0.050)								
Bivalves indet.									103	(127)	0.381	(1.050)	406	(491)	0.021	(0.060)
Thyasira sp.	224	(452)	0.1	(0.169)									177	(289)	0.154	(0.169)
Gari solida									13	(42)	0.905	(3.002)				
Nucula sp.	35	(63)	0.022	(0.046)												
Eunucula sp.									38	(91)	0.141	(0.388)	177	(146)	24.029	(35.313)
Gastropoda													35	(65)	0.773	(2.187)
Scaphopoda sp. A													106	(156)	0.074	(0.105)
Ophiuroidea													71	(106)	0.143	(0.205)
Nemertea	12	(40)	0.004	(0.012)	1201	(3395)	0.268	(0.759)	64	(131)	0.041	(0.089)	141	(151)	0.064	(0.066)
Oligochaeta sp. A					4873	(3622)	0.47	(0.447)	1605	(3058)	0.325	(0.951)	18	(49)	0.007	(0.020)
Anthozoa									26	(57)	4.024	(12.995)	18	(49)	0.005	(0.015)
Celenterata sp. A					18	(49)	0.011	(0.030)								
Sipunculid					18	(49)	0.007	(0.020)	13	(42)	0.001	(0.004)	18	(49)	0.037	(0.105)
Echiuroidea	24	(54)	0.686	(1.608)	71	(199)	0.014	(0.040)					18	(49)	0.039	(0.110)

Units as in Table 3.

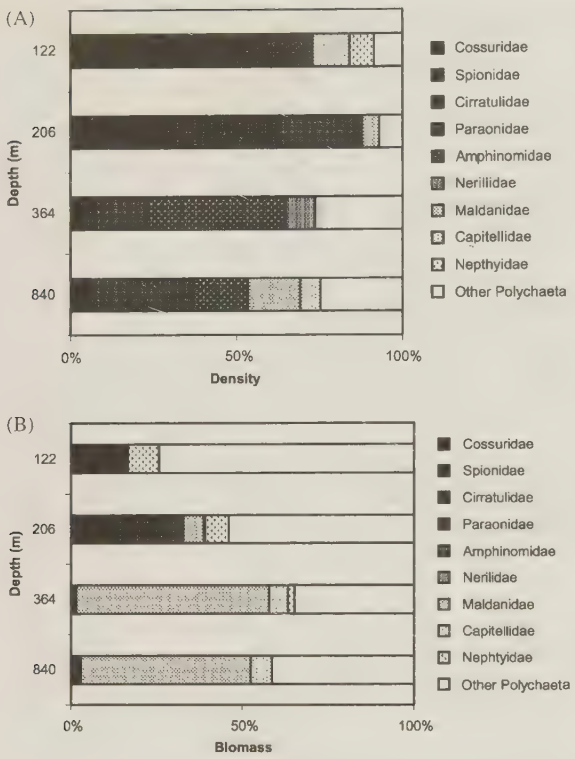

Fig. 4. Representative polychaete families in terms of (A) percent density and (B) biomass at each sampling site.

Fig. 5. Photograph of anterior body of the polychaete worm *Paraprionospio pinnata* with highly developed branchial structures.

also recorded at the OMZ edge ($E[S_{100}] = 18.5$). Both Shannon H' and equitability J' increased with bottom depth (Table 4), a result of increased species richness and reduced dominance. H' was positively correlated with species richness S ($r = 0.981$; $p < 0.05$), rarefaction diversity $E[S_{100}]$ ($r = 0.965$;

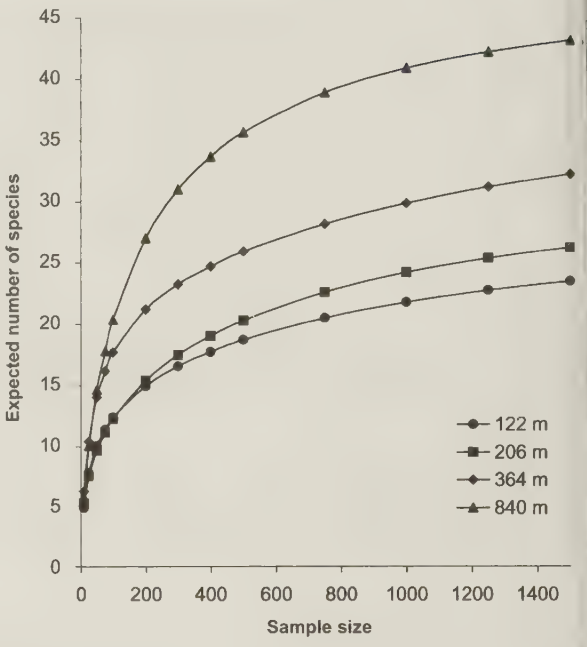

Fig. 6. Sanders–Hurlbert rarefaction diversity curves for the pooled abundance and species richness at each of the sampling sites. The data from all collected taxa were used (see Table 5).

$p < 0.05$), and evenness J' ($r = 0.994$; $p < 0.01$). The Shannon H' reached 55–58% of the maximum theoretical diversity (H'_{max}) within the OMZ and 68–70% of the H'_{max} at the edge of and beneath the OMZ (Table 4). None of the diversity parameters correlated with the total macrofaunal density or biomass, but polychaete density correlated negatively with $E[S_{100}]$ ($r = -0.980$; $p < 0.05$), Shannon H' ($r = -0.958$; $p < 0.05$), and evenness J' ($r = -0.960$; $p < 0.05$). The total number of polychaete species increased moderately from within the OMZ (19 at OS-122 and 22 at SB-206) to its edge (25 at US-364). In contrast, the crustacean species richness increased from 3 per station within the OMZ to 6 at the OMZ edge and 7 beneath the OMZ. Mollusk diversity was low at all four sites; only 1 to 2 mollusk species were found within the OMZ, 3 at the OMZ edge, and 5 beneath the OMZ.

3.5. *Community classification and ordination*

The macrofaunal community composition, as examined by cluster analysis (Fig. 7) and multidimensional scaling (Fig. 8), was clearly distinct at

each station (ANOSIM Pair-wise comparisons, $p<0.05$). Moreover, spatial heterogeneity increased with depth according to the Multivariate Dispersion Index (Fig. 8).

3.6. Faunal relationships with environmental factors

Rarefaction diversity $E[S_{100}]$ correlated positively with bottom depth ($r=0.90$; $p<0.05$) and Shannon H' showed a weak positive correlation with depth ($r=0.79$; $p>0.05$). Although total macrofaunal density and biomass did not correlate with water depth or bottom-water oxygen, polychaete density correlated negatively with water depth ($r=-0.98$; $p<0.05$) and DO ($r=-0.93$; $p<0.05$) and positively with bottom water temperature ($r=0.97$; $p<0.05$). The total macrofaunal species richness $E[S_{100}]$ correlated positively with the DO concentration ($r=0.84$; $p>0.05$). The total species richness $E[S_{100}]$, evenness J', and Shannon H' of the macrofauna correlated positively with the redox potential at the sediment surface (Eh) ($p<0.05$), but polychaete density correlated negatively with this parameter ($r=-0.98$; $p<0.05$). Simpson's dominance D was positively related to chl-*a* ($r=0.95$; $p<0.06$) and Phaeo ($r=0.91$; $p=0.1$).

Together, bottom-water DO and phaeo provide the best explanation ($\rho_w=0.91$) for the patterns seen in macrofaunal community abundance and composition, although the combination of bottom water DO, phaeo, chl-*a*, and sulfide also correlated significantly ($\rho_w=0.96$) with the observed faunal diversity patterns.

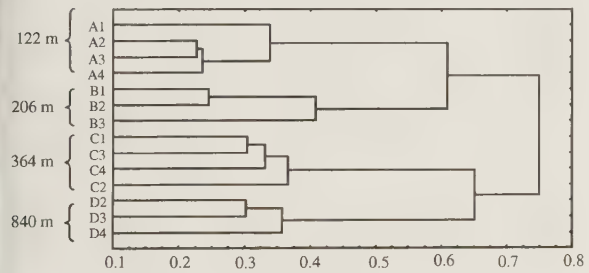

Fig. 7. Cluster analysis of the species abundance for each multicore sample.

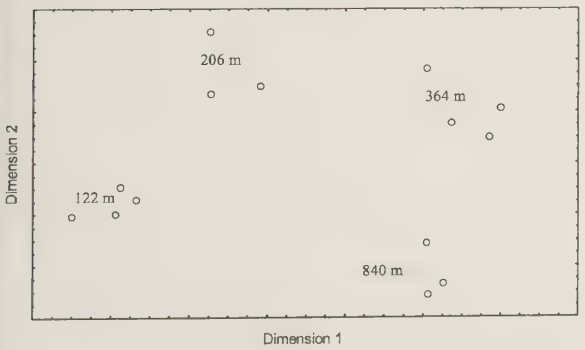

Fig. 8. Plot resulting from the Non-metric Multidimensional Scaling (NMDS) analysis of the mean density of all samples of a multicore (stress = 0.17).

4. Discussion

4.1. Physical settings

Sorting coefficients reflected a poorly sorted, low-energy regime at all sites. Biogeochemical properties of the sediment, temperature, and oxygen varied appreciably across the margin off Concepción Bay and were not significantly correlated. For many parameters, however, the shallower OS-122 differed greatly from the other sites (Table 2). In this study, bottom DO varied from 0.10 to 2.89 ml L^{-1}; thus our sampling was performed within the region's characteristic OMZ (sediments associated with the ESSW) and below the OMZ (sediments associated with the AAIW). Similar low oxygen concentrations have been measured in the Santa Barbara Basin (Bernhard et al., 2000), on the continental margins off Chile (Gutiérrez et al., 2000) and Peru (Levin et al., 2002), at the summit of Volcano 7, Mexico (Levin et al., 1991, 1994), off Oman (Levin et al., 2000), and off west Africa (Sanders, 1969).

4.2. OMZ effects on macrofaunal density, biomass, and body size

Total macrofaunal density across the continental margin off Concepción did not differ significantly among stations and, in fact, exhibited no OMZ effect. Nevertheless, higher densities were registered within the OMZ at SB-206 due to oligochaete worms (4873 ind m^{-2}) (Table 5). In

comparison with previous observations, however, the densities found at OS-122 were relatively low. Gutiérrez et al. (2000) reported densities ranging from 16,400 to 60,000 ind m^{-2} on the continental shelf. The negative impact of the 1997–1998 El Niño (EN) on surface productivity could have triggered downward changes in the eukaryotic density and faunal composition, thereby explaining the low densities observed here. Under non-EN conditions, the high inputs of fresh organic matter that reach the ocean bottom allow for an abundant prokaryote–eukaryote assemblage (Gallardo, 1985). Gutiérrez et al. (2000) reported that the macrofauna of the outer shelf occurred in sediments having more refractory and oxidized organic matter than those further inshore.

This study's macrofaunal densities are higher than those at similar depths in the Rockall Trough, Atlantic Ocean (Paterson and Lambshead, 1995), in the east tropical North Atlantic (Cosson et al., 1997), and on Volcano 7 off Mexico (Wishner et al., 1990) and are comparable to those on the continental margin of the western mid-Atlantic (Schaff et al., 1992), the Oman margin (Levin et al., 2000), and the Peru margin (Levin et al., 2002). The global bathyal data on benthic faunal density and biomass indicate a reduction in density at the OMZ core (Rosenberg et al., 1983; Mullins et al., 1985; Wishner et al., 1990, 1995) and an increase at the OMZ boundaries (0.5 ml L^{-1}) (Mullins et al., 1985; Wishner et al., 1990, 1995; Levin et al., 1991). Although this pattern was not observed off Peru (Levin et al., 2002), maximal macrofaunal densities on the Oman margin and Volcano 7 were observed within the OMZ (Levin et al., 1991, 2000). Whereas our density data are inconclusive in this respect, the biomass data exhibit a concave distribution in which the smallest biomasses are at the OMZ core.

In most OMZs where macrofaunal body size has been measured, the most dense sites are those with the smallest biomass and lowest average body size. This is true for the continental margin off central Chile (this study), Oman (Levin et al., 2000), and Peru (Levin et al., 2002). In this study, estimated body sizes (0.27 mg C ind^{-1}) are larger than those registered in the Arctic hypoxic environments (0.23 mg C ind^{-1}) (Rowe, 1997) and much larger than those found at 400 m depth in the Oman study (0.07 mg C ind^{-1}) (Levin et al., 2000) and at 300 m off Peru (0.05 mg C ind^{-1}) (Levin et al., 2002).

4.3. Taxonomic composition

The macrofaunal zonation across central Chile's margin is evident in the form of shifts in the taxonomic composition and diversity that distinguish the OMZ shelf sites (under the direct influence of the ESSW) from the upper and mid-slope sites (the latter, in particular, under the direct influence of the AAIW).

In a review of mainly shallow water data, Díaz and Rosenberg (1995) found that polychaetes, followed by bivalves and crustaceans, were the macrofaunal invertebrates most tolerant to hypoxia. Nevertheless, exceptions exist; ampeliscid amphipods are sometimes abundant in the OMZs of the Chilean, Peruvian, and Oman margins (Gallardo, 1963; Carrasco and Arcos, 1984; Gallardo et al., 1995; Levin et al., 2000, 2002). However, amphipods appear to be rare at oxygen concentrations <0.15 ml L^{-1} (Levin, 2003; this study). In this study, amphipods did not surpass 2% of the total macrofauna at stations with oxygen levels <0.13 ml L^{-1}.

The macrofauna within central Chile's OMZ consisted mainly of polychaetes of the families Cossuridae, Capitellidae, Spionidae, and Cirratulidae. Although spionids often predominate when oxygen values range between 0.1 and 0.5 ml L^{-1} (Rhoads and Morse, 1971; Thompson et al., 1985; Arntz et al., 1991; Levin et al., 1991; Díaz and Rosenberg, 1995; Levin and Gage, 1998; Levin et al., 2000), in this study, Cossuridae showed the greatest ecological dominance at all OMZ sites. Gutiérrez et al. (2000) described the changes in faunal composition and bioturbation functionality that are induced by the extreme cold and warm phases of the El Niño Southern Oscillation cycle off central Chile. The higher bioturbation potential during EN is due to higher numbers of subsurface deposit feeders (i.e. *Cossura chilensis*). Conversely, the lower bioturbation potential during La Niña and 'normal' cold regimes is due to the predominance of surface deposit feeders (i.e.

Paraprionospio pinnata). The amphipod *Ampelisca araucana* falls into the latter trophic group.

On the slope beneath the OMZ, the dominant forms were polychaetes of the families Paraonidae, Amphinomidae, and Maldanidae. The mid-slope communities off central Chile resembled those of other organic-rich regions at 840 m depth, such as off Cape Hatteras, North Carolina, USA. Key similarities are abundant maldanid polychaetes, dominance by paranoid polychaetes of the genus *Aricidea*, and the presence of common shallower water species (Schaff et al., 1992; Levin et al., 1997).

4.4. Zonation

Cluster analysis (Fig. 7) and NMDS (Fig. 8) confirm the zonation within the OMZ, with relatively distinct assemblages evident at 122, 206, and 364 m. The MVDISP (Fig. 8) corroborates the increased heterogeneity between multicorer casts with increasing depth and bottom water DO. The high homogeneity at the OMZ stations with the lowest DO can be explained by a physical control associated with uniformly high organic inputs and oxygen stress. A transect across the Oman margin OMZ revealed similar zonation and heterogeneity patterns (Levin et al., 2000). In both regions, the increased incidence of burrowing taxa below the OMZ appears to generate more and larger biogenic sediment structures (Smith et al., 2000).

DO, phaeo, chl-*a*, and bottom depth most likely contribute to zonation. The pattern exhibited by the NMDS analysis in the Euclidean space resembles the "horseshoe effect" encountered when a perfect gradient is sampled and analyzed (Digby and Kempton, 1987). The observed zonation across central Chile's margin, including its OMZ, occurs over a highly condensed depth range (122–364 m), exhibiting strong faunal gradients similar to those reported by Sanders (1969) off West Africa but much sharper than those occurring in the 1000 m thick OMZs observed off Oman (Levin et al., 2000) and Mexico (Wishner et al., 1990; Levin et al., 1991). Additional sampling stations are required to determine if the zonation patterns of central Chile's margin are different from those of other regions.

4.5. Community structure and environmental correlations

Sanders (1968) showed that deep-sea benthic communities are highly diverse and that their diversity varies with bathymetry (Sanders et al., 1965; Watts et al., 1992) and geography (Rex et al., 1993). Interesting debates have ensued on the existence of and causes for this high diversity (Rex, 1976, 1981; Rex et al., 1993; Boucher and Lambshead, 1995; Lambshead et al., 2000; Levin et al., 2001). Classic studies indicate that diversity changes with depth due to factors such as reduced food availability and physical disturbances. The generation of patches in a mosaic (Grassle and Maciolek, 1992) or the activities of deep-sea organisms that modify the benthic environment (Jumars, 1976; Thistle, 1979; Levin, 1991; Gage, 1996) also may influence diversity. Etter and Grassle (1992) suggested that diversity patterns in the western Atlantic can be related to sediment heterogeneity, created and maintained by the biota (Jumars, 1976). Levin et al. (2001) reviewed the impact of productivity, a hydrodynamic regime, oxygenation, sediment properties, and catastrophic disturbances of deep sea macrofaunal diversity, pointing out that many of these factors interact to produce the observed diversity patterns. Thus, while bottom-water oxygen gradients are probably a critical element in determining diversity changes on Chile's margin, oxygen is unlikely to be the only significant parameter.

Acknowledgements

We acknowledge the help of J. Sellanes, C. Neira, and other participants in R/V Vidal Gormaz cruise. L.A.L. acknowledges support from NSF grants OCE 98–03861 and INT–0227511. This work was supported in Chile by the FONDAP–Humboldt (CONICYT) Program and is a contribution of the FONDAP–COPAS Center (Project No. 150100007). We thank

three anonymous reviewers for suggestions to improve the manuscript.

References

Ahumada, R., Rudolph, A., Madariaga, S., Carrasco, F., 1989. Descripción de las condiciones oceanográficas de la Bahía San Vicente y antecedentes sobre los efectos de la contaminación. Biología Pesquera 18, 37–52.

Arntz, W.E., Tarazona, J., Gallardo, V.A., Flores, L.A., Salzwedel, H., 1991. Benthos communities in oxygen deficient shelf and upper slope areas of the Peruvian and Chilean Pacific Coast, and changes caused by El Niño. In: Tyson, R.V., Pearson, T.H. (Eds.), Modern and Ancient Continental Shelf Anoxia. Geological Society Special Publication 58, pp. 131–154.

Bernhard, J.M., Buck, K.R., Farmer, M.A., Bowser, S.S., 2000. The Santa Barbara Basin is a symbiosis oasis. Nature 403, 77–80.

Berner, R., 1971. Principles of Chemical Sedimentology. McGraw-Hill, New York, 240pp.

Brey, T., Rumohr, H., Ankar, S., 1988. Energy content of macrobenthic invertebrates: general conversion factors from weight to energy. Journal of Experimental Marine Biology and Ecology 117, 271–278.

Boucher, G., Lambshead, P.J.D., 1995. Ecological biodiversity of marine nematodes in samples from temperate, tropical, and deep-sea regions. Conservation Biology 9, 1594–1604.

Cáceres, M., 1992. Vórtices y filamentos observados en imágenes de satélite frente al área de surgencia de Talcahuano, Chile. Investigación Pesquera 37, 55–66.

Cáceres, M., Arcos, D., 1991. Variabilidad en la estructura espacio-temporal de un área de surgencia frente a la costa de Concepción, Chile. Investigación Pesquera 36, 27–38.

Cañete, J.I., Sievers, H.A., Báez, P., Valdovinos, C., 1999. Macrobenthos of the continental slope off Mejillones peninsula, northern Chile: results of the Atacama Trench International Expedition (September, 1997). Istituto Scienze Ambientali Marine, Facoltá di Scienze, Matemathiche Fisiche e Naturali. Data Report 56, 67–74.

Carrasco, F.D., Arcos, D.F., 1984. Life history and production of a cold temperate population of the sublittoral amphipod *Ampelisca araucana*. Marine Ecology Progress Series 14, 245–252.

Carrasco, F.D., Gallardo, V.A., 1994. Diversidad, distribución y abundancia del macrobentos sublitoral y observaciones sobre la dinámica temporal de corto término de los sedimentos de la Bahía de Concepción, Chile. Gayana (Oceanología) 2, 49–68.

Clarke, K.R., Ainsworth, M., 1993. A method of linking multivariate community structure to environmental variables. Marine Ecology Progress Series 92, 205–219.

Cline, J.D., 1969. Spectrophotometric determination of hydrogen sulfide in natural waters. Limnology and Oceanography 14, 454–458.

Cosson, N., Sibuet, M., Galeron, J., 1997. Community structure and spatial heterogeneity of the deep-sea macrofauna at three contrasting stations in the tropical northeast Atlantic. Deep-Sea Research I 44, 247–269.

Daneri, G., Dellarossa, V., Quiñones, R., Jacob, B., Montero, P., Ulloa, O., 2000. Primary production and community respiration in the Humboldt Current System off Chile and associated oceanic areas. Marine Ecology Progress Series 197, 41–49.

Díaz, R.J., Rosenberg, R., 1995. Marine benthic hypoxia: a review of its ecological effects and behavioral responses of benthic macrofauna. Oceanography Marine Biology Annual Review 33, 245–303.

Digby, P.G.N., Kempton, R.A., 1987. Multivariate Analysis of Ecological Communities. Chapman & Hall, London, 206pp.

Etter, R.J., Grassle, J.F., 1992. Patterns of species diversity in the deep sea as a function of sediment particle size diversity. Nature 360, 576–578.

Farias, L., Graco, M., Molina, V., Gutiérrez, D., Gallardo, V.A., 2002. Nitrogen cycling in sediments from central Chile sediments (36°S): Seasonal and interannual variability. Extended Abstract Investigaciones Marinas, Chile 30, 167–168.

Ferdelman, T.G., Lee, C., Pantoja, S., Harder, J., Bedout, B.D., Fossing, H., 1997. Sulfate reduction and methanogenesis in *Thioploca*-dominated sediment off the coast of Chile. Geochimica et Cosmochimica Acta 61, 3065–3079.

Field, J., Clarke, K., Warwick, R., 1982. A practical strategy for analyzing multispecies distribution patterns. Marine Ecology Progress Series 8, 37–52.

Figueroa, D., Moffat, C., 2000. On the influence of topography in the induction of coastal upwelling along the Chilean coast. Geophysical Research Letters 27, 3905–3908.

Fossing, H., Gallardo, V.A., Jørgensen, B.B., Hüttel, M., Nielsen, L.P., Schulz, H., Canfield, D., Foster, S., Glud, R.N., Gundersen, J.K., Ramsing, N.B., Teske, A., Thamdrup, B., Ulloa, O., 1995. Concentration and transport of nitrate by the mat-forming sulphur bacterium *Thioploca*. Nature 374, 713–715.

Frankenberg, D., Menzies, R.J., 1968. Some quantitative analysis of deep sea benthos off Peru. Deep-Sea Research 15, 623–626.

Gage, J.D., 1996. Why are there so many species in the deep-sea sediments? Journal of Experimental Marine Biology and Ecology 200, 257–286.

Gage, J.D., Tyler, T.A., 1991. Deep Sea Biology. A Natural History of Organisms of the Deep Sea Floor. Cambridge University Press, Cambridge, 504pp.

Gallardo, V.A., 1963. Notas sobre la diversidad de la fauna bentónica sublitoral del norte de Chile. Gayana (Zoología) 10, 3–15.

Gallardo, V.A., 1985. Efectos del fenómeno de El Niño sobre el bentos sublitoral frente a Concepción, Chile. In: Arntz, W., Landa, A., Tarazona, J. (Eds.), El Niño: su impacto en la fauna marina. Boletín Instituto del Mar del Perú (vol. extr.), pp. 79–85.

Gallardo, V.A., Carrasco, F.D., Roa, R., Cañete, J.I., 1995. Ecological patterns in the benthic macrobiota across the continental shelf off central Chile. Ophelia 40, 167–188.

Gauch, H.G., 1982. Multivariate Analysis in Community Ecology. Cambridge University Press, Cambridge, 298pp.

Graco, M., Farias, L., Molina, V., Gutiérrez, D., Nielsen, L.P., 2001. Massive developments of microbial mats following phytoplankton blooms in a naturally eutrophic bay: implications for nitrogen cycling. Limnology and Oceanography 46, 821–832.

Grassle, J.F., Maciolek, N.J., 1992. Deep-sea species richness: regional and local diversity estimates from quantitative bottom samples. The American Naturalist 139, 313–341.

Gray, J.S., Aschan, M., Carr, M.R., Clarke, K.R., Geen, R.H., Pearson, T.H., Rosenberg, R., Warwick, R.M., 1988. Analysis of community attributes of the benthic macrofauna of Friefjord/Langessundfjord and in a mesocosm experiment. Marine Ecology Progress Series 46, 151–165.

Gutiérrez, D., Gallardo, V.A., Mayor, S., Neira, C., Vásquez, C., Sellanes, J., Rivas, M., Soto, A., Carrasco, F., Baltazar, M., 2000. Effects of dissolved oxygen and fresh organic matter on the bioturbation potential of macrofauna in sublittoral bottoms off central Chile, during the 1997–98 El Niño. Marine Ecology Progress Series 202, 81–99.

Hormazábal, S., Shaffer, G., Letelier, J., Ulloa, O., 2001. Local and remote forcing of sea surface temperature in the coastal upwelling system off Chile. Journal of Geophysical Research 106, 16657–16672.

Hurlbert, S.H., 1971. The non-concept of species diversity: a critique and alternative parameters. Ecology 52, 577–586.

Jumars, P.A., 1976. Deepsea species diversity: does it have a characteristic scale? Journal of Marine Research 34, 217–246.

Knap, A., Michaels, A., Dow, R., Johnson, R., Gundersen, K., Sorensen, J., Close, A., Howse, F., Hammer, M., Bates, N., Doyle, A., Waterhouse, T., 1993. Bermuda Atlantic Time-series Study Methods Manual (Version 3). Bermuda biological station for research, Inc., US JGOFS, 108pp.

Lambshead, P.J.D., Tietjen, J., Ferrero, T., Jensen, P., 2000. Latitudinal diversity gradients in the deep sea with special reference to North Atlantic nematodes. Marine Ecology Progress Series 194, 159 167.

Lamont, P.A., Gage, P.J.D., 2000. Morphological responses of macrobenthic polychaetes to low oxygen on the Oman continental slope, NW Arabian Sea. Deep-Sea Research II 47, 9–24.

Legendre, L., Legendre, P., 1979. Ecologie Numerique, Vol. 2. La Structure des patche Données Ecologiques. Masson, Paris and Presses de l'Université du Quebec, 254pp.

Levin, L.A., 1991. Interactions between metazoans and large, agglutinating protozoans: implications for the community structure of deep-sea benthos. American Zoologist 31, 886–900.

Levin, L.A., 2003. Oxygen minimum zone benthos: adaptation and community response to hypoxia. Oceanography and Marine Biology Annual Review 41, 1–45.

Levin, L.A., Gage, J.D., 1998. Relationships between oxygen, organic matter and the diversity of bathyal macrofauna. Deep-Sea Research II 45, 129–163.

Levin, L.A., Huggett, C.L., Wishner, K.F., 1991. Control of deep-sea benthic community structure by oxygen and organic-matter gradients in the eastern Pacific Ocean. Journal of Marine Research 49, 763–800.

Levin, L.A., Plaia, G.R., Huggett, C.L., 1994. The influence of natural organic enhancement on life histories and community structure of bathyal polychaetes. In: Young, C.M., Eckelbarger, K.J. (Eds.), Reproduction, Larval Biology, and Recruitment of the Deep-Sea Benthos. Columbia University Press, New York, pp. 261–283.

Levin, L.A., Blair, N., DeMaster, D.J., Plaia, G., Fornes, W., Martin, C., Thomas, C., 1997. Rapid subduction of organic matter by maldanid polychaetes on the North Carolina slope. Journal of Marine Research 55, 595–611.

Levin, L.A., Gage, J.D., Martin, C., Lamont, P.A., 2000. Macrobenthic community structure within and beneath the oxygen minimum zone, NW Arabian Sea. Deep-Sea Research II 47, 189–226.

Levin, L.A., Etter, R.J., Rex, M.A., Gooday, A.J., Smith, C.R., Pineda, J., Stuart, C.T., Hessler, R.R., Pawson, D., 2001. Environmental influences on regional deep-sea species diversity. Annual Review Ecology and Systematics 132, 51–93.

Levin, L., Gutiérrez, D., Rathburn, A., Neira, C., Sellanes, J., Muñoz, P., Gallardo, V.A., 2002. Benthic processes on the Peru Margin: a transect across the oxygen minimum zone during the 1997–98. El Niño. Progress in Oceanography 53, 1 27.

McAleece, N., Lambshead, P.J., Paterson, G.L., Gage, J.D., 1997. Biodiversity Professional. Natural History Museum, London and Scottish Association for Marine Sciences (Beta version).

Mullins, H.T., Thompson, J.B., McDougall, K., Vercoutere, T.L., 1985. Oxygen minimum zone edges effects: evidence from the central California coastal upwelling system. Geology 13, 491–494.

Neira, C., Sellanes, J., Soto, A., Gutiérrez, D., Gallardo, V.A., 2001. Meiofauna and sedimentary organic matter off Central Chile: response to changes caused by the 1997–1998 El Niño. Oceanologica Acta 24, 313–328.

Nemec, A.F.L., Brinkhurst, R.O., 1998. Using the bootstrap to assess statistical significance in the cluster analysis of species abundance data. Canadian Journal of Fisheries and Aquatic Sciences 45, 965–970.

Nichols, J.A., Rowe, G.T., 1977. Infaunal macrobenthos off Cap Blanc, Spanish Sahara. Journal of Marine Research 35, 525–536.

Paterson, G.L., Lambshead, P.J., 1995. Bathymetric patterns of polychaetes diversity in Rockall Trough, northeast Atlantic. Deep-Sea Research I 42, 1199–1214.

Pearson, T.H., Rosenberg, R., 1978. Macrobenthic succession in relation to organic enrichment and pollution of the marine environment. Oceanography Marine Biology Annual Review 16, 229–311.

Pielou, E., 1966. The measurement of diversity in different types of biological collections. Journal Theoretical Biology 13, 131–144.

Pizarro, O., Shaffer, G., Dewitte, B., Ramos, M., 2002. Dynamics of seasonal and interannual variability of the Peru–Chile Undercurrent. Geophysical Research Letters 29, 22–1, 22–4.

Rex, M.A., 1976. Biological accommodation in the deep-sea benthos. Annual Review of Ecology and Systematics 12, 331–353.

Rex, M.A., 1981. Community structure in the deep-sea benthos. Annual Review of Ecology and Systematics 12, 331–353.

Rex, M.A., Stuart, C.T., Hessler, R.R., Allen, J.A., Sanders, H.L., Wilson, G.D.F., 1993. Global scale latitudinal patterns of species diversity in the deep-sea benthos. Nature 365, 1419–1424.

Rhoads, D.C., Morse, J.W., 1971. Evolutionary and ecologic significance of oxygen-deficient marine basins. Lethaia 4, 413–428.

Rosenberg, R., Arntz, W.E., Chumán de Flores, E., Flores, L.A., Carbajal, G., Finger, I., Tarazona, J., 1983. Benthos biomass and oxygen deficiency in the upwelling system off Peru. Journal of Marine Research 41, 263–279.

Rowe, G.T., 1971a. Benthic biomass in the Pisco, Perú upwelling. Investigación Pesquera 35, 127–135.

Rowe, G.T., 1971b. Benthic biomass and surface productivity. In: The Fertility of the Sea, vol. 11. Gordon and Breach, New York, pp. 441–454.

Rowe, G.T., 1997. The structure and function of Arctic benthic communities: are high-latitude ecosystems different? Korean Journal Polar Research 8, 85–95.

Rullkötter, J., 2000. Organic matter: the driving forces for early diagenesis. In: Schulz, H.D., Zabel, M. (Eds.), Marine Geochemistry. Springer, Berlin, pp. 129–172.

Schaff, T., Levin, L., Blair DeMaster, D., Pope, R., Boehme, S., 1992. Spatial heterogeneity of benthos on the Carolina continental slope: large (100 Km) scale variation. Marine Ecology Progress Series 88, 143–160.

Sanders, H.L., 1968. Marine benthic diversity: a comparative study. The American Naturalist 102, 243–282.

Sanders, H.L., 1969. Benthic marine diversity and stability-time hypothesis. Brookhaven Symposium on Biology 22, 71–81.

Sanders, H.L., Hessler, R.R., Hampson, G.R., 1965. An introduction to the study of deep-sea benthic faunal assemblages along the Gay Head. Bermuda Transect. Deep-Sea Research 12, 845–867.

Smith, C.R., Levin, L.A., Hoover, D.J., McMurty, G., Gage, J.D., 2000. Variations in bioturbation across the oxygen minimum zone in the northwest Arabian Sea. Deep-Sea Research II 47, 227–257.

Sneath, P.H.A., Sokal, R.R., 1973. Numerical taxonomy. The Principles and Practice of Numerical Classification. W.H. Freeman, San Francisco, 573pp.

Sokal, R.R., Rohlf, F.J., 1981. Biometry, second ed. Freeman, New York, 859pp.

Strub, P.T., Mesias, J.M., Montecino, V., Rutllant, J., Salinas, S., 1998. Coastal ocean circulation of western South American. In: Robinson, A.R., Brink, K.H. (Eds.), The Global Coastal Ocean. Wiley, New York, pp. 273–314.

Thamdrup, B., Canfield, D., 1996. Pathways of carbon oxidation in continental margin sediments off central Chile. Limnology and Oceanography 41, 1629–1650.

Thistle, D., 1979. Deep-sea harpacticoid copepod diversity maintenance: the role of polychaetes. Marine Biology 52, 371–376.

Thompson, J.B., Mullins, H.T., Newton, C.R., Vercoutere, T., 1985. Alternative biofaces model for dysaerobic communities. Lethaia 18, 167–179.

Tyson, R.V., Pearson, T.H. (Eds.), 1991. Modern and ancient continental shelf anoxia. Geological Society Special Publication No. 58, Blackwell, Oxford, 470pp.

Watts, M.C., Etter, R.J., Rex, M.A., 1992. Effects of spatial and temporal scale on the relationship of surface pigment biomass to community structure in the deep-sea benthos. In: Rowe, G.T., Pariente, V., (Eds.), Deep-Sea Food Chains and the Global Carbon Cycle, NATO ASI Series 360, pp. 245–254.

Wishner, K.L., Ashijan, C.J., Gelfman, C., Gowing, M.M., Kann, L., Levin, L.A., Mullineaux, L.S., Saltzman, J., 1995. Pelagic and benthic ecology of the lower interface of the Eastern Tropical Pacific oxygen-minimum zone. Deep-Sea Research II 42, 93–115.

Wishner, K., Levin, L., Gowing, M., Mullineaux, L., 1990. Involvement of the oxygen minimum in benthic zonation on a deep seamount. Nature 346, 57–59.

ELSEVIER

Deep-Sea Research II 51 (2004) 2491–2505

DEEP-SEA RESEARCH
PART II

www.elsevier.com/locate/dsr2

Temporal variability of nitrogen cycling in continental-shelf sediments of the upwelling ecosystem off central Chile

Laura Farías[a,b,c,*], Michelle Graco[a,b], Osvaldo Ulloa[a,b,c]

[a]*Departamento de Oceanografía, Universidad de Concepción, Casilla 160-C, Concepción 3, Chile*
[b]*Programa Regional de Oceanografía Física y Clima (PROFC), Universidad de Concepción, Casilla 160-C, Concepción 3, Chile*
[c]*Centro de Investigación en el Pacífico Sur–Oriental (FONDAP–COPAS), Universidad de Concepción, Casilla 160-C, Concepción 3, Chile*

Accepted 28 July 2004

Abstract

The continental shelf region off central Chile (~36 °S), one of the widest and most productive areas of the eastern South Pacific, is an important site of coastal upwelling. In order to understand how seasonal and inter-annual variability in bottom-water physical and chemical conditions affect benthic nutrient regeneration and sediment characteristics in this area, ammonium (NH_4^+) and nitrate (NO_3^-) fluxes at the water sediment interface were experimentally quantified (March 1998 April 2001), along with net NH_4^+ production, potential nitrification and denitrification rates (November 1998–August 2000). NH_4^+ fluxes to the overlying water up to 10.4 mmol m^{-2} d^{-1}, occurred during the upwelling season (i.e. austral spring and summer), while NH_4^+ removal from the water column up to -5.7 mmol m^{-2} d^{-1} during non-favorable upwelling conditions was observed (i.e., austral winter and the 1997–1998 El Niño condition). The fate of the benthic N regenerated as NH_4^+ appears to be controlled by the amount of labile organic carbon (here indexed as chlorophyll-*a*) in the surface sediment and, indirectly, by the bottom-water oxygen concentration. The balance between net NH_4^+ production and potential nitrification (4.4–34.3 and 0.3–2.9 mmol m^{-2} d^{-1}, respectively) does not support the observed NH_4^+ fluxes, suggesting the occurrence of other NH_4^+ dissamilative (by dissolved metal or anammox) or assimilative consuming processes. Throughout the entire study period, the sediments acted as a large sink for NO_3 (-3.4 ± 1.4 mmol m^{-2} d^{-1}) and as an important denitrification site (0.6–2.9 mmol m^{-2} d^{-1}) coupled with NO_3^- produced by nitrification (58–97%). Other processes such as NO_3^- ammonification or active NO_3^- uptake by *Thioploca* mats could account for NO_3^- uptake from the water column.
© 2004 Elsevier Ltd. All rights reserved.

1. Introduction

Along the Chilean coast, the poleward Peru Chile Undercurrent transports Equatorial Subsurface Water (ESSW), which is rich in nutrients but

*Corresponding author. University of Concepcion, P.O. Box 160-C, Correo 3, Concepcion, Chile. Tel.: +56 41 203738; fax: +56 41 239900.
E-mail address: lfarias@profc.udec.cl (L. Farías).

0967-0645/$ - see front matter © 2004 Elsevier Ltd. All rights reserved.
doi:10.1016/j.dsr2.2004.07.029

poor in oxygen. The presence of the ESSW creates an oxygen minimum zone (OMZ) that extends between 50 and 300 m depth. The OMZ impinges on the shelf sediments and creates a benthic environment with extended periods of suboxic conditions. Off central Chile, the upwelling of ESSW to the euphotic zone from late spring through early autumn produces a strong increase in phytoplankton biomass and primary production rates (e.g., Daneri et al., 2000) followed by high organic particle sedimentation toward the seafloor that also could cause anoxic conditions in the sediments or even in the bottom water. Conversely, a downwelling regime, occurring mainly in winter, produces an efficient vertical mixing of the water column. This regime is also characterized by the presence of Subantarctic Waters (SAAW), which have higher dissolved oxygen (O_2) and lower nutrient concentrations (Strub et al., 1998), and therefore less capacity to fertilize the euphotic zone. Besides this seasonal fluctuation, dissolved O_2, nutrients, and productivity levels also can vary in this area on inter-annual time scales (e.g., the El Niño–Southern Oscillation [ENSO] cycle, with a 2–7 year periodicity), as reported by Morales et al. (1999) and Ulloa et al. (2001) for the north of Chile.

The O_2 concentration in the overlying water and the organic carbon deposition, which is associated with O_2 demand, determines the chemical status of the sediments (Klump and Martens, 1983). When the O_2 supply falls or its demand increases, marked changes occur in the dominant metabolic pathways of the benthic microbial processes in the sediments. These changes affect the delicate balance between nitrogen (N) processes (basically organic N mineralization, nitrification, and nitrate reduction like denitrification) determining the form of the N species being exported from the sediments to the water column (Risgaard-Petersen et al., 1994; Rysgaard et al., 1994). Sedimentary N balances have received substantial attention because the release of nitrogenous compounds to the water column can contribute to the nutrient requirements of pelagic primary producers (Rowe et al., 1975; Klump and Martens, 1983). Morover, benthic denitrification, mainly that occuring in continental shelves, could represent about 75% of the global ocean N sink (Codispoti et al., 2001).

Most of the extensive research associated with benthic N cycling comes from coastal ecosystems, such as estuaries and bays (Kemp et al., 1990; Lohse et al., 1993; Cowan et al., 1996). In continental shelf sediments, the dominant N regeneration processes and exchange rates with the water column have been less studied (Hopkinson et al., 2001), particularly in wind-driven coastal upwelling areas, such as in the North East Pacific shelf (Devol and Christensen, 1993). Nutrient regeneration in upwelling regions takes place primarily through bacterial regeneration at the sediment–water interface and in the water column, as well as by the excretion activities of pelagic organisms. In general, it is accepted that sediments beneath upwelling zones receive a high organic matter sedimentation (Hebbeln et al., 2000) and accumulate large reservoirs of C and N (Summerhayes, 1983) and thus influence global C and nutrient cycles (Walsh, 1991). For the continental shelf sediments off central Chile, high rates of organic matter remineralization by anaerobic pathways have been observed (Thamdrup and Canfield, 1996; Ferdelman et al., 1997; Glud et al., 1999; Gutiérrez et al., 2000; Molina et al., 2004). However, these studies considered only spatial variability in the processes and rates, so there is still a need for understanding their changes with time.

Another characteristic of coastal upwelling ecosystems is the presence of large nitrate-storing, sulfide-oxidizing bacteria (Jørgensen and Gallardo, 1999), such as *Thioploca* off central Chile, a massive mat-forming bacteria. The nitrate-storing, sulfide-oxidizing bacteria are found along the continental shelf off Chile and Peru (Rosenberg et al., 1983; Schulz et al., 1996), off Namibia (Schulz et al., 1999), and in the Arabian sea (Schmaljohann et al., 2001). They are thought to play a major role in coupling the biogeochemical N and sulfur (S) cycles in upwelling areas (Farías, 1998; Otte et al., 1999). However, little is known about temporal variations of these bacteria, and their apparently widespread capacity to respond to changes in productivity and dissolved O_2.

This study reports on N fluxes and processes involved in N transformation in the continental shelf sediments off central Chile. The observed changes in flux directions and rates are interpreted in terms of possible pathways of N regeneration, dependent on the O_2 and nutrient conditions in the bottom water, and on the organic matter availability in the sediments. We discuss these results in relation to the temporal variability of the oceanographic conditions in the area, mainly in relation to the seasonality of upwelling and the occurrence of the 1997–1998 El Niño (EN) event, and the biogeochemical consequences of this variability.

2. Methods

2.1. Field site and sample collection

The sampling station (Station 18; 36°31′S–73°08′W) was located ≈28 km northwest of the mouth of Concepción Bay, in a water depth of 85 m (Fig. 1). Sediment samples were obtained during March, June, and November 1998; January, March, and August 1999; March and September 2000; and April 2001 onboard the R.V. *Kay Kay*. A SMBA mini–Multicorer was used to collect sediment cores of 50–60 cm in length. Triplicate undisturbed cores (inner diameter of 7.2 cm) were subsampled from the multicorer tube for experimental measurements back in the laboratory. At the same time, samples of the water overlying the sediments were taken and placed in plastic bottles for later analysis. A vertical hydrocast was made using Niskin bottles, and water samples were drawn from each bottle for determination of temperature (T), salinity, dissolved O_2, and nutrient concentrations. To complement these observations, concurrent measurements were made of ^{14}C primary production (PP) in the water column at five depths within the euphotic zone, as well as chlorophyll-*a* (chl-*a*) in the surface sediment (top 1 cm). Two cores (3.6 cm in diameter, 20 cm in length) were subsampled for the determination of vertical profiles of nitrite (NO_2^-), nitrate (NO_3^-), and ammonium (NH_4^+) in the pore waters. The cores were sliced into 1–2 cm segments under N_2, and the pore-water was obtained by pressure filtration. One core was used for determining sediment porosity and C and N composition, and the other for determining redox potential and pH.

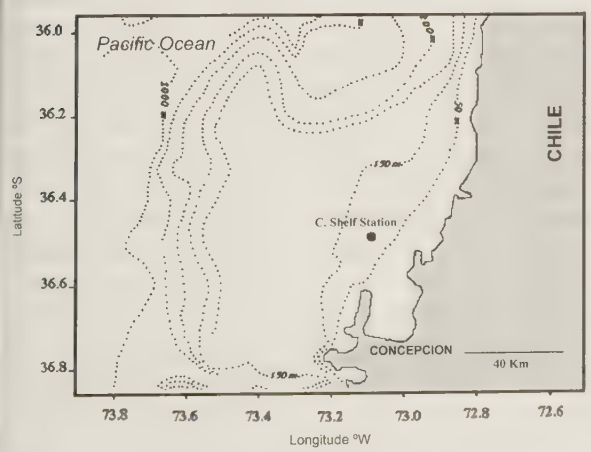

Fig. 1. Location of sampling station on the continental shelf off Concepción, Chile (Station 18).

2.2. Benthic flux and N processes

The cores were transported to the laboratory within 3 h of sampling, wrapped in aluminum foil to exclude light, and placed in a thermo-regulated water bath at the in situ bottom T. The core samples were left to re-equilibrate for 6–12 h, with the bottom water taken from above the sediments; the O_2 level was kept at the in situ concentration by bubbling with a mixture of O_2 and Argon (Ar). The overlying water was continuously monitored for pH, T, and dissolved O_2 concentration. Net rates of sediment–water exchange of dissolved N nutrients (NH_4^+, NO_3^-, and NO_2^-) were measured by triplicate in short incubations (3–6 h). A magnetic stirrer gently mixed the water in order to maintain the in situ dissolved O_2 and nutrient distributions adjacent to the sediment surface.

Net NH_4^+ production rates were obtained by measuring dissolved NH_4^+ accumulation in the pore water through time using slurry incubations corrected for the NH_4^+ adsorbed into sediment particles with a coefficient of $K = 1.3$ (Mackin and Aller, 1984). Homogenized sediment slurries (without macrofauna) from different depths (0–1, 3–4, 5–6, and 9–10 cm) were placed in plastic tubes

(45 ml) under a N_2 atmosphere and diluted 1:1 with filtered and sterilized bottom seawater. The tubes were incubated for 10 days in a dark, temperature-controlled, N_2 atmosphere simulating in situ conditions. Samples for NH_4^+ analysis were taken at 0, 6, 12, 18, and 24 h (day 1), after which one sample was taken per day until day 10. Potential nitrification (PN) in the upper 2 cm depth was measured by incubating 2–3 g of homogenized fresh sediment with filtered, sterilized seawater enriched with NH_4^+ (1 mM final concentration). A concentration of 10 mM $NaClO_3$ was used to block the oxidation of NO_2^- to NO_3^- and the time course of NO_2^- accumulation in the slurry was measured to obtain the nitrification rate (Henriksen and Kemp, 1988). Incubations took place at room temperature (~18–20 °C) in plastic tubes placed on a gently rotating shaker with optimum aeration. The experiments lasted for about 12 h.

Total denitrification rates (D_t), which included denitification from NO_3^- produced by nitrification (D_n) and from NO_3^- diffusing from bottom water (D_w), were determined using the Isotope Pairing technique (IPT), following Nielsen (1992). Four sediment cores in Plexiglas tubes (3.6 cm diameter, 10 cm water height, and 5 cm sediment height) were selected for this purpose. In each core, $^{15}NO_3^-$ was added (10 mM stock solution, 99.6% $^{15}NO_3^-$) to the overlying water to obtain a final concentration of 30–50 μM. The cores were closed with rubber stoppers, mixed with a magnetic stirrer, and incubated in the dark for 3–4 h at the in situ temperature. After incubation, the microbial activity was stopped at 1.5–2 h intervals by the addition of 3 ml $ZnCl_2$ solution (50% w/w) and the whole core was mixed with a rod. Duplicate slurry samples were then gently transferred with a syringe to 6-ml glass vials (Exatainer, Labco) containing 250 μl of $ZnCl_2$ solution. The samples were analyzed by mass spectrometry at the National Environmental Research Center (NERI) in Silkeborg, Denmark.

2.3. Chemical analysis

NO_2^-, NO_3^-, and NH_4^+ concentrations were initially measured using a TRAACS 800 Auto-analyser (March 1998). Later, NO_2^- and NO_3^- were determined spectrophotometrically using standard colorimetric methods (Parsons et al., 1984), and NH_4^+ was determined using the technique of Solorzano (1969), modified for 1-ml samples. Dissolved O_2 measurements were made using a semi-automatic version of the Winkler method (Williams and Jenkinson, 1982) based on a photometric end-point detector, a Dosimat 665 (Metrohom), and a chart recorder. The coefficient of variation of the measurements of dissolved O_2 was $<0.1\%$. Sediment porosity was determined by water loss after drying to a constant temperature (110 °C). Redox potential and pH in the sediments were measured with platinum and glass electrodes, respectively, inserted into intact sediment cores at 1-cm intervals along the core liner. Pelagic PP was derived from the in situ ^{14}C incubations (Parsons et al., 1984) and chl-*a* fluorometric measurements were made by a modified acidification procedure (Gutiérrez et al., 2000) and calibrated using a standard solution (Sigma) of chl-*a*.

2.4. Data and statistical analysis

Data on the increase or decrease of N-pools (NO_2^-, NO_3^-, and NH_4^+) in the water overlying the experimental sediment cores were plotted against time and fitted to a linear model $[A(t) = A_0 + mt]$ using the least-squares method; where t is the incubation time, A_0 is the nutrient concentration at $t = 0$ and m is the slope. The fluxes were calculated from the slope, considering the specific volume/area ratio of the corer. Flux uncertainties were calculated from the errors in the linear regressions, as the square root of the sum of the variance of each flux rate. NH_4^+ production rates were estimated by using a linear fit and the standard errors by Monte Carlo confidence intervals. The rates were expressed as depth-integrated rates (10 cm depth for the cases of NH_4^+ production and 3 cm for the case of PN) in units of $mmol\,m^{-2}\,d^{-1}$. Denitrification rate (D_t) was obtained based in the production of the labeled N_2 species: $D_{15} = {}^{14}N^{15}N + 2({}^{15}N^{15}N)$ from the $^{15}NO_3^-$ added to the overlying water. The methods also allows to evaluate a denitrification rate produced from denitrification coupled to nitrification (D_n),

based on unlabelled NO_3^-, relies on the assumption of binomial distribution, and is derived from: $D_{14} = [D_{15}\ (^{14}N^{15}N/2)(^{15}N^{15}N)]$. The rate of D_{14} is supported by NO_3^- diffusing into the sediment from the overlying water: $Dw = (100\text{-}e15)/(e15)D_{15}$ (where e15 is the percentage of $^{15}NO_3^-$ enrichment of the total NO_3^- pool in the overlying water), and by NO_3^- that is produced by nitrification: $D_{15} = D_{14} - D_w$ (Nielsen, 1992). Spearman correlation (rs) between environmental variables (T, dissolved O_2, and PP in the water column; chl-*a* and N-pool sizes in the pore water), fluxes, and net NH_4^+ production, PN and Dn also were performed.

3. Results

3.1. Primary production and bottom-water column characteristics

Temperature, salinity, nutrients, and dissolved O_2 concentrations in the bottom water together with pelagic PP at Station 18 are presented in Table 1. The temperature and salinity ranged between 10.0 and 11.8 °C and 34.38 and 34.55, respectively, values that are characteristic for the ESSW ($10 < T < 12; 34.4 < S < 34.9$) (Strub et al., 1998). Near-bottom dissolved O_2 concentrations were maximum in wintertime (16.5–50 μM) and minimum in summertime (2–9.4 μM, excluding March 1998). The lower value represents the limit of the analytical method, so that dissolved O_2 in summertime could have been much lower, even zero. During spring–summer, NO_2^- and NO_3^- concentrations in the bottom water were variable (Table 1). NO_3^- values ranged between 1.2 and 25.0 μM. There was significant NO_3^- consumption in the bottom water during the summer period (i.e., March 1998 and January 1999), indicated by significantly lower concentrations of NO_3^- in the bottom waters than those expected in the presence of ESSW (e.g., NO_3^-, 15–25 μM) (Ahumada et al., 1983). Primary production rates varied between 188 and ~4000 mg $C\,m^{-2}\,d^{-1}$, those measured during the summer of 1998 (March) and winter periods (e.g., June 1998 and August 1999) being an order of magnitude lower than those measured during the summer of 1999 (March).

3.2. Sediment characteristics

Surface chl-*a*, the depth of the discontinuity redox layer (DRL), and the N-pool sizes (NH_4^+, NO_3^-, and NO_2^-) in the sediments are presented in

Table 1
Hydrographic characteristics of the bottom water and PP rates during the sampling period on the continental shelf off Concepción (Station 18)

Sampling period	Bottom water						PP ($mg\,C\,m^{-2}\,d^{-1}$)
	Temperature (°C)	Salinity	Oxygen (μM)	Nutrients			
				NH_4^+	NO_3^- (μM)	NO_2^-	
Mar 1998	11.70	34.523	20.00	n.m.	1.17	1.16	188
Jun 1998	11.70	34.411	50.00	n.m.	18.70	0.35	166
Nov 1998	10.00	34.427	2.12	0.88 (2.1)	25.05	0.44	1,200
Jan 1999	11.80	34.555	2.50	2.51 (6.0)	1.76	4.22	3,986
Mar 1999	11.20	34.389	9.37	0.00 (20.0)	14.50	0.00	620
Aug 1999	10.00	34.510	37.39	0.29 (16.2)	17.90	0.27	398
Mar 2000	10.80	34.380	3.59	0.10 (12.0)	10.0	0.45	249
Sep 2000	11.40	n.m.	16.50	0.2 (20.0)	24.70	0.49	n.m.
Apr 2001[a]	11.40	34.530	6.24	1.40	25.0	0.27	n.m.

n.m. = not measured; numbers in parentheses correspond to initial values of NH_4^+ (measured in the overlying water of cores) in the experiments.

[a]Taken from Molina (2002).

Table 2. The sediments from Station 18 consisted of brown to black mud with high porosity (0.88–0.93, ~80% clay minerals with a mean grain size of 7.05 phi). The DRL revealed oxidizing characteristics between 3 and 11 cm depth (Table 2). The pH varied from 7.4 to 7.9 (not shown). Surface sediment chl-*a* concentrations showed a large fluctuation during the sampling period, from 16 to 110 $\mu g\, g^{-1}$ dry weight (Table 2). The marked difference between the surface chl-*a* from March to June 1998 and winter 1999 ($<25\ \mu g\, g^{-1}$) and the spring–summer (November 1998–March 2000) period (89–110 $\mu g\, g^{-1}$) indicated a higher flux of organic matter to the sediment during the latter period. A positive significant Spearman correlation ($rs = 0.86$, $p = 0.01$) between PP and surface sediment chl-*a* concentrations was observed. Both variables, however, showed a significant negative correlation with dissolved O_2 ($rs = 0.79$ and -0.90, respectively; $p < 0.05$).

The vertical NH_4^+ and NO_3^- profiles in the pore water are shown in Fig. 2. Dissolved NH_4^+ was always the prevailing N-component in the interstitial water, ranging from 37 to 121 μM at the surface (0–1 cm depth) and from 66 to 376 μM at 15 cm depth. The estimated NH_4^+ pool size (0–15 cm depth) ranged from 8 to 44 $mmol\, m^2$, being larger during summer 1999 and 2000 than during summer 1998 (Table 2). The NO_3^- profiles of summer 1999 and 2000 showed maximum subsurface concentrations (2–4 cm depth) up to 270 μM, one order of magnitude higher than the NO_3^- concentrations in the bottom waters. These concentrations were probably artifacts produced by the core-squeezing technique due to the presence of NO_3^--rich filamentous bacteria, such as *Thioploca* spp. Hence, the pore water NO_3^- data should be viewed with caution when *Thioploca* spp. trichomes are present in the sediment. However, during the entire study period, *Thioploca* biomass values were low, fluctuating between 0.5 and 20 $g\, m^{-2}$ (V.A. Gallardo, pers. comm.). The NO_3^- pools varied from 1.2 to 12.4 $mmol\, m^{-2}$, being between 3 and 9 times lower than those of NH_4^+ pools (Table 2).

3.3. Nitrogen fluxes across the sediment–water interface and N processes within the sediments

Nutrient fluxes (mean rates ± standard deviations) are shown in Table 3. Mean NH_4^+ flux across the sediment–water interface showed a temporal variability between the winter and summer periods. NH_4^+ influxes (negative flux) were observed in summer 1998 ($-14.7\ mmol\, m^{-2}\, d^{-1}$) and winter ($-5.7\ mmol\, m^{-2}\, d^{-1}$), while NH_4^+ effluxes (positive fluxes) up to 10.4 $mmol\, m^{-2}\, d^{-1}$ were characteristic of summer 1999 and 2000. NO_3^- fluxes were directed into the sediment throughout the sampling period. The sediment NO_3^- uptake did not vary significantly during the annual cycle ($p > 0.01$), having an average rate

Table 2
Geochemical and biological features of the sediments during the sampling period on the continental shelf off Concepción (Station 18)

Sampling period	Eh 0–1 cm (mV)	DRL[a,b] (cm)	Sediment Chl-*a*[b] ($\mu g\, g^{-1}$)	N-pool sizes 0–15 cm depth ($mmol\, m^{-2}$)		
				NH_4^+	NO_3	NO_2^-
Mar 1998	195	9[b]	22.0 ± 0.3[b]	8.33	1.20	0.18
Jun 1998	86	6[b]	16.3 ± 2.9[b]	9.48	1.64	0.11
Nov 1998	101	5[b]	110.0 ± 56.0[b]	20.30	3.20	1.11
Jan 1999	66	3[b]	96.9 ± 39.0[b]	29.80	10.20	0.69
Mar 1999	115	8[b]	47.7 ± 19.0[b]	28.10	3.70	0.32
Aug 1999	158	10	24.8 ± 3.0	20.90	2.80	0.40
Mar 2000	114	11	88.7 ± 6.0	44.00	4.90	0.70
Sep 2000	173	6	20.9	29.00	4.90	0.40
Apr 2001[b]	n.m.	n.m.	n.m.	62.00	12.40	0.40

[a]Discontinuity redox layer.
[b]Data from Gutiérrez et al. (2000); other abbreviations as in Table 1.

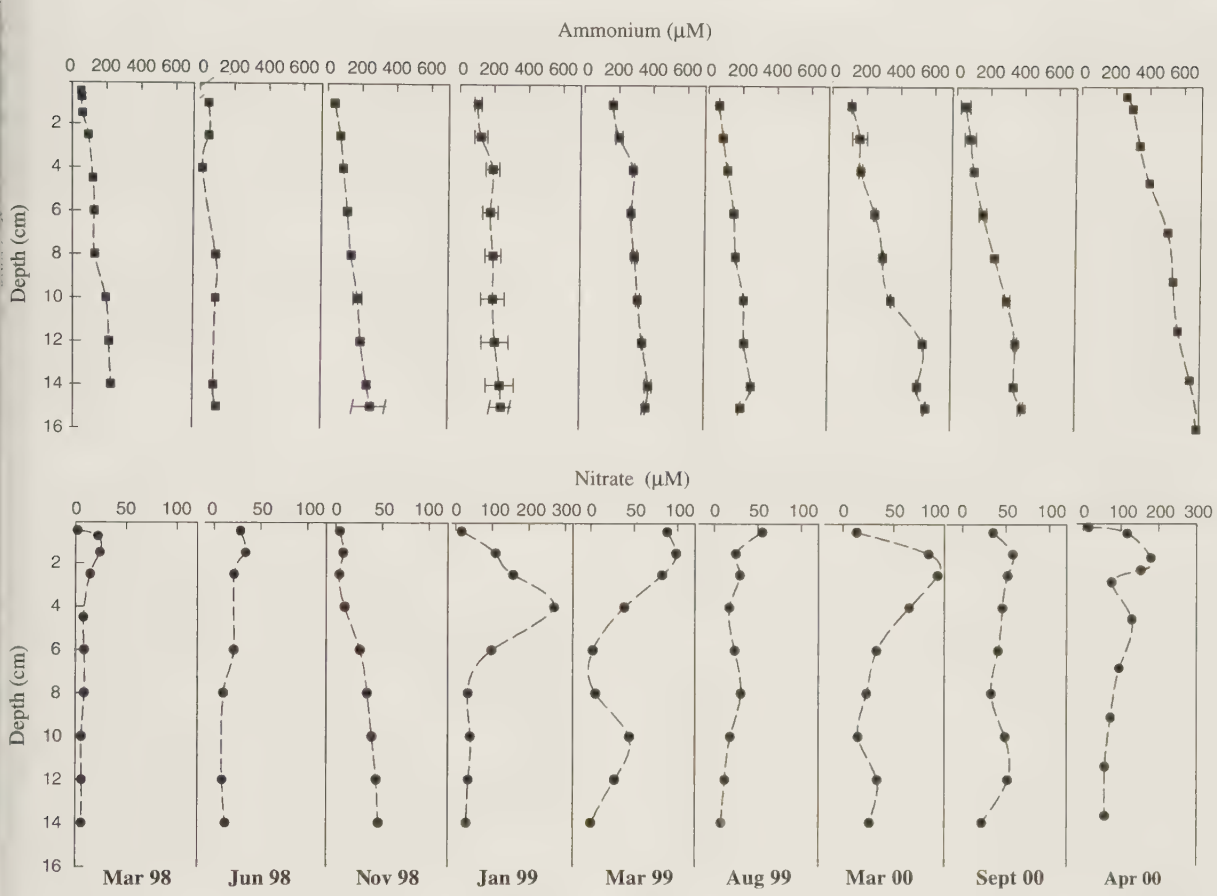

Fig. 2. Vertical distributions of NH_4^+ and NO_3^- in the sediment pore water during the study period. Bars represent ±1 SD.

Table 3
Average NH_4^+ and NO_3^- fluxes and net N exchange on the continental shelf off Concepción (Station 18)

Sampling period	NH_4^+ flux ($mmol\,m^{-2}\,d^{-1}$)		NO_3 flux ($mmol\,m^{-2}\,d^{-1}$)		Net N exchange ($mmol\,m^{-2}\,d^{-1}$)
	Mean	SD	Mean	SD	
Mar 1998	−14.7	3.7	−2.8	0.3	−17.5±3.7
Jun 1998	−4.7	2.8	−4.9	1.7	−8.9±3.2
Nov 1998	2.9	1.1	−3.9	1.0	−1.2±1.6
Jan 1999	10.4	2.7	−4.0	1.5	4.4±3.1
Mar 1999	10.4	1.8	−3.3	1.4	7.1±2.3
Aug 1999	−5.7	1.8	−4.9	1.2	−10.6±2.2
Mar 2000	6.6	1.1	−4.2	1.3	2.4±1.7
Sep 2000	−0.4	0.7	−2.2	0.8	−2.6±1.1
Apr 2001*	2.1	0.1	−0.6	0.1	1.5±0.2

Abbreviations as in Table 1

of $3.4\pm1.4\,mmol\,m^{-2}\,d^{-1}$. The NH_4^+ and NO_3^- fluxes were not significantly correlated with T, dissolved O_2, or nutrient concentrations in the bottom water. Changes in chl-*a* concentration, an index of labile organic matter availability in the sediments ($rs = 0.62$, $p = 0.05$), and pelagic PP rates

Table 4
Rates of different N processes measured on the continental shelf off Concepción (Station 18)

Sampling period	Net NH_4^+ production[a] ($mmol\,m^{-2}\,d^{-1}$)	Potential nitrification ($mmol\,m^{-2}\,d^{-1}$)	D_n coupled to nitrification ($mmol\,m^{-2}\,d^{-1}$)	Total denitrification ($mmol\,m^{-2}\,d^{-1}$)
Mar 1998	n.m.	n.m.	n.m.	n.m.
Jun 1998	n.m.	0.19±0.12	n.m.	n.m.
Nov 1998	4.4 (4.1–4.8)	0.26±0.04	1.68±0.34	2.90±0.5 (58%)
Jan 1999	15.4 (14.9–15.9)	1.94±0.57	2.78±0.42	2.87±1.11 (97%)
Mar 1999	28.5 (24.6–31.9)	1.03±0.14	0.91±0.39	1.27±0.45 (72%)
Aug 1999	5.7 (4.6–6.7)	1.52±0.12	0.42±0.07	0.58±0.14 (72%)
Mar 2000	34.3 (31.9–36.1)	2.31±0.11	0.41±0.08	0.64±0.12 (64%)
Sep 2000	5.9 (5.3–6.4)	2.95±0.80	n.m.	n.m.

Values in brackets represent the 95% confidence interval.
Values in parentheses represent percent of nitrate produced by nitrification and used during D_n.
[a]Net ammonification values represent the ammonium accumulated in the pore water corrected by adsorption obtained from Graco et al. (2004).

(rs = 0.88, $p = 0.00$) were found to be the best predictors for the NH_4^+ fluxes.

Net NH_4^+ production, PN, D_t and D_n rates are presented in Table 4. Net NH_4^+ production, integrated from 0 to 10 cm depth, fluctuated between 4.4 and 34.3 mmol $N\,m^{-2}\,d^{-1}$. During favorable upwelling conditions (i.e. austral spring–summer), the estimates were at least 7 times higher than during unfavorable upwelling conditions (i.e. winter ca. 5 $mmol\,m^{-2}\,d^{-1}$). With the exception of 1998, net NH_4^+ production rates followed the same seasonal signal of surface sediment chl-*a* concentrations. These rates were strongly correlated with NH_4^+ pools (rs = 0.94, $p = 0.00$), and with NH_4^+ fluxes (rs = 0.65, $p = 0.05$) during the study period. The relationships between pelagic PP, surface chl-*a* in sediment, and the NH_4^+ production and exchange are presented in Fig. 3.

The PN rate, an estimator of nitrifying bacteria activity when dissolved O_2 and NH_4^+ are not limiting factors, varied from 0.2 to 2.9 mmol $N\,m^{-2}\,d^{-1}$ in the upper 0–2 cm. The data did not show any temporal patterns. D_n coupled with nitrification rates, which may be taken as an indicator of the minimum rates of nitrification expected in the sediment, were lower than potential nitrification rates with the exception of January 1999. The D_t rates varied between 0.6 and 2.9 $N\,mmol\,m^{-2}\,d^{-1}$, the highest values being

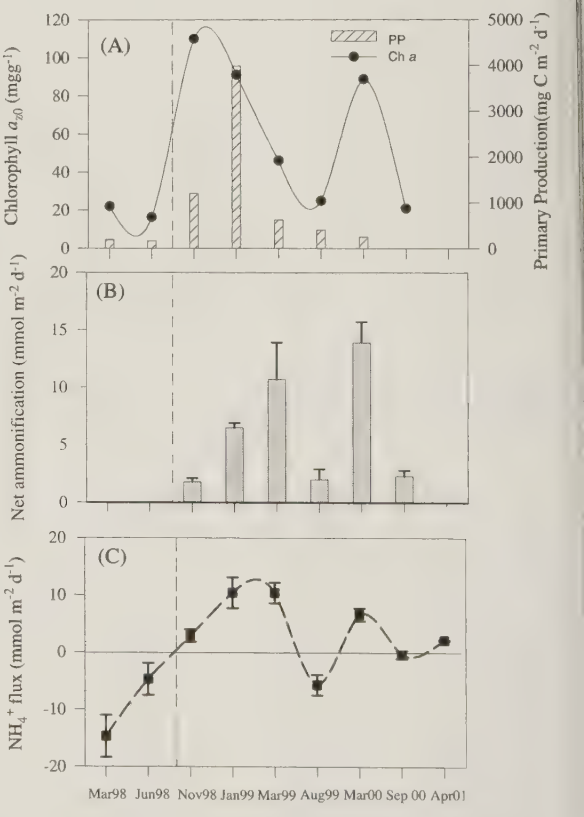

Fig. 3. Temporal variation of (A) chlorophyll-*a* in the sediment surface and primary production in the water column (PP); (B) rates of net NH_4^+ production; and (C) NH_4^+ exchange across water–sediment interface during the study period. The vertical dashed line indicates the end of the 1997–1998 El Niño event.

found during upwelling periods and the lowest (~2–5 times lower) in non-upwelling periods. NO_3^- produced by nitrification within sediments represented 58–97% of the NO_3^- source used by denitrifying bacteria in the different periods (Table 3). The D_t rates showed a negative correlation with dissolved O_2 ($rs = -0.89$; $p = 0.01$) and a positive correlation with chl-*a* ($rs = 0.94$, $p = 0.00$), indicating its dependency as an anaerobic heterotrophic process by C source and low O_2 concentration.

4. Discussion

4.1. Variability in the environmental variables

Several factors influence N cycling (T, dissolved O_2, organic matter input, bottom-water nutrients, and benthic community structure). T and dissolved O_2 have been shown to be the best predictors for many ecosystems (Cowan et al., 1996). In addition, in the upwelling area associated with the OMZ discussed here, it is also necessary to consider the large NO_3^- content of the bottom water and the high organic matter sedimentation. The temporal variability of the N fluxes in this area (in particular NH_4^+) could not be explained by changes in T ($\Delta T < 3\,^{\circ}C$ during the sampling period) nor by the macrofauna-standing stock, which did not show significant changes during the study period (V.A. Gallardo, unpublished data). Our data suggest that both the amount of labile organic matter reaching the sediment surface and dissolved O_2 in the bottom water could be the most important factor controlling the benthic N exchange, as has been shown before in other benthic systems (e.g., Caffrey et al., 1993). Both variables in the study area depend on the temporal variability of oceanographic conditions in the water column, mainly ascribed as favorable (spring–summer) and not favorable (fall–winter) coastal upwelling. In fact, a close coupling between PP, labile organic matter in the sediment (as chl-*a*), and dissolved O_2 in the bottom water was observed during the upwelling periods of 1999 and 2000 as a product of the intensification of wind stress favorable to the upwelling (data not shown). In the same sense, the significant negative correlation found between the pelagic PP and surface sediment chl-*a* versus the dissolved O_2 concentration indicates that the latter is modulated or masked by the aerobic oxidation of organic loading in both bottom water and sediments, and by the reoxidation of metabolic products such as HS^-. Although the sediments are bathed all year with hypoxic or even suboxic waters, they showed oxidizing characteristic, evidenced through a deep DRL (see Table 2). They also had low pore water HS^- concentrations ($<2\,\mu M$) but held high SO_4^{2-} reduction rates (data not shown). These results suggest that metals could be acting as important oxidizing agents as it was found in the area by Thamdrup and Canfield (1996) and Ferdelman et al. (1997).

During the summer 1998, PP rates and the organic matter loading to the sediments (chl-*a*) were significantly lower than during upwelling periods (Table 1), even if they are compared with previous reports for the area (Fossing et al., 1995; Daneri et al., 2000; Gutiérrez et al., 2000); and the bottom waters were more oxygenated ($20\,\mu M$) than expected for the typical presence of ESSW during upwelling process ($<10\,\mu M$, Table 1). These data, together with those observed by Gutiérrez et al. (2000) in and off the Bay of Concepción, suggest that the change was probably associated with the presence of the 1997–1998 EN in the central Chile (~36 °S). During EN events, the thermocline and oxycline deepen, so that any upwelling tends to be of warm, nutrient-poor, oxygen-rich waters from above the depressed thermocline, with a potential reduction in the PP (Huyer et al., 1987). We expect these characteristics to determine a lower nutrient regeneration in the sediments and also a lower exchange of this nutrient with the water column, as was observed during this periods (Tables 3 and 4). In accord with a lower nutrient remineralization, the sulfate reduction rates measured during EN 1997–1998 were an order of magnitude lower than those of the post EN summer periods (Gutiérrez et al., 2000). Conversely, in the summers 1999 and 2000, the sediment surface chl-*a* content increased significantly, suggesting a high remineralization in the sediments and nutrient production (mainly

NH_4^+), with the concomitant effluxes toward the water column, as were observed in this study (Fig. 3).

4.2. Ammonium cycling

The continental shelf off central Chile present a clear temporal pattern in the NH_4^+ fluxes. During the upwelling periods, with the exception of March 1998, a high sediment NH_4^+ flux into the water columns was observed, whereas a net sediment NH_4^+ uptake dominated during the non-upwelling season (Fig. 3). This temporal pattern also has been found in sediments of the Concepción Bay by Farías et al. (1996) and Graco et al. (2001), and it is expected considering the temporal changes in the organic matter input that increase during upwelling periods and also the oxygen deficiency in the bottom waters favorable to export of N reduced species to the water column. In contrast, a NH_4^+ influx was observed during March 1998 and non-upwelling conditions (Fig. 3). The NH_4^+ uptake by the sediment has been previously observed in the study area (Farías et al., 1996; Graco et al., 2001; Molina, 2002), as well as in hyper-nutrified water bodies, such as estuaries and coastal lagoons (e.g. Callender and Hammond, 1982; Simon, 1989; Blackburn et al., 1996; Ogilvie et al., 1997).

The NH_4^+ cycling in the sediment has been explained by a balance between NH_4^+ production and NH_4^+ oxidation by nitrification (Blackburn and Henriksen, 1983; Klump and Martens, 1983; Blackburn, 1986). In our case, the NH_4^+ cycling responds to such balance only during upwelling periods, with the exception of March 1998. In fact, during March 1998 and non-upwelling periods, particularly in August 1999, D_n and even the PN rates cannot explain the observed strong NH_4^+ uptake. This imbalance could be the result of an overestimation in the NH_4^+ production rates, associated with slurry experiments versus the whole core experiments (Hansen et al., 2000) or other NH_4^+ consuming processes.

In relation with an overestimation in the NH_4^+ production by the experimental setup, the net NH_4^+ production was significant lower than the total NH_4^+ production found in the same study area (Graco, 2002). The imbalance between total and net NH_4^+ production appears as indirect evidence that NH_4^+ consumption by the sediments is higher than would be expected from NH_4^+ oxidation by nitrification (Graco, 2002). In fact, other processes may have become important, such as NH_4^+ bacterial uptake/assimilation in periods where the sediments have a low organic content (Fenchel et al., 1998), conditions observed in early 1998 and non-upwelling periods (August 1999 and September 2000), with 2 and 8 times lower organic matter content in the sediments (see chl-*a*, Table 2), C:N were between 8 and 10, the phaeopigment/chl-*a* ratio was higher than 11 (Gutiérrez et al., 2000), and NH_4^+ pools were low. All of this may indicate that the substrate was relatively low in N, and probably a large fraction of the remineralized NH_4^+ was assimilated explaining the negative direction of nutrient fluxes (Sumi and Koike, 1990; Blackburn and Blackburn, 1993; Pedersen et al., 1999).

The anaerobic oxidation of NH_4^+ by NO_2^- (or NO_3^-) respiration produces N_2 in a process called "the anammox reaction" (Strous et al., 1999), which could also explain part of the measured NH_4^+ and NO_3^- uptake in the continental shelf sediments studied (see below). The anammox reaction would be favored in anoxic conditions where NH_4^+ and NO_3^- concentrations are high (Mulder et al., 1995). This process, recently measured in marine sediment by Thamdrup and Dalsgaard (2002), could account for 24–67% of the total N_2 production in two typical shelf sediments. The relative importance of the anaerobic NH_4^+ oxidation and denitrification appears to be regulated by the availability of the reduced substrates, and can explain NH_4^+ deficiencies in anoxic water and sediment contributing significantly to ocean N budget (Thamdrup and Dalsgaard, 2002; Devol, 2003). Another possible mechanism for removing NH_4^+ from sediment is the oxidation (anaerobic nitrification) with metals, a process thermodynamically favorable with Mn and Fe at a low pH (Luther et al., 1997). This possibility in the study area is discussed in more detailed by Molina et al. (2004). Although the anaerobic processes just mentioned could explain the observed NH_4^+ influxes, they were not quantified in this study.

4.3. Nitrate cycling

In contrast to the NH_4^+ fluxes, NO_3^- fluxes were always directed to the sediments and did not show any significant relationship with environmental variables. NO_3^- cycling in sediments could be explained by a balance between nitrification and denitrification. In our case, however, NO_3^- exchange across water–sediment interface could not be accounted by these processes. The difference between the PN and D_t suggests a NO_3^- exchange across the sediment–water interface fluctuating from -1.4 to $2.6\,mmol\,m^{-2}\,d^{-1}$, that significantly differs from our measured fluxes, which were always directed towards the sediment (Table 3).

In addition, our results indicate that 58–97% of the overall estimated denitrification was supported directly by the NO_3^- supplied from nitrification within the sediments (Table 4). This is in accordance with several investigations that show denitrification to be directly coupled with benthic nitrification (Jenkins and Kemp, 1984; Kemp et al., 1990; Lohse et al., 1993; Rysgaard et al., 1994). Consequently, denitrification can only account for up to 25% of the observed NO_3^- influx (i.e., $-3.4\pm1.8\,mmol\,m^{-2}\,d^{1}$). The NO_3^- imbalance, as well as those from the NH_4^+ cycling, could indicate that processes were not well measured or the occurrence of other processes, not quantified here, and involved in NO_3^- transformation.

In the first case, the measured D_t rates could have been not well estimated. The IPT assumption that NO_3^- is the only electron acceptor used by denitrifying bacteria (Nielsen, 1992), a situation that is not really true, could result in an underestimation of total denitrification. In fact, intermediate compounds as NO_2^- and N_2O can be used directly as electron acceptor during denitrification, which suggests the important consumption of N_2O by the sediment ($15\,mmol\,m^{-2}\,d^{-1}$) observed in the study area (Zopfi et al., 2001). Recently, measurements of N_2O recycling in sediments, using sediment slurry (Cornejo and Farías, unpublished data), confirms that N_2O can be used as an electron acceptor during denitrification, but at a rate significant lower than the NO_3^- uptake (ca. $0.3\,mmol\,m^{-2}\,d^{-1}$), and indicates a high potential for sedimentary N_2 formation not yet quantified. On the other hand, the possible co-existence of anammox along with denitrification produces an overestimation of N_2 production calculated by the IPT. The percentage of overestimation depends on how much does anammox account for N_2 production, which according to Risgaard-Petersen et al. (2003) could vary between 0% and 82%. Although much attention has been given to anammox measurement in marine sediment as well as suboxic–anoxic water column (Thamdrup and Dalsgaard, 2002; Kuypers et al., 2003; Dalsgaard et al., 2003.), no enough data are available to scale, temporal and spatially, this process to continental shelf sediments of the upwelling ecosystems; thus it is necessary to evaluate experimentally this process in the area.

Among other processes associated with NO_3^- uptake and then determining the influxes of this nutrient from the bottom water to the sediment in the area, is NO_3^- reduction to NH_4^+ (NO_3^- ammonification), which, for example, is shown to be important in coastal sediments by Sørensen (1978). In particular, NO_3^- ammonification by *Thioploca* could have important biogechemical implication in the study area (Farías, 1998). However a low *Thioploca* biomass, with an average of 6 g wet weight m^{-2} (up to 20 g wet weight m^{-2}), was found from 1998 to 2000 (V.A. Gallardo, unpublished), one order of magnitude lower than previous values recorded in the area (Gallardo, 1977; Fossing et al., 1995; Schulz et al., 1996, 2000). This biomass could be associated with a NO_3^- uptake lower of $0.2\,mmol\,m^{-2}\,d^{-1}$ (up to $0.63\,mmol\,m^{-2}\,d^{-1}$; Graco, 2002), and therefore this process could represent 6% (up to 18%) of the observed average of NO_3^- uptake by sediments. However, it is necessary to remark that the high capacity of these bacteria to accumulate nitrate can determine a lag between the uptake of nitrate and the observed fluxes. Another explanation of the observed NO_3^- influx in the area could be associated with a HS^- oxidation coupled with NO_3^- reducing activity in the sediments (Brettar and Rheinheimer, 1991). In fact, recent data associated with microbial communities in sediments under oxygen deficiency suggest the presence of large populations of species capable of

sulfur oxidation using NO_3^- as electron acceptor (e.g., *Pseudomonas stutzeri*, Nold et al., unpublished data).

Finally, our observed D_t rates in the Chilean continental shelf sediments were similar to those reported for estuaries and other coastal ecosystems (review in Seitzinger, 1990) and comparable with model predictions for areas subjected to strong organic loading and low oxygen conditions (Middelburg et al., 1996; Seitzinger and Giblin, 1996). They were also of the same order of magnitude as those found by Devol (1991) in the eastern North Pacific continental margin, supporting the idea that the capacity of the shelf sediments to act as an N sink due to greater denitrification processes than previously thought.

In continental shelf sediments off Central Chile, very high supply of electron donors from primary production in conjunction with a particular microbial community characterized by heterotrophic (e.g., SO_4^{2-} reducers) and chemolitotrophic (e.g., *Thioploca* mats) communities suggest that alternative acceptor electrons are used other besides the classical NO_3^- and SO_4^{2-}, whose abundance seems to be limited. Thus a complex and intricated coupling between C, N, and S cycles, and maybe Fe, seems to be working in the area.

5. Conclusions

The sediments of the upwelling system off central Chile act as a large NH_4^+ source or sink, depending principally on the amount of labile organic C reaching the sediments. Seasonal upwelling locally modulates the amount of labile organic C in the surface sediments. However, during the ending phase of the 1997–1998 EN (summer, 1998), PP in the water column was lower than expected for an upwelling period. Also, the sediment chl-*a* values indicated a lower input of organic matter to the sediment, and oxygen conditions underlying the sediments were unexpectedly higher than during non-EN years. In this period, the sediment could act as a NH_4^+ sink not explained by nitrification processes and possibly driven more by assimilatory than by dissimilatory microbial processes. The sediments of the continental shelf off central Chile act as a nitrogen NO_3^- sink and are major denitrification sites. Denitrification processes are mainly coupled to nitrification (58–99%) and explain only up to 25% of the NO_3^- flux into the sediment.

Acknowledgements

The authors thank A. Davies (MBA, UK) and C. Morales for their critical readings of this manuscript; V. Dellarossa for laboratory availability during the experimental analysis; V.A. Gallardo, D. Gutierrez, and other collaborators for the sediment parameters provided for this research (FONDECYT Grant No. 1971336). We greatly appreciate the help and support that we received from R. Castro in the laboratory analyses. Financial assistance was provided by the Directorate of Research of the University of Concepción (P.I. 98.112.050), Fundación Andes, and the Chilean National Commission for Scientific and Technological Research (CONICYT) through FONDECYT Grant No. 198-0544, the FONDAP-Humboldt Program, and the FONDAP-COPAS Center (Project No. 150100007).

References

Ahumada, R., Rudolph, A., Martínez, V., 1983. Circulation and fertility of waters in Concepción Bay. Estuarine, Coastal and Shelf Science 16, 95–105.

Blackburn, T.H., 1986. Nitrogen cycle in marine sediments. Ophelia 26, 65–76.

Blackburn, T.H., Blackburn, N.D., 1993. Rates of microbial processes in sediments. Philosophical Transactions of the Royal Society of London, Series A 344, 49–58.

Blackburn, T.H., Henriksen, K., 1983. Nitrogen cycling in different types of sediments from Danish waters. Limnology and Oceanography 28, 477–493.

Blackburn, T.H., Hall, P.J., Hulth, S., Landén, A., 1996. Organic-N loss by efflux and burial associated with a low efflux of inorganic N and with nitrate assimilation in Arctic sediments (Svalbard, Norway). Marine Ecology Progress Series 141, 283–293.

Brettar, I., Rheinheimer, G., 1991. Denitrification in the Central Baltic: evidence for H_2S oxidation as motor of denitrification at the oxic–anoxic interface. Marine Ecology Progress Series 77, 157–169.

Caffrey, J.M., Sloth, N.P., Kaspar, H.F., Blackburn, T.H., 1993. Effect of organic loading on nitrification and denitrification in a marine sediment microcosm. FEMS Microbiology Ecology 12, 159–167.

Callender, E., Hammond, D.E., 1982. Nutrient exchange across the sediment–water interface in the Potomac River Estuary. Estuarine, Coastal and Shelf Science 15, 395–413.

Codispoti, L.A., Brandes, J.A., Christensen, J.P., Devol, A.H., Naqvi, S.W.A., Paerl, H.W., Yoshinari, T., 2001. The oceanic fixed nitrogen and nitrous oxide budgets: moving targets as we enter the anthropocene? Scientia Marine 65 (Suppl. 2), 85–105.

Cowan, J.L., Pennock, J.R., Boynton, W.R., 1996. Seasonal and interannual patterns of sediment-water nutrient and oxygen fluxes in Mobile Bay, Alabama (USA): regulating factors and ecological significance. Marine Ecology Progress Series 141, 229–245.

Dalsgaard, T., Canfield, D.E., Petersen, J., Thamdrup, B., Acuña-González, J., 2003. N_2 production by the anammox reaction in the anoxic water column of Golfo Dulce, Costa Rica. Nature 422, 606–611.

Daneri, G., Dellarossa, V., Quiñones, R., Jacob, B., Montero, P., Ulloa, O., 2000. Primary production and community respiration in the Humboldt current system off Chile and associated areas. Marine Ecology Progress Series 197, 41–49.

Devol, A.H., 1991. Direct measurement of nitrogen gas fluxes from continental shelf sediments. Nature 349, 319–321.

Devol, A.H., 2003. Solution to a marine mystery. Nature 422, 575–576.

Devol, A.H., Christensen, J.P., 1993. Benthic fluxes and nitrogen cycling in sediments of the continental margin of the eastern North Pacific. Journal Marine Research 51, 345–372.

Farías, L., 1998. Potential role of bacterial mats in the nitrogen budget of marine sediments: the case of *Thioploca* spp. Marine Ecology Progress Series 170, 291–292.

Farías, L., Chuecas, L.A., Salamanca, M.A., 1996. Effect of coastal upwelling on nitrogen regeneration from sediments and ammonium supply to the water column in Concepción Bay. Estuarine, Coastal and Shelf Science 43, 137–155.

Fenchel, T., King, G.M., Blackburn, T.H., 1998. Bacterial Biogeochemistry: The Ecophysiology of Mineral Cycling, second ed. Academic Press, London, 307pp.

Ferdelman, T.G., Lee, C., Pantoja, S., Harder, J., Bebout, B.M., Fossing, H., 1997. Sulfate reduction and methanogenesis in a Thioploca-dominated sediment off the coast of Chile. Geochimica and Cosmochimica Acta 61, 3065–3079.

Fossing, H., Gallardo, V.A., Jørgensen, B.B., Huttel, M., Nielsen, L.P., Schulz, H., Canfield, D.E., Foster, S., Glud, R.N., Gundersen, J.K., Kuver, J., Ramsing, N.B., Teske, A., Thamdrup, B., Ulloa, O., 1995. Concentration and transport of nitrate by mat-forming sulphur bacterium *Thioploca*. Nature 374, 713–715.

Gallardo, V.A., 1977. Large benthic microbial communities in sulphide biota under Peru–Chile subsurface countercurrent. Nature 268, 331–332.

Glud, R.N., Gundersen, J.K., Lobby, O., 1999. Benthic in situ respiration in the upwelling area off central Chile. Marine Ecology Progress Series 186, 9–18.

Graco, M., 2002. Sedimentos del área de surgencia de Chile central (36°S) ¿Fuente o sumidero de nitrógeno? Ph.D Thesis. University of Concepcion, Concepción, Chile, 224 pp.

Graco, M., Farías, L., Molina, V., Gutiérrez, D., Nielsen, L.P., 2001. Massive developments of microbial mats following phytoplankton blooms in a naturally eutrophic bay: implications for nitrogen cycling. Limnology and Oceanography 46 (4), 821–832.

Gutiérrez, D., Gallardo, V.A., Mayor, S., Neira, C., Vásquez, C., Sellanes, J., Rivas, M., Soto, A., Carrasco, F., Baltazar, M., 2000. Effects of dissolved oxygen and organic matter reactivity on macrofaunal bioturbation potential in sublittoral bottoms off central Chile during 1997–1998 El Niño. Marine Ecology Progress Series 202, 81–99.

Hansen, J.W., Thamdrup, B., Jorgensen, B.B., 2000. Anoxic incubation of sediment in gas-tight plastic bags: a method for biogeochemical process studies. Marine Ecology Progress Series 208, 273–282.

Hebbeln, D., Marchant, M., Freudenthal, F., Wefer, G., 2000. Surface sediment distribution along the Chilean continental slope related to upwelling and productivity. Marine Geology 164, 119–137.

Henriksen, K., Kemp, M., 1988. Nitrification in estuarine and coastal marine sediments. In: Blackburn, T.H., Sorensen, J. (Eds.), Nitrogen Cycling in Coastal Marine Sediments. Wiley, New York, pp. 207–249.

Hopkinson, C.S., Giblin, A.E., Tucker, J., 2001. Benthic metabolism and nutrient regeneration on the continental shelf of Eastern Massachusetts, USA. Marine Ecology Progress Series 224, 1–19.

Huyer, A., Knoll, M., Paluszkiewicz, T., Smith, R.L., 1987. The Peru undercurrent: a study in the variability. Deep-Sea Research 38 (Suppl. 1), 247–279.

Jenkins, M.C., Kemp, W.M., 1984. The coupling of nitrification and denitrification in two estuarine sediments. Limnology and Oceanography 29, 609–619.

Jørgensen, B.B., Gallardo, V.A., 1999. *Thioploca* spp.: filamentous sulfur bacteria with nitrate vacuoles. FEMS Microbiology Ecology 28, 301–313.

Kemp, W.M., Sampou, P., Caffrey, J., Mayer, M., 1990. Ammonium recycling versus denitrification in Chesapeake Bay sediments. Limnology and Oceanography 33, 1545–1563.

Klump, J.V., Martens, C.S., 1983. Benthic nitrogen regeneration. In: Carpenter, C., Capone, D.G. (Eds.), Nitrogen in the Marine Environment. Academic Press, Inc., London.

Kuypers, M.M., Sliekers, A.O., Lavik, G., Schmid, M., Jorgensen, B.B., Kuenen, J.G., Damste, J.S., Strous, M., Jetten, S.M., 2003. Anaerobic ammonium oxidation by anammox bacteria in the Black Sea. Nature 422, 608–611.

Lohse, L., Malschaert, J.F.P., Slomp, C.P., Helder, W., Raaphorst, W.V., 1993. Nitrogen cycling in North Sea sediments: interaction of denitrification and nitrification in

offshore and coastal areas. Marine Ecology Progress Series 101, 283–296.

Luther III, G.W., Sundby, B., Lewis, B.L., Brendel, P.J., Silverberg, N., 1997. Interactions of manganese with the nitrogen cycle: alternative pathways to dinitrogen. Geochimica and Cosmochimica Acta 61, 4043–4052.

Mackin, J.E., Aller, R.C., 1984. Ammonium adsorption in marine sediments. Limnology and Oceanography 29, 250–257.

Middelburg, J.J., Soetaert, K., Herman, P.M.J., Heip, C.H.R., 1996. Denitrification in marine sediments: a model study. Global Biogeochemical Cycles 10 (4), 661–673.

Molina, V., 2002. Flujos de Nitrógeno Orgánico Disuelto (NOD), un indicador de la capacidad degradadora de los sedimentos costeros de Chile central (36°S). Master Thesis, Department of Oceanography, Concepción, Chile, 152pp.

Molina, V., Farías, L., Graco, M., Rivera, C., Pinto, L., Gallardo, V.A., 2004. Benthic nitrogen regeneration under oxygen and organic matter spatial variability off Concepción (~36°S), central Chile. Deep-Sea Research II, this issue [doi:10.1016/j.dsr2.2004.08.014].

Morales, C.E., Hormazabal, S.E., Blanco, J.L., 1999. Interannual variability in the mesoscale distribution of the depth of the upper boundary of the oxygen minimum layer off northern Chile (18–24°S): implications for the pelagic system and biogeochemical cycling. Journal of Marine Research 57, 909–932.

Mulder, A., van de Graf, A.A., Roberson, L.A., Kuenen, J.G., 1995. Anaerobic ammonium oxidation discovered in a denitrifying fluidized bed reactor. FEMS Microbiology Ecology 16, 177–184.

Nielsen, L.P., 1992. Denitrification in sediments determined from nitrogen isotope pairing. FEMS Microbiology Ecology 86, 357–362.

Ogilvie, B., Nedwell, D.B., Harrison, R.M., Robinson, A., Sage, A., 1997. High nitrate, muddy estuaries as nitrogen sinks: the nitrogen budget of the River Colne estuary (United Kingdom). Marine Ecology Progress Series 150, 217–228.

Otte, S., Kuenen, J.G., Nielsen, L.P., Paerl, H.W., Zopfi, J., Schulz, H.N., Teske, A., Strotmann, B., Gallardo, V.A., Jørgensen, B.B., 1999. Nitrogen, carbon and sulfur metabolism in natural *Thioploca* samples. Applied Environmental Microbiology 65, 3148–3157.

Parsons, T.R., Maita, Y., Lalli, C.M., 1984. A Manual of Chemical and Biological Methods for Seawater Analysis. Pergamon Press, Oxford.

Pedersen, A.-G.U., Berntsen, J., Lomstein, B.A.a., 1999. The effect of eelgrass decomposition on sediment carbon and nitrogen cycling: a controlled laboratory experiment. Limnology and Oceanography 44, 1978–1992.

Risgaard-Petersen, N., Rysgaard, S., Nielsen, L.P., Revsbech, N.P., 1994. Diurnal variation of denitrification and nitrification in sediments colonised by benthic microphytes. Limnology and Oceanography 39, 573–579.

Risgaard-Petersen, N., Nielsen, L.P., Rysgaard, S., Dalsgaard, T., Meyer, R.L., 2003. Application of the isotope pairing technique in sediments where anammox and denitrification coexist. Limnology and Oceanography: Methods 1, 63–73.

Rosenberg, R., Arntz, W.E., Flores, E.C., Flores, L.A., Carvajal, G., Finger, Y., Tarazona, J., 1983. Benthos biomass in an oxygen deficiency in the upwelling system off Peru. Journal of Marine Research 41, 263–279.

Rowe, G.T., Clifford, C.H., Smith, K.L., 1975. Benthic nutrient regeneration and its coupling to primary productivity in coastal water. Nature 255, 215–217.

Rysgaard, S., Risgaard-Pedersen, N., Sloth, N.P., Jensen, K., Nielsen, L.P., 1994. Oxygen regulation of nitrification and denitrification in sediments. Limnology and Oceanography 39, 1643–1652.

Schmaljohann, R., Drews, M., Walter, S., Linke, P., von Rad, U., Imhoff, J.F., 2001. Oxygen-minimum zone sediments in the northeastern Arabian Sea off Pakistan: a habitat for the bacterium *Thioploca*. Marine Ecology Progress Series 211, 27–42.

Schulz, H.N., Jørgensen, B.B., Fossing, H., Ramsing, N.B., 1996. Community structure of filamentous sheath-building sulfur bacteria *Thioploca* spp. off the coast of Chile. Applied Environmental Microbiology 62, 1855–1862.

Schulz, H., Brinkhoff, T., Ferdelman, T.G., Hernández Mariné, M., Teske, A., Jørgensen, B.B., 1999. Dense populations of giant sulfur bacterium in Namibian shelf sediments. Science 284, 493–495.

Schulz, H.N., Strotmann, B., Gallardo, V.A., Jørgensen, B.B., 2000. Population study of the filamentous sulfur bacteria *Thioploca* spp. off the Bay of Concepción, Chile. Applied Environmental Microbiology 62, 1855–1862.

Seitzinger, S.P., 1990. Denitrification in aquatic sediments. In: Revsbech, N.P., Sorensen, J. (Eds.), Denitrification in Soil and Sediment. Plenum Press, New York.

Seitzinger, S.P., Giblin, A.E., 1996. Estimating denitrification in North Atlantic continental shelf sediments. Biogeochemistry 35, 235–260.

Simon, N.S., 1989. Nitrogen cycling between sediment and the shallow-water column in the transition zone of the Potomac river and estuary. 2. The role of wind-driven resuspension and adsorbed ammonium. Estuarine, Coastal and Shelf Science 28, 531–547.

Solorzano, L., 1969. Determination of ammonium in natural waters by the phenol hypochlorite method. Limnology and Oceanography 14, 799–801.

Sørensen, J., 1978. Capacity for denitrification and reduction of nitrate to ammonia in coastal marine sediment. Applied Environmental Microbiology 35, 301–305.

Strous, M., Fuerst, J.A., Kramer, E.H.M., Logemann, S., Muyzer, G., Van de Pas-Schoonen, K., Webb, R., Kuenen, J.G., Jetten, M.S.M., 1999. Missing lithotroph identified as new planctomycete. Nature 400, 446–449.

Strub, P.T., Mesias, J., Montecinos, V., Rutllant, J., Salinas, S., 1998. Coastal ocean circulation off Western South America. In: Robinson, A.R., Brink, K.H. (Eds.), The Sea, vol. 11. Wiley, London.

Sumi, T., Koike, I., 1990. Estimation of ammonification and ammonium assimilation in surface coastal and

estuarine sediments. Limnology and Oceanography 35 (2), 270–286.

Summerhayes, C.P., 1983. Sedimentation of organic matter in upwelling regimes. In: Thiede, J., Suess, E. (Eds.), Coastal Upwelling: Sedimentary Record of Ancient Coastal Upwelling (Part B). Plenum Press, New York, pp. 29–72.

Thamdrup, B., Canfield, D.E., 1996. Pathway of carbon oxidation in the continental margin off central Chile. Limnology and Oceanography 41, 1629–1650.

Thamdrup, B., Dalsgaard, T., 2002. Dinitrogen production through anaerobic ammonium oxidation—a shunt in the marine nitrogen cycle. Applied Environmental Microbiology 68, 1312–1318.

Ulloa, O., Escribano, R., Hormazabal, S., Quiñones, R., Gonzalez, R., Ramos, M., 2001. Evolution and biological effect of the 1997-98 El Niño in the upwelling ecosystem off northern Chile. Geophysical Research Letters 28 (7), 1591–1594.

Walsh, J.J., 1991. Importance of continental margins in the marine biogeochemical cycling of carbon and nitrogen. Nature 350, 53–55.

Williams, P.J., Jenkinson, N.W., 1982. A transportable microprocessor controlled precise Winkler titration suitable for field station and shipboard use. Limnology and Oceanography 27, 576–584.

Zopfi, J., Kjaer, T., Nielsen, L.P., Jorgensen, B.B., 2001. Ecology of *Thioploca* spp.: nitrate and sulfur storage in relation to chemical microgradients and influence of *Thioploca* spp. on the sedimentary nitrogen cycle. Applied Environmental Microbiology 67, 5530–5537.

ELSEVIER

Deep-Sea Research II 51 (2004) 2507–2522

DEEP-SEA RESEARCH
PART II

www.elsevier.com/locate/dsr2

Benthic nitrogen regeneration under oxygen and organic matter spatial variability off Concepción (~36°S), central Chile

Verónica Molina[a,b,*], Laura Farías[b,c,d], Michelle Graco[b], Cecilia Rivera[e], Luis Pinto[c], Victor A. Gallardo[c,d]

[a]*Programa de Postgrado, Departamento Oceanografía, Universidad de Concepción, Concepción, Chile*
[b]*Programa Regional de Oceanografía Física y Clima (PROFC), Universidad de Concepción, Casilla 160-C, Concepción, Chile*
[c]*Departamento de Oceanografía, Facultad de Ciencias Naturales y Oceanográficas, Universidad de Concepción, Casilla 160-C, Concepción, Chile*
[d]*Centro de Investigación Oceanográfica en el Pacífico Sur-Oriental (FONDAP-COPAS), Universidad de Concepción, Casilla 160-C, Concepción, Chile*
[e]*Departamento de Química, Facultad de Ciencias Químicas, Universidad de Concepción, Casilla 160-C, Concepción, Chile*

Accepted 30 July 2004

Abstract

The effects of dissolved oxygen (DO) and organic matter (OM) on several geochemical parameters and nitrogen cycling were evaluated in the upwelling region off central Chile (~36°S). The sediments of the study area presented: (i) nearly anoxic conditions (2.68 μM) and high chlorophyll-*a* content (1112 mg g^{-1}) within the Concepción Bay (29 m water depth); (ii) suboxic to oxic conditions (10–129 μM), and from moderate to low chlorophyll-*a* levels (47–13 mg g^{-1}), in a depth transect outside the bay (88–820 m depth); and (iii) suboxic conditions (5.75–8.9 μM) and low chlorophyll-*a* content (~13 mg g^{-1}) in the Itata Canyon area (209 and 362 m depth). Nitrogen processes (in mmol m^{-2} d^{-1}) varied with depth, in association with changes in fresh OM input and DO content at the transect stations: i.e. decreased ammonification (from 12.9 to 1.0), NH_4^+ efflux (from 4.8 to 1.2) and denitrification (from 1.3 to 0.3), and increased potential nitrification (from 1.0 to 2.4). Concepción Bay and one of the Itata Canyon stations (209 m) were notably different from the others, indicating heterogeneity of benthic nitrogen cycling in this upwelling region. The bay presented the highest ammonification and lowest denitrification rates. Itata Canyon sediments showed high urea influxes at both sites, although high NH_4^+ influxes and the highest potential nitrification were only found at the 209 m station. Patterns such as the occurrence of dissolved organic nitrogen effluxes (4.9–75) and higher ammonification rates were found at stations < 30 km offshore; influxes (9.7–20.5) and lower ammonification rates were observed at stations > 52 km offshore. All the stations presented $NO_3^- + NO_2^-$ influxes (0.6–4.3). A nitrogen-cycling

*Corresponding author. Programa de Postgrado, Departamento Oceanografia, Universidad de Concepcion, Concepcion, Chile. Tel.: +56 41 20 4239; fax: +56 41 22 5400.
E-mail address: vemolina@udec.cl (V. Molina).

0967-0645/$ - see front matter © 2004 Elsevier Ltd. All rights reserved.
doi:10.1016/j.dsr2.2004.08.014

imbalance in the NH_4^+ benthic cycle was found at four stations: NH_4^+ excesses (30–>100%) at two transect and one of the canyon stations, and a deficit (>100%) at the other canyon station. A small proportion of the $NO_3^- + NO_2^-$ influxes (<42%) was explained by the processes studied herein. These imbalances indicated potential incubation biases and the presence of other N processes not accounted for in this study.
© 2004 Elsevier Ltd. All rights reserved.

1. Introduction

The Peru Chile Current System, also known as the Humboldt Current System (HCS), presents high primary productivity associated with coastal wind-driven upwelling events of different intensities and frequencies along the South American coast (Strub et al., 1998). An important fraction (~40–50%) of the organic matter (OM) produced in the euphotic zone of the HCS is exported toward the depths (Farías et al., 1996; González et al., 2000), fueling benthic mineralization processes (Thamdrup and Canfield, 1996; Glud et al., 1999; Gutiérrez et al., 2000).

Intense seasonal upwelling events off central Chile (~36°S) fertilize the euphotic zone with high-nutrient waters (e.g., NO_3^-: 15–25 μM) (Ahumada and Chuecas, 1979), creating suitable conditions for primary producers and supporting production rates of up to 19.9 g C m^{-2} d^{-1} (Daneri et al., 2000). The area's complex coastline and topography (i.e. bays, canyons, and rivers) create different depositional environments. Sea-surface temperature satellite images reveal upwelling centers and offshore projections of upwelled waters (Cáceres, 1992), and SeaWiFS images show chlorophyll-*a* (Chl-*a*) filaments projecting offshore (Graco, 2002). These coastal–oceanic physical interactions potentially mediate the export of primary production offshore, thus increasing OM deposition from the euphotic zone towards deeper sediments situated far from the coast. In addition, the sediments of the continental margin off central Chile are exposed to various dissolved oxygen (DO) concentrations, due mainly to water-mass distribution: (1) Sub-Antarctic Water (SAAW; 0–80 m depth), (2) Equatorial Subsurface Water Mass (ESSW; 80–400 m depth) with minimum DO concentrations of <44.6 μM, and (3) Antarctic Intermediate Water (AAIW; 400–800 m depth). DO concentrations in both SAAW and AAIW are >90 μM (Brandhorst, 1971; Silva and Konow, 1975; Strub et al., 1998).

OM and DO are controlling factors for benthic mineral cycling rates and OM preservation (e.g., Summerhayes, 1983; Pedersen and Calvert, 1990; Canfield, 1994). Despite the fact that both, the quantity and quality of OM, changes during its sinking from the euphotic zone (Lee and Cronin, 1982; Wakeham and Lee, 1993), sediment nitrogen (N) cycling is mainly sustained by the particulate organic nitrogen (PON) reaching the sediment surface (Rowe et al., 1975). Briefly, the first step of N cycling involves PON transformation, by dissolution and hydrolytic processes, to dissolved organic nitrogen (DON). The next steps involve DON transformation to "dissolved inorganic nitrogen" (DIN) in several interdependent reactions, i.e. ammonification, nitrification, and denitrification. Each of these processes is more or less (or not at all) sensitive to DO concentrations (Henriksen and Kemp, 1988; Hansen and Blackburn, 1991; Sloth et al., 1995).

To elucidate how the benthic N cycle responds to different OM loadings and DO concentrations off the central Chilean continental margin, OM and DO related parameters were measured in the sediment pore-water [i.e. surface total organic carbon (TOC_{z0}), total nitrogen (TN_{z0}), Chl-*a* (chl-a_{z0}), Redox, Mn^{2+}, and Fe^{2+}], together with water-mass indicator parameters (i.e. salinity, temperature, DO, nutrients). These parameters were analyzed against benthic-N exchange rates (DON, urea, NH_4^+, and $NO_3^- + NO_2^-$ fluxes), N process rates (denitrification, ammonification, and potential nitrification), and pore-water DIN distribution (NH_4^+, NO_3^-, and NO_2^-).

2. Material and methods

2.1. Study site and sampling

The study area (Fig. 1) is located at the widest portion of central Chile's continental margin, the so-called "Itata Terrace" (~50 km), which is limited by two submarine canyons and their corresponding rivers: the Itata Canyon (Itata River) to the north and the Bio-Bio Canyon (Bio-Bio River) to the south. This area also includes an embayment system, among which is the Bay of Concepción. Four of the six stations sampled were located in an onshore–offshore

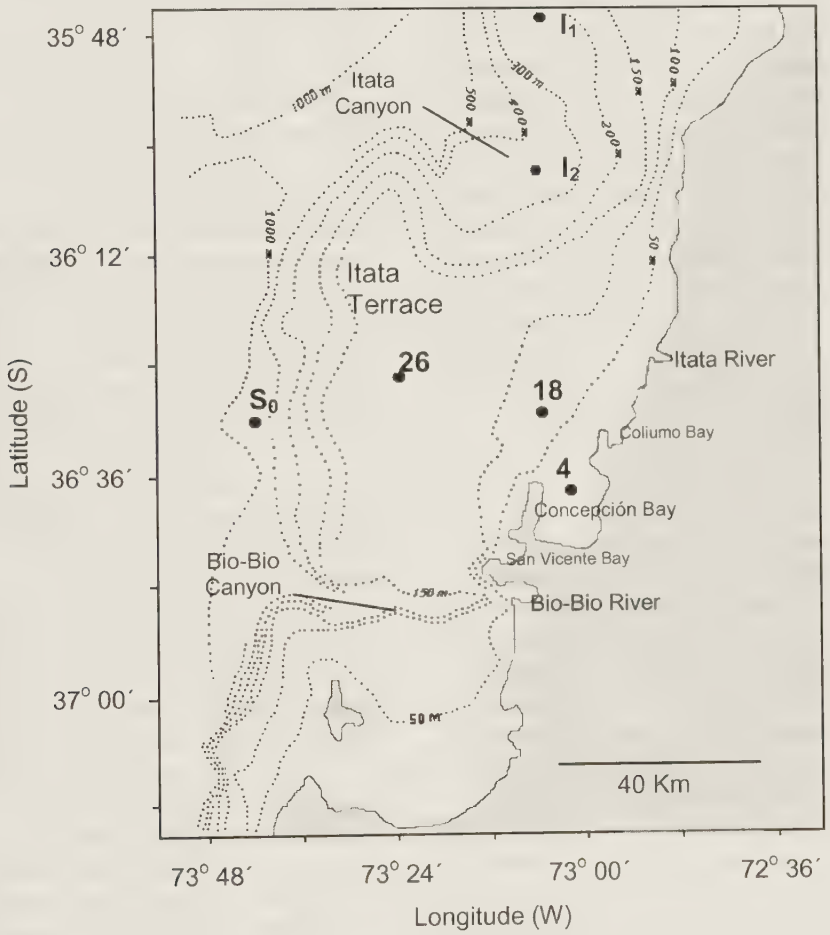

Stations	Geographical Position	Distance off the coast km	Water depth m
4	36°38′S, 73°02′W	7.4	29
18	36°31′S, 73°0.2′W	25.9	88
26	36°26′S, 73°23′W	51.8	120
S_0	36°32′S, 73°40′W	83.3	820
I_1	35°44′S, 73°04′W	51.8	209
I_2	35°03′S, 73°04′W	29.6	368

Fig. 1. Geographical location of the sampling sites and their approximate distances from the coast. Dotted lines are depth contours.

transect (Station 4 in the inner bay; Stations 18 and 26 on the shelf; and Station S_0 on the slope), and two were within (I_2) and on the northern edge (I_1) of the Itata Canyon (Fig. 1). The stations were visited between 11 and 13 March 1999 on board the R/V *Kay Kay*, and between 30 March and 04 April 1999 on board the R/V *Vidal Gormaz*.

Sediments were collected using a SMBA mini–multicorer 600 with six sampling tubes of 9.5-cm internal diameter (i.d.) and 60 cm height. The multicorer tubes were then carefully sub-sampled by introducing acrylic cores of lesser diameter for geochemical parameters and incubation experiments. Water-column samples were obtained using Niskin bottles from a CTD rosette. Water samples for DO and NH_4^+ determinations were immediately fixed following collection (Williams and Jenkinson, 1982; Solorzano, 1969, respectively); for $NO_3^- + NO_2^-$, ~250 mL were filtered (0.45 μm, Millipore filter) and frozen for later analysis. Water temperature, salinity, and density were recorded in situ with a CTD.

2.2. General sediment features

In order to recover pore-water, two cores (3.6 cm i.d., 25 cm height) from the same multicorer tube were cut into slices of 1–2 cm up to 14 cm deep under a N_2 atmosphere. The sediment slices were squeezed at 0.2 bar and immediately filtered "on-line" with 0.45-μm membrane Millipore filters. The pore-water aliquots from one core were used for dissolved nutrients (NH_4^+, NO_3^-, NO_2^-) and those from the other for metal (Mn^{2+}, Fe^{2+}) determinations. Another core (4 cm i.d., 25 cm height) was sectioned (as mentioned above), and the sediment slices were used to determine porosity (Φ) and bulk density according to Håkanson and Jansson (1983).

An undisturbed sediment core (7.2 cm i.d., 30 cm height) was used to measure redox potential (Eh) with a standard combination electrode with a calomel internal reference (Mettler Toledo). The electrode was slowly introduced from the sediment–water interface towards the upper 1 cm (Eh_{z0}). Homogenized sediment samples from the sediment surface (1 cm height, $z0$) of two cores (3.6 cm i.d., 25 cm height) were used to estimate Chl-a_{z0} and phaeopigments ($Phaeo_{z0}$), following Stal et al. (1984). One core (4 cm i.d., 25 cm height) was used for TOC_{z0} and TN_{z0} determinations. The samples for elemental CHN determinations were treated with 2% HCl to remove inorganic carbon, thoroughly washed with distilled water to remove salt and acid (allowing material to settle so as to avoid OM loss), and then freeze-dried. Two to five milligrams of treated sediment were analyzed in a Carlo Erba NA-1500 CNS analyzer.

2.3. Benthic fluxes and nitrogen processes

Three cores (5.5 cm i.d., 20 cm height) taken from a second multicorer cast were used to subsample sediments and overlying water (~300 mL); DIN (NH_4^+, $NO_3^- + NO_2^-$), DON, and urea fluxes across the sediment–water interface were determined. At the same time, a syringe (60 mL) was used to sample the overlying sediment water for initial DIN and DON concentrations. After this procedure, the cores were immediately incubated for 6 h, on board and in the dark, in a water-bath maintained at 10 °C (all stations). Water overlying the sediment was kept homogenous by a stirring magnetic bar (hanging from the top). After 6 h, a final sample was taken from the overlying water of each core. Oxygen, pH, and temperature were measured at the beginning and end of the incubation using a sensor (Oxi 323-B/SET).

NH_4^+ accumulation rates were obtained by measuring the accumulation of dissolved NH_4^+ in slurry incubations. Homogenized sediments (2–3 g) from different depths (0–1, 3–4, 5–6, and 9–10 cm) of a 7.2 cm i.d. core were placed in plastic tubes (45 mL) under a N_2 atmosphere and diluted 1:1 with autoclaved bottom seawater. The tubes were incubated for 10 d in a N_2 atmosphere, in the dark and under controlled temperature simulating in situ bottom water conditions. Samples were taken for NH_4^+ analysis at 0 and 12 h, and then once a day until day 10.

Potential nitrification rates were obtained by measuring NO_2^- accumulations in experimental slurry incubations, according to Henriksen and Kemp (1988). Briefly, sediment slurries (2–3 g) from homogenized fresh-surface sediments (first

1 cm of a 7.2 cm i.d. core) were enriched with NH_4^+ (1 mM, prepared with filtered-UV sterilized seawater) and treated with chlorate (10 mM final concentration) to block out further NO_2^- oxidation to NO_3^-, and incubated for 9 h at room temperature under slow agitation.

Direct denitrification rates were estimated, following the isotope pairing method (IPM; Nielsen, 1992), using four sediment cores (3.6 cm i.d.) from a third multicorer cast. $^{15}NO_3^-$ (10 mM stock solution 99.6% $^{15}NO_3^-$) was added to the overlying water of each core to obatin a 30–50 μM final concentration. The sediments were incubated for 3–4 h, in the dark at 10 °C. After the incubation, 3 mL $ZnCl_2$ (50% v/v) were added at 1.5–2 h intervals to each well-mixed core to block out microbial activity. Duplicate samples were transferred from the core into 6-mL glass vials (previously filled with 250 μL of $ZnCl_2$) with a syringe. Analysis was then carried out in a mass spectrometer at the National Environmental Research Center (NERI) in Silkerborg (Denmark).

2.4. Analytical procedure and calculations

DO was determined on board by a modified Winkler method following Williams and Jenkinson (1982). A semi-automatic system, consisting of an end-point photometric detector and a Dosimat (Metrohm burette 665) connected with a chart recorder (0.03–1% variation) was used. NO_3^- and NO_2^- samples were frozen until analysis was performed by standard colorimetric methods (Parsons et al., 1984). NH_4^+ was immediately fixed and maintained, on board, at 4 °C until color development reaction was carried out (1 day maximum), according to Solorzano (1969). Porewater Mn^{2+} and Fe^{2+} samples were acidified to pH = 2 with HCl and refrigerated until analysis was performed by atomic absorption spectrometry (AAS GBC model 902).

Samples for urea and DON determinations were filtered through GF/F millipore filters (previously ignited at 450 °C) and frozen until analysis. Urea was determined following Newell et al. (1967), modified for a 2.5 mL sample, and DON by the persulfate wet-oxidation technique according to Parsons et al. (1984), adapted to suit a 10-mL sample. Calibration curves for the DON persulfate wet oxidation technique were constructed with NH_4^+, urea and glycine standards were prepared by adding spikes from a concentrated solution to 10 mL of synthetic seawater for a final concentration of 5–30 μM ($P<0.05$). Inter-calibrations (Stations S_0 and 4) were carried out by a modified high-temperature oxidation (HTO) technique (e.g., Burdige and Zheng, 1998); the wet oxidation technique was found to underestimate DON flux determination by >12% in comparison with the HTO method.

Nutrients and metal pool sizes (mmol m^{-2}) were obtained by first, multiplying the pore-water concentrations at each depth with the porosity and height of the sediment slice (1 or 2 cm), and then, integrating the result into the whole sediment height (14 cm). The benthic flux rate was calculated from each replicate (mmol m^{-2} d^{-1}) by means of a linear regression (slope and error). The flux value reported here is the average and propagation error (square root of the square slope errors sum) of the three replicates. A negative value indicates a flux from the overlying water towards the sediment (an influx). NH_4^+ accumulation rates were estimated using a linear model and the standard errors by Monte Carlo confidence intervals. Ammonification rates were calculated by multiplying the NH_4^+ accumulation rates with $1+k$, where k is the adsorption coefficient for muds (1.3), according to Mackin and Aller (1984). The ammonification rates were expressed at depth-integrated rates (10 cm depth), in mmol m^{-2} d^{-1}. Denitrification rates (D_{15}) were calculated according to Nielsen (1992), based on the production of N_2-labeled species ($D_{15} = {}^{14}N^{15}N + 2({}^{15}N^{15}N)$) from the $^{15}NO_3^-$ added to the overlying water. This method also allows the evaluation of a denitrification rate produced from denitrification coupled to nitrification (D_{14}), which was obtained indirectly from D_{15} ($D_{14} = D_{15}$ $({}^{14}N^{15}N/2({}^{15}N^{15}N))$. Using a non-parametric Spearman rank correlation, two correlations were performed (e.g., Zar, 1999); one included the data (see Tables 1 and 2, and Fig. 4) from all the stations and the other only the data from the transect stations.

Table 1
Bottom water temperature, salinity, dissolved oxygen, and nutrient concentrations of the sampled stations

Station	Depth (m)	Temperature (°C)	Salinity (psu)	Oxygen (μM)	NO_3^- (μM)	NO_2^- (μM)	NH_4^+ (μM)
Transect							
4	29	11.80	34.31	2.7	0.96	0.47	28.5
18	88	11.00	34.38	10.0	14.5	n.d.	n.d.
26	120	10.78	34.59	4.5	9.5	0.07	0.31
S_0	820	3.70	34.43	129.4	24.8	0.11	0.23
Itata canyon							
I_1	209	10.00	34.61	5.8	25.5	0.12	0.03
I_2	362	8.90	34.53	8.9	12.5	0.25	n.d.

n.d. = not detected.

3. Results

3.1. Water column

Data from a CTD cast at station S_0 are presented in a T–S diagram (Fig. 2A). The influence of three different water masses (SAAW, ESSW, and AAIW) can be seen, according to the original source T(°C)/S(psu) values: 11.5/33.8 (SAAW), 12.5/34.9 (ESSW), and 3/34 (AAIW) (e.g., Silva and Konow, 1975; Strub et al., 1998). In the DO distribution, the oxycline was situated in the upper 50 m at almost all the stations (Fig. 2B). Below the oxycline, between 100 and 300 m depth, DO was near 0, indicating an ESSW influence (DO < 44.6 μM). At Station S_0, more oxygenated AAIW was clearly discernible (> 350 m depth).

Bottom-water temperature, salinity, DO, and nutrient concentrations (Table 1) show a greater influence of ESSW at Stations 18, 26, I_1, and I_2, whereas AAIW influenced Station S_0. Using the bottom-water DO content, the stations can be grouped into three zones: (i) Station 4, with almost anoxic conditions (< 4 μM), (ii) Stations 18, 26, and Itata Canyon with suboxic conditions (5–10 μM), and (iii) Station S_0, with oxic conditions (~130 μM). At all stations, except Station 4, higher NO_3^- concentrations were observed (9.5–25.5 μM) in the bottom water, together with lower NO_2^- and NH_4^+ concentrations (reaching the detection limit in some cases). Higher nutrient concentrations of benthic flux incubations were found in the water directly overlying the sediment than in the bottom water; NO_3^-, NO_2^-, and NH_4^+ ranged between 17–45, 1–45, and n.d.–1 μM, respectively (data not shown).

3.2. General sediment features

The sediments at all stations consisted of greenish-brown to gray mud, except for the Concepción Bay station, where a conspicuous black soupy layer ~5 cm thick was found. The sediments were poorly sorted, with > 90% of the silty clay minerals having a mean grain size between 8.5 and 13.0 μm (Gallardo et al., 2004). The surface porosity (cm^3 water cm^{-3} sediment, Φ_{z0}) decreased from 0.95 to $0.87\Phi_{z0}$, and wet bulk density increased from 1.1 to 1.23 g cm^{-3} along the transect stations (data not shown). Porosity and wet bulk density in Itata Canyon stations presented lower and higher values, respectively [$0.75\Phi_{z0}$ and 1.43 g cm^{-3} (Station I_1) and $0.84\Phi_{z0}$ and 1.29 g cm^{-3} (Station I_2)].

The analysis of the geochemical characteristics of the sediments (Table 2) showed that redox potential values at the sediment surface (Eh_{z0}) agree with an increase in bottom-water DO concentrations in the depth transect (from negative values within the bay towards higher and positive values at Station S_0). Chl-a_{z0} decreased, whereas its ratio to other OM parameters (i.e. C:Chl-a_{z0} and phaeo:Chl-a_{z0}) increased with depth along the transect. Other OM parameters (TOC_{z0}, TN_{z0}, $C{:}N_{z0}$) were unrelated to depth. At the Itata

Table 2
Geochemical and organic matter parameters measured and calculated for the sampled stations

Station	Depth (m)	Eh_{z0} (mV)	Chl-a_{z0} ($\mu g\,g^{-1}$ ws)	TOC_{z0} ($mg\,g^{-1}$)	TN_{z0} ($mg\,g^{-1}$)	C:Chl-a_{z0} ($mg\,g^{-1}$)	Phaeo:Chl-a_{z0} ($mg\,g^{-1}$)	$C:N_{z0}$ (molar ratio)	NH_4^+ ($mmol\,m^{-2}$)	NO_3^- ($mmol\,m^{-2}$)	NO_2 ($mmol\,m^{-2}$)	Fe^{+2} ($mmol\,m^{-2}$)	Mn^{+2} ($mmol\,m^{-2}$)
Transect													
4	29	−148	1112.0±285.0	32.8	5.0	30	2.5±0.5	8.0	150.0	5.6	0.30	1.9	0.49
18	88	115	47.7±19.4	36.8	5.0	771	6.5±0.6	8.6	28.1	4.3	0.30	3.3	0.42
26	120	135	35.5±2.9	43.0	5.8	1211	7.8±0.7	8.6	46.0	0.31	0.09	2.1	0.27
S_0	820	257	13.4±1.4	21.0	3.0	1567	11.2±1.6	8.2	23.3	0.28	0.03	3.3	0.22
Itata canyon													
I_1	209	121	12.9±8.5	11.0	1.7	853	10.6±2.4	7.5	14.5	0.83	0.04	1.1	0.35
I_2	362	198	13.3±2.9	31.0	4.1	2331	9.9±0.1	8.8	19.0	0.82	0.04	12.3	0.24

$z0$ = surface sediments (0–1 cm).
± = standard deviation (SD).

Canyon stations, Chl-a_{z0} and phaeo:Chl-a_{z0} values were comparable with the Station S_0 values, whereas TOC_{z0}, TN_{z0}, $C:N_{z0}$, and C:Chl-a_{z0} ratios were different, and also dissimilar between Stations I_1 and I_2.

3.3. Pore-water distribution and pool-size trends

NH_4^+, NO_3^-, NO_2^-, Mn^{2+}, and Fe^{2+} pore-water profiles are shown in Fig. 3, and their respective pool sizes in Table 2. NH_4^+ concentrations varied between 46 and 1323 μM. The highest concentrations were measured at Station 4, increasing from 1080 μM at the surface to 1323 μM at 4 cm, and then decreasing to 892 μM at 14 cm. At Stations 18, 26, and S_0, NH_4^+ concentration profiles increased from 46–226 μM at the surface to 305–467 μM at 14 cm depth. In contrast, NH_4^+ profiles were nearly homogeneous throughout the sediment column (<200 μM) at the Itata Canyon stations. NO_3^- concentrations fluctuated between 0 and 98 μM (Fig. 3); the highest magnitude was observed at Station 18. NO_2^- concentrations varied between 0 and 21 μM; the highest value was found at Station 4. In general, the NO_2^- pore-water distribution coincided with the NO_3^- distribution within the sediment column of the sampled stations, except for Stations 4, S_0, and I_1, where several peaks appeared at depth.

Dissolved Mn^{2+} and Fe^{2+} concentrations varied between 0 and 15 and 1 and 189 μM, respectively, with the highest magnitudes at the Itata Canyon stations (Fig. 3). In general, the Mn^{2+} and Fe^{2+} content presented a variable distribution, with higher surface concentrations and peaks at depth at all stations. Within the transect stations, the position of the Mn^{2+} and Fe^{2+} surface peaks in the sediment column were in agreement with the surface redox status of the sediment (Eh_{z0}), getting deeper as Eh_{z0} increased towards Station S_0.

Pool sizes were calculated from the same pore-water data for easy evaluation of the main DIN and metal trends among the stations (Table 2). NH_4^+, NO_3, and NO_2^- pool sizes decreased along the transect stations. The Itata Canyon stations presented the lowest NH_4^+ pool size values among all the stations; NO_3^- and NO_2^- pool sizes were

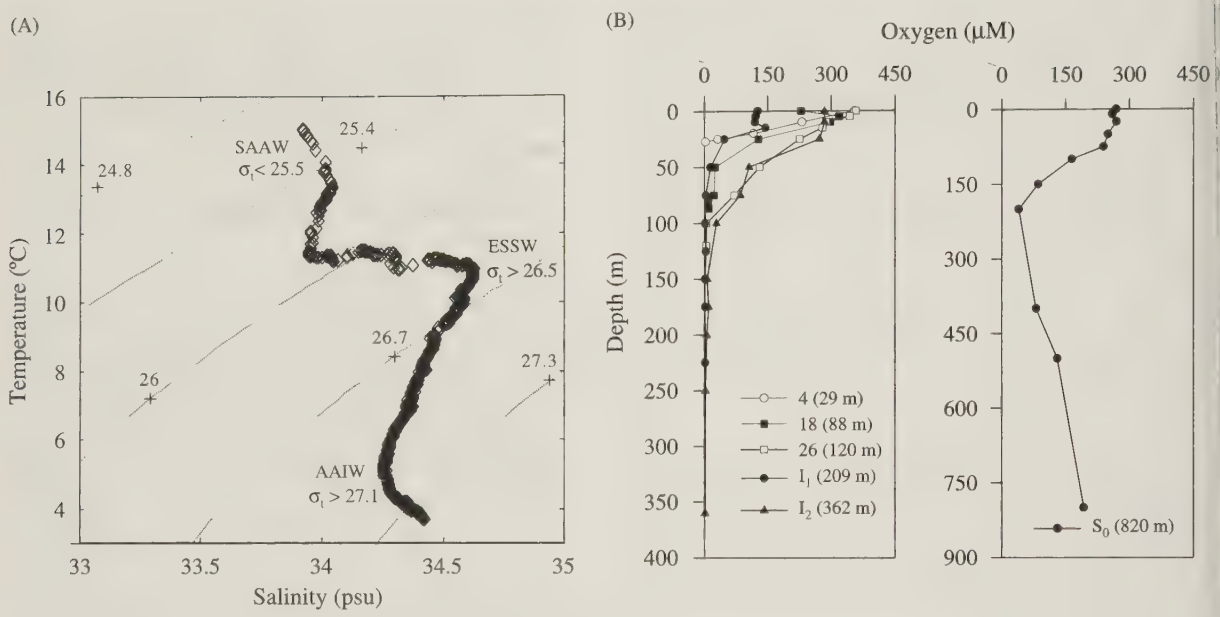

Fig. 2. (A) T/S diagram for Station S_0 and water masses in the study area. (B) Vertical distribution of DO at the sampling stations.

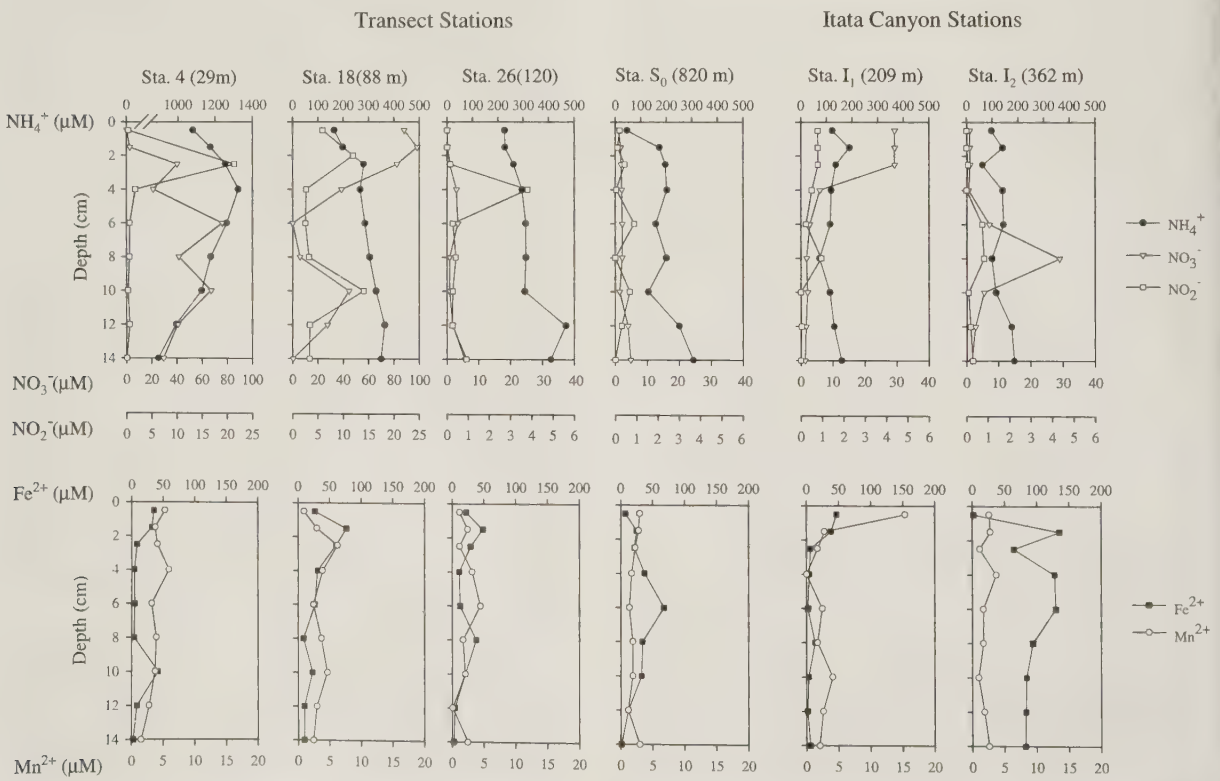

Fig. 3. Nutrient and metal pore-water profiles: ammonium (●), nitrate (▽), nitrite (□), iron (■), and manganese (○). (Note different scale for nutrients of Stations 4 and 18).

equal at both Itata stations. Mn^{2+} pool sizes decreased with depth along the transect, whereas Fe^{2+} pool sizes were unrelated to depth. Mn^{2+} pool sizes at the Itata Canyon stations were comparable to the transect values, whereas Fe^{2+} pool size magnitudes were lower (I_1) and higher (I_2) than the calculated pools.

3.4. Benthic nitrogen fluxes

Fig. 4A summarizes the benthic fluxes of DIN, urea, and DON. In general, NH_4^+ benthic fluxes were towards the water column (effluxes), ranging from 1.2 to 5.6 mmol $m^{-2} d^{-1}$, and decreased with depth along the transect stations. The value at Station I_2 was similar to that of the bay, whereas Station I_1 presented an influx (-5.3 mmol $m^{-2} d^{-1}$). Benthic fluxes of $NO_3^- + NO_2^-$ were always influxes, varying from -0.6 to -4.3 mmol $m^{-2} d^{-1}$. These fluxes presented an increasing uptake with depth at the transect stations, considering that the high error for Station 4 results in a near-zero rate. At the Itata Canyon stations, the influx was higher at Station I_2 than at Station I_1.

Low-magnitude (near zero) benthic fluxes of urea were observed at the transect stations (-0.03 to -0.14 mmol $m^{-2} d^{-1}$), whereas, at the Itata Canyon stations, these rates were higher (-1.67 to -2.77 mmol $m^{-2} d^{-1}$). Benthic fluxes of DON showed a high heterogeneity in direction and magnitude among the stations, with effluxes (4.9 to 75 mmol $m^{-2} d^{-1}$) at coastal stations (4, 18, and I_2) and influxes (-9.7 to -20.5 mmol $m^{-2} d^{-1}$) at offshore stations (26, S_0 and I_1).

3.5. Nitrogen processes

Nitrogen rate processes (i.e. ammonification, denitrification, and potential nitrification) are presented in Fig. 4B. Ammonification rates ranged from 2.4 to 46.8 mmol $m^{-2} d^{-1}$ and decreased with depth along the transect stations. At the Itata Canyon stations, the rate was highest at Station I_2. Denitrification varied from 0.2 to 0.9 mmol $m^{-2} d^{-1}$, and except for Station 4, these rates decreased with depth at the transect stations and were lower at Station I_2 than at Station I_1. Potential nitrification ranged from 0.9 to 4.4 mmol $m^{-2} d^{-1}$, presenting the opposite spatial pattern than denitrification.

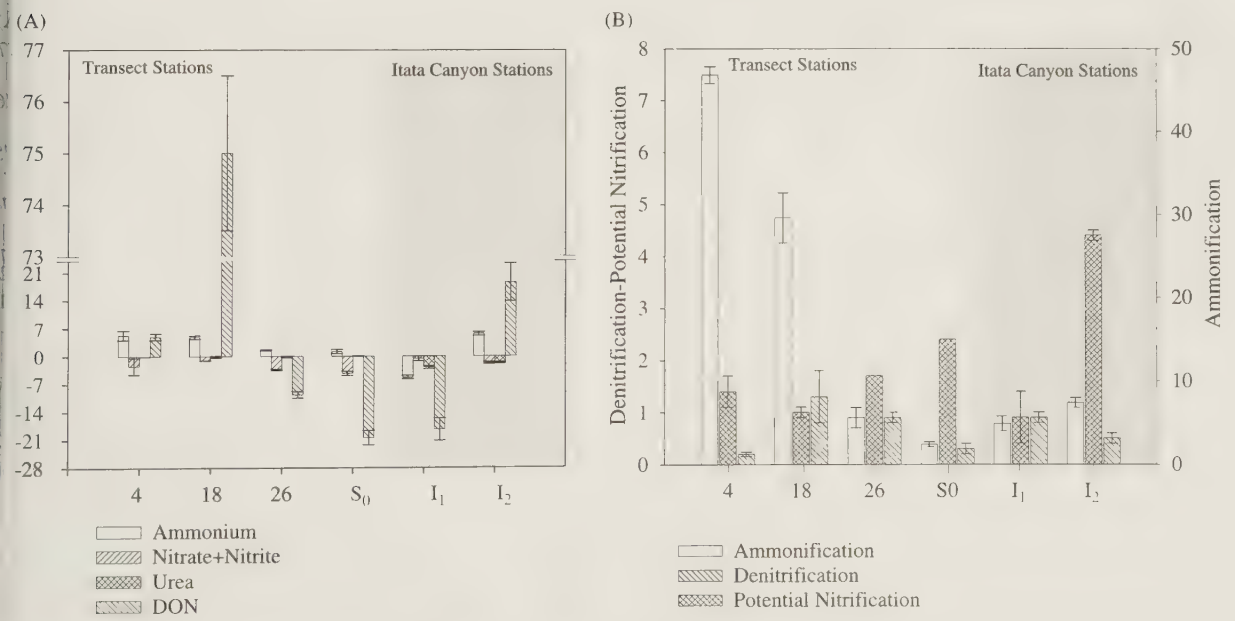

Fig. 4. (A) Average dissolved inorganic and organic nitrogen benthic fluxes (± propagation error); (B) nitrogen processes (±SD) evaluated for the sampled stations 4 (29 m), 18 (88 m), 26 (120 m), S_0 (820 m), I_1 (209 m) and I_2 (362 m).

4. Discussion

4.1. Organic matter and dissolved oxygen influence on geochemical sediment parameters and nitrogen processes

OM (Chl-a_{z0}) and DO conditions were found to group the sampling stations into three distinct environments (Table 3): (i) Concepción Bay, with high OM and anoxic conditions; (ii) the stations off the bay, with moderate to low OM and suboxic to oxic conditions; and (iii) the Itata Canyon stations, with low OM and suboxic conditions. Concepción Bay is also characterized by the presence of a flocculent layer at the sediment–water interface, which Graco et al. (2001) described as consisting of fresh OM aggregates (e.g., diatoms) and *Beggiatoa* spp. mats. Chl-a_{z0} was the only OM parameter that showed a clear trend with depth at the transect stations (Table 2); this is expected due to its sensitivity as an indicator of the fresh OM produced in the euphotic zone (Graf, 1992; Gutiérrez et al., 2000). However, the similarity of the Chl-a_{z0} magnitudes and phaeo:Chl-a_{z0} ratios of Station S_0 with the Itata Canyon stations, despite depth differences of ~500 m, indicate that different OM deposition-transport mechanisms could be affecting the Itata Canyon stations. These could include an OM income from a different origin, via lateral transport by bottom water currents, and/or OM loss due to the funnel effect of the canyons (Seibold and Berger, 1996).

It is likely that topographic effects in the Itata Canyon stations influenced the geochemical conditions, especially at Station I_1, located on the northern break of the 200 m isobath. Station I_1 sediments presented the lowest TOC_{z0}, TN_{z0}, and porosity, and the highest bulk density. The latter parameter is only comparable with >15 cm sediment horizons of the other stations (data not shown), suggesting a different sediment composition, e.g., heavy minerals. Thus, the low C:N_{z0} and C:Chl-a_{z0} ratios at this station were not related to high OM reactivity, as indicated by their low ammonification rates and NH_4^+ pool sizes. The location of the Itata Canyon station I_2, mid-canyon and nearer to the coast, could explain its

Table 3
Relevant geochemical aspects of the study stations and nitrogen remineralization processes balance

Station	Depth (m)	OM	DO	Amonification → nitrified (%)	Nitrification* → denitrificated (%)	Amonification-nitrication from Dn -NH_4^+ fluxes (mmol m^{-2} d^{-1})	Adsorption** (mmol m^{-2} d^{-1})	$NO_3^- + NO_2^-$ fluxes → denitrificated–Dn (mmol m^{-2} d^{-1})
Transect								
4	29	+ + +	+	3.0* (0.4)	14 [94]	41.3	26.3	2.5
18	88	+ +	+ +	3.4 * (3.1)	>100 [72]	23.9	16.8	0.7
26	120	+ +	+ +	30.4* (13.7)	53 [85]	3.2	3.1	3.3
S_0	820	+	+ + +	100* (11.4)	13 [91]	0.9	1.3	4.3
Itata canyon								
I_1	209	+	+ +	18.4* (13.2)	100 [72]	9.6	2.7	0.35
I_2	362	+	+ +	59.5* (5.5)	11 [81]	1.4	4.2	1.6

OM = organic matter, DO = dissolved oxygen.
+ (low), + + (moderate), + + + (high).
→ Coupled to.
*Potential nitrification was used.
Dn = denitrification coupled to nitrification obtained from IPT.
Values in round parentheses are obtained using nitrification from Dn.
Values in square parentheses are Dn.
**Adsorption – NH_4^+ accumulation rate*k (k = 1.3; Mackin and Aller, 1984).

higher TOC_{z0} and TN_{z0} content, ammonification rates, and NH_4^+ benthic efflux in comparison with Station I_1. On the other hand, both Itata Canyon stations presented the highest pore-water Mn^{2+} and Fe^{2+}, which may be attributed to high concentrations of labile Fe and Mn (hydroxy) oxides, entering via river runoff and only noticeable as a reduced form because of the low DO concentrations and biological utilization.

OM and DO also were found to control the sediment geochemical conditions (e.g., Eh_{z0}, Mn^{2+}, and Fe^{2+} first subsurface peak) and N regeneration processes. Ammonification and other related processes (NH_4^+ pool sizes and NH_4^+ benthic fluxes) varied according to fresh OM content, as evidenced by the significant correlation found between these variables and Chl-a_{z0}, ($r = 0.94, P < 0.05$) in the transect stations. Therefore, OM remineralized to NH_4^+ in the sediments was mainly produced in the euphotic zone, denoting a close coupling between primary production and the OM sediment oxidation process, as previously reported for this area (Thamdrup and Canfield, 1996; Glud et al., 1999; Gutiérrez et al., 2000; Graco, 2002). At some stations, however, NH_4^+ production could be linked to a chemoautotrophic *Thioploca* and *Beggiatoa* dissimilatory NO_3^- reduction to NH_4^+ (DNRA) (Graco et al., 2001; Zopfi et al., 2001). These NO_3^--storing, filamentous, sulfide-oxidizing bacteria were observed during the same cruise, with biomass ranging between 0.8 and 29.2 g wet m^{-2} (Fig. 5).

Except for within Concepción Bay, potential nitrification and denitrification seem to be influenced mainly by the DO gradient in the transect stations. Although a low DO value was observed at Station 26, previous data indicate that they are normally higher or similar to values at Station 18 (Gutiérrez, 2000). Optimal DO conditions are thought to immediately activate nitrification (Henriksen et al., 1981). In fact, higher potential nitrification rates were found toward deeper stations, where DO is higher. In addition, the negative correlation between DO and NH_4^+ pool sizes ($r = -1.00, P < 0.05$) provides indirect evidence of more active nitrification towards the deepest stations. The spatial DO trend also could be associated with denitrification rates that decrease towards the deeper stations. The potential nitrification and denitrification at the Itata Canyon stations presented the same patterns associated with a DO change.

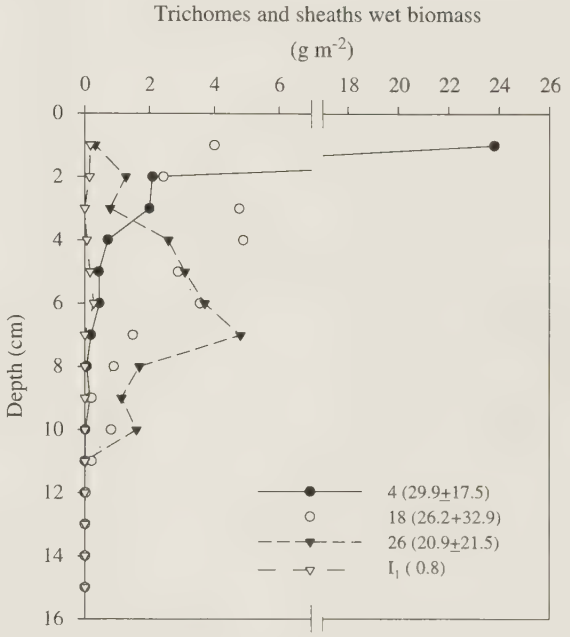

Fig. 5. *Thioploca* wet biomass distribution in the sediments of Stations 4 (29 m), 18 (88 m), 26 (120 m) and I_1 (209 m). In parenthesis, total wet biomass (g m^{-2}), ± = SD. Data provided by Pamela González.

In the case of Concepción Bay, where the conditions of the water overlying the sediment are anoxic and show higher NO_3^-, the lowest denitrification rates and high-potential nitrification rates were observed. This odd situation was previously reported by Graco et al. (2001) and two potential explanations were given: sulfide inhibition mechanisms and/or substrate competition between denitrifiers and *Beggiatoa* spp. Indeed, the low denitrification rate in the bay sediments could be associated with high biomass of filamentous bacteria (Fig. 5), which probably consume NO_3^- through storage and/or DNRA activity. The high potential nitrification rate in the bay could be explained by a fast response of the nitrifying microbial community to favorable changes, like oxygenation. Periodic oxygenation is expected in the bay due to mixing in the water column, mainly

during fall–winter but also during the relaxation phase of spring–summer upwelling (e.g., Ahumada and Chuecas, 1979).

4.2. Benthic nitrogen fluxes

In general, during the study period, the sediments off central Chile consumed DIN as $NO_3^- + NO_2^-$ and produced DIN as NH_4^+ at a mean rate ($\pm$SD) of -2.3 ± 1.4 and $3.7 \pm 2.1\,mmol\,m^{-2}\,d^{-1}$, respectively (values averaged from Fig. 4A). DON fluxes were more variable in magnitude and direction, being produced and consumed at a mean rate of 32.8 ± 37.2 and $-16.2 \pm 5.7\,mmol\,m^{-2}\,d^{-1}$, respectively. Urea was mainly consumed in the sediments at an average rate of $-0.96 \pm 1.2\,mmol\,m^{-2}\,d^{-1}$. The magnitudes and benthic flux directions of DIN, DON and urea followed their concentrations in the overlying water. DIN concentrations in the bottom water were lower than in the overlying water, probably because the rosette sampled at ~0.5 m above the sediment.

Potential biases during sediment incubations also could influence DIN benthic fluxes (discussed below), especially those related to a decrease or even depletion of DO. The DO sensor determinations showed non-significant changes after the incubations (data not shown). However, DO depletion at concentrations $<10\,\mu M$ (Table 1) was undetectable because of the limited sensitivity of the sensor used. In addition, DO consumption during the incubations was evaluated through the Winkler method (data not shown), but, except for Station S_0, we failed to obtain representative DO values due to oxygenation during sampling of water overlying the sediment. At Station S_0, DO Winkler data showed no depletion after the incubation (initial DO ~150 and final DO $\sim 100\,\mu M$). If DO depletion occurred during the incubations at the stations with DO $<10\,\mu M$, this should not interfere with NH_4^+ regeneration processes, and consequently not with NH_4^+ benthic fluxes, since they are mainly driven by anaerobic processes such as SO_4^{2-} reduction (Thamdrup and Canfield, 1996). Conversely, nitrification still could be active at DO $<10\,\mu M$, as was evidenced by denitrification coupled to nitrification (Dn, Table 3). For this reason, DO depletion could stop nitrification and overestimate NH_4^+ fluxes and NO_3^- influxes, at a magnitude similar to that of the denitrification coupled to nitrification process (Dn, i.e. $0.19–0.9\,mmol\,m^{-2}\,d^{-1}$).

DON benthic fluxes were high (despite an underestimation of >12% by the wet oxidation technique), but comparable with previously reported rates for the study area (Molina, 2002) and for estuaries and coastal sediments (e.g., Burdige and Zheng, 1998). DON fluxes and ammonification rates were significantly correlated when all the stations data were pooled (Spearman rank test, $r = 0.83, P < 0.05$). This can be attributed to the fact that DON effluxes were found at stations situated <30 km offshore (Stations 4, 18, and I_2), where high ammonification rates were measured. DON effluxes usually have been observed in coastal environments and in enrichment studies after a fresh OM addition (e.g., Hansen and Blackburn, 1991; Enoksson, 1993; Burdige and Zheng, 1998). On the other hand, DON influxes were measured at the most offshore stations (>52 km). DON could be a reactive fraction of dissolved OM, and has even been used as a quality indicator in comparison to dissolved organic carbon (Burdige and Zheng, 1998; Pedersen et al., 1999). Therefore, DON could be used for remineralization processes and also as a N source for marine bacterial growth. The DON influx at Station I_1 also coincided with a high urea influx. Urea has been considered a poor C source (Goldman et al., 1987) but a good N source for marine bacteria (Lomstein et al., 1989; Pedersen et al., 1999).

4.3. Nitrogen cycling imbalances and its possible explanations

A nitrogen process balance was constructed to evaluate the NH_4^+ fate in the study area (Table 3). First, the amount of NH_4^+ oxidized from the ammonification (ammonification → nitrification) was calculated using independently measured potential nitrification rates; the resulting values varied between 3.0 and 100%. However, potential nitrification may overestimate in situ rates because

nitrifiers are incubated under optimal DO and substrate conditions. When the nitrification rate obtained from denitrification coupled to nitrification process (Dn) was used, the coupling between ammonification–nitrification was lower (0.4–13.7%). The balance was obtained by subtracting the nitrification (obtained from Dn) and NH_4^+ fluxes rates from the ammonification rates. These results were compared with the expected NH_4^+ sediments adsorption (Table 3). The results indicated that Stations 26 and S_0 were in balance, while the sediments of Stations 4, 18, and I_1 presented an NH_4^+ excess (30–>100%) compared with adsorption. At Station I_2, an NH_4^+ deficit (>100%) was obtained, indicating that the adsorption requirement was not accomplished.

Following the traditional DIN transformation pathways (nitrification→denitrification), the denitrification rates presented a wide degree of coupling with the potential nitrification rates (11–>100%), whereas Dn showed a high degree of coupling at all the stations (>72%, Table 3). Denitrification rates, uncoupled with nitrification (−Dn), could explain a lower fraction of $NO_3^- + NO_2^-$ influxes (0.5–42%). If nitrification was stopped during the benthic flux incubations, then total denitrification could explain >100% of the $NO_3^- + NO_2^-$ influxes at Stations 18 and I_1, and from 7% to 29% at the rest.

The imbalances between NH_4^+ production and consumption processes indicates potential incubation biases associated with slurry versus whole-core experiments (Hansen et al., 2000) but also the presence of other benthic processes. The NH_4^+ excess observed in some sediment samples suggests that the slurry experiments could stimulate remineralization over NH_4^+ consumption processes, in comparison with the benthic flux incubations. Higher ammonification rates were observed in sediments with higher OM availability (i.e. Station 4 vs.18). In fact, during the slurry incubations, a higher interaction between microorganisms and substrates, macrofaunal decay, and/or viral influence is expected and this could determine higher ammonification rates than in the in situ or benthic fluxes incubations (Hansen et al., 2000).

The ammonification experiments were carried out under anoxic conditions, thus only anaerobic NH_4^+ consumption processes could be balancing its accumulation; adsorption is almost invariant in the sediment of the study area (Graco, 2002). The anaerobic NH_4^+ consumption potential in the sediments of the study area is evidenced by the unbalanced N processes, the NH_4^+ influx observed (e.g., Station I_1), and by the almost homogeneous NH_4^+ vertical distribution in the sediments. The last feature was observed especially at the Itata Canyon stations (Fig. 3) and cannot be attributed to macrofaunal bioturbation activities. The predominant macrofauna are preferentially surface deposit feeders (~5 cm) at the prevalent DO conditions (data from the same cruise, Gallardo et al., 2004).

The questions that arise from this study are related to which anaerobic NH_4^+ consumption processes are going unnoticed during these incubations and what potential influence they could have in the sediments of the study area. Anaerobic NH_4^+ consumption pathways, like anammox (e.g., Thamdrup and Dalsgaard, 2002) and NH_4^+ oxidation to NO_3- and N_2 by Fe and Mn oxides (Luther et al., 1997; Hulth et al., 1999; Anschutz et al., 2000), have been studied in marine environments. According to Risgaard-Petersen et al. (2003), an overestimation of IPT denitrification rates occurs when anammox and denitrification coexist (Mn oxides NH_4^+ oxidation end in N_2, thus are also included in IPT estimations). Considering the low denitrification rates observed in the area, the anammox and/or metal NH_4^+ oxidation leading to N_2 production should play a minor role.

On the other hand, NO_3^- pore-water subsurface peaks could signal the occurrence of anoxic nitrification using Mn and Fe oxides (Hulth et al., 1999; Anschutz et al., 2000). In these sediments, NO_3^- peaks did not coincide with Mn^{2+} but with Fe^{2+} peaks at Station I_2 (>4 cm, Fig. 3). However, a low feasibility of this process is expected given the sediment geochemical conditions in the study area (Anschutz et al., 2000). Finally, NH_4^+ assimilation, a DO independent process, could also influence benthic fluxes (Blackburn et al., 1996; Pedersen et al., 1999). NH_4^+ assimilation could be occurring at Station I_1, where a presumably high microbial N demand also is expected due to the high urea, and also

DON, benthic influxes. Finally, the NH_4^+ deficit found after balancing at Station I_2 could indicate an additional NH_4^+ source being more important than OM remineralization. A possible explanation is DNRA, a process that could be more active in the benthic flux incubations than in the slurry incubations; NO_3^- availability in the former is higher than in the latter. The slurry incubations were amended with bottom water with less NO_3^- content.

The predominance of $NO_3^- + NO_2^-$ influxes (not explained by denitrification) and NH_4^+ benthic effluxes are features associated with DNRA (Childs et al., 2002). In the ocean, DNRA is carried out by several microorganisms as an anaerobic pathway (Samuelsson and Rönner, 1982), with rates ranging from 0.1 to $5.5\,mmol\,m^{-2}\,d^{-1}$ (or even higher $\sim 55\,mmol\,m^{-2}\,d^{-1}$) (An and Gardner, 2002). In the study area, a benthic NO_3^- consumption not directly coupled with denitrification has been attributed to *Thioploca* NO_3^- accumulation and/or DNRA metabolism (Thamdrup and Canfield, 1996; Zopfi et al., 2001). In fact, a slightly lower *Beggiatoa* total wet biomass ($17.9\,g\,m^{-2}$) than that found in this study ($\sim 25\,g\,m^{-2}$), can produce $0.63\,mmol\ NH_4^+\,m^{-2}\,d^{-1}$ by DNRA (Graco et al., 2001), values that are in the range of $NO_3^- + NO_2^-$ influxes observed in our study.

Acknowledgments

The authors thank. D. Burdige for his help with DON inter-calibration, the Max Planck Institute for Marine Microbiology for the CHN analysis. The crews of the R.V. *Vidal Gormaz* and the R.V. *Kay Kay* are acknowledged for their help during the cruises, and D. Gutiérrez, R. Castro and the "Benthos group" for collaboration during the cruises and sediment analyses. P. González provided data on filamentous sulfide-oxidizing bacteria. The comments of three anonymous reviewers and the editors helped improve this manuscript. Financial assistance was provided by the Comisión Nacional de Investigaciones Científicas y Tecnológicas (CONICYT) through FONDECYT Grant No. 198-0544, the FONDAP-Humboldt Program and the FONDAP-COPAS Center (Project No. 150100007). V.M. was supported by a graduate fellowship from Fundación Andes and the MECESUP UCO0002 project.

References

Ahumada, R., Chuecas, L., 1979. Algunas características hidrográficas de Bahía de Concepción (36° 40′S; 73° 02′W) y áreas adyacentes. Gayana Miscelanea 8, 3–56.

An, S., Gardner, W.S., 2002. Dissimilatory nitrate reduction to ammonium (DNRA) as a nitrogen link, versus denitrification as a sink in a shallow estuary (Laguna Madre/Baffin Bay, Texas). Marine Ecology Progress Series 237, 41–50.

Anschutz, P., Sundby, B., Lefrancois, L., Luther III, G.W., Mucci, A., 2000. Interactions between metal oxides and species of nitrogen and iodine in bioturbated marine sediments. Geochimica et Cosmochimica Acta 64, 2751–2763.

Blackburn, T.H., Hall, P.O., Hulth, S., Landen, A., 1996. Organic-N loss by efflux and burial associated with a low efflux of inorganic N and with nitrate assimilation in Arctic sediments (Svalbard, Norway). Marine Ecology Progress Series 141, 283–293.

Brandhorst, W., 1971. Condiciones oceanográficas estivales frente a la costa de Chile. Revista de Biologia Marina, Valparaiso 4, 34–84.

Burdige, D., Zheng, S., 1998. The biogeochemical cycling of dissolved organic nitrogen in estuarine sediments. Limnology and Oceanography 43, 1796–1813.

Cáceres, M., 1992. Vórtices y filamentos observados en imágenes de satélite frente al área de surgencia de Talcahuano, Chile Central. Investigación Pesquera (Chile) 37, 55–66.

Canfield, D.E., 1994. Factors influencing organic carbon preservation in marine sediments. Chemical Geology 114, 315–329.

Childs, C.R., Rabalais, N.N., Turner, R.E., Proctor, L.M., 2002. Sediment denitrification in the Gulf of Mexico zone of hypoxia. Marine Ecology Progress Series 204, 285–290.

Daneri, G., Dellarrosa, V., Quiñones, R., Jacob, B., Montero, P., Ulloa, O., 2000. Primary production and community respiration in the Humboldt Current System off Chile and associated oceanic areas. Marine Ecology Progress Series 197, 41–49.

Enoksson, V., 1993. Nutrient recycling by coastal sediments: effects of added algal material. Marine Ecology Progress Series 92, 245–254.

Farías, L., Chuecas, L., Salamanca, M., 1996. Reactividad y remineralización de carbono orgánico total y nitrógeno total en sedimentos anóxicos de Bahía de Concepción. Gayana Oceanológica 4, 117–127.

Gallardo, V.A., Palma, M., Carrasco, F.D, Gutiérrez, D., Levin, L.A., Cañete, J.I., 2004. Macrobenthic zonation caused by the oxygen minimum zone on the shelf and slope

off central Chile. Deep-Sea Research II, this issue [doi:10.1016/j.dsr2.2004.07.028].

Glud, R.N., Gundersen, J.K., Holby, O., 1999. Benthic in situ respiration in the upwelling area off central Chile. Marine Ecology Progress Series 186, 9–18.

Goldman, J.C., Caron, D.A., Dennett, M.R., 1987. Regulation of gross growth efficiency and ammonium regeneration in bacteria by substrate C:N ratio. Limnology and Oceanography 32, 1239–1252.

González, H.E., Ortiz, V.C., Sobarzo, M., 2000. The role of faecal material in the particulate organic carbon flux in the northern Humboldt Current, Chile (23°S), before and during the 1997–1998 El Niño. Journal of Plankton Research 22, 499–529.

Graco, M., 2002. Sedimentos del área de surgencia costera de Chile central (36°S): Fuente o sumidero de nitrógeno? Ph.D. Thesis, Universidad de Concepción, Chile.

Graco, M., Farías, L., Molina, V., Gutiérrez, D., Nielsen, L.P., 2001. Massive developments of microbial mats following phytoplankton blooms in a naturally eutrophic bay: implications for nitrogen cycling. Limnology and Oceanography 46, 821–832.

Graf, G., 1992. Benthic–Pelagic coupling: a benthic view. Oceanography and Marine Biology: An Annual Review 30, 140–190.

Gutiérrez, D., 2000. Tasas de bioperturbación en sedimentos de un área de surgencia de Chile central (36°S). Ph.D. Thesis, Universidad de Concepción, Chile.

Gutiérrez, D., Gallardo, V.A., Mayor, S., Neira, C., Vásquez, C., Sellanes, J., Rivas, M., Soto, A., Carrasco, F., Baltazar, M., 2000. Effects of dissolved oxygen and fresh organic matter on the bioturbation potential of macrofauna in sublitoral sediments off Central Chile during the 1997/1998 El Niño. Marine Ecology Progress Series 202, 81–99.

Håkanson, L., Jansson, M., 1983. Principles of Lake Sedimentology. Springer, Berlin, 316pp.

Hansen, L.S., Blackburn, T.H., 1991. Aerobic and anaerobic mineralization of organic material in marine sediment microcosms. Marine Ecology Progress Series 75, 283–291.

Hansen, J.W., Thamdrup, B., Jorgensen, B.B., 2000. Anoxic incubation of sediment in gas-tight plastic bags: a method for biogeochemical process studies. Marine Ecology Progress Series 208, 273–282.

Henriksen, K., Kemp, W.M., 1988. Nitrification in estuarine and coastal marine sediments. In: Blackburn, T.H., Sorensen, J. (Eds.), Nitrogen Cycling in Coastal Marine Environments. Wiley, New York, pp. 207–249.

Henriksen, K., Hansen, J.I., Blackburn, T.H., 1981. Rates of nitrification, distribution of nitrifying bacteria and nitrate fluxes in different sediment from Danish water. Marine Biology 61, 299–304.

Hulth, S., Aller, R.C., Gilbert, F., 1999. Coupled anoxic nitrification/manganese reduction in marine sediments. Geochimica et Cosmochimica Acta 63, 49 66.

Lee, C., Cronin, C., 1982. The vertical flux of particulate organic nitrogen in the sea: decomposition of amino acids in the Peru upwelling area and equatorial Atlantic. Journal of Marine Research 40, 227–251.

Lomstein, B.A., Blackburn, T.H., Henriksen, K., 1989. Aspects of nitrogen and carbon cycling in the northern Bering Shelf sediment. I. The significance of urea turnover in the mineralization of NH_4^+. Marine Ecology Progress Series 57, 237–247.

Luther III, G.W., Sundby, B., Lewis, B.L., Brendel, P.J., Silverberg, N., 1997. Interactions of manganese with the nitrogen cycle: alternative pathways to dinitrogen. Geochimica et Cosmochimica Acta 61, 4043–4052.

Mackin, J.E., Aller, R.C., 1984. Ammonium adsorption in marine sediments. Limnology and Oceanography 29, 250–257.

Molina, V., 2002. Flujos de Nitrógeno Orgánico Disuelto (NOD), un indicador de la capacidad degradadora de los sedimentos costeros de Chile Central (36°S). M.Sc. Thesis, Universidad de Concepción, Chile.

Newell, B.S., Morgan, B., Cundy, J., 1967. The determination of urea in seawater. Journal of Marine Research 25, 201–202.

Nielsen, L.P., 1992. Denitrification in sediments determined from nitrogen isotope pairing FEMS. Microbiology Ecology 86, 357–362.

Parsons, T., Maita, Y., Lalli, C.M., 1984. A Manual of Chemical and Biological Methods for Seawater Analysis. Pergamon Press, New York, 173pp.

Pedersen, T.F., Calvert, S.E., 1990. Anoxia vs. productivity: What controls the formation of organic-carbon-rich sediments and sedimentary rocks? The American Association of Petroleum Geologist Bulletin 74, 454–466.

Pedersen, A-G.U., Berntsen, J., Lomstein, B.A., 1999. The effect of eelgrass decomposition on sediment carbon and nitrogen cycling. A controlled laboratory experiment. Limnology and Oceanography 44, 1978–1992.

Risgaard-Petersen, N., Nielsen, L.P., Rysgaard, S., Dalsgaard, T., Meyer, R.L., 2003. Application of the isotope pairing technique in sediments where anammox and denitrification coexist. Limnology and Oceanography Methods 1, 63–73.

Rowe, G.T., Clifford, C.H., Smith, K.L., Hamilton, P.L., 1975. Benthic nutrient regeneration and its coupling to primary productivity in coastal waters. Nature 255, 215–217.

Samuelsson, M-O., Rönner, U., 1982. Ammonium production by dissimilatory nitrate reducers isolated from Baltic sea water, as indicated by ^{15}N study. Applied and Environmental Microbiology 44, 1241–1243.

Seibold, E., Berger, W.H., 1996. The Sea Floor. An Introduction to Marine Geology, third ed. Springer, New York, 356pp.

Silva, N., Konow, D., 1975. Contribución al conocimiento de las masas de agua del Pacífico Sudoriental. Revista Pacífico Sur 3, 63 75.

Sloth, N.P., Blackburn, H., Hansen, L.S., Risgaard-Petersen, N., Lomstein, B.A., 1995. Nitrogen cycling in sediments with different organic loading. Marine Ecology Progress Series 116, 163–170.

Solorzano, L., 1969. Determination of ammonium in natural waters by the phenol hypochlorite method. Limnology and Oceanography 14, 799–801.

Stal, L.J., Van Gamerden, H., Krumbein, W.E., 1984. The simultaneous assay of chlorophyll and bacteriochlorophyll in natural microbial communities. Journal of Microbial Methods 2, 295–306.

Strub, P.T., Mesías, J.M., Montecino, V., Rutllant, J., Salinas, S., 1998. Coastal ocean circulation off western South America. In: Robinson, A.R., Brink, K.H. (Eds.), The Sea, vol. 11. Wiley, New York, pp. 273–313.

Summerhayes, C.P., 1983. Sedimentation of organic matter in upwelling regimes. In: Thiede, J., Suess, E. (Eds.), Coastal Upwelling: Its Sediment Record. Part B. Plenum Press, New York, pp. 29–72.

Thamdrup, B., Canfield, D.E., 1996. Pathways of carbon oxidation in continental margin sediments off central Chile. Limnology and Oceanography 41, 1629–1650.

Thamdrup, B., Dalsgaard, T., 2002. Production of N_2 through anaerobic ammonium oxidation coupled to nitrate reduction in marine sediments. Applied and Environmental Microbiology 68, 1312–1318.

Wakeham, S.G., Lee, C., 1993. Production, transport, and alteration of particulate organic matter in the marine water column. In: Engel, M.H., Macko, S.A. (Eds.), Organic Geochemistry. Plenum Press, New York, pp. 145–169.

Williams, P.J., Jenkinson, N.W., 1982. A transportable microprocessor controlled precise Winkler titration suitable for field station and shipboard use. Limnology and Oceanography 27, 576–584.

Zar, J.H., 1999. Bioestatistical Analysis, fourth ed. Prentice-Hall, Englewood Cliff, NJ, 718pp.

Zopfi, J., Kjaer, T., Nielsen, L.P., Jorgensen, B.B., 2001. Ecology of *Thioploca* spp.: nitrate and sulfur storage in relation to chemical microgradients and influence of *Thioploca* spp. on the sedimentary nitrogen cycle. Applied and Environmental Microbiology 67, 5530–5537.

ELSEVIER

Deep-Sea Research II 51 (2004) 2523–2541

DEEP-SEA RESEARCH
PART II

www.elsevier.com/locate/dsr2

Recent sedimentation and mass accumulation rates based on ^{210}Pb along the Peru–Chile continental margin

P. Muñoz[a,b,*], C.B. Lange[b,c], D. Gutiérrez[d], D. Hebbeln[e], M.A. Salamanca[c], L. Dezileau[b,f], J.L. Reyss[g], L.K. Benninger[h]

[a]*Departamento de Biología Marina, Universidad Católica del Norte, Larrondo 1281, Coquimbo, Chile*
[b]*Centro de Investigación Oceanográfica en el Pacífico Sur-Oriental (FONDAP-COPAS), Casilla 160-C, Concepción, Chile*
[c]*Departamento de Oceanografía, Universidad de Concepción, Casilla 160-C, Concepción, Chile*
[d]*Dirección de Investigación Oceanográfica, Instituto del Mar del Perú (IMARPE), Casilla 22, Callao, Lima, Perú*
[e]*Fachbereich Geowissenschaften, Research Center Ocean Margins (RCOM), Universität Bremen, Postfach 33044, D-28334 Bremen, Germany*
[f]*Laboratoire de Dynamique de la Lithosphère (LDL), Bâtiment 22, 1er étage, Université de Montpellier 2, Place Eugène Bataillon, 34095 Montpellier Cedex 05, France*
[g]*Laboratoire des Sciences du Climat et de l'Environnement, Laboratoire mixte C.E.A-C.N.R.S., 91198 Gif sur Yvette Cedex, France*
[h]*Department of Geological Sciences, University of North Carolina, Chapel Hill, NC 27599-3315, USA*

Accepted 21 July 2004

Abstract

The concentrations of the natural radionuclide ^{210}Pb were measured in sediment samples collected with a multicorer, boxcorer, and gravity corers along the Chilean continental margin (20–45 °S) in order to estimate sedimentation rate (SR) and mass accumulation rate. This database was compared with previously obtained results from central Peru (Callao). ^{210}Pb activities decreased exponentially with core depth and profiles showed a deepening of the ^{210}Pb in excess (unsupported) in the sediments from north to south (~6–18 cm sediment depth off Peru and northern Chile vs. 8–35 cm off central and southern Chile. An onshore–offshore decrease of surface activities was observed off central Peru whereas the reverse was true for surface activities along the Chilean margin. SRs increased from north (0.04–0.17 cm yr^{-1}) to south (0.09–0.29 cm yr^{-1}). Across the shelf, higher rates were observed at deeper sites, especially at those close to submarine canyons, except off central Peru, where SRs showed similar values through the slope area. Off northern Chile and central Peru, SRs seem to reflect the export of particles over the shelf and redistribution processes such as slumps and lateral transport. In contrast, SRs in central and southern Chile seem to be controlled by several additional factors that modulate the settling particles, such as onshore precipitation and river runoff. In addition, the more complex topography of the southern Chile margin allows for settling or winnowing areas.
© 2004 Elsevier Ltd. All rights reserved.

*Corresponding author. Centro de Investigación Oceanográfica en el Pacífico Sur-Oriental (FONDAP-COPAS), Casilla 160-C, Concepción, Chile. Tel.: +56 51 209802; fax: +56 51 209812.
E-mail address: praxedes@ucn.cl (P. Muñoz).

0967-0645/$ - see front matter © 2004 Elsevier Ltd. All rights reserved.
doi:10.1016/j.dsr2.2004.08.015

1. Introduction

Sediment rate and mass accumulation rate (MAR) are useful to understand sediment-transport processes and the flux of the major constituents of the sediments, as lithogenic and organic components, both important for geochemical studies (Alperin et al., 2002; Borole, 2002; Gorgas and Wilkens, 2002; Masqué et al., 2002, 2003; Oguri et al., 2003). Export of particles derived from primary production together with terrestrial input through river runoff and coastal erosion are the main sources of the material deposited in the sediments. In addition, eolian transport of lithogenic particles could constitute an important input to the deep-sea sediments, as has been described for the Atlantic and Pacific oceans (e.g., Blank et al., 1985; Chester, 1990). Size, shape, and composition of settling particles are important factors that determine transport and preservation in the sediments. Moreover, morphologic characteristic of the seafloor, such as the presence of canyons, slope terraces, and ridges, govern sediment accumulation patterns (Masqué et al., 2003).

^{210}Pb has been extensively used in studies of sedimentation processes and, despite some limitations of the methodology, it has demonstrated to be a useful tool to estimate recent sedimentation rates (SRs) (McCaffrey and Thomson, 1980; Cochran, 1982; Smoak et al., 2000; Lewis et al., 2002; Masqué et al., 2002, 2003; Oguri et al., 2003). ^{210}Pb is a natural product of the ^{238}U decay series with a half-life of 22.3 yr. It enters the oceans predominantly by the decay of ^{226}Ra in seawater, and by the decay of ^{222}Rn in the atmosphere and subsequent rainout to the ocean surface. ^{210}Pb is efficiently scavenged by suspended fine particles and thus actively removed from seawater on timescales comparable to its half-life (Henderson and Maier-Reimer, 2002); it is deposited on the seafloor, producing an excess with respect to ^{226}Ra decay within the sediments. This allows the estimation of mass accumulation and SRs in environments where productivity and advective processes are considered to be important aspects in the distribution and removal of ^{210}Pb in the water column (Thomson and Turekian, 1976; Cochran, 1982; Nozaki et al., 1997; Henderson and Maier-Reimer, 2002).

Little is known about SR and accumulation rate over the past ~100 yr in the eastern South Pacific margin. Here, the Humboldt Current System (HCS), one of the most productive eastern boundary systems in the world resulting from persistent wind-driven upwelling cells occurring along the Peruvian and Chilean coasts (e.g., Berger et al., 1987; Dellarosa, 1998; Strub et al., 1998), can constitute an important source of particles for the shelf sediments. However, differences in mass accumulation and SRs can be expected along the continental margin due to (a) latitudinal variability of primary productivity and upwelling, (b) distinct hydrological regimes, and (c) topography.

Biological, physical, chemical, and geological characteristics define four distinct areas in the coastal HCS: (A) Peru coast (7–12 °S), with sustained upwelling during the year and high average primary production rates (3.8 g C m^{-2} d^{-1}) (Chávez et al., 1989) and a well-developed mid-water oxygen minimum zone (OMZ; <22 μM or 0.5 ml l^{-1}, 50–600 m depth). (B) Northern Chile (~18–30°), with relatively low primary productivity in spite of permanent upwelling (it is considered a high nutrient–low chlorophyll area; Torres, 1995), although there are distinct upwelling cells with relatively high productivity (i.e., off Antofagasta, 9.3 g C m^{-2} d^{-1}) (Daneri et al., 2000). A well-developed, strong OMZ dominates the water column from 100 to 450 m depth (Blanco et al., 2001). (C) Central Chile (~35–38 °S), with the presence of an important upwelling center due to the predominance of southwesterly winds (Arcos and Wilson, 1984) and high primary productivity (maximum values of 9.9–19.9 g C m^{-2} d^{-1}) during the upwelling-favorable summer period (Bernal et al., 1989; Fossing et al., 1995; Dellarosa, 1998; Daneri et al., 2000). The OMZ is less intense (>0.5 ml l^{-1}) and its upper boundary is deeper (>100 m). (D) Southern Chile (south of 37 °S), where low-salinity waters at the surface are derived from the Chilean fjord region (Silva and Neshyba, 1979) and very high and persistent pigment concentrations (> 2 mg m^{-3}) have been reported (Thomas et al., 2001); the OMZ is not well-established here.

These areas present distinct hydrological regimes. The central Peru–northern Chile area, with the Atacama desert, is an extremely arid zone without relevant fluvial inputs into the ocean. The maximum amount of precipitation in Peru is 20 mm yr^{-1} and in northern Chile, 2 mm yr^{-1}. This is significantly lower than in central and southern Chile (300 to >1000 mm yr^{-1}) (www.meteochile.cl), where fluvial drainage basins can be large and river discharges are high (1–5 to ~23–100 km^3 yr^{-1}, respectively) (Arcos et al., 1996; Parra and Habit, 1998; DGA-Dirección General de Aguas, Chile, www.dga.cl). Such rivers are an important source of sediment from the Andes and the Coastal Range to the ocean (Habit et al., 1998; Lamy et al., 1998, 1999; Pineda, 1999).

Finally, even the topography of the margin is widely variable. The shelf is relatively wide off central Peru (40–60 km) (Strub et al., 1998), extremely narrow from southern Peru to northern Chile (10–15 km), and wide and interrupted by submarine canyons off central and southern Chile (~65 km) (Scholl et al., 1970; Thornburg and Kulm, 1987a, b). The prominent canyons in this area are the San Antonio (33 °S) and Bio-Bio Canyons (37 °S) (Hagen et al., 1996; Pineda, 1999; Sobarzo et al., 2001; Laursen and Normark, 2002). South of 42 °S, the Chilean margin is highly complex due to the presence of fjords, the drowned forearc basin, and the dissection of the coastal range into numerous islands (Lamy et al., 1998).

In this study, we present new estimates on SR and MAR along the Chilean margin between 20 and 42 °S using ^{210}Pb as a particle tracer; we then compare these estimates with those previously made for the area off Callao, Peru (12 °S). Our data set spans across a broad range of sedimentation regimes and includes very distinct areas differentiated by their primary production, continental input, and topography. We provide important information for a better understanding of the sedimentary processes along the Peru–Chile continental margin, which can then be used to evaluate fluxes of other major elements and help estimate mass balances of organic carbon, metals, or any particle-reactive element that is relevant to geochemical processes.

2. Material and methods

2.1. Collection and sampling of sediments

We report on sediment samples obtained from four margin areas: (a) central Peru (12 °S); (b) northern (20–22 °S); (c) central (36 °S); and (d) southern Chile (42 °S) (Fig. 1). Sediment samples from the Chilean margin were collected during several cruises between 1999 and 2002, using various coring devices (multicorer, MUC; box corer, BC; rhumor corer, RC) (Table 1). Sediments from off Callao, Peru, were retrieved during the Panorama III cruise onboard the R./V. *Melville* in December 1997–January 1998. Some of the data obtained during this cruise have already been published by Levin et al. (2002).

Sediment cores were sliced into 1-cm intervals and stored at −20 °C. Each sample was dried at 60°C to a constant weight (Cochran et al., 1998) and homogenized to determine: (i) organic matter content, by ignition at 550 °C in a muffle furnace (% loss of ignition, LOI); (ii) bulk sediment density, estimated from mass percent water and density of solids (2.65 g cm^{-3}); and (iii) ^{210}Pb activities, determined mainly by alpha spectrometry of its daughter, ^{210}Po (Flynn, 1968). Some samples were analyzed for ^{210}Pb and ^{226}Ra by Gamma counting in a high-resolution "well-type" Ge-detector at the Laboratoire de Sciences du Climate et l'Environnement (LSCE) at Gif-Sur-Yvette, France. ^{226}Ra analyses for samples from Peru were done by Gamma counting at the Department of Geological Sciences, University of North Carolina, Chapel Hill-NC, USA.

2.2. Chemical analysis

For ^{210}Pb chemical analysis, ~0.5 g of dry sediment was placed in a Teflon beaker and digested with a mixture of concentrated HCl, HNO_3, and HF spiked with ^{209}Po. The solutions were auto-plated onto silver disks at ~75 °C for 2.5 h in the presence of ascorbic acid. The activities obtained were corrected by the decay of ^{210}Po (half-life: 138 d) between plating and counting. Since a short time elapsed between sampling and

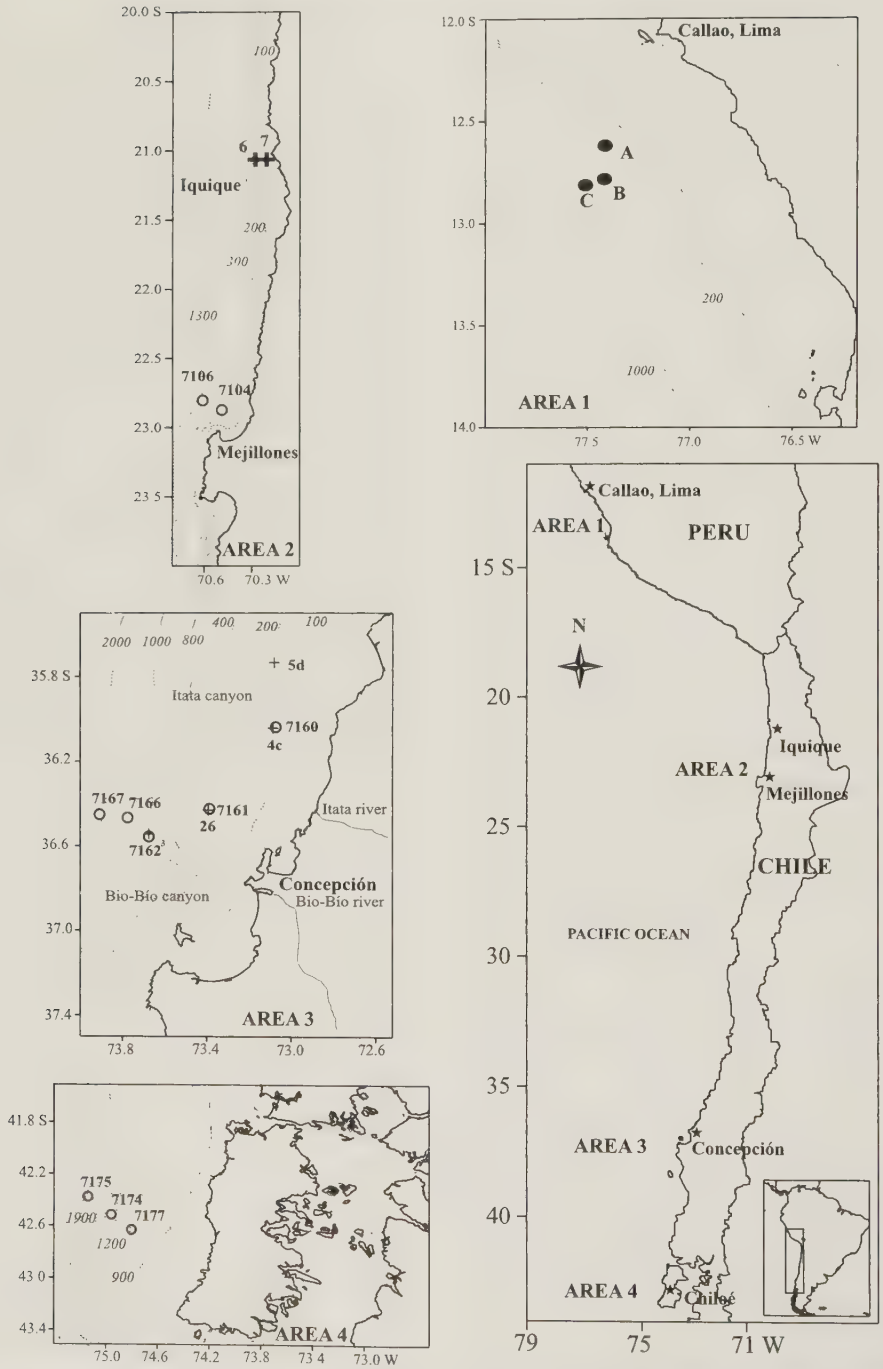

Fig. 1. Position of sampling stations off Peru (Area 1), northern Chile (Area 2), south-central Chile (Area 3), and southern Chile (Area 4) collected during several cruises: Peru, R./V. *Melville* Panorama III, December 1997–January 1998 (●); Chile, R./V. *Vidal Gormaz* Thioploca, March 1999 (+); R./V. *Sonne* SO 156, March–May 2001 (○); L./C. *Kay Kay* FONDAP-COPAS, March 2002 (○); L./C. *Carlos Porter* FONDAP-COPAS, April 2002 (+).

Table 1
Sampling locations along the Peru–Chile continental margin

Station	Location	Water depth (m)	Cruise	Sediment sampler	Core length (cm)
Callao					
Sta. A	12°22.7′S–77°29.1′W	305	A	MUC	50
Sta. B	12°32.5′S–77°29.6′W	562	A	MUC	18
Sta. C	12°32.8′S–77°34.8′W	830	A	MUC	25
Iquique					
Sta. 6	21°03.82′S–70°12.99′W	103	D	RC	16
Sta. 7	21°03.82′S–70°16.79′W	86	D	RC	37
Mejillones					
GEOB 7104	22°52.03′S–70° 29.39′W	312	C	MUC	30
GEOB 7106	22°48.02′S–70° 36.71′W	1351	C	MUC	25
Concepción					
5d	35°44.34′S–73°04.49′W	201	B	MUC	57
4c	36°02.38′S–73°05.10′W	364	B	MUC	70
GEOB 7160	36°02.34′S–73°04.39′W	365	C	MUC	34
26A	36°25.53′S–73°23.32′W	122	B	MUC	68
26B	36°25.67′S–73°23.34′W	123	E	BC	39
GEOB 7161	36°25.52′S–73°23.34′W	125	C	MUC	40
3	36°32.37′S–73°40.26′W	815	B	MUC	33
GEOB 7162	36°33.42′S–73°40.45′W	879	C	MUC	24
GEOB 7166	36°27.99′S–73°46.48′W	1294	C	MUC	19
GEOB 7167	36°27.10′S–73°54.48′W	2065	C	MUC	34
Chiloé					
GEOB 7177	42°34.96′S–74°50.21′W	905	C	MUC	28
GEOB 7174	42°32.66′S–75°01.10′W	1221	C	MUC	24
GEOB 7175	42°27.12′S–75°12.65′W	1961	C	MUC	25

A: Peru, R./V. *Melville*, Scripps Institution, Panorama III December 1997–January 1998 (from Levin et al., 2002).
B: Chile, R./V. *Vidal Gormaz*, SHOA-Chile, Thioploca, March 1999.
C: Chile, R./V. *Sonne* SO 156, Universität Bremen, March–May 2001.
D: Chile, L./C. *Carlos Porter*, Universidad de Antofagasta, Fondap-Copas, April 2002.
E: Chile, L./C. *Kay Kay*, Universidad de Concepción, Fondap-Copas, March 2002.
MUC: multicorer; BC: box corer; RC: Rhumor corer.

plating (0.5 yr), compared to the half-life of ^{210}Pb (22.3 yr), the activities were not corrected for this time lag. Analysis and counting were performed at the radioisotope laboratory of the Universidad de Concepción, Chile. Chemical assurance was evaluated by analyzing three replicates of International Atomic Energy Agency reference material (IAEA-326). The precision was 3.4%, corresponding to a reasonable deviation of the mean measured value ($49.5 \pm 1.7\,\mathrm{Bq\,kg^{-1}}$) with respect to the certified mean value ($53.3\,\mathrm{Bq\,kg^{-1}}$; range: 48.8–57.8).

2.3. Data analyses

Inventories (I) of $^{210}Pb_{xs}$ (unsupported) are expressed in $\mathrm{dpm\,cm^{-2}}$ and were calculated according to Turekian et al. (1980):

$$I = \Sigma A_i \rho_i h_i,$$

where A_i is the $^{210}Pb_{xs}$ ($\mathrm{dpm\,g^{-1}}$), ρ_i the bulk density in the i interval ($\mathrm{g\,cm^{-3}}$), and h the thickness of the interval (cm).

$^{210}Pb_{xs}$ activities were determined from the total ^{210}Pb minus the activity of its parent, ^{226}Ra. In

those cases where ^{226}Ra measurements were lacking, we used the ^{210}Pb asymptotic activity at depth, assumed to be in equilibrium with ^{226}Ra in the sediment, to determine unsupported activities ($^{210}Pb_{xs}$) (McCaffrey and Thomson, 1980; Cochran et al., 1998). The distribution of ^{210}Pb activities allowed us to obtain a good exponential fit ($r^2 \sim 0.95-0.99$, $n = 6-16$, Table 2) and the low variability of activities at depth (constant values), determined significant supported ^{210}Pb values at $0.01 < p < 0.1$. Although supported ^{210}Pb values estimated from the exponential fit have a higher uncertainty (±standard error, SE) tha values derived from ^{226}Ra measurements (±1 SD, σ), they are in agreement with ^{226}Ra value obtained at close-by stations off Concepción an Chiloé (Table 2). Standard deviations of ^{210}P inventories were estimated by propagating th counting uncertainties of ^{210}Pb and ^{226}Ra and th error introduced by the estimated supported ^{210}P (Bevington and Robinson, 1992). The highe uncertainty of the estimated supported ^{210}P implies higher standard errors in the inventor calculations (Table 2).

Table 2
Inventories and fluxes (±SD) determined from $^{210}Pb_{xs}$

Station	Supported ^{210}Pb (dpm g_{ash}^{-1})	Exp. fit r^2	^{226}Ra (dpm g_{ash}^{-1}) Surface	^{226}Ra (dpm g_{ash}^{-1}) Deep	Depth of excess (cm)	Inventory (dpm cm^{-2})	Flux (dpm cm^{-2} yr^{-1})
Callao							
Sta. A	—		7.8±0.90	23.6±0.14	16	103.9±1.75	3.2±0.1
Sta. B	—		33.8±0.20	3.8±0.07	—	—	—
Sta. C	—		4.9±0.08	7.1±0.11	6	23.2±0.5	0.7±0.01
Iquique							
Sta. 6	2.2±0.2	0.97	n.m.	n.m.	6	55.6±5.8	1.7±0.2
Sta. 7	1.7±0.1	0.95	n.m.	n.m.	4	37.3±3.7	1.2±0.1
Mejillones							
GEOB 7104			6.6±0.21	3.9±0.05	4	22.6±4.1	0.7±0.1
GEOB 7106	—		6.2±0.21	3.4±0.12	10	50.3±6.6	1.6±0.2
Concepción							
5d	1.4±0.1	0.98	n.m.	n.m.	23	116.7±11.4	3.6±0.4
4c	1.4±0.4	0.99	n.m.	n.m.	>20	288.2±48.7	9.0±1.5
GEOB 7160	—		1.6±0.07	1.4±0.07	35	132.5±7.3	4.1±0.2
26A	0.95±0.10	0.95	n.m.	n.m.	10	140.1±17.2	4.3±0.5
26B	1.10±0.15	0.98	n.m.	n.m.	10	78.1±3.9	2.4±0.1
GEOB 7161	—		1.4±0.05	0.8±0.04	8	54.1±2.6	1.7±0.1
3	2.3±0.1	0.95	n.m.	n.m.	20	265.5±17.4	8.3±0.5
GEOB 7162	—		2.3±0.21	2.4±0.02	20	169.8±9.9	5.3±0.3
GEOB 7166	—		3.9±0.29	2.5±0.07	24	165.3±5.0	5.1±0.2
GEOB 7167	4.9±1.8	0.99	n.m.	n.m.	18	153.9±61.3	4.8±1.9
Chiloé							
GEOB 7177	—		2.7±0.04	2.9±0.05	20	141.1±6.5	4.4±0.2
GEOB 7174	—		3.4±0.15	2.2±0.01	15	135.2±8.1	4.2±0.3
GEOB 7175	3.7±1.9	0.97	n.m.	n.m.	15	119.0±61.5	3.7±1.9

Note: Unsupported ^{210}Pb values were estimated at $0.01 < p < 0.1$ when no data of ^{226}Ra were available (^{226}Ra values ±σ). These data are shown for surface and deep sections to compare with estimated values. No ^{210}Pb excess to estimate the inventory was observed at Sta. B.
n.m.: Not measured.

SR and MAR were calculated from excess activities ($^{210}Pb_{xs}$) according to Christensen (1982), who assumed an exponential distribution of the density in the absence of mixing:

$$\rho = \rho_0 - \rho_1 e^{-az},$$

where ρ is the bulk density (g cm^{-3}), ρ_0 the bulk sediment density at infinite depth, ρ_1 the difference between the surface and the deep value, a the compaction coefficient, and z the depth in sediment. Most stations showed good density exponential fits ($r^2 = 0.83-0.98$, $n = 9-40$, $p < 0.01$, Table 3) to estimate MAR (r):

$$A = A_0 \exp(-\lambda/r[\rho_0 z - (\rho_1/a)(1 - e^{-az})]),$$

where $r = \rho v$ is the constant under steady-state conditions, expressed in g cm^{-2} yr^{-1}, and v the SR in cm yr^{-1}, λ the decay constant of ^{210}Pb (0.031 yr^{-1}), and z the depth (cm), A and A_0 are the unsupported $^{210}Pb_{xs}$ activities (dpm g^{-1}). A_0 is

Table 3
SR and MAR, and bulk density parameters from the exponential fit according to Christensen (1982)

Station	Bulk density parameters				Sediment mixed layer[a] (cm)	Accumulation rate (g cm^{-2} yr^{-1})	SR (cm yr^{-1})	Model r^2	CPE (μg/g)
	a	ρ_0	ρ_1	r^2					
Callao									
Sta. A	—	—	—	—	4–8	0.06±0.03	0.13±0.02[b]	0.96	99.4±2.3[b]
Sta. B	—	—	—	—	—	—	—	—	11.2±0.6[b]
Sta. C	0.91	0.51	0.27	0.97	[c]	0.04±0.01	0.10±0.01[b]	0.98	23.3±2.0[b]
Iquique									
Sta. 6	—	—	—	—	[c]	0.05±0.01	0.10±0.01	0.97	n.a.
Sta. 7	3.06	2.85	0.03	0.83	—	0.04±0.01	0.08±0.01	0.95	n.a.
Mejillones									
GEOB 7104	—	—	—	—	[c]	0.05±0.01	0.04±0.01	0.88	42.0±4.0[d]
GEOB 7106	1.29	0.61	0.07	0.98	[c]	0.12±0.02	0.17±0.03	0.85	25.1±0.6[d]
Concepción									
5d	1.33	0.52	0.06	0.91	4	0.18±0.04	0.24±0.05	0.98	n.a.
4c	1.88	1.46	0.01	0.98	8	0.11±0.01	0.26±0.03	0.99	n.a.
GEOB 7160	1.14	0.73	0.04	0.97	4	0.10±0.03	0.24±0.07	0.96	29.9±0.7[d]
26A	1.28	0.95	0.02	0.92	6	0.05±0.01	0.09±0.01	0.95	n.a.
26B	1.02	0.71	0.03	0.92	2	0.05±0.01	0.14±0.02	0.98	n.a.
GEOB 7161	1.05	0.73	0.03	0.92	—	0.05±0.004	0.15±0.01	0.96	85.3±12.0[d]
3	2.00	1.47	0.01	0.98	10	0.13±0.05	0.26±0.10	0.95	n.a.
GEOB 7162	0.70	0.36	0.24	0.95	10	0.08±0.01	0.25±0.04	0.96	24.5±2.3[d]
GEOB 7166	0.64	0.35	0.22	0.89	3	0.06±0.01	0.18±0.02	0.96	27.2±1.0[d]
GEOB 7167	0.59	0.35	0.12	0.96	1	0.04±0.004	0.18±0.02	0.99	31.9±5.5[d]
Chiloé									
GEOB 7177	0.57	0.36	0.19	0.99	1	0.05±0.003	0.22±0.01	0.98	27.9±4.6[d]
GEOB 7174	0.64	0.40	0.10	0.97	—	0.05±0.005	0.22±0.02	0.98	23.8±3.7[d]
GEOB 7175	1.15	0.86	0.05	0.95	0.5	0.05±0.01	0.29±0.04	0.97	17.8±0.3[d]

Note: Chloroplastic pigment equivalents (CPE in μg g^{-1}) at the top 0–1 cm±SD; and depth of sediment mixed layer (cm). n.a., Not available data.

[a]Homogeneous mixed layer.

[b]Previously published by Levin et al. (2002).

[c]Clear mixed layer not identified.

[d]J. Sellanes (unpublished data, Centro de Investigación Oceanográfica en el Pacífico Sur-Oriental, COPAS).

the activity at the water–sediment interface. This model uses the compaction coefficient a derived from the exponential fit to the density used to estimate the MAR r; therefore, the SR v shows an apparent exponential distribution downcore, satisfying the assumption of constant MAR. We report SR for surface sediments (not affected by compaction), while MAR corresponds to the accumulation of material deposited in the recent sediments (~last 100 yr), established by the half-life of ^{210}Pb.

In those cases where bulk density did not show an exponential distribution, SRs were estimated directly from:

$$A = A_0 e^{-(\lambda/v)z}$$

neither estimation considers the mixing effect. Since other radionuclides are not available for this study, we worked with the ^{210}Pb activities below the mixing layer as described by others (Lewis et al., 2002; Masqué et al., 2002; Oguri et al., 2003). Thus, our estimates on SR and MAR assume that mixing is negligible below the mixed layer, where sedimentation is the dominant process. The values reported here should be considered as upper limits. On the other hand, the use of a constant value to estimate the unsupported ^{210}Pb (in excess) where no ^{226}Ra data are available does not greatly affect SR estimations; ^{226}Ra is usually constant with depth and ^{226}Ra values agree well with ^{210}Pb values at the base of the sediment cores (Cochran et al., 1998; Radakovitch and Heussner, 1999; Oguri et al., 2003).

3. Results

3.1. Sediment characteristics

The sediments collected off Callao, Peru (Stations A at 305 m and B at 562 m) were dark, olive-green muds. At the deeper station (Station C at 830 m); the sediments consisted of a mixture of phosphoritic sand, foraminifera sand, and olive-green mud. At Station B, irregular phosphorite nodules were common. Off northern Chile, at Station GEOB7106 (1351 m) near Mejillones, the sediments were dark, muddy sands, whereas organic detritus and fish remains were observed at the shallower Station GEOB7104 (312 m) and in the sediments off Iquique (Stations 6 and 7 at 10 and 83 m, respectively). The latter contained significant amounts of poorly consolidated phosphorite nodules. Sediments from central (Concepción) and southern (Chiloé) Chile were olive-green

In general, sediment bulk density increased downcore (Fig. 2). Exceptions were Station B off Callao (Fig. 2A), where bulk density decreased from about 1.2 to 0.9 g cm^{-3}, and site GEOB7104 (Fig. 2C) off Mejillones, where it decreased strongly from 1.2 to 0.4 g cm^{-3}. Also, there was no downcore variation at Station 7 off Iquique (Fig. 2B) and values fluctuated around 0.6 g cm^{-3}. In the south (Figs. 2D–H), densities reached maximum values at depth (around 0.6–0.9 g cm^{-3}). Off Concepción, the stations sampled during the 1999 Thioploca cruise (26A, 3, 4c, 5d) showed slightly higher densities than those sites sampled during the 2001 R./V. *Sonne* cruise, even at similar locations (Figs. 2D–F).

Total organic matter (TOM) contents, expressed as the percentage obtained by LOI, had a distinct latitudinal pattern at the sediment surface, with higher values in the north than in the south (Fig. 3). Specifically, the highest values were observed at Station A off Callao (30–35%) (Fig. 3A) and at Station 7 off Iquique (25–30%) (Fig. 3B). Downcore, a sharp decrease was noted at Station 6 off Iquique, where TOM values dropped from >20% at the surface to <5% at 10 cm depth in the core (Fig. 3B). Off Mejillones, TOM fluctuations with depth were minimal (Fig. 3C). At all other stations, TOM content varied between 10% and 20%, decreasing with depth to <10%, except at Station GEOB7161 off Concepción, which showed two anomalous peaks at 50 and 70 cm depth (Fig. 3E). Another exception in this area was Station 5d, where the TOM content was low throughout the core (~6%) (Fig. 3D).

3.2. ^{210}Pb activities

In general, ^{210}Pb activities decreased exponentially with depth (Fig. 4), reaching constant values at ~6–18 cm depth off Callao (Fig. 4A), at 4–10 cm depth off Iquique (Fig. 4B) and Mejillones

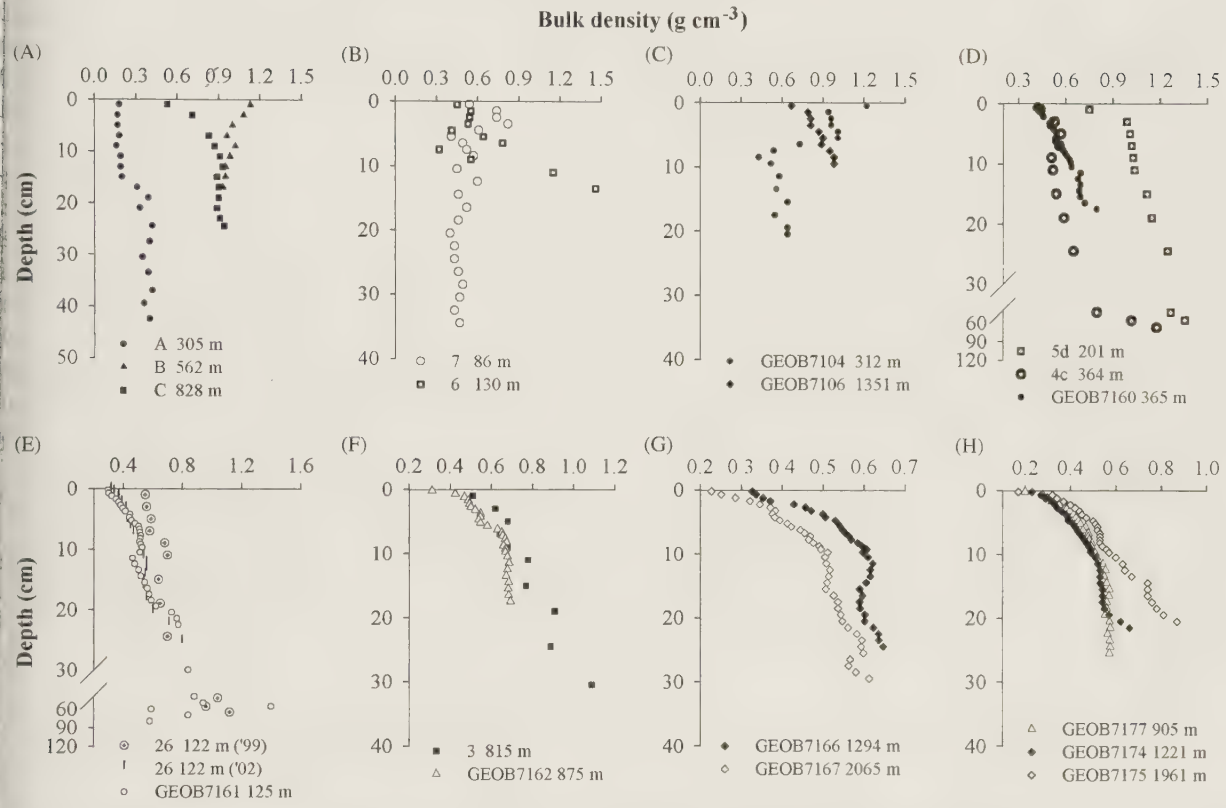

Fig. 2. Bulk sediment density profiles. Cores from central Peru: Callao (A), northern Chile; Iquique (B) and Mejillones (C), south-central Chile; Concepción (D–G, from north to south); southern Chile, Chiloé (H).

(Fig. 4C), and at 8–35 cm off Concepción (Fig. 4D) and Chiloé (Fig. 4E), showing a deepening of the ^{210}Pb in excess (unsupported) in the sediments toward southern areas (Table 2). An onshore–offshore decrease of surface activities was observed off central Peru, from ~60 dpm g^{-1} at coastal Station A to 32 and 14 dpm g^{-1} at the deeper sites. In contrast, surface activities along the Chilean margin increased, in general, from shallower to deeper areas (from ~12 to >80 dpm g^{-1}).

The activity profiles showed a slight subsurface increase at ~5 cm depth at Station 6 off Iquique and at Stations GEOB7104 and GEOB7106 off Mejillones (Figs. 4B and C). Constant surface activities (0–4 cm depth) were seen at the shallow Station A off Callao, and an abrupt subsurface drop at 6–8 cm depth (Fig. 4A). Off Concepción, subsurface increments of activities also were observed (Stations 26A, 5d, 3, and GEOB7162), with relatively constant values in the upper 4–8 cm (Stations 4c, GEOB7160, and GEOB7166) (Fig. 4D, Table 3).

^{226}Ra values at Station A off Callao were between 7.8 and 7.9 dpm g^{-1} from the surface to 38 cm depth. At Station C, these values varied between 4.9 at the surface to 7.1 at depth (Table 2). Both stations showed similar ^{226}Ra values to those measured in sediments off Mejillones (3.4–6.6 dpm g^{-1}). Anomalously high ^{226}Ra activities were observed at Station A between 38 and 54 cm depth (14.4–23.6 dpm g^{-1}), and at Station B (between 33.8 dpm g^{-1} at the surface and 3.8 dpm g^{-1} at depth). Supported ^{210}Pb activities estimated from the constant values at the base of the cores for Iquique were lower (~1.7–2.2 dpm g^{-1}). Off Concepción for stations visited in 1999 were in agreement with ^{226}Ra

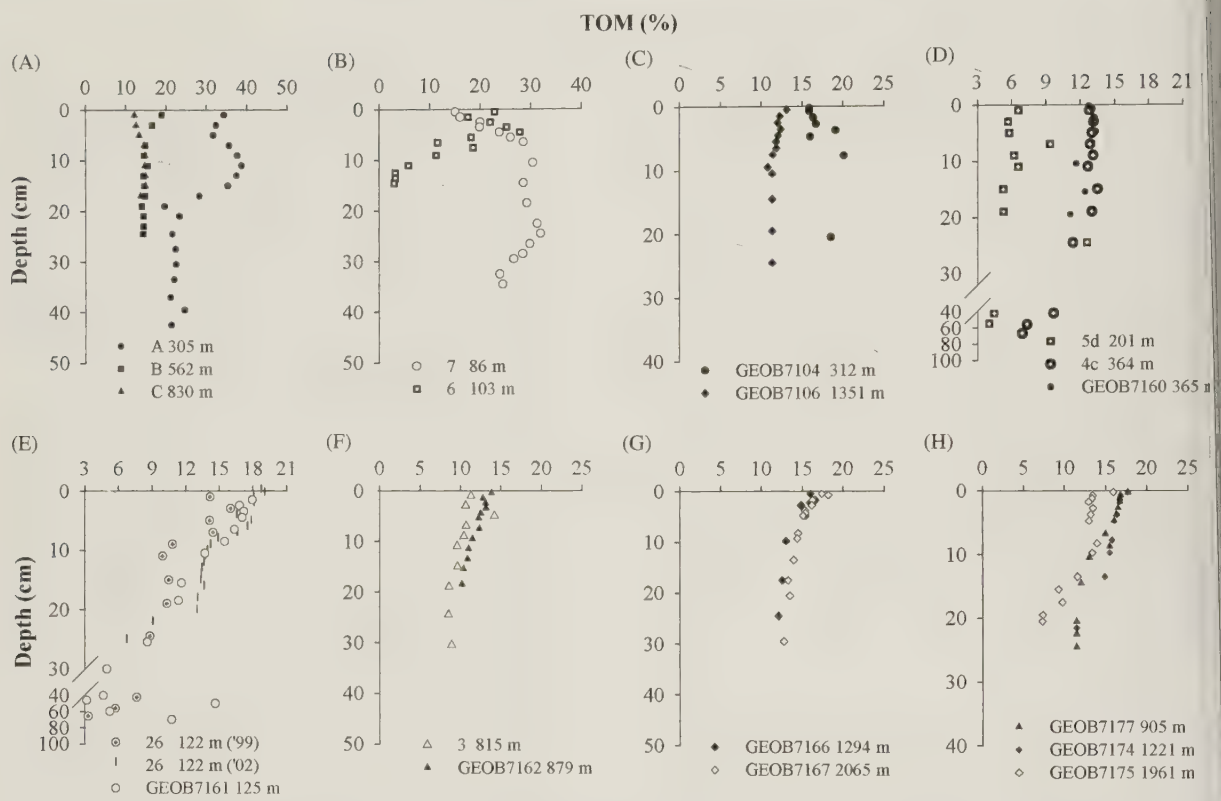

Fig. 3. TOM (%) profiles. Cores from central Peru: Callao (A), northern Chile; Iquique (B) and Mejillones (C), south-central Chile; Concepción (D–G, from north to south); southern Chile, Chiloé (H).

values measured at nearby stations occupied in 2001 (Stations 4c and GEOB7160; Stations 26A, 26B, and GEOB7161; Stations 3 and GEOB7162). These values ranged between 0.8 and 1.6 dpm g^{-1} at the shallower stations and between 2.3 and 4.9 dpm g^{-1} at the deeper sites (Table 2, Fig. 4D). Off Chiloé, the supported ^{210}Pb activity estimated at Station GEOB7175 (3.7 ± 1.9 dpm g^{-1}) lies within the range of ^{226}Ra values measured at nearby Stations GEOB7174 and 7177 (3.4–2.2 and 2.7–2.9 dpm g^{-1}, respectively) (Table 2, Fig. 4E).

3.3. ^{210}Pb inventories and fluxes and resulting sedimentation rates

^{210}Pb inventories and fluxes showed a lower range in values among the northern stations. Lowest values were observed at the deep Station C off Callao and at Station GEOB7106 off Mejillones (inventories: 22.6–23.2 dpm cm^{-2} and flux: 0.7 dpm cm^{-2} yr^{-1}). Values increased at shallow stations (off Mejillones and Iquique, 37.3–55.6 dpm cm^{-2} and 1.2–1.7 dpm cm^{-2} yr^{-1}) to reach maximum numbers at Station A off Callao (117.1 dpm cm^{-2} and 3.5 dpm cm^{-2} yr^{-1}). To the south, the range was even larger. Lowest inventories were observed at shallow sites off Concepción (Stations 26B and GEOB7161, 78.1–54.1 dpm cm^{-2} and 1.7–2.4 dpm cm^{-2} yr^{-1}), except at Station 26A, which showed a higher inventory and flux (140.1 dpm cm^{-2} and 4.3 dpm cm^{-2} yr^{-1}). All other deep stations showed higher inventories (116.7–288.2 dpm cm^{-2}) and fluxes (>3.6 dpm cm^{-2} yr^{-1}) (Table 2). Resulting SRs showed the same trend, with lower values and ranges in the north (0.04–0.17 cm yr^{-1}; Callao, Iquique, and Mejillones), and higher in the

south (0.09–0.29 cm yr^{-1}; Concepción and Chiloé) (Table 3).

4. Discussion

4.1. ^{210}Pb distribution

4.1.1. Central Peru and northern Chile margins

The overall trend of decreasing ^{210}Pb surface activities downslope observed at the transect off Peru could be related to deposition rates of organic mater. Organic matter serves as a carrier for ^{210}Pb, as has been reported for phytoplankton post-bloom situations by Thomson and Turekian (1976) and Nozaki et al. (1997). Chloroplastic pigment content (CPE, i.e., chlorophyll-*a* + phaeopigments) in surface sediments is an indicator of deposited organic material that originated from primary productivity in surface waters (Pfannkuche and Soltwedel, 1998). The higher CPE and TOM content observed at Station A off Callao (Figs. 4A and 5C, Table 3) could be interpreted as reflecting higher primary productivity closer to the coast, high deposition rate to the bottom and, thus, higher surface ^{210}Pb activities. The sediments at the deeper sites off Callao revealed higher compaction, lower ^{210}Pb activities, CPE and TOM contents, and phosphorite nodules, especially at Station B. This has been previously explained as a result of sediment transport by slumping and winnowing (Levin et al., 2002), processes commonly observed along the Peru margin (Kim and Burnett, 1988). The anomalously low surface activities at deep Station C, as well as the fact that the sediments reach supported ^{210}Pb levels at shallower depths in this core (6 cm) than at Station A (16 cm, Table 2) also may suggest a loss of surface sediments in the area. On the other hand, these sediments could be a relict of erosive

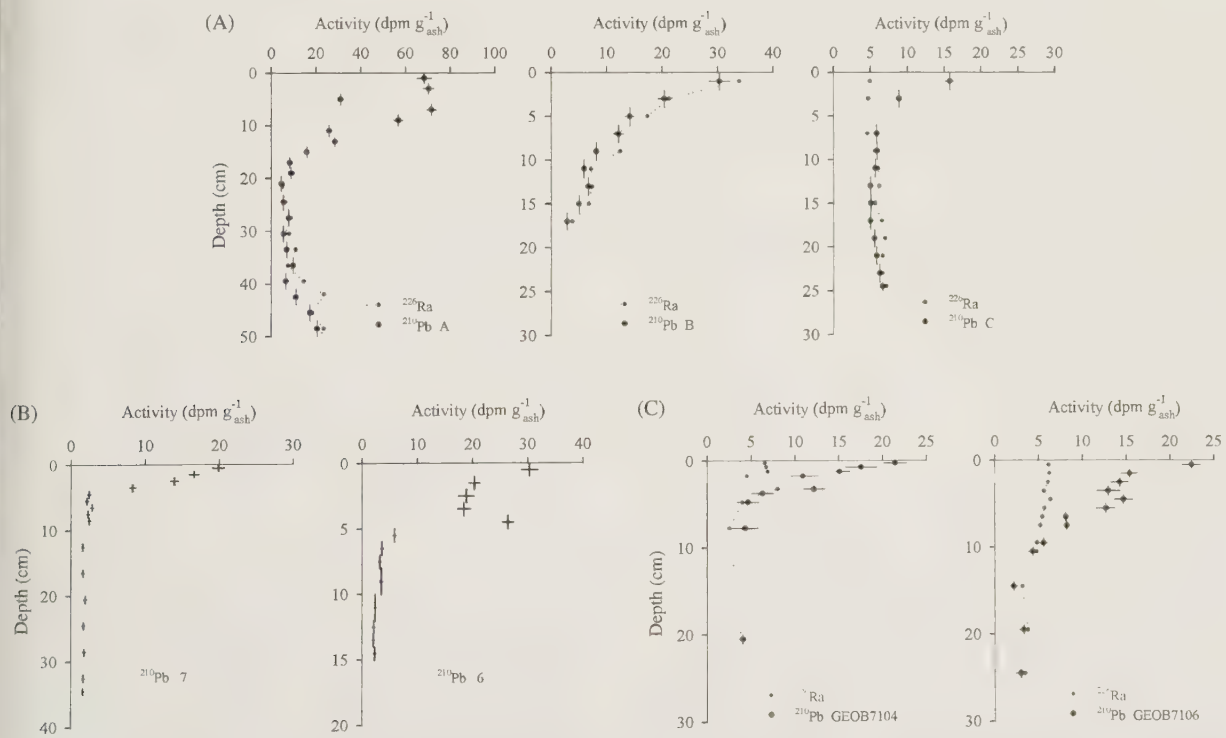

Fig. 4. ^{210}Pb distribution in sediment profiles. Dotted lines indicate the ^{226}Ra distribution; dotted symbols represent the effective measurement. Horizontal lines indicate ±SD and vertical lines the thickness. (A) Callao; (B) Iquique: Stations 6 and 7; (C) Mejillones: Stations GEOB7104 and 7106; (D) Concepción: several stations; (E) Chiloé: Stations GEOB7174, 7175, and 7177.

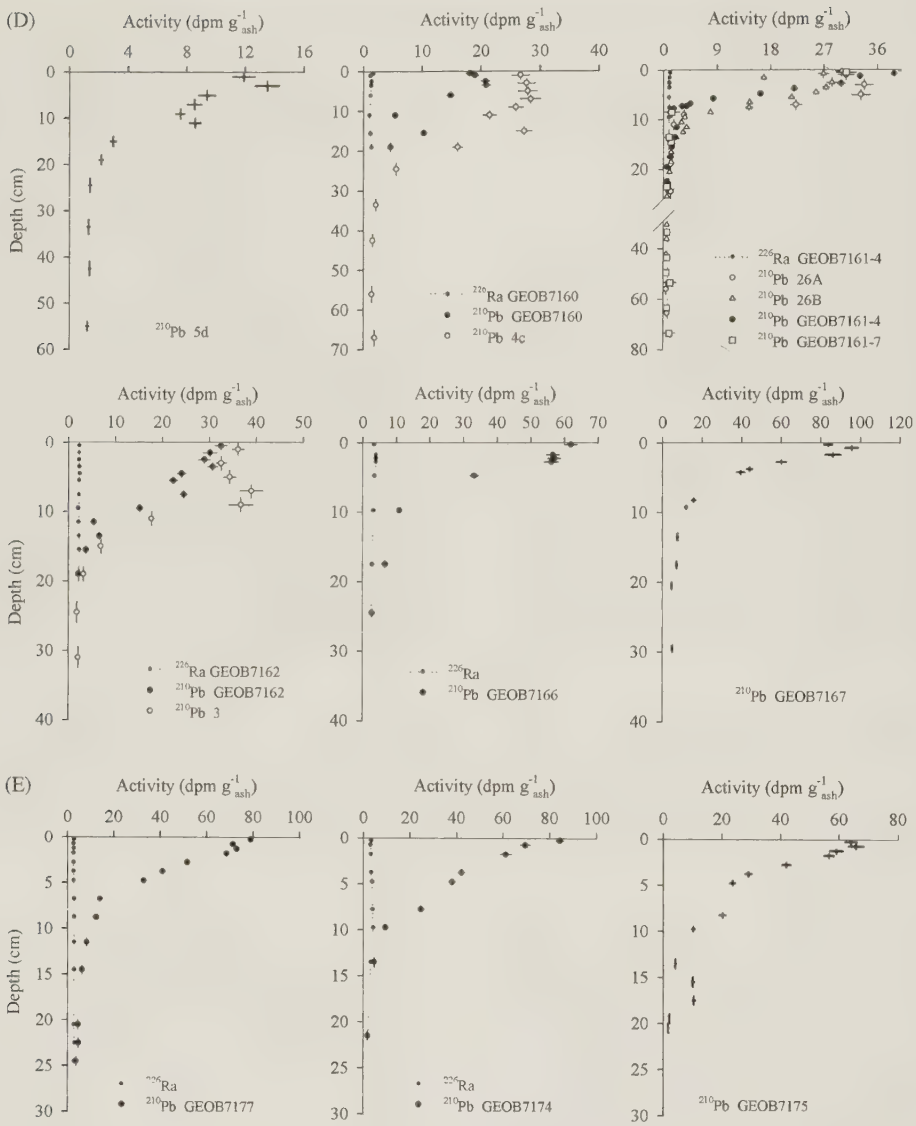

Fig. 4. (*Continued*)

processes, which may explain their higher densities (lower porosity) and the presence of phosphorite nodules at the surface (Krauskopf, 1982). No excess of ^{210}Pb is observed at Station B due to the anomalously high ^{226}Ra activity (both radioisotopes parent and daughter are in equilibrium) (Fig. 4A). We suggest that these high activities could be attributed to an effective removal of ^{226}Ra by biological particles that are large enough to promote an excess at surface sediments in upwelling areas (Cochran, 1982). Because Ra is strongly involved in the biogeochemical cycling of Ba and Si that are present in the hard parts of organisms (Bruland et al., 1974; Rhein and Schlitzer, 1988; Nozaki et al., 1998), an alternative explanation for this high ^{226}Ra activity could be the formation of authigenic minerals (Krauskopf, 1982), enriched in Ra and Th (Cochran, 1982).

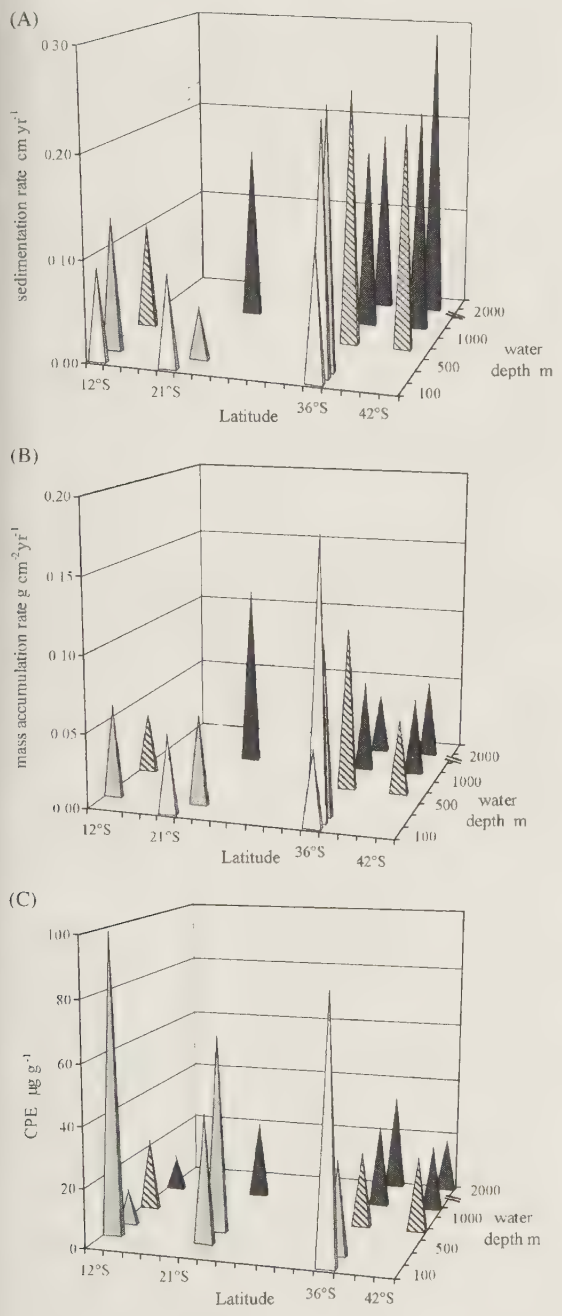

Fig. 5. SR (A) and MAR (B) along and across the sampled continental margin. (C) Chloroplastic pigment equivalent concentrations (CPE) provided by J. Sellanes (unpublished data). Shallow areas: 0–200 m (white cones), 200–500 m (light gray cones); deep areas: >500–800 m (striped cones), >800 m (black cones). Average values for sites located close to each other were used. SR for shallow site at 12 °S (Callao, Peru) was obtained from Kim and Burnett (1988).

Phosphorite nodules and carbonate rocks have been described for this area (Kim and Burnett, 1988; Levin et al., 2002), suggesting that some radionuclides could be concentrated in these sediments by biological and diagenetic processes.

In contrast to the situation off Peru, surface activities at all stations (including the deeper sites) off northern Chile (Figs. 4B and C) showed a shorter range in activity values (20–32 dpm g^{-1}) and the unsupported ^{210}Pb (excess) values were reached at similar depths (4–6 cm), except at Station GEOB7106 (10 cm) (Table 2). This pattern seems to be independent from variations in organic matter deposition (Fig. 5C). However, a definite pattern cannot be proposed here since we lack CPE information for the area off Iquique and SR for a station at 500 m off Antofagasta (22 °S) (Table 3, Figs. 5A and C).

The ^{210}Pb distribution in all cores showed lowest exponential distribution at Station C, attributed to greater mixing in these sediments (Levin et al., 2002). In contrast, stations in northern Chile had a better exponential distribution (Figs. 4B and C), except at Station 6 off Iquique where a subsurface maximum (4–5 cm depth) interrupted the pattern. This could be attributed to slight sediment mixing by non-local transport; i.e., the organisms may ingest recently settled particles with higher activities at the sediment surface and excrete them at depth (Boudreau, 1997). However, such activities produce fewer disturbances in ^{210}Pb profiles than biodiffusion (Wheatcroft et al., 1990; Dauwe et al., 1998). High compaction of these sediments (Fig. 2B) suggests low bioturbation activity and no disturbance was observed at the close-by Station 7.

Differences between the stations off Mejillones (Fig. 4C) could be attributed to changes in the sediment composition or slumps that normally produce erratic $^{210}Pb_{xs}$ distribution profiles (Lewis et al., 2002). The shallow Station GEOB7104 shows anomalously high densities at the surface (0–5 cm, 1.2–0.9 g cm^{-3}) and lower values at depth (around 0.6 g cm^{-3}) (Fig. 2C) coincident with a slight increase in ^{210}Pb and ^{226}Ra activities (Fig. 4C). ^{226}Ra tends to diminish with depth at both Stations GEOB7104 and GEOB7106, but a more erratic distribution is observed at Station

GEOB7104. Here, the increment in ^{226}Ra is accompanied by an increment in ^{210}Pb, which could be related to ^{226}Ra and/or ^{222}Rn diffusion in pore water, as was observed by Suckow et al. (2001) in their bioturbation study in the Peru margin. The authors argue that the anomalies in the radionuclide profiles could be misinterpreted as non-local mixing. In our case, Station GEOB7104 seems to be more affected by diffusion of the radionuclides than by bioturbation. In contrast, ^{226}Ra distribution at Station GEOB7106 did not show strong evidence for diffusion, and we believe that the subsurface increments in the ^{210}Pb profile should be the result of slight bioturbation.

4.1.2. Central-south Chilean margin

At the shelf off Concepción, the lowest ^{210}Pb activities in surface sediments are observed at the northernmost station (Station 5d) (Fig. 4D), where highest bulk densities (Fig. 2D) and lowest TOM contents (Fig. 3D) suggest a relatively coarse grain size distribution. Lamy et al. (1998) report an increase in sand (from 13% to 85%) between 90 and 400 m water depth at close-by stations just north of our Station 5d. A large supply of siliciclastic sediment on the upper continental margin in this area results from rivers that drain the mountain regions of the Andes and the Coastal Range (Scholl et al., 1970; Hebbeln et al., 2000). It is known that adsorption of organic matter is related to particle size and surface area (Mayer, 1994; Fisher et al., 1987), being lower for larger fractions, similar to that observed for ^{210}Pb (Turekian et al., 1980). In this sense, coarse sediments maintain lower activities than those composed of fine particles.

Two stations on the upper slope in this area (Stations 4c and GEOB7160), just southeast of Station 5d (Fig. 1), have higher ^{210}Pb activities. Cores from these stations were collected during two different sampling periods, Station 4c during the 1999 Thioploca cruise and GEOB7160 during the 2001 SONNE cruise. They have similar compositions (density and TOM content) (Figs. 2D and 3D) and similar ^{210}Pb distribution with depth. A subsurface peak in activity also is observed at the same depth (~15 cm) (Fig. 4D). These higher activities could be associated with particle advection from shallower depths where sediments are easily resuspended. Particles are enriched in ^{210}Pb during repeated resuspension events (Radakovitch and Heussner, 1999; Smoal et al., 2000; Lewis et al., 2002). Reworked benthic diatoms have been reported at nearby ODP Site 1235 (Mix and Shipboard Scientific Party, 2002) suggesting that resuspension and advection might play a significant role in this area. The reason for the difference in activity values observed between these stations is not clear. Deeper sites to the south, located close to the maximum depth of the submarine Bio-Bio Canyon (Stations 3 and GEOB7162), have similar ^{210}Pb profiles but also slight differences in activities between them (Fig. 4D).

Radakovitch and Heussner (1999), in their study of the Bay of Biscay, suggested that the biological activity in the axis of the canyons could be responsible for the ^{210}Pb redistribution. They attributed the differences within cores from the same stations to small-scale variability in the mixing processes. This also was observed by Suckow et al. (2001) at shallow depths off Peru. In the case of our Stations GEOB7162 and 3, non-local mixing seems to affect the first 10 cm. The effect of mixing decreases substantially toward deeper sites (Stations GEOB7166 and GEOB7167).

Stations GEOB7161 and 26B (locations separated by <40 m) show mostly similar ^{210}Pb activities (Fig. 4D), TOM contents (Fig. 3E), and bulk densities (Fig. 2E). However, the upper 6–8 cm core depth at Station 26A sampled during the 1999 Thioploca cruise has lower TOM contents and, consequently, higher bulk densities, suggesting that the differences observed in activity distribution may be attributable to textural differences. In addition, mixing is affecting the upper 6 cm in 1999, while in 2002 only the uppermost 2 cm of Station 26B are affected; there is no evidence of mixing at near-by Station GEOB7161 obtained in 2001 (Table 3). This points to the intensity of bioturbation being highly variable in time and space, as observed at shallow depths in the area (Gutiérrez, 2000). In spite of the observed surface differences, all cores from the Concepción area show similar ^{210}Pb distribution patterns with depth. As expected, surface activities are higher in

the deeper cores (GEOB7166 and GEOB7167), since particles reaching the seafloor at greater depths may be more enriched in ^{210}Pb due to longer residence times in the water column (Masqué et al., 2003).

4.1.3. Southern Chilean margin

In general, ^{210}Pb surface activities and depth distribution off Chiloé (Fig. 4E) are similar to those observed at the deep sites off Concepción (Fig. 4D). Station GEOB7175, the deepest of these sites, shows a 0.5 cm mixed layer at the surface and an anomalous increase at 15–17 cm depth. In a gravity core from this station (Core 7175–6) (Hebbeln et al., 2001), a burrow of about 40 cm in length filled with soft sediment was observed. As mentioned above, such burrows can produce typical radionuclide profiles with higher subsurface activities (non-local mixing) (Boudreau, 1997), as seen at site GEOB7175. If we do not consider the anomalously high activity at 15 cm depth in core GEOB7175, and compare it with GEOB7174 and GEOB7177, all three cores seem to reach supported ^{210}Pb values at ~15 cm depth. This suggests that these sites receive particulate material with similar ^{210}Pb content with the same deposition rate.

4.2. Sedimentation and mass accumulation rates

In general, SRs along the Peru–Chile margin increase from north to south (Fig. 5A, Table 3). No significant differences in SR were observed among shallow sites away from canyons and, in general, higher SRs occur at the deeper sites. The high CPE values at Station A off Peru and at Station GEOB7161 off Concepción (99 and 85 $\mu g\,g^{-1}$, respectively) (Table 3, Figs. 5A and C) do not correspond with higher SRs, suggesting that other processes besides primary production in the water column are at play (see below). No clear latitudinal pattern emerges when plotting MAR; trends are more evident across the shelf than along the margin (Fig. 5B, Table 3). MARs are lower at greater depths, except off northern Chile, and high near the canyons off central-south Chile.

Since MAR is related to the density of the sediments, changes in particle composition could somewhat complicate data interpretation. Strong precipitation and high river discharges transport huge amounts of terrigenous matter to the ocean off central-south Chile (35–39 °S) (river flux mode = 40–500 $m^3\,s^{-1}$ and suspended particles = 600–2500 ton $month^{-1}$; http://www.dga.cl; http://lauca.usach.cl/ima/cap10.htm). This constitutes an additional source of particles, increasing SRs and MARs, with a predominance of siliciclastic material over organic particles. Off northern Chile, on the other hand, the high MAR at deep site GEOB 7106 (Fig. 5B) is most probably related to lateral transport since there are no important river outflows in this area (river flux mode = 0.6–6.6 $m^3\,s^{-1}$; http://www.dga.cl).

It is evident that the different topographic settings of the sampled areas also contribute to the differences in SR and MAR. Off Callao, low SRs on slope Stations A and C are comparable to low values reported for the Peru shelf (0.07–0.32 $cm\,yr^{-1}$) (Koide and Goldberg, 1982; Kim and Burnett, 1988), where erosive processes play an important role in the distribution of the sediment (Kim and Burnett, 1988; Froelich et al., 1988). The increase of SR and MAR at deeper sites on the northern Chilean margin (off Mejillones) (Figs. 5A and B) can be attributed to the narrow shelf, which promotes downslope transportation of eroded material (slumps) or turbidity current flows, transporting huge amounts of particles. In contrast to the Peru shelf and slope, the wider shelf off central Chile is crossed by canyons. This determines higher SR and MAR that result from both river discharges and lateral transport (Lewis et al., 2002; Xu et al., 2002; Oguri et al., 2003). Canyons act as particle conduits, and the low currents found at their maximum depths allow for rapid settling of particles resulting in a zone of preferential accumulation and highest MAR (Radakovitch and Heussner, 1999). This can be observed at stations close to the maximum depth of the Bio-Bio Canyon (~800 m, Stations 3 and GEOB7162) and Itata Canyon (~450 m, Stations 4c and GEOB7160).

All stations located at the deepest sites off Concepción (not within canyons) and Chiloé showed comparable CPE (24.5–31.9 $\mu g\,g^{-1}$) and MAR (0.04–0.06 $g\,cm^{-2}\,yr^{-1}$) values (Figs. 5B

and C), suggesting that they are influenced by similar processes. Here, the currents should be an important source of particles to deep sediments along the margin. In the south (40 °S), Hebbeln et al. (2001) reported strong shelf currents that sweep all fine-grained material, which is then canalized through the numerous canyons directly into the deep sea.

4.3. The mixing effect on sedimentation rate in the study area

When mixing is intense and burial velocity is low, the effect on ^{210}Pb profiles is significant, creating a typical homogeneous surface layer (Lewis et al., 2002); this is observed at some stations off Concepción, affecting the upper 4–10 cm of the sediment column. At other stations, a slight bioturbation is evident only for the first centimeters (Table 3). Our SR estimations are related to the sediments below the mixing layer, where bioturbation coefficients can be one order of magnitude lower than those measured at the surface, as reported by Salamanca (1989) in shallow areas off Concepción (<100 m water depth, 0.45 $cm^2 yr^{-1}$). Other authors have shown a significant decrease in the mixing coefficient (Db) in shallow areas, of 10–20% that of surface values (Silverberg et al., 1986). However, the potential of bioturbation is highly variable, depending on dissolved oxygen concentrations and the quality of organic carbon at the bottom. For example, in the area off Concepción, temporal oxygenation events such as those during El Niño promote an increase in bioturbating species compared to those periods when a hypoxic environment is dominant (Gutiérrez et al., 2000). Other studies using Uranium series disequilibrium techniques (as in this study), which include mixing effects below the mixing layer, report SR between 0.07 and 0.11 $cm\,yr^{-1}$ at shallow water depths (100–200 m, ~12 °S) (Kim and Burnett, 1988). Our estimates fall within the upper range of these data, probably because we did not consider this mixing effect. We propose that ignoring this effect below the mixed layer does not cause serious overestimation of SRs and is a good approach to "real" SRs, as also stated by Nittrouer et al. (1983/1984) for the Washington continental shelf and by Lewis et a (2002) for shelf sediments in Monterey Bay.

Although ^{210}Pb profiles provide low resolutio in those cases where mixing is observed, we believ that they are a useful tool for first-order approx imation of sediment-transport parameters, espe cially for a study area like ours, where availabl information on the seafloor environment is stil very scarce.

Acknowledgments

We thank the captains and crew members of the R./V. *Sonne*, R./V. *Vidal Gormáz*, L./C. *Carlos Porter*, and L./C. *Kay Kay* for their efforts and support at sea. We extend our special thanks to the technicians and students for their help during sampling and analyses. We thank O. Parra and R. Urrutia for laboratory facilities and working space in the EULA Center, Universidad de Concepción, Chile, as well as personnel of the Sciences du Climat et l'Environnement (LSCE) laboratory at Gif-Sur-Yvette, France. O. Ulloa, V.A. Gallardo, and R. De Pol kindly supplied several sediment samples for this project. We are indebted to J. Sellanes for sharing unpublished CPE data. The final version of this manuscript greatly benefited from reviews by three anonymous referees. This work was supported by the FONDAP-COPAS Center (Project No. 150100007) and by the ECOS-SUD Program.

References

Alperin, M., Suayah, I., Benninger, L.K., Martens, C.S., 2002. Modern organic carbon burial fluxes, recent sedimentation rates, and particle mixing rates from the upper continental slope near Cape Hatteras, North Carolina (USA). Deep-Sea Research II 49, 4645–4665.

Arcos, D.F., Wilson, R.C., 1984. Upwelling and distribution of chlorophyll *a* within the bay of Concepción, Chile. Estuarine, Coastal and Shelf Science 18 (1), 25–35.

Arcos, D.F., Núñez, S.E., Acuña, A., 1996. Variabilidad de pequeña escala en la zona nerítica del sistema de surgencia de Talcahuano (Chile Central): identificación y dinámica de áreas de retención larval. Gayana Oceanológica 4 (1), 21–58.

Berger, W.H., Fisher, K., Lai, C., Wu, G., 1987. Ocean productivity and organic carbon flux. Part I. Overview and

maps of primary production and export production. SIO Reference, pp. 87–30.

Bernal, P., Ahumada, R., Gonzáles, H., Pantoja, S., Troncoso, A., 1989. Carbón flux in a pelagic trophic model for Concepción Bay, Chile. Biología Pesquera 18, 5–14.

Bevington, P., Robinson, K., 1992. Error analysis. In: Bevington, P., Robinson, K. (Eds.), Data Reduction and Error Analysis for the Physical Sciences. WCB/McGraw-Hill, New York, USA, pp. 38–52.

Blanco, J.L., Thomas, A., Carr, M.E., Strub, P.T., 2001. Seasonal climatology of hydrographic conditions in the upwelling region off northern Chile. Journal of Geophysical Research 106 (C6), 11451–11467.

Blank, M., Leinen, M., Prospero, J.M., 1985. Major Asian aeolian inputs indicated by the mineralogy of aerosols and sediments in the Western North Pacific. Nature 314, 84–86.

Borole, D.V., 2002. Analysis of ^{210}Pb in sediment trap samples and sediments from northern Arabian Sea: evidence for boundary scavenging. Deep-Sea Research I 49, 1055–1069.

Boudreau, B., 1997. Model construction. In: Boudreau, B. (Ed.), Diagenetic Models and Their Implementation. Springer, Berlin, Germany, pp. 23–90.

Bruland, K.W., Koide, M., Goldberg, E., 1974. The comparative marine geochemistries of lead and radium 226. Journal of Geophysical Research 79 (21), 3083–3086.

Chávez, F.P., Barber, R.T., Sanderson, M.P., 1989. The potential primary production of the Peruvian upwelling ecosystem, 1953–1984. In: Pauly, D., Muck, P., Mendo, J., Tsukayama, I. (Eds.), The Peruvian Upwelling Ecosystem: Dynamics and Interactions, vol. 18. ICLARM Conference Proceedings, Manila, pp. 50–63.

Chester, R., 1990. Marine Geochemsitry. Chapman & Hall, London, p. 698.

Christensen, E.R., 1982. A model for radionuclides in sediments influenced by mixing and compaction. Journal of Geophysical Research 87 (C1), 566–572.

Cochran, K., 1982. The oceanic chemistry of the U- and Th-series nuclides. In: Ivanovich, M., Harmon, R. (Eds.), Uranium Series Disequilibrium. Clarendon Press, Oxford, pp. 384–430.

Cochran, J.K., Frignani, M., Salamanca, M., Belluci, L.G., Guerzoni, S., 1998. Lead-210 as a tracer of atmospheric input of heavy metals in the northern Venice Lagoon. Marine Chemistry 62 (1–2), 15–29.

Daneri, G., Dellarossa, V., Quiñones, R., Jacob, B., Montero, P., Ulloa, O., 2000. Primary production and community respiration in the Humboldt Current System off Chile and associated oceanic areas. Marine Ecology Progress Series 197, 41–49.

Dauwe, B., Herman, P.M.J., Heip, C.H.R., 1998. Community structure and bioturbation potential of macrofauna at four North Sea stations with contrasting food supply. Marine Ecology Progress Series 173, 67–83.

Dellarosa, V., 1998. Producción primaria anual en sistemas de alta producción biológica. Ph.D. Thesis, Universidad de Concepción, Chile, Unpublished.

Fisher, N.S., Teyssié, J.-L., Krishnaswami, S., Baskaran, M., 1987. Accumulation of Th, Pb, U, and Ra in marine phytoplankton and its geochemical significance. Limnology and Oceanography 32 (1), 131–142.

Flynn, W.W., 1968. The determination of low levels of polonium-210 in environmental materials. Analytica Chimica Acta 43, 221–227.

Fossing, H., Gallardo, V.A., Jørgensen, B.B., Hüttel, M., Nielsen, L.P., Schulz, H.N., Canfield, D.E., Forster, S., Glud, R.N., Gundersen, J.K., Küver, J., Ramsing, N.B., Teske, A., Thamdrup, B., Ulloa, O., 1995. Concentration and transport of nitrate by the mat-forming sulfur bacterium Thioploca. Nature 374, 713–715.

Froelich, P.N., Arthur, M.A., Burnett, W.C., Deakin, M., Hensley, V., Jahnke, R., Kaul, L., Kim, K.-H., Roe, K., Soutar, A., Vathakanon, C., 1988. Early diagenesis of organic matter in Peru continental margin sediments: phosphorite precipitation. Marine Geology 80, 309–343.

Gorgas, T.J., Wilkens, R.H., 2002. Sedimentation rates off SW Africa since the late Miocene deciphered from spectral analyses of borehole and GRA bulk density profiles: ODP Sites 1081–1084. Marine Geology 180, 29–47.

Gutiérrez, D., 2000. Bioperturbación y macrofauna en fopndos sublitorales de un área de surgencias frente a Chile Central (36°30′S): Variación espacial y temporal en el período 1997–1999. Ph.D. Thesis, Universidad de Concepción, Casilla 160-C, Concepción, Chile.

Gutiérrez, D., Gallardo, V.A., Mayor, S., Neira, C., Vásquez, C., Sellanes, J., Rivas, M., Soto, A., Carrasco, F., Baltasar, M., 2000. Effects of dissolved oxygen and fresh organic matter on the bioturbation potential of macrofauna in sublittoral bottoms off central Chile, during the 1997–98 El Niño. Marine Ecology Progress Series 202, 81–99.

Habit, E., Bertrán, C., Arévalo, S., Victoriano, P., 1998. Benthonic fauna of the Itata river and irrigation canals (Chile). Irrigation Science 18, 91–99.

Hagen, R.A., Vergara, H., Naar, D., 1996. Morphology of San Antonio submarine canyon on the central Chile forearc. Marine Geology 129, 197–205.

Hebbeln, D., Shipboard Scientific Party, 2001. Report and preliminary results of R/V *Sonne* cruise SO 156, Valparaíso (Chile)–Talcahuano (Chile), March 29–May 14, 2001. Berichte aus dem Fachbereich Geowissenschaften der Universität Bremen, No. 182 (195pp) (boelen@uni-bremen.de).

Hebbeln, D., Marchant, M., Freudenthal, T., Wefer, G., 2000. Surface sediment distribution along the Chilean continental slope related to upwelling and productivity. Marine Geology 164, 119–137.

Henderson, G.M., Maier-Reimer, E., 2002. Advection and removal of ^{210}Pb and stable Pb isotopes in the oceans: a general circulation model study. Geochimica et Cosmochimica Acta 66 (2), 257–272.

Kim, K.H., Burnett, W., 1988. Accumulation and biological mixing of Peru margin sediments. Marine Geology 80, 181–194.

Koide, M., Goldberg, E.D., 1982. Transuranic nuclides in two coastal marine sediments off Peru. Earth & Planetary Science Letters 57, 263–277.

Krauskopf, K.B., 1982. Carbonate sediments. In: Emery, K.O., Legget, R.F., Murray, B., Sloss, L. (Eds.), Introduction to Geochemistry, second ed. McGraw-Hill Book Company, New York, pp. 51–78.

Lamy, F., Hebbeln, D., Wefer, G., 1998. Terrigenous sediment supply along Chilean continental margin: modern regional patterns of texture and composition. Geologische Rundschau 87, 477–494.

Lamy, F., Hebbeln, D., Wefer, G., 1999. High-resolution marine record of climatic change in mid-latitude Chile during the last 28,000 years based on terrigenous sediment parameters. Quaternary Research 51, 83–93.

Laursen, J., Normark, W.R., 2002. Late Quaternary evolution of the San Antonio Submarine Canyon in the central Chile forearc (~33°S). Marine Geology 188, 365–390.

Levin, L., Gutiérrez, D., Rathburn, A., Neira, C., Sellanes, J., Muñoz, P., Gallardo, V., Salamanca, M., 2002. Benthic processes on the Peru margin: a transect across the oxygen minimum zone during the 1997-1998 El Niño. Progress in Oceanography 53, 1–27.

Lewis, R.C., Coale, K.H., Edwards, B.D., Marot, M., Douglas, J.N., Burton, E.J., 2002. Accumulation rate and mixing of shelf sediments in the Monterey Bay National Marine Sanctuary. Marine Geology 181, 157–169.

Masqué, P., Isla, E., Sanchez-Cabeza, J.A., Palanques, A., Bruach, J.M., Puig, P., Guillén, J., 2002. Sediment accumulation rates and carbon fluxes to bottom sediments at the Western Bransfield Strait (Antarctica). Deep-Sea Research II 49, 921–933.

Masqué, P., Fabres, J., Canals, M., Sanchez-Cabeza, J.A., Sanchez-Vidal, A., Cacho, I., Calafat, A.M., Bruach, J.M., 2003. Accumulation rates of major constituents of hemipelagic sediments in the deep Alborean Sea: a centennial perspective of sedimentary dynamics. Marine Geology 3242, 1–27.

Mayer, L.M., 1994. Relationships between mineral surfaces and organic carbon concentrations in soils and sediments. Chemical Geology 114 (3–4), 347–363.

McCaffrey, R., Thomson, J.A., 1980. Record of the accumulation of sediment and trace metals in the Connecticut salt marsh. Advances in Geophysics 22, 165–236.

Mix, A., Shipboard Scientific Party, 2002. In: Shipboard Scientific Party (Ed.), Leg 202 Preliminary Report Southeast Pacific Paleoceanographic Transects, 29 March–30 May 2002. Ocean Drilling Program, Texas A&M University, USA, 154pp. (www-odp.tamu.edu/publications/prelim/202_prel).

Nittrouer, C.A., DeMaster, D.J., McKee, B.A., Cutshall, N.H., Larsen, I.L., 1983/1984. The effect of sediment mixing on ^{210}Pb accumulation rates for the Washington Continental Shelf. Marine Geology 54, 201–221.

Nozaki, Y., Zhang, J., Takeda, A., 1997. ^{210}Pb and ^{210}Po in the equatorial Pacific and the Bering Sea: the effects of biological productivity and boundary scavenging. Deep-Sea Research II 44 (9–10), 2203–2220.

Nozaki, Y., Dobashi, F., Kato, Y., Yamamoto, Y., 1998. Distribution of Ra isotopes and the ^{210}Pb and ^{210}Po balance in surface seawaters of the mid Northern Hemisphere. Deep-Sea Research I 45, 1263–1284.

Oguri, K., Matsumoto, E., Yamada, M., Saito, Y., Iseki, K., 2003. Sediment accumulation rates and budgets of depositing particles of the East China Sea. Deep-Sea Research II 50, 513–528.

Parra, O., Habit, E., 1998. In: Parra, O., Habbit, E., (Eds.), Documento de síntesis, estudio de línea base para la evaluacón de impacto ambiental del Complejo Forestal Industrial Itata (celulosa Arauco y Constitución, S.A.). Centro Eula-Chile, Universidad de Concepción, Chile, 172pp.

Pfannkuche, O., Soltwedel, T., 1998. Small benthic size classes along the western European continental margin: spatial and temporal variability in activity and biomass. Progress in Oceanography 42, 189–207.

Pineda, V., 1999. El cañón submarino del Bio-Bío: Aspectos dinámicos y ambientales. Ph.D. Thesis, Centro EULA, Universidad de Concepción, Concepción-Chile, Unpublished.

Radakovitch, O., Heussner, S., 1999. Fluxes and budget of ^{210}Pb on the continental margin of the Bay of Biscay (Northeastern Atlantic). Deep-Sea Research II 46, 2175–2203.

Rhein, M., Schlitzer, R., 1988. Radium-266 and barium sources in the deep East Atlantic. Deep-Sea Research 35 (9), 1499 1510.

Salamanca, M.A., 1989. El efecto de la bioperturbación en la distribución del exceso de ^{210}Pb y ^{239,240}Pu en sedimentos de Bahía Concepción. Ciencia y Tecnología del Mar, CONA 13, 43–56.

Scholl, D.W., Christensen, M.N., Von Huene, R., Marlow, M.S., 1970. Peru–Chile trench sediments and sea-floor spreading. Geological Society of America Bulletin 81, 1339–1360.

Silva, N., Neshyba, S., 1979. On the southernmost extension of the Peru–Chile undercurrent. Deep-Sea Research 26 (12A), 1387–1393.

Silverberg, N., Nguyen, H.V., Delibrias, G., Koide, M., Sundy, B., Yokoyama, Y., Chesselet, R., 1986. Radionuclide profiles, sedimentation rates, and bioturbation in modern sediments of the Laurentian Trough, Gulf of St. Lawrence. Oceanologica Acta 9 (3), 285–290.

Smoak, J.M., Moore, W.S., Thunell, R.C., 2000. Influence of boundary scavenging and sediment focusing on ^{234}Th, ^{228}Th and ^{210}Pb fluxes in the Santa Barbara basin. Estuarine, Coastal and Shelf Science 51 (3), 373–384.

Sobarzo, M., Figueroa, D., Djurfeldt, L., 2001. Upwelling of subsurface water into the rim of the Biobío submarine canyon as a response to surface winds. Continental Shelf Research 21, 279–299.

Strub, P.T., Mesias, J.M., Montecino, V., Ruttlant, J., Salinas, S., 1998. Coastal ocean circulation off Western South

America. In: Robinson, A.R., Brink, K.H. (Eds.), The Global Coastal Ocean. Regional Studies and Syntheses. Wiley, New York, USA, pp. 273–314.

Suckow, A., Treppké, U., Wiedicke, M.H., Weber, M.E., 2001. Bioturbation coefficients of deep-sea sediments from the Peru Basin determined by gamma spectrometry of $^{210}Pb_{exc}$. Deep-Sea Research II 48, 3569–3592.

Thomas, A.C., Carr, M.E., Strub, P.T., 2001. Chlorophyll variability in eastern boundary currents. Geophysical Research Letters 28 (18), 3421–3424.

Thomson, J., Turekian, K., 1976. ^{210}Po and ^{210}Pb distribution in ocean water profiles from the Eastern South Pacific. Earth Planetary Science Letters 32, 297–303.

Thornburg, T., Kulm, L.D., 1987a. Sedimentation in the Chile Trench: depositional morphologies, lithofacies and stratigraphy. Geological Society of America Bulletin 98, 33–52.

Thornburg, T., Kulm, L.D., 1987b. Sedimentation in the Chile Trench: petrofacies and provenance. Journal of Sedimentary Petrology 57, 55–74.

Torres, R., 1995. Condiciones oceanográficas y baja concentración de clorofila frente a Coquimbo-Chile (Lat. 30°S) durante 1992–1994. M.Sc. Thesis, Universidad de Concepción, Chile, 123pp.

Turekian, K., Cochran, K., Benninger, L., Aller, R., 1980. The sources and sinks of nuclides in Long Island Sound. Advances in Geophysics 22, 129–163.

Wheatcroft, R.A., Jumars, P.A., Smith, C.R., Nowell, A.R.M., 1990. A mechanistic view of the particulate biodiffusion coefficient: step lengths, rest periods and transport directions. Journal Marine Research 48, 177–207.

Xu, J.P., Noble, M., Eittreim, S.L., 2002. Suspended sediment transport on the continental shelf near Davenport, California. Marine Geology 181, 171–193.

Deep-Sea Research Part II – Instructions to Authors

A more detailed set of instructions can be found in the journal's home page at http://www.elsevier.com/locate/dsr2

1. Submission of Papers

Authors are requested to submit their original manuscript and figures with two copies to the Guest Editor of their Special Issue. Authors should ensure that they submit manuscripts and meet any additional requirements in line with deadlines set by the Guest Editor(s) to ensure that the entire issue can be published in a timely fashion. In most instances, revised manuscripts must be resubmitted within six months of receipt by the author. Failure to do so may lead to additional review, in some instances, rejection of the paper. Submission of a paper implies that it has not been published previously, that it is not under consideration for publication elsewhere, and that if accepted it will not be published elsewhere in the same form, in English or in any other language, without the written consent of the publisher.

2. Manuscript Preparation

General: Manuscripts must be typewritten, double-spaced with wide margins on one side of white paper. Good quality printouts with a font size of 12 or 10 pt are required. The corresponding author should be identified (include a Fax number and E-mail address). Full postal addresses must be given for all co-authors. Authors should consult a recent issue of the journal for style if possible. An electronic copy of the paper should accompany the final version. The Editors reserve the right to adjust style to certain standards of uniformity. Authors should retain a copy of their manuscript since we cannot accept responsibility for damage or loss of papers. Original manuscripts are discarded one month after publication unless the Publisher is asked to return original material after use.

Paper Length: Authors should try to confine the text to no more than 25–30 pages, with a total manuscript length (including figures and tables) of 45–50 pages.

Abstracts: The essential contents of each paper should be recapitulated briefly in an abstract of no more than 500 words at the head of the paper.

Keywords: Please provide up to six subject keywords, plus regional index terms. At least four of the subject keywords should be selected from the *Aquatic Science & Fisheries Thesaurus*. An eletronic version of the Thesaurus can be found at: http://www.csa.com/ helpV3/ ab.html. The Regional terms should be provided as a hierarchical string, eg; USA, California, Monterey Bay.

Text: Follow this order when typing manuscripts: Title, Authors, Affiliations, Abstract, Keywords, Main text, Acknowledgements, Appendix, References, Vitae, Figure Captions and then Tables. The corresponding author should be identified with an asterisk and footnote. All other footnotes (except for table footnotes) should be identified with superscript Arabic numbers.

Units: In general, metric units should be used, preferably the Systeme International (SI). If other units are used (fathoms, F, knots, etc), the metric equivalents must be given in parentheses ( ) or by presenting the dimensionally correct conversion factors as a footnote.

References: All publications cited in the text should be presented in a list of references following the text of the manuscript. In the text refer to the author's name (without initials) and year of publication (e.g. "Since Peterson (1993) has shown that ..." or "This is in agreement with results obtained later (Kramer, 1994)". For three or more authors use the first author followed by "et al.", in the text. The list of references should be arranged alphabetically by authors' names. The manuscript should be carefully checked to ensure that the spelling of authors' names and dates are exactly the same in the text as in the reference list. The title of the journal should not be abbreviated; titles of journals in Russian language should be transliterated and not translated. References should be given in the following form:

Gooday, A.J., Bett, B.J., Shires, R., Lambshead, P.J.D., 1998. Deep-sea benthic foraminiferal species diversity in the NE Atlantic and NW Arabian Sea: a synthesis. Deep-Sea Research Part II 45 (1–3), 165–201.

Hessler, R.R., Wilson, G.D.F., 1983. The origin and biogeography of malacostracan crustaceans in the deep sea. In: Sims, R.W., Price, J.H., Whalley, P.E.S. (Eds.), Evolution, time and space: the emergence of the biosphere. Academic Press. London, pp. 227–254. Thiel, H., 1983. Benthos size classification. Deep-Sea Newsletter 20, 8–11.

References to unpublished literature should be set out in the format detailed below. The following information needs to be provided: Names and initials of all authors., year. Title of work. All other relevant information needed to identify items (e.g., technical report, Ph.D. Thesis, institute, current status, i.e. in press/unpublished, etc).

Marstakas, N., 1990. Relationships of morphological and physicochemical properties of vertisols under Greek climate conditions. Ph.D. Thesis, Agricultural University Athens, unpublished.

Examples of appropriate citation formats for non-text and electronic-only information can be found in the Guide for Authors at the Deep-Sea Research Part II website. However, it is requested that a web site address, or listserver message is given as a reference only where the information is unavailable in a more permanent form. If such sources are given, then please give as complete information as is possible. All references to such material in the text of the article must be supported by a full entry in the bibliography.

Illustrations: All illustrations should be provided in camera-ready form, suitable for reproduction (which may include reduction) without retouching. Photographs, charts and diagrams are all to be referred to as "Figure(s)" and should be numbered consecutively in the order to which they are referred. They should accompany the manuscript, but should not be included within the text. All illustrations should be clearly marked on the back with the figure number and the author's name. All figures are to have a caption. Captions should be supplied on a separate sheet.

Line drawings: Good quality printouts on white paper produced in black ink are required. All lettering, graph lines and points graphs should be sufficiently large and bold to permit reproduction when the diagram has been reduced to a size suitable for inclusi in the journal. Dye-line prints or photocopies are not suitable for reproduction. Do not use any type of shading on computer-generat illustrations.
Photographs: Original photographs must be supplied as they are to be reproduced (e.g. black and white or colour). If necessary, a sc should be marked on the photograph. Please note that photocopies of photographs are not acceptable. Half-tone illustrations shou be kept to a minimum.
Fold-charts: The cost of fold-charts or diagrams must be borne by the author or his institution. *Colour:* Authors will be charged f colour reproduction as follows: €350 (or US$350) for the first page, €175 (or US$175) for subsequent pages.
Submit colour illustrations as original photographs, high-quality computer prints or transparencies, close to the size expected publication, or as 35 mm slides. Polaroid colour prints are not suitable. If, together with your accepted article, you submit usab colour figures then Elsevier will ensure, at no additional charge, that these figures will appear in colour on the web (e.g., ScienceDire and other sites) regardless of whether or not these illustrations are reproduced in colour in the printed version. For colour reproductio in print, you will receive information regarding the costs from Elsevier after receipt of your accepted article. For further information c the preparation of electronic artwork, please see *Artwork Instructions*. Please note: Because of technical complications which can ari by converting colour figures to 'grey scale' (for the printed version should you not opt for colour in print) please submit in additio usable black and white prints corresponding to all the colour illustrations.
Tables: Tables should be numbered consecutively and given a suitable caption and each table typed on a separate sheet. Footnotes tables should be typed below the table and should be referred to by superscript lowercase letters. No vertical rules should be use Tables should not duplicate results presented elsewhere in the manuscript, (e.g. in graphs).

Authors in Japan kindly note: Upon request Elsevier Japan will provide a list of people who can check and improve the English of a article (*before submission*). Please contact our Tokyo office: Elsevier Japan K.K., 1-9-15 Higashi Azabu, Minato-ku, Tokyo 106-004 Japan; tel.: +81-3-5561-5032; fax: +81-3-5561-5045; e-mail: jp.info@elsevier.com

3. Electronic Submission

Authors should submit an electronic copy of their paper with the final version of the manuscript. The electronic copy should match th hardcopy exactly. For authors using LaTex, the document style files, as well as the instructions "Preparing articles with LaTex" in th form of a dvi file, can be obtained free of charge from any host on the Comprehensive Tex Archive Network (CTAN) using anonymou ftp. The primary CTAN hosts are ftp.dante.de and ftp.tex.ac.uk. The Elsevier macros are in /pub/tex/macros/latex/contrib/supporte elsevier. These can also be downloaded from the Internet site http://www.tex.ac.uk. Always keep a back up copy of the electronic fil for reference and safety. Full details of electronic submission and other formats can be obtained from http://authors.elsevier.com o from Author Support at Elsevier.

4. Proofs

Proofs will be sent to the author (first named author if no corresponding author is identified of multi-authored papers) and should b returned within 48 hours of receipt. Corrections should be restricted to typesetting errors; any others may be charged to the author Any queries should be answered in full. Please note that authors are urged to check their proofs carefully before return, since th inclusion of late corrections cannot be guaranteed. If authors are expecting to be away from their office when the proofs arrive arrangements should be made with colleagues for the proofs to be checked in the authors absence. Proofs are to be returned to th Log-in Department, Elsevier, Stover Court, Bampfylde Street, Exeter, Devon EX1 2AH, UK.

5. Offprints

Twenty-five offprints and a copy of the issue will be supplied free of charge to each corresponding author of a paper. Additiona offprints can be ordered at a specially reduced rate using the order form sent to the corresponding author after the manuscript has beer accepted. Orders for reprints will incur a 50% surcharge.

6. Copyright

All authors must sign the "Transfer of Copyright" agreement before the article can be published. This transfer agreement enables Elsevier Ltd to protect the copyrighted material for the authors, but does not relinquish the author's proprietary rights. The copyright transfer covers the exclusive rights to reproduce and distribute the article, including reprints, photographic reproductions, microfilm or any other reproductions of similar nature and translations. Includes the right to adapt the article for use in conjunction with computer systems and programs, including reproduction or publication in machine-readable form and incorporation in retrieval systems. Authors are responsible for obtaining from the copyright holder permission to reproduce any figures for which copyright exists.

7. Author Enquiries

For enquiries relating to the submission of articles (including electronic submission), the preparation of electronic artwork, the status of accepted articles, author Frequently Asked Questions and any other enquiries relating to Elsevier Science, please consult http:// authors.elsevier.com
Contact details for questions arising after acceptance of an article, especially those relating to proofs, are provided when an article is accepted for publication.
Authors can also keep a track on the progress of their accepted article, and setup e-mail alerts informing them of changes to their manuscripts status, by using the "Track a paper" feature of Elsevier's Author gateway (http://authors.elsevier.com).

(*Continued from outside back cover*)

M. Marchant, D. Hebbeln, S. Giglio, C. Coloma and H.E. González	2441	Seasonal and interannual variability in the flux of planktic foraminifera in the Humboldt Current System off central Chile (30°S)
H.E. González, D. Hebbeln, J.L. Iriarte and M. Marchant	2457	Downward fluxes of faecal material and microplankton at 2300 m depth in the oceanic area off Coquimbo (30°S), Chile, during 1993–1995
		Section III: Benthic systems, sedimentation and elemental cycling in sediments
V.A. Gallardo, M. Palma, F.D. Carrasco, D. Gutiérrez, L.A. Levin and J.I. Cañete	2475	Macrobenthic zonation caused by the oxygen minimum zone on the shelf and slope off central Chile
L. Farías, M. Graco and O. Ulloa	2491	Temporal variability of nitrogen cycling in continental-shelf sediments of the upwelling ecosystem off central Chile
V. Molina, L. Farías, M. Graco, C. Rivera, L. Pinto and V.A. Gallardo	2507	Benthic nitrogen regeneration under oxygen and organic matter spatial variability off Concepción (~36°S), central Chile
P. Muñoz, C.B. Lange, D. Gutiérrez, D. Hebbeln, M.A. Salamanca, L. Dezileau, J.L. Reyss and L.K. Benninger	2523	Recent sedimentation and mass accumulation rates based on ^{210}Pb along the Peru–Chile continental margin

CONTENTS Direct This journal is part of **ContentsDirect**, the *free* alerting service which sends tables of contents by e-mail for Elsevier books and journals. You can register for **ContentsDirect** online at: **www.elsevier.com/locate/contentsdirect**

Indexed/abstracted in: *Curr Cont/Agri Bio Env Sci. Cirr Cont/Phys. Chem. Earth Sci, Curr Cont Sci Cit Ind, Res Alert, Global Change, Curr Aware BioSci, Geobase, Ocean Lit Rev, Awuat Sci. Fish Abstr, Meteor, Geoastrophys Abstr*

ISSN 0967–0645

ELSEVIER

DEEP-SEA RESEARCH PART II

Topical Studies in Oceanography

Oceanography in the eastern South Pacific: Part I

Volume 51, Numbers 20–21, 2004

CONTENTS

		Editorial
C.E. Morales and C.B. Lange	2345	Oceanographic studies in the Humboldt current syste off Chile: an introduction
		Section I: Physical oceanogaphy
O. Leth, G. Shaffer and O. Ulloa	2349	Hydrography of the eastern South Pacific Ocea results from the Sonne 102 cruise, May–June 1995
A. Valle-Levinson, W. Schneider, M. Sobarzo, M. Bello, L. Bravo, M. Castillo, L. Duarte, R. Fuenzalida, J.M. Gallegos, J. Garcés–Vargas, J. González, D. Gutiérrez, C. Molinet, M.S. Navarro, J. Pierini, E. Rodríguez-Rubio, A. Valdenegro, L. Vera and L. Zenteno	2371	Wind-induced exchange at the entrance Concepción Bay, an equatorward facing embayment central Chile
		Section II: Pelagic system and bentho-pelag coupling
R. Escribano, G. Daneri, L. Farías, V.A. Gallardo, H.E. González, D. Gutiérrez, C.B. Lange, C.E. Morales, O. Pizarro, O. Ulloa and M. Braun	2389	Biological and chemical consequences of th 1997–1998 El Niño in the Chilean coastal upwellin system: a synthesis
V. Montecino, R. Astoreca, G. Alarcón, L. Retamal and G. Pizarro	2413	Bio-optical characteristics and primary productivit during upwelling and non-upwelling conditions in highly productive coastal ecosystem off centra Chile (~36°S)
L.A. Cuevas, G. Daneri, B. Jacob and P. Montero	2427	Microbial abundance and activity in the seasona upwelling area off Concepción (~36°S), central Chile: comparison of upwelling and non-upwelling condition

(*Continued on inside back cover*)

Visit our home page:
http://www.elsevier.com/locate/dsr2

Printed in Great Britain by Alden Press Ltd., Osney Mead, Oxford OX2 OEF

Also available on
SCIENCE DIRECT®
www.sciencedirect.com

0967-0645(200410)51:20-21;1-8